INSTITUTE *of* TECHNOLOGY SLIGO

The Effect of Organic Fibres on the Undrained Shear Strength of Soil

Raymond Mark Grennan

This project is submitted in fulfilment of Quality and Qualifications
Ireland requirements for the Degree of Master of Engineering

Supervisor: Dr. Patrick J. Naughton

Submitted to Institute of Technology Sligo, December 2013

ABSTRACT

Accurate determination of soil's undrained shear strength is essential to make informed decisions regarding construction or maintenance problems. Reduced scale modelling can achieve accurate predictions of in-situ field conditions without intensive field investigations. Geotechnical centrifuge modelling replicates in-situ conditions by accelerating a reduced *1/n* scale model to a multiple *n* of earth's gravity, thereby replicating the stress level of a *1:1* prototype. In this study bearing capacity testing and penetrometer profiling were carried out on normally and over consolidated kaolin clay models, with various fibre contents. Construction of fibrous models in the drum centrifuge ensured a homogenous soil and a random orientation of fibres during the consolidation process. Bearing capacity testing was carried out in flight with different size and shaped foundations. The undrained shear strength was back calculated from the foundation bearing capacity at two locations; at maximum resistance and at the resistance corresponding to depths of 0.5 times the width (B) or diameter (D) of the foundation; cone and piezoball penetrometers were also conducted in flight. Shear vane testing and soil characterisation was performed on samples retrieved from the centrifuge models.

Analysis of the fibrous models determined that with increased fibre content the undrained shear strength increased; no optimum fibre content was determined in the testing undertaken. Undrained shear strength increased once 4 % and 2-3% fibre content was reached in normally and over consolidated models respectively. Maximum resistance of the models occurred within the initial 5-10 mm of the model surface. Determination of the undrained shear strengths at depths corresponding to 0.5 B/D of the foundation showed that shear strength increased with increasing depth in the majority of cases. Back calculations of undrained shear strength from bearing capacity testing in normally consolidated and over consolidated models corresponded well with that of the penetrometers; while the shear vane results produced a poor correlation. On average piezoball results gave higher undrained shear strength, with reduced scatter, compared to CPT results. Over consolidated models produced greater undrained shear strengths than normally consolidated models. Atterberg limits and plasticity index was found to increase with increased fibre content; models were seen to change from clays of intermediate plasticity at 0 % fibre content to clays of high plasticity at 4 % fibre content.

ACKNOWLEDGEMENTS

Firstly, I would like to thank my supervisor Dr. Patrick Naughton, whose guidance and support were vital to the accomplishment of this study. I found myself very fortunate to have a supervisor that provided such excellent tutelage.

I would like to thank Cathal Colreavy, whose technical knowledge and advice were invaluable.

Thanks to my colleagues and friends at IT Sligo whose good will and support throughout my time there were very much appreciated.

I would like to thank my family for their encouragement and support.

Finally I would like to acknowledge the support I received from the Technological Sector: Strand III programme. This initiative allowed me to prioritise my research and expand my knowledge.

TABLE OF CONTENTS

Chapter 1: Introduction

Chapter 2: Literature review

Chapter 3: Methodology

Chapter 4: Results

Chapter 5: Analysis and discussion

Chapter 6: Conclusions and recommendations

LIST OF TABLES

LIST OF FIGURES

NOTATION

Symbol	*Meaning (units)*
n	Scaling factor relating prototype to centrifuge model.
CPT	Cone penetrometer test.
g	Gravity (m/s).
h_m	Centrifuge model depth (m).
h_p	Prototype depth (m).
ρ	Density (kN/m^3).
σ_{vm}	Model vertical stress (kPa).
σ_{vp}	Prototype vertical stress (kPa).
ω	Angular acceleration (Radians/s).
r	Centrifuge radius (m).
CPTu	Cone penetration test with pore pressure measurement.
s_u	Penetrometer undrained shear strength (kPa).
q_{net}	Net CPT tip resistance (kPa).
N_{kt}	Resistance factor associated with the CPT.
q_c	Measured cone tip resistance (kPa).
q_t	Total measured cone tip resistance (kPa).
u_2	Measured pore pressure (kPa).
α	Unequal area ratio.
$q_{full\ flow}$	Total measured ball/T-bar tip resistance (kPa).
q_{ball}	Net piezoball tip resistance (kPa).
σ_{vn}	Overburden stress at location n (kPa).
u_n	Pore water pressure at location n (kPa).
A_s/A_p	Shaft area to penetrometer area ratio.
N_{ball}	Resistance factor associated with the piezoball.
COV	Coefficient of variation.
MPa	Mega pascals.
µm	Micro meters.
Mg/m^3	Mega grams per cubic meter.
s_{ur}/σ'_{vc}	Ratio of undrained peak shear strength to effective vertical consolidation stress.

OCR	Over-consolidation ratio.
q/p_o	Deviator stress against mean effective stress ratio.
ϕ	Soil internal angle of friction (˚).
q'_c	Surcharge to achieve a state of plastic equilibrium.
q''_c	Surcharge to push a foundation into soil of a plastic equilibrium state.
β	Equivalent free surface.
q_o, s_o	Equivalent free surfaces stresses.
q	Bearing capacity (Meyerhof 1951).
N_c, N_q, N_y	Bearing capacity factors.
D	Depth of soil above foundation (m).
y	Unit weight of soil (kN/m^3).
c	Cohesion of soil.
σ	Total normal stress (kPa).
M	Degree of mobilization of shear strength.
q_r	Bearing capacity of a circular foundation (kPa)(Meyerhof 1951).
N_{cqr}	Bearing capacity factor for a circular foundation (Meyerhof 1951).
K_s	The coefficient of earth pressure
Q_{Dr}	Bearing capacity of a circular foundation (kPa)(Terzaghi (1943).
n_c, n_q, n_γ	Bearing capacity factors dependent upon the angle of shearing resistance (Terzaghi (1943).
q_l	Bearing capacity for a rectangular foundation (kPa) (Meyerhof 1951).
N_{cql}	Bearing capacity factor for a rectangular foundation (Meyerhof 1951).
N_{cq}	Bearing capacity factor for a strip foundation (Meyerhof 1951).
B	Width of foundation (m).
L	Length of foundation (m).
d_c, d_q, d_y	Foundation depth factors.
s_c, s_q, s_y	Foundation shape factors.
i_c, i_q, i_y	Load inclination factors.
B	Foundation width (m).
L	Foundation length (m).
B’	Effective foundation width (m).
L’	Effective foundation length (m).
τ_f	Shear stress at failure (kPa).

σ_q	Surcharge pressure (kPa)(Craig 2012).
d	Depth of the foundation base (m)(Craig 2012).
q_f	Undrained bearing capacity (kPa)(Whitlow 2001).
q_{ult}	Ultimate bearing capacity (kPa)(Eurocode 7).
ITS	Institute of Technology, Sligo.
rpm	Revolutions per minute.
DAS	Data acquisition system.
Nm	Newton meter.
V	Voltage.
KW	Kilowatt.
v.E./F.S	Ratio of excitation voltage to full scale.
mV/V	Millivolts per volt.
COFS	Centre for Offshore Foundation Systems.
DC	Direct current (V).
PPT	Pore pressure transducer.
C	Degrees celsius. (˚).
w	Moisture content (%)
NC	Normally consolidated.
OC	Over consolidated.
w_{LL}	Liquid limit (%).
w_{PL}	Plastic limit (%).
I_{p}	Plasticity index (%).
C_c	Compression Index
C_s	Swelling Index.
c_v	Coefficient of consolidation (m^2/yr).
c_u	Undrained shear strength for shear vane and bearing capacity (kPa).
σ_v’	Vertical effective stress (kPa).
k	Factor relating torque to vane undrained shear strength.
D, H	Shear vane blade width and height (mm).
μ	Bjerrum’s correction value.
0.5B/D	Depth of penetration equal to 0.5 times the foundation width or diameter.

CHAPTER 1

INTRODUCTION

1.1 Introduction

Peats and highly organic soils have a higher percentage content of fibrous material due to the breakdown of plant matter. From the level of decomposition present in peat there is a high portion of matter that possess little or no shear strength, yet peat overall possesses notable shear strength when tested with traditional field investigation techniques. It is the presence of these fibres that result in higher strengths than expected for material with such low densities. The shear vane is one method that allows quick estimation of soil properties by relating torque to the undrained shear strength. However as the shear vane is inserted into the soil, the soil stress levels surrounding the blades are known to be elevated hence the shear strength can be overestimated (Kallstenius 1963). Correction factors based upon the peat or soil characteristics along with the dimensions of the shear vane can result in an adequate estimation of the undrained shear strength (Edil 2001).

Numerous studies, such as Maher and Ho (1994), have investigated the effects of fibres on the improved tensile strength of soils. Various types of fibrous material have been added to clays and soil in an effort to eliminate weak plane that can develop when utilizing directional reinforcement. In most cases where organic fibres have been trialled, the tensile soil strength was found to be greater than that of comparable cases where synthetic fibres were used, due in part to the surface texture of organic material (Attom *et al* 2009). Introducing short discrete fibres into a soil mass is seen as an effective way of ensuring strength isotropy. Strength isotropy is usually seen in soil samples taken at great depths, where comparison between strengths determined in the vertical and horizontal directions are practically identical.

In order to accurately determine the in-situ stress of soil at depth without significant excavation or laborious large scale test models, geotechnical centrifuge modelling permits an accurate relationship to be made between a reduced scale model and a full-scale prototype. The centrifuge model is reduced to a *1/n* scale corresponding to a specific problem and subjected to an acceleration gravitational field; hence the soil stresses are increased by a factor of *n*. The model will then have the same stress state corresponding to that of a 1:1 scale prototype (Taylor 1995).

1.2 Aims and objectives

The aim of this study is to determine whether increased organic fibre content contributes to greater undrained shear strength of soil. The objectives are as follows;

- To examine the effect of fibre content on the undrained shear strength of normally and over consolidated models in the IT Sligo geotechnical centrifuge.
- To identify a fibrous material and to develop a suitable methodology to create a homogenous fibre soil sample that can be placed and tested in a centrifuge.
- To conduct modelling in a geotechnical centrifuge investigating the effect of fibre content on the undrained shear strength of normally and over consolidated soils.
- To compare the undrained shear strength from the cone penetration test (CPT) and piezoball profiling, laboratory shear vane and values back calculated from bearing capacity testing in the geotechnical centrifuge.

1.3 Layout of thesis

Following this introduction chapter, Chapter 2 presents the literature review, with particular attention placed on constructing a homogenous fibre soil sample for consolidation and testing purposes. Bearing capacity analysis and penetrometer tests such as the Cone and piezoball were investigated as a means of determining the undrained shear strength.

In Chapter 3, the methodology chapter, the process of geotechnical centrifuge modelling is outlined, which includes the process of model construction and test set up. Characteristics of the materials utilized in this investigation are also presented.

Chapter 4, the results of the centrifuge modelling are presented with some preliminary analysis and discussion.

In depth analysis and discussion is carried out in Chapter 5 on the results of centrifuge modelling and classification studies of the soil models constructed. The conclusions of the study along with recommendations for future work are presented in Chapter 6.

CHAPTER 2

LITERATURE REVIEW

2.1 Introduction

In recent years a number of upland peat slides have occurred in Ireland. In 2003 a peat slide as a result of wind farm construction in Derrybrien Co. Mayo, lead to significant damage in the surrounding area (Lindsay and Bragg 2003). As a result there is now a strong emphasis and planning requirement for developments in upland peat or any area with a high organic soil, to proceed following a thorough assessment. Various techniques have been utilized to determine the strength of soil, both in-situ and within geotechnical laboratories. It is the purpose of this literature review to study the present knowledge on fibrous organic soils and the methods employed to determine the undrained shear strength. The chapter shall detail the areas relevant to the present study;

i. Centrifuge technology
ii. Profiling equipment
iii. Properties of organic soils and peats
iv. Model preparation methods
v. Bearing capacity analysis and failure modes.

2.2 Centrifuge technology

Geotechnical centrifuge modelling allows the study of geotechnical events within a controlled environment. Taylor (1995) details how this technique allows accurate relationships to be drawn between events at reduced model scale and those of a full scale prototype. In-situ stresses and events which are dependent upon gravity can be related directly from the prototype to the centrifuge model; without any reduction in magnitude. For example, a *1/n* scale model constructed and accelerated to *n* time's gravity (g), will have the same stress corresponding to a full scale *1:1* prototype. This can be accomplished by utilizing well established scaling factors, Table 2.1. Centrifuge modelling has proven to be particularly useful for gaining a better understanding of deformations and failure mechanisms, while also proving a useful validation of numerical models (Taylor 1995). Specific problems can be investigated with the objective of design and construction, where determinations of safety factors against failure are extremely useful. Serviceability of structures over their life span can also be studied. Popularity of reduced scale centrifuge modelling is growing as shown by the number of recent studies such as Cassidy (2009), Tessari *et al* (2010), Gaudin *et al* (2011) and Kim *et al* (2013). Such popularity can be attributed to events being free from influence, provided that the necessary model construction and setup protocols are followed (Taylor 1995).

Table 2.1: Scaling factors for centrifuge modelling, Taylor (1995).

Parameter	Dimension	Scale Factor (Model:Prototype)
Acceleration	LT^{-2}	$1{:}n^{-1}$
Length	L	$1{:}n$
Area	L^2	$1{:}n^2$
Stress	$ML^{-1}\,T^{-2}$	1:1
Strain	Dimensionless	1:1
Force	MLT^{-2}	$1{:}n^2$
Mass	$ML^2\,T^{-2}$	$1{:}n^3$
Velocity	LT^{-1}	1:1
Time (Diffusion)	T	$1{:}n^2$
Time (Dynamic Events)	T	$1{:}n$

2.2.1 Principles of modelling

Geotechnical centrifuge modelling technology essentially allows the strength and stiffness of a prototype soil to be reproduced accurately in a geotechnical laboratory. In-situ stresses and soil mechanical properties are known to change with depth. The geotechnical centrifuge provides an accurate way to model these characteristics without laborious and expensive in situ investigations (Taylor 1995). During testing the centrifuge model is subjected to an acceleration field of n times the earth's gravity, so that the vertical stress at a depth h_m will correspond identically to h_p. Taylor (1995) summarized the relationship in Equation 2.1:

$$h_p = nh_m \qquad \text{Equation 2.1}$$

The same principle applies to the stress of the model. If a model of density (ρ) was subjected to n time gravity (g), the vertical stress (σ_{vm}) at a depth h_m in the model can be referred to by Equation 2.2 (Taylor 1995):

$$\sigma_{vm} = \rho ngh_m \qquad \text{Equation 2.2}$$

When in reality, or the prototype situation, the vertical stress (σ_{vp}) is represented by:

$$\sigma_{vp} = \rho gh_p \qquad \text{Equation 2.3}$$

The scale factor for linear dimensions within a geotechnical centrifuge is *1:n*. It should be noted that strains have a scale factor of 1:1, so the strain mobilized in the model will be identical to that of the prototype (Taylor 1995). The acceleration field within a geotechnical centrifuge environment is given by $\omega^2 r$ where ω is the angular rotational speed of the centrifuge and r is the radius to any element in the soil. The principle of geotechnical modelling and the relation to prototype stress is presented in Figure 2.1. When using the centrifuge to generate an acceleration field n time greater than earth's gravity, there will be a slight variation in stress through the model due to changes in radius r, Figure 2.2. Taylor (1995) outlined that variation can be neglected if care is taken to select the correct value of the centrifuge radius, which corresponds to the scale factor n.

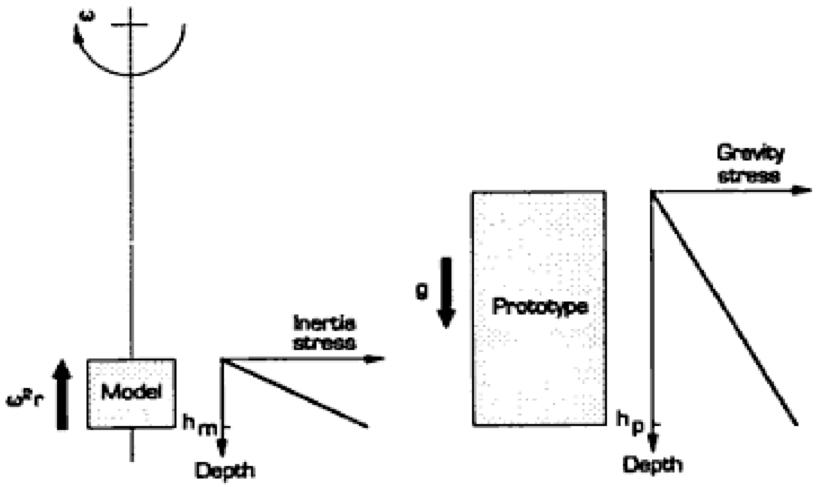

Figure 2.1: Diagrammatic representation of the principle of centrifuge modelling (Taylor 1995).

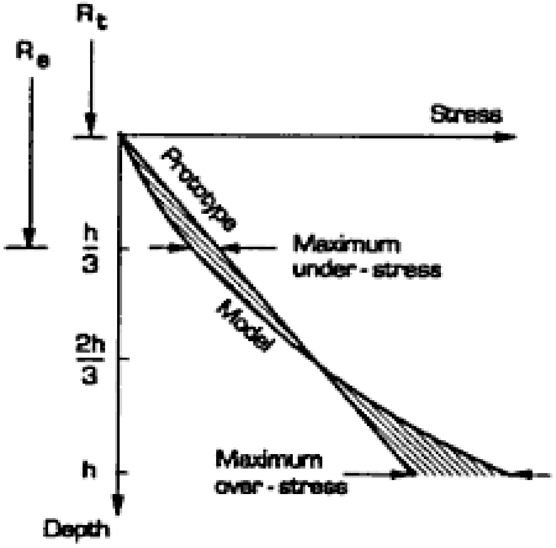

Figure 2.2 Stress v depth relationships within the geotechnical centrifuge model and corresponding prototype (Taylor 1995).

2.2.2 Scale effects

A common misconception regarding centrifuge modelling is that material particles used in modelling should be reduced in size by an appropriate scaling factor (Taylor 1995). If fine sand could be used to represent the characteristics of gravel for a model at scale *n*, the same logic would apply to clay being representative of fine sand. This is clearly problematic as the characteristic behaviour of clay, sand and gravel are different. There are also likely to be problems if a model event was constructed of coarse grained gravel. Taylor (1995) describes that in such cases grain dimensions would be rather large in relation to the model dimensions and as such the mobilization of the internal stresses would be influenced by boundary effects associated with the model container. Taylor (1995) stated that such events would be uncharacteristic of those in the field.

The g-force experienced by the sample in the containment area is related to the radius of rotation. Taylor (1995) describes how the g-force or acceleration field is directed towards the centre of rotation; hence there is a change in its direction in the horizontal plane in relation to the vertical which is across the model width. This can have significant effects on events which take place at the container wall or viewing window. Taylor (1995) thought it prudent that model testing should be confined to the container centre.

2.3 Profiling equipment

The following sections outline profiling equipment used to determine undrained shear strength in soil and peat deposits. Studies detailing each penetrometer's performance while testing in peat are also outlined.

2.3.1 Cone penetration test

The cone penetrometer test (CPT) was first used to evaluate bearing capacities of piles, by recording cone tip resistance. Modern cones record resistance to penetration along with sleeve friction and pore water pressure. CPTu or Piezocone are terms given to penetration tests that record pore water pressures. Boylan *et al* (2011) details the standard cone as sloping at 60˚ from the apex, with a surface contact area of 10 to 25 cm^2, Figure 2.3. The cone penetrometer is used in initial site investigation to determine mechanical properties of soil strata. Factors such as temperature and changes in pore water pressure caused by the penetrating rod can affect the accuracy of CPT results (Lunne *et al* 1997). Pore pressure corrections are especially important in soils where pore pressures can be considerable in relation to cone resistance. Aas *et al* (1986) showed the value of making such corrections to piezocone data and the resultant improvements in accuracy. Net cone resistance, q_{net}, requires correction for unequal pore pressure effects and overburden pressure. The cone tip resistance is related to the undrained shear strength of the soil by an empirically derived resistance factor N_{kt}, Equation 2.4. The N_{kt} factor is site dependent and must be determined from site soil samples. Quality sampling methods are essential to ensure an accurate determination of the N_{kt} factor through laboratory testing.

$$s_u = \frac{q_{net}}{N_{kt}} \qquad \text{Equation 2.4}$$

where; s_u is the undrained shear strength.

The unequal pore pressure effects on the cone penetration test are caused by the pore pressure acting on the shoulder area of the cone. Boylan *et al* (2011) details how the measured cone resistance, q_c, is corrected to give, q_t, the total measured tip resistance using Equation 2.5:

$$q_t = q_c + u_2(1 - \alpha) \qquad \text{Equation 2.5}$$

where; u_2 is the measured pore pressure behind the cone shoulder

α is the unequal area ratio

A minimum α is required in order to limit the number of corrections. Its value should ideally be close to unity but can vary widely from 0.55 to 0.9 (Lunne *et al* 1997).

2.3.2 Full flow penetrometers

Full flow penetrometers allow soft soils to flow around the instrument equalizing the overburdened pressure above and below; ignoring the area of the shaft. Stewart and Randolph (1991) studied how initial T-bar tests resulted in improved measured resistance to penetration compared to standard cone penetrometers. Subsequent developments lead to the production of the ball penetrometer, which reduced the non-symmetrical loading associated with the T-bar, Figure 2.3. Thus overestimation of the penetration resistance was greatly reduced. Boylan *et al* (2011) outlined how the greater surface area of full flow penetrometers, 28 to 100 cm^2 compared to 10 to 25 cm^2 of the cone, improved accuracy in soft soils. Results obtained using full flow instruments therefore require minimal correction (Randolph 2004). This is due primarily to the shaft area to penetrometer area ratio (A_s/A_p) adjustment; which is approximately 0.1. Such minor adjustments to piezoball resistance can be made, according to Boylan *et al* (2011) by using Equation 2.6:

$$q_{full-flow} = q_c - [\sigma_{vn} - u_n(1-\alpha)]\, A_s/A_p \qquad \text{Equation 2.6}$$

where; σ_{vn} is the overburden stress at location n

u_n is the pore water pressure at location n

A_s is the shaft area

A_p is the penetrometer projected area

Long and Gudjonsson (2004) also found that full flow penetrometers provide a more uniform measurement of resistance, compared to CPT data. This was due to large failure plain mobilization during penetration, which averages out the local peaks in resistance that influence the cone resistance. Lunne *et al* (2005) states that the results of full flow penetrometers require little calibration and are uniform with depth.

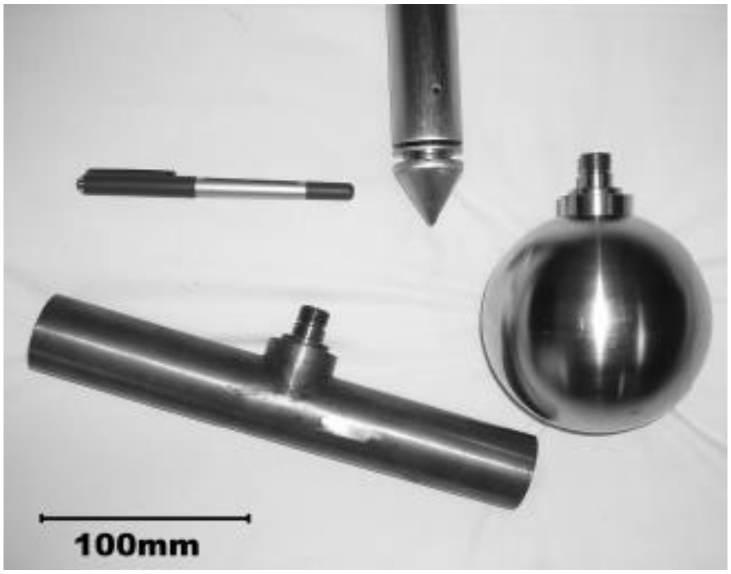

Figure 2.3: CPT along with full flow T-bar and piezocone penetrometers (Boylan *et al* 2011).

The undrained shear strength of the soil is derived from the net resistance of the full flow penetrometer, in Equation 2.7 the piezoball is used as an example. Boylan *et al* (2011) assumed a slightly roughened surface of the penetrometer being used and therefore assumed a value of 13 for the resistance factor of the ball (N_{ball}). Values of resistance factors have been calculated assuming full undrained conditions of the soil and non-softening behaviour of soil by studies including Randolph *et al* (2004).

$$s_u = \frac{q_{ball}}{N_{ball}} \qquad \text{Equation 2.7}$$

where; s_u is the undrained shear strength.

2.3.3 Variations in penetrometer results

Boylan *et al* (2011) carried out a study using full flow penetrometers to access the measured resistance in peats compared to the cone penetrometer. T-bar and ball penetrometers with equal bearing area ratios, where A_s/A_p amounts to 0.1, were used. Testing was carried out at two sites in the Netherlands at penetration rates of 0.2, 2 and 10 cm/s. At the first site in Vinkeveen, Boylan *et al* (2011) found the average T-bar penetration results were higher than the ball penetrometer from 1 to 2 m, whereas below 3 m the average ball resistance was greater. The coefficient of variation (COV), the ratio of standard deviation to the mean, was

15 and 20 % for the T-bar and ball tests respectively, whereas it was 35 % for the cone. The higher coefficient of variation for the cone was attributed to its smaller surface area (10 cm^2), (Boylan *et al* 2011). This smaller surface area interacts with the fibrous material to a greater extent than full flow penetrometers. The geometry of the cone transmits a consolidation effect and as such testing was conducted in a modified peat (Boylan *et al* 2011).

At the Bodegraven site, Boylan *et al* (2011) found the net resistances below 1 m were approximately 0.2 MPa and uniform with depth. The ball penetrometer had a higher resistance approaching 2.5 m depth whereas the T-bar resistances were greatest between 3.5 and 4.5 m. Pore water pressure ranged between 0 and 0.2 MPa and was consistent throughout the peat deposit. It was observed during testing at both sites that penetration occurred in partially drained to drained conditions. Wood layers encountered at the Bodegraven site resulted in a higher COV (25% for both full flow penetrometers), which contrasts with the 20% COV for the cone. This can be attributed to the greater area of the full flow penetrometers interacting with the irregular wood content. Outside the wood layers the cone gave a resistance to penetration 30% greater than the full flow penetrometers. Boylan *et al* (2011) concluded that full flow penetrometers facilitate the flow of soil around the penetrometer, which in Bodegraven deposits allowed large pieces of fibres and wood to influence readings. Conversely the cone displaces material from its path as it flowed, which would otherwise result in higher resistances.

2.4. Shear strength of peat

This section will evaluate the contribution of fibre to the overall strength of peat. In particular the failure mechanics of peat associated with the shear vane test shall be examined.

2.4.1 Fibres in peat

Peats are found to exist with low densities and therefore have low effective stresses. Shear strength testing in organic and highly organic deposits such as peat, result in unique shear strengths compared with mineral soils (Landva 1980). Undrained shear strengths are invariably higher when compared to inorganic clays. Helenelund (1967) proposed that the composition of the peat fibres is responsible for its shear strength rather than frictional resistance compared to soils or clays.

2.4.2 Background on peat

Peat is a material that consists of decomposed or decomposing organic material from plants. Peat formation started in Ireland some 10 000 years ago and is generally found in areas of high rainfall and under poor drainage conditions. Peat differs from mineral soils, according to Boylan *et al* (2008) in three important aspects:

i. The particles are connected to each other on a microscopic level.
ii. The majority of particles are likely to be compressible.
iii. Plant material continues to decaying with time.

The overall nature of peat consists of an assembly of decaying plant cell structures interconnected with frequent fibres and other organic matter (Connolly *et al* 2007). Boylan *et al* (2008) discussed the micro-fabric connectivity between the major plant particles, which creates an open cellular structure. This leads to the pore spacing of peat being defined as large, with regular pores up to 10 μm in size, leading to high permeability. Hobbs (1986) stated that where peat is free of minerals, ash content can be as low as 2 %. In certain areas the mineral content of peat may be as high as 30 %, according to Lefebvre *et al* (1984). Mitchell (1993) showed that the thickness of particles in peat, which are not of a fibrous nature, ranges from 0.03 to 0.2 μm. Bulk density of peat is typically equal to or less than that of water. Values of bulk density tend not to vary with the peat properties and instead remain relatively constant at 1.03 Mg/m^3 (Hobbs 1986). This low value can be attributed to trapped gases, as a result of the decomposition process. According to Hobbs (1986), the gas introduces a buoyancy effect in the peat, keeping the matter in suspension until such time as the gas dissipates. Hobbs (1986) stated that moisture content (w) of peat can vary from 300 % to 2000 %, yet given the small amount of solid plant matter that is present in peat, there is significant shear strength (Boylan *et al* 2008).

2.4.3 Shear vane testing in peat and organic soils

The vane test is a method of directly testing the undrained shear strength of soil. This test is predominantly used during the course of a site investigation. The objective is to obtain realistic data relating to soil failure. The apparatus consists of a vane cross, which will vary in height relative to the stiffness of the soil. The vane in all cases has a height to width ratio of 2 (Flaate 1966). The vane is attached to a series of extension rods and torque is applied at a rate of 0.1 degree per second until the soil fails. In soft soils the vane rod can be pushed directly into the soil. In some cases the vane test is preformed from the bottom of an augered drillhole. Cadling and Odenstad (1950) recommended that the vane extend approximately 50 cm below the bottom of the drillhole, to avoid recording any changes in stress levels due to auguring. Measurements taken by Kallstenius (1963) and Flaate (1965b) show that the elevation in soil stress in the immediate vicinity of the vane was between 8 and 10 times that of the shear strength of the soil. The exposed extension rod can be fitted with a friction coupling to overcome the influences of friction or allowances are made in subsequent calculations. The torque required to cause failure is measured through various spring loaded devices. Any drainage during the test is also ignored, i.e. the test is assumed to be undrained.

The area ratio of the vane can be influenced by the characteristics of the soil. The area ratio is defined as the cross sectional area of the vane in relation to the cross sectional area of the cylindrical shearing zone. Eden and Hamilton (1957) reported that when using vanes with an area ratio of between 10 to 25% differences in readings were negligible. Vey (1955) investigated the effects of vane size on the determination of shear strength and found a 10 % decrease in strength of inorganic clay as the vane height increases from 38 mm to 57 mm. MacFarlane and Rutka (1962) reached similar conclusions.

Failure of the soil is assumed to occur along the cylindrical circumference of the shear vane and is assumed to be fully mobilised and equal in all directions. This is necessary to be able to determine the shear strength at a particular depth in one reading. With high fibrous organic soils, it has been presumed that the presence of discrete fibres reinforces the soil to a degree that is not a true representation of the global strength (Landva 1980). Such instances can be related to deposits of fibrous peat. Landva (1980) highlighted the problems of testing in deposits of fibrous peat with the shear vane. In particular the peat fibres provided resistance to rotation of the vane. Helenlund (1967) reported that the rotation between the vane and peat interface will not shear any peat fibres present. These fibres are merely entangled around the surface area of the vane blade. As the test continues more fibrous material is drawn into the path of the vane, causing a resistance to rotation. Landva (1980) also observed that as the rotation of the vane continues so too will the collection of the fibrous material in front of the vane. This will lead to the formation of a modified peat, Figure 2.4.

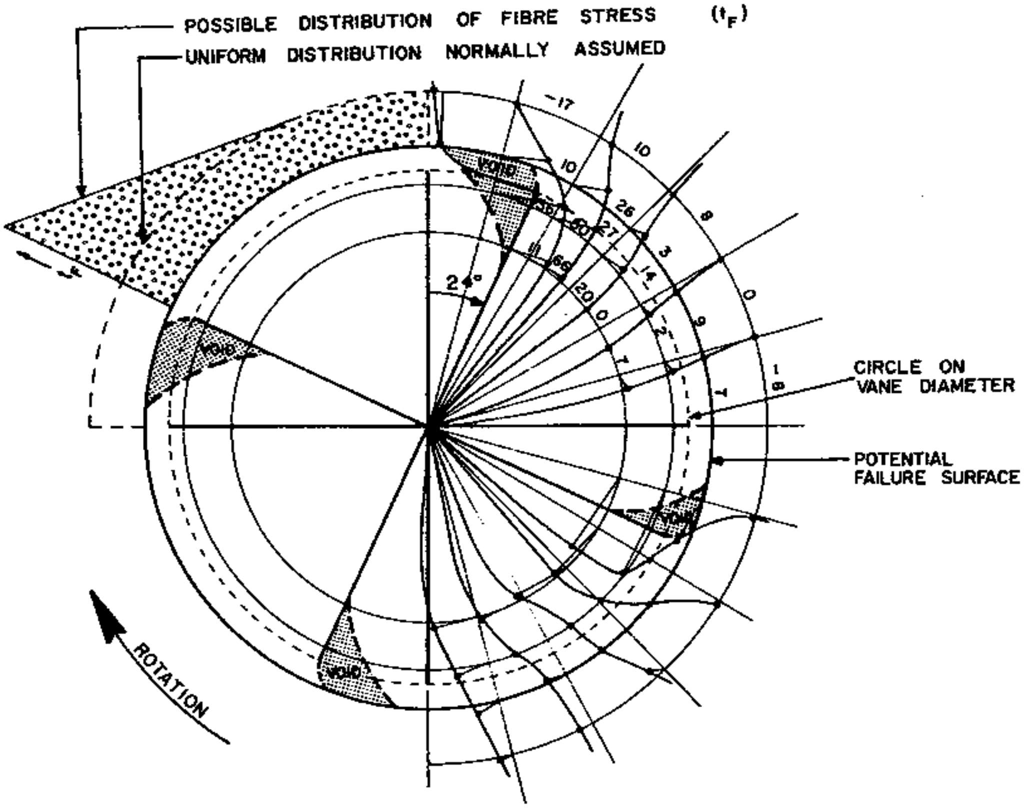

Figure 2.4: Distribution of fibre stress along shear face (Landva 1980).

Landava (1980) observed that the shear face occurred at a distance outside the periphery of the blade vane path and was found to be in the region of 7 to 10mm. Factors such as the change in stress level of a soil with the insertion of the vane and the degree of remoulding during the course of the test, contribute to inaccurate representations of the undrained shear strength of soil. However, with the implementation of correction factors, the shear vane test can be used as an adequate estimation. Edil (2001) recommends that the strength of an organic soil or peat be taken as a maximum 60% of the value determined through the use of the shear vane. Through subsequent investigations, correction factors have been defined to produce a more accurate estimation of peat strength. These factors vary greatly in respect of peat and soil types encountered (Edil 2001). In the case of granular soils, vane results require correction factors for disturbance, anisotropy and strain rate effects in order to use undrained shear strengths measured.

One of the most widely used correction factors was put forward by Bjerrum (1973), which relate to the process of consolidation and dynamic events such as in situ testing, along with soil that is anisotropic. Factors of safety were determined by using undrained shear strengths determined from shear vane tests where documented failures of excavations and footings occurred in clays. Safety factors were back calculated using the failure data and a plot of the shear strength data against plasticity indices of soil was created. The author believed that the best method of correcting shear vane results was to determine correction factors for anisotropy and strain rate effects separately. Bjerrum also estimated a value for the correction factor that related to strain rate effects and found that corrections for the effects of anisotropy were dependent upon the orientation of the failure surface. In order to carry out a successful plasticity index test in peat, a certain percentage of clay would be required, as the humus present does not contribute to effective testing alone (Edil 2001). It is extremely difficult to carry out such a test on a pure peat sample, with no current record of plastic index determined for peat with a 1000 % liquid limit or greater (Edil 2001). Bjerrum's plasticity index correction chart is therefore unsuitable for purely organic peat deposits.

2.5. Properties of soil affected by the presence of fibres

The following sections outline the effects of introducing fibres into soil. Properties such as strength and ductility are directly improved; fibres can also absorb large amounts of moisture present in the soil.

2.5.1 Strength of fibrous soil

The mechanical property that is most influenced when considering fibrous soil is strength. Freitag (1986) demonstrated that strength increased with increasing fibre content. Maher and Ho (1994) also found an increase in the tensile strength with increasing fibre content, along with increases in hydraulic conductivity. Attom *et al* (2009) focused on the effects of short, discrete, randomly orientated fibres introduced into a clayey soil. The fibres included synthetic nylon and organic fibrous materials. The purpose behind using randomly orientated fibres was to eliminate weak planes that can develop when implementing directional reinforcement, hence ensuring strength isotropy. The soil used by Attom *et al* (2009) was extracted from within 1 m below ground level. Three soil types were mixed with percentages of 1 %, 2 %, 3 %, 4 % and 5 % synthetic and natural fibres, by dry weight. All fibres used in that study were selected based on their ratio of length to diameter being equal to 75. As the samples were laboratory prepared, varying water contents were used to investigate the effects on unconfined strength. A water repellent bitumen admixture was used to eliminate natural fibre swelling. The unconfined compressive strength increased with increasing fibre content, Figure 2.8. For samples containing nylon fibres the increase in strength was 25 %, 50 %, 75 %, 88 % and 100 % for fibre contents 1 %, 2 %, 3 %, 4 % and 5 % respectively. Comparison between two soils enhanced with 5 % nylon and 5 % natural fibres showed a difference of 263 kPa and 272 kPa respectively, Figure 2.5. This increase in strength can be attributed to the surface texture of natural fibres producing a better interlock between the soil and the fibre surface.

Al–Khafaji (1979) also carried out an investigation on consolidated soil samples with increasing degrees of fibre content. In that study, artificial organic clay was produced by utilizing pulp fibre and kaolin clay. Here when test samples underwent an increase in organic content as high as 80 %, results showed considerable increase in shear strength, Figure 2.6. That study conducted shear vane tests at separate consolidation pressures and illustrated that an increase in the consolidation of a given sample, along with an increase in fibrous content, resulted in an increase in the resistance to shear.

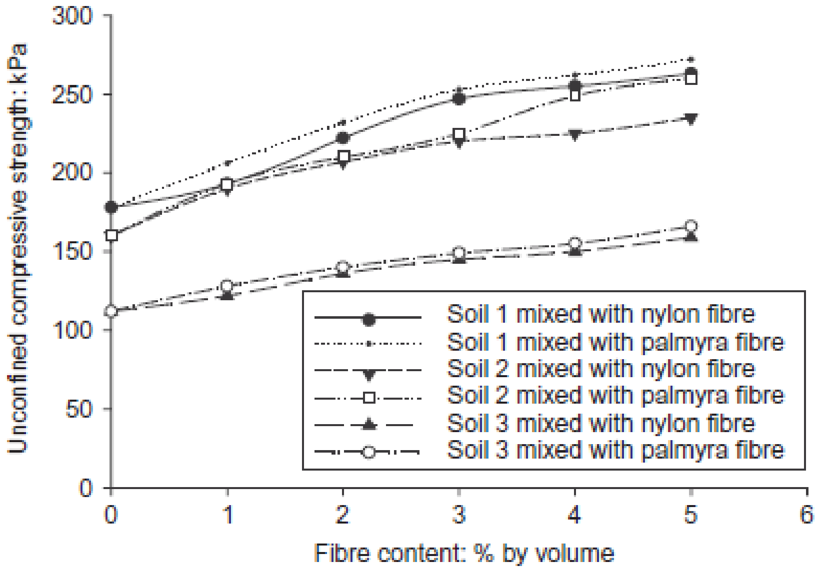

Figure 2.5: The effects of natural and synthetic fibres on the unconfined compressive strength of three soil samples (Attom *et al* 2009).

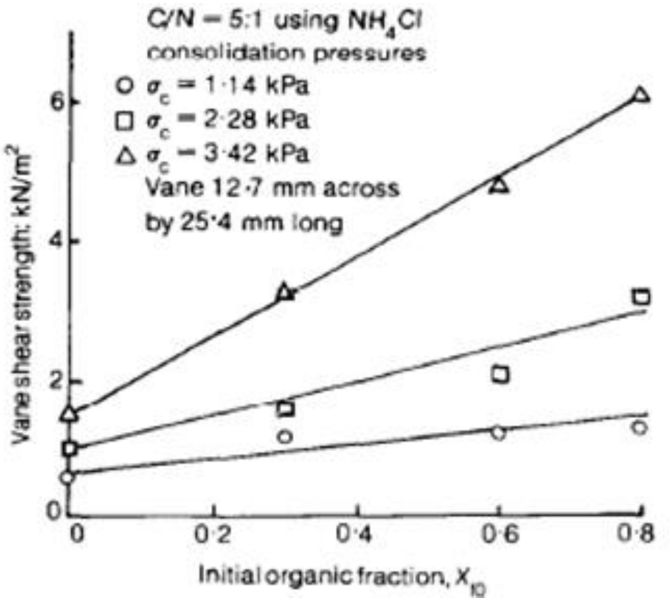

Figure 2.6: Influence of organic content on vane shear strength (Al–Khafaji 1979).

2.5.2. Effect of water content on fibrous soil

Mattone (2005) investigated the effects of moisture on soils which contained different percentage fibres. It was discovered that during mixing fibres absorbed water leading to swelling, which pushed soil away from the fibre surface. Mattone (2005) stipulated that this occurred at the micro-level. Once the process of mixing was completed, the drainage of the mass began almost immediately. Completion of this process showed the fibres had lost moisture leading to a return, approximately to their original dimensions. This event was attributed to the formation of fine voids around the reinforcing fibres, assisting in drainage with progressive drying. Ghavami *et al* (1999) investigated a similar method of introducing organic fibres into soil for the achievement of greater strength, using sisal and coconut fibres. An accelerated intake of water through capillary action or the process of absorption was found to increase with increasing organic content.

2.6. Effects of consolidation on soil strength

Clay deposits are formed through a process of weathering and deposition. Consolidation occurs with overlying sedimentary deposits or other forms of variable loading (Ling *et al*

2002). This deposition and consolidation process generally produces soils that are anisotropic, where the horizontal stresses are invariably weaker than the vertical stresses (Sivakumar *et al* 2001). That study noted that in such cases the principle stresses are aligned with axis of anisotropy. Sivakumar *et al* (2002) detailed the behaviour of consolidated soils and showed that the shape and orientation of the soil particles will have an effect on its anisotropic nature. Some soils display isotropic tendencies or characteristics which display uniformity in all directions (Jacobson 1955). When dealing with the resistance to failure of a soil, it is important to be aware of the vertical and horizontal shear strength. The strength of a soil can affect such characteristics as compressibility and permeability (Clough and Hansen 1981).

2.6.1 Undrained shear strength of consolidated organic mud

Schule *et al* (2011) quantified the undrained shear strength of organic harbour mud and outlined the attempts to reuse dredged organic mud from the port city of Bremen, Germany, as a fill material. Numerous difficulties arose in choosing appropriate consolidation techniques, as the soil was subjected to large vertical movements. During the subsequent investigation, samples were consolidated in cylindrical tubes with increasing pressures of 2, 4, 8 and 16 kPa, this covered the stress range to which the mud was subjected to during the consolidation phase of construction. Schule *et al* (2011) conducted 36 shear vane tests within 460 days of the test duration. Undrained shear strength was observed with increasing vertical consolidation. It was also discovered that the rate of application of shear strain influenced the peak and residual shear strengths. It was found that the relationship between undrained shear strength and water content was exponential. Water contents lay between 110 % and 185 % for that range of oedometer testing (Schule *et al* 2011). The relationship between undrained peak shear strength and vertical consolidation stress, s_{ur}/σ'_{vc}, was found to be 0.25: along with a value for undrained residual shear strength and vertical consolidation stress, s_{ur}/σ'_{vc}, of 0.054, Figure 2.7.

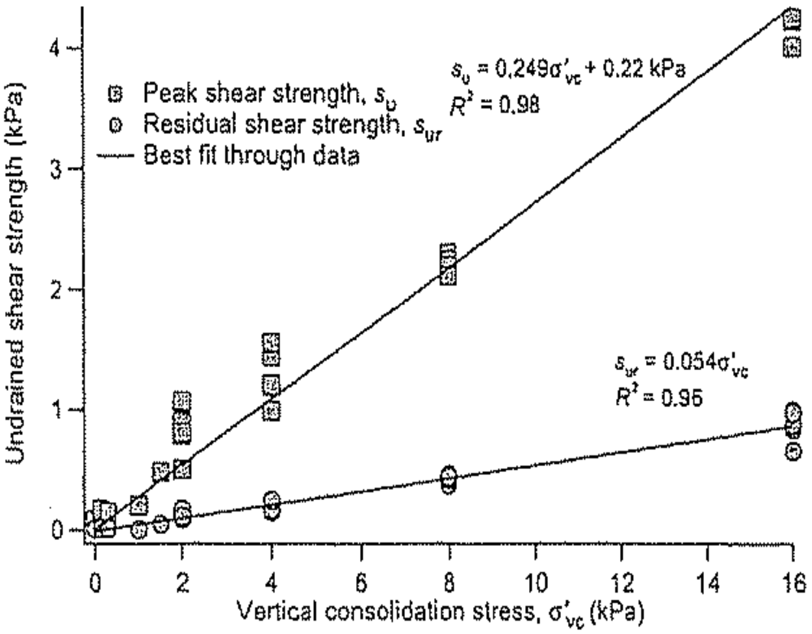

Figure 2.7: Corrected undrained peak and residual shear strength verses vertical consolidation stress (Schule *et al* 2011).

2.6.2 Effects of anisotropy on soil strength

Attom and Al-Akhras (2008) investigated anisotropy or the influence of direction when investigating the characteristics of soil. Undisturbed soil samples were obtained from a selection of sites based upon known clay contents and plasticity indexes. At fifteen locations three samples were taken in three directions; horizontal, vertical and inclined at 45°. Unconfined compression tests were carried out to determine the failure strains of soils and the unconfined compression strengths. From results obtained soil samples taken in the vertical direction displayed the greatest unconfined compressive strength followed by the inclined samples, with horizontal samples showing the weakest strength profiles. An increase in depth up to 5 m resulted in an increase in compressive strength, Figure 2.8. Between 1 and 2 m the unconfined compressive strength values were 105, 130 and 150 kPa for the horizontal, inclined and vertical directions respectively. However at a sampling depth of 5 m, the compressive strength increased to 145, 150 and 170 kPa respectively.

Attom and Al-Akhras (2008) found that the depth at which the samples were extracted influenced the anisotropy of the soil. At depths approaching 10 m the soil tended to become isotropic. That was observed when the values of the unconfined compressive strength in the horizontal and inclined directions approached the vertical strength (Attom and Al-Akhras

2008). It also became obvious that the horizontal samples had a higher rate of increase in strength than the inclined. As sampling depth increased the horizontal and inclined anisotropic strengths become closer and approach unity.

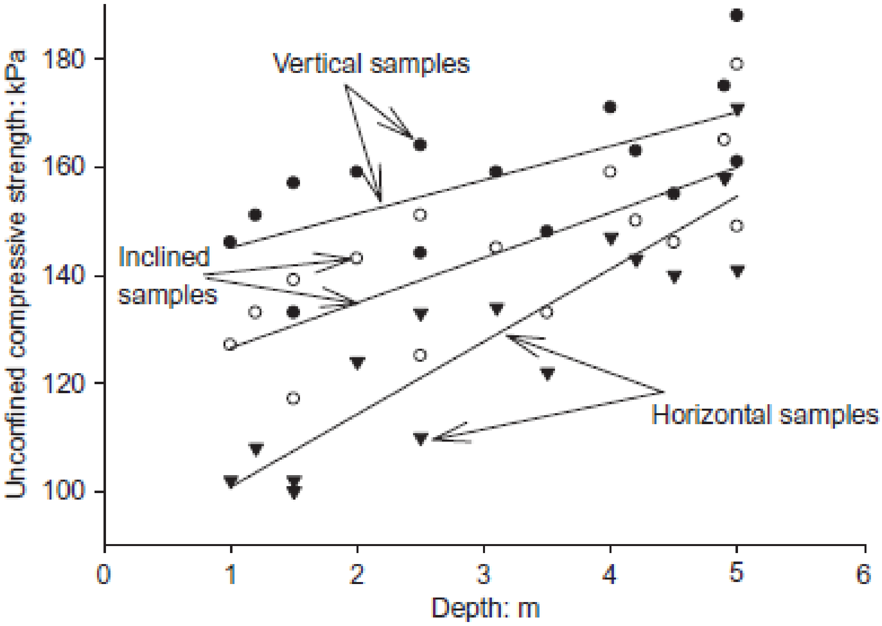

Figure 2.8: Comparison of soil samples with unconfined compressive strength for the horizontal, inclined and vertical direction (Attom and Al-Akhras 2008).

Anisotropic strength was also influenced by the consolidation experienced by the soil, known as over-consolidation ratio (OCR). Where a low OCR was present, shear strength in the horizontal and inclined directions approached unity (Attom and Al-Akhras 2008).

2.6.3 Over consolidated soils

Ling *et al* (2002) studied the results of isotropic and anisotropic conditions on over consolidated kaolin samples. Over consolidated ratio (OCR) ranged from 1 to 8 for isotropic and 1 to 4 for anisotropic tests. Extension and compression tests were carried out using a triaxial apparatus. Results showed that low OCR consistently produced greater values of deviator stress against mean effective stress (q/p_o) irrespective of the change in cell pressure, when compared to higher OCR samples, Figure 2.9. Li and Meissner (2002) noticed a similar trend when looking at a plasticity model for the behaviour of undrained clays. The clay used in that investigation was 60% kaolinite. Plots of effective mean stress against strain, showed a reduction in effective stress with an increase in OCR, Figure 2.10. Li and Meissner attributed this directly to the over consolidation of the samples and argued that during loading, positive pore water pressures build up in normally or lightly over-consolidated soil. Whereas in over consolidated samples, due to soil particle dilatation during loading and shearing, negative pore pressure along with a negative change in volume was induced.

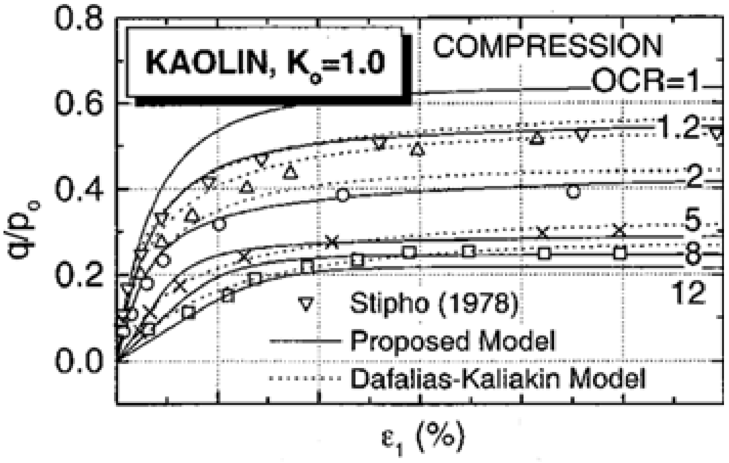

Figure 2.9: q/p$_o$ against strain for kaolin clay with increasing OCR (Ling *et al* 2002).

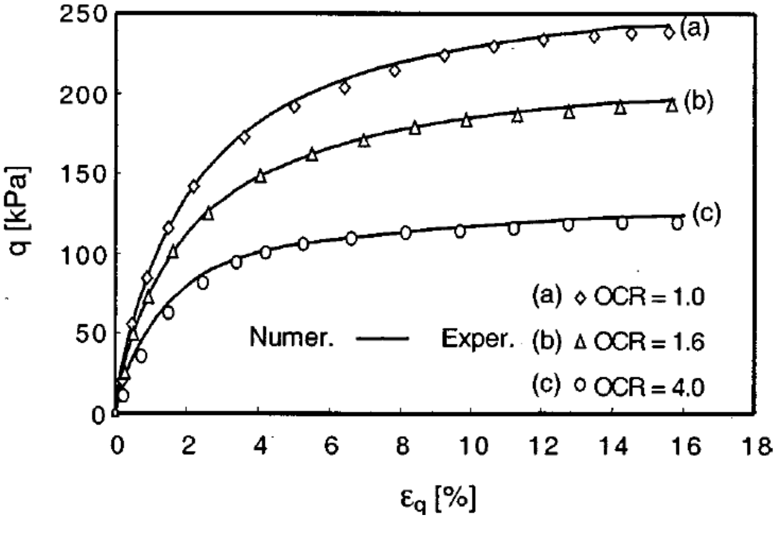

Figure 2.10: Deviator stress against direct strain for isotropically consolidated clay (Li and Meissner 2002).

2.7. Sample preparation methods

Achieving a homogeneous sample, while ensuring that the preparation process yields consistent specimens, is a primary objective for any experimental investigation. This is especially important when constructing soil/fibre samples.

2.7.1 Achieving repeatable homogeneous samples

Puppala and Musenda (2000) along with Das *et al* (2009) are two examples of investigations that carried out initial dry mixing of composite materials to achieve a homogeneous fibre sample. Saturation of the sample to twice the liquid limit or the addition of water to achieve optimum moisture contents then followed. The former investigation carried out a dry mixing process by hand, and states that a uniform mix was obtained. With the addition of specific water dosages as the mixing process continued, accumulation or balling of the fibres in the mixture was kept to a minimum (Puppala and Musenda 2000). Das *et al* (2009) advise that the water content should be added to the fibre/soil mix in two allotments, separated by a fifteen minute mixing period. Das *et al* (2009) believed the addition of fibres into slurry was the more optimum method of achieving a composite sample. That method was employed by Heineck *et al* (2005) as prevention against floating of the fibres. There a post-test examination of the prepared specimens was carried out, where sample variability was deemed to be low.

Freitag (1986) investigated the strength characteristics of discrete synthetic fibre reinforced soils. That study implemented a hand mixing method to achieve a consistent sample. The synthetic fibres were mixed into a moist soil using a stirring action. This had the effect of fibre clumps forming during the process. Freitag (1986) observed that when the mixing process was minimizing and ensuring fibre dispersion by constant visual inspection, a consistent sample could be achieved.

In geotechnical centrifuge modelling, a number of studies that include Dean *et al* (1997), Hossain (2003) and Chia (2004) conducted tests on clay samples that have already been consolidated. Consolidating kaolin slurry one-dimensionally to 100kPa before being strategically placed and tested in the centrifuge was the method used other than forming models in flight. Studies, such as Stewart and Finnie (2001), Rattley (2008) and Cassidy (2009), proceed to construct models with minimal preparation to the clay. In these cases the clay, usually kaolin slurry, had been prepared to the desired specifications and was simply poured into the testing area. In some of the above studies the slurry was subjected to a vacuum before placement in the centrifuge, in an effort to eliminate or reduce to a negligible level air bubbles entrained during mixing.

2.7.2 Segetin *et al* (2006)

Fibre reinforcement is a method of introducing natural or synthetic material into a soil with the end objective of increasing shear strength. Fibre reinforcement can often be referred to as discrete reinforcement, which replicates the effects that vegetation roots play in binding a soil mass together (Hejazi *et al* 2012). A comparator study was conducted by Segetin *et al* (2006) into the optimum method of mixing fibre into soil. The fibre utilized was from a flax plant, referred to as *Harakeke*. The mixing methods that were investigated in the study include; hand mixing, cultivator or rotary-hoe, concrete mixer and a tumble mixer.

The tumble mixer and the hand mixing method provided the best results for fibre dispersion in soil (Segetin *et al* 2006). The cultivator and concrete mixer both caused some fibre damage, with the cultivator leading to over-mixing and consequently separation of the fibres from the slurry. Using the concrete mixer resulted in the fibres floating on the surface of the sample and also fibre tangles forming around the mixing blades. It was also noticed that the buoyancy of the fibres inhibited the mechanical mixing process. In such cases, the fibres were not dragged to the bottom of the mixer, resulting in what Segetin *et al* (2006) defined as an inconsistent sample. In contrast to the hand mixing method, mechanical mixing with the tumble mixer did not fully entrain the fibres into the slurry of pre-mixed soil.

2.8 Modes of foundation failure

Shear failure of soil under a foundation is a result of the ultimate bearing capacity being surpassed. There are three modes of shear failure associated with foundations (Knappett and Craig 2012);

i. General shear failure
ii. Punching shear failure
iii. Local shear failure

General shear failure can be identified by the existence of a continuous slip surface from foundation edge to the ground surface, Figure 2.11(a). Failure is often quick with catastrophic effects. Failure of this nature is followed by tilting of the footing (Vesić 1973). The soil adjacent to the foundation will have a tendency to bulge, and will be visible on both sides throughout loading. However the final collapse of the soil will only occur on one side of the foundation (Vesić 1973).

Local shear failure can be characterized by a failure pattern found immediately below the foundation. The local shear pattern is similar to that of general shear, where the slip surface starts at the periphery of the footing ending at an unknown location in the soil mass, Figure 2.11(b). A substantial amount of vertical displacement of the foundation is required before the slip surfaces appear on the ground surface (Knappett and Craig 2012). There is also bulging of the soil, similar to that of general failure characteristics. In this instance there is no collapse or tilting of the foundation, which will remain embedded in the soil mass as it mobilizes the resistance of the deeper soil strata (Vesić 1973).

The third mode of failure is punching shear; in this case the shearing pattern is not easily identifiable, Figure 2.11(c). During the loading stage of the foundation, the tendency to move vertically is accompanied by compression of the soil directly underneath the foundation (Knappett and Craig 2012). This can be characterized by a vertical shear failure pattern adjacent to the periphery of the footing (Vesić 1973). There is only soil movement directly adjacent to the footing, with equilibrium in both the vertical and horizontal direction is maintained.

For a foundation to fail in one of the three modes of failure outlined above, a number of conditions must be present. The failure mode is directly linked with the compressibility of the soil. In the event that the soil is relatively incompressible and has infinite shear strength, the mode of failure will be general shear failure (Vesić 1973). However if the soil is relatively compressible and has a limited shear strength, then the failure mode will be punching shear.

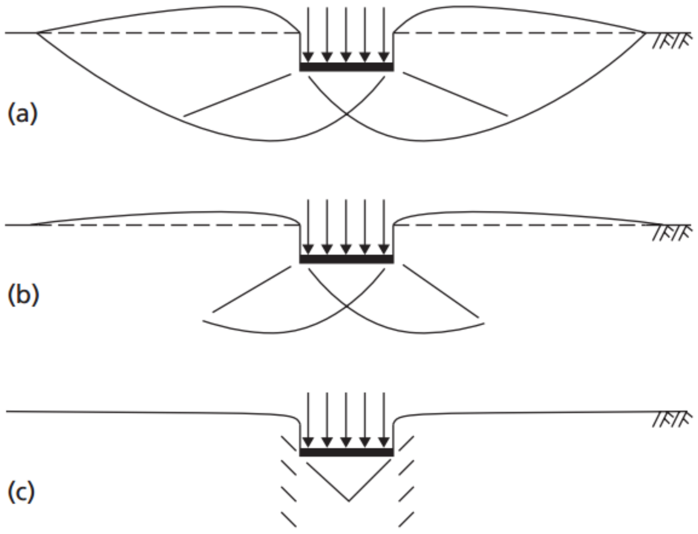

Figure 2.11: Modes of shear failure; (a) general failure (b) local failure (c) punching failure, (Knappett and Craig 2012).

2.9 Plastic equilibrium theory

Before a load is placed upon an area of soil, the underlying soil itself is said to be in a state of elastic equilibrium. In this state a small increase in stress will result in a small increase in strain. According to Terzaghi (1943) it was necessary to disregard such characteristics as friction and adhesion on the base of the foundation for this state to exist. When a load is placed upon the soil and increased beyond a limiting value the soil passes into a state of plastic equilibrium. In this state a small increase in stress will produce a significant increase in the strain. When plastic materials fail in shear, the failure is followed by shear flow, also known as plastic flow, which is continuous deformation at constant stress (Terzaghi 1943).

Terzaghi (1943) claimed that to establish a state of plastic failure at every point in a soil it must be subjected to deformation which is orientated at right angles to the surface of the soil. Plastic equilibrium can be reached by compressing or tensioning the soil body uniformly. If the soil is placed under tension, the soil weight aids in the process of soil expansion horizontally, such failure is called *active failure*. Horizontal compression of the soil is resisted by the weight of the soil, so subsequent failure is known as *passive failure*, Figure 2.12. In either case, Rankine (1857) found that slip lines through the soil mass will occur at an angle of 45˚- $\phi/2$ or 45˚+ $\phi/2$ to the horizontal respectively, where ϕ is defined as the internal angle of friction of the soil in question.

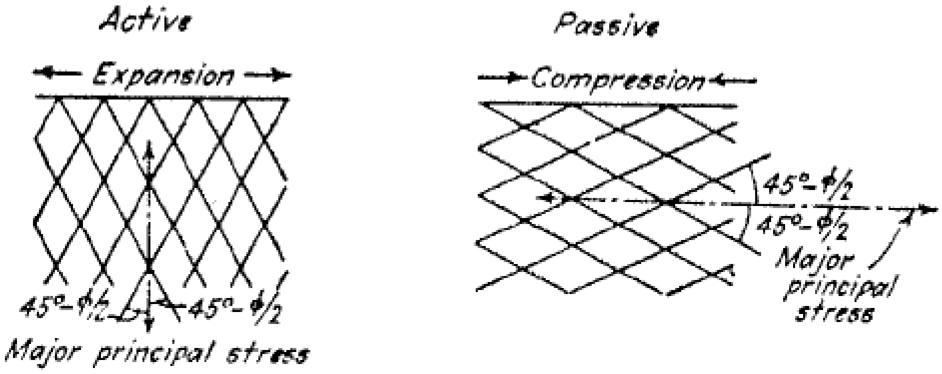

Figure 2.12: Shear pattern for the active and passive stress states and the orientation of the principle stresses (Terzaghi 1943).

2.9.1 Terzaghi's plastic theory

The transition from a state of elastic equilibrium to a state of plastic equilibrium in a semi-infinite mass can be achieved by a constant surcharge (Terzaghi 1943). This surcharge was denoted by the expression q'_c in Figure 2.13. For a foundation to penetrate into the soil, the weight of soil above the slip line bcde will have to be displaced, Figure 2.14. This can be achieved if a second surcharge q''_c is located within a distance of 2B from the foundation edge (Terzaghi 1943). Prandtl (1920) presented a solution for the problem of determining the extent of plastic failure, by assuming that the soil mass in question had no unit weight. The state of plastic equilibrium can be divided into three zones, which border the failure surfaces emanating from the periphery of the foundation in the case of general shear. These borders are essentially where the active and passive zones cease, Figure 2.13. Located directly under the foundation, is the active Rankine zone *abc*. This zone is encompassed by the active shear plane which descends at an angle of 45˚+ $\phi/2$ from the foundation (Terzaghi 1943). In ideal soil conditions during loading, the soil within this zone tends to spread laterally. However, if the foundation base is considered to be rough, the tendency to spread laterally is counteracted by friction and adhesion. The soil within zone one will then remain in a state of elastic equilibrium, sinking into the soil mass as if it was part of the footing (Terzaghi 1943). The second shear plane also emanates from the foundation edge, but travels away from the active zone at an angle of $45^\circ-\phi/2$. Passive Rankine zone *ade* is encapsulated above this shear plane and terminates at ground level, Figure 2.13. Within the active and passive zones the major principal stresses as found to be orientated vertically and horizontally respectively. This means the active zone moves downwards as a result of the formation of vertical slip lines, while the passive rankine zone moves horizontally from horizontal slip lines. The Rankine zones are separated by a zone of radial shear. Figure 2.14 shows within this zone the slip lines are a combination of straight lines with their origin at the foundation edges, while the intersecting slip lines are represented as logarithmic spirals which cross the straight lines at an angle of $90^\circ-\phi$ (Prandtl 1920).

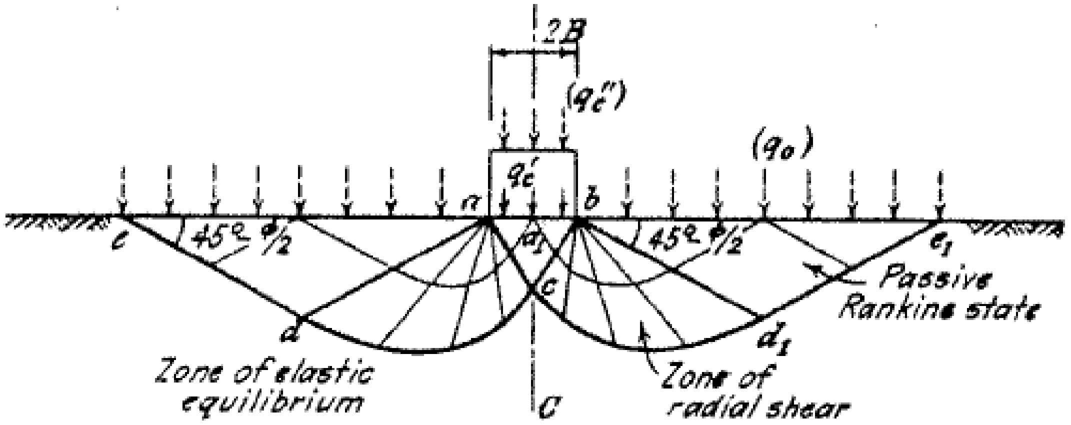

Figure 2.13: The occurrence of plastic flow with a uniform surcharge and a loaded strip foundation (Prandtl 1920).

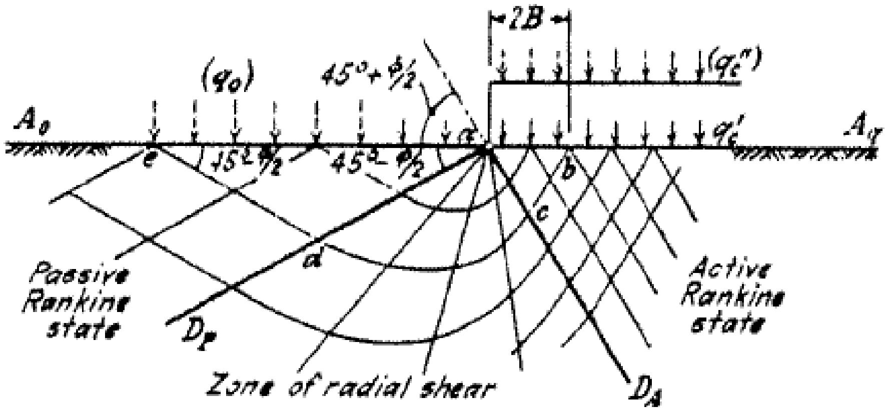

Figure 2.14: Detail of a loaded strip foundation with the induced state of plastic flow (Prandtl 1920).

2.9.2 Meyerhof’s plastic theory

Meyerhof (1951) extended the work of Terzaghi (1943) to cater for foundations that are shallow and deep. Meyerhof (1951) was concerned only with single vertical loads acting centrally on a foundation. This theory proposed that the zone of plastic equilibrium increased with depth and size of the plastic zones varied with the roughness and foundation shape. Meyerhof (1951) extended the failure surface to take account of the overburdened soil which Terzaghi excluded. In this theory the central zone *abc* remains and adjacent to that lies a radial shear zone proposed to cover an area of *bcd*, Figure 2.15. Meyerhof also proposed that a mixed shear zone lay between the radial zone and the horizontal soil surface, zone *bdef*. In the mixed shear zone the limits of shear depend on the size, shape and roughness of the foundation and lie between the extent of the radial and shear stresses. Meyerhof (1951) treated the boundary between the radial and mixed zones as an equivalent free surface, inclined at an angle β. This surface is subjected to the equivalent free surfaces stresses q_o and s_o which are normal and tangential to the free surface respectively, Figure 2.15. The bearing capacity can be calculated using the same expression as Terzaghi’s, Equation 2.8, but with the bearing capacity factors are now dependent upon the depth and shape of the foundation as well as the roughness of the base and angle of internal friction ϕ. The subscripts c, q and y on each individual bearing capacity factor N in Equation 2.8 relate to the cohesion, over burden stress and soil unit weigh respectively.

$$q = cN_c + \gamma DN_q + \frac{1}{2}\gamma BN_\gamma \qquad \text{Equation 2.8}$$

Where: c is the value of cohesion for the soil

N_c, N_q and N_y are bearing capacity factors

D is the foundation depth

y is the unit weight of the soil

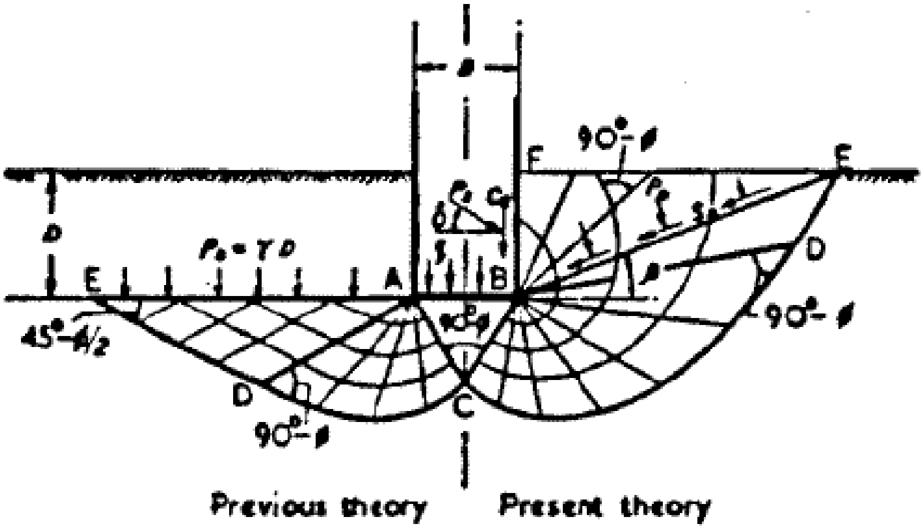

Figure 2.15: Comparison of the Terzaghi theory and the Meyerhof theory of plastic equilibrium (Meyerhof 1963).

In the plane shear zone, the state of plastic equilibrium requires that the shear strength, under normal pressure, is fully mobilized and equal to c + σtan ϕ. Where c represents the cohesion of the soil and σ is the total normal stress. Meyerhof (1951) calculated a range of values for N_c and N_q which lie between the lower and the upper limit of the shearing stress, (m=0, m=1). M denotes the degree of mobilization of the shear strength on the equivalent free surface and is described as having no effect to full mobilization of the shear strength (0 to 1). The degree of mobilization has little effect on the values of N_c and N_q, however, they are very sensitive to changes in β and ϕ. Meyerhof (1951) produced a set of graphs to determine N_c and N_q based on changes in β and ϕ. The Meyerhof (1951) method produced results that were identical to those of Prandtl (1920) and Reissner (1924) respectively.

For determining a minimum value of bearing capacity factor N_y for a strip foundation, Meyerhof (1951) proposed using a logarithmic spiral method drawn from the work of Ohde (1938). As with the bearing capacity factors of N_c and N_q, N_y was calculated for the upper and lower limits (m=0, m=1), where it was found to vary little but was effected greatly by changes in β and ϕ. N_y is therefore independent of the equivalent free surface, m. Meyerhof recommended a value of 22.5 for N_y.

2.10 Bearing capacity of circular foundations

Meyerhof (1951) determined bearing capacity of a circular foundation, using Equation 2.9. The procedure for determining the value of N_{cqr} was similar to that used to determine N_c for a strip foundation. The bearing capacity for a circular foundation, at depth D was determined in a similar manner as that for a strip foundation, taking account of the hoop stresses.

$$q_r = cN_{cqr} + \gamma K_s D \qquad \text{Equation 2.9}$$

where: N_{cqr} is the resultant bearing capacity factor for a circular foundation

K_s is the coefficient of earth pressure, taken as 1.

Meyerhof (1951) proposed that the value of N_{cqr} varies with depth from 6.18 at surface level to 9.74 at a depth twice the diameter of the foundation. Vesic (1970) also compiled shape factors for circular foundations shown in Table 2.2, and can be compared to values of shape factors given by Meyerhof (1963).

Table 2.2: Shape factors required for shallow foundations.

Parameter	Meyerhof (1963), ϕ=0°	de Beer (1967), modified by Vesic (1970)
Shape factor s_c	1.2	$1 + \left(\frac{N_q}{N_c}\right)$
Shape factor s_q	1.0	$1 + tan\phi$
Shape factor s_y	-	0.6

Terzaghi (1943) adopted his equation from the bearing capacity of a strip foundation and produced Equation 2.10, for a foundation with radius R. Terzaghi (1943) stated that beyond a distance of 5R the soil deformation was undefinable. In Equation 2.11, Terzaghi (1943) produced an expression for circular foundation bearing capacity from experimental data;

$$Q_{Dr} = \pi R^2 (cn_c + qn_q + \gamma R n_\gamma) \qquad \text{Equation 2.10}$$

where: n_c, n_q and n_γ are values dependent upon the angle of shearing resistance.

$$Q_{Dr} = \pi R_{qd}^2 = \pi R^2(1.3cN_c + qN_q + 0.6\gamma RN_\gamma) \quad \text{Equation 2.11}$$

where: N_c, N_q and N_γ are the bearing capacity factors for continuous foundations supported on the same soil.

2.11 Bearing capacity of rectangular and square foundations

Equation 2.12 expresses Meyerhof's (1951) solution for q_l, the bearing capacity for a rectangular foundation.

$$q_l = cN_{cql} + \gamma K_s D \quad \text{Equation 2.12}$$

where: N_{cql} is the resultant bearing capacity factor for a rectangular foundation

Meyerhof (1951) found that the ratio of N_{cqr}/N_{cql} (factors for circular and strip foundations respectively) varied from 1.10 to 1.20 and was dependent upon the foundation depth and roughness. Equation 2.13 was used as a method for determining the bearing capacity factor N_{cql} in terms of N_{cq} (bearing factor for strip foundations) as follows:

$$N_{cql} = \left(1 + 0.15\frac{B}{L}\right)N_{cq} \quad \text{Equation 2.13}$$

Meyerhof (1963) complied expressions for depth factors, where rectangular foundation depth was equal to or less than foundation width, Table 2.3. As the embedment depth of the foundation increases, the value of the depth factors will also increase, however this occurs at a decreasing rate (Meyerhof 1963). Shape factors are applied to bearing capacity equations to account for the varying shape of foundations. Powrie (2004) referred to s_q as an enhancement factor to account for foundations having a finite length. Table 2.4 compares shape factors associated with rectangular foundations compiled by Meyerhof (1963), Hansen (1970) and Vesic (1970). The depth and shape factor subscripts *c*, *q* and *y* relate to the cohesion, over burden stress and soil unit weight respectively.

Table 2.3: Depth factors required for shallow foundations.

Parameter	Meyerhof (1963)	Hansen (1970) $\boldsymbol{\phi}$=0˚
Depth factor d_c	$1 + 0.2\sqrt{N_\phi}\frac{D}{B}$ $where\ N_\phi = tan^2\left(\frac{1}{4}\pi + \frac{1}{2}\phi\right)$	$1 + 0.4\frac{D}{B}$
Depth factor d_q	$1 + 0.1\sqrt{N_\phi}\frac{B}{L}$	1.0
Depth factor d_y	$= d_q$	-

Table 2.4: Shape factors required for rectangular foundations.

Parameter	Meyerhof (1963) ($\boldsymbol{\phi}$'>10)	Hansen (1970)	Vesic (1970)
Shape factor s_c	$1 + 0.2N_\phi\frac{B}{L}$	$0.2\frac{B}{L}$	$1 + \frac{B}{L}\left(\frac{N_q}{N_c}\right)$
Shape factor s_q	$1 + 0.1N_\phi\frac{B}{L}$	$1 + \frac{B}{L}tan\phi'$	$1 + \frac{B}{L}tan\phi$
Shape factor s_y	$= s_q$	$1 - 0.4\frac{B}{L}$	$1 - 0.4\frac{B}{L}$

Meyerhof (1963) proposed Equation 2.14 for determining the bearing capacity of a foundation with an inclined eccentric vertical load at a depth within the soil. For comparison purposes the shape factors defined by Hansen (1970) and Vesic (1970) are shown along with Meyerhof (1963) in Table 2.5. B' and L' are the effective foundation dimensions. In the case of a shallow foundation the bearing capacity factors can be defined in terms of depth by substituting in the corresponding factors given in Table 2.4.

$$q = \frac{Q}{B'L'} = cN_C d_c i_c + \gamma D N_q d_q i_q + \gamma B' N_y d_y i_y$$

Equation 2.14

Similar to the equation produced for the establishment of the bearing capacity of circular foundations, Equation 2.15 was designed for a square foundation.

$$Q_D = 4B_{qD}^2 = 4B^2(1.3cN_c + qN_q + 0.8\gamma B N_\gamma)$$

Equation 2.15

The bearing capacity factors outlined in Eurocode 7 for spread foundations are presented in Table 2.5. This code also stipulates that expressions from experimental results may be used and that allowances should be made for site specific ground conditions.

Table 2.5: Eurocode 7 bearing capacity factors.

Parameter	Bearing Resistance
Bearing capacity factor N_q	$e^{\pi tan\phi} tan^2\left(45+\frac{\phi'}{2}\right)$
Bearing capacity factor N_c	$(N_q-1)\ cot\phi'$
Bearing capacity factor N_y	$2(N_q-1)\ tan\phi'$ (rough base)

2.12 Undrained bearing capacity

Knappett and Craig (2012) stated that when shear failure occurs in an undrained soil, the failure lines also known as slip lines are found to be circular or straight, and may be a combination of the two depending on the underlying soil and foundation type. At all locations in a soil mass where undrained conditions are present, the shear stress at failure equates to the undrained shear strength, $\tau_f = c_u$. The bearing capacity of a shallow foundation may be as written in Equation 2.16, and depending on soil characteristics undrained shear strength is known to vary with depth in certain cases (Knappett and Craig 2012).

$$q = s_c N_C c_u + \sigma_q$$ Equation 2.16

where; s_c is a factor accounting for foundation shape

N_c is the bearing capacity factor

c_u is the undrained shear strength

σ_q is the surcharge pressure

Analysis of foundation bearing capacity at depth ignores the undrained shear strength of soil above the footing base; however the weight of the soil is taken into account in subsequent analysis in the form of a surcharge (Knappett and Craig 2012). Exceptions arise in cases where the depth of the foundation, d, is greater than the foundation width. In circumstances where the foundation is surrounded by a surcharge, the bearing capacity factor, N_c, can be taken as 5.14 (Knappett and Craig 2012). For circular foundations, the value of N_c for a square foundation can be substituted into any calculations. The value for N_c has an upper limit of 9 for deep foundations that are both circular and square in shape. Salgado *et al* (2004) produced an expression for the determination of N_c in undrained conditions, shown in Equation 2.17

and values for a range of d/B is presented in Figure 2.16 along with values determined by Skempton (1951) for comparison. Skempton (1951) proposed that the basic from of Terzaghi's bearing capacity expression, Equation 2.18 should be used. The N_c value is related to the foundation shape and depth, and a value for this factor could be found by using the chart in Figure 2.16 or by using Equation 2.19. In Equation 2.19, for the lower limit of B/L (breath/length), N_c is taken as 7.5 for a strip foundation and 9.0 for a circular foundation in the upper limit of B/L.

$$N_C = (2+\pi)\left(1+0.27\sqrt{\frac{d}{B}}\right) \qquad \text{Equation 2.17}$$

$$q = c_u N_C + \gamma D \qquad \text{Equation 2.18}$$

where; γ is the unit weight of the soil in question

D is the depth to the foundation

$$N_C = 5.14\left(1+0.2\frac{B}{L}\right)\left(1+\sqrt{0.053\frac{d}{B}}\right) \qquad \text{Equation 2.19}$$

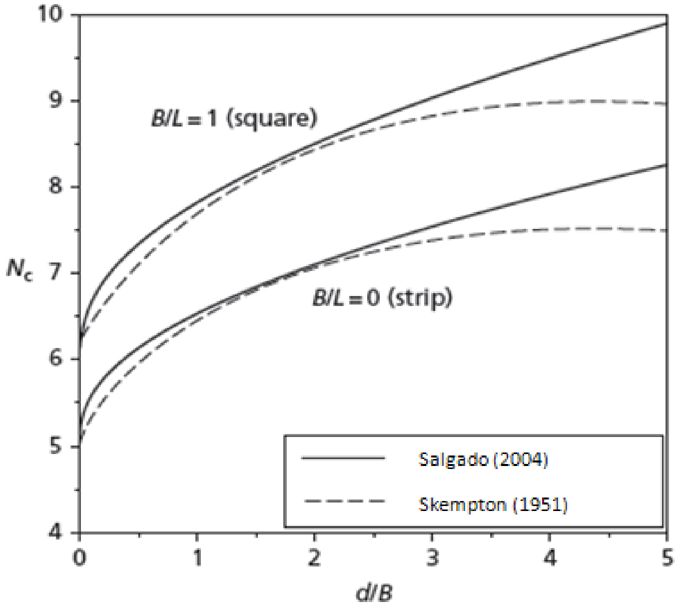

Figure 2.16: Range of N_c factor values for foundations in undrained conditions (Knappett and Craig 2012).

For the radial zones of shear between the Rankine passive and active zone in undrained conditions, the curve failure lines for drained conditions shown by studies such as Terzaghi (1943) and Meyerhof (1963) are replaced with circular arcs in undrained conditions, Figure 2.17 (Whitlow 2001). An expression to determine the bearing capacity, q_f, in undrained conditions as defined by Whitlow (2001) is outlined in Equation 2.20.

$$q_f = (\pi + 2)c_u + \sigma_o \qquad \text{Equation 2.20}$$

where; c_u is the undrained shear strength

σ_o is the surcharge pressure

An increase in the vertical stress at a given depth due to the overlaying soil, coupled with an increase in depth beneath the foundation base will not increase the bearing capacity of the soil in question according to Powrie (1997), since the bearing capacity is expressed in terms of the difference between the vertical stresses in the active and passive zones.

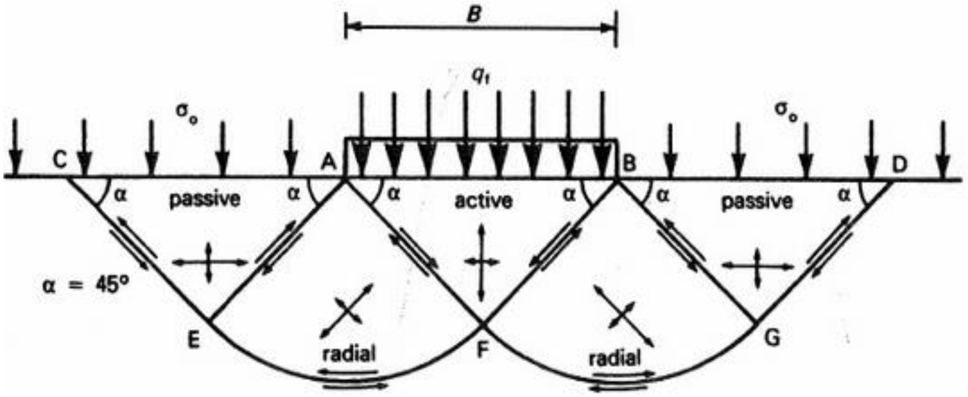

Figure 2.17: Shear failure slip lines within undrained conditions (Whitlow 2001).

2.13 Undrained bearing capacity from Eurocode 7

According to Eurocode 7, the bearing capacity of foundations in undrained conditions may be calculated by utilising Equation 2.21. Shape s_c factor changes with foundation shape as outlined in Table 2.4. The shape factors b_c and i_c are dependent upon the foundation base inclination and inclination of the load to the foundation respectively. Determination of these factors can be carried out by following the expressions outlined in Table 2.5 and Table 2.6.

$$\frac{R}{A'} = (\pi + 2)c_u b_c s_c i_c + q$$ Equation 2.21

Where; $\frac{R}{A`}$ is the ultimate loading, written as q_{ult}

c_u is the undrained shear strength

b_c and i_c are equal to 0

s_c is the foundation shape factor

q is the value of the surcharge loading

Table 2.6: Shape factors required for undrained conditions, Annex D, Eurocode 7 (2003).

Foundation Type	Associated shape factor
Strip Foundation	$s_c = 1.0$
Rectangular foundation	$s_c = 1 + 0.2\frac{B}{L}$
Circular or square foundation	$s_c = 1.2$

Table 2.7: Inclination factors required for undrained conditions, Annex D, Eurocode 7 (2003).

Parameter	Eurcode 7
b_c	$\frac{1 - 2\alpha}{(\pi + 2)}$
i_c	$\frac{1}{2}\left(1 + \sqrt{1 - \frac{H}{A'c_u}}\right)$

2.14 Summary

Relevant literature which assisted in the completion of this study has been presented. Geotechnical centrifuges allow for accurate relations to be drawn between events in reduced scale laboratory models and full scale prototypes. A *1/n* model is accelerated to a multiple *n* of earth's gravity so that internal stress are the same as that experienced in a *1:1* prototype (Taylor 1995). Penetrometers are used for determining the undrained shear strength of a prototype soil and can also be used within a centrifuge environment. Full flow penetrometers equate the over burden pressure above and below the tip resulting in a more accurate determination of undrained shear strength (Boylan *et al* 2011). A considerable number of studies have assessed the contribution of fibres which influence the physical and mechanical properties of soil (Freitag 1986). In controlled studies fibres have shown to increase the shear strength of soil. In the case of peat, the presences of fibres lead to an elevated stress level when assessments are made using the shear vane (Landva 1980). This elevated stress results in unrealistic determination of undrained shear strength. Investigations have also looked at the effects of consolidation, with and without directionally dependent means of application, when determining the shear strength of soils. Various methods have been investigated to determine the optimum methods for creating a homogenous fibre soil, with differing opinions in regard to the more accurate method (Segetin *et al* 2006). There is however a lack of knowledge regarding consolidation and testing of a fibrous soil within a centrifuge environment. There has also been little investigation regarding the application of fibres with the objective of improving the bearing capacity of mineral soils.

There are three modes of shear failure associated with foundations; general, punching and local shear failure (Knappett and Craig 2012).When a load is placed upon soil and increased beyond the ultimate strength, a state of plastic equilibrium occurs. Terzaghi (1943) theorized that when plastic materials fail in shear, plastic flow occurs, which is continuous deformation at constant stress. Terzaghi's plastic theory concerning drained conditions was based on studies completed by Rankine (1857) who established the formation of slip lines relative to ground level and Prandtl (1920) who presented a solution for determining the extent of plastic failure. Meyerhof (1951) extended the work of Terzaghi and focused on foundations that are shallow and deep. Meyerhof proposed that the zone of plastic equilibrium increased with depth and the size of plastic zones varied with foundation shape. In soil where undrained conditions are present, the shear stress at failure equates to the undrained shear strength, $\tau_f = c_u$ (Knappett and Craig 2012). Skempton (1951) proposed that the basic from of Terzaghi's bearing capacity expression could be used to determine bearing capacity in undrained conditions. Eurocode 7 includes in the expression for determining the bearing capacity of foundations in undrained conditions shape factors which are dependent upon the foundation base inclination and inclination of the load to foundation. Undrained shear strength in this study shall be determined by utilizing the formula set out in Eurocode 7.

CHAPTER 3

METHODOLOGY

3.1 Introduction

The objective of this study was to determine the shear strength of various fibre reinforced soil models. This study was broken into three stages; stage 1 involved the identification of a suitable fibre material; stage 2 comprised of testing various fibre models at an accelerated g-level and in stage 3 the analysis of the gathered data.

Initially this study was concerned with producing a homogenous soil fibre mass suitable for testing in a geotechnical centrifuge environment. A suitable organic fibrous material which could be prepared with relative ease was evaluated, along with an adequate method of producing homogenous fibre slurry. Reinforced fibrous models were consolidated at g-level and the influence of peat fibres on kaolin clay was evaluated by conducting bearing capacity tests, profiling using penetrometers and assessing the fibre soil characteristics from Atterberg limits. The load bearing tests involved foundations of varying sizes and shape. The size of the foundations was based upon the maximum number of tests that could be completed within the testing area without mobilising any boundary effects. Ten models were constructed which looked at the effects of varying parameters on the undrained shear strength of a modified soil: normal consolidation, over consolidation and varying peat fibre content (0-4%). Profiling was carried out once bearing capacity tests were completed and were located between sites of the foundation plate tests. Various characteristics of the reinforced soils were ascertained by conducting classification tests on samples taken of the test models. The Atterberg limits were determined from bulk samples while laboratory shear vane tests were carried out on cores retrieved from the centrifuge models.

The methods of testing used to achieve the outlined objectives are contained within this chapter.

3.2 Geotechnical centrifuge modelling

The following sections describe the physical equipment used during the course of geotechnical centrifuge modelling undertaken in this study.

3.2.1 IT Sligo geotechnical centrifuge facility

The geotechnical centrifuge facility established at the Institute of Technology, Sligo (ITS), had the ability to use either a beam or drum method of testing. The drum application of the centrifuge, Figure 3.1, was utilised in the course of this study to test homogeneous clay-fibre models. The ITS centrifuge had a maximum rotational speed of 638 rpm and a maximum acceleration level of 300g. The centrifuge was fully enclosed by a 12 mm steel casing with an external diameter of 1.7m and height of 750 mm.

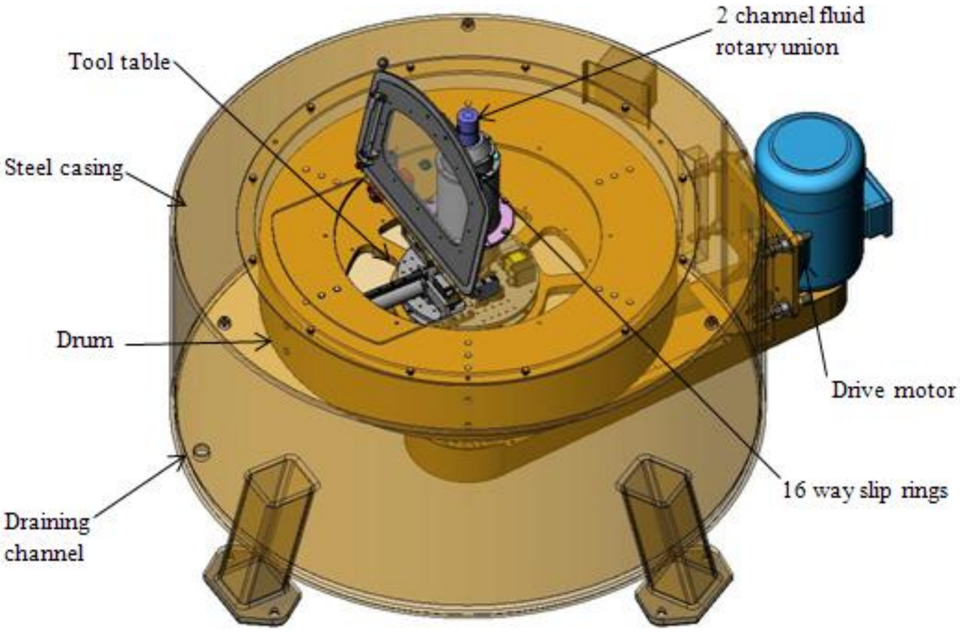

Figure 3.1: Layout of centrifuge equipped with drum, actuator, viewing window and rotary stack (Broadbent & Sons 2010).

The steel drum had a 1.17 m external diameter and a height of 245 mm. The drum had a testing channel of 200mm depth with an available model surface testing area of 1.38 m^2 and was equipped with a 600 mm diameter tool table; located centrally about the drum axis of rotation which could rotate independently of the drum. The table was housed within a steel container for protection during testing; this container was also equipped with a dispersion plate for sample placing. The required instrumentation such as the data acquisition system (DAS), actuator etc. were attached to the tool table during flight, Figure 3.2. A wireless router and motors for control of the actuator and tool table were operated remotely from the laboratory PC. Power was supplied to the instrumentation via slip rings contained within the centrally located rotary stack.

A more comprehensive analysis of the ITS centrifuge testing facility and data acquisition systems may be found in a summary of O' Loughlin *et al.* (2010), Establishing a beam centrifuge facility at the Institute of Technology, Sligo, Ireland, in Appendix A.

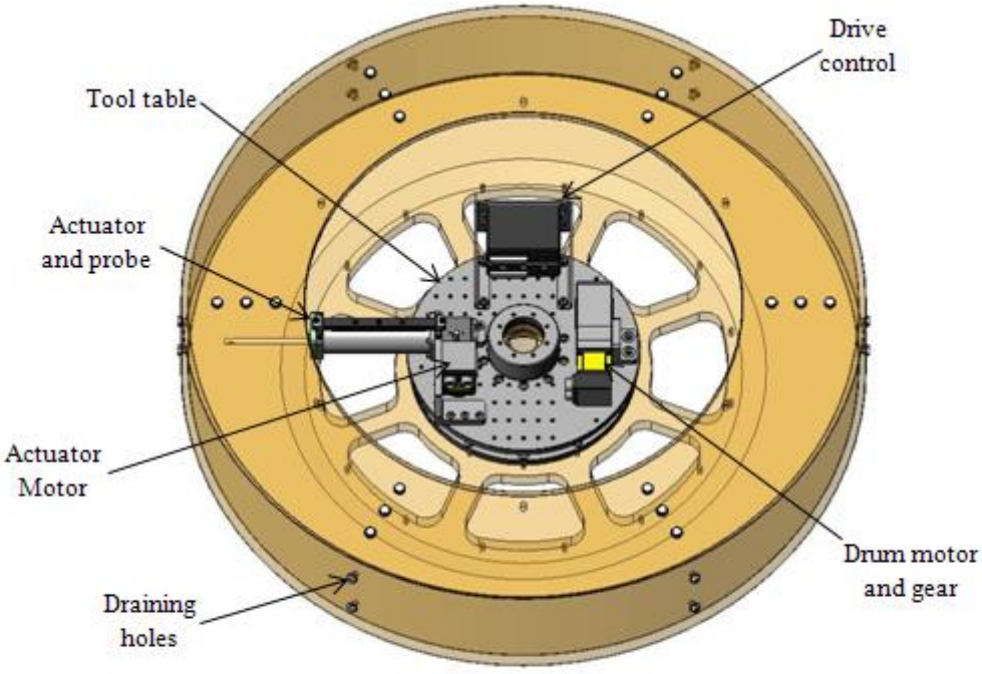

Figure 3.2: Cut-away of drum showing tool table, actuator and drive assembly (Broadbent & Sons 2010).

3.2.2 Motor driven actuator

The actuator used in this study, was electrically powered and was designed specifically to accommodate linear geotechnical sample characterisation and bearing capacity design. The ITS actuator was a combination of a Parker Hannifin BE series servo motor, a housing unit and motion inducing mechanism. Due to weight restrictions that apply when testing within an accelerated g-level, lightweight aluminium was used in construction where possible. The housing unit was comprised of a 225 x 60 mm diameter column, which held the worm nut screw, plus a linear transducer (baluff) attached externally for position sensing, Figure 3.3. A U-bracket measuring 195 x 85 x 70 mm was connected to the top of the column, for attaching to the tool table. A gear system for inducing motion to the worm nut screw, along with the servo motor was located on the U-bracket. The principle function of the actuator was to induce motion of the loading plate or probe through the model, thereby simulating shear failure by loading or by fulfilling characterisation of the soil. Motion was supplied by the worm screw or roller screw to the specific probe, which moved the worm screw nut in a positive or negative linear direction. The rate of penetration for all tests was fixed at 1 mm/s. Vertical stroke length of the actuator was limited to 145 mm. Control of the actuator motion was carried out remotely from the laboratory PC.

Motor function was controlled by a ViX250IE Intelligent Digital Servo Drive, which provided resolver feedback and a programmed mode. A direct current of 24V was required to run the system. Table 3.1 presents a list of the motor characteristics. This drive, located on the on-board tool table, was linked directly to the laboratory PC via a connection through the centrifuge slip rings. Communication between the operator and servo drive and by extension the actuator was facilitated by the Easi-V software programme. The drive was required to be set up and installed for use with a particular motor type. Once installed, Easi-V software enabled downloading of control commands to the drive. Basic operation of the actuator system was carried out by utilising the terminal buttons displayed at the bottom of the command screen. Situations arose where programmes were required to be written by the operator and saved to the drive. Housing the drive in the on-board hardened steel cabinet provided the ideal protected environment from mixture splashes and other debris. Ventilation through the cabinet was problematic, however the relatively short duration of the tests and the need to manually retrieve the loading plates resulted in a sufficient cooling down period.

Table 3.1: Characteristics of a BE 230GJ Motor.

Parameter	Value
Stall Torque (Nm)	0.38
Rated Voltage (V)	340
Rated Power (KW)	0.186
Rated Speed (RPM)	4990

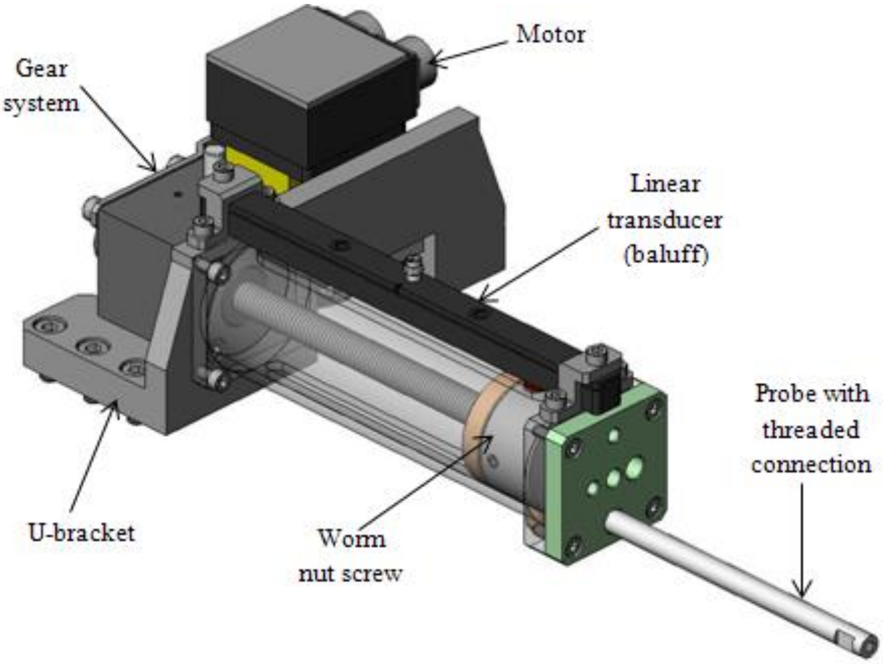

Figure 3.3: Section through the radial actuator used for bearing capacity and penetrometer testing (Broadbent & Sons 2010).

3.2.3 Subminiture load cell

A Burster subminiture strain gauge load cell was used in this study to measure the load imparted to the penetrating load plate. This particular load cell was a full bridge, i.e. containing four strain gauges. Table 3.2 provides the technical data of the burster load cells. Two loads cells were used, a 1kN and 2kN, depending on the force expected during testing, Figure 3.4. A threaded male to female connector located along the load cell's axis of symmetry allowed ease of connection to the actuator probe, plus other attachments where required. A cable connected radially to the load cell provided for transmission of data from the sensor, while also providing a range of motion. The load cell was calibrated before testing and was subsequently checked periodically during the testing programme. Load cells were calibrated by hanging 10 kg weight plates from a suitable threaded attachment. The average cumulative output was used to determine a calibration factor. The output of the load cell was in millivolts and thus required an electric amplifier before the data could be used. This amplification and digitising process was carried out on the data acquisition system (DAS) circuit board.

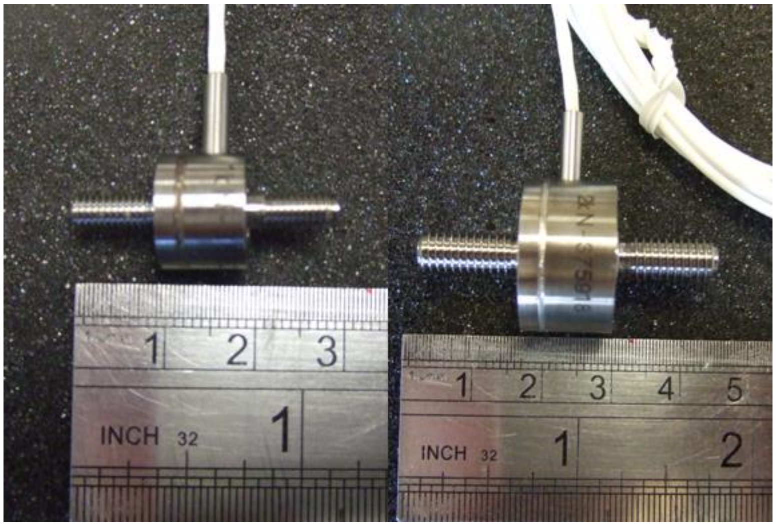

Figure 3.4: 1 and 2 kN burster load cells used during bearing capacity testing.

Table 3.2: Technical data of a Burster 1kN and 2kN subminiture load cell.

Parameter	1kN	2 kN
Dimensions (mm)	12Ø x 10H	20Ø x 12H
Force Range (kN)	0-1	0-2
Accuracy (%)	≤ 0,5	≤ 0,5
Max force operating (% v.E./F.S)	100	100
Reference Excitation (V)	5,0	5,0
Output signal (sensitivity) (mV/V)	1,1235	1,1731
Zero output (mV/V)	-0,0181	-0,0023

3.2.4 DAS and wireless system

The data acquisition system (DAS) used on the ITS centrifuge was developed at the Centre for Offshore Foundation Systems (COFS), part of the University of Western Australia, Perth. The ITS system was similar to the detailed description outlined by Gaudin *et al* (2009). This piece of equipment allowed for high speed data collection and was connected directly to a wireless router, which transferred data to the laboratory PC. O'Loughlin *et al* (2010) outlined the benefits of this wireless system. Data could be viewed and recorded in real time. The system unit was equipped with 8 different transducer connections, to accommodate several different sensors within the drum at any one time, Figure 3.5. The unit was comprised of a metallic box 150 x 60 x 40 mm with power input and Ethernet output.

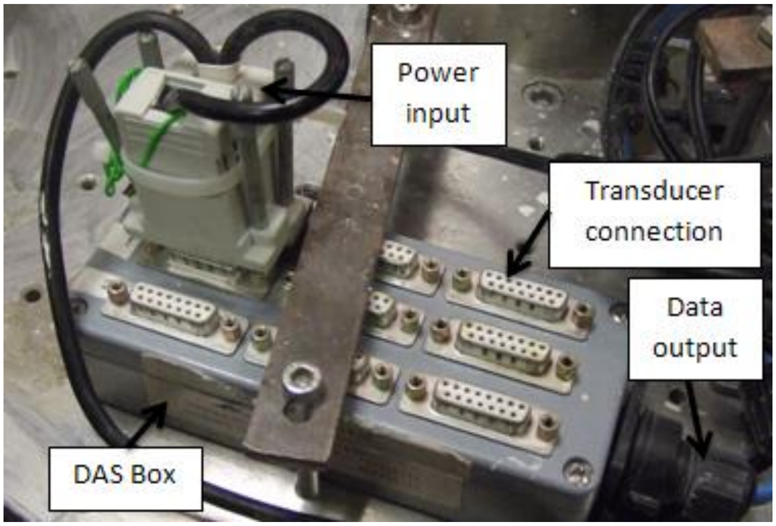

Figure 3.5: DAS box restrained on the centrifuge tool table.

Data was transmitted using a Linksys 2.4 GHz wireless-G Ethernet Bridge. The system was powered by 12 V DC brought through the slip rings. All of the on board systems were located as close to the centrifuge axis of rotation as possible to minimise stress on components. Streamed data was viewed using DigiDAQ software, which had a circulating memory system. Once the system was turned on, data logging was continuous. When event capture was required the data was saved to the PC hard drive.

3.2.5 Cone penetrometer

The cone penetration test (CPT) is a standard method used in geotechnical investigation to determine the properties of soils and identification of soil stratification (Lunne *et al* 1997). The ITS electric cone penetrometer was manufactured by COFS at the University of Western Australia. The electric CPT was used in this investigation as a method of determining the undrained shear strength of the fibre reinforced soil. Comprised of a cone at the top of a steel shaft, the probe was pushed into the model at a continuous rate with a continuous data feed transmission. The test proceeded at a rate of 1 mm/s. With this probe only tip resistance of the cone was measured, there was no facility to measure sleeve friction or pore pressure. The probe shaft was 175 mm in length and has a uniform diameter of 10 mm, Figure 3.6. The cone tip was inclined at 60 degrees to the apex. A communication cable was connected radially to the base of the shaft, allowing great flexibility. The cable connected with the DAS via a D-Type connection. Extension pieces were available to increase the length of the shaft where necessary by attaching to the base of the probe. The cone load cell was calibrated by the manufacturer and was fixed at 13021.42 kPa/V for the duration of the testing programme.

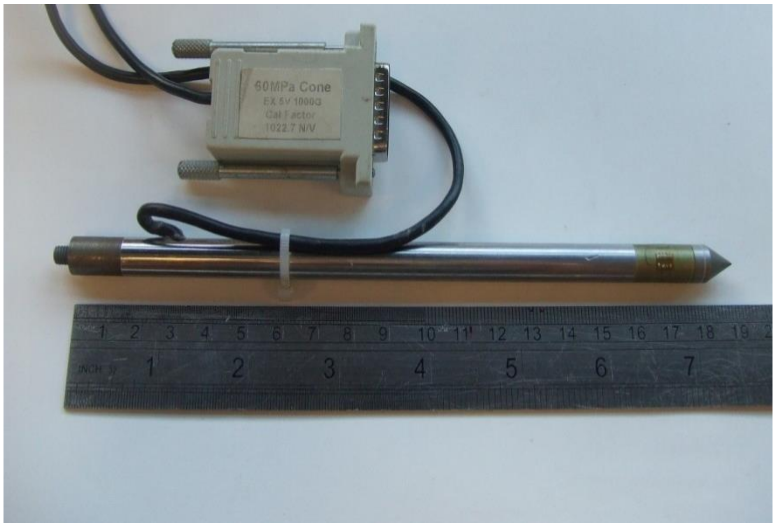

Figure 3.6: CPT probe used during profiling, shown with extension piece.

The probe was attached to the worm screw nut; if an extension piece was required this was attached to the base of the probe. The test locations for the penetrometer tests were chosen as being approximately half the distance between loaded foundation sites. The tool table was rotated to the desired location. The probe was lowered to the model surface; this was the start position of the test. The centrifuge was programmed and spun at 25g-level. Once the probe had equated to the acceleration field i.e. load cell drift had dissipated, the test began. The probe was driven to a depth of 100-120 mm into the model. On completion of the test, the model was spun down and the probe was cleaned of kaolin and fibres. The tool table was rotated to the next test site and the procedure was repeated. A total of three CPT tests were conducted on each model.

The total measured tip resistance, q_t, of the CPT was determined from the net tip resistance data, q_c, using Equation 3.1. As there was no facility to determine the pore water pressure generated during testing there was no correction undertaken. The net tip resistance is presented as the total measured tip resistance for the following CPT data.

$$q_t = q_c \qquad \text{Equation 3.1}$$

3.2.6 Piezoball penetrometer

The second probe used to investigate the characteristics of the reinforced fibre model was the ball penetrometer or piezoball. The piezoball is a full flow penetrometer and facilitates the flow of soil around the sensor, thus giving a more accurate strength indication compared to the cone due to a greater surface area (Boylan and Long 2007). This was seen as an advantage for the ball due to the fibrous nature of the soil and the likelihood of fibres entangling around the cone. The ball penetrometer was chosen to carry out full flow profiling due to the non-existent bending effects. Such effects are associated with the T-Bar. The piezoball shown in Figure 3.7 had a 14 mm ball with a 3 mm porous filter at mid-face to facilitate pore pressure measurements. Like the CPT it was designed and manufactured by COFS. Located behind the filter of the ball was a pore pressure transducer (PPT), described by Kelleher and Randolph (2005) as producing a greater sensitivity than that of the cone. The load cell was also contained within the ball and was calibrated by the manufacturer at 2611.556 kPa/V, while the PPT was calibrated at 234.9 kPa/V. As was the case with the CPT, the piezoball was calibrated by COFS and these factors were assumed to remain constant during testing. The probe was 175 mm in length from tip to base, and had the capacity to be fitted with several extension pieces similar to the CPT. The probe shaft tapered from 4 mm behind the ball to 8 mm one third of the shaft length, and finally 10 mm at the base.

The process for attaching the piezoball penetrometer to the actuator and selection of adequate test sites was the same as that described for the cone penetrometer outlined in the previous section. A total of three piezoball tests were conducted on each model, Figure 3.8. In the case of the piezoball, prior to testing the probe was saturated for a period of 24 hours in a sealed chamber. The probe was immersed in silicone oil to fully saturate the filter. This was undertaken to remove any entrapped air around the load cell, to avoid compromising the test data.

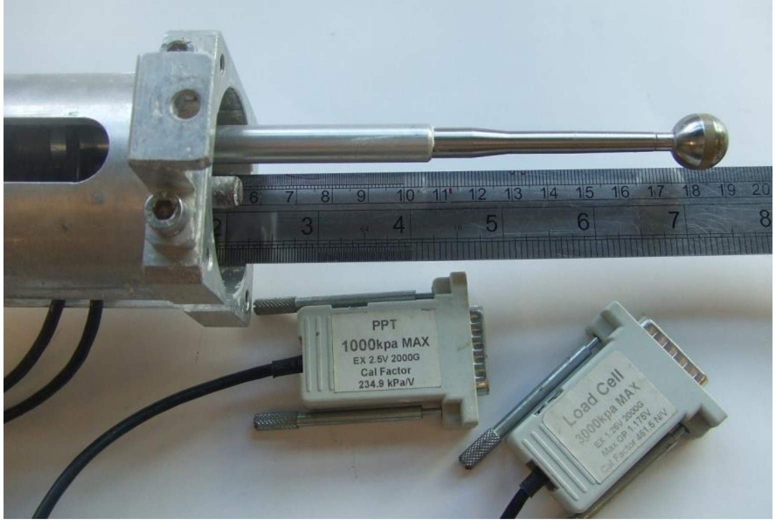

Figure 3.7: Piezoball attached to the actuator nut screw. PPT and load cell connections are also shown.

The net tip resistance of the piezoball was determined from the tip resistance data using Equation 3.2. The factors associated with the unequal area ratio and the ratio of the surface area to shaft area for the cone and piezoball probe are shown in Table 3.3. Such factors were used during the calculation of shear strength to improve the accuracy of the associated penetrometer.

$$q_{full-flow} = q_c - [\sigma_{nv} - u_n\,(1-\alpha)]\,A_s/A_p \qquad \text{Equation 3.2}$$

where; σ_{vn} is the overburden stress at location n

u_n is the pore water pressure at location n

α is the unequal area ratio

A_s is the shaft area

A_p is the penetrometer projected area

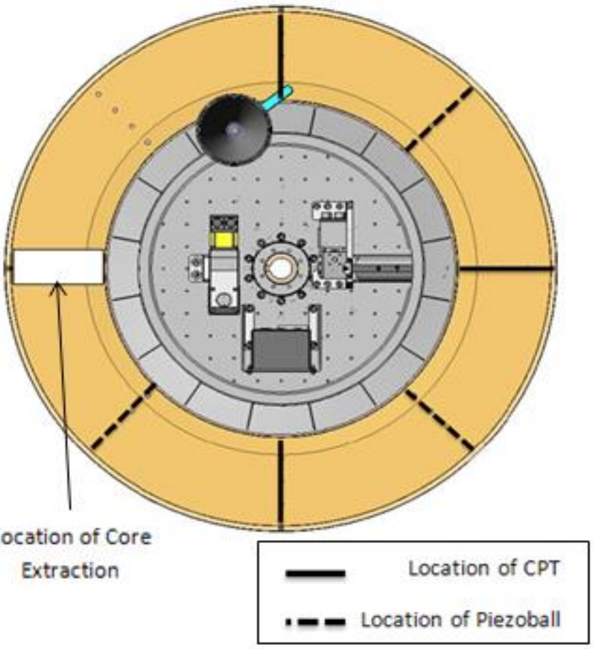

Figure 3.8: Location of CPT and piezoball testing positions, along with core extraction position (Broadbent & Sons 2010).

Table 3.3: Factors required for penetrometer correction.

Factor	Denotation	Piezoball
Unequal area ratio	α	0.80
Area of Shaft/ Area of Probe	A_s/A_p	0.16

3.3 Development of a centrifuge model

The reinforced soil models created in this study had a vertical cross section of 200 x 200 mm. The 200 mm depth of the model corresponded to a depth of 5 m at 25g. The model was formed by pouring a slurry pre mixture consisting of kaolin clay at twice its liquid limit and a known mass of peat fibres per dry weight of kaolin, into the drum channel while the centrifuge was at a low g-level, typically 5g. The slurry was poured externally through a funnel onto a spiral dispersion plate, and spread along the channel. This ensured a random orientation of fibres throughout the model. To facilitate the consolidation process and to allow the production of a slurry mixture between loads, the channel was filled in 20 kg increments, corresponding to a height of approximately 20 mm. The drum was then accelerated to 25g in the case of a normally consolidated sample or 50g for an over consolidated sample. Once the drum had reached its capacity load, consolidation continued uninterrupted. During consolidation water was poured over the model surface to retard the establishment of a crust in the upper portion.

Upon completion of consolidation the centrifuge was spun down to 1 g and the testing arrangements were attached to the tool table. The actuator was fitted with a calibrated load cell plus a socket piece and lowered until it just came into contact with a loading plate resting on the sample surface. A ball bearing was located between the recessed portion of the foundation and the socket attached to the actuator shaft to facilitate possible rotation of the foundation during testing. The centrifuge was then accelerated to the testing g-level, where the foundation was pushed into the model at a rate of 1 mm/s, to a depth corresponding to twice the width of the foundation. The load during testing was measured. This data was transferred from the data acquisition system (DAS), via a wireless router to a laboratory PC. The centrifuge was decelerated to 1 g, where the actuator probe was extracted remotely. The bearing plate, ball bearing and socket were required to be manually removed from the model. The tool table was remotely rotated clockwise along the model face. A new testing location was established at a distance of 3B away from initial site and the process repeated.

The characteristics of the modified soil were also accessed by conducting piezoball and CPT tests on the consolidated sample. These penetrometers were attached to the actuator and lowered until directly above the model surface at 1g. The tests were also conducted at a rate of 1 mm/s and data processed in the same manner while the model was at the test g-level.

Test data was exported into Microsoft Excel which facilitated analysis and back calculation of the model's shear strength. Descriptions of each testing procedure, along with the processes involved in creating the centrifuge testing model are outlined in the following sections.

3.3.1 Creating fibrous slurry

Kaolin clay was chosen as a preferable testing material due to ease of application and its proven record in geotechnical modelling (Lowmass 2006). The kaolin powder was turned into slurry form by saturation to twice its liquid limit corresponding to a moisture content of 120 %. The mixer available had a capacity of 30 kg. Mixing of kaolin slurry took place for a 24 hour period. Segetin *et al* (2006) and Freitag (1986) produced a consistent and repeatable slurry, using a hand mixing method where fibre was added to a wet soil and mixed to form a homogenous mass. Das *et al* (2009) and Viswanadham *et al* (2009) proposed dry mixing of the fibre/clay prior to saturation produced the best results, whereas others like Heineck *et al* (2005) championed the addition of fibres into slurry. For practical reasons it was decided to adopt the hand mixing method. The most consistent mixtures were produced when working with 10 kg quantities of kaolin slurry and the corresponding percentage fibres. Fibres were introduced into the slurry mixture by percentage dry weight of kaolin. Addition of fibre was conducted incrementally to ensure even dispersal throughout the clay mass. A homogenous 10 kg load of 1 % fibre and clay slurry could be prepared within 30 minutes.

For 2 % or higher percentage fibre concentrations, the 1% fibre model was reconstituted and remixed with additional fibres. This involved breaking the used model up into pieces of approximately 30 mm diameter, saturating these to twice the liquid limit as before, along with mixing of additional fibres. Moisture contents of the tested model were required to determine the percentage water required to saturate to 120%. The most effective way to re-saturate the used model was by using an electric blade mixer. This method did have an undesirable effect in that the fibres already contained within the sample when remixed clumped together around the mixer blades. This event was well documented in literature when Segetin *et al* (2006) used blade or spiral mixing devices. This could not be avoided during reconstituting of the sample. To re-disperse the fibres, a portion approximately 10 kg of the mixture, was taken and mixed by hand before additional fibres were added. By being vigilant when reconstituting samples, consistent homogenous samples were achieved.

Perpetration time for 2 % or higher was increased to between 40 to 50 minutes, to produce a homogenous sample. This preparation time remained constant for the 3 % and 4 % fibrous slurry.

3.3.2 Filling the drum channel

Once the slurry had been satisfactorily mixed, filling of the drum channel began. The centrifuge was spun at a g-level of 5g to facilitate ease of application. Filling the drum at an acceleration level greater than 7g resulted in a considerable portion of the sample failing to be directed onto the drum channel base. Unwanted quantities of the slurry were thus deflected onto the outer protective steel casing or alternatively the mixture fell between the drum and the tool table. The funnel arrangement in Figure 3.10 was attached rigidly to the outer steel casing. The funnel was equipped with a viewing section below the tapering to facilitate inspection of the mixture as it entered the drum. The slurry mixture was poured into the funnel and allowed to fall under gravity onto the spiral dispersion plate. When filling with high percentages of fibre slurry, the mixtures were seen to gather along the funnel neck and exit, thus increasing time taken to fill the drum. When handling the 3 % and 4 % fibre slurry mixture a perspex extension, Figure 3.9, was added to the funnel. This allowed a greater quantity of slurry to be placed in the funnel; assisting the clearing of sample gathering at the exit or along the funnel section. By using the mixtures self-weight to push itself onto the dispersion plate, filling continued at pace. A decision was made prior to filling the drum that no rodding or compacting of the slurry should take place while in the funnel in the event that such an action could cause clumping or gathering of the fibres.

The sample preparation method adopted worked reasonably well for fibre contents up to and including 4 %. Hypothetically, if a fibre content of 5 % or higher was used it is highly unlikely that such a mixture would pass through the funnel without clumping or localising of the fibres in the slurry. To ensure the drum would fill correctly compaction or rodding of the slurry in the funnel would be required. Therefore, it would be likely that the model formed would not be homogenous.

Figure 3.9: Fibrous sample fed into the funnel and descending onto the dispersion blades.

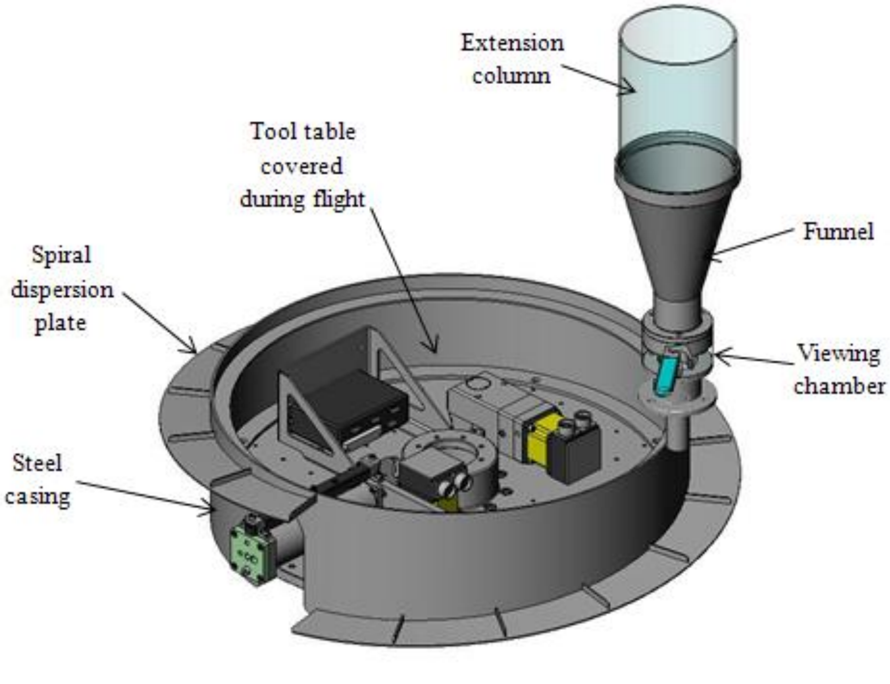

Figure 3.10: Funnel and spiral dispersion blade apparatus used to fill drum channel (Broadbent & Sons 2010).

3.3.3 Sample consolidation

The maximum depth of model contained within the channel was 200 mm. Once this depth had been achieved, loading of the channel ceased. To ensure the upper portion of the sample did not dry out and crust, a method of keeping the model surface moist during consolidation was implemented. This was needed to ensure unrealistic strengths were not experienced during testing; also excessive scraping of the model surface could be avoided by ensuring a moist surface. Water was supplied through a special conduit inside the fluid rotary union and onto the model surface via a small hose located on the periphery of the dispersion plate. During flight the tool table was rotated independently to the drum rotation at 1 mm/s. This ensured that localising of the water feed was avoided and the entire surface length of the model was keep moist. The sample was spun down daily during the consolidation process for a visual inspection of the model; checking of the centrifuge and to record the current depth of sample. This process took approximately 5 to 10 minutes. The centrifuge then remained in flight to allow consolidation to continue unimpaired. The time taken to complete the process of filling and consolidation varied between 15 and 18 days depending on the fibrous content and the desired consolidation ratio required. Consolidation reduced the final depth of the models, by up to 15 mm in the case of the 4% fibre. Once consolidation was complete, loading of the model began.

3.4 Characterisation of fibres used to create testing models

Peat fibres were used to create the reinforced soil models tested in this study. The ease of sourcing sufficient quantities and the relative quickness of fibre extraction were decisive factors in choosing this material. A bulk shipment of peat was obtained from a Bord na Mona Environmental Plant, located at Timahoe, Coill Dubh, Naas in Co. Kildare. The sample contained peat from a number of different sites in the midlands and north Tipperary.

3.4.1 Fibrous nature of peat

Boylan *et al* (2008) described peat as being comprised of organic plant material in various states of decay. The structure of peat is interconnected on a microscopic level. In mineral soils or clays, the skeletal structure has frictional contact between its particles. Connolly *et al* (2007) discusses the decaying process of plant cellular structures and other material is frequently interconnected with fibres. These fibres are created as a result of the natural break down in plant structure during decomposition. It is these fibres and their ability to act as reinforcement in a peat mass that is of interest to this study.

The length of the peat fibre contributes directly to the shearing resistance found in the peat mass; a study by Segetin *et al* (2006) have shown the link between fibre lengths and shear resistance for a soil/fibre mixture. The bond formed between the soil and fibre is invariably a result of surface texture of fibres. These bonds can be affected by the fluctuation in moisture content during consolidation, with expansion or contraction of the fibres. Drainage can also occur at a faster rate in a reinforced soil due to fibre strands acting as conduits for the moisture.

3.4.2 Preparation of fibrous material

Peat is a material in which an abundance of fibrous material can be found. Owing to the accessibility of waste peat from briquette production facilities around Ireland, a decision was made to utilise this material. The by-product obtained from one of these facilities contained large quantities of decomposing material, humus material, debris from illegal dumping and other unwanted material. To remove the undesirables from the fibres, Figure 3.11, the quantities of peat were first checked for large debris and sieved on a 10 mm sieve. The sieved portion was washed to remove remaining peat and smaller fragments of wood etc. and also to break dried and crusted peat from fibre clumps. The washed fibres were then oven dried at 50˚ C. After drying was completed, the fibres were free of peat and other material; however, they remained in a clumped or tangled state. Fibres were required to be separated individually. Through trial and error the most effective way of achieving this was found to consist of a grating action. The fibre clumps were rubbed repeatedly against a coarse surface, thus by "tearing" the fibrous clumps individual fibre strands separated from the collective. The fibres were again sieved on a 0.5 mm sieve to remove dust and fine particles. After which the fibres could be easily pulled apart by hand and as such were ready for mixing with the kaolin slurry. The prepared fibres, Figure 3.12, were stored until required.

Figure 3.11: Peat showing contaminants before the separation process was completed.

Figure 3.12: Peat fibres post washing and sieving.

At the start of a centrifuge test a representative sample of the prepared fibres was taken from storage and used to determine the physical properties. The sample weighed 10 grams and was taken from various containers of the prepared material. Using a digital Caliper, the length and diameter of the fibres were measured, Table 3.4.

Table 3.4: Average physical properties of peat fibres.

Property	Value
Diameter (mm)	0.02-0.1
Length (mm)	10-60

3.5 Characterisation of clay used to create testing models

Kaolin clay was used to create fibrous models for the purpose of this study, due to its availability, quality and ease of handling. The clay was purchased in bulk and was tested in accordance with BS1377 (1990) Part 2 to determine its characteristics.

3.5.1 Overview of kaolin clay

Kaolin clay was used for many laboratory investigations, owing to its attractive properties. Kaolin is soft, plastic clay, white in colour and comprises a low iron content. This clay is hydrophilic and thus will readily disperse when contact is made with water (Ciullo 2003). The hydrophilic property of kaolin renders it an extremely useful medium to create slurry mixtures within which the dispersion of the peat fibres can be achieved. The powder kaolin clay was required to be saturated to twice its liquid limit to create a suitable slurry. Mixing the slurry/fibre composite by hand was seen as the most suitable method to achieve random fibre dispersion throughout the sample.

3.5.2 Moisture content

The moisture content, *w*, of a soil is a measure of the water contained within the soil structure. Powrie (2004) defined the moisture content as the ratio of the mass of water to the mass of soil solid. The moisture content is vital when determining the nature of soils. Determination of moisture contents on the prepared soil fibre models in the centrifuge were carried out using the procedure outlined in BS1377-2 (1990). Moisture contents were carried out on core samples from centrifuge models and on cores after shear vane testing. For the centrifuge models, samples were taken at four separate locations around the model face; the four sample locations were orientated at 90 degrees to each other. At each location three sample at depths of 10, 100 and 190 mm were extracted. In relation to model cores, samples were taken at depths of 51, 102 and 153 mm where shear vane testing was performed. Single moisture contents were determined at each depth where the core was sheared. Figure 3.13 shows the range of moisture contents with sample depth determined from the centrifuge models after testing. Normally consolidated and over consolidated models are abbreviated as NC and OC respectively. A trend was apparent with both NC and OC samples where an increase in fibre content leads to a reduction in moisture content. There was a noticeable moisture increase with depth for the samples, with over consolidated samples showing lesser moisture retention than normally consolidated. The 1 % NC sample was an exception; however, this was attributed to a mechanical failure in the centrifuge, where the sample was stationary and with limited watering for a period of 48 to 72 hours.

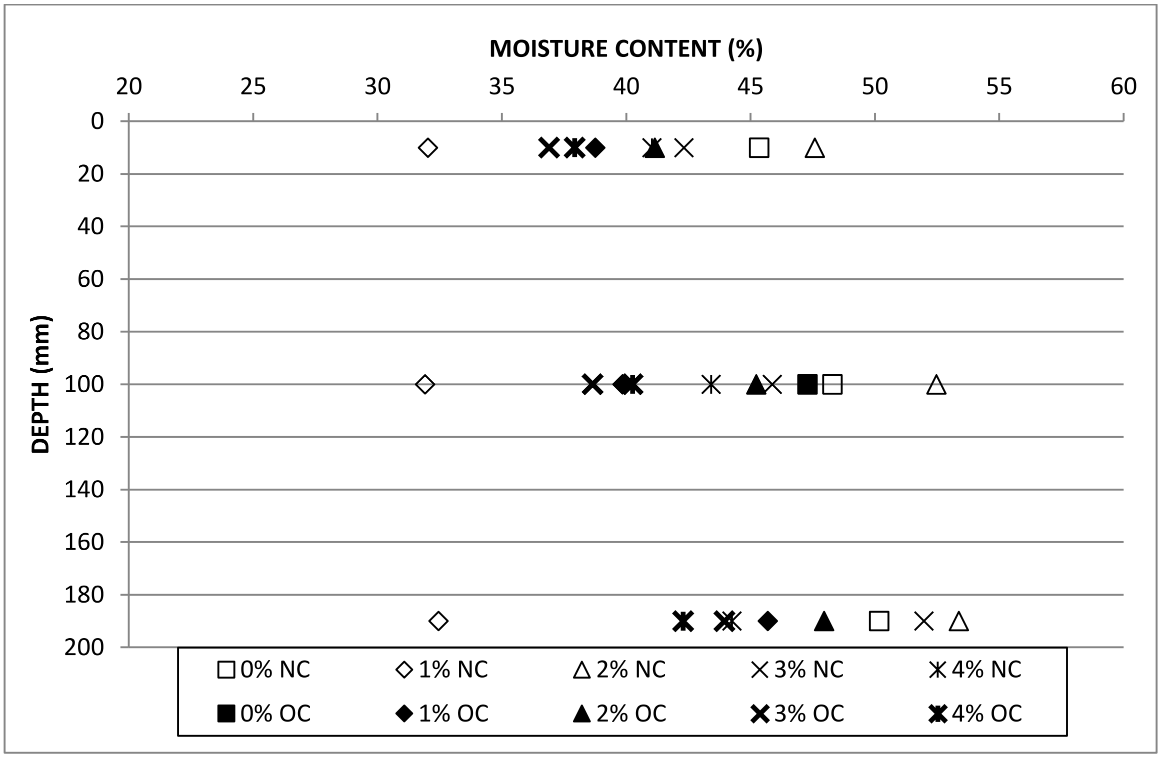

Figure 3.13: Average moisture content from locations within the centrifuge models.

3.5.3 Liquid limit

According to Powrie (2004), where clay has the characteristics of a liquid, at or above a particular water content, is known as the liquid limit, w_{LL}. The liquid limit of kaolin clay was determined using BS1377-2 (1990). Determination of w_{LL} followed the loading plate and penetrometer tests. The specific method used was the one-point cone penetrometer method. Samples of the all fibrous and non-fibrous models were taken at mid-face along the drum surface, for liquid limit determination. These samples were kept submersed in water until required. A paste was formed of the clay-fibre sample, which allowed for penetration of the cone between 15 and 25 mm. A portion of the paste was pushed into a container and placed under the cone penetrometer. The cone was released and the penetration depth was recorded. This process was repeated until two consecutive readings of 20 +/- 0.5 mm were obtained. The moisture content of the tested paste was then determined. Determination of the average liquid limit was carried out on core samples extracted from tested centrifuge models and the results are presented in Table 3.5. The liquid limit was found to increase linearly with increased fibre content in the soil mass.

Table 3.5: Average liquid limit values of kaolin with different percentage by dry weight of fibres.

Specimen	Average Liquid Limit (%)
0% Sample	58.38
1% Sample	59.89
2% Sample	61.79
3% Sample	64.36
4% Sample	67.26

3.5.4 Plastic limit

At or below the water content where clay displays brittleness or crumbles to the touch is known as the plastic limit, $w_{PL.}$ The plastic limit for the models in this study was determined using the hand rolling method described in BS1377-2 (1990). Samples of each fibrous and non-fibrous model were taken at mid-face of the drum surface once testing was completed. These samples were wrapped in tinfoil and submerged in water until required. The average plastic limit, w_{PL} values from centrifuge models tested are presented in Table 3.6. The plastic limit was also observed to increase linearly with increasing fibre content in the soil mass.

Table 3.6: Average plastic limit values of kaolin with different percentage by dry weight of fibres.

Specimen	Average Plastic Limit (%)
0% Sample	28.50
1% Sample	29.12
2% Sample	29.86
3% Sample	30.72
4% Sample	31.81

3.5.5 Plasticity index

The behaviour of clay over a range of water contents, where its characteristics are representative of a plastic material, is called the plasticity index, I_{p}. Plasticity index is the difference in moisture content between the liquid limit and plastic limit:

$$I_P = w_{LL} - w_{PL} \qquad \text{Equation 3.3}$$

The plasticity chart, Figure 3.14, was used to determine the nature of the models produced. Classification of the samples showed that an increase in plasticity occurred with increase in fibre material. All samples placed above the A-line and ranged from intermediate plasticity to high plasticity clays. Table 3.7 shows the value of plastic index for varying samples tested. The characteristics of kaolin clay determined by Stewart (1991) are shown in Table 3.8. The values of liquid limit and plastic limit compare well with the values of kaolin clay determined during this study. No other properties of the kaolin clay were calculated for the purposes of characterising the centrifuge models.

Table 3.7: Average plasticity index values of kaolin with different percentage by dry weight of fibres.

Specimen	Average Plasticity Index (%)
0% Sample	29.88
1% Sample	30.67
2% Sample	31.94
3% Sample	33.64
4% Sample	35.46

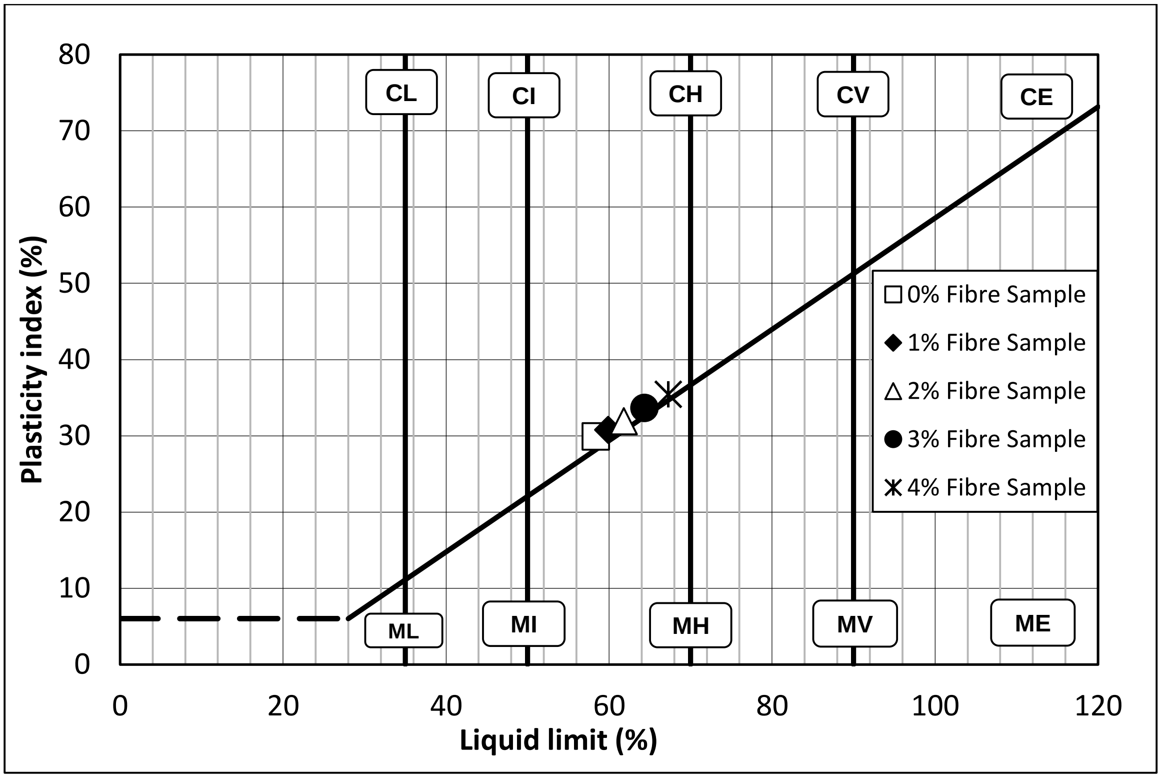

Figure 3.14: Plasticity chart showing transition of fibrous samples from clay to silt with high plasticity (BS5930 1999).

Table 3.8: Properties of kaolin clay (Stewart 1991).

Property	Stewart 1991	This Study
Specific Gravity, *Gs*	2.60	2.53
Liquid Limit, *LL* (%)	61	58.38
Plastic Limit, *PL* (%)	27	28.50
Compression Index, C_c	0.47	-
Swelling Index, C_s	0.1	-
Internal Friction Angle, φ (˚)	23	-
Coefficient of consolidation, c_v (m^2/yr)	3.9	-

3.5.6 Liquid limit, plastic limit and plasticity index

BS1377-2 (1990) was used to determine the liquid limit, plastic limit and plasticity index of the clay/fibre centrifuge models. Figure 3.15 showed that with increasing fibre content the liquid limit increased almost linearly. The liquid limit increased on average 3.6 % with each 1 % increase in fibre content. The plastic limit was also found to increase by 2.8 % per model over the 0 to 4 % fibre range. Plasticity index experienced a near linear increase as a result of increased fibre content and on average increased by 4.4 % through the range of models from 0 % to 4 %, Figure 3.15. Difficulty in determining the Atterberg limits according to the specifications set out in BS1377-2 (1990) increased with increasing fibre content.

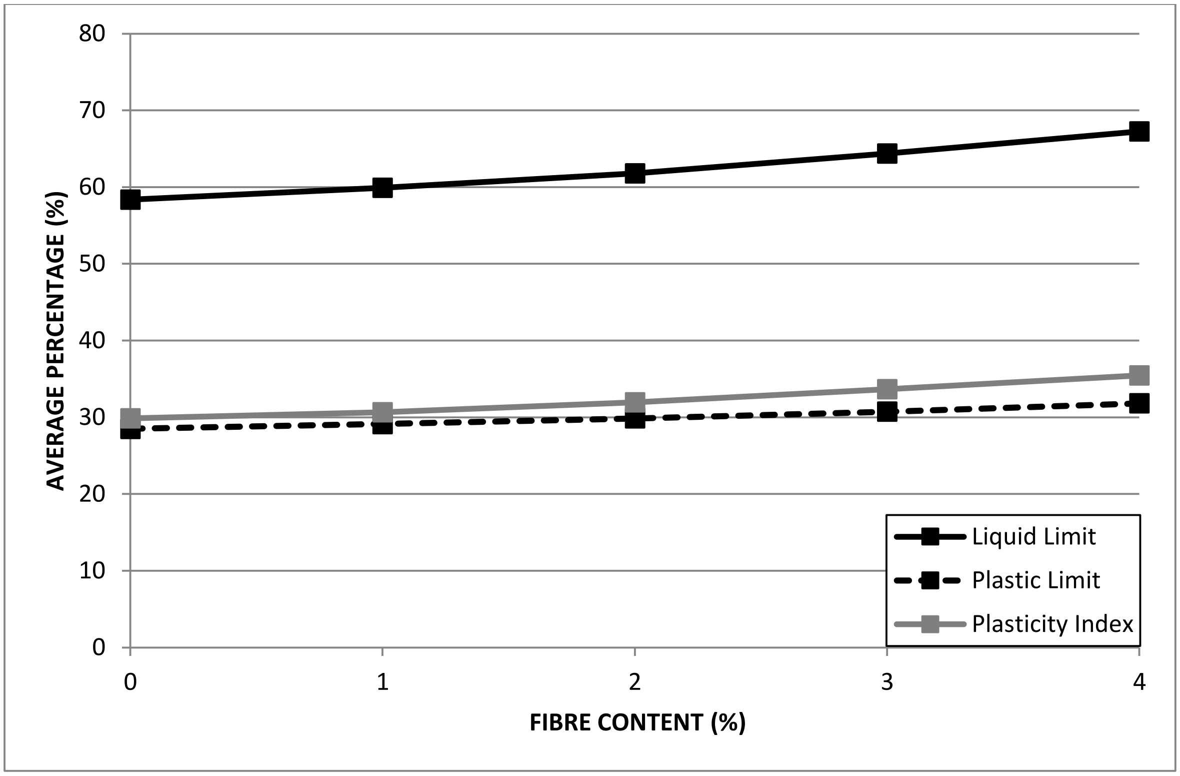

Figure 3.15: Influence of percentage fibre on liquid limit, plastic limit and plasticity index.

3.5.7 Shear vane testing

The vane test was carried out in accordance with BS1377-7 (1990). The vane used in this study was an electric Laboratory Vane Apparatus SL800, designed and manufactured by Impact Test Equipment, Figure 3.16. Core samples were first retrieved from the model, once geotechnical centrifuge testing was completed, and were either sheared immediately or stored. Storage consisted of wrapping cores in cling-film and tin foil, while submersed in water.

Figure 3.16: Electric Laboratory Vane Apparatus SL800, with accompanying blade and spring attachments.

The cores taken were approximately 110 x 110 mm in horizontal cross section by approximately 195 mm in length, i.e. the depth of the reinforced model contained within the centrifuge drum. Cores were taken at locations providing the greatest surface area between testing sites. This usually occurred where the 40 mm diameter foundation plates had been tested. One core was taken per model. The number two spring was chosen as the apparent shear strength of the core sample was less than 40kPa. The selected blade face measured 12.7 x 12.7 mm, with a length of 20 mm. The dial was zeroed and the assembly was lowered into the core to a depth 51 mm, corresponding to 4 times the blade width. The blade was rotated until the sample sheared i.e. no further increase in angular rotation was observed and the value recorded. The blade was rotated manually counter clockwise for two full revolutions and the location was sheared once more to determine the remoulded shear strength. This process was carried out at a total of five locations on the sample core retrieved from the centrifuge model. Testing was carried out for a total of three depths, 51 mm, 102 mm & 153 mm, through each sample. Samples extracted from both the normally and over consolidated models with fibre contents of 2 %, 3 % and 4 % were tested. The shear strength for a normally consolidated core sample with no fibre content was used as a control.

The torque M causing shear failure was determined by expressing the measured angular vane rotation by a calibration factor. Data sheets provided by Impact Test Equipment allowed for interpolation of the calibration factor; No.2 vane required a factor of 1.833. The vane shear strength was determined using Equations 3.4 and 3.5.

$$c_u = \frac{1000(M)}{k} \qquad \text{Equation 3.4}$$

where k is constant:

$$k = \pi D^2 \left[\frac{H}{2} + \frac{D}{6}\right] \qquad \text{Equation 3.5}$$

where D is the blade width and H is the blade height.

It has been established by Helenelund (1967) and Edil (2001) that the results from the shear vane test can lead to an overestimation of the mobilised shear strength. This study, which uses a fibrous clay sample, required the implementation of such a correction factor. Using Bjerrum's chart from Terzaghi *et al* (1996), Figure 3.17, values of the correction factor μ, were plotted against plasticity index. The Bjerrum correction chart, in relation to the I_p, was used to determine a correction factor for each shear strength calculated.

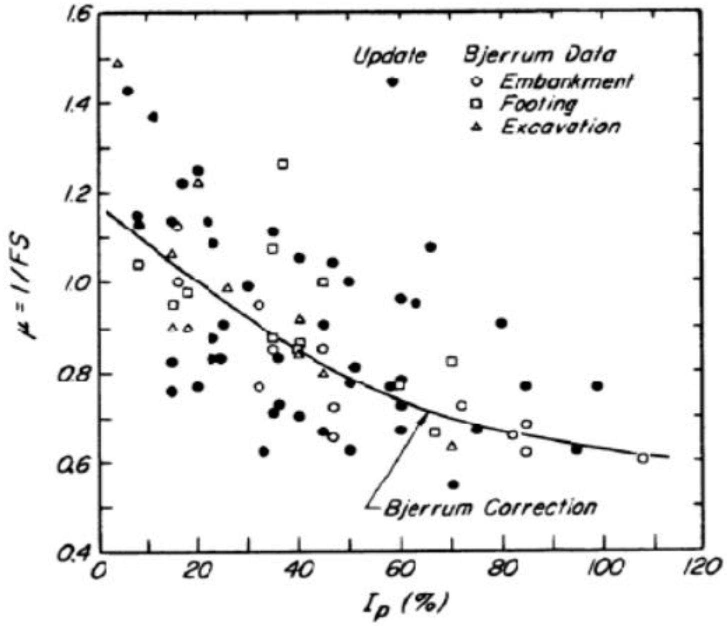

Figure 3.17: Bjerrum's correction factors accounting for the plasticity of a soil **(**Terzaghi *et al* 1996).

3.6. Testing programme

Bearing capacity testing was carried out with plates consisting of three shapes; circular, square and rectangular. Each category had two plates of different sizes, with the size of the plates influenced by the space along the channel surface, Table 3.9. The surface length of the channel and the size of the loading plates limited the number of tests per model. A total of three tests were performed using each plate, accounting for a spacing of 3 times the foundation width to avoid boundary effects. A series of eighteen load plate tests were conducted on each fibre reinforced model. Penetrometer testing of the model was carried out once the bearing capacity tests were completed. Locations for conducting profiling tests were situated between the plate bearing sites. All models were tested at 25g. Normally consolidated samples were consolidated and tested at 25g, while over consolidated samples were first consolidated at 50g before reducing the centrifuge acceleration to 25g to obtain over consolidation ratio of 1:2.

Table 3.9: Summary of foundation types used in bearing capacity testing.

Foundation	Size 1	Size 2
Rectangular (mm)	30x60	40x80
Square (mm)	30x30	40x40
Circular d (mm)	30	40

3.6.1 Bearing capacity testing

The loading plate was placed centrally on the model surface to prevent boundary effects distorting the test data. The distance between the foundation and the channel wall was 60 to 70 mm for rectangular foundations, corresponding to 2B and 2.3B; a distance of 80 to 85 mm corresponding to 2B and 2.1B, was left for square and circular foundation between the footing edge and container wall. All plates used during testing had a centrally located recess, into which a ball bearing sat, Figure 3.18. The resistance of the soil mobilised during loading was recorded via a 1 or 2 kN calibrated load cell, which was placed in contact with the loading plate through the ball bearing and socket piece, Figure 3.19. This joint was essential to allow a range of motion as the foundation was forced through the model. In the event that loading plate slipped during testing or orientated itself at an angle which would otherwise put the load cell under a twisting or bending moment, damage to the instrument would be avoided. The joint also prevented the plate being driven in a preordained way by the actuator, as could be the case with a rigidly fixed plate. Thus failure would be a result of failure in the soil under a uniform load.

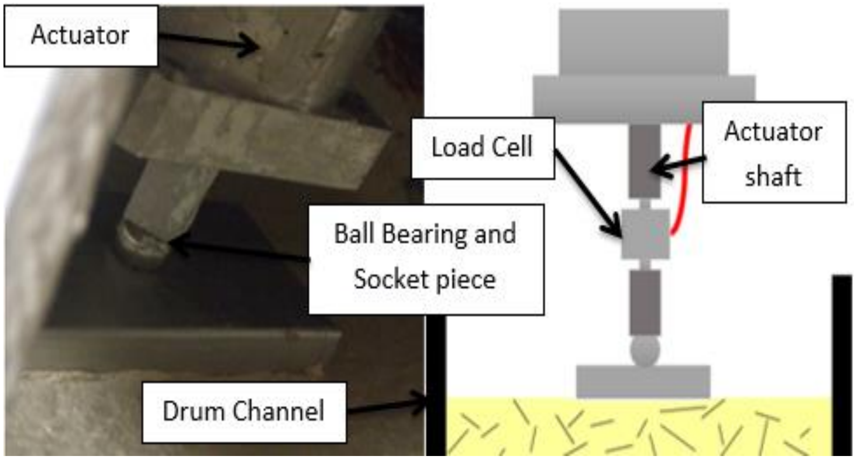

Figure 3.18: 3D and 2D depiction of the bearing capacity test set-up, showing socket piece, ball bearing and foundation plate on the model surface.

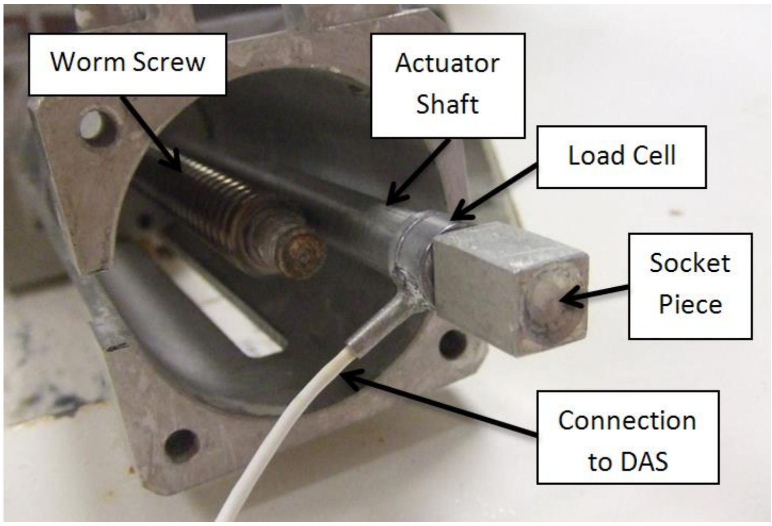

Figure 3.19: Burster load cell attached to the actuator probe and socket piece. The probe shaft runs parallel to the worm screw.

Once the testing arrangement was set, the centrifuge was closed and accelerated to 25g for testing. The test proceeded once the load cell had equilibrated to the accelerated gravitation field and background noise levels could be neglected. The loading plate was pushed via the actuator to a depth twice that of the plate width. Data from the test was sent through wireless router to the laboratory PC. This allowed mobilised loads to be viewed in real time. Sending data in this way greatly reduced the inherent noise levels encountered if such signals were sent through the centrifuge slip rings. The depth at which the foundation travelled through the model was recorded by the baluff censor. Alternatively penetration could be timed as the actuator was rated at 1 mm/s. Upon completion of the test the centrifuge was decelerated and the actuator probe and load cell was moved to its initial position. The tool table was turned sufficiently to allow the loading plate and ball bearing to be extracted manually. Rotation of the tool table clockwise facilitated positioning of the actuator in a new testing location approximately 3B away from the initial site. Thus the boundary of slip lines from neighbouring tests would not overlap. The equipment was cleaned and the testing arrangement was reassembled. Tests were repeated three times on each plate, Figure 3.20.

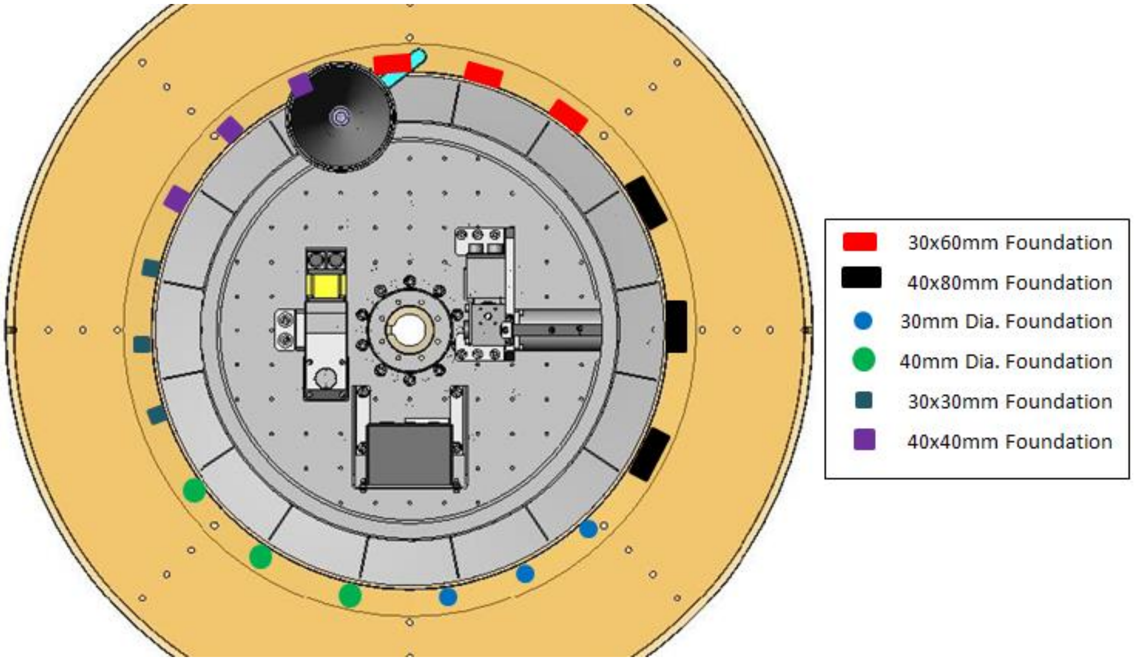

Figure 3.20: Location of various foundations along the model surface during each testing phase (Broadbent & Sons 2010).

The drum apparatus and the model testing arrangement ensured that the models were undrained during the loading procedure. The undrained shear strength was back calculated from the load bearing data by utilising Equation 3.7 which was derived from Equation 3.6 the undrained bearing capacity equation given in Annex D, EN 1997:(2005). This coincided with the work carried out by Skempton (1951) and Salgado *et al* (2004) to determine an expression for the undrained shear strength and the bearing capacity factor N_c. The inclination of the foundation base and the inclination of the load have been removed, as the load acts perpendicular to the foundation and the foundation base is parallel to the model surface. Therefore, only the shape factor s_c was relevant in Equation 3.7. Rearranging of Equation 3.6 allowed the undrained shear strength to be determined in Equation 3.7 from the bearing resistance and foundation shape.

$$q_{ult} = (\pi + 2)c_u b_c s_c i_c + q \qquad \text{Equation 3.6}$$

$$\frac{q_{ult} - q}{(\pi + 2)s_c} = c_u \qquad \text{Equation 3.7}$$

where; q_{ult} is the ultimate loading.

b_c and i_c are equal to 0.

q is the value of the surcharge loading

Shape factors accounting for the various foundation types were required to be included in the undrained shear strength calculations. Such factors used in back calculations and the relevant foundation types are shown in Table 3.10.

Table 3.10: Shape factors required for undrained conditions, Annex D, Eurocode 7 (2003).

Foundation Type	Calculation of shape factor	Shape Factor
Rectangular foundation	$s_c = 1 + 0.2\frac{B}{L}$	1.14
Circular or square foundation	$s_c = 1.2$	1.2

3.7 Summary

The test methods used in this study have been described in this chapter. The first series of tests were carried out where models were induced to an accelerated gravitational field in the IT Sligo geotechnical centrifuge. The drum mode of the centrifuge was utilized to create a series of soil models that were homogenous and to ensure the orientation of the peat fibre content was completely random throughout each model. The large surface testing area of the drum channel allowed a large number of bearing capacity and profiling tests to be completed quickly and with relative ease. Various foundation types and sizes were tested on each model allowing direct comparisons to be drawn between the undrained shear strengths generated. CPT and piezoball penetrometers were also used to characterise the clay fibre models and to provide a comparison with results of the bearing capacity analysis. Two differing types of penetrometer were used to account for the effects of fibre content acting upon the probe shape. The data acquisition system (DAS) and the actuator/load cell arrangement were used to record the resistance to penetration of the fibrous models. Descriptions of all testing equipment have been provided in this chapter and in Appendix A. The series of desk top classification tests were carrying out, including Atterburg limit tests, on samples taken throughout each model and laboratory shear vane tests conducted on extracted model cores. Completion of the Atterburg limits proved difficult with samples containing high levels of organic peat fibre. Moisture contents were also determined at three depths throughout each model.

A series of fibrous models were created using a mixture of kaolin slurry and varying quantities of peat fibres. Fibrous material was extracted from a bulk quantity of peat and suitably prepared. The fibrous slurry was created by hand mixing the required quantity of fibrous material into kaolin clay with a moisture content of 120 %. The prepared slurry was fed into the drum channel by a feeder apparatus while a low g-level was maintained. Models were consolidated at 25g and 50g to produce both normally consolidated and over consolidated samples, with steps taken to ensure that all models were undrained. All bearing capacity and penetrometer tests were conducted at 25g. Cores were taken from the consolidated models, allowing desk top shear vane tests to be carried out after bearing capacity and profiling analysis. The extracted cores were sheared at five locations and the average value of the unconfined undrained shear strength was taken.

CHAPTER 4

RESULTS

4.1 Introduction

This chapter presents the results generated during the geotechnical centrifuge modelling. Bearing capacity and penetrometer testing of fibrous models were carried out to investigate the effects of random organic fibres on shear strength of kaolin clay. The bearing capacity testing was divided into two series; Test Series 1 examined the bearing capacity of normally consolidated models, while for Test Series 2 the models were over consolidated. The fibre content of the models was varied from 0 to 4 % by dry weight of kaolin. Undrained shear strength of the fibre/clay centrifuge models was back calculated from loads measured during bearing capacity tests. Shear strength of the model was determined at two points: at the maximum curvature of the resistance profile and at a depth corresponding to a penetration of 0.5 times the breath or diameter of the foundation. Profiling of the models, with cone and ball penetrometers was carried out immediately after bearing capacity testing to determine the variation in shear strength with depth.

Additional shear strength characterisation of the fibrous centrifuge models was performed on extracted cores, following centrifuge testing. Cores were sheared using a standard laboratory shear vane. Samples were also taken at various depths and locations throughout the model to determine the liquid limit, plastic limit and plastic index for each fibre content model tested, to further characterise the fibrous soils. Atterberg limits and moisture content data from the experimental test programme were already presented in Chapter 3.

4.2. Model profiling

Model profiling using CPT and piezoball penetrometers was carried out to determine the variation in undrained shear strength with depth.

4.2.1 Cone testing

The cone penetration test was carried out on all fibrous centrifuge models to ascertain the undrained shear strength. Figures 4.1 to 4.4, relate to 0 % and 4 % fibre content models in Test Series 1 and 2. The CPT profiles of models with other fibre contents, in Test Series 1 and 2, can be found in Appendix B and C. The average net tip resistance of three tests conducted per model are shown along with the undrained shear strengths, Table 4.1. In Figures 4.1 to 4.4 for 0 % and 4 % normally consolidated (NC) and over consolidated (OC) models the CPT resistance profiles decreased with increased depth for NC and OC models, as can be seen in Figure 4.1, or remained relatively constant with depth, shown by test results in Figure 4.2. The reduction in tip resistance may be attributed to increased moisture contents towards the bottom of some of the models. Figure 4.1 showed excellent repeatability between Tests 1 and 2, while Test 3 displayed a greater reduction in resistance. The initial 20 mm of the model show a wide variation in resistance which could be attributed to the load cell equalising in the model. CPT results for the 0 % OC model showed poor repeatability between the tests conducted, with a spread of 70 kPa separating the resistance profiles of Tests 1 and 3. Tests 1 and 2 showed better correlation, however there was still a considerable discrepancy between results. Considerable variation was present in the resistance profiles for the 4 % NC model, where Tests 1 and 3 showed a decrease in shear strength. For the 4 % OC model, repeatability between Tests 1 and 2 was excellent with both exhibiting a decrease in shear strength. Test 3 resulted in a relatively constant resistance profile with depth and began converging with the previous tests at a depth of 80 mm, Figure 4.4.

With increased fibre content the CPT results showed increased resistance to penetration, there was also increased variation in the resistance profiles, comparing 0 % NC and 4 % NC, Figures 4.1 and 4.3 respectively. The increased resistance may be attributed to the presence of fibrous matter, while variation in resistance profile may be attributed to fibres interacting with the CPT probe. The fluctuation of the CPT profiles in Figures 4.3 and 4.4 suggest that the fibres gathered in front and around the probe as the test proceeded, influencing the resistance to penetration as discussed by Boylan *et al* (2011).

Table 4.1 comprises the results of the CPT profiling carried out for all fibrous centrifuge models. The maximum values of shear strength encountered are presented with the associated depths. The repeatability of the CPT results ranged from good to poor over the range of normally and over consolidated models tested and in the majority of cases the validity of the data did not appear to be affected by the fibre content of the models. The strength profiles were, however, influenced by the fibre content, with the strength generally increasing with fibre content. The results of CPT data are presented as the net tip resistance rather than the total tip resistance due to the inability to measure pore water pressure with the CPT.

Table 4.1: Summary of CPT results for normally and over consolidated models.

Test No.	Fibre (%)	Consolidation ratio	Net Tip Resistance (max) (kPa)	Standard Deviation Net Tip resistance	CPT Undrained shear strength (max) (kPa)	Depth of max c_u (mm)
19-21	0	1	102.0	0.34	9.7	39.6
43-45	0	2	218.9	0.58	20.8	21.5
67-69	1	1	219.2	0.40	20.9	22.5
91-93	1	2	105.3	0.42	10.3	48.3
115-117	2	1	91.8	0.26	7.9	79.6
139-141	2	2	230.9	0.64	22.0	30.0
163-165	3	1	186.4	0.52	17.8	41.1
187-189	3	2	321.3	2.03	30.6	73.9
211-213	4	1	417.1	0.95	39.7	76.0
235-237	4	2	521.6	0.90	49.7	41.6

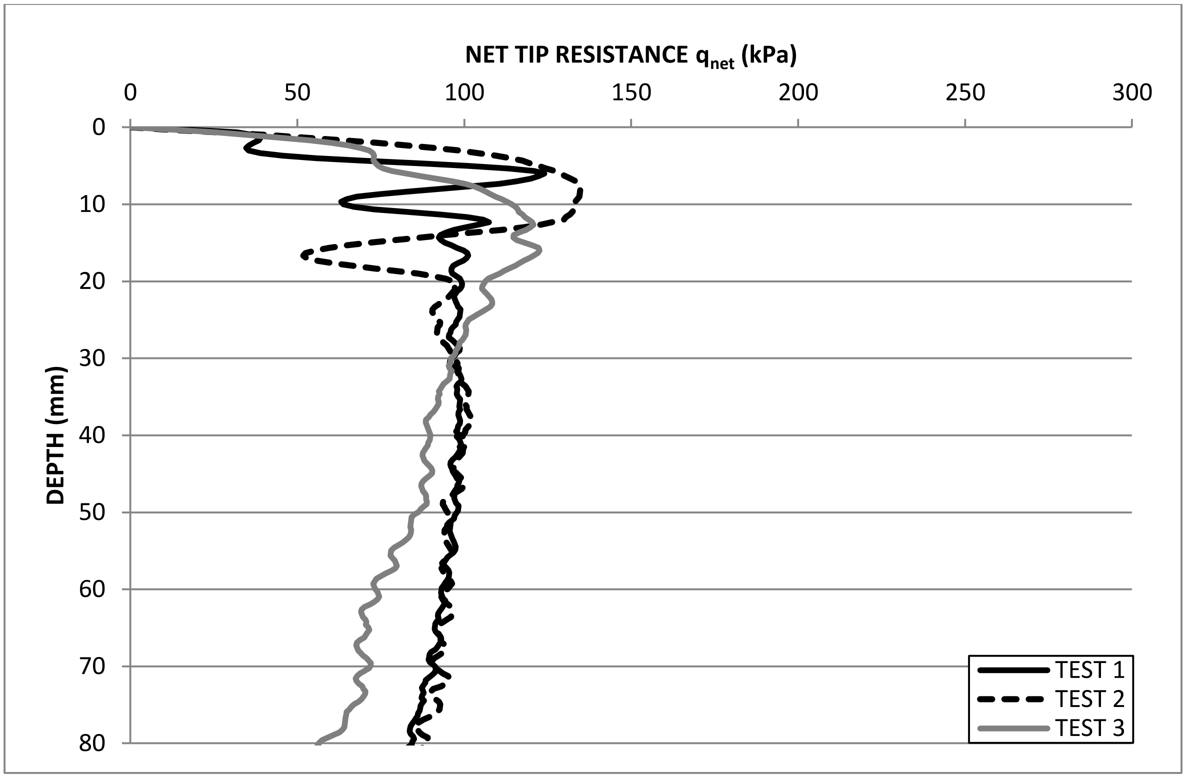

Figure 4.1: CPT net tip resistance profile for 0 % fibre normally consolidated model.

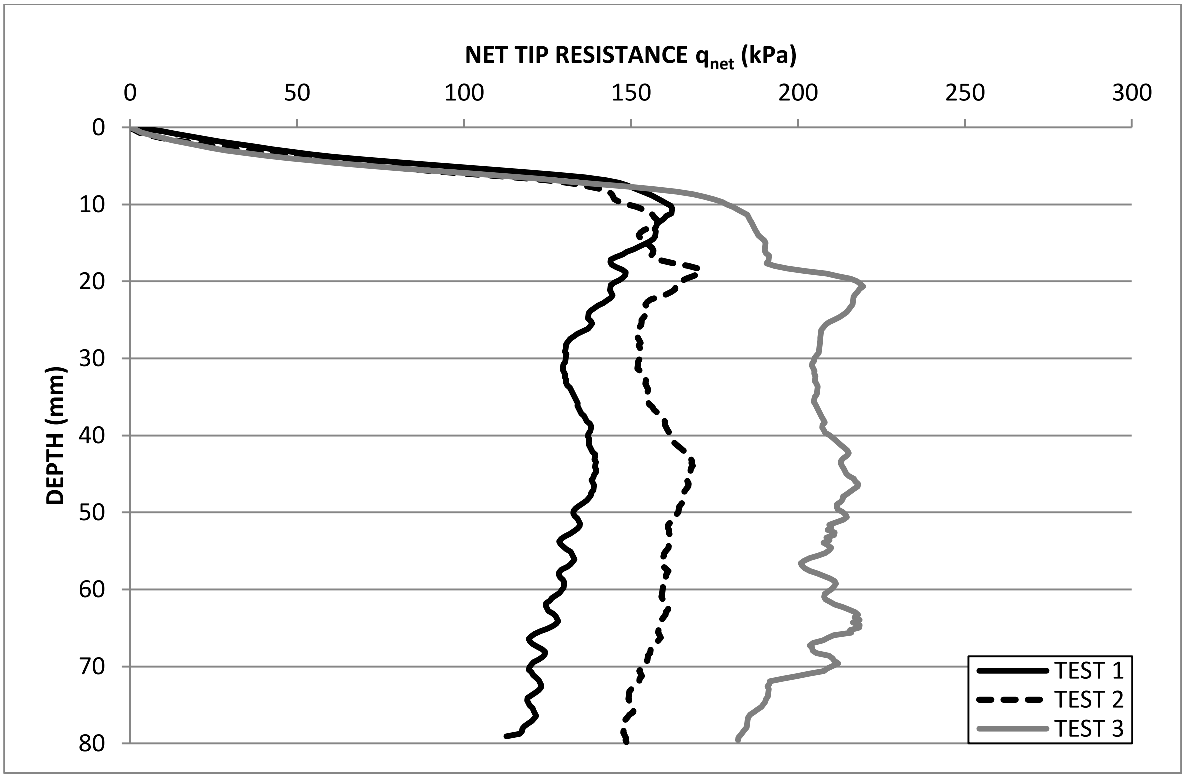

Figure 4.2: CPT net tip resistance profile for 0 % fibre over consolidated model.

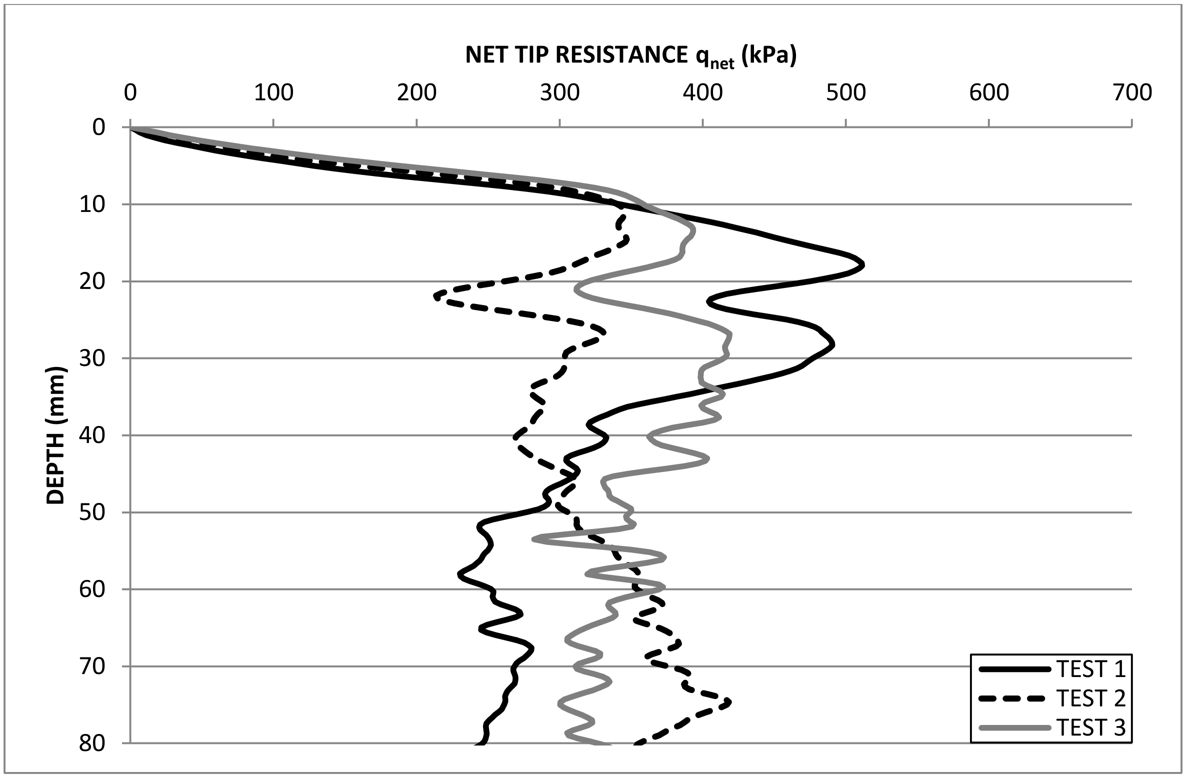

Figure 4.3: CPT net tip resistance profile for 4 % fibre normally consolidated model.

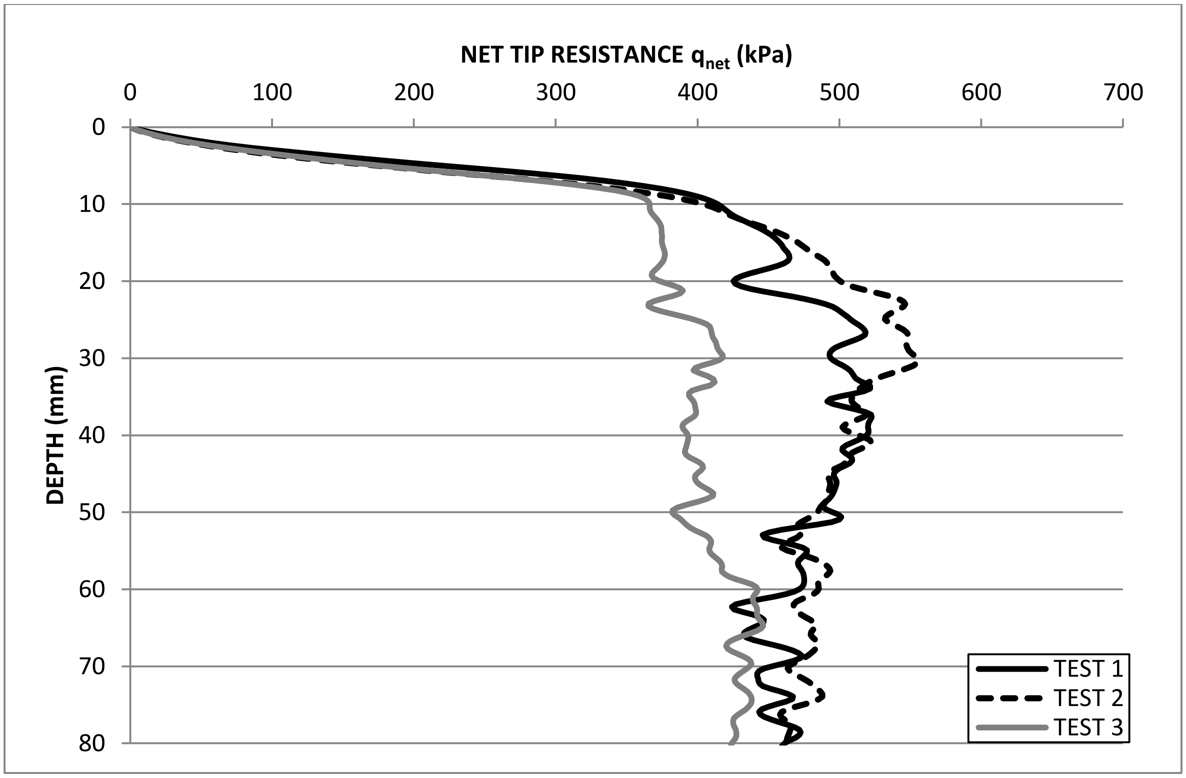

Figure 4.4: CPT net tip resistance profile for 4 % fibre over consolidated model.

4.2.2 Piezoball testing

Piezoball profiling was also undertaken to facilitate comparison with the results of CPT profiling and back calculations of shear strength from bearing capacity tests. Figures 4.5 to 4.8 present the net tip resistance from the piezoball for 0 % and 4 % fibre models from NC and OC cases. Appendix D and E contain piezoball tip resistance profiles for Test Series 1 and 2. The 0 % NC model showed relatively constant model resistance with depth but average repeatability for all 3 tests conducted. An increase in resistance with depth was evident for tests on the 0 % fibre OC model, Figure 4.6. The profiles showed increased resistance with increasing depth, Tests 2 and 3 upon reaching 70 mm depth the resistance profiles remained constant. The 4 % NC model showed increased strength with depth in the top 25 mm of the model, Figure 4.7. The net resistance of the piezoball decreased once the peak resistance has been surpassed. There was some recovery in strength with depth in the case of Tests 1 and 2 once 60 mm had been passed. Overall repeatability of tests in Figure 4.7 was poor. Results of 4 % OC models tests showed relatively consistent resistance, with some increased resistance in Tests 1 and 3. Repeatability of tests in Figure 4.8 was average. Variation in the strength profile for the piezoball was reduced considerably compared to that experienced by the cone penetrometer in Section 4.3.1. This can be attributed to the nature of full flow penetrometers when testing in soils of a fibrous nature, (Boylan *et al* 2011). In all tests conducted with the CPT and piezoball there is reasonably good agreement between q_{ball} and q_{net}, with the average piezoball data giving a higher value of undrained shear strength compared to that of the CPT. The study carried out by Boylan *et al* (2011) also found similarity of results between these two penetrometers. This finding concurs with that of Boylan et al (2011). Table 4.2 summarises the results gathered from this penetrometer.

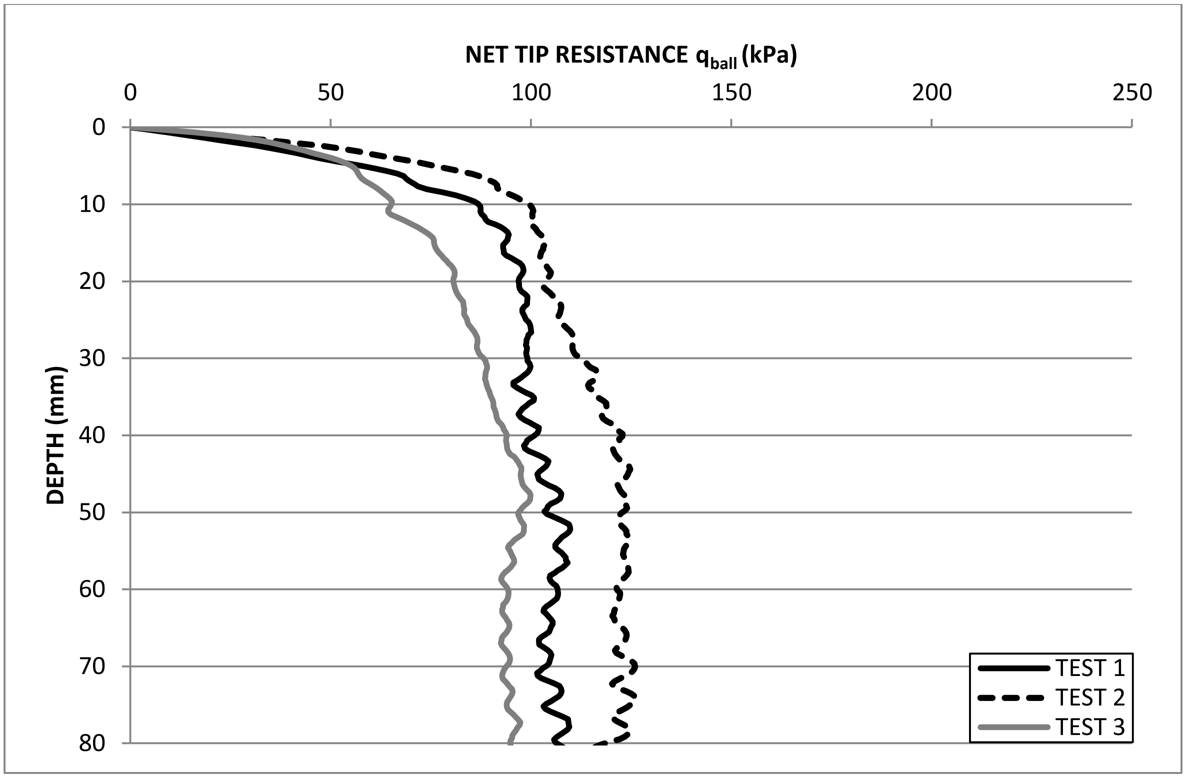

Figure 4.5: Piezoball net tip resistance profile for 0 % fibre normally consolidated model.

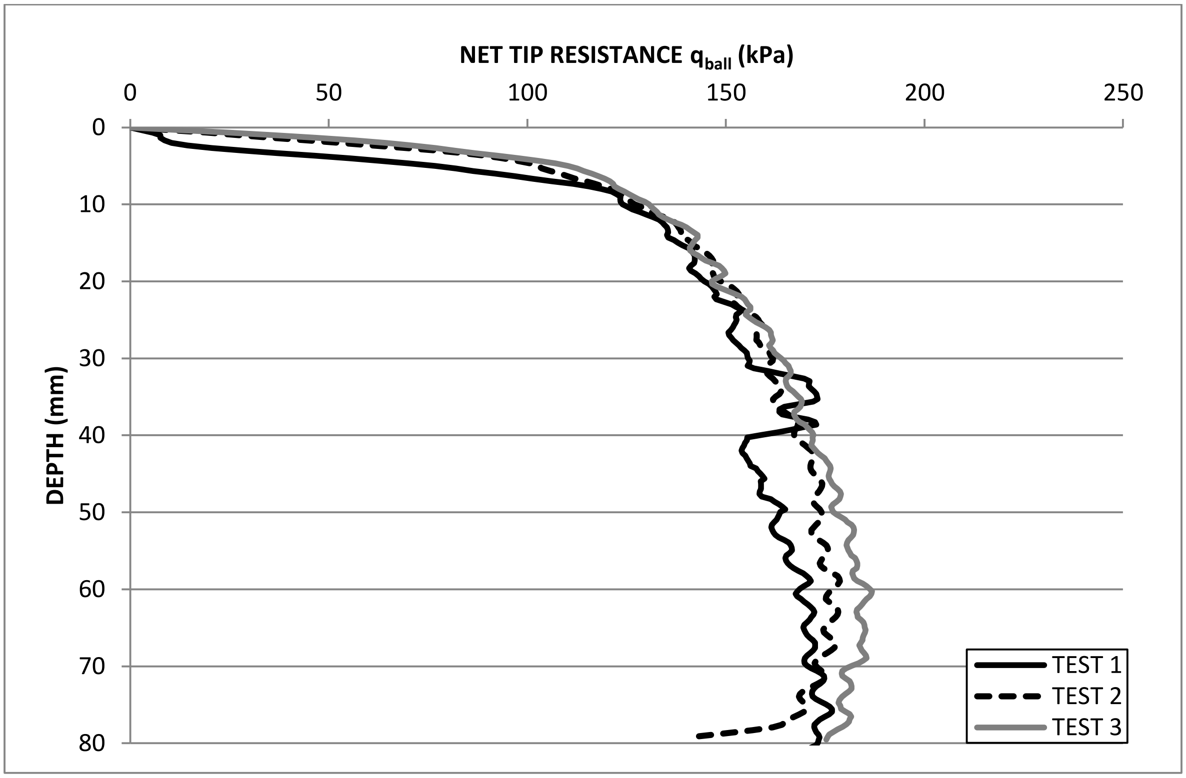

Figure 4.6: Piezoball net tip resistance profile for 0 % fibre over consolidated model.

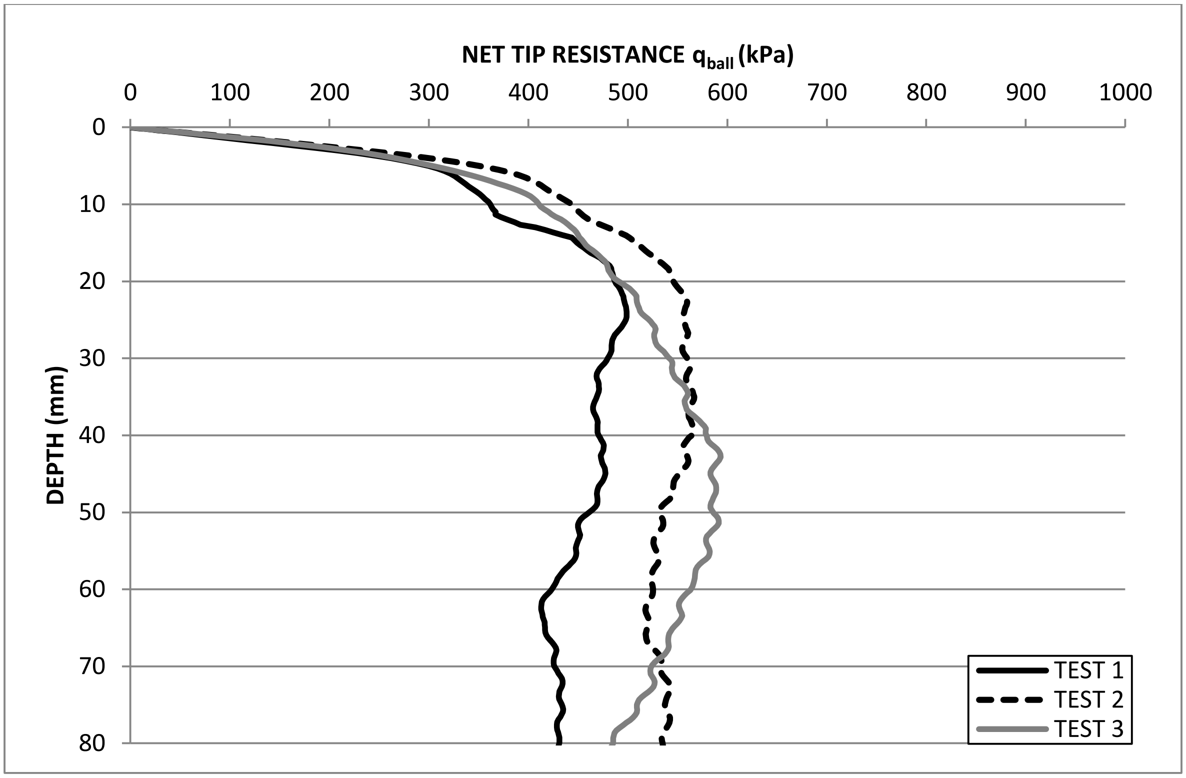

Figure 4.7: Piezoball net tip resistance profile for 4 % fibre normally consolidated model.

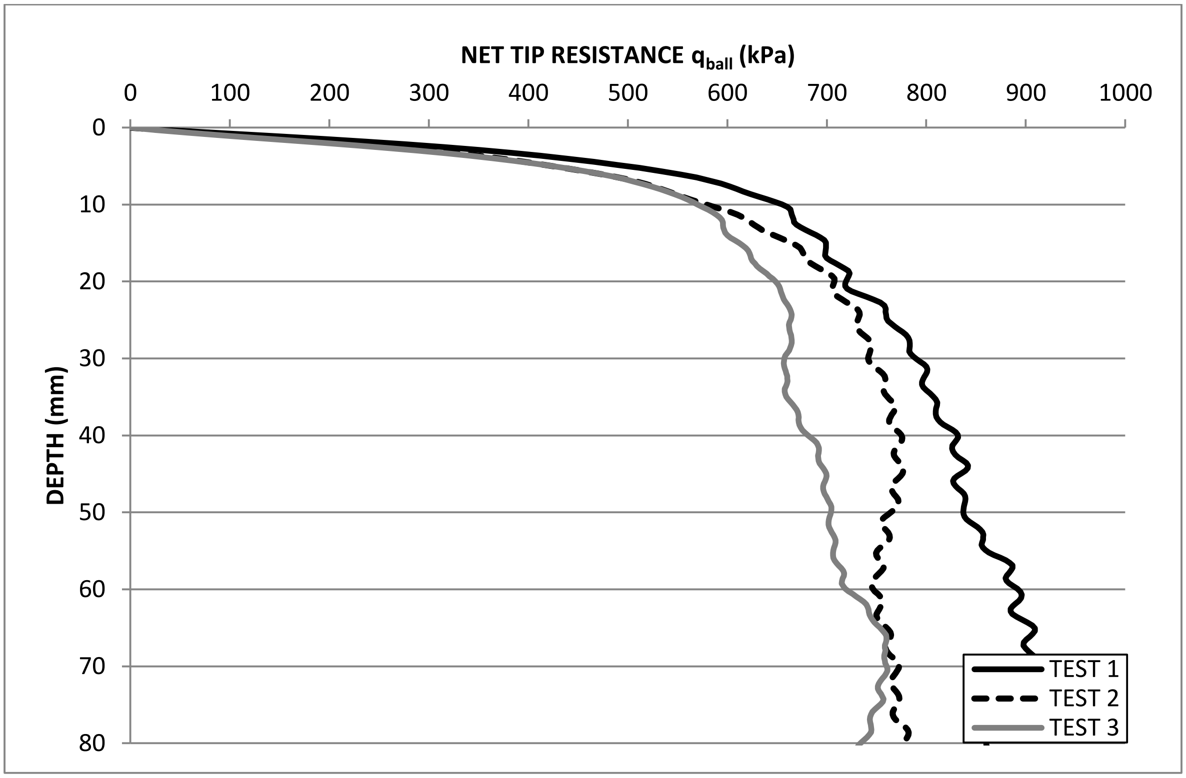

Figure 4.8: Piezoball net tip resistance profile for 4 % fibre over consolidated model.

Table 4.2: Summary of piezoball results for normally and over consolidated models.

Test No.	Fibre (%)	Consolidation ratio	Net Tip Resistance (max) (kPa)	Standard Deviation Net Tip resistance	Undrained shear strength (max) (kPa)	Depth (mm)
22-24	0	1	125.9	0.13	12.0	70.9
46-48	0	2	186.5	0.32	17.8	60.3
70-72	1	1	170.2	0.61	16.2	66.9
94-96	1	2	160.7	0.16	15.3	78.7
118-120	2	1	145.9	0.13	13.9	89.2
142-144	2	2	215.5	0.27	20.5	76.7
166-168	3	1	176.5	0.14	16.8	87.6
190-192	3	2	481.6	0.36	45.9	58.6
214-216	4	1	587.2	1.33	55.9	47.8
238-240	4	2	910.8	0.80	86.7	69.5

The pore water pressure profiles remained consistent in the majority of piezoball tests conducted and appeared to be independent of depth, Figures 4.9 to 4.11. Appendix D and E contains the pore pressure figures for all piezoball tests conducted in Test Series 1 and 2. Significant positive spiked pore pressure was found in the profiles for the 0 % fibre model tests in Figure 4.9 and in the remaining figures of this section. Such spikes may be attributed to the possibility of the fibrous material intermittently blocking the probe filter and disrupting the pore pressure sensor. Negative pore pressures were recorded during testing and could be attributed moisture being drawn into micro cavities between the soil and the fibres; increased depth had little effect on the pressure profiles. There was no pore pressure data recorded for the 0 % fibre over consolidated sample due to an equipment fault. Figure 4.10 typifies the profile of the pore pressure in most cases with scatter in the upper portion of the models. This scatter reduced as negative pore pressure became pronounced and fluctuations to positive pressure were encountered during piezoball testing. This may be seen in the 4 % NC model, Figure 4.10. The 4 % fibre OC model depicted an increase in pore water pressure of approximately 10 kPa for Test 1 at 60 mm depth, while Test 2 recorded 5 kPa pore pressure at the same depth. Following this the pore water pressure dropped to a value slightly in excess of 0 kPa and remained constant. There was very good repeatability between Tests 2 and 3 for this model, which showed the effects of depth on pore pressure in some cases.

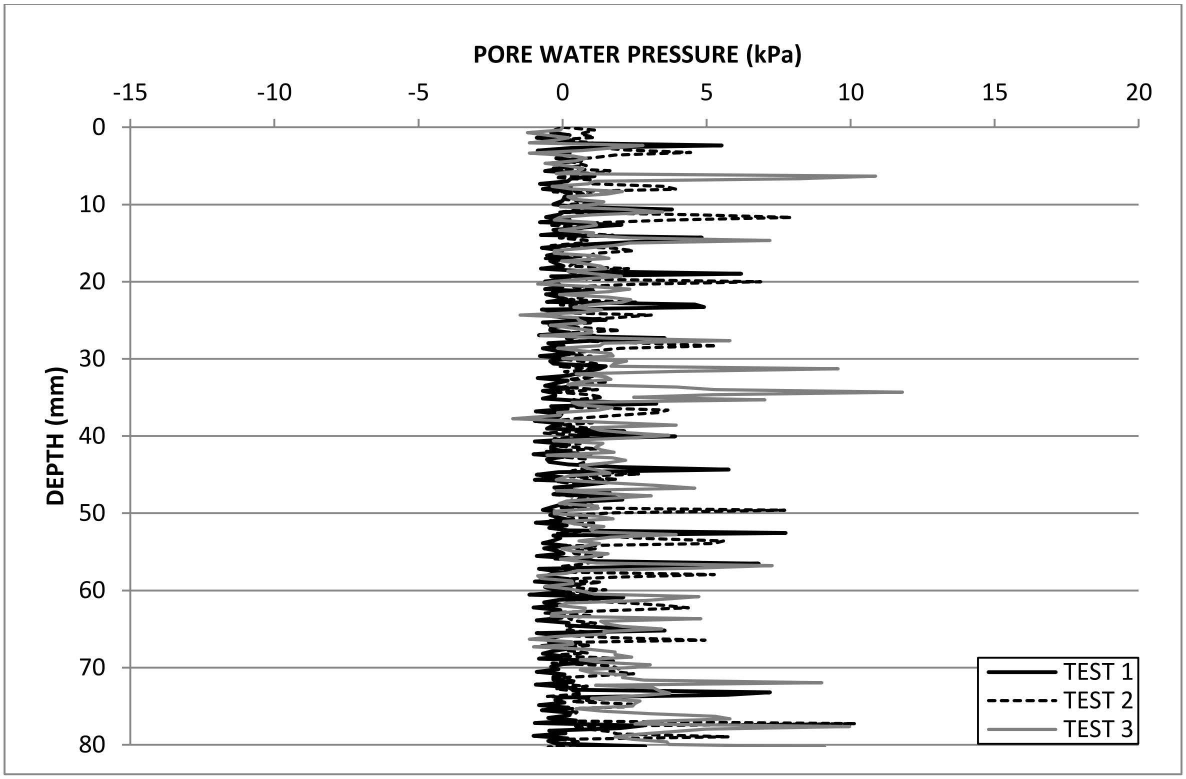

Figure 4.9: Pore water pressure profile for 0 % fibre normally consolidated model.

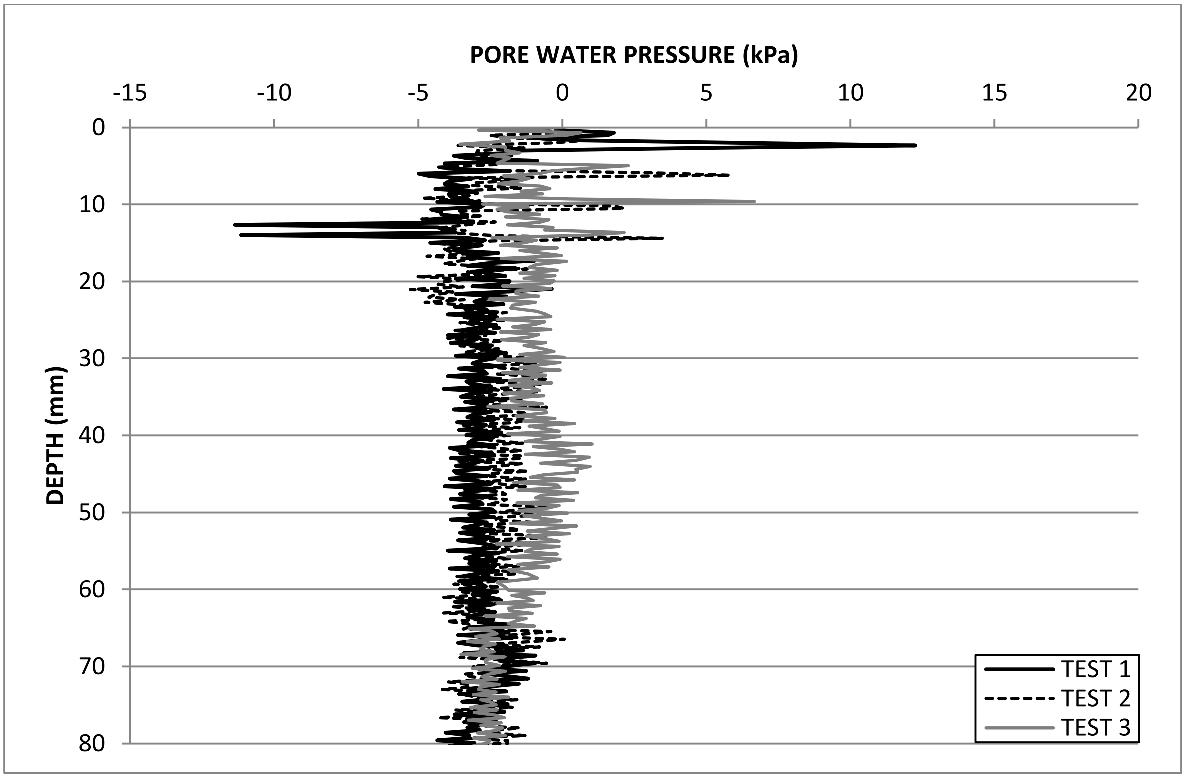

Figure 4.10: Pore water pressure profile for 4 % fibre normally consolidated model.

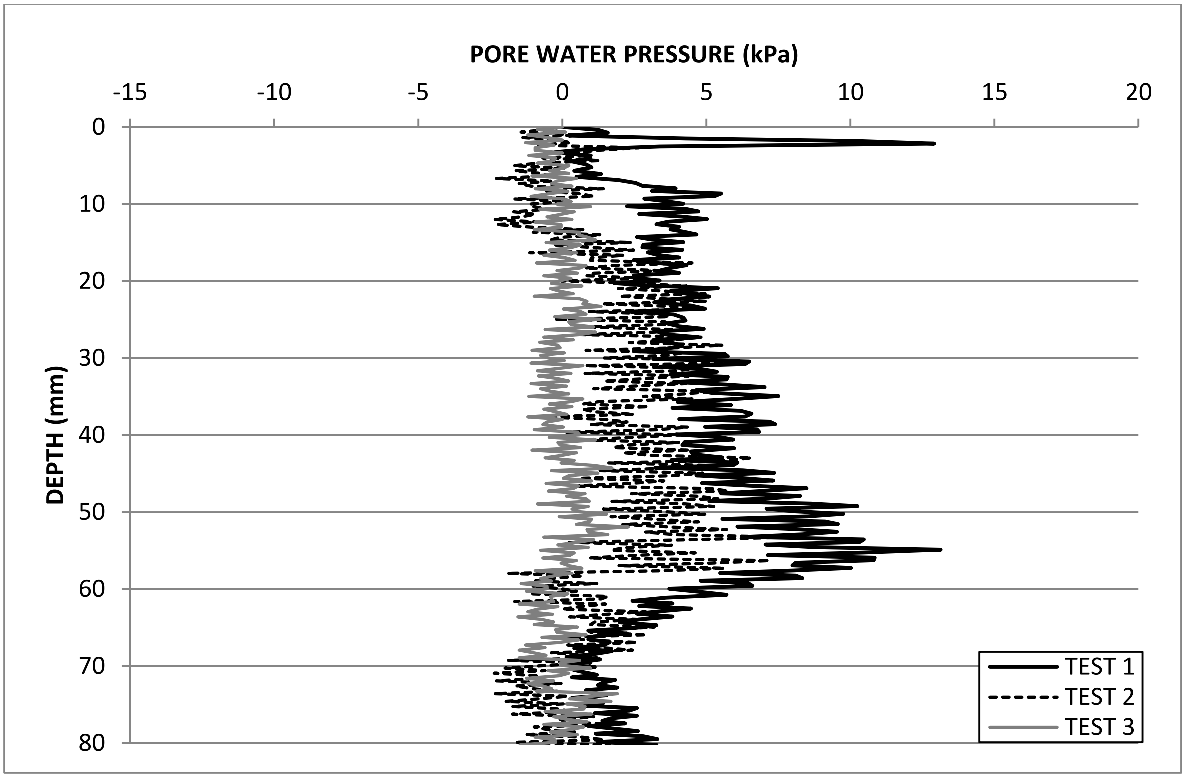

Figure 4.11: Pore water pressure profile for 4 % fibre over consolidated model.

Overall repeatability varied from very good to poor for the piezoball tip resistances encountered throughout the fibre reinforced model range. The tip resistance data appeared to be affected by fibre content more than the pore pressure. Repeatability also appeared to vary in the majority of cases as fibre content increased, and in some cases of normally consolidated models of low fibre content. Repeatability of the pore water pressure was good throughout the model range tested, while increased fibre content did not appear to effect repeatability. Spiked data and negative pressures were recorded which may be attributed to the location of the pore pressure filter at the probe mid face.

4.2.3 Shear vane testing

The shear vane results from the fibrous models in Test Series 1 and 2 are presented in the following section. Cores from over consolidated models with 0 % and 1 % fibre content were not extracted, that also included the 1 % normally consolidated model. The resulting values of μ from Bjerrum's correction chart were used to correct the shear vane results for plasticity effects. The values of μ along with the corrected average shear strength and remoulded shear strengths for each model in the normally and over consolidated cases are presented in Table 4.3 and Table 4.4 respectively.

Table 4.3: Summary of the average shear vane calculations for the normally consolidated fibrous model cores.

Fibrous Model (%)	0	2	3	4
Calibration factor for vane No.2	1.8			
Average Torque (Nmm)	42.1	53.2	61.0	69.7
Remoulded Avg. Torque M (Nmm)	20.6	25.6	29.4	33.5
k	5931.4			
Correction Factor	0.93	0.91	0.87	0.85
Corrected Avg. Shear Strength (kPa)	6.6	8.1	8.9	9.9
Corrected Remoulded Avg. Shear Strength (kPa)	3.2	3.9	4.3	4.7
Sensitivity (C_u/C_u remoulded)	2.1	2.1	2.1	2.1

Table 4.4: Summary of the average shear vane calculations for the over consolidated fibrous model cores.

Fibrous Model (%)	2	3	4
Calibration factor for vane No.2	1.8		
Average Torque (Nmm)	54.7	61.4	71.6
Remoulded Avg. Torque M (Nmm)	26.4	29.4	33.7
k	5931.4		
Correction Factor	0.91	0.86	0.84
Corrected Avg. Shear Strength (kPa)	8.4	8.9	10.1
Corrected Remoulded Avg. Shear Strength (kPa)	4.0	4.3	4.8
Sensitivity (C_u/C_u remoulded)	2.1	2.1	2.1

An increase in fibre content led to an increase in shear strength. Consolidation ratio also affected the shear strength mobilised during vane testing, with OC models producing slightly greater strengths. The correction factors were applied to these values of shear strength and plotted as corrections in Figures 4.12 and 4.13. Sensitivity for both the normally consolidated and over consolidated models is presented in Figure 4.14. Some scatter was observed in the sensitivity data, the soil classified as being low in sensitivity.

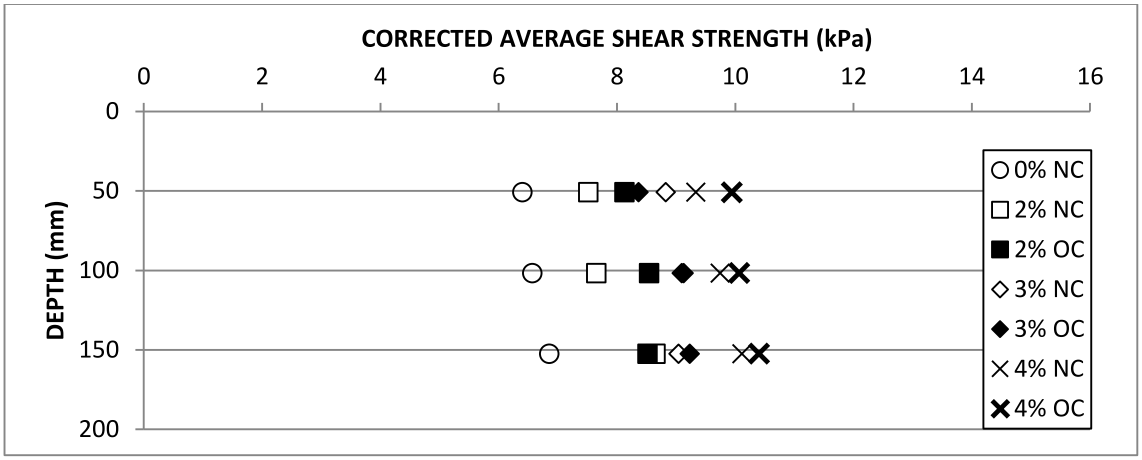

Figure 4.12: Depth against corrected average shear strength from shear vane testing.

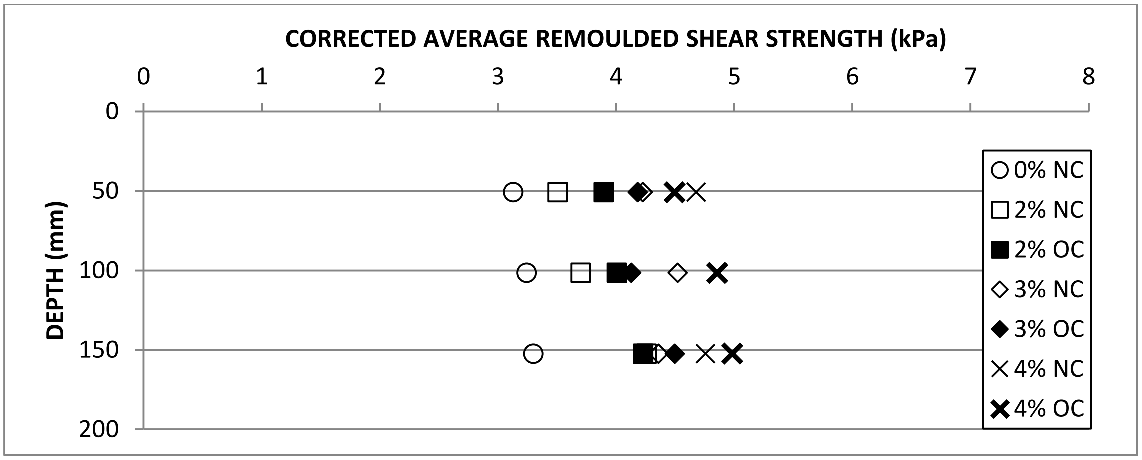

Figure 4.13: Depth against corrected average remoulded shear strength from shear vane testing.

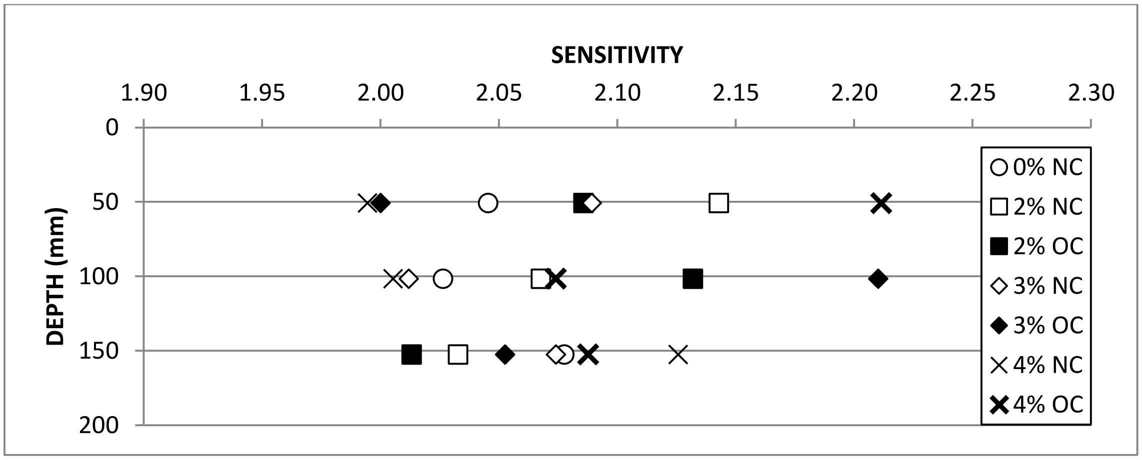

Figure 4.14: Depth against sensitivity from shear vane testing.

4.3 Geotechnical centrifuge modelling

The geotechnical centrifuge modelling process consisted of two test series. Test Series 1 investigated the bearing capacity of normally consolidated models with 0 % to 4 % fibre content. The models in this series were consolidated and tested at 25 g to achieve a normal consolidation ratio of 1. Test Series 2, investigated the bearing capacity of over consolidated models with the same fibre contents as Test Series 1. The models were consolidated at 50 g with the gravitation acceleration reduced to 25g for testing, which resulted in the models having an over consolidation ratio of 2. A full list of tests carried out in each Test Series along with relevant data may be found in Tables 4.5 and 4.6. The maximum resistance for each model test was synonymous with the maximum curvature of the relevant bearing capacity profile. Typically, after 2 to 5 mm penetration the load penetration relationship changed. Curvature at this point varied from a relatively slow transition in some tests to a sharp spike for others. The maximum point of curvature in the load-penetration relationship was taken as the apex of the spike or in the case of the transitional curve, where the plot immediately exited the curve. A secondary location for the determination of undrained shear strength at a depth equal to 0.5 times the breath or diameter of the footing (0.5B/D) was also chosen to provide a comparison to the maximum resistance of the model.

Following initial analysis of the test data, some trends became apparent in the load penetration relationship. Three separate profiles emerged from the bearing capacity tests;

1. The model displayed an increase in strength (strain hardening)
2. The model displayed a constant residual strength
3. The model displayed a reduction in strength (strain softening)

Table 4.5: Summary of Test Series 1, normally consolidated models.

Test No.	Fibre (%)	Foundation size (mm)	Average resistance at max curvature (kPa)	Standard Deviation at max curvature	Average resistance at deformation of 0.5B/0.5D (kPa)	Standard Deviation at deformation of 0.5B/0.5D (kPa)
1-3	0	30 x 60	71.7	0.31	75.6	0.38
4-6	0	40 x 80	62.4	0.08	69.8	0.11
7-9	0	30	62.8	0.67	65.7	0.21
10-12	0	40	60.7	0.24	67.1	0.48
13-15	0	30 x 30	69.5	0.44	72.3	0.41
16-18	0	40 x 40	67.0	0.50	69.8	0.76
25-27	1	30 x 60	112.4	0.82	115.6	0.58
28-30	1	40 x 80	93.2	0.20	98.0	0.20
31-33	1	30	134.2	0.75	138.4	1.31
34-36	1	40	94.2	0.418	103.4	0.37
37-39	1	30 x 30	95.8	0.50	103.9	0.66
40-42	1	40 x 40	89.3	0.48	90.5	0.25
49-51	2	30 x 60	66.6	0.13	67.8	0.12
52-54	2	40 x 80	56.5	0.05	55.4	0.09
55-57	2	30	71.0	0.06	68.5	0.13
58-60	2	40	50.9	0.10	50.8	0.11
61-63	2	30 x 30	103.2	0.10	100.0	0.12
64-66	2	40 x 40	113.8	0.08	115.6	0.20
73-75	3	30 x 60	98.9	0.21	95.3	0.14
76-78	3	40 x 80	98.2	0.06	93.3	0.16
79-81	3	30	134.3	0.17	126.0	0.17
82-84	3	40	132.8	0.11	121.1	0.09
85-87	3	30 x 30	89.9	0.15	92.9	0.13
88-90	3	40 x 40	130.5	0.19	128.5	0.16
97-99	4	30 x 60	384.5	0.14	374.3	0.21
100-102	4	40 x 80	303.6	0.26	291.3	0.07
103-105	4	30	236.5	0.25	236.8	0.10
106-108	4	40	227.6	0.21	230.1	0.06
109-111	4	30 x 30	225.1	0.18	231.8	0.16
112-114	4	40 x 40	216.8	0.14	216.0	0.12

Table 4.6: Summary of Test Series 2, over consolidated models.

Test No.	Fibre (%)	Foundation size (mm)	Average resistance at max curvature (kPa)	Standard Deviation at max curvature	Average resistance at deformation of 0.5B/0.5D (kPa)	Standard Deviation at deformation of 0.5B/0.5D (kPa)
121-123	0	30 x 60	72.0	0.63	88.3	0.79
124-126	0	40 x 80	91.1	0.13	103.5	0.18
127-129	0	30	121.8	0.53	125.1	0.43
130-132	0	40	100.1	0.56	112.4	0.44
133-135	0	30 x 30	113.6	0.79	119.3	0.87
136-138	0	40 x 40	101.1	0.56	117.0	0.25
145-147	1	30 x 60	104.6	0.50	102.5	0.31
148-150	1	40 x 80	101.8	0.19	103.9	0.44
151-153	1	30	90.1	0.43	93.1	0.61
154-156	1	40	86.1	0.28	90.4	0.39
157-159	1	30 x 30	102.5	0.86	103.9	0.34
160-162	1	40 x 40	86.2	0.68	88.9	0.38
169-171	2	30 x 60	260.1	0.16	254.9	0.13
172-174	2	40 x 80	130.6	0.12	162.6	0.11
175-177	2	30	149.8	0.16	149.5	0.54
178-180	2	40	163.5	0.21	174.8	0.14
181-183	2	30 x 30	212.4	0.29	236.8	0.16
184-186	2	40 x 40	162.9	0.11	171.5	0.13
193-195	3	30 x 60	399.7	0.15	365.6	0.37
196-198	3	40 x 80	309.0	0.07	265.0	0.09
199-201	3	30	411.6	0.10	372.7	0.26
202-204	3	40	355.6	0.08	329.9	0.25
205-207	3	30 x 30	261.3	0.37	226.7	0.28
208-210	3	40 x 40	353.6	0.16	330.8	0.31
217-219	4	30 x 60	510.7	0.37	549.5	0.13
220-222	4	40 x 80	379.9	0.15	377.4	0.13
223-225	4	30	344.8	0.10	356.3	0.09
226-228	4	40	419.4	0.12	421.7	0.20
229-231	4	30 x 30	410.7	0.29	427.1	0.26
232-234	4	40 x 40	374.9	0.36	398.4	0.10

4.3.1 Bearing capacity Test Series 1

Test Series 1 investigated the effects of fibres on normally consolidated kaolin clay models with fibre content varied from 0 to 4 %. For this section, tests on the 4 % normally consolidated (NC) model are outlined. The resistance of the model to penetration is shown in Figures 4.15 to 4.20. Test data for other fibre contents of this Test Series may be found in Appendix F.

Figure 4.15 summarises the 30 x 60 mm foundation tests completed on the 4 % NC model. Repeatability between the 3 tests in this case was excellent. Tests 2 and 3 had very similar peak resistance; Test 1 peaked slightly higher. There was little scatter present in the test data and the model resistance to penetration decreased once the peak resistance had been surpassed. The model resistance to the 40 x 80 mm footing also produced very good repeatability for tests conducted. There was some variation in the profiles between 40 and 65 mm model depth and approximately 20 kPa differential between peak resistances. The resistance profile corresponding to the 30 mm diameter footing showed significant variation in the resistance to penetration but poor repeatability for all tests conducted, Figure 4.17. Peak resistance varies by 60 kPa between the 3 tests, Tests 2 and 3 converged with increasing depth.

Figure 4.18 showed the 40 mm diameter tests, where Tests 1 and 3 showed little scatter in their respective profiles. Test 2 showed a reduced resistance after a depth of 20 mm had been passed, however with increased depth the model showed increasing resistance and appeared to converge with the other tests. Tests 2 and 3 with the 30 x 30 mm foundation exhibited excellent repeatability, with some scatter. Test 1, however, possessed higher peak strength with significant variation in the resistance profile. Once Test 1 had passed a depth of 30 mm the resistance profile decreased and appeared to converge with Tests 2 and 3, Figure 4.19. Tests 1 and 3 conducted with the 40 mm square foundation showed good repeatability with some scatter present between the two profiles. Test 2 of the 40 mm square foundations demonstrated increased resistance once the peak resistance was passed. The profile increased to a depth of 50 mm, after which it receded to a resistance similar to that of Tests 1 and 3 at a depth of 80 mm, Figure 4.20.

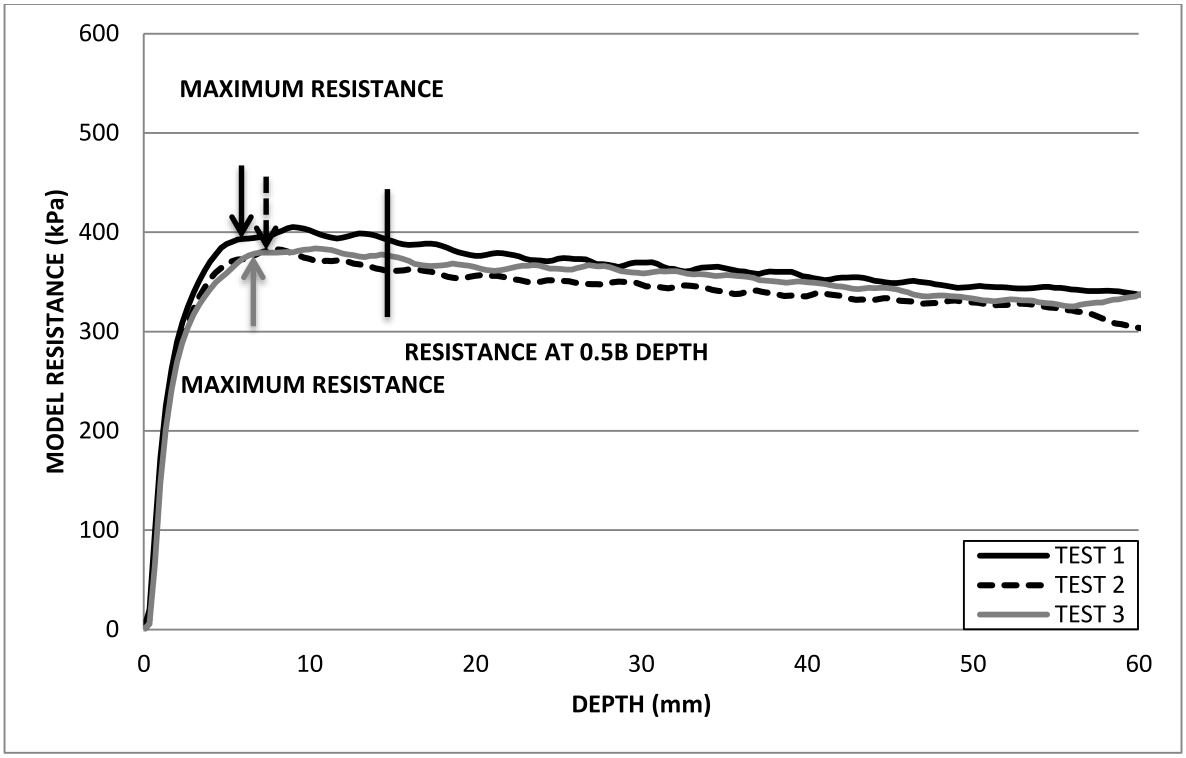

Figure 4.15: Resistance profile for a 30 x 60 mm rectangular foundation tested on 4 % fibre normally consolidated model.

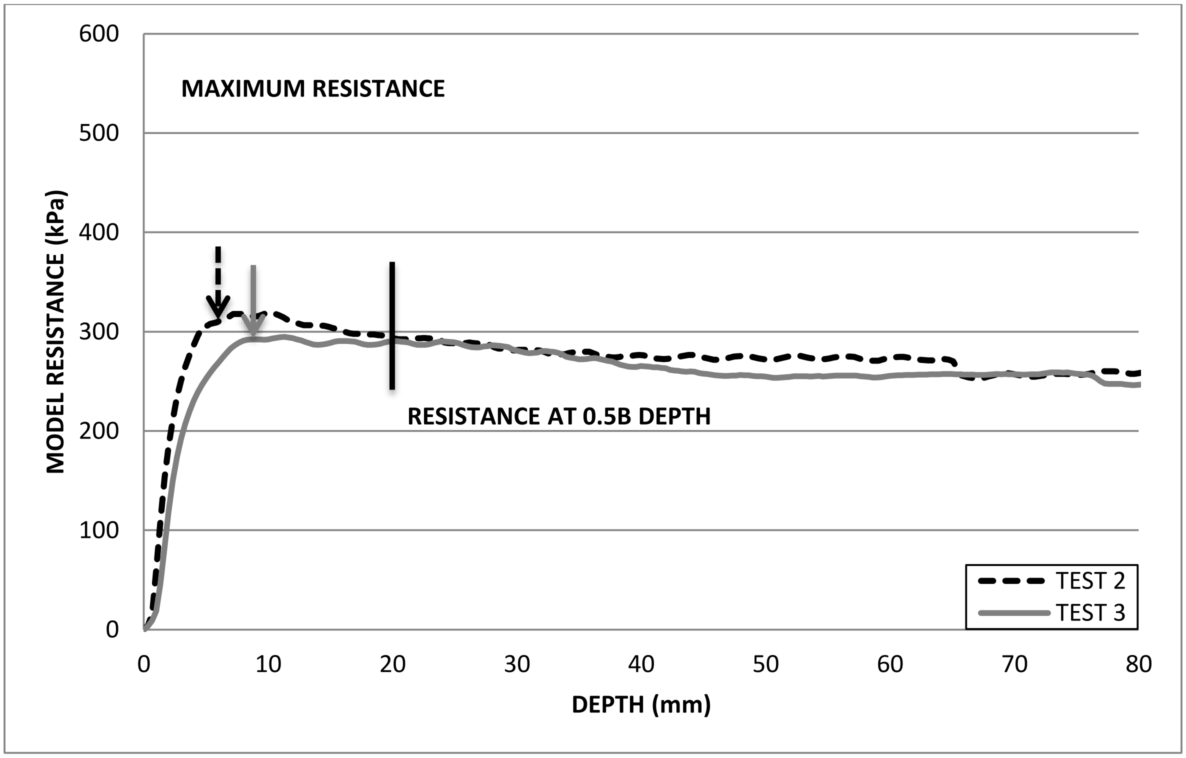

Figure 4.16: Resistance profile for a 40 x 80 mm rectangular foundation tested on 4 % fibre normally consolidated model.

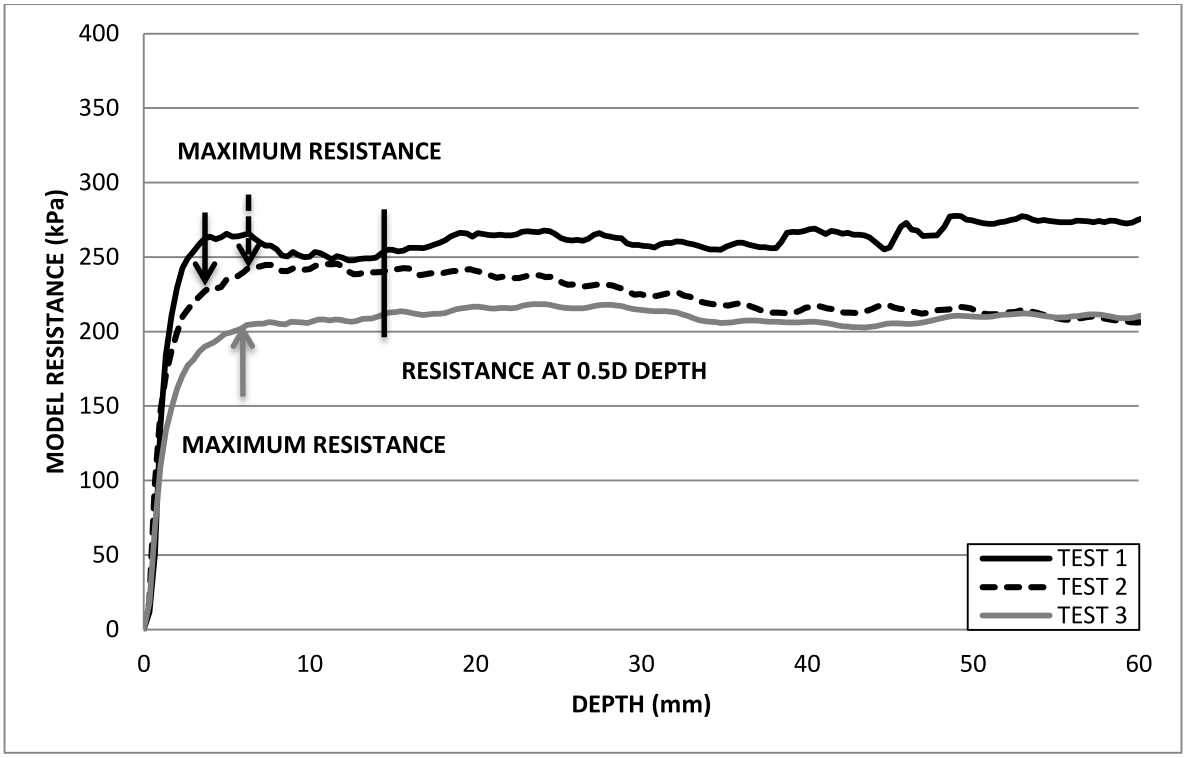

Figure 4.17: Resistance profile for a 30 mm circular foundation tested on 4 % fibre normally consolidated model.

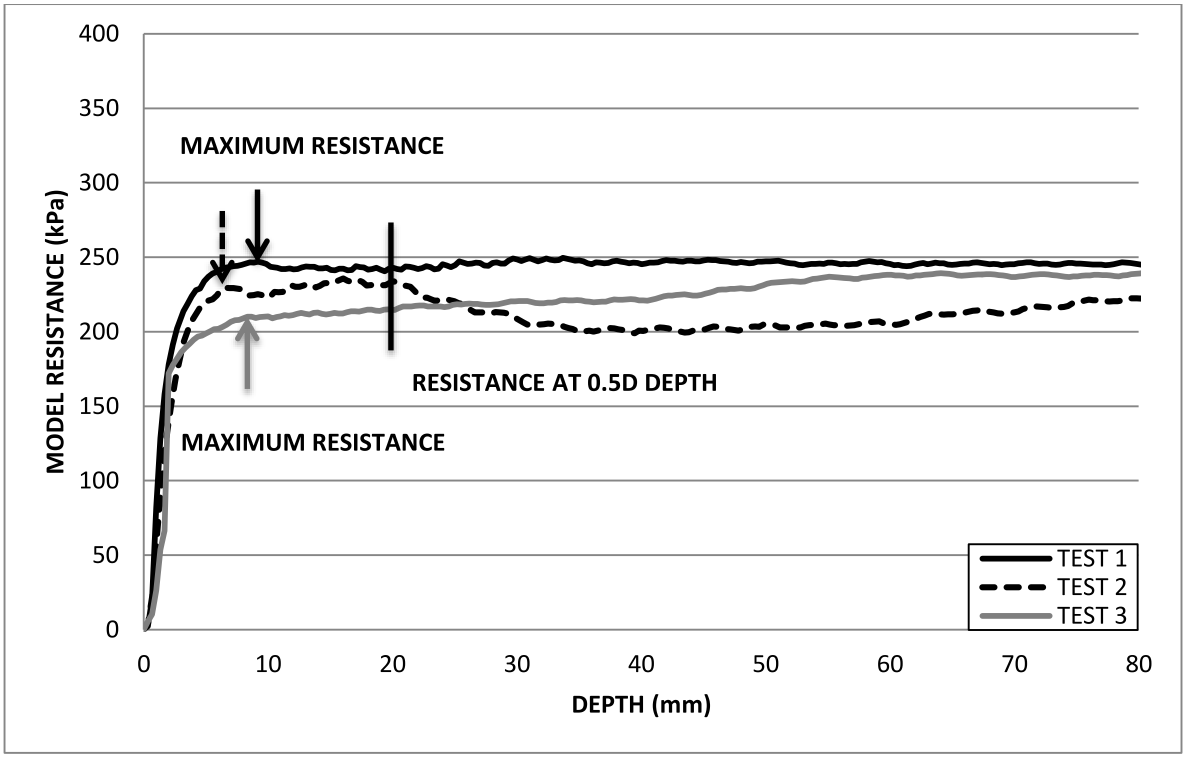

Figure 4.18: Resistance profile for a 40 mm circular foundation tested on 4 % fibre normally consolidated model.

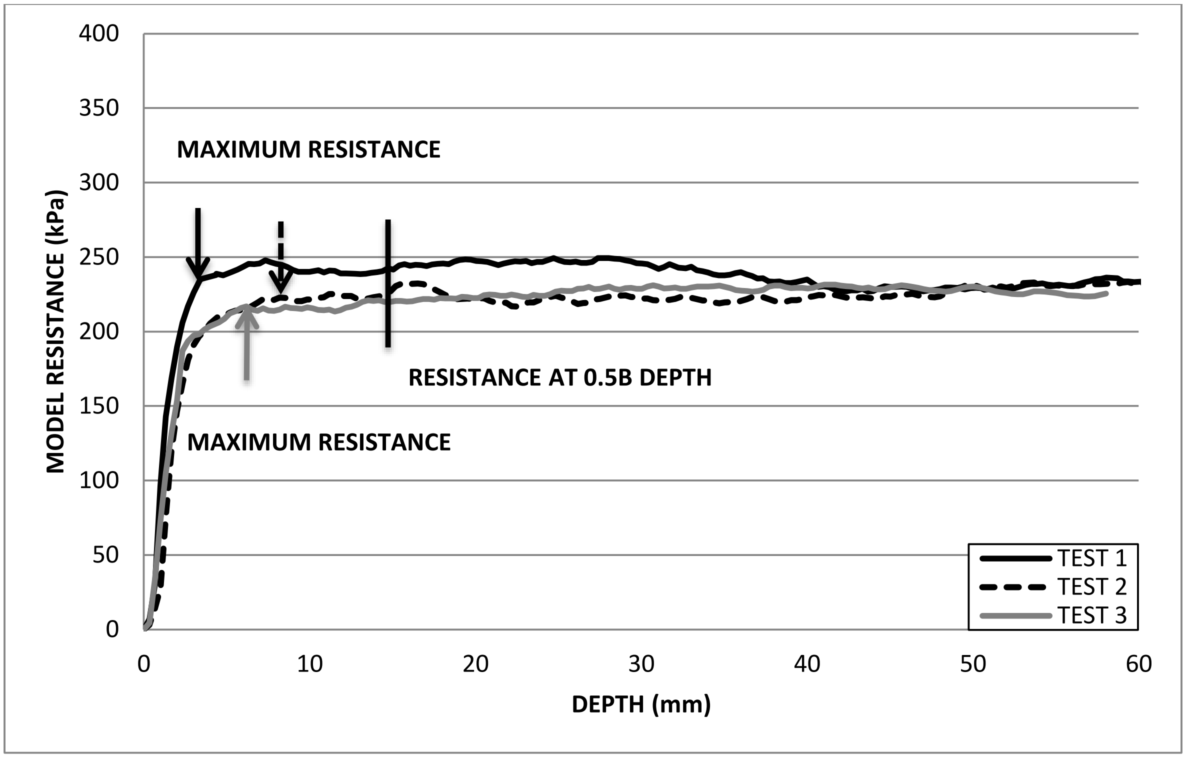

Figure 4.19: Resistance profile for a 30 x 30 mm square foundation tested on 4 % fibre normally consolidated model.

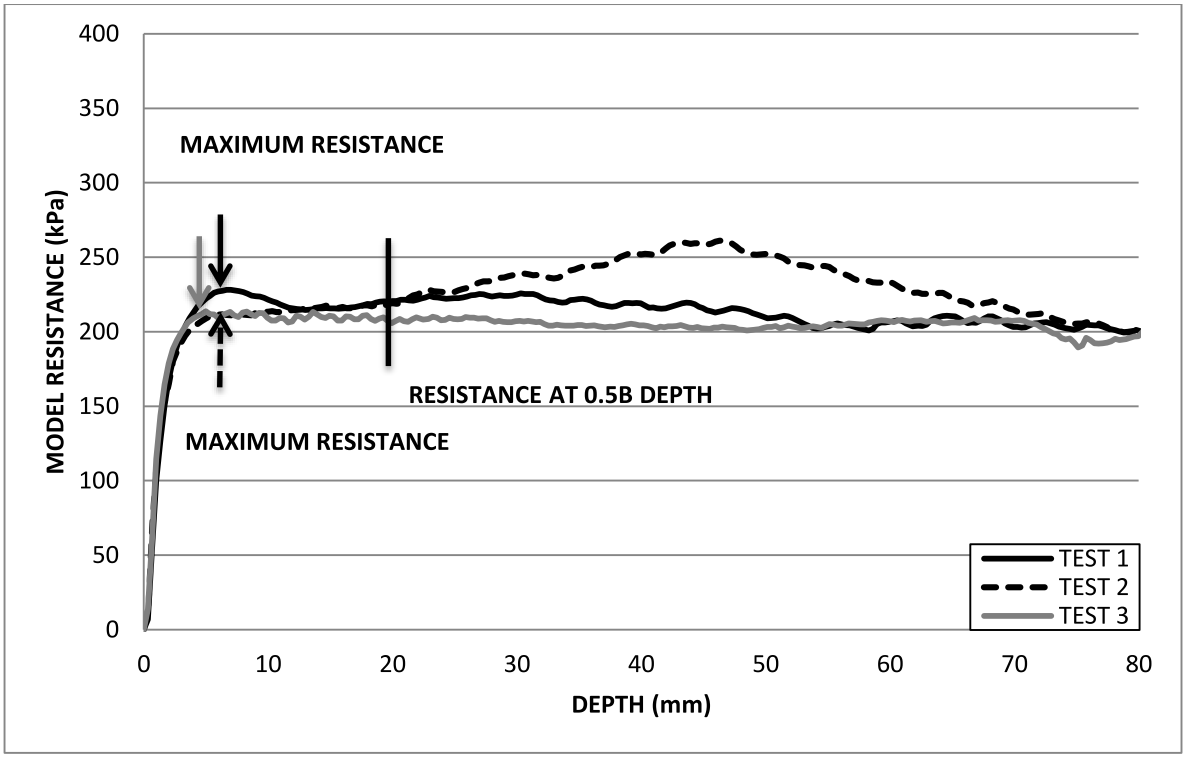

Figure 4.20: Resistance profile for a 40 x 40 mm square foundation tested on 4 % fibre normally consolidated model.

4.3.2 Bearing capacity Test Series 2

Test Series 2 investigated the effects of fibre content on over consolidated kaolin clay models having an over consolidated ratio of 2. The fibre content ranged from 0 to 4 % per dry weight of kaolin clay. The following section details the reaction of the 4 % normally consolidated (OC) model when tested with various foundation types and sizes, Figures 4.21 to 4.24. Test data for other fibre contents of Test Series 2 may be found in Appendix G.

Figure 4.21 shows poor repeatability for tests conducted with the 30 x 60 mm foundation. Peak resistance varied by approximately 170 kPa between the 3 tests. Tests conducted in Test Series 2 showed a reduction in scatter for the resistance data compared to Test Series 1. Similarly tests with the 40 x 80 mm foundation produced resistance profiles with poor repeatability, Figure 4.22. The difference in peak resistance between the two tests was approximately 60 kPa. Test 2 showed a reduction in resistance once the peak value had been passed but resistance did increase once a depth of 30 mm was reached. Test 1 depicted an increasing resistance profile with depth; however beyond 60 mm the resistance began to decrease to a value of 433 kPa at 80 mm model depth. A plate slip during Test 3 resulted in a poor resistance profile and therefore was excluded from subsequent analysis. Figure 4.23 shows very good repeatability for the 3 tests conducted with the 30 mm diameter foundation. Maximum resistance varied by approximately 30 kPa when compared to Tests 1 and 3, however the resistance profiles were very similar beyond 25 mm depth. Test 2 yielded a maximum resistance similar to that of Test 3, while the resistance profile was weaker when compared to the aforementioned tests.

Tests conducted with the 40 mm diameter foundation produced excellent repeatability to a depth of 40 mm, after which Test 1 showed increased resistance that was not mirrored by Tests 2 and 3, Figure 4.24. Peak resistance for Tests 1 and 2 were approximately 420 kPa each, while the peak resistance for Test 3 was 402 kPa. Figure 4.25 shows excellent repeatability between the resistance profiles for the 30 x 30 mm foundation. Some scatter was present in the resistance profiles for the initial 20 mm of the model. As depth increased during testing the variation between the resistance profiles reduced and the tests converged thereafter. Repeatability for the 40 mm square foundation tests was excellent, shown by variation of 4 kPa in peak resistance over the test range. The profiles for Tests 2 and 3 were practically the same, with Test 1 showing very close correlation, Figure 4.26.

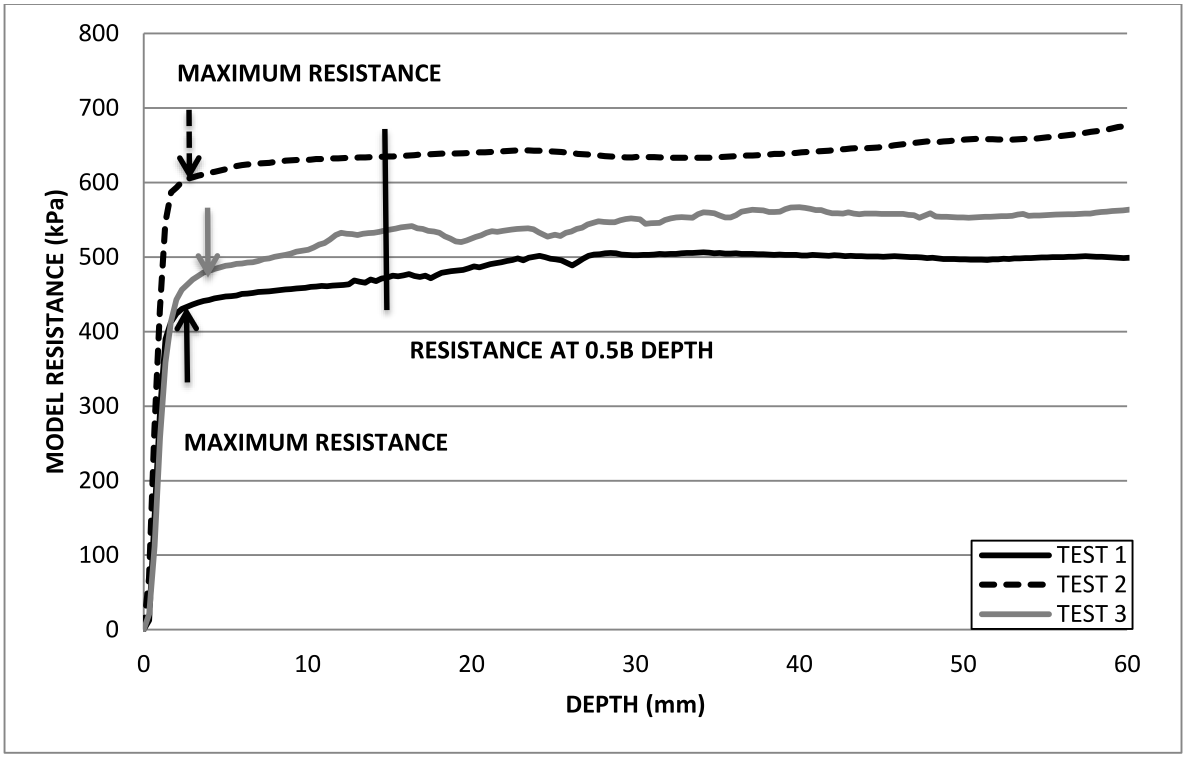

Figure 4.21: Resistance profile for a 30 x 60 mm rectangular foundation tested on 4 % fibre over consolidated model.

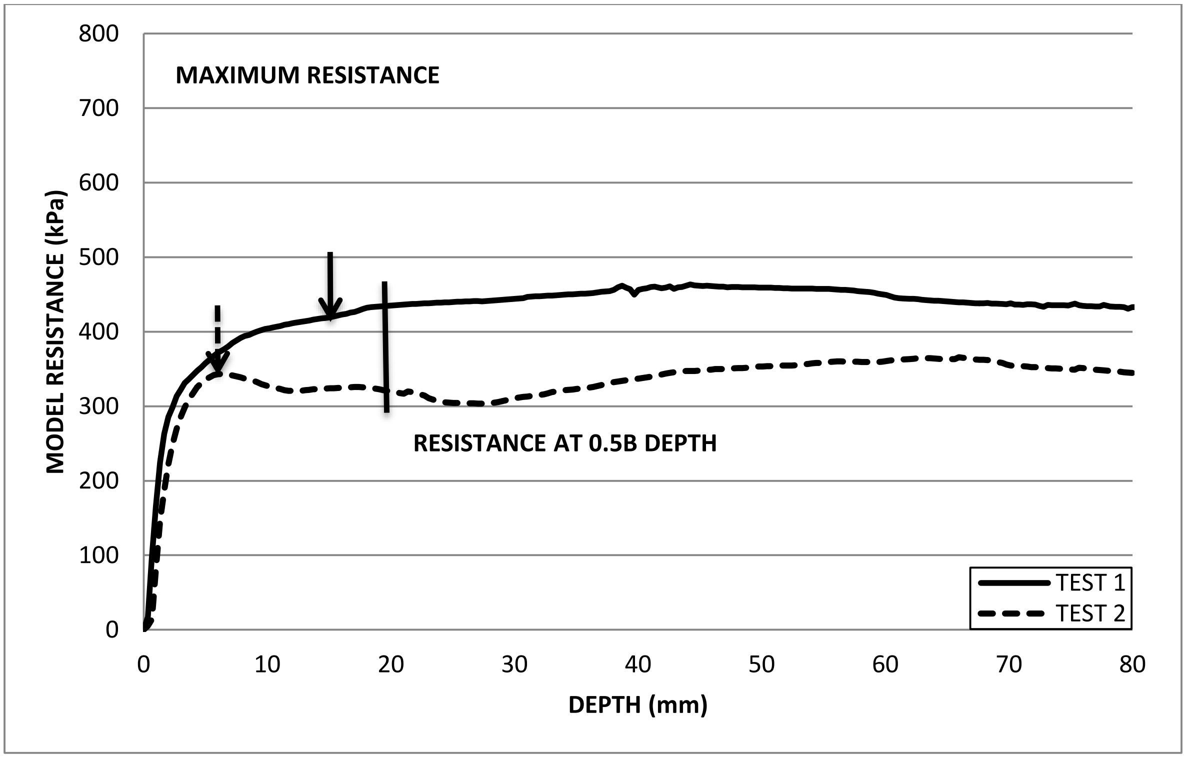

Figure 4.22: Resistance profile for a 40 x 80 mm rectangular foundation tested on 4 % fibre over consolidated model.

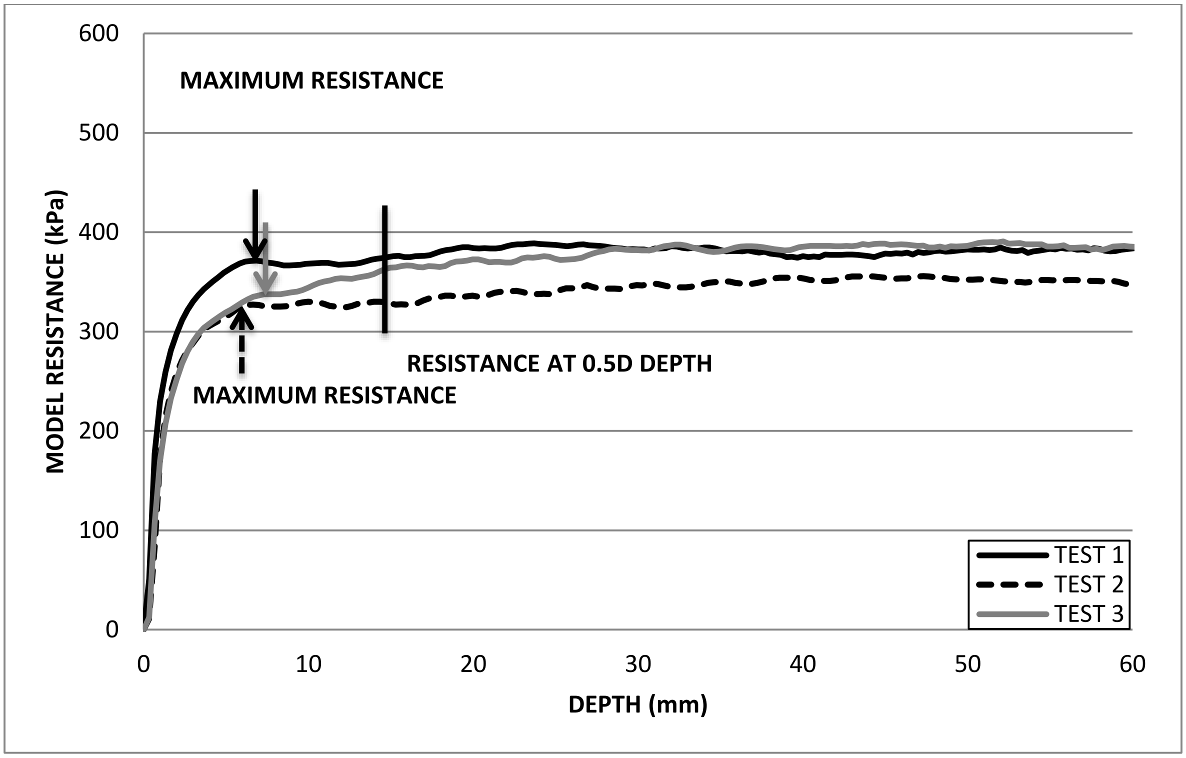

Figure 4.23: Resistance profile for a 30 mm circular foundation tested on 4 % fibre over consolidated model.

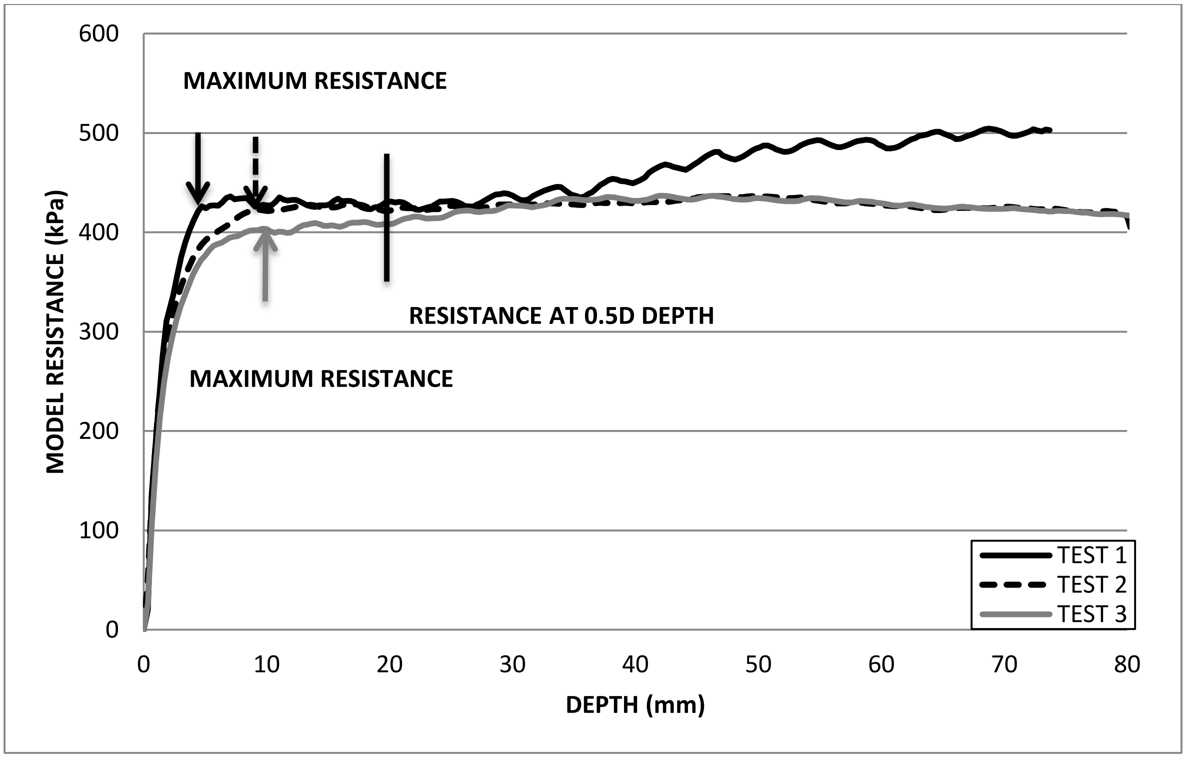

Figure 4.24: Resistance profile for a 40 mm circular foundation tested on 4 % fibre over consolidated model.

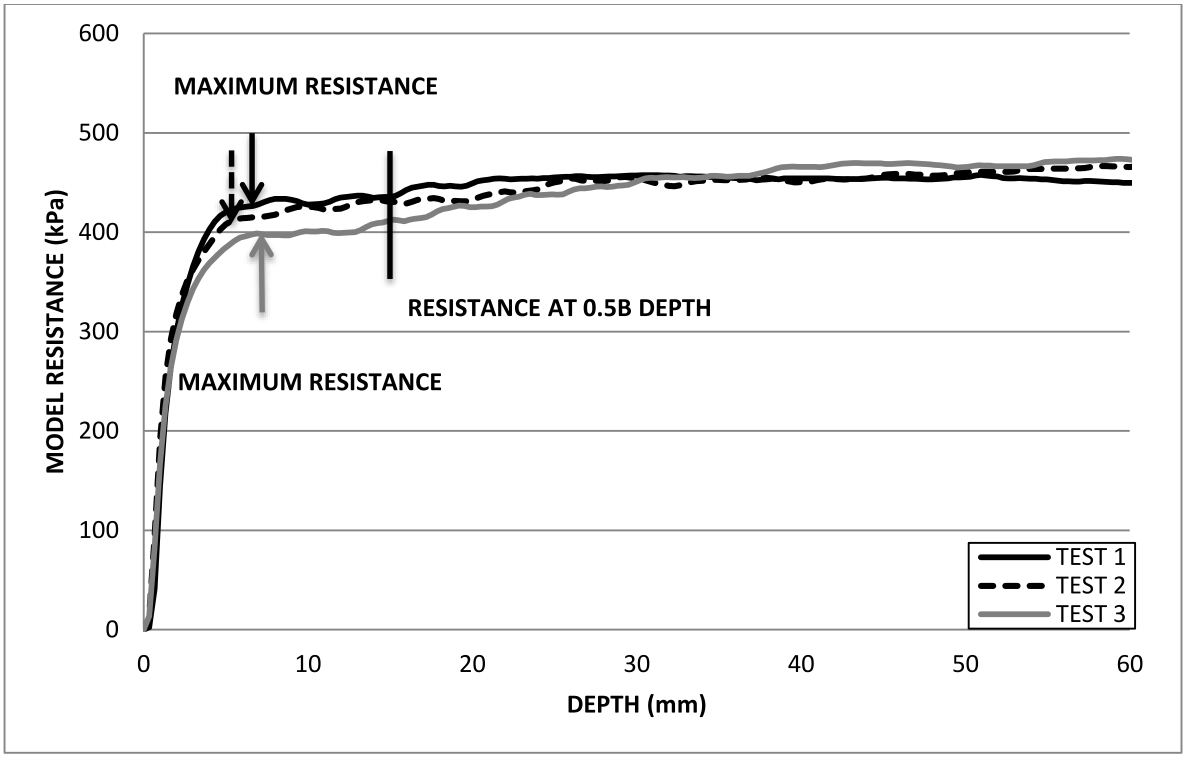

Figure 4.25: Resistance profile for a 30 x 30 mm square foundation tested on 4 % fibre over consolidated model.

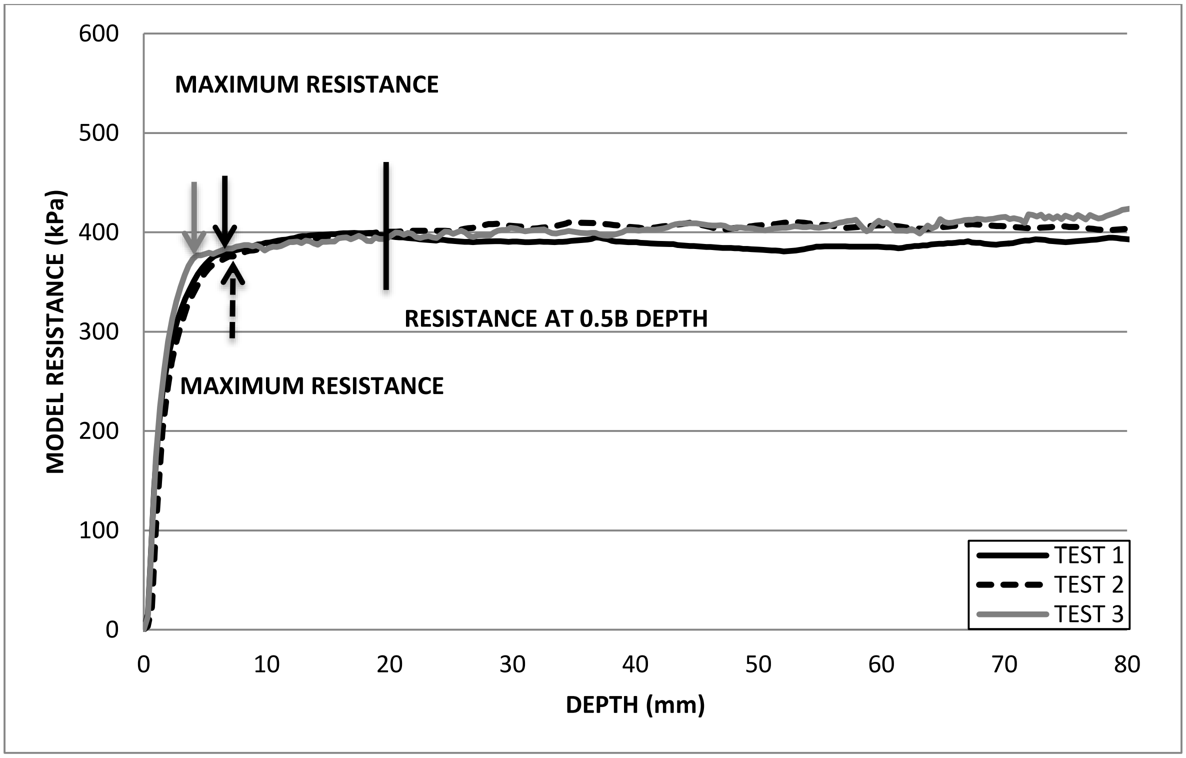

Figure 4.26: Resistance profile for a 40 x 40 mm square foundation tested on 4 % fibre over consolidated model.

4.3.3 Bearing capacity with increasing residual strength

This section presents bearing capacity data which resulted in an increased residual resistance of a model to load. The 30 mm circular foundation tests on the 0 % OC model illustrated this increase in resistance, Figure 4.27. Test data for other fibre contents may be found in Appendix F and G.

A summary of tests conducted with various foundation types and sizes that resulted in increased resistance in relation to the 0 % fibre OC model, is compiled in Table 4.7. The 30 mm circular foundation produced very good repeatability between Tests 2 and 3, while the results of Test 1 were offset slightly from the previous profiles. In Figure 4.27 as Test 1 progressed the resistance profile converged with that of the other tests. Scatter was more pronounced in Test 1 at shallow depths compared to Tests 2 and 3; however with greater depth the scatter was equally apparent between all 3 tests. The difference in resistance at maximum curvature and at depth 0.5 times the diameter varied slightly and was found to increase by 3.2 kPa with increased depth for Test 1. Resistance to load was found to increase by 6.5 kPa for Test 3 and 6.2 kPa for Test 2, when compared to resistances at 0.5 D depth. After a depth of 20 mm was reached in Test 1, resistance to load began to pick up and increased by approximately 25 kPa over the next 40 mm depth. The resistance to load was less pronounced in Test 2 and 3, while the rate of increase in resistance remained constant through the remainder of each test.

Table 4.7: Summary of tests conducted displaying an increase in strength (strain hardening).

Test No.	Fibre (%)	OCR	Foundation size (mm)	Average resistance at max curvature (kPa)	Standard Deviation at max curvature	Average resistance at deformation of 0.5B/0.5D (kPa)	Standard Deviation at deformation of 0.5B/0.5D (kPa)
1-3	0	1	30 x 60	71.7	0.31	75.6	0.38
13-15	0	1	30 x 30	69.5	0.44	72.3	0.41
28-30	1	1	40 x 80	93.2	0.20	98.0	0.20
34-36	1	1	40	94.2	0.418	103.4	0.37
40-42	1	1	40 x 40	89.3	0.48	90.5	0.25
49-51	2	1	30 x 60	66.6	0.13	67.8	0.12
52-54	2	1	40 x 80	56.5	0.05	55.4	0.09
55-57	2	1	30	71.0	0.06	68.5	0.13
58-60	2	1	40	50.9	0.10	50.8	0.11
64-66	2	1	40 x 40	113.8	0.08	115.6	0.20
85-87	3	1	30 x 30	89.9	0.15	92.9	0.13
88-90	3	1	40 x 40	130.5	0.19	128.5	0.16
121-123	0	2	30 x 60	72.0	0.63	88.3	0.79
124-126	0	2	40 x 80	91.1	0.13	103.5	0.18
127-129	0	2	30	121.8	0.53	125.1	0.43
130-132	0	2	40	100.1	0.56	112.4	0.44
133-135	0	2	30 x 30	113.6	0.79	119.3	0.87
136-138	0	2	40 x 40	101.1	0.56	117.0	0.25
145-147	1	2	30 x 60	104.6	0.50	102.5	0.31
148-150	1	2	40 x 80	101.8	0.19	103.9	0.44
151-153	1	2	30	90.1	0.43	93.1	0.61
154-156	1	2	40	86.1	0.28	90.4	0.39
157-159	1	2	30 x 30	102.5	0.86	103.9	0.34
160-162	1	2	40 x 40	86.2	0.68	88.9	0.38
172-174	2	2	40 x 80	130.6	0.12	162.6	0.11
175-177	2	2	30	149.8	0.16	149.5	0.54
178-180	2	2	40	163.5	0.21	174.8	0.14
181-183	2	2	30 x 30	212.4	0.29	236.8	0.16
184-186	2	2	40 x 40	162.9	0.11	171.5	0.13

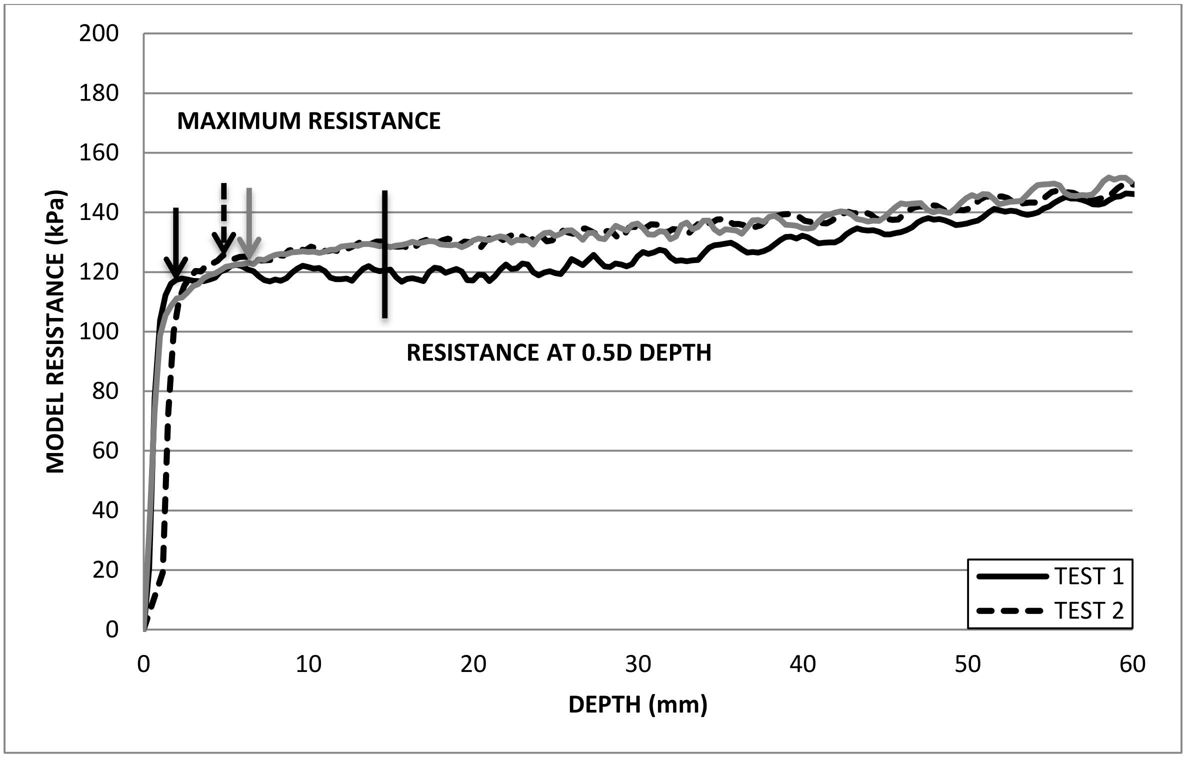

Figure 4.27: Resistance profile for a 30 mm circular foundation tested on 0 % fibre over consolidated model.

4.3.4 Bearing capacity with constant residual strength

The following section details the bearing capacity results that exhibited constant residual resistance. The 30 mm circular foundation results for the 4 % OC fibrous model shall be used to demonstrate this behaviour in the following section, Figure 4.28. Test data for other fibre contents may be found in Appendix F and G.

Table 4.8 summarises the tests conducted along with the resistances encountered for the constant profiles of the 4 % OC model. The 30 mm circular foundation resistance profiles showed little variation between Tests 1 and 3, Figure 4.28. Variation was present in Test 2, while there was similar resistance to Test 3 at maximum curvature, Figure 4.28. There was some variation in resistance between locations of maximum curvature and 0.5 times the foundation diameter, Table 4.8. As expected resistance to load increased somewhat with depth; however this slight increase plateaus approaching 30 mm depth with the profiles remaining relatively constant thereafter. Some fluctuation was evident in the profile that may be attributed to the shearing of the fibres present. For the 40 mm circular foundation, Tests

2 and 3 produced repeatable resistance profiles; whereas Test 1 increased somewhat in resistance profile.

Table 4.8: Summary of tests conducted displaying constant strength.

Test No.	Fibre (%)	OCR	Foundation size (mm)	Average resistance at max curvature (kPa)	Standard Deviation at max curvature	Average resistance at deformation of 0.5B/0.5D (kPa)	Standard Deviation at deformation of 0.5B/0.5D (kPa)
4-6	0	1	40 x 80	62.4	0.08	69.8	0.11
7-9	0	1	30	62.8	0.67	65.7	0.21
10-12	0	1	40	60.7	0.24	67.1	0.48
16-18	0	1	40 x 40	67.0	0.50	69.8	0.76
25-27	1	1	30 x 60	112.4	0.82	115.6	0.58
31-33	1	1	30	134.2	0.75	138.4	1.31
37-39	1	1	30 x 30	95.8	0.50	103.9	0.66
61-63	2	1	30 x 30	103.2	0.10	100.0	0.12
103-105	4	1	30	236.5	0.25	236.8	0.10
106-108	4	1	40	227.6	0.21	230.1	0.06
169-171	2	2	30 x 60	260.1	0.16	254.9	0.13
217-219	4	2	30 x 60	510.7	0.37	549.5	0.13
220-222	4	2	40 x 80	379.9	0.15	377.4	0.13
223-225	4	2	30	344.8	0.10	356.3	0.09
226-228	4	2	40	419.4	0.12	421.7	0.20
229-231	4	2	30 x 30	410.7	0.29	427.1	0.26
232-234	4	2	40 x 40	374.9	0.36	398.4	0.10

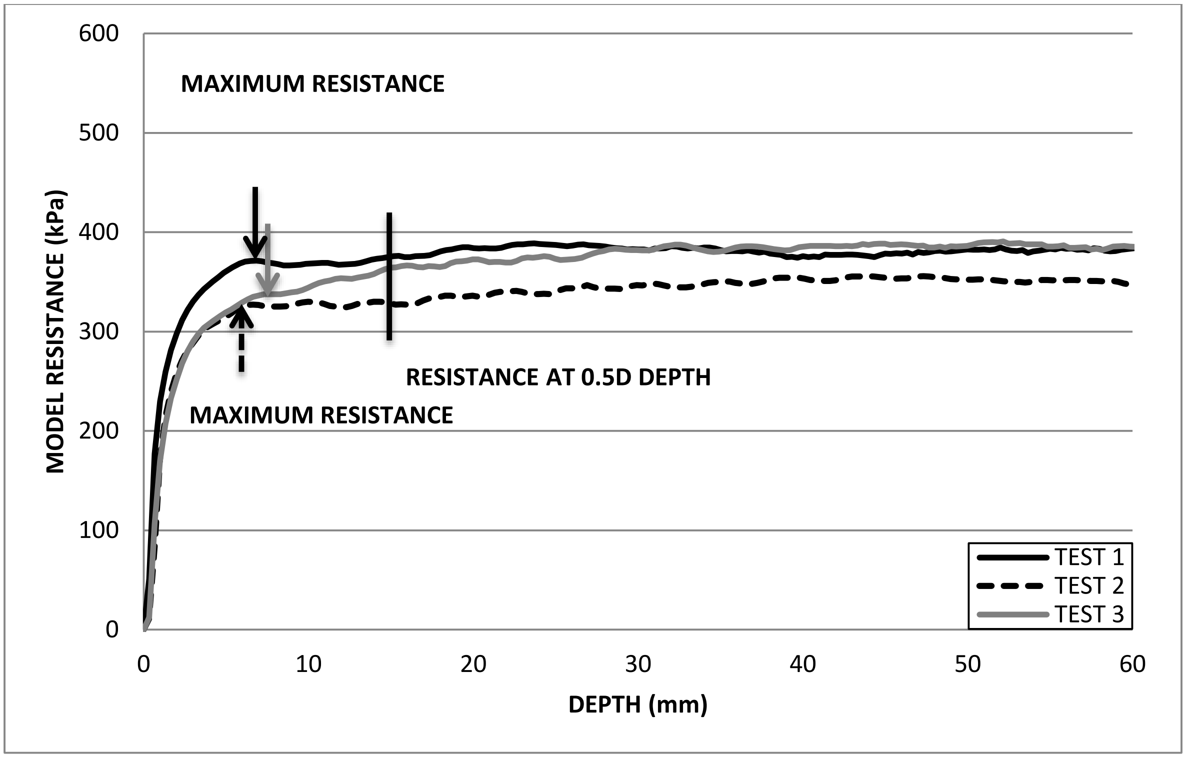

Figure 4.28: Resistance profile for a 30 mm circular foundation tested on 4 % fibre over consolidated model.

4.3.5 Bearing capacity with decreasing residual strength

A decreasing resistance with depth profile was the third trend found in the bearing capacity results. Figure 4.29 shows one set of tests that demonstrated this behaviour and was taken from normally consolidated models with 3 % fibre reinforcement, Tests 73 to 84 in Table 4.9. Test data for other fibre contents may be found in Appendix F and G.

The decreasing resistance profiles for all tests displaying this trend are summarised in Table 4.9. Comparisons were drawn between the resistance at maximum curvature and resistance at a model depth of 0.5 B/D. Repeatability between the tests conducted in Figure 4.29 was average. The 30 mm circular foundation showed significant scatter in the resistance profiles for each test, with approximately 25 kPa between the maximum resistance for Tests 2 and 3, Figure 4.29. Resistance profiles decreased once the maximum load had been reached. Comparisons between resistance at maximum curvature in the profiles and at depth equal to 0.5 B/D showed a decrease in resistance. As depth of penetration increased the profiles appeared to exhibit a constant resistance with some fluctuation from 35 to 60 mm depth in the model.

Table 4.9: Summary of tests conducted displaying a reduction in strength (strain softening).

Test No.	Fibre (%)	OCR	Foundation size (mm)	Average resistance at max curvature (kPa)	Standard Deviation at max curvature	Average resistance at deformation of 0.5B/0.5D (kPa)	Standard Deviation at deformation of 0.5B/0.5D (kPa)
73-75	3	1	30 x 60	98.9	0.21	95.3	0.14
76-78	3	1	40 x 80	98.2	0.06	93.3	0.16
79-81	3	1	30	134.3	0.17	126.0	0.17
82-84	3	1	40	132.8	0.11	121.1	0.09
97-99	4	1	30 x 60	384.5	0.14	374.3	0.21
100-102	4	1	40 x 80	303.6	0.26	291.3	0.07
109-111	4	1	30 x 30	225.1	0.18	231.8	0.16
112-114	4	1	40 x 40	216.8	0.14	216.0	0.12
193-195	3	2	30 x 60	399.7	0.15	365.6	0.37
196-198	3	2	40 x 80	309.0	0.07	265.0	0.09
199-201	3	2	30	411.6	0.10	372.7	0.26
202-204	3	2	40	355.6	0.08	329.9	0.25
205-207	3	2	30 x 30	261.3	0.37	226.7	0.28
208-210	3	2	40 x 40	353.6	0.16	330.8	0.31

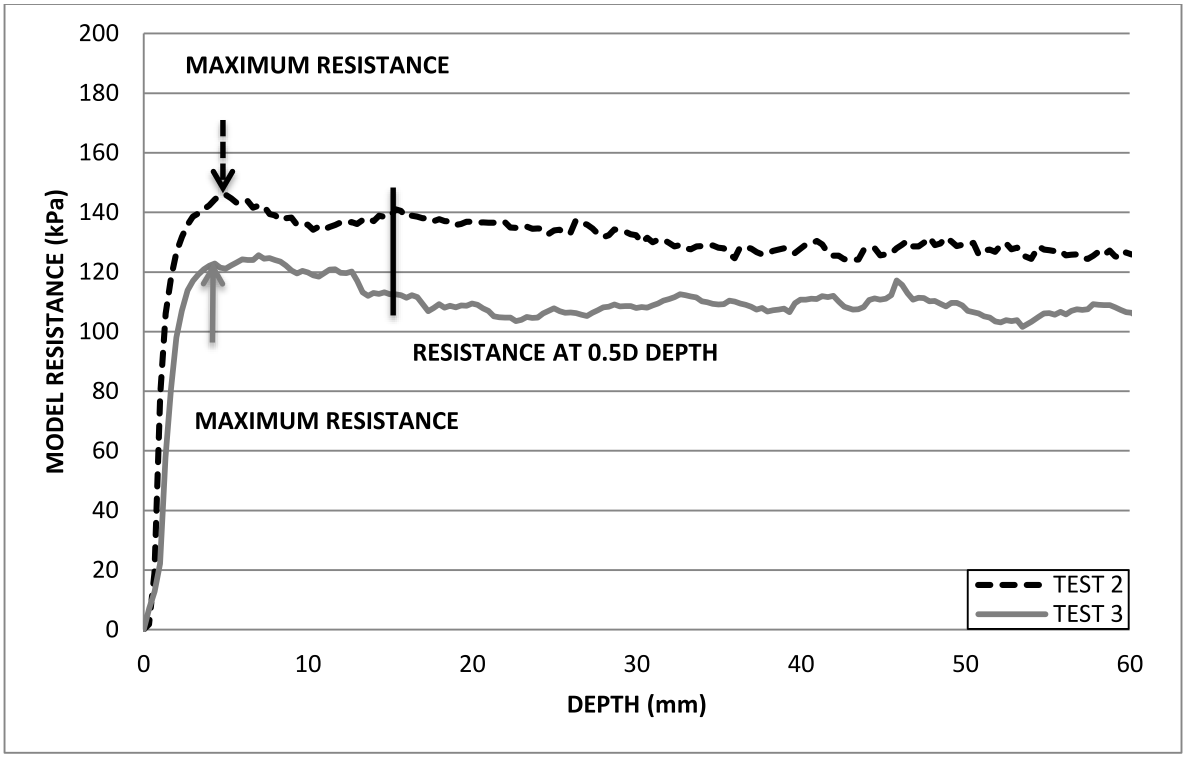

Figure 4.29: Resistance profile for a 30 mm circular foundation tested on 3 % fibre normally consolidated model.

4.4 Summary

The results of classification tests, shear vane tests and the geotechnical centrifuge modelling process have been presented in this chapter along with some initial analysis. Centrifuge modelling was divided into two Test Series, which looked at the effects of normally and over consolidated fibrous models respectively. The fibre content in each test series varied from 0 to 4 %. Bearing capacity tests and penetrometer profiling was completed to ascertain the undrained shear strength of the various models. Shear vane tests were carried out on cores extracted from the centrifuge models for comparison with bearing capacity values obtained from centrifuge modelling. Samples were taken at various depths in order to classify the fibrous soils.

Bearing capacity results showed that with increasing fibre content the undrained shear strength increased. Consolidation ratio also affected the shear strength determined. Over consolidated models were found to produce higher strengths than those of normally consolidated models of corresponding fibre content. The effects of strain hardening contributed to increased undrained shear strength with increased depth, particularly for over consolidated models. Undrained shear strength reduced for some models at depths of 0.5B/D and may be related to the effects of strain softening. Strain softening occurred in both Test Series 1 and 2. The third strength profile encountered was a constant strength profile and was also found in normally and over consolidated models. The CPT results also showed that on average increasing the fibre content improved the shear strength of the reinforced models. In the case of the 2 and 3 % fibre models, CPT results showed low shear strength due to high moisture contents remaining in the model, becoming particularly evident with depth. Piezoball results demonstrated less variation in the shear strength profiles compared to CPT results. The full flow penetrometer showed increased shear strength with increasing fibre content, with over consolidated model results greater than that of normally consolidated results. Piezoball testing also showed a decrease in shear strength for the 2 % NC fibre model. Repeatability of tip resistance in each of the profiling devices ranged from very good to poor and in the majority of cases appeared to be independent of the fibre content present. Scatter in the strength profiles for each penetrometer became more pronounced with increasing fibre content, while the pore water pressure from piezoball tests showed good repeatability and therefore appeared to be independent of any effects of fibre content.

Shear vane results corrected for the effects of plasticity increased the associated scatter in some cases. Shear vane tests also indicated increases in shear strength with some variation, for fibre contents 0 to 4 %. Sensitivity of the soils spanned from 2 to 2.21 for the range of fibrous soils sampled and can be classed as a soil of low sensitivity.

CHAPTER 5

ANALYSIS AND DISCUSSION

5.1 Introduction

The purpose of this chapter is to analyse and discuss the results gathered during the experimental testing undertaken as part of this study. The centrifuge modelling process was divided into two test series, which assessed the influence of the over consolidation ratio on the strength of fibrous soil models. For Test Series 1 and 2, the percentage fibre, by dry weight, added to each sample ranged from 0 to 4 % for each model constructed. Test Series 1 looked at the bearing capacities of normally consolidated soil models, while Test Series 2 studied soil models with an over consolidation ratio of 2.

The undrained shear strength of the fibre soil mixture was back calculated from plate loading tests on the centrifuge models. Bearing capacity testing was carried out on each soil model using a range of foundation types and sizes. CPT and piezoball profiling was also conducted after bearing capacity testing, to determine the variation of strength both around the circumference of the test area and also with depth, to validate the results of the bearing capacity tests. Samples and cores for additional testing and classification purposes were extracted from each model once centrifuge modelling was completed. Additional tests conducted include laboratory vane testing and moisture content determination.

The results of tests carried out on the centrifuge models are analysed under the following headings:

i. Undrained shear strength from CPT, piezoball and laboratory vane.
ii. Influence of foundation shape on c_u
iii. Influence of fibre content on c_u
iv. Comparison of results from normally and over consolidated models

5.2 Undrained shear strength from CPT, piezoball and shear vane

Figures 5.1 and 5.3 present the variation in undrained shear strength at maximum curvature for normally consolidated models with fibre contents of 0 and 4 %. For comparison, the ratios of undrained shear strength to vertical effective stress (c_u/σ_v') are presented in Figures 5.2 and 5.4 respectively. Figures 5.5 and 5.7 show the undrained shear strength profiles at maximum curvature for over consolidated models, also with fibre content of 0 and 4 %, with the relevant ratios of c_u/σ_v' presented in Figures 5.6 and 5.8 respectively. Strength profiles at 0.5 B/D can be found in Figures 5.9 to 5.12.

For the 0 % fibre normally consolidated model, Figure 5.1, the corrected shear strength determined from shear vane results showed a poor correlation with results from penetrometer data and back calculated strength from bearing capacity testing. This poor correlation may be attributed to the fact that shear vane analysis was carried out on unconfined samples where effective stress was low compared to the centrifuge models. The shear vane analysis was conducted at three depths through the model cores; the shear vane profile lines in the following figures are an average of the corrected shear vane strength in the respective consolidated model. The average results of each penetrometer profiling showed a relatively consistent profile through the depth of the model tested. In Figure 5.1 the piezoball results produced a consistent strength profile with minimal scatter. The CPT results showed a reduction in strength with depth with less scatter compared to the piezoball. The undrained shear strength profiles of various foundation types presented in Figure 5.1 correspond to the strength at maximum curvature in the resistance displacement relationships in Chapter 4, and as such are only valid for undrained shear strength near surface level. The back calculated undrained shear strength from foundation tests showed a very good correlation for all footing types utilized. Undrained shear strengths mobilized by the larger foundations were found to be weaker than strengths determined for the smaller footing sizes; this trend was consistence for all foundation types.

The ratio of undrained shear strength to vertical effective stress, Figure 5.2, decreased with depth for both the piezoball and CPT, with close correlation between sets of results for each penetrometer. The shear vane c_u/σ_v' ratios are shown as vertical lines in Figure 5.2. There was some variation of c_u/σ_v' in the upper 20 mm of the model, with a high value for this ratio recorded through the model.

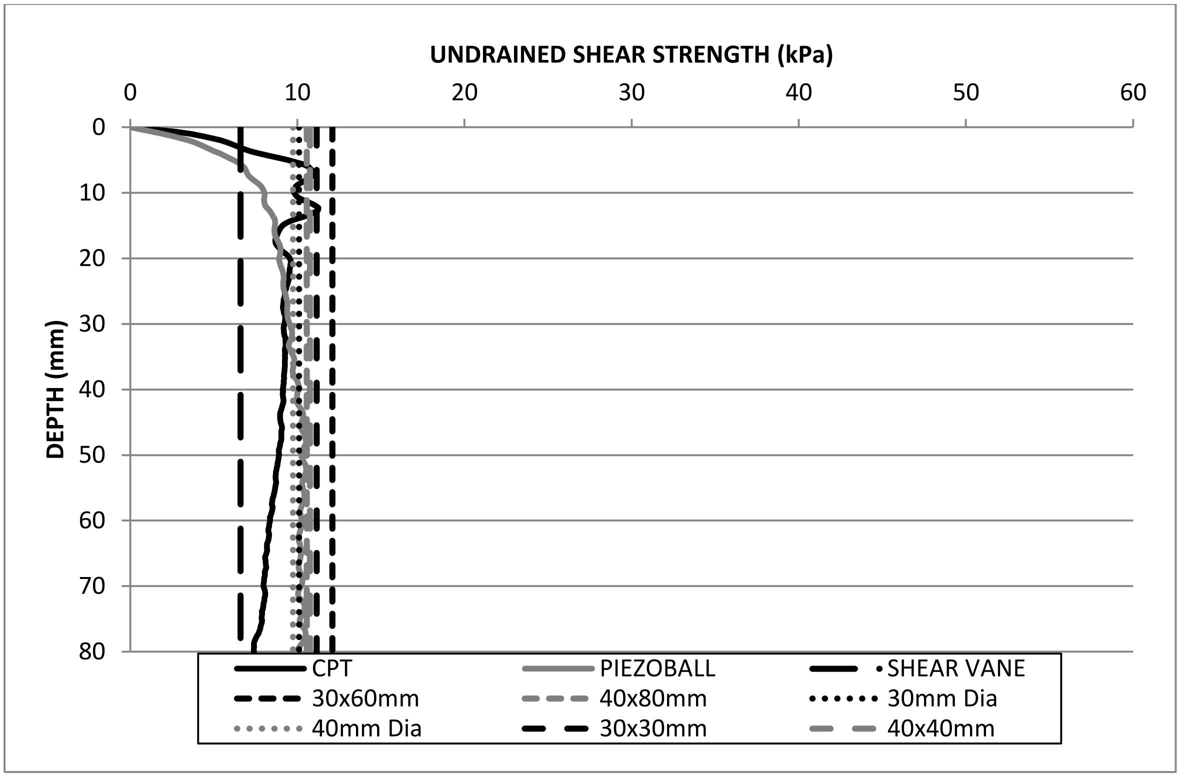

Figure 5.1: Undrained shear strength at maximum curvature for 0 % fibre normally consolidated model.

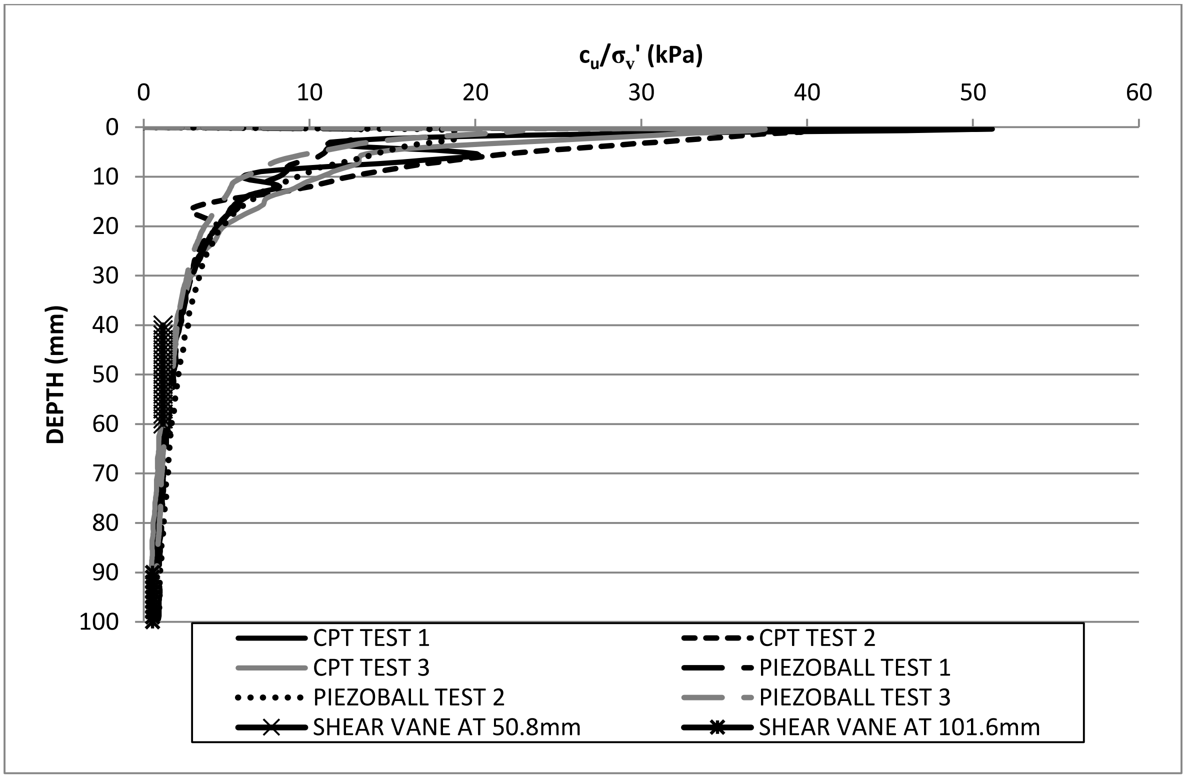

Figure 5.2: CPT/piezoball c_u/σ_v’ profile for 0 % fibre normally consolidated model.

Figure 5.3 shows the undrained shear strength profile determined for the 4 % fibre normally consolidated model. The corrected results from the shear vane did not compare well with either of the penetrometers or the back calculated undrained shear strengths from bearing capacity testing as the vane tests were carried out on samples with low effective stress. Corrected shear vane results of approximately 9 kPa were consistent with other shear vane results for the fibre models, where the undrained shear strength was under estimated relative to the other methods. Penetrometer strength varied considerably between the cone and piezoball probes used, with a discrepancy of 20 kPa at some depths; however each shear strength profile showed a relatively consistence strength profile with depth. Foundation profiles, as before, relate to the undrained shear strength near model surface. Results from the square and circular foundations compare well with each other; undrained shear strength determined for these foundation types reduced slightly with increases in size of the bearing area, Figure 5.3. The 30 x 60 mm foundation mobilised an average undrained shear strength of 65 kPa in the 4 % fibre content model, which was in excess of the 51 kPa mobilized by the 40 x 80 foundation. The trend of smaller bearing areas mobilising greater undrained shear strength was consistence throughout testing on the 4 % model.

The ratio of undrained shear strength to vertical effective stress for the 4 % normally consolidated model is shown in Figure 5.4. The piezoball produced the greater peak c_u/σ_v' ratio near the model surface, compared to the CPT. The ratio decreased with depth for both the piezoball and CPT results, with close correlations between each penetrometer. The shear vane values of c_u/σ_v' are shown as vertical lines corresponding to depths. Again the ratio of c_u/σ_v' is high through the model, higher than the 0.3 experienced in most cases. The presence of fibres increasing the undrained shear strength can account for the increase in ratio of c_u/σ_v'.

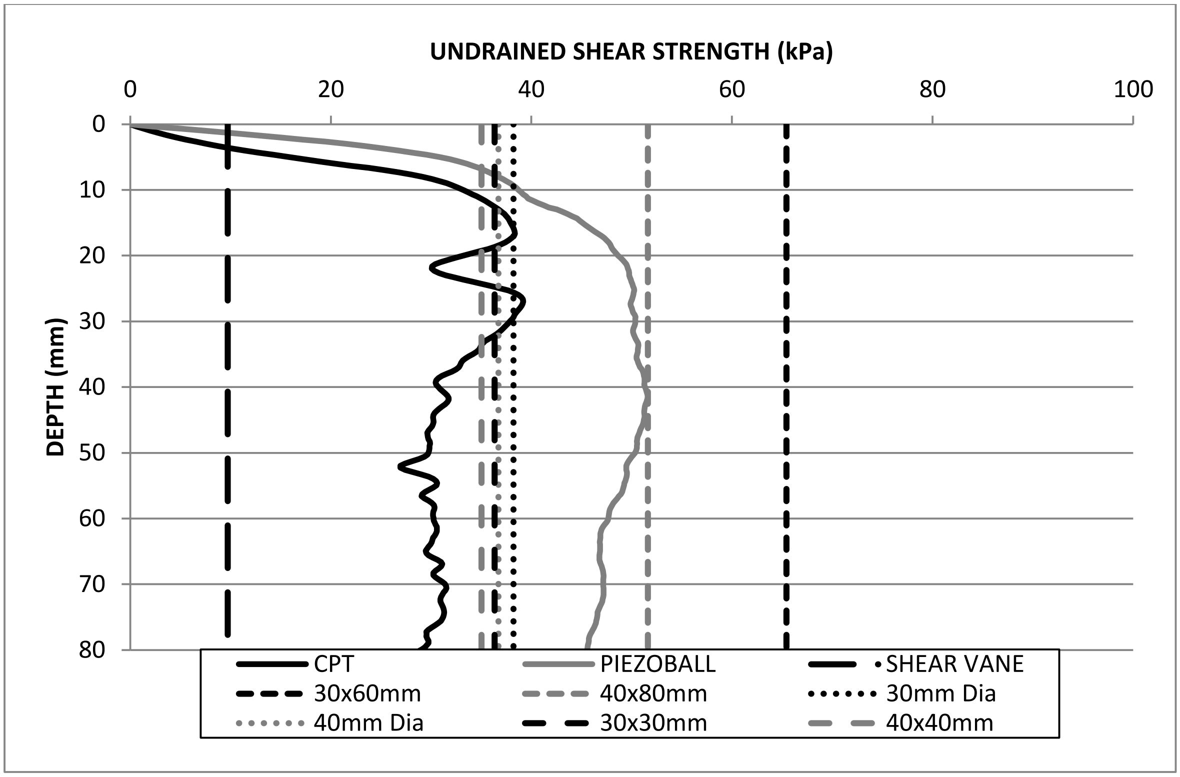

Figure 5.3: Undrained shear strength at maximum curvature for 4 % fibre normally consolidated model.

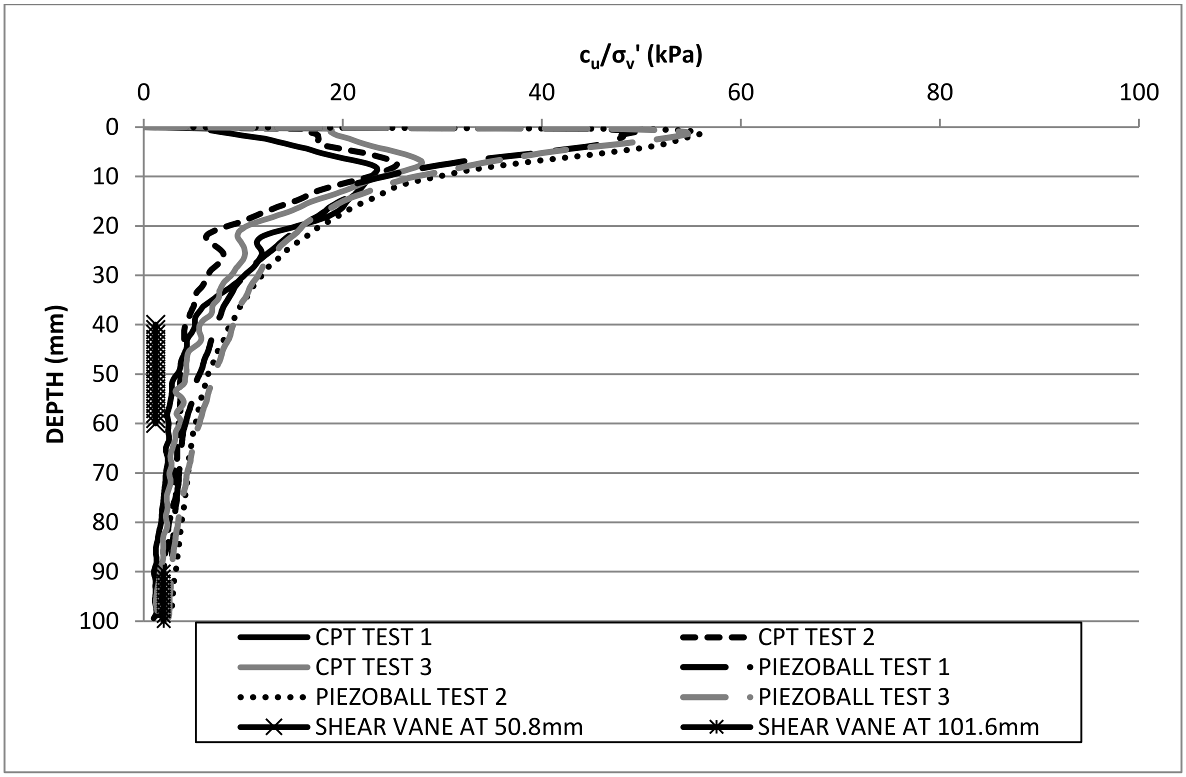

Figure 5.4: CPT/piezoball c_u/σ_v’ profile for 4 % fibre normally consolidated model.

In Figure 5.5, the undrained shear strengths determined for the 0 % fibre content over consolidated model are presented. Shear vane tests were unable to be carried out on a core of the 0 % fibre model. The CPT and piezoball penetrometers were in close agreement, showing constant undrained shear strength with depth. The piezoball averaged the peaks and troughs associated with the CPT in fibrous soils (Boylan *et al* 2011). The 40 mm width rectangular, square and 40 mm diameter circular foundations mobilised similar maximum undrained shear strengths of approximately 15 to 16 kPa in the 0 % model, which compared very well with the shear strength profile determined from CPT and piezoball testing. The 30 mm square and 30 mm diameter foundations determined undrained shear strength in the 0 % fibre content over consolidated model slightly higher than the 40 mm foundations and penetrometer tests results, at approximately 18 and 19 kPa respectively. The maximum undrained shear strength mobilised by the 30 x 60 mm foundation did not correlate well with undrained shear strengths mobilized by foundations where the width or diameter was 30 mm. The trend of smaller foundation bearing areas producing higher undrained shear strength mobilization was reversed in the case of the rectangular foundations for the 0 % fibre content over consolidated model.

In Figure 5.6 the ratio of c_u/σ_v' for both cone and piezoball penetrometers is shown; the piezoball results on average exhibited a greater peak c_u/σ_v' than the results generated from cone penetration testing. However comparison of the residual c_u/σ_v' ratio showed close correlation between the two sets of results with increased depth.

Undrained shear strength profiles corresponding to the 4 % fibre content over consolidated model are displayed in Figure 5.7. Strengths determined using bearing capacity and profiling methods for the 4 % fibre content model showed considerably more variation than those of the 0 % fibre content over consolidated model. Such variation may be attributed to the fibrous matter interacting with the penetrometers. The shear vane analysis showed peak strength of approximately 10 kPa, considerably less compared to those from profiling and back calculated from bearing capacity tests. The penetrometer profiles showed consistent shear strength with depth, where the piezoball results determined the undrained shear strength to be greater than that of the CPT. Foundations with 30 mm width or diameter showed considerable variation in undrained shear strengths mobilized for the 4 % fibre content over consolidated models, over a range of 32 kPa. The 30 x 60 mm foundation mobilised the greatest shear strength of 87 kPa for the foundations tested.

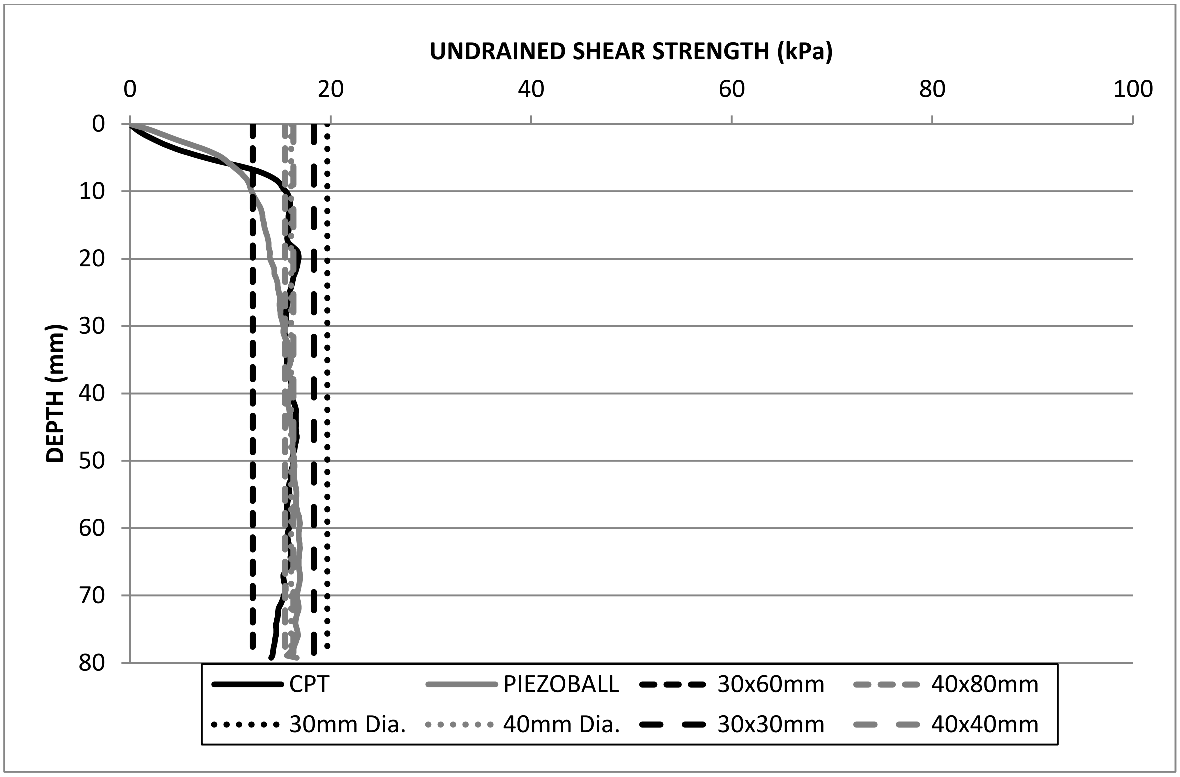

Figure 5.5: Undrained shear strength at maximum curvature for 0 % fibre over consolidated model.

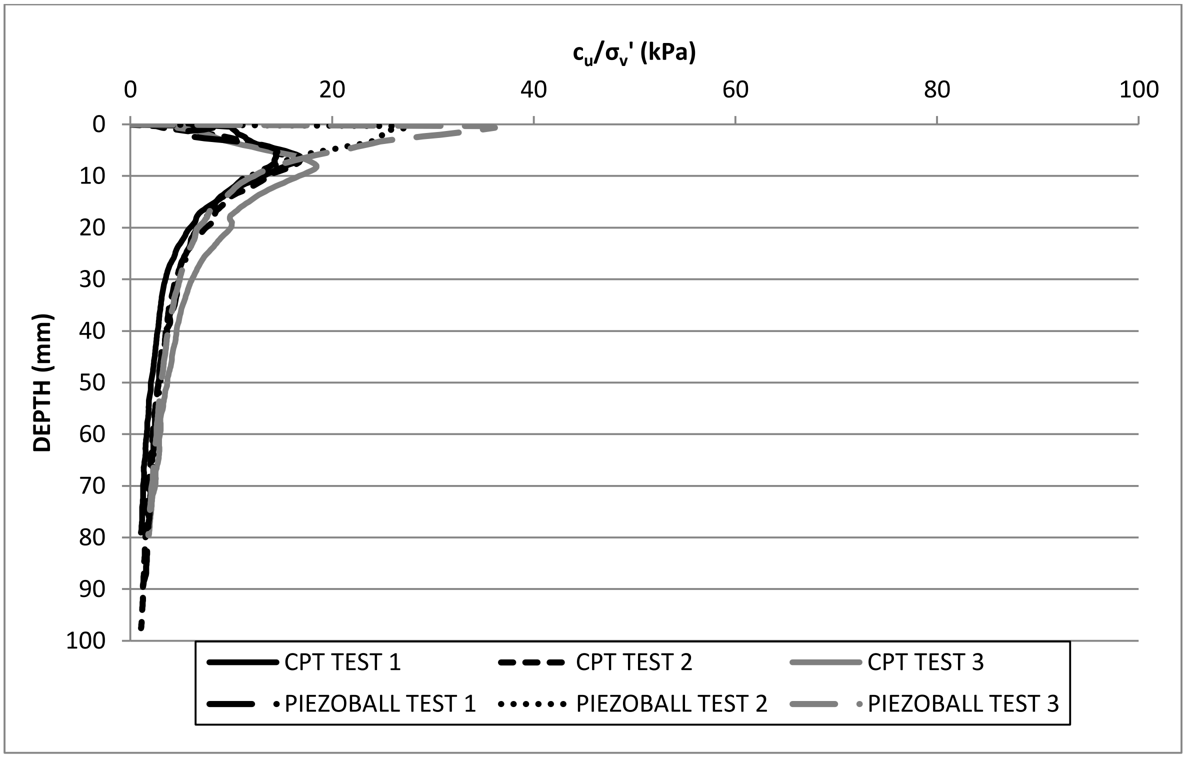

Figure 5.6: CPT/piezoball c_u/σ_v' profile for 0 % fibre over consolidated model.

The 30 mm diameter foundation mobilized the lowest undrained shear strength for the 0 % fibre content over consolidated model, less than the strength achieved with the 40 mm foundation. Foundations where the greatest dimensions was equal to 40 mm showed a closer correlation to other measured undrained shear strength mobilized, and was within a range of 60 to 67 kPa. Smaller foundation bearing areas produced greater undrained shear strengths for all foundation tests; the 30 mm diameter footing was an exception.

Figure 5.8 displays the ratios of c_u/σ_v' for both cone and piezoball penetrometers. Values for c_u/σ_v' were again high due to increased undrained shear strength as a result of the fibre content present. The piezoball results showed a greater peak c_u/σ_v' than the CPT near surface level, while the residual c_u/σ_v' also showed piezoball results generating a greater strength ratio. The analysis of shear vane results showed that the residual strength ratios were lower than the CPT and piezoball profiles.

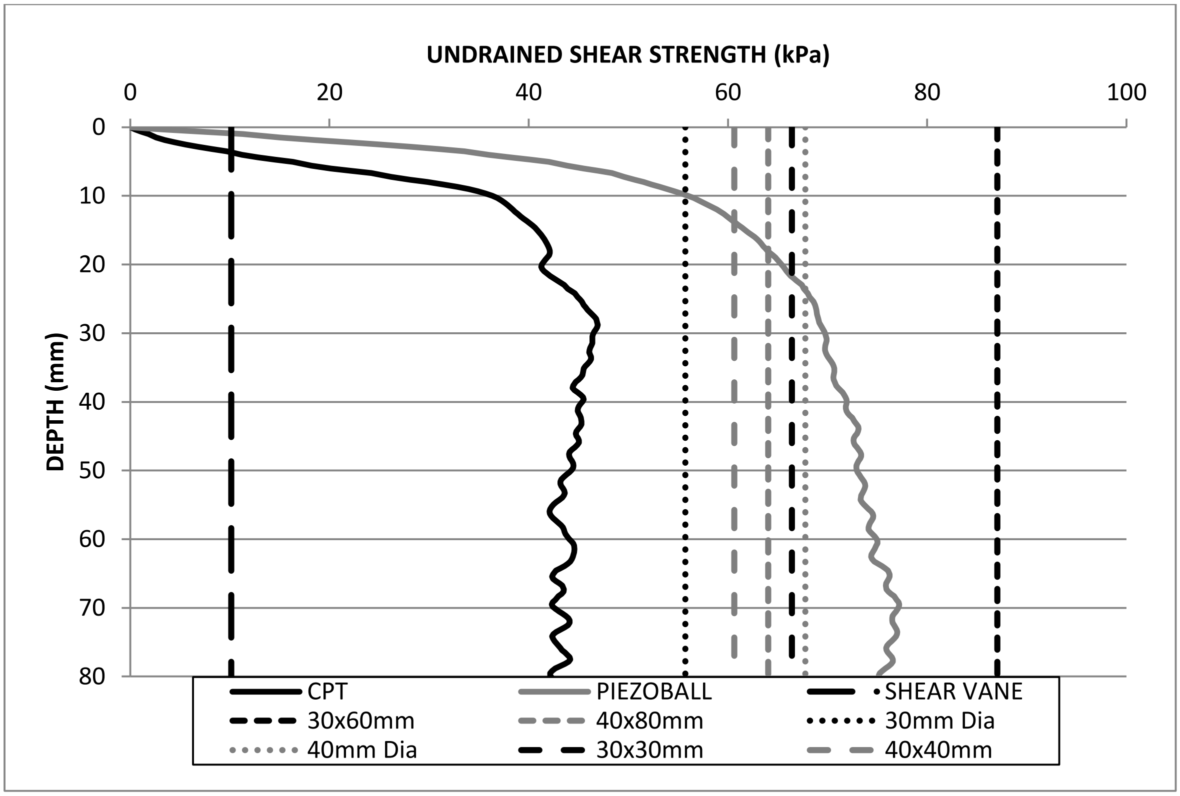

Figure 5.7: Undrained shear strength at maximum curvature for 4 % fibre over consolidated model.

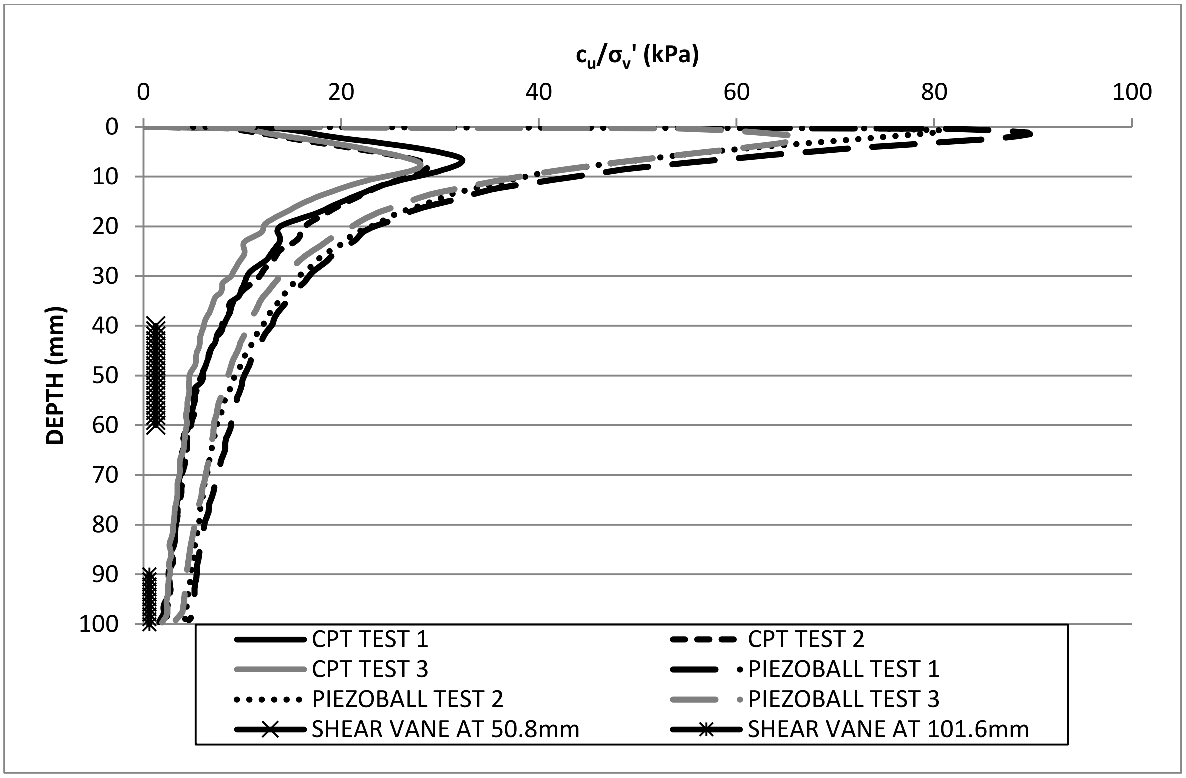

Figure 5.8: CPT/piezoball c_u/σ_v’ profile for 4 % fibre over consolidated model.

Comparison of undrained shear strength back calculated from bearing capacity testing in the 0 % fibre content normally consolidated model at locations of maximum curvature and 0.5 B/D, Figure 5.1 and 5.9, showed an increase in undrained shear strength with depth. The back calculated strengths at 0.5 B/D demonstrated improved correlation compared to the strengths at maximum load, for the majority of foundations tested. Foundations with a greater bearing area mobilized lower undrained shear strengths compared to the smaller foundations. At a depth of 0.5 B the 40 x 80 mm foundation mobilized undrained shear strength greater than both square foundations (30 x 30 mm and the 40 x 40 mm).

For the 0 % fibre content over consolidated model undrained shear strength was observed to increase at a depth of 0.5 B/D, Figure 5.10, compared to that at maximum curvature, Figure 5.5. The square foundations showed the greatest improvement in strength profile correlation when compared to the circular and rectangular foundations. The undrained shear strength mobilized by the 30 x 60 mm foundation remained the weakest of any foundation for the 0 % fibre content over consolidated model.

The undrained shear strength of the 4 % fibre content normally consolidated model increased for the 40 mm diameter and 40 mm square foundations only. The remaining foundations experienced a minimal decrease in shear strength mobilized. Increased variation in undrained shear strength mobilized for the square foundations at 0.5 B/D, Figure 5.11, was present compared to the strength at maximum curvature, Figure 5.3.

In relation to the 4 % over consolidated model at depths of 0.5 B/D, Figure 5.12, greater undrained shear strength was mobilization for all foundations apart from the 40 x 80 mm, compared to values at maximum curvature, Figure 5.7. Increased shear strength ranged from 6 kPa in the case of the 30 x 60 mm foundation to a constant undrained shear strength for the 40 mm diameter foundation.

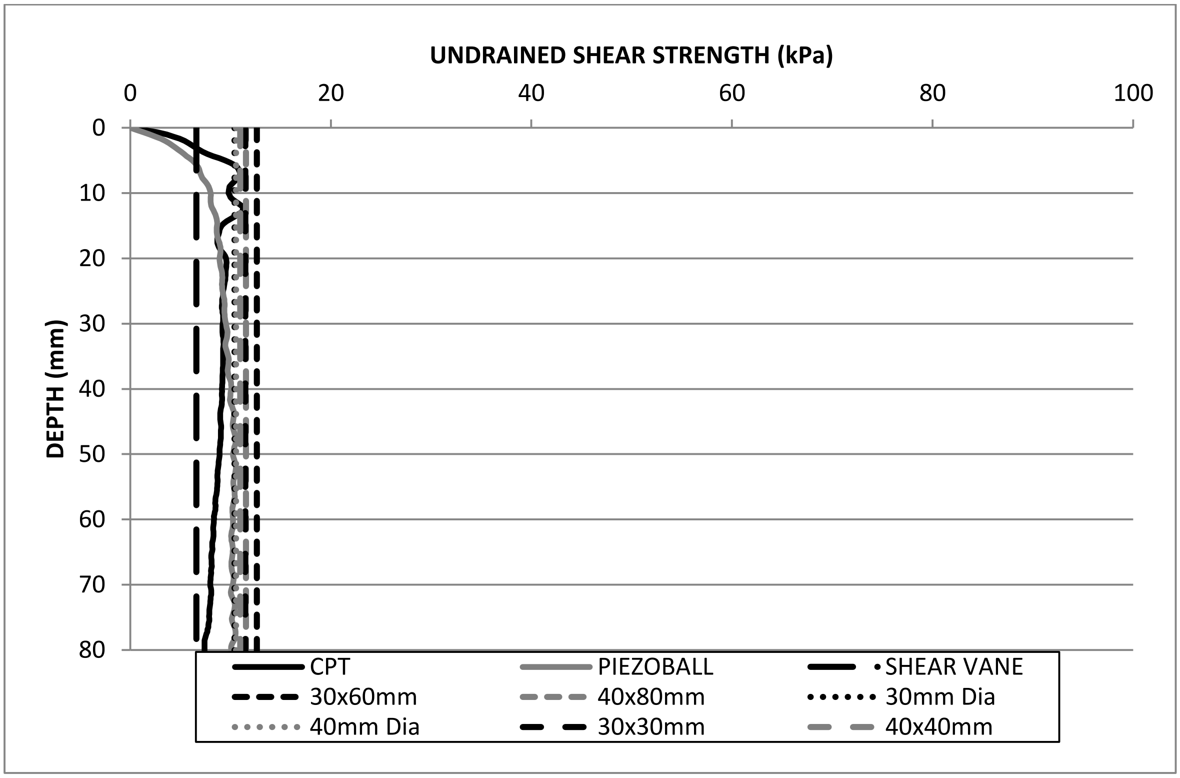

Figure 5.9: Undrained shear strength at 0.5B/D for 0 % fibre normally consolidated model.

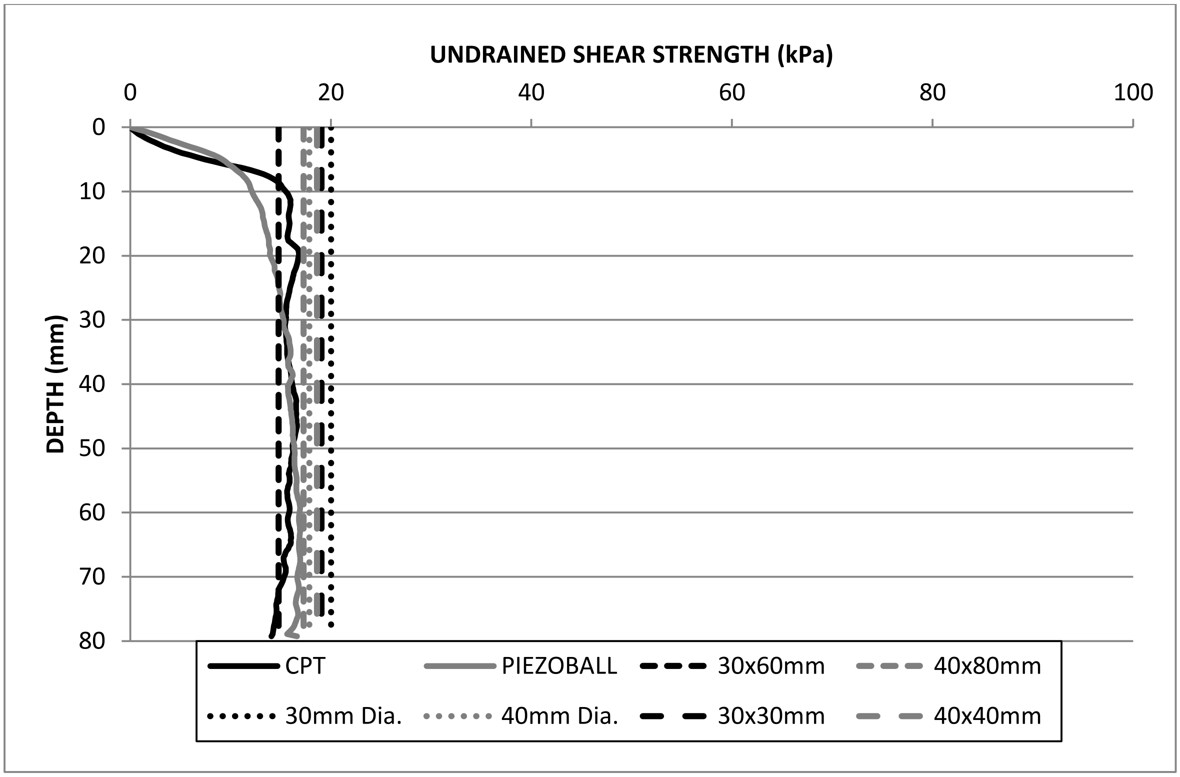

Figure 5.10: Undrained shear strength at 0.5B/D for 0 % fibre over consolidated model.

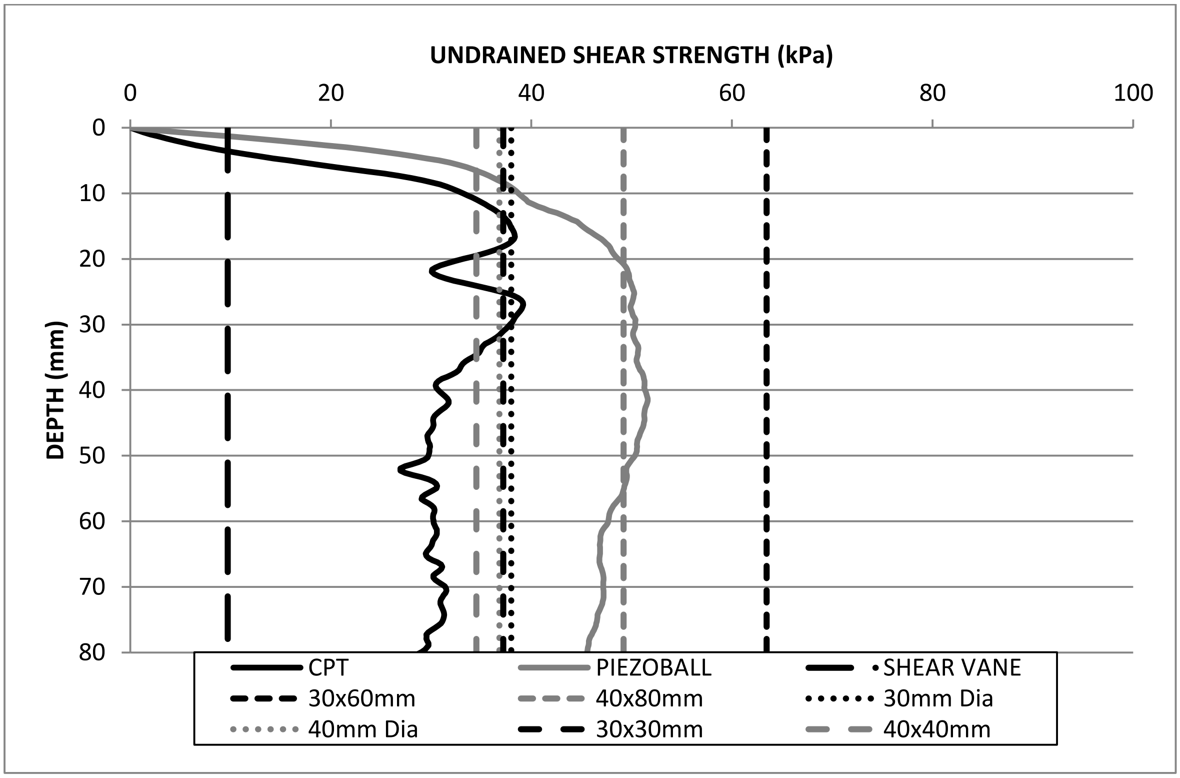

Figure 5.11: Undrained shear strength at 0.5B/D for 4 % fibre normally consolidated model.

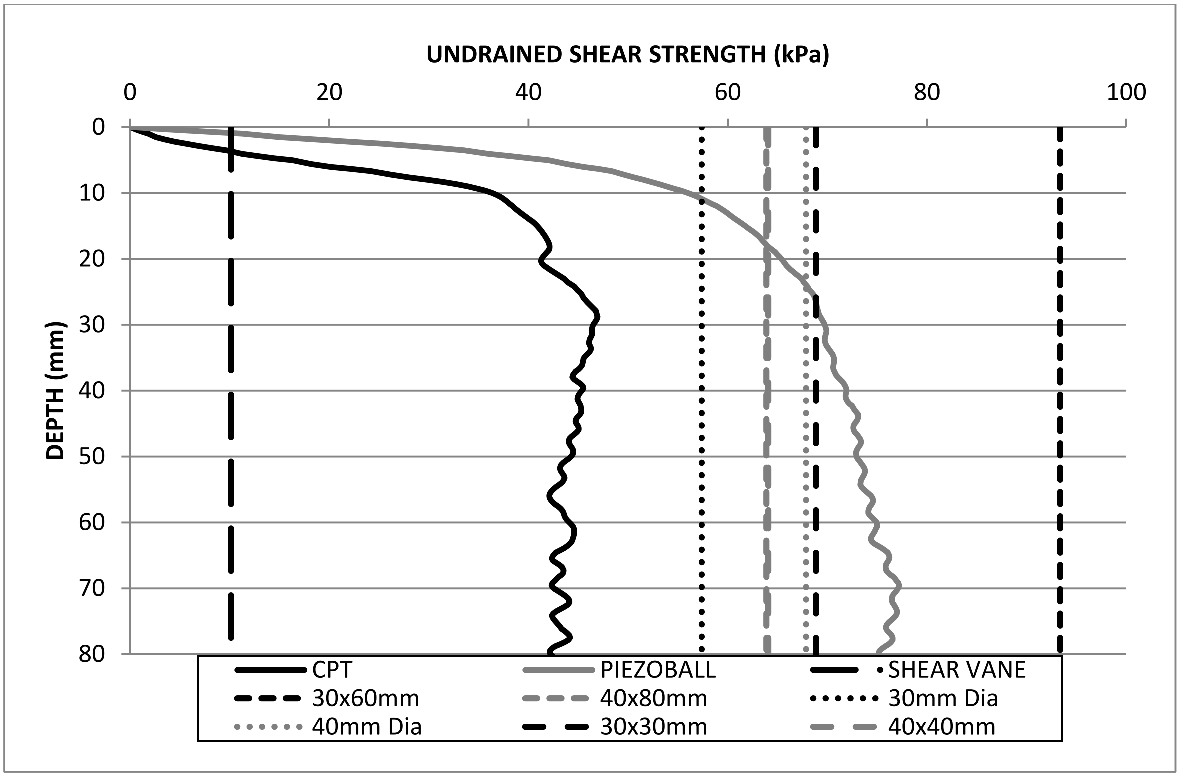

Figure 5.12: Undrained shear strength at 0.5B/D for 4 % fibre over consolidated model.

5.3 Influence of fibre content on undrained shear strength

The following sections examine the effect of fibre content on the different undrained shear strengths determined in this study. Comparisons are drawn between the strengths determined by bearing capacity analysis, penetrometer profiling and shear vane testing.

5.3.1 Penetrometer determination of undrained shear strength

Figure 5.13 and 5.14 display the variation in the undrained shear strength with fibre content for Test Series 1 and 2. The undrained shear strengths were determined by penetrometer profiling during the centrifuge modelling programme, laboratory shear vane tests were also carried out on model cores for comparison. The maximum tip resistance encountered during profiling was used to determine the maximum undrained shear strength for a particular fibre model. Shear vane tests were carried out at 3 depths in the extracted cores, the average values of strength through each model are presented in Figures 5.13 and 5.14.

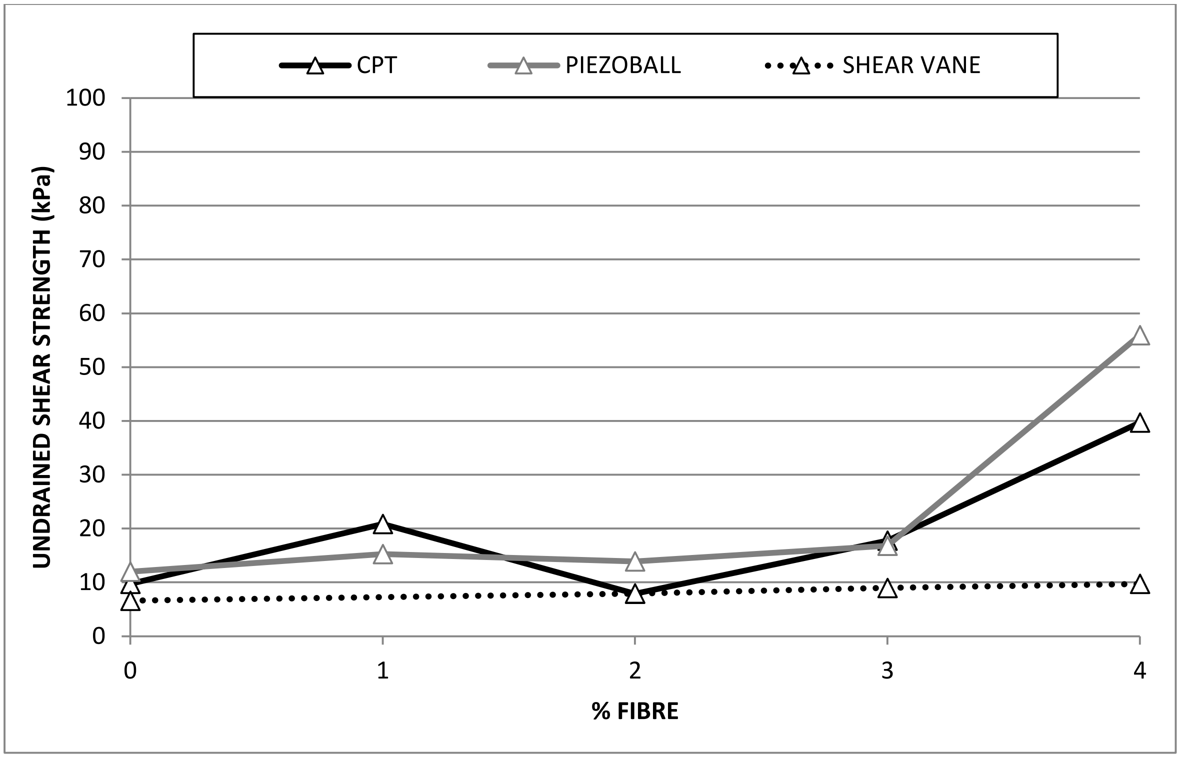

Figure 5.13: Shear strength results from profiling and shear vane testing in normally consolidated models.

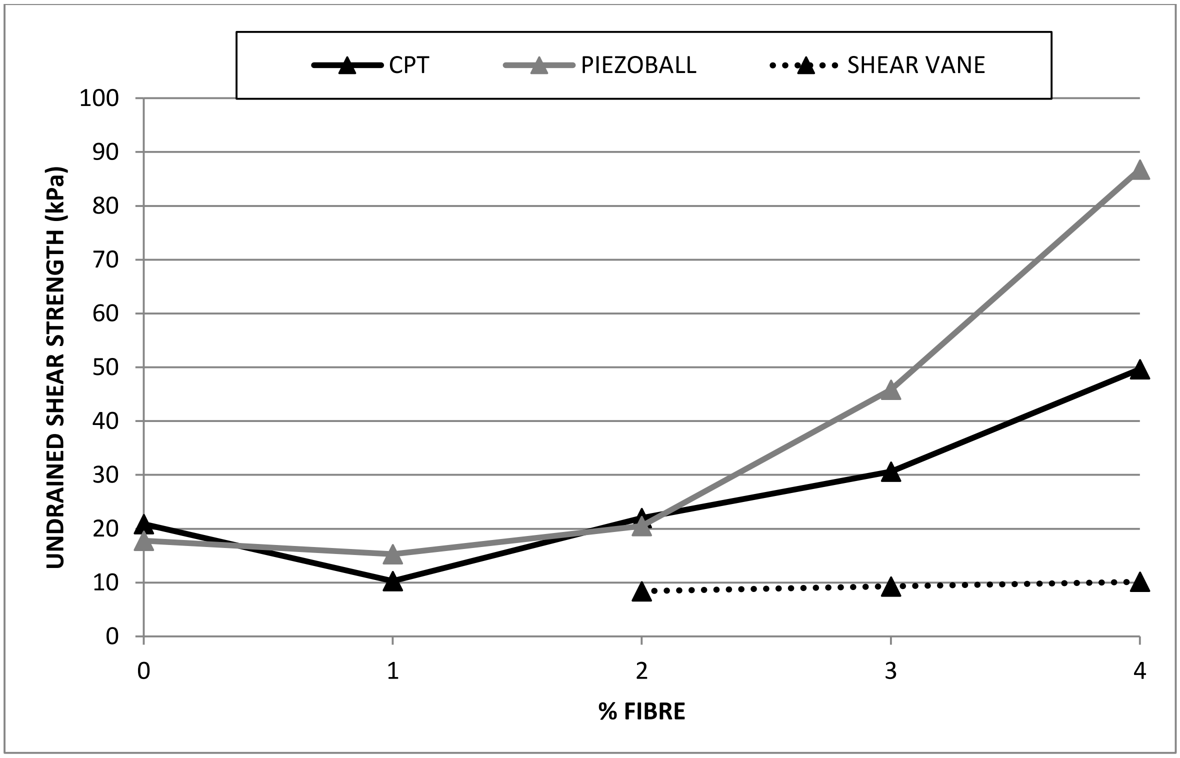

Figure 5.14: Shear strength results from profiling and shear vane testing in over consolidated models.

The penetrometer data in Test Series 1 was consistent throughout the model range tested, with minimal strength increase from 1 % to 3 % fibre content. Undrained shear strength increased dramatically with 4 % fibre content along with divergence in strength determined for the two penetrometers used, Figure 5.13. The shear vane tests conducted showed a rise in undrained shear strength with increased fibre content. Strength increase was gradual, each 1 % increase in fibre content resulted in less than 1 kPa increase in strength for all models tested. Vane tests on the 0 % model were in close agreement with the results from the penetrometers, however profiling recorded significant rises in strength for the 1 % fibre content normally consolidated model which was not seen in the vane results, Figure 5.13. For the 2 % fibre content model, strength decreased for both penetrometers when compared to the 1 % fibre content model. The CPT results showed shear strength for the 3 % model had increased but was still less than the 1 % model strength; the piezoball recorded a slightly higher strength than the CPT. At 4 % fibre content, the CPT showed shear strength had increased by 400 % of the vane results, while the piezoball strength had increased by approximately 550 % from the same level. Shear strength determined by the shear vane continued to increase with increased fibre content, reaching 9.7 kPa at 4 % fibre content, significantly lower than strength measured in the CPT and piezoball for the same model.

Results of Test Series 2 were consistent throughout the model range profiled, with the penetrometers showing very good correlation of results at 2 % fibre content or less; scatter in the data became apparent for 3 % and 4 % fibre content, Figure 5.14. Shear vane analysis of model cores showed an increase in shear strength with increased fibre content, with peak shear strength of 10.1 kPa at 4 % fibre content. Vane tests on over consolidated models determined strengths to be slightly higher than that of normally consolidated models. The profiling results of the 1 % fibre content over consolidated model displayed a reduction in shear strength for both penetrometers when compared to the 0 % fibre content. This was in contrast to that observed for normally consolidated models where undrained shear strength increased. For the 2 % model the piezoball and CPT results were in close agreement, and exhibited a strength level comparable to the 0 % model. CPT and piezoball data for the 3 % model showed a considerable increase in strength, with the piezoball mobilising a maximum strength 15 kPa greater than that of the CPT, Figure 5.14. Profiling on the 4 % model resulted in shear strengths of 50 and 87 kPa for the CPT and piezoball respectively.

5.3.2 Influence of fibre content on back calculated undrained shear strength

Figure 5.15 shows the back calculated undrained shear strength for bearing resistance taken from Test Series 1. Shear strength was consistent throughout the models tested with 3 % fibre content or less, showing that such models displayed constant undrained shear strength; some variation was present which can be attributed to the various shape and size of foundations utilized. Strength increased dramatically for 4 % fibre content, with rectangular footings mobilizing the greatest strengths. There was reduced scatter in the circular and square foundation strengths mobilized for the 4 % fibre content model, compared to the rectangular foundations. Results for the rectangular foundation mobilized consistent undrained shear strength profiles for the two sizes investigated in the 4 % fibre content model; the 30 x 60 mm foundation produced slightly greater mobilization of shear strength for each fibre model tested. The undrained shear strength reduced for tests carried out on models with 2 and 3 % fibre content. The circular footing tests exhibited similar behaviour to the rectangular, where the smaller bearing areas produced greater strength mobilization in most cases. Undrained shear strength increased by approximately 50 % between the 3 % and 4 % fibre content models for circular foundation tests. Undrained shear strength for models tested with the 30 mm square foundation showed a linear increase in strength, with some reduction in the 3 % fibre content model. The 40 x 40 mm foundation showed a near linear increase in shear strength mobilization with increased fibre content, however, on average strength was slightly lower than that mobilized for the 30 mm square footing.

Comparisons drawn between the shear strengths at maximum curvature and strengths at a depth of 0.5 B/D showed a modest increase in undrained shear strength for most cases, Figure 5.16. Such increased undrained shear strengths may be attributed to the effects of strain hardening. Where strength mobilization was weaker, this corresponded to the occurrence of constant residual shear strength or models that displayed strain softening.

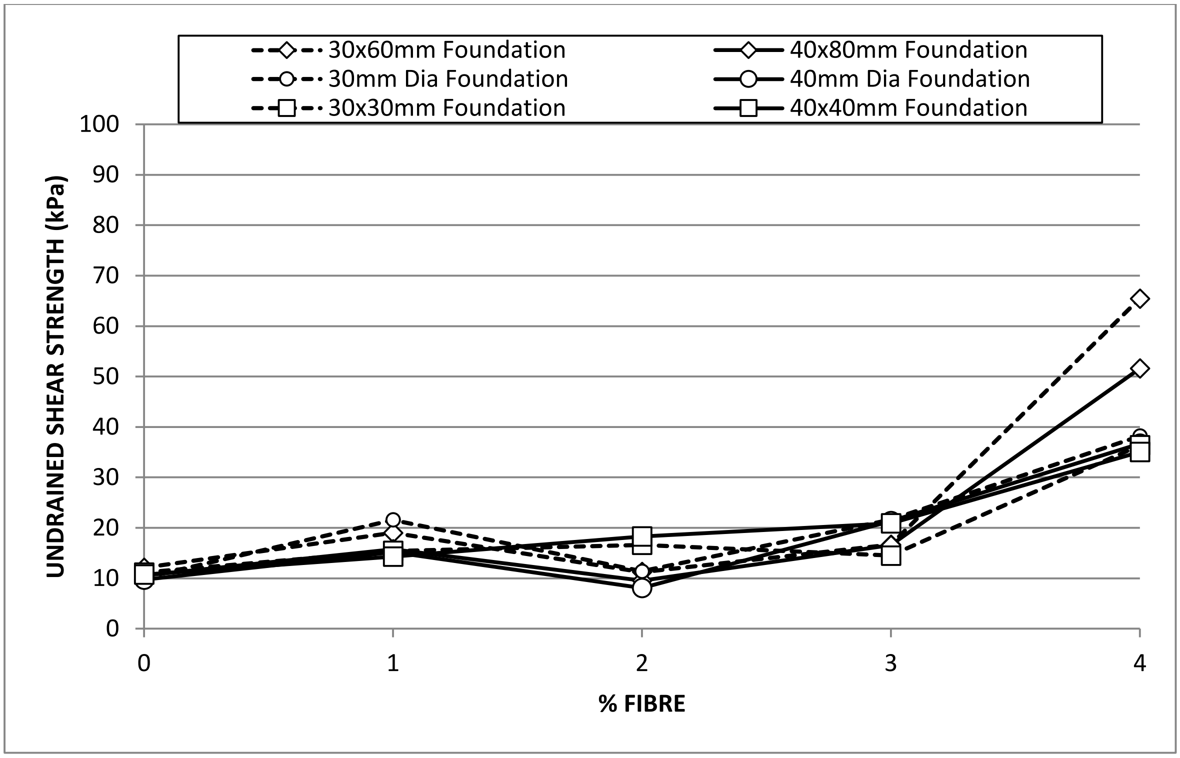

Figure 5.15: Shear strength from bearing capacity results at maximum curvature in normally consolidated models.

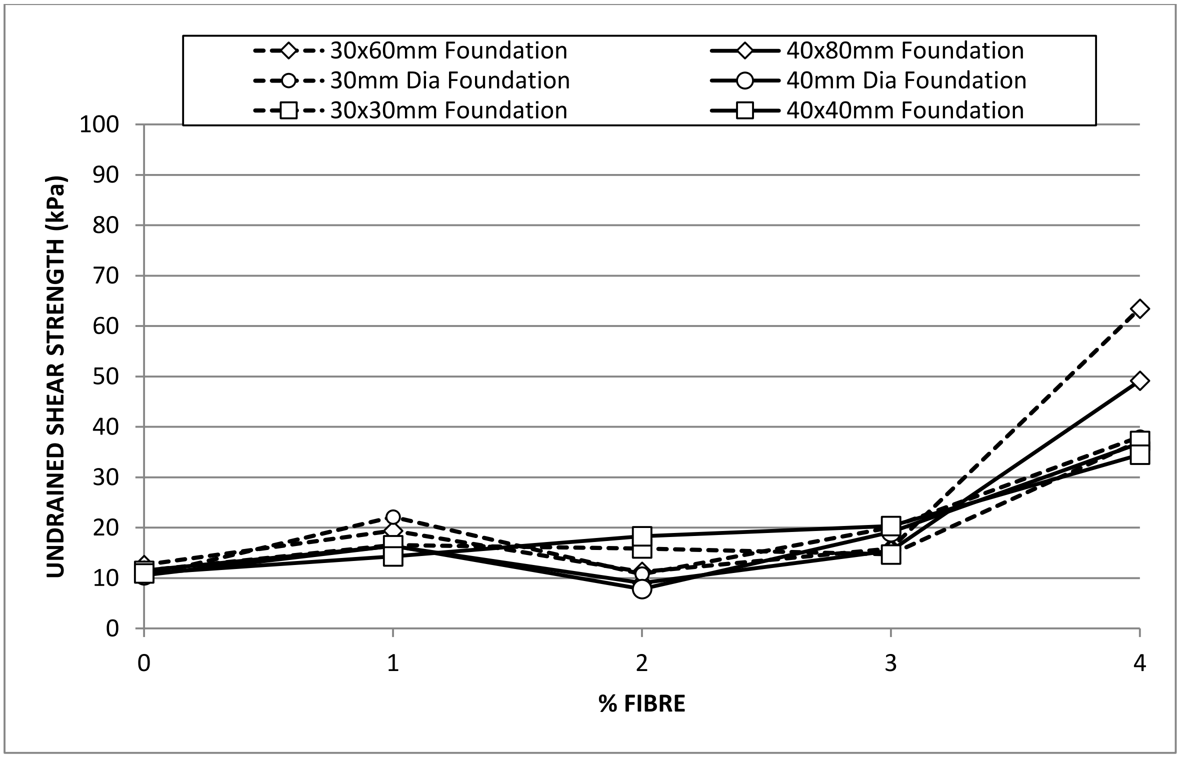

Figure 5.16: Shear strength from bearing capacity results at 0.5B/D depth in normally consolidated models.

The influence of fibres on the undrained shear strength of over consolidated models can be seen in Figure 5.17. Shear strength increased with increasing fibre content with a more pronounced increase than that observed in the normally consolidated models. The effects of strain hardening in the over consolidated models also contributed to rise in undrained shear strength compared to the normally consolidated models. Scatter in the undrained shear strengths increased dramatically at 3 % fibre content or greater. Strength profiles of the same foundation types showed good correlation with each other throughout Test Series 2. The undrained shear strength mobilized for tests conducted with the 30 x 60 mm foundation showed an almost linear increase in strength with increasing fibre content. The 40 x 80 mm footing failed to mobilise shear strength levels comparable with those of the 30 x 60 mm and on average was 12 kPa less. The undrained shear strength mobilized by the 30 mm diameter foundation decreased from 67 kPa in the 3 % fibre content over consolidated model to 57 kPa when tested on the 4 % model, which may indicate that the strength mobilised at 3 % fibre content was abnormally high. Shear strength for the 4 % fibre model when tested with the 40 mm foundation appeared to be reaching a plateau of 68 kPa. Tests conducted with square foundations showed a gradual increase in undrained shear strength with increasing fibre content. In contrast to the rectangular and circular foundations, the strength profiles for the square foundations did not show a dramatic increase in strength for the 3 % fibre content model. However shear strength increased rapidly with 4 % fibre content with a difference of almost 40 kPa mobilised between the 40 mm and 30 mm square foundations when fibre content was increased from 3 % to 4 %, Figure 5.17.

The undrained shear strength results at a depth of 0.5 B/D were found to increase in magnitude for the majority of models tested, Figure 5.18. Strain hardening effects became more prominent with increasing depth. Undrained shear strength reduced almost uniformly for tests conducted on the 3 % fibre model, Figure 5.18. Such reduction in strength was minimal, but consistence, and may be a result of strain softening in the 3 % fibre model.

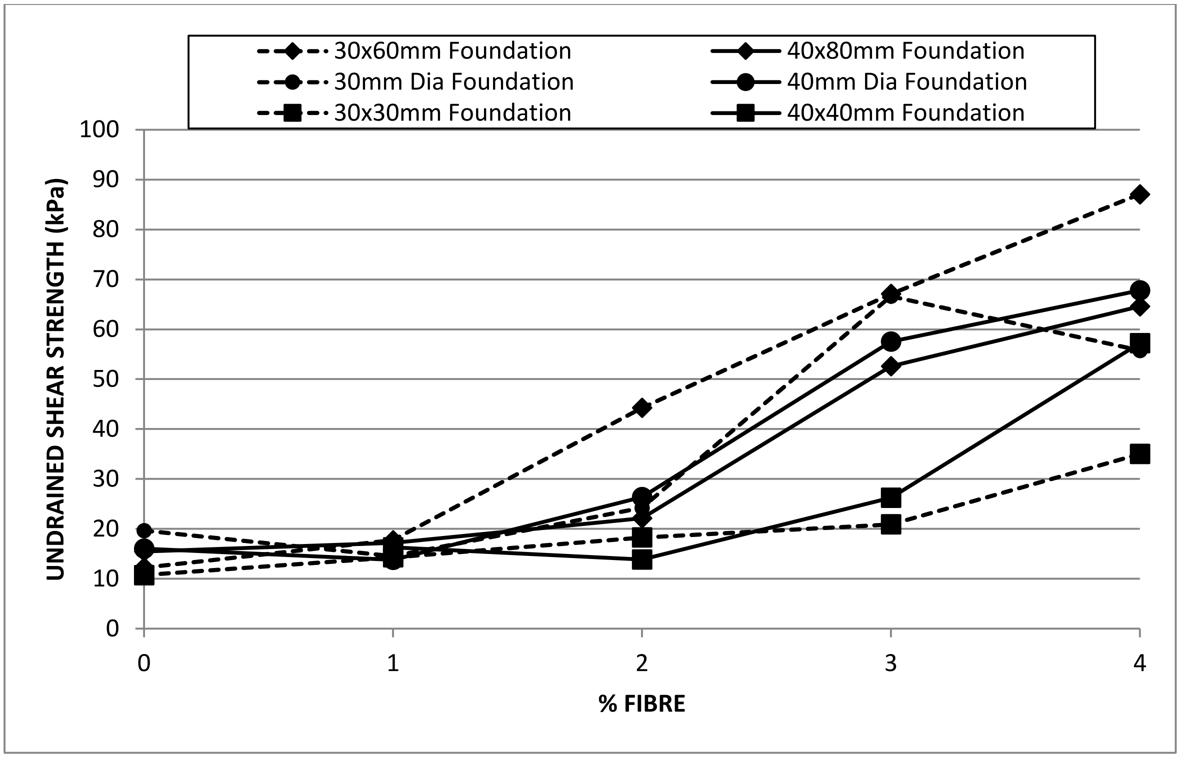

Figure 5.17: Shear strength from bearing capacity results at maximum curvature in over consolidated models.

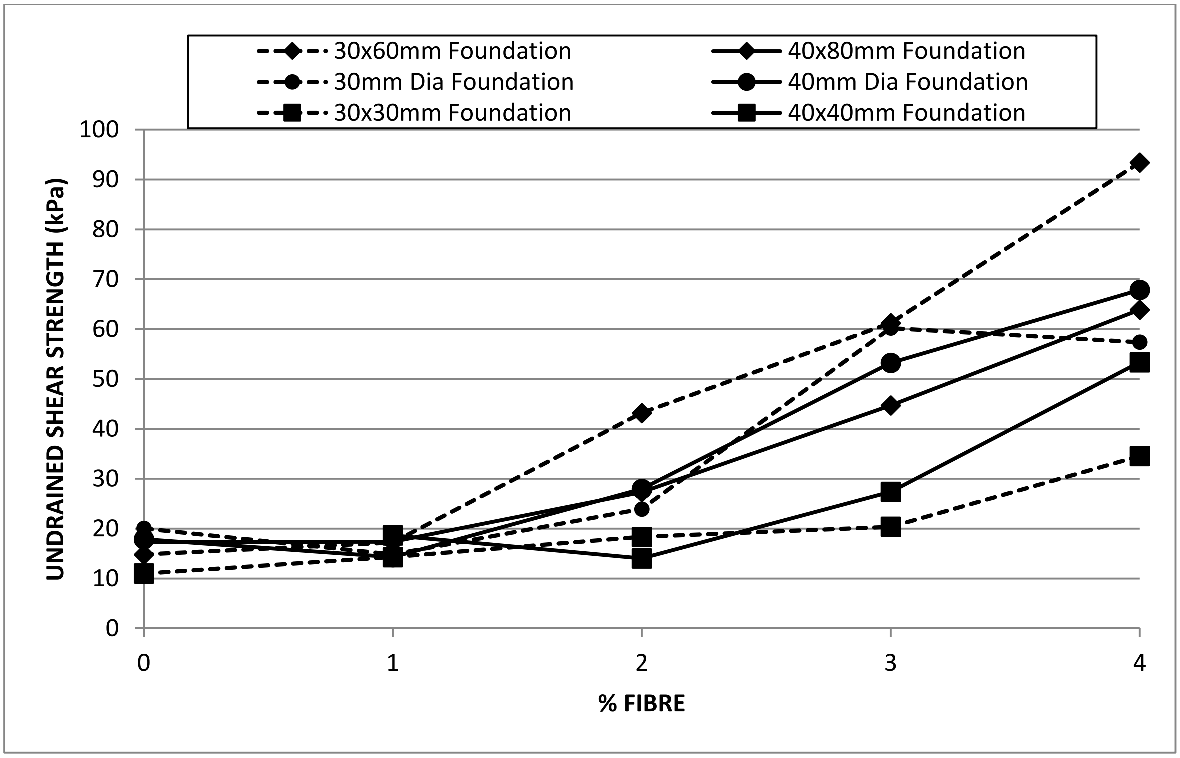

Figure 5.18: Shear strength from bearing capacity results at 0.5B/D depth in over consolidated models.

5.3.3 Comparison of undrained shear strength from shear vane and bearing capacity analysis

Determination of undrained shear strengths at maximum curvature from back calculated bearing capacity testing and shear vane tests are presented in Figures 5.19 to 5.24. Both methods of strength determination showed that increased fibre content resulted in increased undrained shear strength. Back calculation of undrained shear strength, using the method described in Section 3.6.1 of Chapter 3, resulted in significantly higher shear strength when compared to the shear vane data of corresponding fibrous models. Back calculated values for over consolidated models showed increased undrained shear strength compared to normally consolidated models for bearing tests; shear vane tests also produced higher peak strengths for over consolidated models. Undrained shear strengths determined at depths equal to 0.5 times the breath or diameter of foundations showed increased back calculated undrained shear strength from bearing capacity tests, Figures 5.25 to 5.30. Models where the undrained shear strength reduced at maximum curvature or at depths of 0.5 B/D correspond to cases of constant residual strength or strain softening outlined in Sections 4.3.4 and 4.3.5, of Chapter 4.

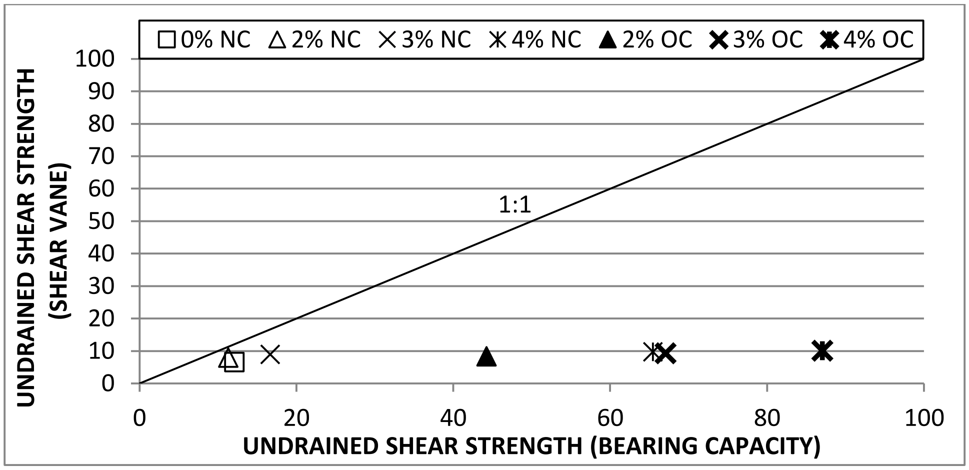

Figure 5.19: Undrained shear strength estimated from shear vane and bearing capacity at maximum curvature for a 30x60 mm foundation.

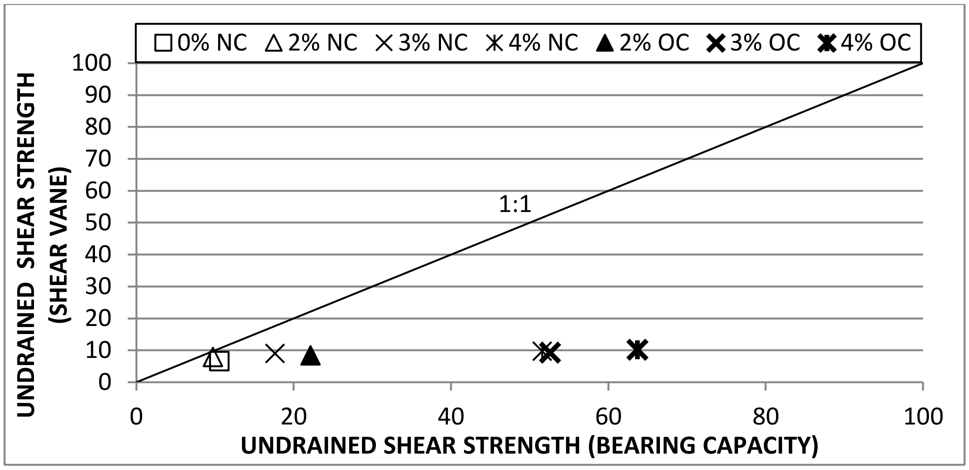

Figure 5.20: Undrained shear strength estimated from shear vane and bearing capacity at maximum curvature for a 40x80 mm foundation.

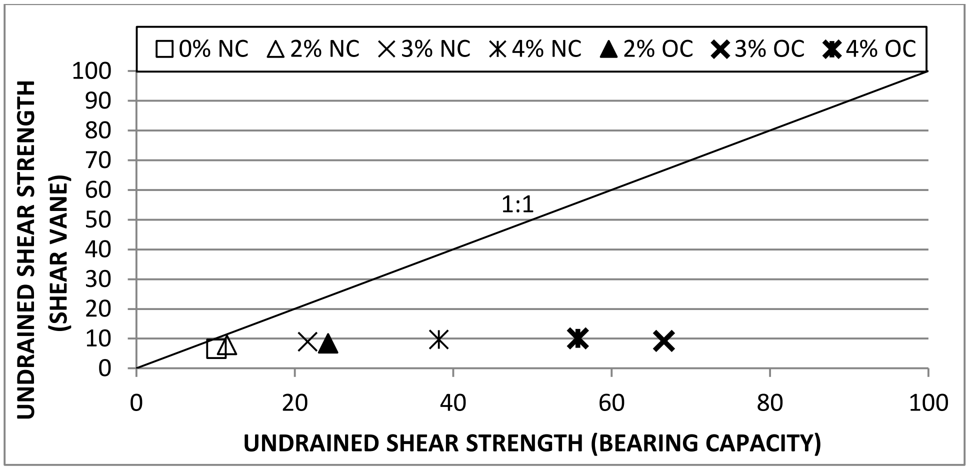

Figure 5.21: Undrained shear strength estimated from shear vane and bearing capacity at maximum curvature for a 30 mm diameter foundation.

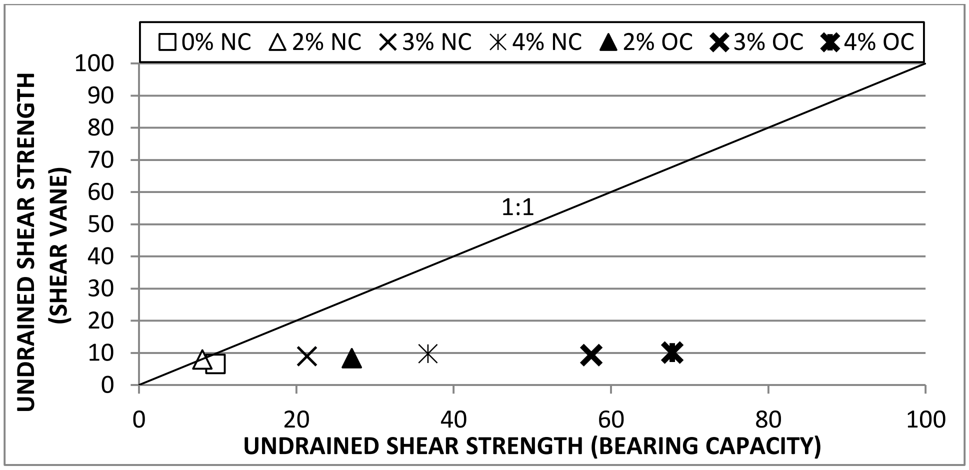

Figure 5.22: Undrained shear strength estimated from shear vane and bearing capacity at maximum curvature for a 40 mm diameter foundation.

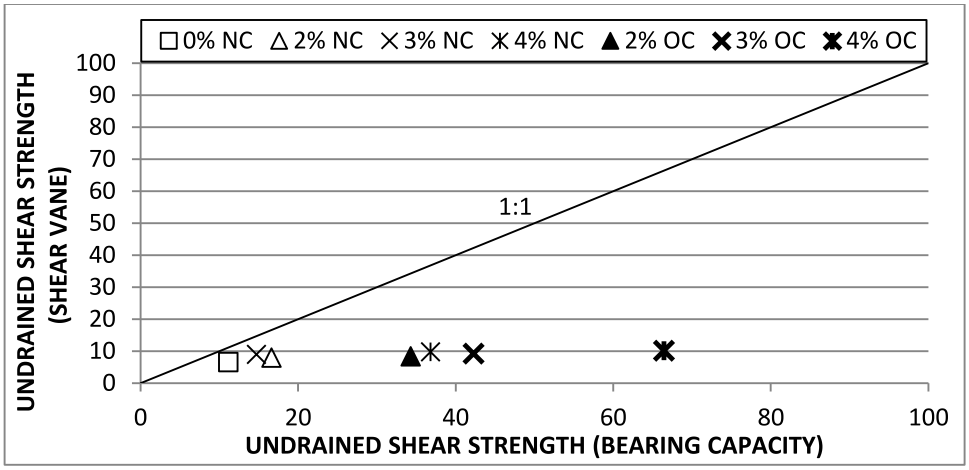

Figure 5.23: Undrained shear strength estimated from shear vane and bearing capacity at maximum curvature for a 30x30 mm foundation.

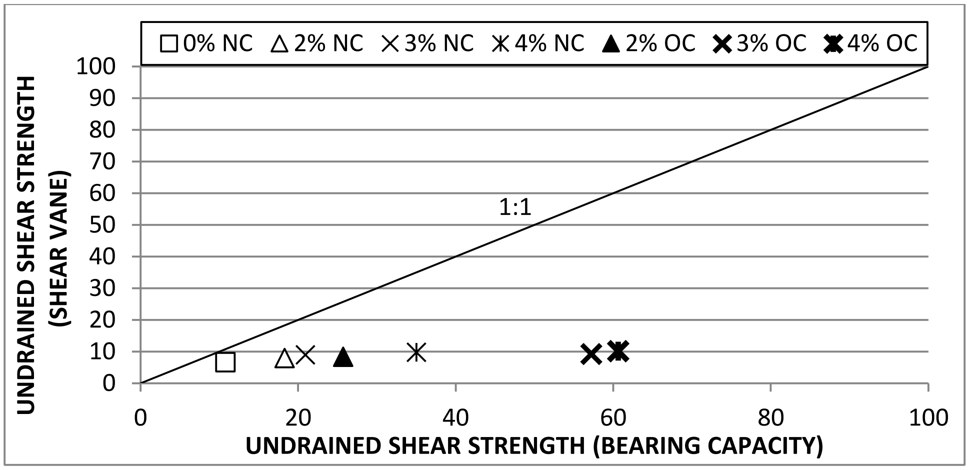

Figure 5.24: Undrained shear strength estimated from shear vane and bearing capacity at maximum curvature for a 40x40 mm foundation.

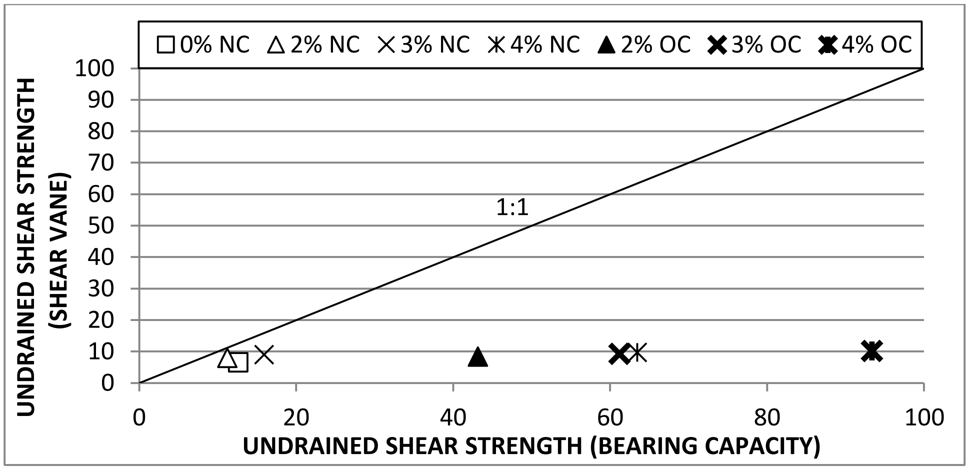

Figure 5.25: Undrained shear strength estimated from shear vane and bearing capacity at a depth of 0.5B for a 30x60 mm foundation.

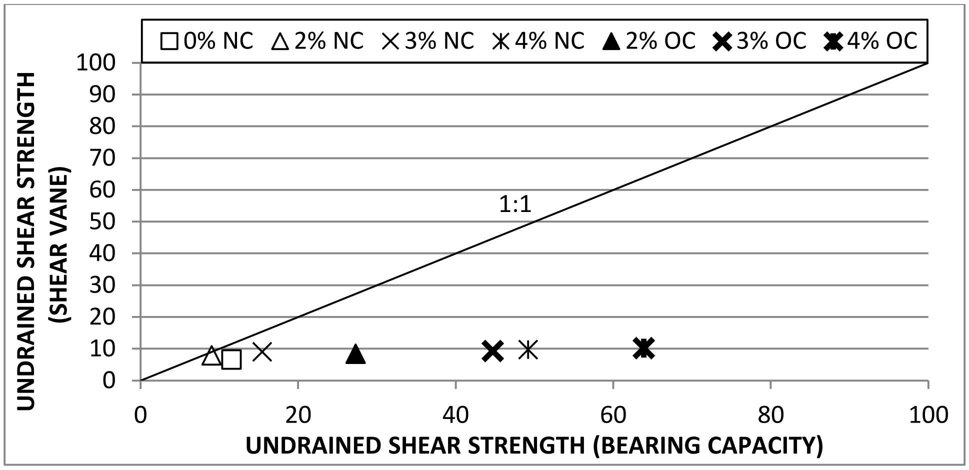

Figure 5.26: Undrained shear strength estimated from shear vane and bearing capacity at a depth of 0.5B for a 40x80 mm foundation.

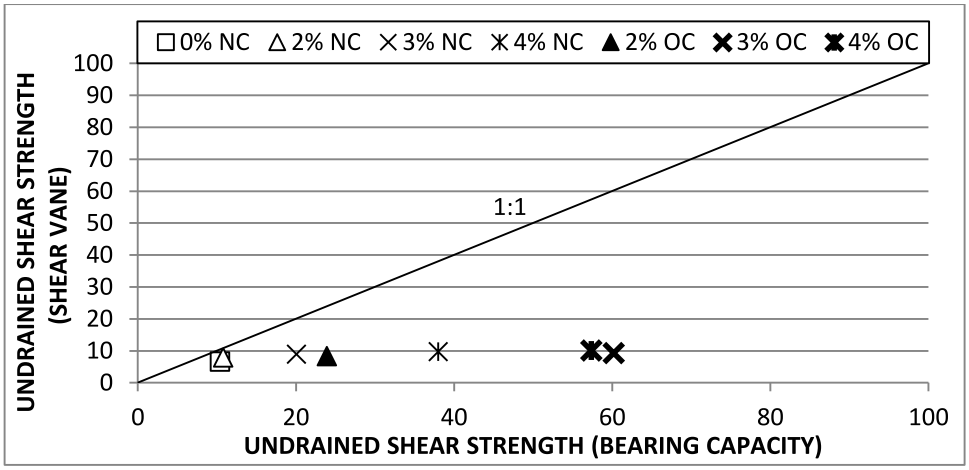

Figure 5.27: Undrained shear strength estimated from shear vane and bearing capacity at a depth of 0.5D for a 30 mm diameter foundation.

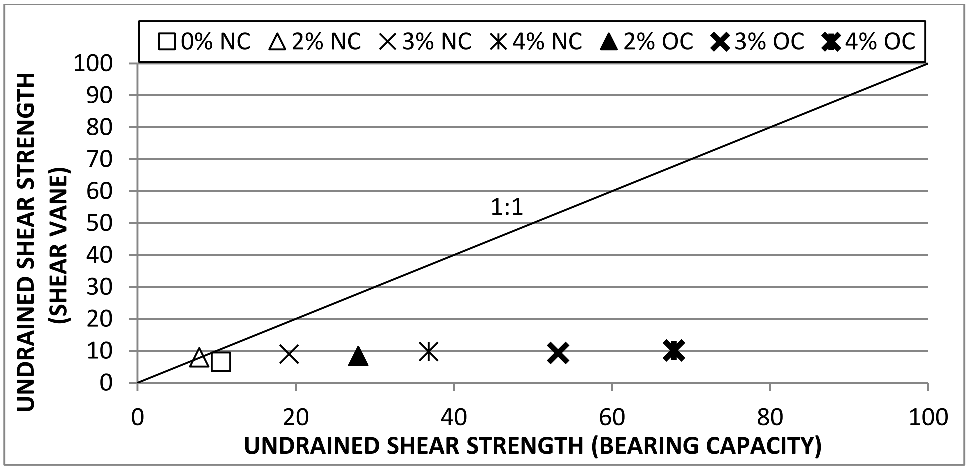

Figure 5.28: Undrained shear strength estimated from shear vane and bearing capacity at a depth of 0.5D for a 40 mm diameter foundation.

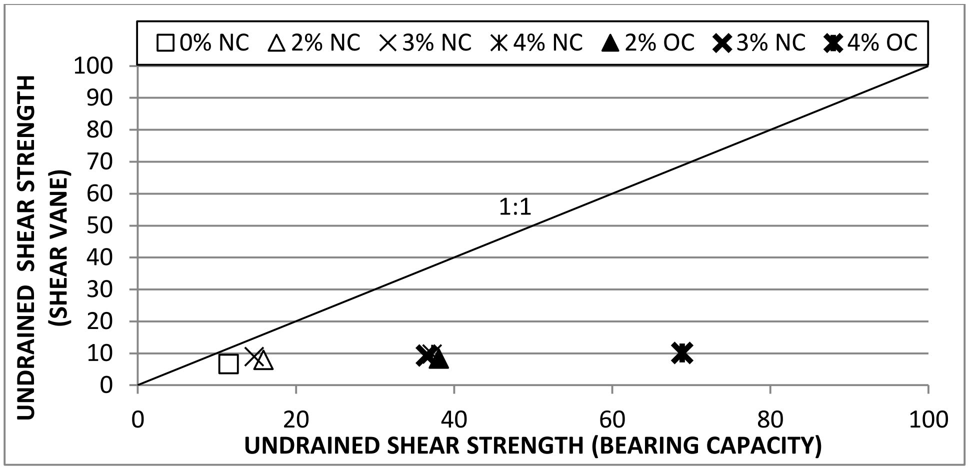

Figure 5.29: Undrained shear strength estimated from shear vane and bearing capacity at a depth of 0.5B for a 30x30 mm foundation.

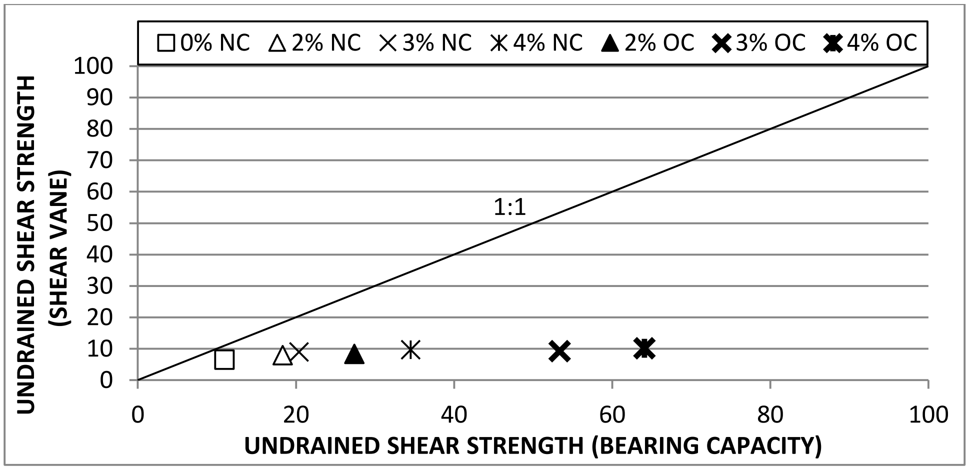

Figure 5.30: Undrained shear strength estimated from shear vane and bearing capacity at a depth of 0.5B for a 40x40 mm foundation.

5.3.4 Comparison of undrained shear strength from CPT and bearing capacity analysis

Figures 5.31 to 5.36 show the comparison between the undrained shear strength determined at maximum curvature in bearing resistance analysis and shear strength determined from CPT profiling of the same models. In the majority of over consolidated models the back calculated values of shear strength were greater than CPT results, Figure 5.31 and 5.32. Normally consolidated models showed a close correlation to the CPT undrained shear strength; however in the majority of cases the back calculated undrained shear strength was greater than that from the CPT analysis. Over consolidated models with fibre content of 1, 2, 3 and 4 %, along with the 4 % fibre content normally consolidated model, exhibit undrained shear strength back calculated from tests with the 30 x 60 mm foundation approximately twice that of the strength determined using the CPT, Figure 5.31. The remaining models tested showed some scatter in the results, with a close correlation in the majority of cases. The normally consolidated model of 4 % fibre content and over consolidated models with 3 % and 4 % fibre content exhibit greater undrained shear strengths from bearing capacity calculations compared to CPT results. The undrained shear strength results back calculated from the 30 mm diameter foundation tests showed a good correlation with the CPT results, for both normally and over consolidated models, Figure 5.33.

The undrained shear strength mobilized by the 40 mm diameter foundation showed good correlation for the majority of models, Figure 5.34, but with slightly more scatter than the 30 mm diameter footing, Figure 5.53. The undrained shear strength mobilized by the 30 mm square foundation showed mixed correlations in Figure 5.35; the 1, 2, and 3 % fibre content over consolidated models, along with the 2 % fibre content normally consolidated model, showed back calculated undrained shear strengths almost double the CPT values. The remaining model results showed good correlation, with some scatter. The undrained shear strength results from the 40 mm square foundation tests, Figure 5.36, showed scatter between the CPT and back calculated results of undrained shear strength, similar to the 30 x 30 mm foundation. The 3 % fibre content over consolidated and 2 % fibre content normally consolidated models exhibited back calculated undrained shear strength to be almost twice that of CPT values. Figures 5.37 to 5.42 summarises the comparison between back calculated undrained shear strength at a depth corresponding to 0.5 B/D and strength determined from CPT results. The back calculated undrained shear strength increased with depth. The effects of strain hardening resulted in increased undrained shear strength, particularly in the case of over consolidated models.

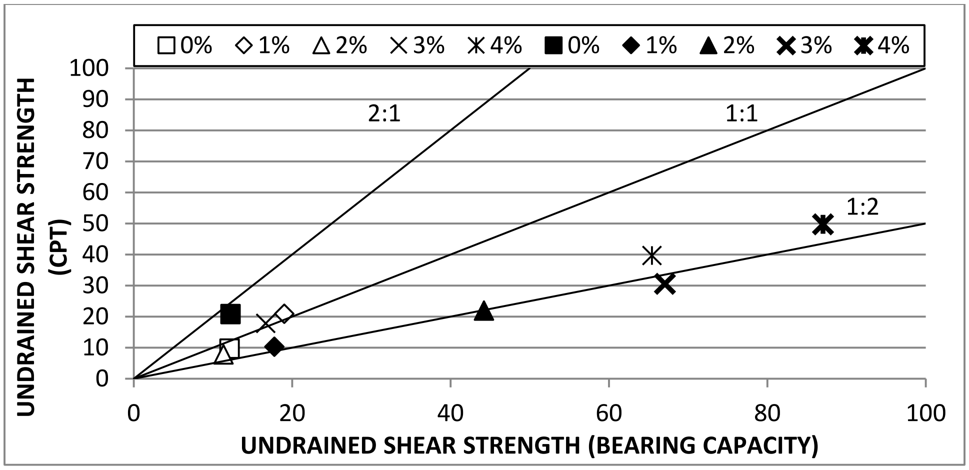

Figure 5.31: Undrained shear strength estimated from CPT and bearing capacity at maximum curvature for a 30x60 mm foundation.

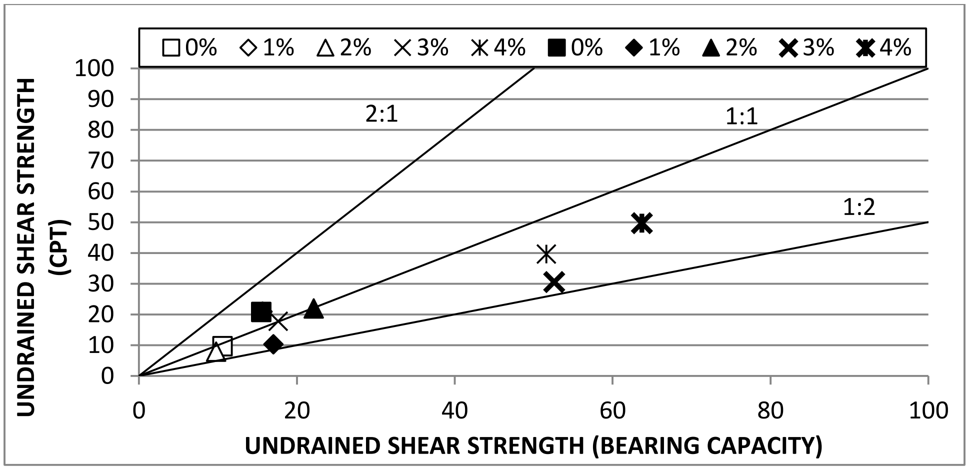

Figure 5.32: Undrained shear strength estimated from CPT and bearing capacity at maximum curvature for a 40x80 mm foundation.

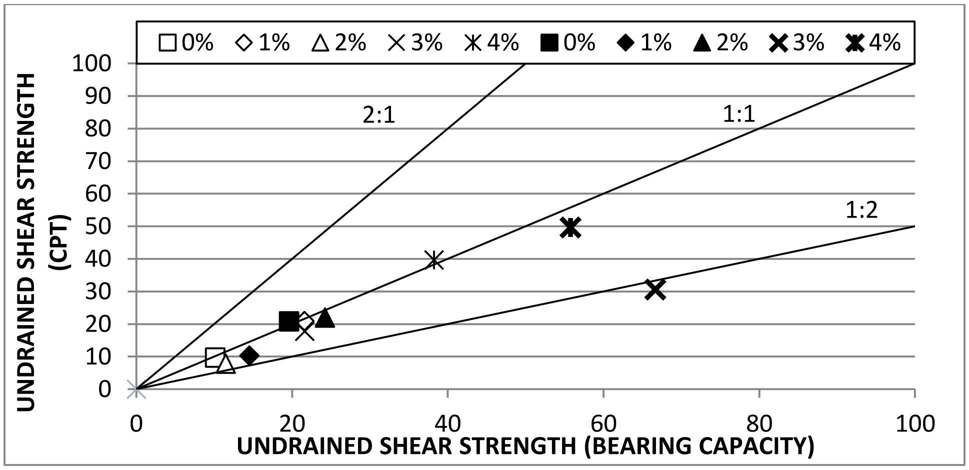

Figure 5.33: Undrained shear strength estimated from CPT and bearing capacity at maximum curvature for a 30 mm diameter foundation.

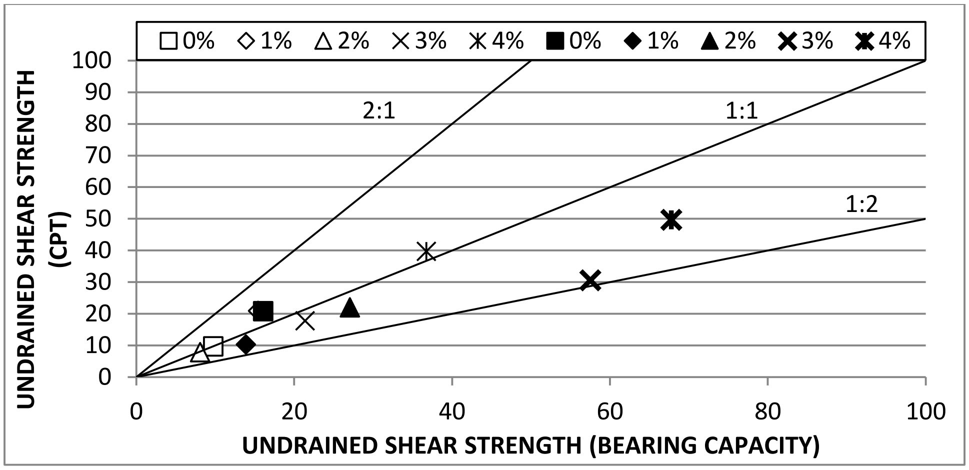

Figure 5.34: Undrained shear strength estimated from CPT and bearing capacity at maximum curvature for a 40 mm diameter foundation.

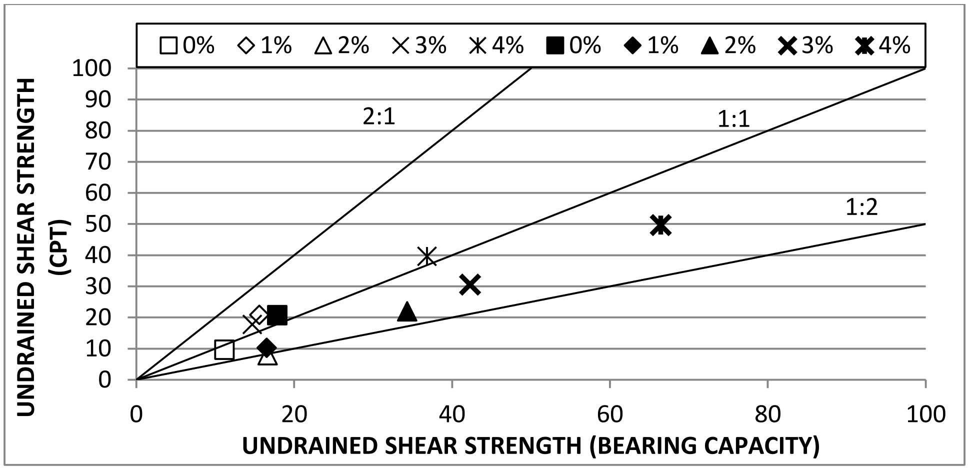

Figure 5.35: Undrained shear strength estimated from CPT and bearing capacity at maximum curvature for a 30x30 mm foundation.

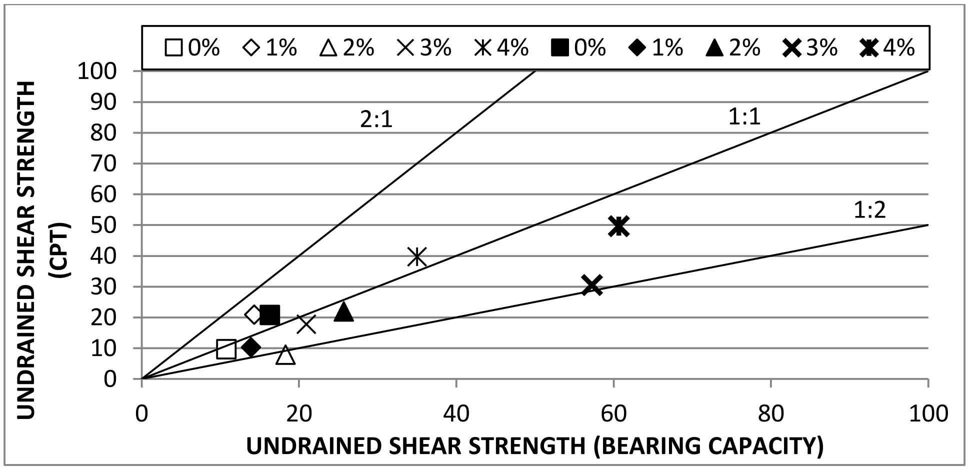

Figure 5.36: Undrained shear strength estimated from CPT and bearing capacity at maximum curvature for a 40x40 mm foundation.

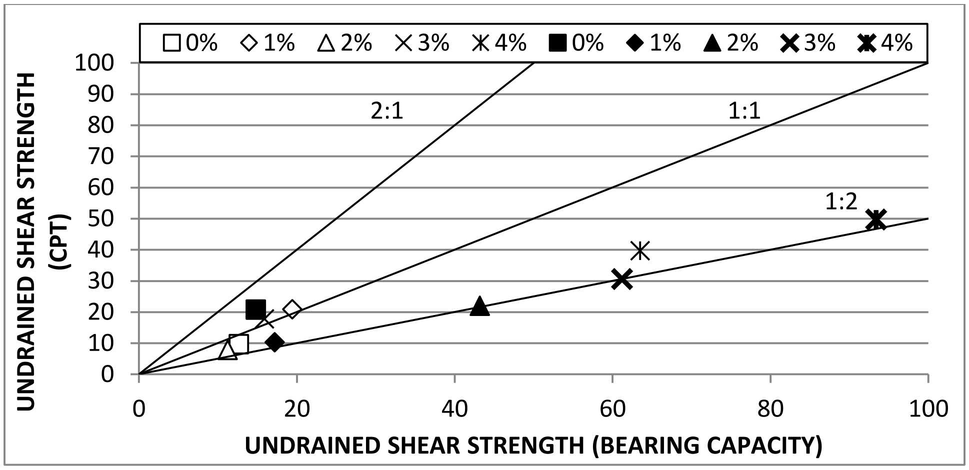

Figure 5.37: Undrained shear strength estimated from CPT and bearing capacity at a depth of 0.5B for a 30x60 mm foundation.

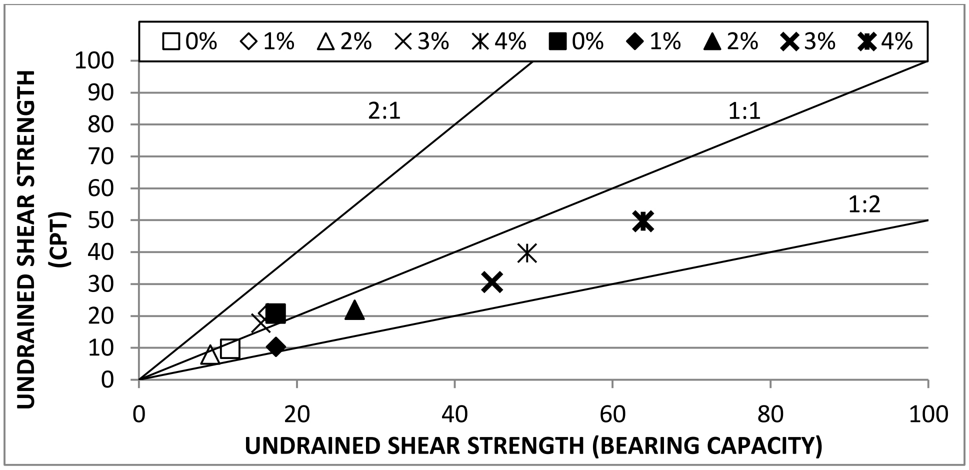

Figure 5.38: Undrained shear strength estimated from CPT and bearing capacity at a depth of 0.5B for a 40x80 mm foundation.

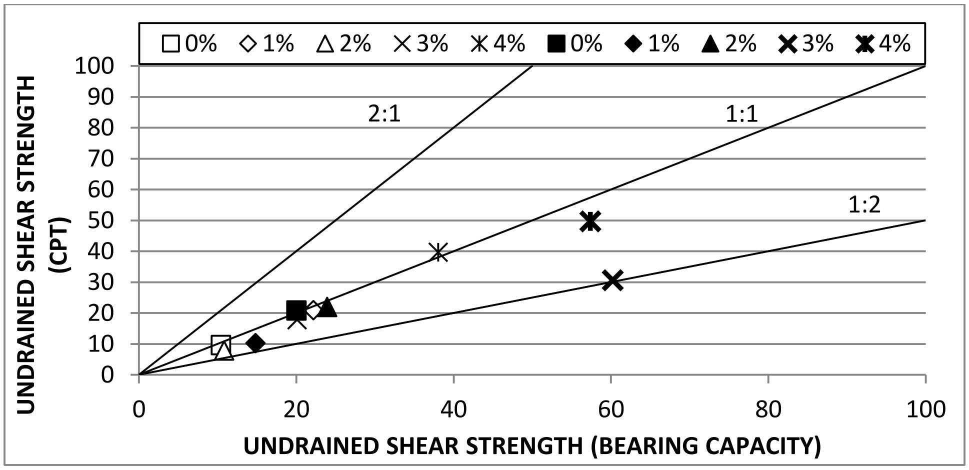

Figure 5.39: Undrained shear strength estimated from CPT and bearing capacity at a depth of 0.5D for a 30 mm diameter foundation.

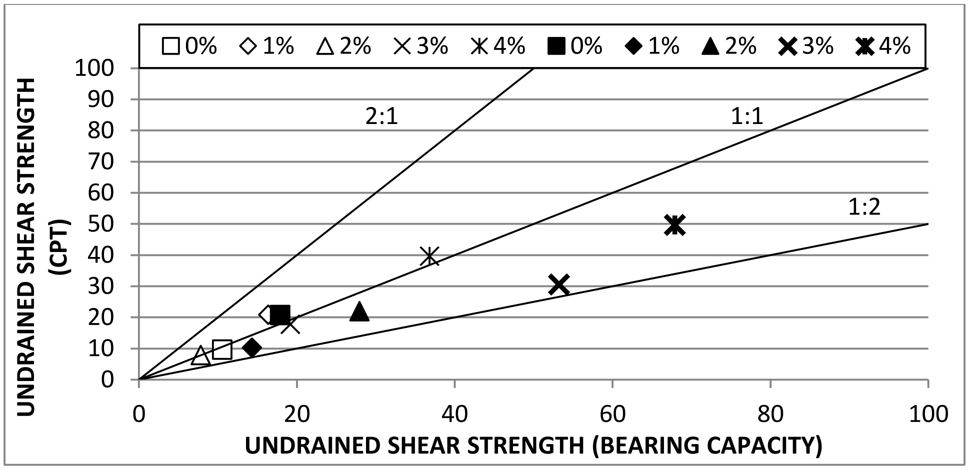

Figure 5.40: Undrained shear strength estimated from CPT and bearing capacity at a depth of 0.5D for a 40 mm diameter foundation.

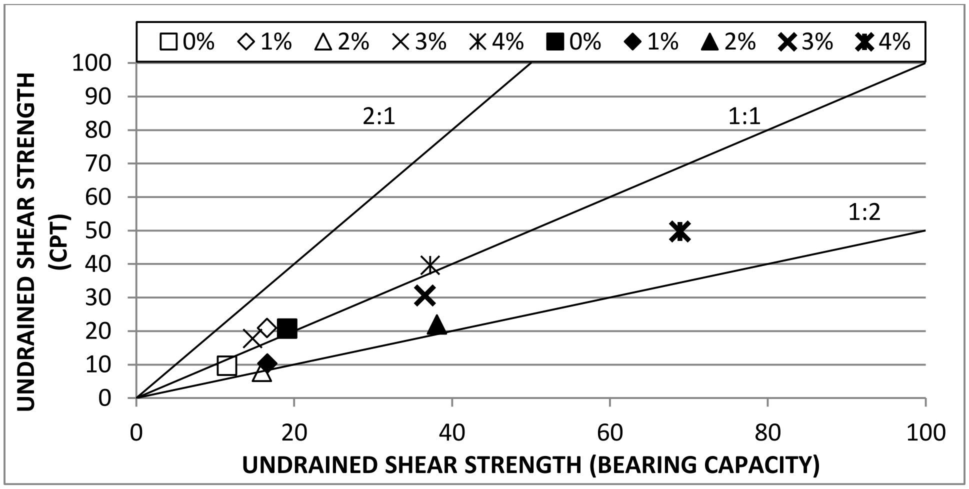

Figure 5.41: Undrained shear strength estimated from CPT and bearing capacity at a depth of 0.5B for a 30x30 mm foundation.

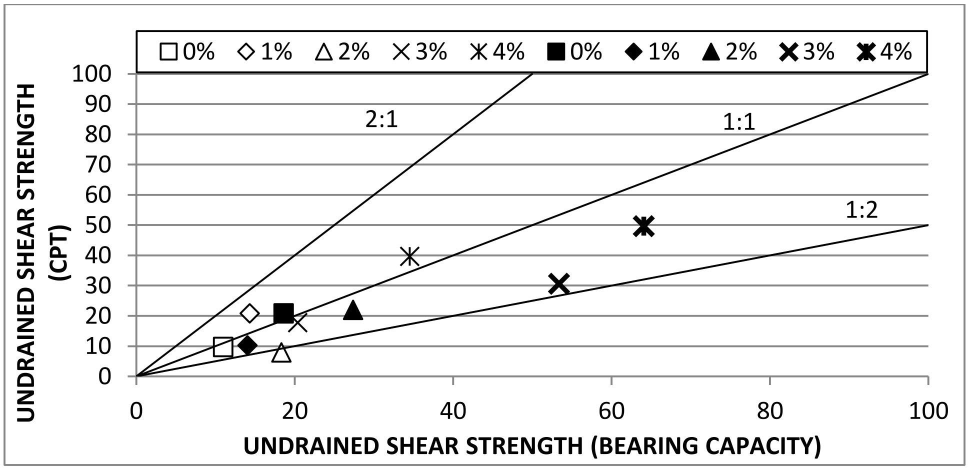

Figure 5.42: Undrained shear strength estimated from CPT and bearing capacity at a depth of 0.5B for a 40x40 mm foundation.

5.3.5 Comparison of undrained shear strength from piezoball and bearing capacity analysis

Undrained shear strengths determined from the piezoball and bearing capacity testing are presented in Figures 5.43 to 5.48. The shear strength determined from piezoball and back calculated from bearing resistance showed a good correlation. Scatter of the test data increased with an increase in fibre content. For the 30 x 60 mm foundation, the undrained shear strengths mobilized by the 2 and 3 % fibre content over consolidated models were double that of the piezoball values of undrained shear strength, Figure 5.43. The remaining models showed good correlation between strength determination methods with some scatter. There was also a good correlation between the undrained shear strength results of the 40 x 80 mm foundation and piezoball, Figure 5.44. The undrained shear strength back calculated for the 30 mm circular foundation also showed a near linear relationship with the ball penetrometer, Figure 5.45, with some scatter in the results. The normally and over consolidated models with 4 % fibre content, showed significant increased shear strength from piezoball data. The 4 % fibre content normally and over consolidated models tested with the 40 mm square foundation resulted in a decrease in the undrained shear strength compared to the piezoball, Figure 5.46; similar to what was found with the results of 30 mm circular foundation. Results of undrained shear strength mobilized by the 30 mm square footing showed a good correlation with piezoball data; the 4 % fibre content models normally and over consolidated models showed greater strength for piezoball tests. The 2 % fibre content over consolidated model however, showed undrained shear strength from the bearing capacity testing double those of the penetrometer, Figure 5.47. The 40 mm square foundation results, in comparison with the ball penetrometer, were found to be similar to those for the 40 mm diameter circular foundation. The 3 % over consolidated and 4% normally and over consolidated fibre content models showed almost the same strength relationships; however there was some variation for low fibre content samples, Figure 5.48.

Variation of shear strength with depth at 0.5 B/D of the foundation showed an increase in the shear strength back calculated from bearing capacity testing, Figure 5.49 to 5.54. Strength reduction in some models may be attributed to strain softening, the 3 % fibre model for example. The results at 0.5 B/D showed a good correlation between the shear strength from the bearing capacity testing.

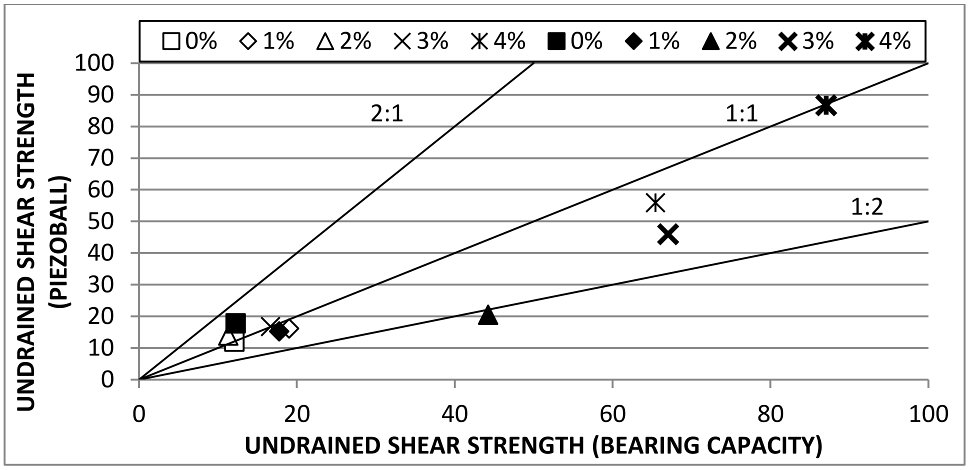

Figure 5.43: Undrained shear strength estimated from piezoball and bearing capacity at maximum curvature for a 30x60 mm foundation.

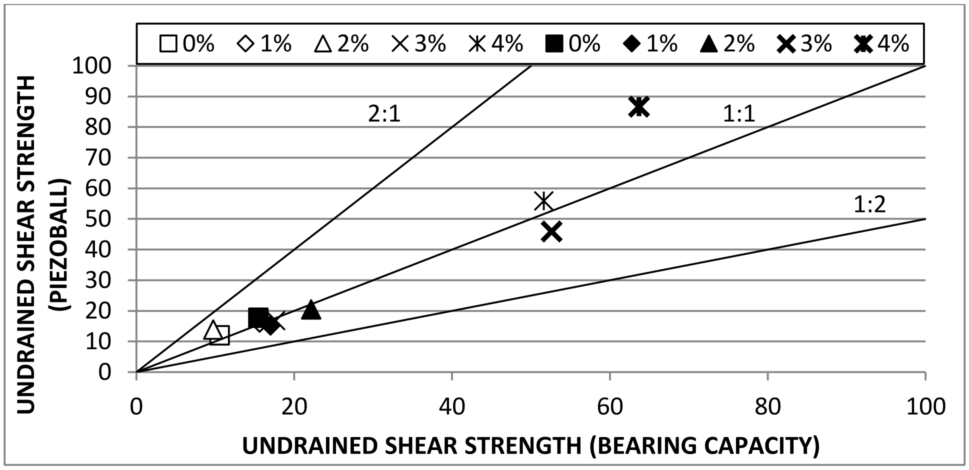

Figure 5.44: Undrained shear strength estimated from piezoball and bearing capacity at maximum curvature for a 40x80 mm foundation.

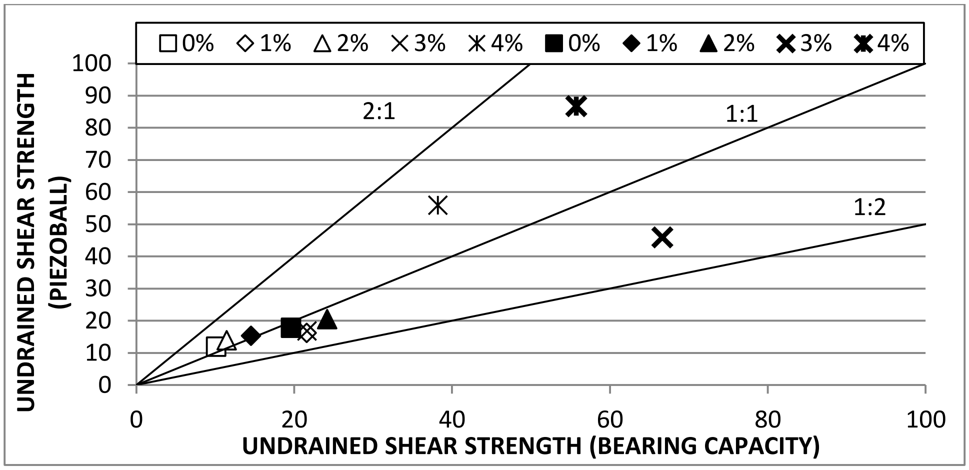

Figure 5.45: Undrained shear strength estimated from piezoball and bearing capacity at maximum curvature for a 30 mm diameter foundation.

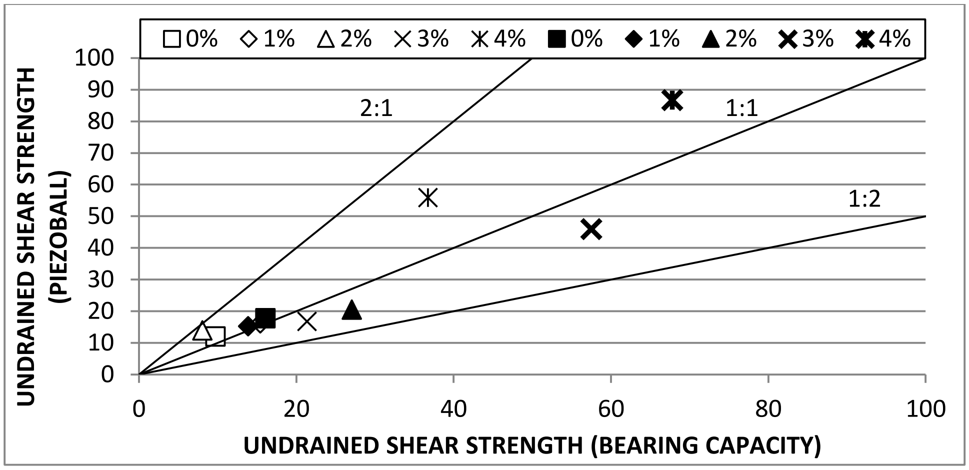

Figure 5.46: Undrained shear strength estimated from piezoball and bearing capacity at maximum curvature for a 40 mm diameter foundation.

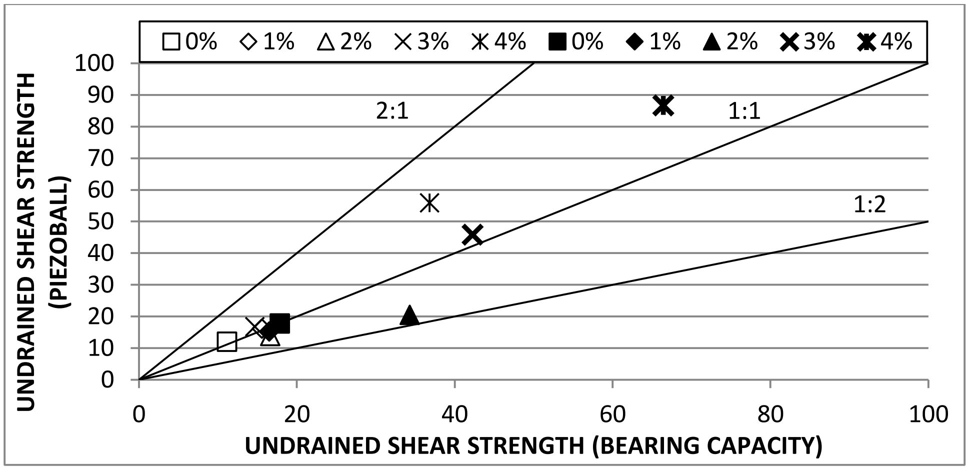

Figure 5.47: Undrained shear strength estimated from piezoball and bearing capacity at maximum curvature for a 30x30 mm foundation.

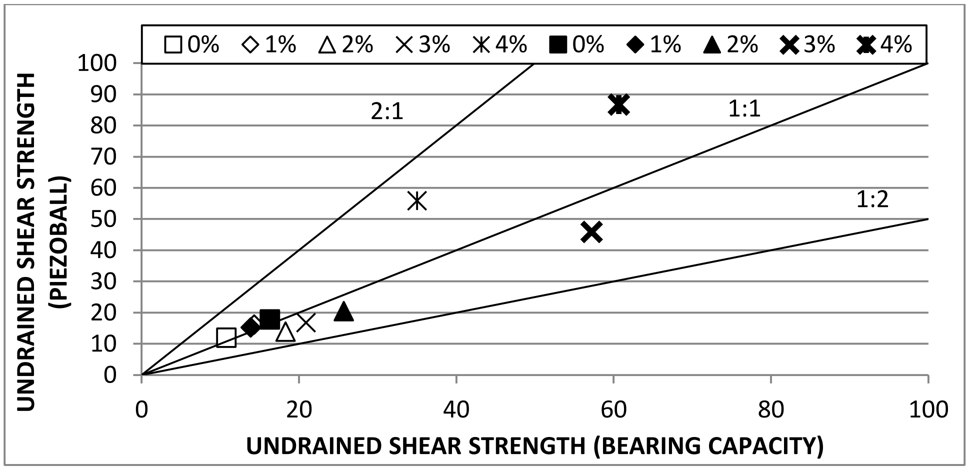

Figure 5.48: Undrained shear strength estimated from piezoball and bearing capacity at maximum curvature for 40x40 mm foundation.

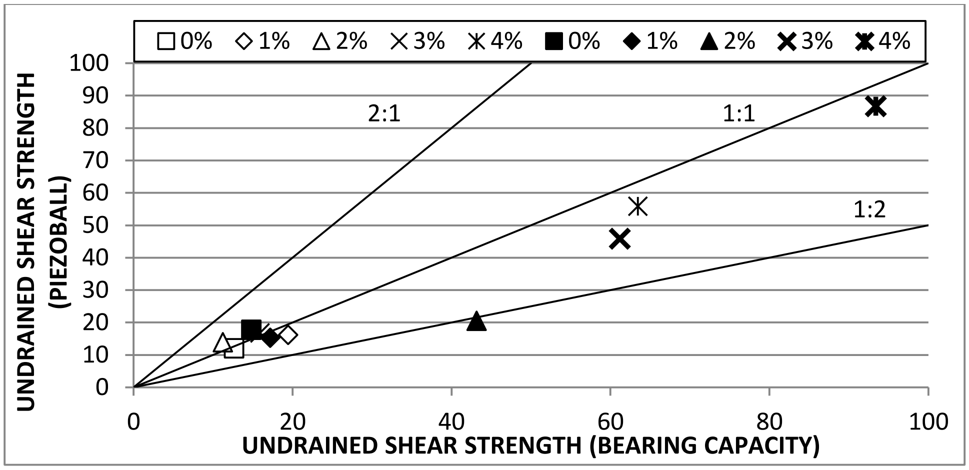

Figure 5.49: Undrained shear strength estimated from piezoball and bearing capacity at a depth of 0.5B for a 30x60 mm foundation.

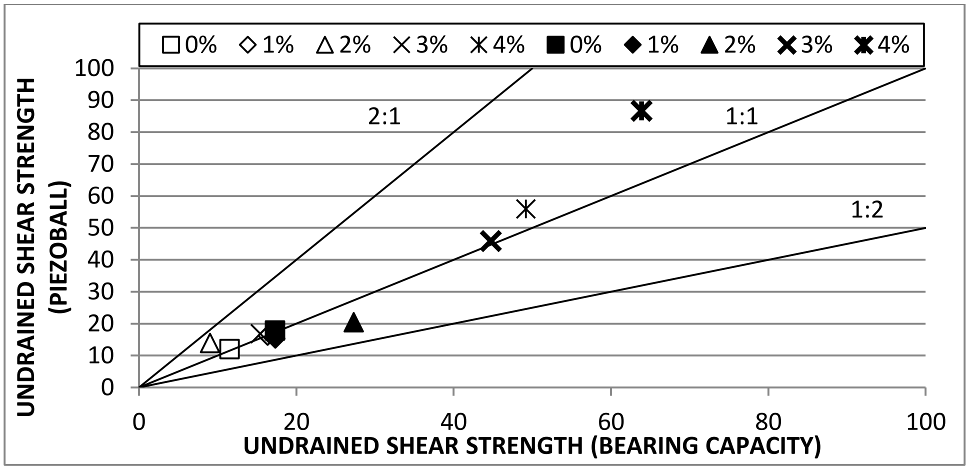

Figure 5.50: Undrained shear strength estimated from piezoball and bearing capacity at a depth of 0.5B for a 40x80 mm foundation.

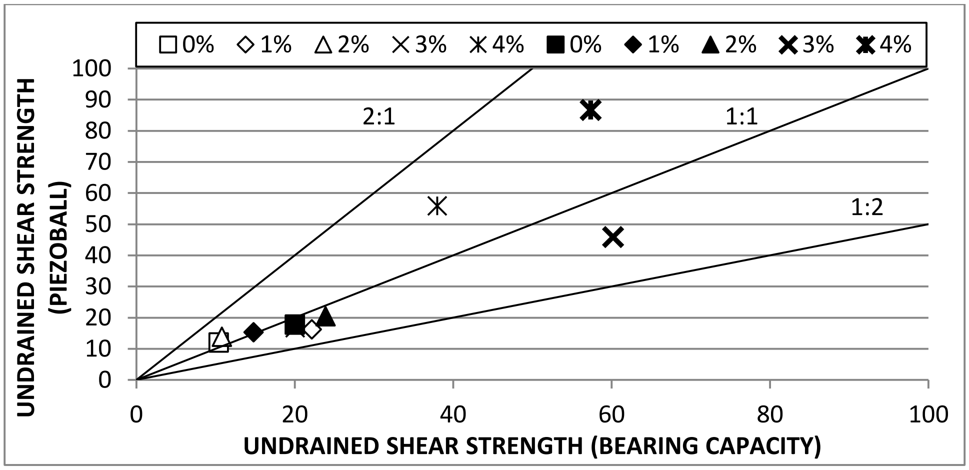

Figure 5.51: Undrained shear strength estimated from piezoball and bearing capacity at a depth of 0.5D for a 30 mm diameter foundation.

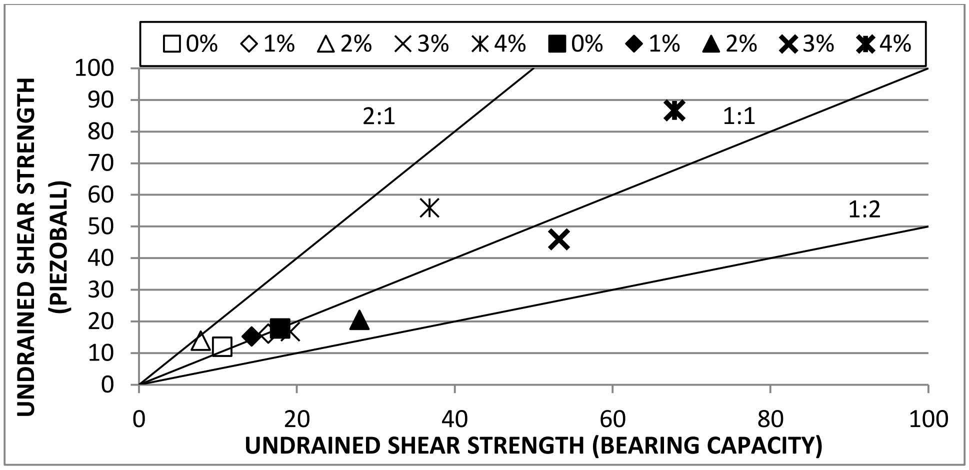

Figure 5.52: Undrained shear strength estimated from piezoball and bearing capacity at a depth of 0.5D for a 40 mm diameter foundation.

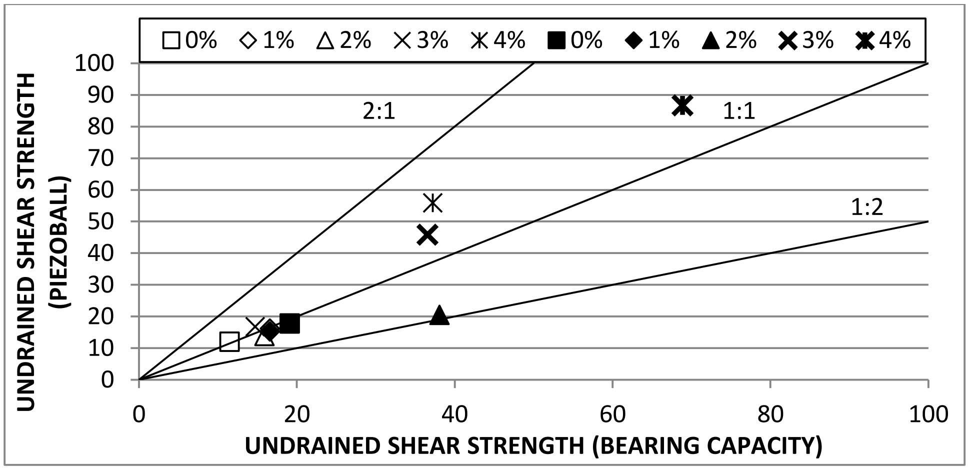

Figure 5.53: Undrained shear strength estimated from piezoball and bearing capacity at a depth of 0.5B for a 30x30 mm foundation.

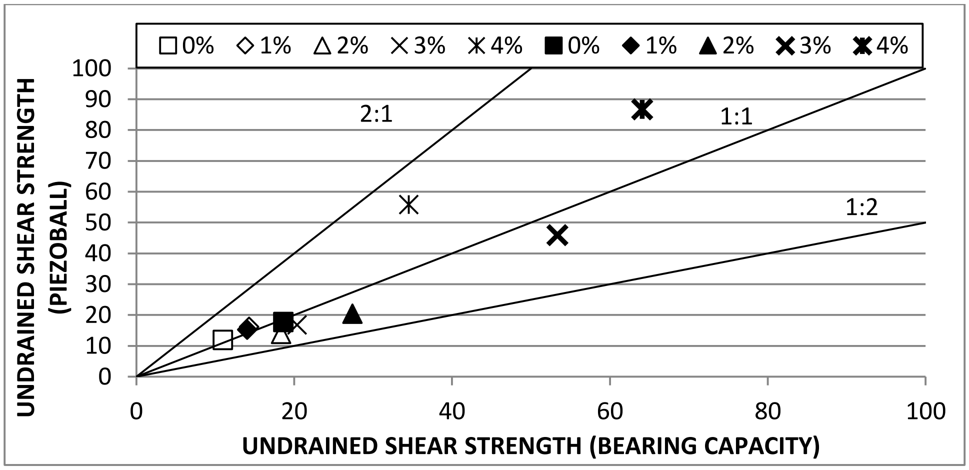

Figure 5.54: Undrained shear strength estimated from piezoball and bearing capacity at a depth of 0.5B for a 40x40 mm foundation.

5.4 Influence of foundation shape on undrained shear strength

The following section investigates the effect of foundation shape on the mobilization of undrained shear strength for each test series. Figure 5.55 represents the undrained shear strength determined for each foundation size in Test Series 1, while Figure 5.56 looks at test data for over consolidated models in Test Series 2. The average mobilized undrained shear strength was calculated for each foundation, penetrometer and shear vane from three sets of resistance data.

In Figure 5.55 the 0 % fibre content normally consolidated model demonstrated relatively constant undrained shear strengths of between 9.7 and 12.1 kPa, irrespective of the foundation shapes and sizes used during testing. Penetrometer data correlated well with the findings of bearing capacity tests. A slight reduction in undrained shear strength became apparent when tests were completed with larger foundation sizes. The 1 % fibre content normally consolidated model showed on average 64 % increase in strength from 0 % fibre content across the range of foundations used. The 30 mm diameter foundation mobilised the greatest proportional undrained shear strength increase of 21.6 kPa for the 1 % fibre content model, compared to 10 kPa for 0 % fibre content. A reduction in the undrained shear strength mobilized with an increase in foundation size for each category was recorded for the 1 % fibre content model. The piezoball data correlated well with the average bearing capacity shear strength, while the CPT results determined undrained shear strength to be above the average of the back calculated values, Figure 5.55. The 2 % fibre model showed a reduction in undrained shear strength mobilized for rectangular and circular foundations compared to the 1 % fibre model and on average was less than the shear strengths of the 0 % fibre content model. However, the 30 mm and 40 mm square foundations for the 2 % fibre content model showed an average increase of 2.7 and 3.8 kPa in strength compared to the 0 % and 1 % fibre contents respectively. CPT and piezoball data did indicate a decrease in shear strength for the 2 % fibre content, when compared to the 1 % model.

Rectangular and circular foundations tests on 3 % fibre content models mobilized shear strengths that were on average 1.2 kPa greater than those of the 1 % fibre content model. The model strength mobilized with rectangular and circular foundation tests, diminished slightly with increased foundation size. Shear strength of the 3 % fibre content model when tested with square footings was found to increase significantly with increased bearing area.

Profiling results on average correlated well with the average bearing capacity data for all foundation types; shear vane tests however underestimated shear strength for the 3 % content models. Tests on the 4 % fibre content model produced the highest shear strength for all models, Figure 5.55. The 30 x 60 mm and 40 x 80 mm rectangular foundations mobilised shear strengths of 65 and 51 kPa respectively. Undrained shear strength decreased with increasing foundation size for all foundation types in the 4 % model, which was comparable to the 0 %, 1 % and 3 % models. Piezoball results showed good correlation with the rectangular foundation data, the CPT data showed above average strength for circular and square footings. Shear vane results did not compare well with the bearing capacity or penetrometer results as vane tests were carried out on unconfined samples.

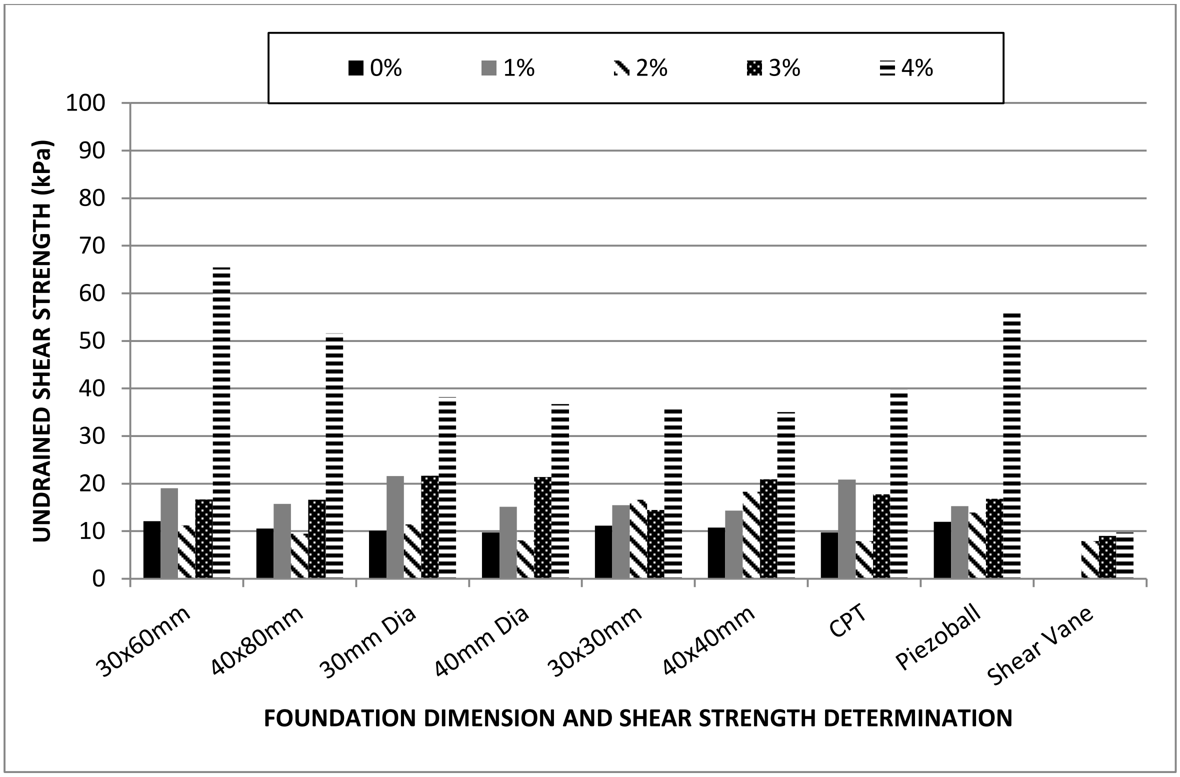

Figure 5.55: Effect of foundation size and shape on the undrained shear strength in normally consolidated models.

Figure 5.56 displays the response of over consolidated models in terms of shear strength to various foundation shapes and direct methods of strength determination. The 0 % fibre content model on average had shear strengths of 16.3 kPa and correlated well with the results of the penetrometers. Undrained shear strength was found to increase with increased size of rectangular footings and reduced with increasing size for circular and square footings. For the 1 % fibre content model, increased shear strength was observed for rectangular foundations while the circular and square foundations exhibited a decrease in strength when compared to the 0 % fibre content model. Undrained shear strength increased dramatically for the 30 x 60 mm foundation in the 2 % fibre content model; however strength drops approximately 50 % when the 40 x 80 mm foundation testing was included. Increase in the size of square foundations from 30 to 40 mm also resulted in undrained shear strength falling from 34 kPa to 26 kPa respectively. In contrast the 30 and 40 mm diameter foundations shear strength increased from 24 to 26 kPa respectively.

For the 3 % fibre content over consolidated model, a decrease in shear strength of 14 kPa and 9 kPa was observed with increased size for rectangular and circular foundations respectively. Penetrometer determination of the undrained shear strength was found on average to be less than the strength mobilized during plate bearing tests. The 4 % fibre content model mobilized the greatest undrained shear strength when tested for the complete foundation range, with the exception of the 30 mm diameter foundation; for this foundation the 3 % fibre content model mobilized greater undrained shear strength, Figure 5.55. The undrained shear strength dropped for the rectangular and square foundations when the bearing area was increased, but rose when the 40 mm circular foundation tests were conducted on the 3 % fibre content model. For the 4 % fibre content over consolidated model the CPT determined the shear strength to be lower than the average shear strength from footing tests, while the piezoball was slightly greater than the undrained shear strength determined from the bearing capacity testing. The shear vane results for the range of over consolidated models did not correlate with the undrained shear strength determined from the bearing capacity testing or with undrained shear strength from the penetrometers. This can be attributed to the low effective stress of the model samples when removed from the accelerated gravitational field generated within the centrifuge.

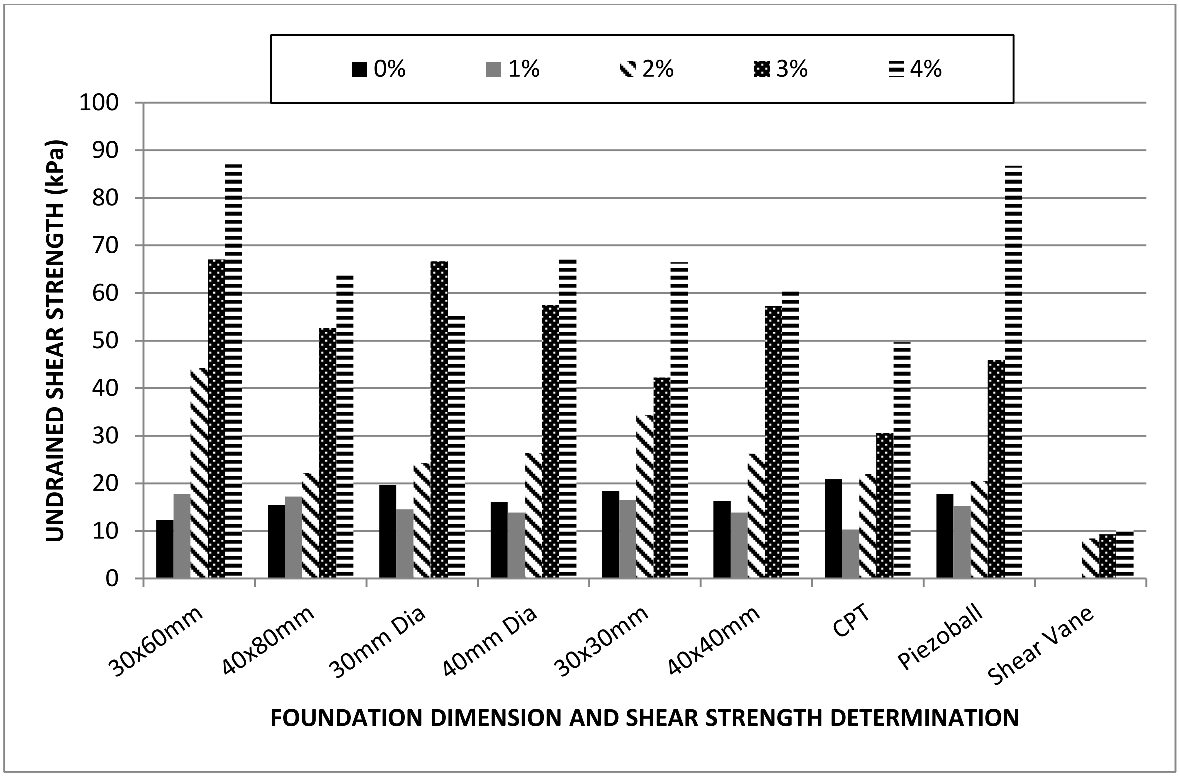

Figure 5.56: Effect of foundation size and shape on the undrained shear strength in over consolidated models.

5.5 Comparison of normally and over consolidated models

Analysis of the results gathered from Test Series 1 and 2 are presented in the following section; comparisons are drawn between the undrained shear strengths encountered at maximum curvature (primary failure location) and at depths equal to 0.5 B/D (secondary failure location). Figures 5.57 and 5.58 show the increased undrained shear strength at maximum curvature with increased fibre content in the normally and over consolidated models. Figure 5.57 details the 30 mm foundation widths and Figure 5.58 shows the strength increases associated with the 40 mm width foundations.

The 30 mm width foundation tests carried out on over consolidated models showed greater undrained shear strength than normally consolidated models, Figure 5.57. Scatter of the footing shear strength became more pronounced in the case of over consolidated models at 2 % fibre content, Figure 5.57. For Test Series 2, the undrained shear strength mobilized for circular and square foundations decreased for 1 % fibre content. Test Series 2 models also exhibited more scatter in the strength profiles, with 2 % fibre content and greater, compared to Test Series 1, Figure 5.57. The undrained shear strength mobilized for all foundations increased with 1 % fibre reinforcement for all normally consolidated models. Undrained shear strength for circular and rectangular foundation tests in the 2 % fibre content normally consolidated model were approximately the same as those in the 0 % model, and remained relatively constant up to 3 % fibre content. For the 3 % over consolidated model with the circular foundation, a dramatic rise in undrained shear strength was recorded. The undrained shear strength of the 4 % fibre content model tested with the circular foundation reduced, Figure 5.57. Scatter of all undrained shear strength results for the 4 % fibre content over consolidated model increased. The unexpected peak at 3 % fibre content may be attributed to a random event within the test series and therefore not a true reflection of the capabilities of that foundation. For the normally consolidated 4 % fibre content model, both undrained shear strength and scatter of the results increased.

For foundations with a 40 mm dimension, the undrained shear strength for over consolidated models increased with increasing fibre content, Figure 5.58. In contrast to the 30 mm foundation, the 1 % fibre content over consolidated model mobilized increased shear strength when tested with the rectangular foundations, Figure 5.58. The circular and square footings yielded lower undrained shear strengths than the 0 % fibre content model, Figure 5.58. Undrained shear strength in over consolidated models increased dramatically for the 3 % fibre content model, however, the scatter of the strength data was minimal compared to the 30 mm foundation results. The rate of strength increase reduced for the 4 % fibre content over consolidated model, while strength scatter remained within 10 kPa for the 3 foundations tested. Square foundation in the normally consolidated models produced very consistence results up to 3 % fibre content, upon 4 % fibre content shear strength increased dramatically, Figure 5.58. Circular and rectangular foundations produced relatively consistent shear strength for 3 % fibre content or less. All strength mobilized on normally consolidated models increased substantially for the 4 % fibre content model, scatter of the strength results also increased.

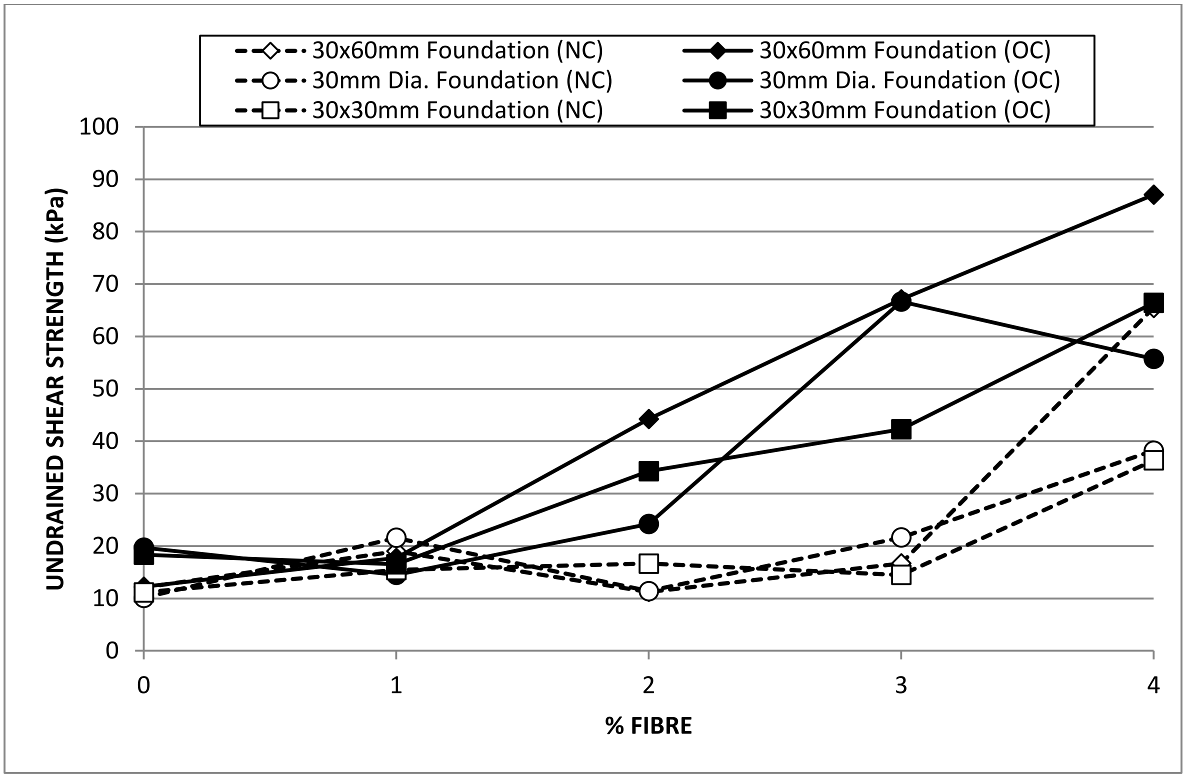

Figure 5.57: Undrained shear strength at maximum curvature for 30mm width foundations.

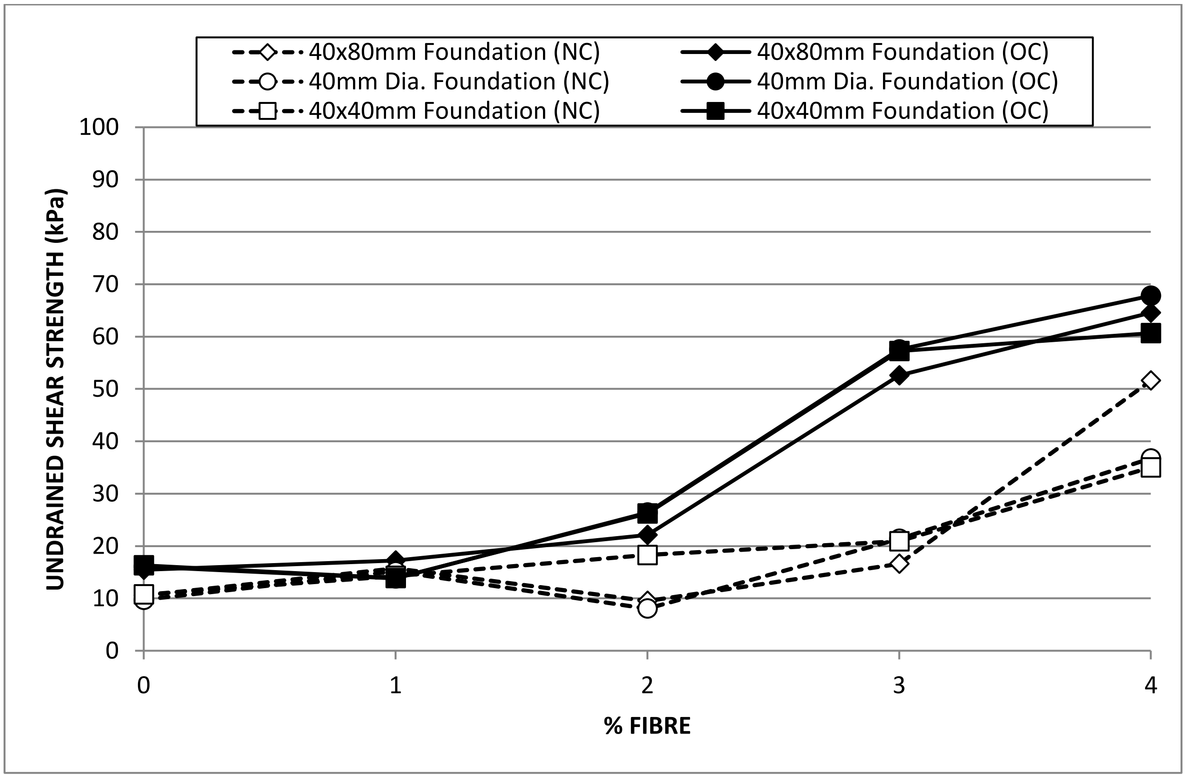

Figure 5.58: Undrained shear strength at maximum curvature for 40mm width foundations.

At depths of 0.5 B/D for the 30 mm foundations, Figure 5.59, the back calculated undrained shear strength increased compared to the values at the primary failure locations at maximum curvature. The undrained shear strength for over consolidated models at 0.5 B/D had very similar trends to those found for shear strengths at maximum curvature. One noticeable difference was a reduction of shear strength for the 30 x 30 mm foundation tested in the 3 % fibre content over consolidated model. That reduction also appeared when examining the circular and rectangular foundation results for 3 % fibre content, Figure 5.59. When the undrained shear strength increased for over consolidated models at the secondary failure locations, increases were minimal in the majority of cases with the upper range of strength increase not exceeding 12 kPa. From examination of the undrained shear strength profiles it became clear that strain hardening was prominent in the majority of over consolidated models. The undrained shear strength determined at a depth of penetration equal to 0.5 B/D showed less scatter than that determined at the point of maximum curvature in the normally consolidated models, Figure 5.59.

At depths of 0.5 B/D for foundations with 40 mm widths, Figure 5.60, the undrained shear strength was found to have little scatter in the minority of cases, suggesting a relatively constant undrained shear strength profile. The average undrained shear strength reduced for all foundation tests on the 3 % fibre content over consolidated model; the 40 x 80 mm foundation mobilized undrained shear strength approximately 8 kPa weaker, Figure 5.60, than that found at maximum curvature. For 4 % fibre content there was constant undrained strength mobilized at depths of 0.5 B/D penetration for the circular and rectangular foundations, with an increase in undrained shear strengths mobilized with the square footing. There was some variation in undrained shear strength when examining the normally consolidated models; however such variations were relatively small. Undrained shear strength reduction for normally consolidated models at 0.5 B/D in bearing capacity testing may be attributed to strain softening of the models.

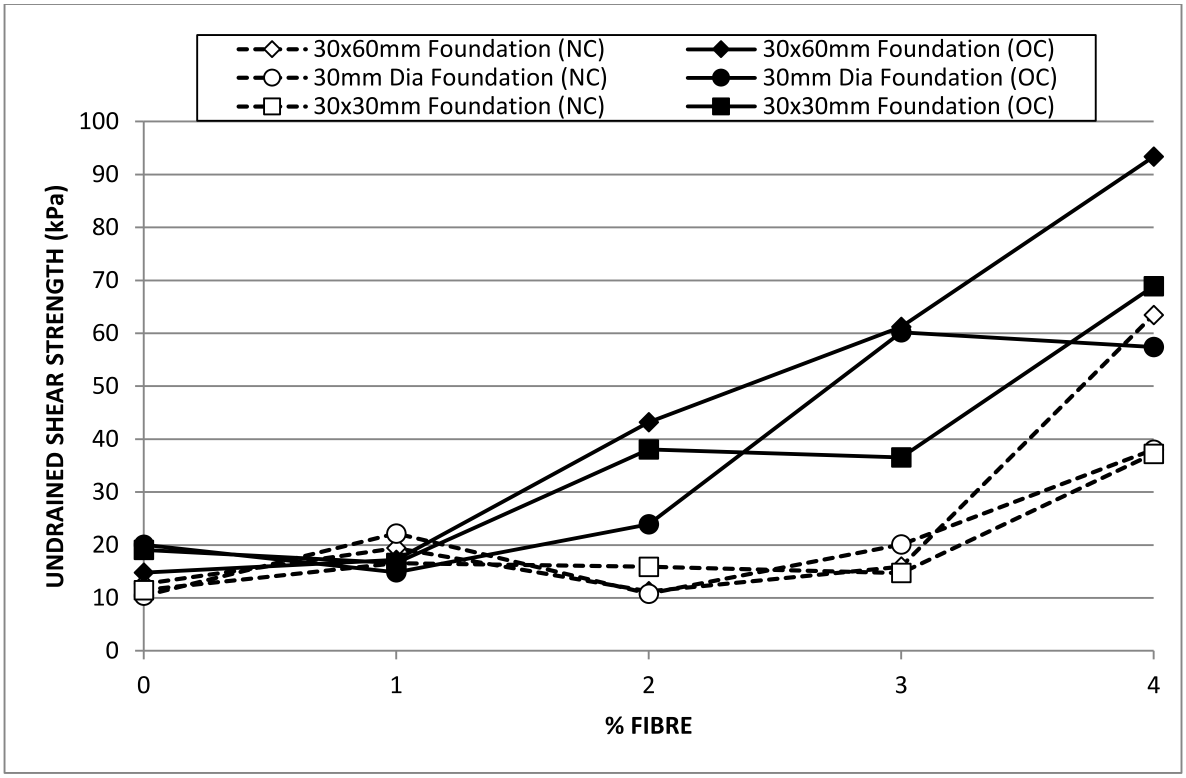

Figure 5.59: Undrained shear strength at a depth of 0.5B/D for 30mm width foundations.

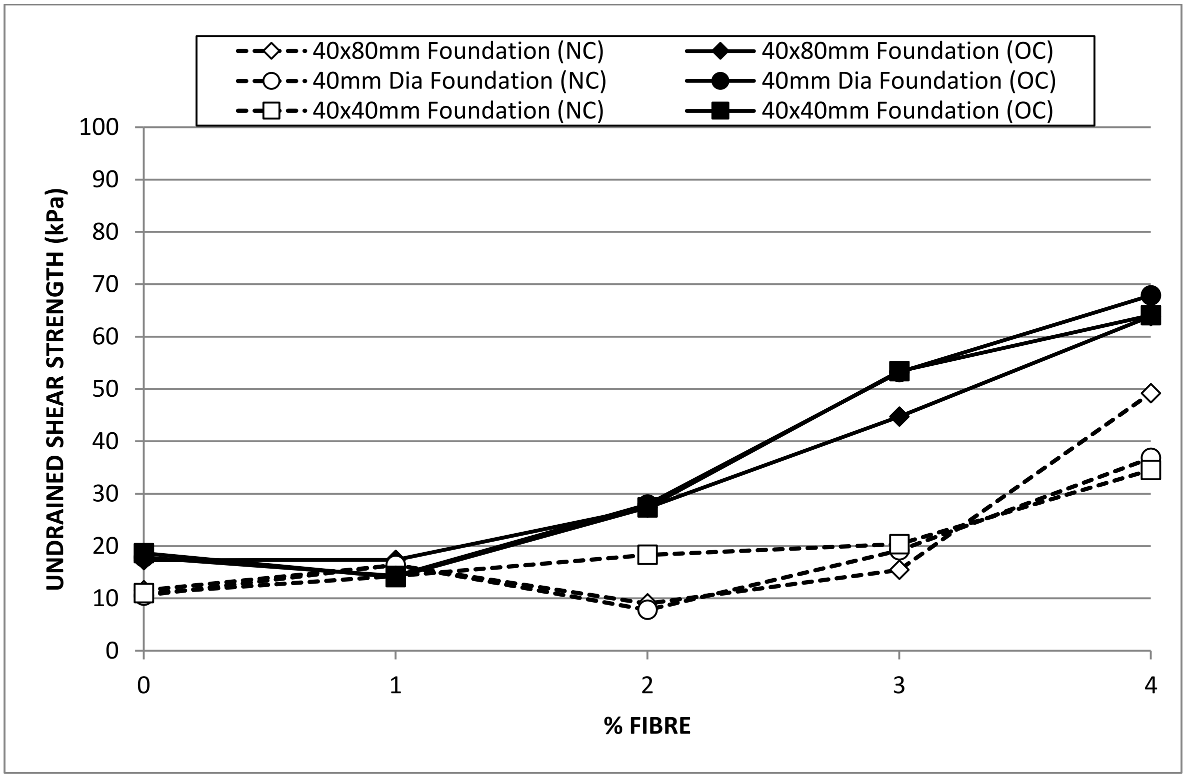

Figure 5.60: Undrained shear strength at a depth of 0.5B/D for 40mm width foundations.

The average back calculated undrained shear strengths at maximum curvature along with the average profiling and vane shear data in Test Series 2, yielded higher results than results of Test Series 1, Figure 5.61 to 5.66. The undrained shear strength back calculated from bearing capacity results were higher for over consolidated models compared to normally consolidated cases. The effects of strain hardening contributed to the greater strength mobilization in Test Series 2. Scatter was present throughout the various foundation strength profiles; however it was clear that with an increase in fibre content the undrained shear strength for the 30 x 60 mm foundation increased dramatically, Figure 6.61. The CPT results showed that, with the exception of the 1 % fibre content normally consolidated model, the undrained shear strengths determined for the over consolidated models were higher, Figure 5.62. Comparison between the CPT and back calculated undrained shear strength results showed a scattered correlation which can be attributed to the interaction of the fibre content on the cone tip and face during CPT testing, Figure 5.63. Piezoball results showed that over consolidated models produced the greater undrained shear strengths, while at 1 % fibre content the strengths exhibited a good correlation between normally and over consolidated shear strengths, Figure 5.64. Piezoball results showed, in the majority of cases, a higher undrained shear strength for the range of fibrous models. The shear vane results showed a near linear relationship between the normally and over consolidated models, but at lower undrained shear strength compared to other methods of strength determination, Figure 5.66.

At depths corresponding to 0.5 B/D, Figure 5.67 to 5.72, the undrained shear strength increased in the majority of cases which may be attributed to the effects of strain hardening with depth; undrained shear strength increases were minimal in the majority of cases. Instances where shear strength dropped below the level determined from the point of maximum curvature, may be attributed to models that experienced strain softening, 40 x 80 mm foundation tests in the 3 % over consolidated model, Figure 5.68. Some models with a relatively constant shear strength profile may also contribute to a slight reduction in undrained shear strength at depths corresponding to 0.5 B/D.

An attempt was made to relate the undrained shear strength of normally consolidated models to the undrained shear strength of over consolidated models using the Ladd and Foott (1974) expression, see Equation 5.1. The best relationship was found with the Piezoball test results where data from Test Series 1 and 2 correlated within an accuracy of 15 to 20 %, see Figure 5.73 and 5.74. Appendix H contains the remaining figures of the Ladd and Foott analysis.

$$\left(\frac{c_u}{\sigma_v{}'}\right)_{OC} = OCR^{0.8}\left(\frac{c_u}{\sigma_v{}'}\right)_{NC}$$ Equation 5.1

where; c_u is the undrained shear strength

σ_v' is the effective vertical stress

OCR is the over consolidation ratio

OC denote the over consolidated equation terms

NC denote the normally consolidated equation terms

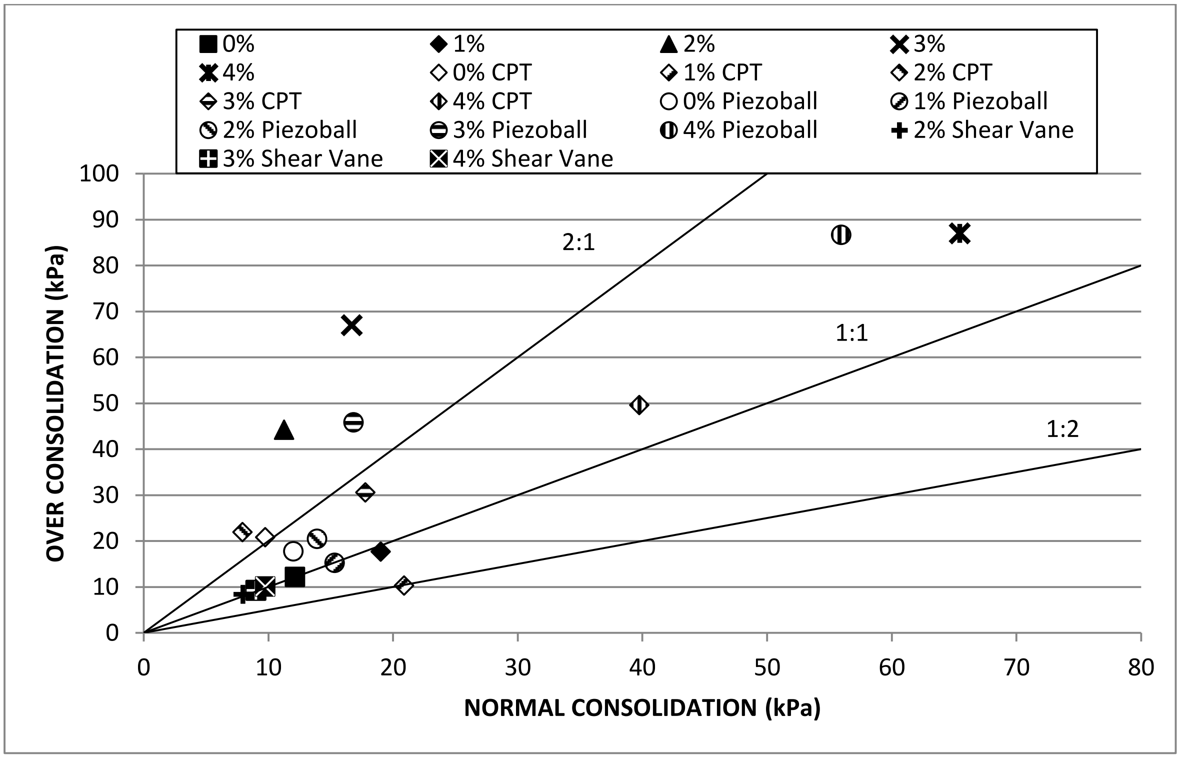

Figure 5.61: Over consolidation v normal consolidation at maximum curvature for models tested with a 30x60mm foundation.

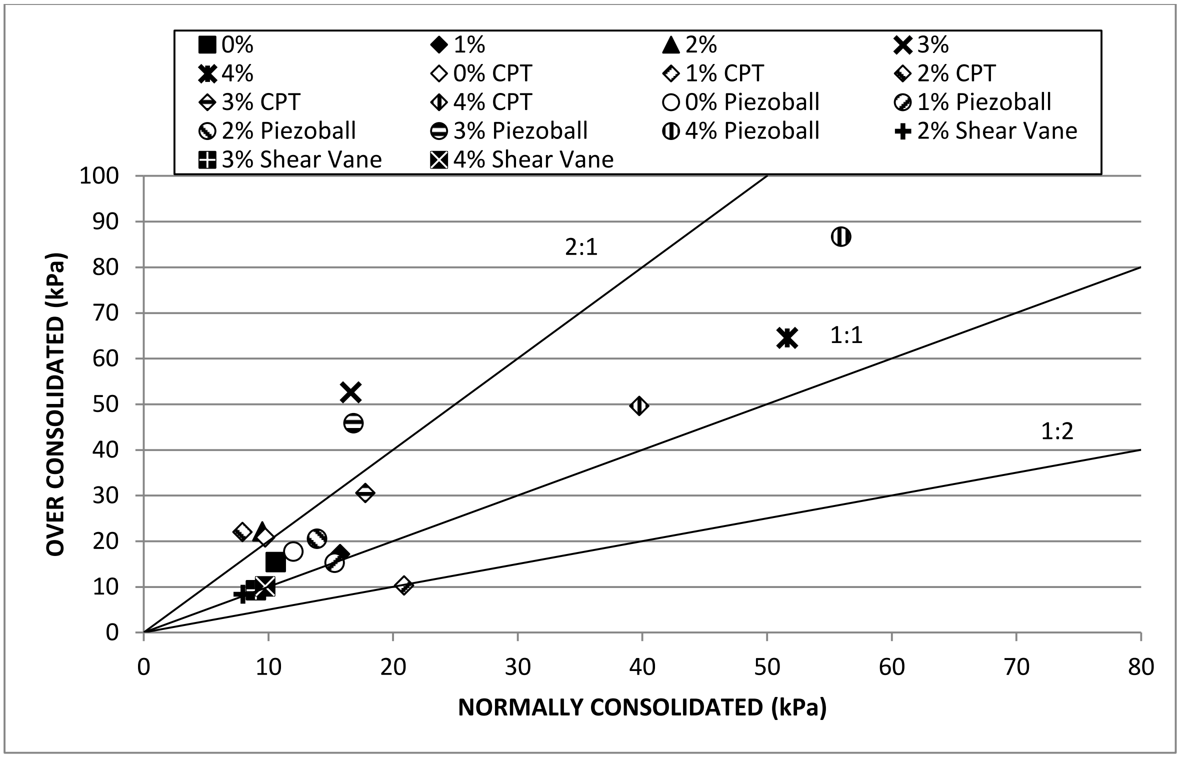

Figure 5.62: Over consolidation v normal consolidation at maximum curvature for models tested with a 40x80mm foundation.

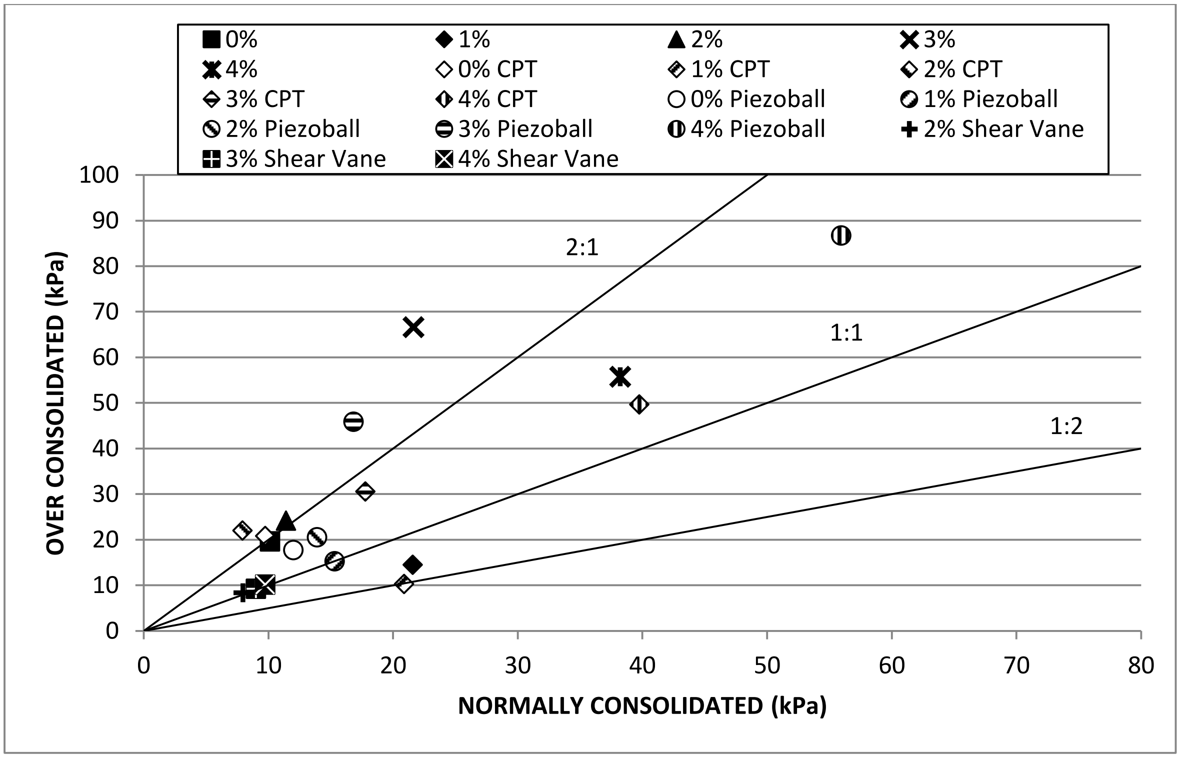

Figure 5.63: Over consolidation v normal consolidation at maximum curvature for models tested with a 30mm diameter foundation.

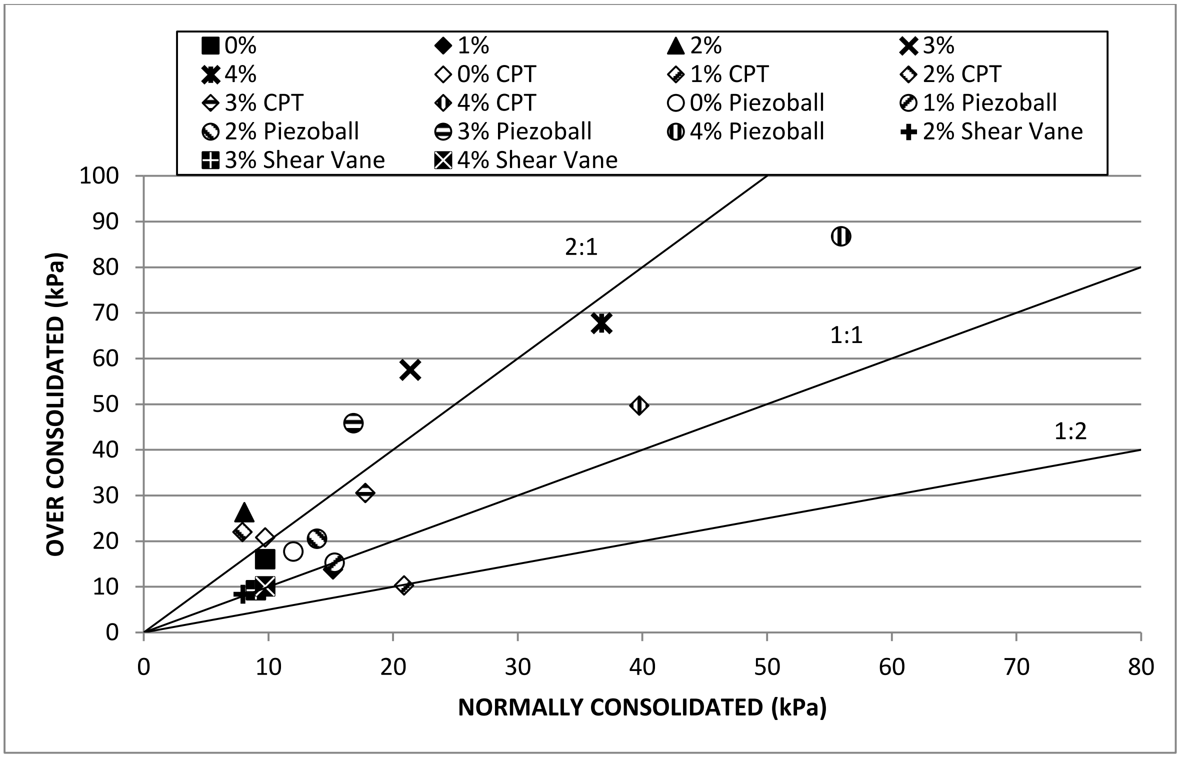

Figure 5.64: Over consolidation v normal consolidation at maximum curvature for models tested with a 40mm diameter foundation.

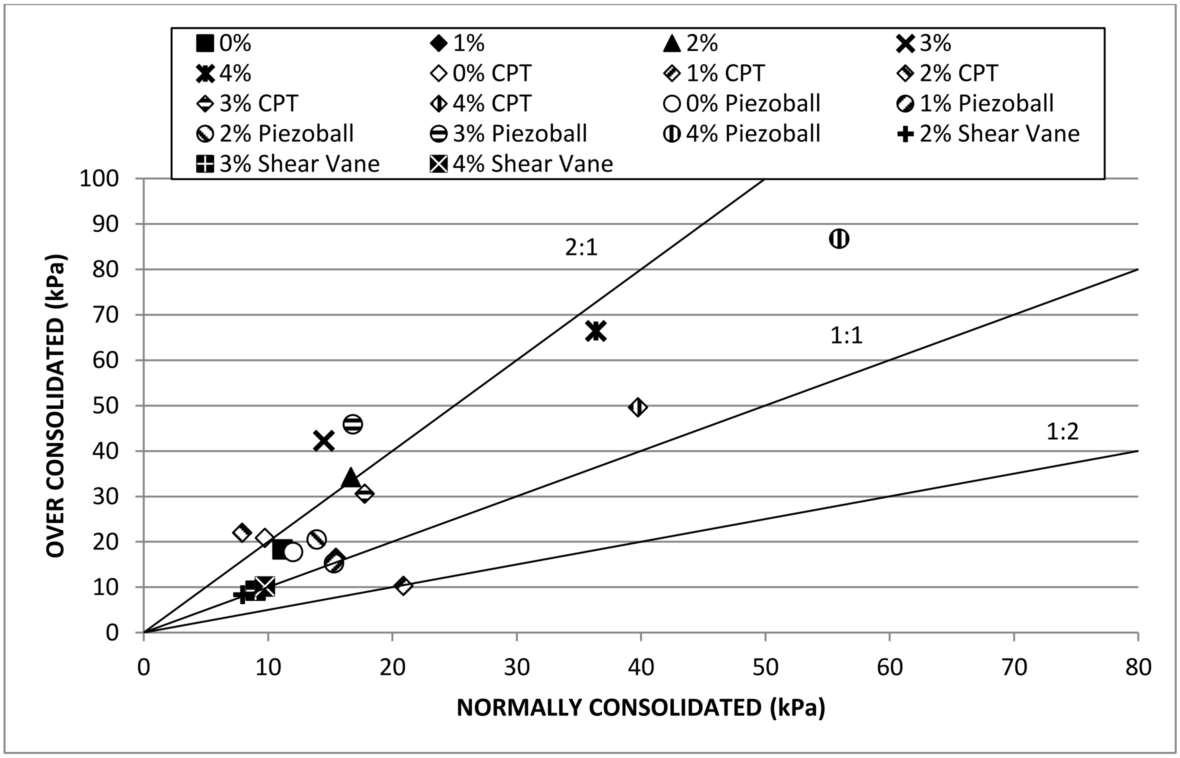

Figure 5.65: Over consolidation v normal consolidation at maximum curvature for models tested with a 30x30mm foundation.

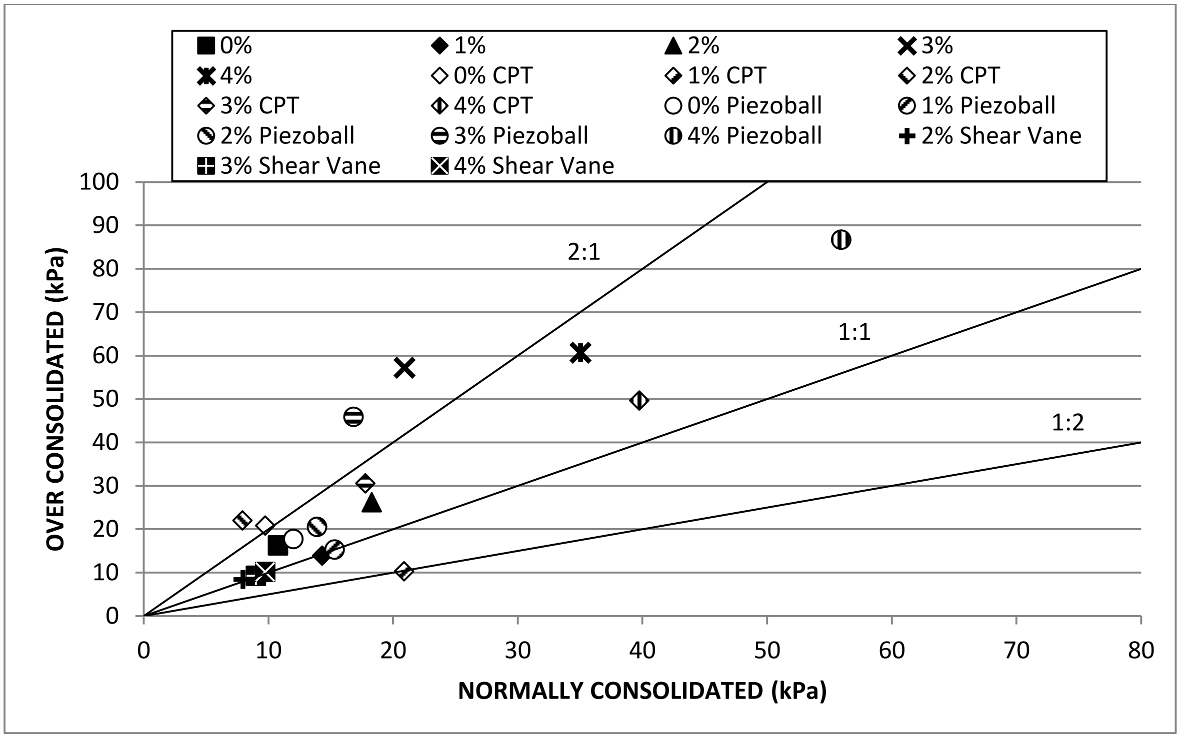

Figure 5.66: Over consolidation v normal consolidation at maximum curvature for models tested with a 40x40mm foundation.

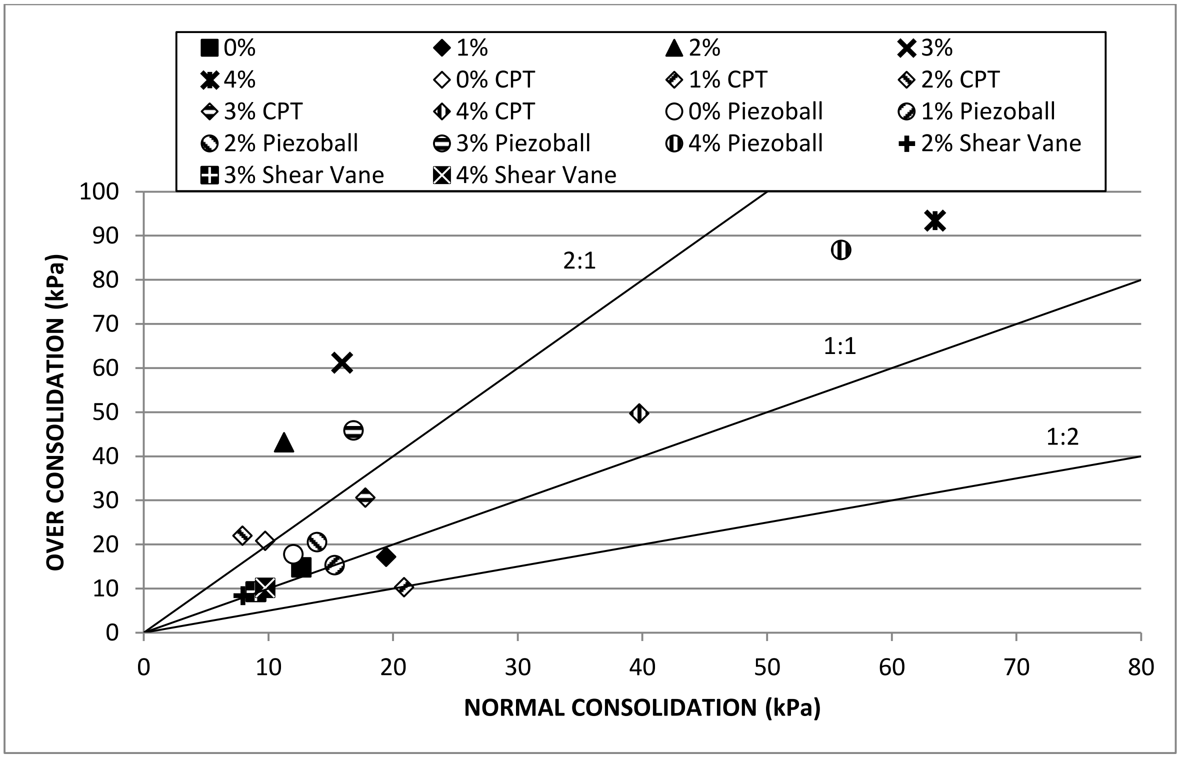

Figure 5.67: Over consolidation v normal consolidation at 0.5B depth for models tested with a 30x60mm foundation.

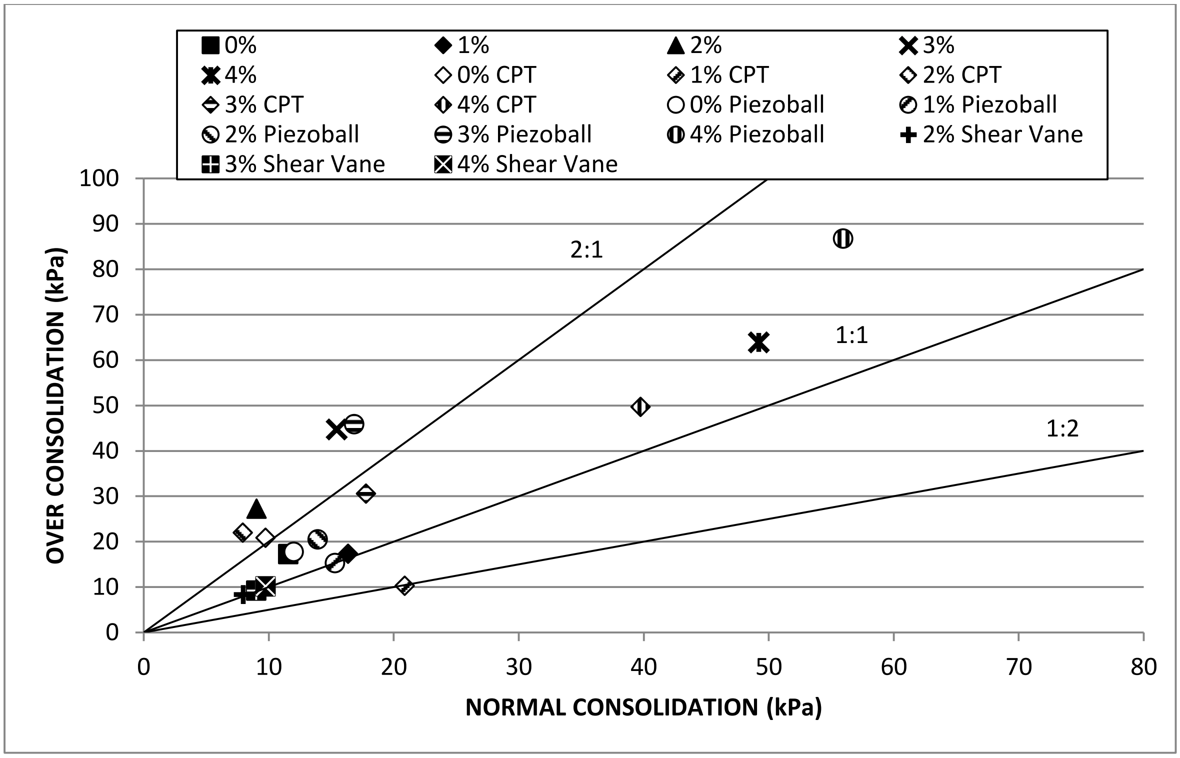

Figure 5.68: Over consolidation v normal consolidation at 0.5B depth for models tested with a 40x80mm foundation.

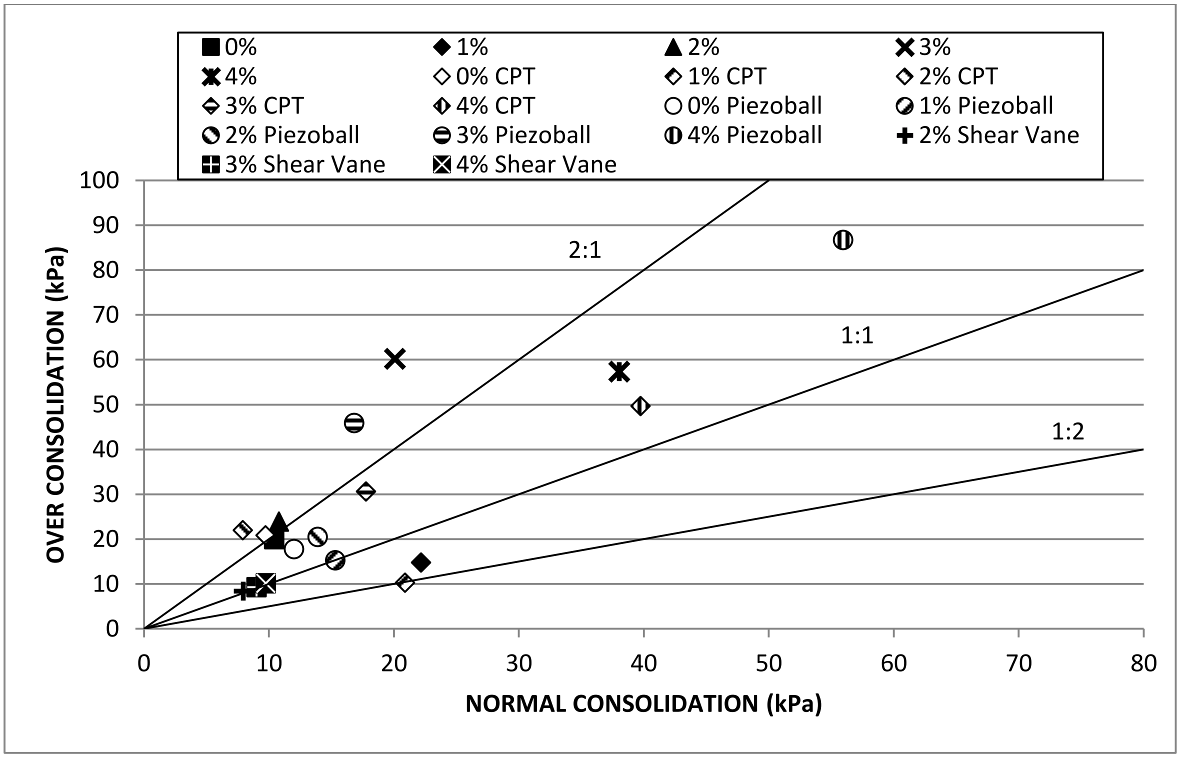

Figure 5.69: Over consolidation v normal consolidation at 0.5D depth for models tested with a 30mm diameter foundation.

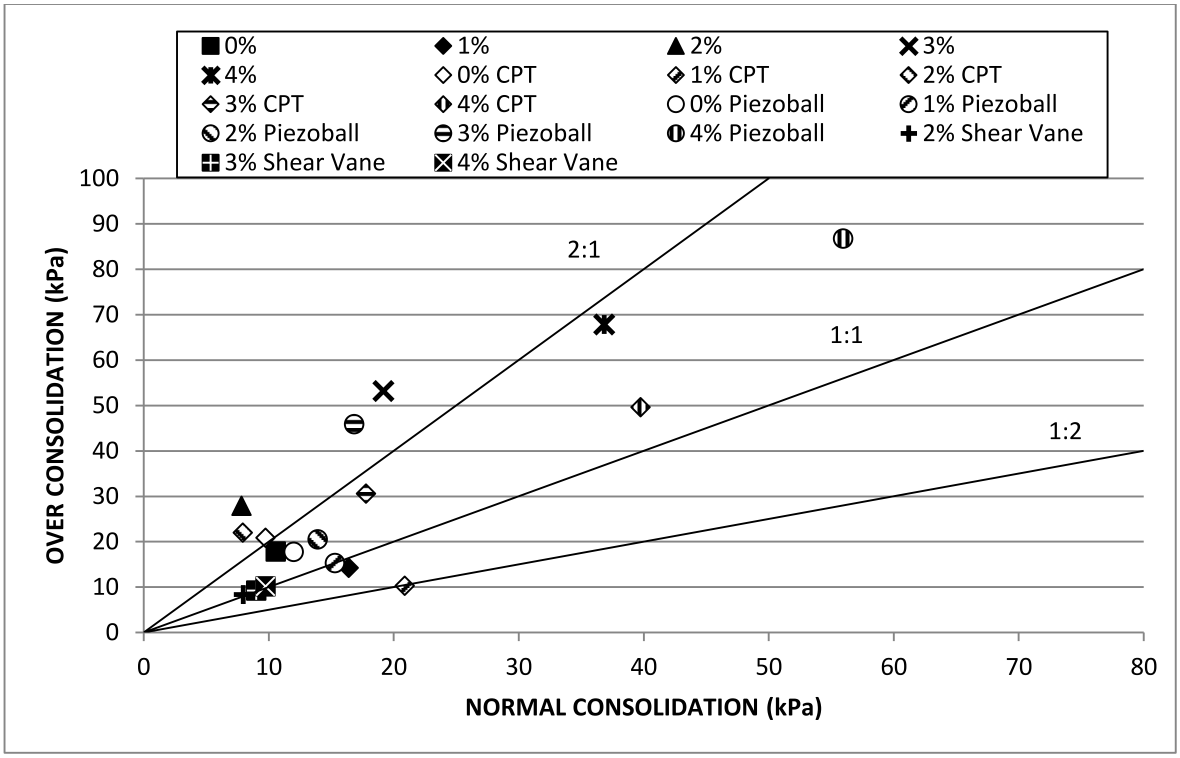

Figure 5.70: Over consolidation v normal consolidation at 0.5D depth for models tested with a 40mm diameter foundation.

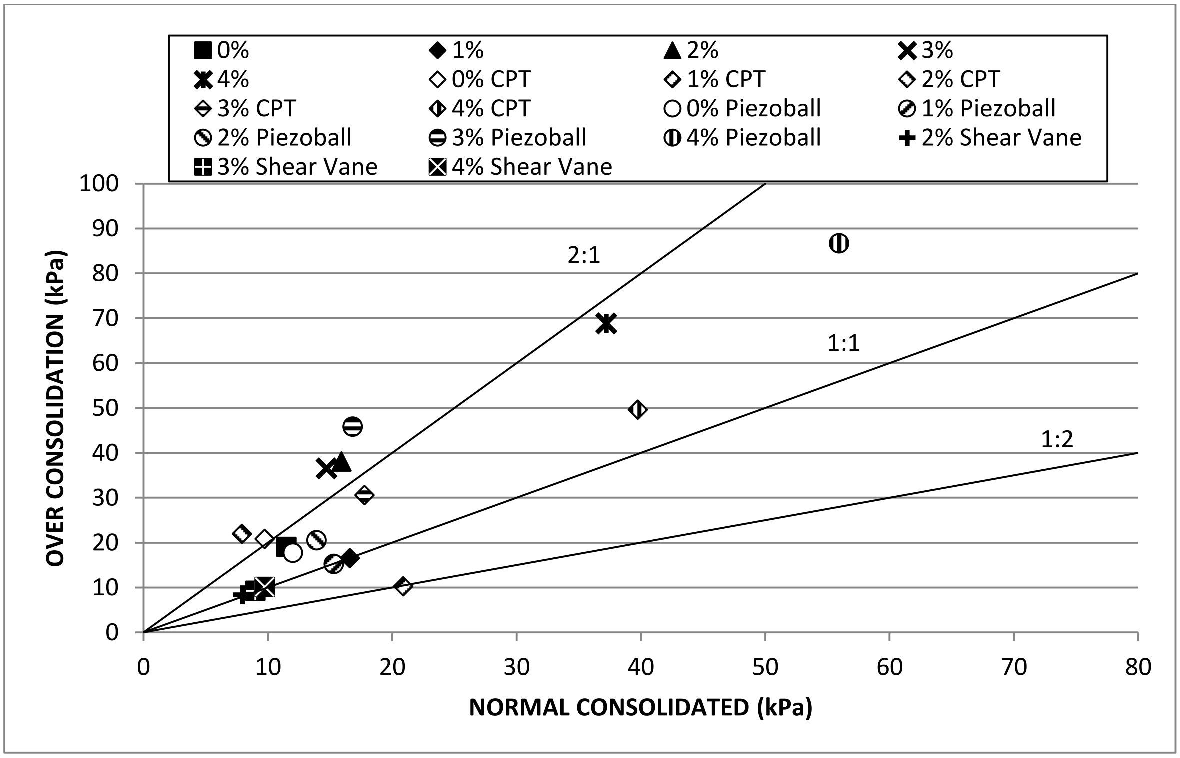

Figure 5.71: Over consolidation v normal consolidation at 0.5B depth for models tested with a 30x30mm foundation.

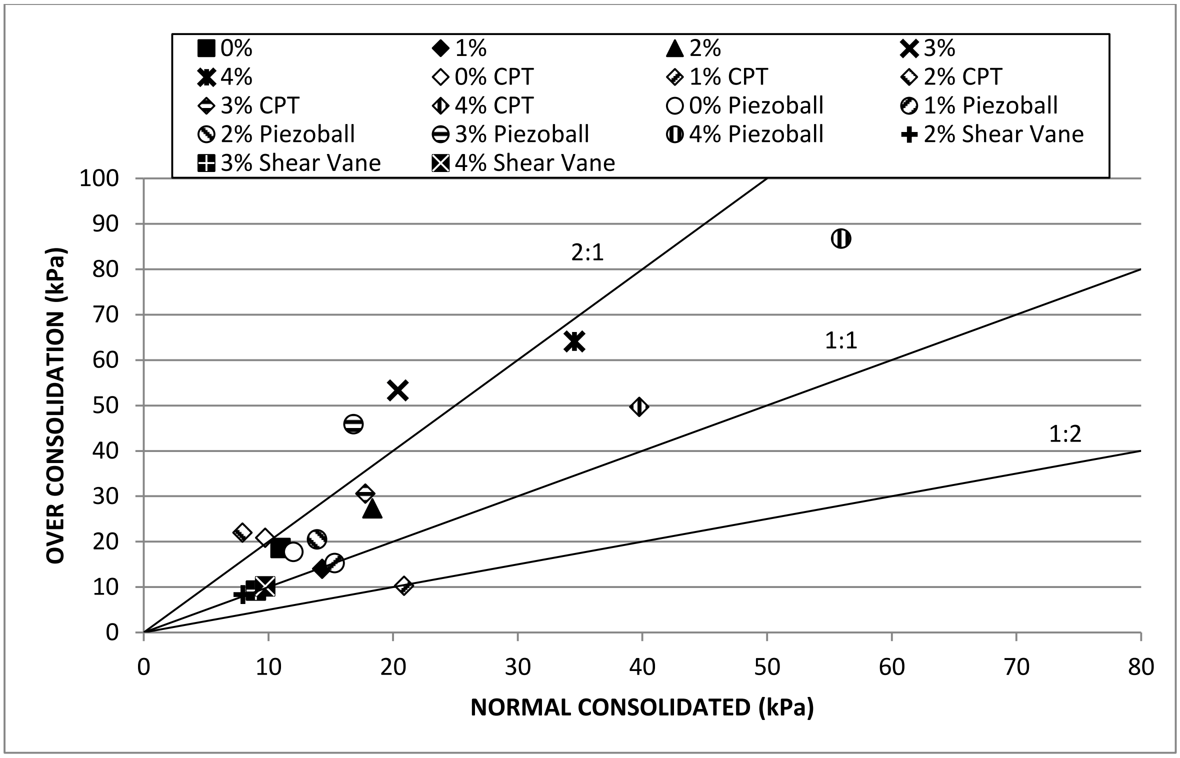

Figure 5.72: Over consolidation v normal consolidation at 0.5B depth for models tested with a 40x40mm foundation.

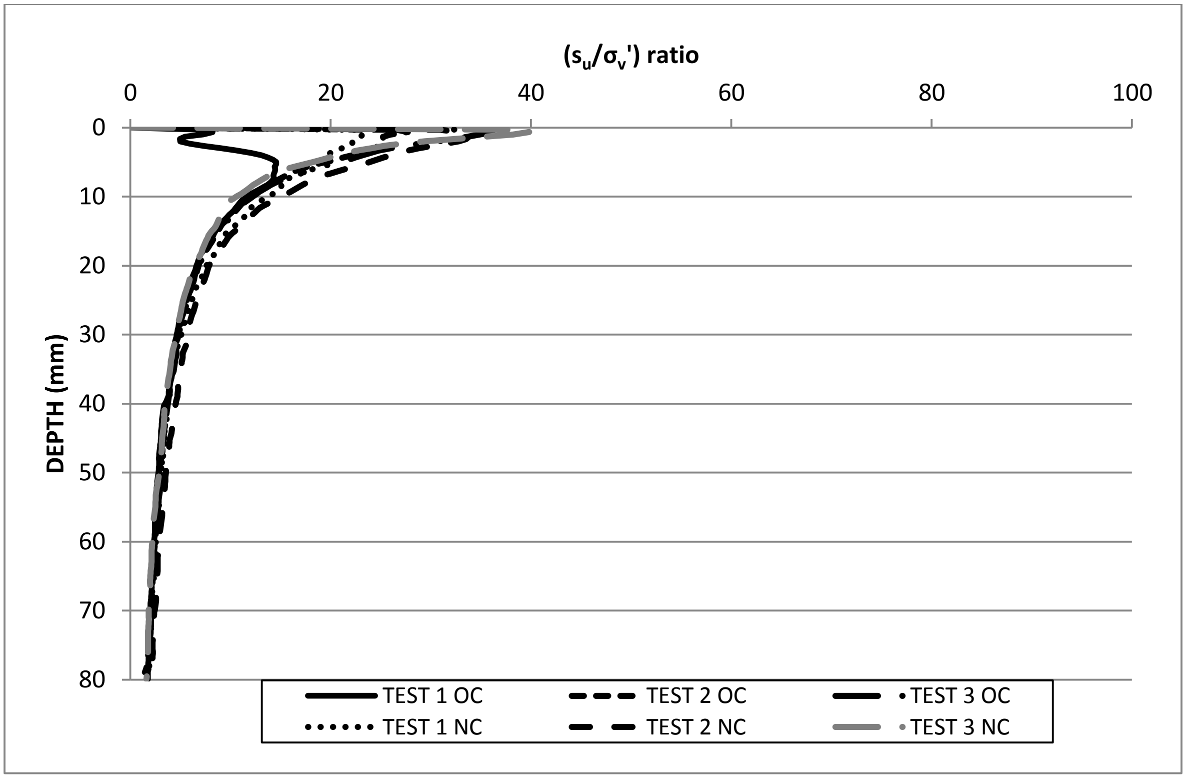

Figure 5.73: $(s_u/\sigma_v')_{oc}$ and $OCR^{0.8}\,(s_u/\sigma_v')_{nc}$ comparator profiles for Piezoball tests completed on 0 % fibre normally and over consolidated models.

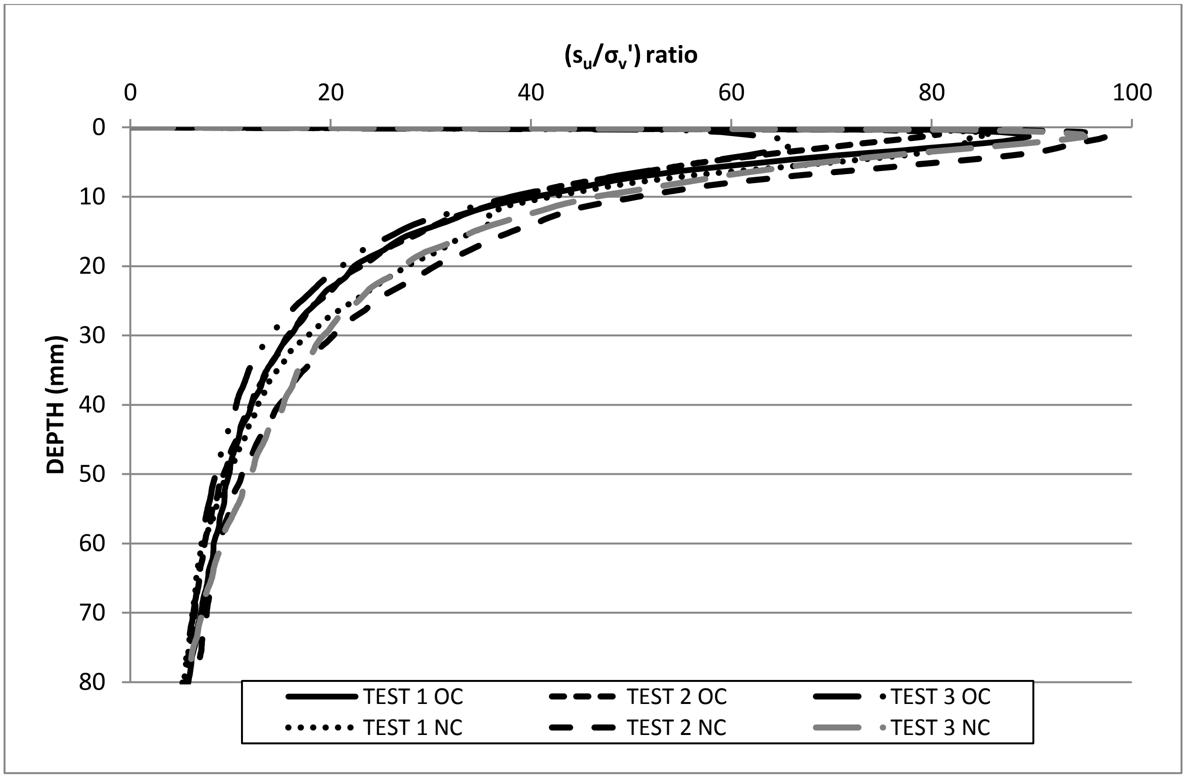

Figure 5.74: $(s_u/\sigma_v')_{oc}$ and $OCR^{0.8}\,(s_u/\sigma_v')_{nc}$ comparator profiles for Piezoball tests completed on 4 % fibre normally and over consolidated models.

5.5.1 Characterisation of fibrous models

The models produced for this study showed that when a fibrous organic material was added to material such as kaolin clay, the undrained shear strength increases once an optimum fibre content was exceeded. The effects of consolidation play a significant role in the strengths attained, where over consolidated models produced significantly greater values of undrained shear strength compared to normally consolidated models. Generally speaking, greater percentage fibre content resulted in lower moisture retention in the centrifuge models, Figure 5.75. This would suggest that drainage of moisture through the model was influenced by the fibre content. Normally consolidated models in contrast to over consolidated models retained a greater percentage of moisture, which may be an attribute of the consolidation ratio. In the case of the 0 % fibre content over consolidated model, moisture content was determined at the centre of the model only. In all other cases moisture content was determined at 10, 100 and 190 mm depths in the models. It was not possible to separate low undrained shear strength with high moisture content from the relationship between low undrained shear strength and low fibre content.

Moisture content tests were carried out on each centrifuge model to assist in characterisation. In Figure 5.75, the 4 % fibre content over-consolidated model showed an increase in moisture content with increased depth. This trend became more pronounced for the 3 % fibre content normally consolidated model. The increase in moisture content with depth may be attributed to the presence of fibrous material channelling moisture to the model base. Moisture was continuously expelled from the model during consolidation; however high moisture content in the lower region of the model suggests that the properties of the fibrous material inhibited this from occurring. There was the possibility that fibres are in some way blocking the drainage paths through the filter layer of the drum channel. This would seem logical as the base of the model has experienced a longer consolidation time than the upper regions and should therefore possess lower moisture content.

The reduction in undrained shear strength for the 2 % fibre content normally consolidated model, may be attributed to a higher percentage of moisture inherent in this model compared to any other. The high moisture content in this case may be attributed to high levels of absorbed moisture in the fibres resulting in insufficient consolidation of the model, that had equal consolidation time with the 1 % fibre content normally consolidated model. However, when the 1 % fibre content over consolidated model was examined a similar trend existed where undrained shear strength was weaker than that of 0 % fibre content over consolidated model, for certain types of foundations.

The liquid limit determined for this study correlated well with the value determined by (Stewart 1991). For low fibre contents of 1-2 % the increases in the liquid limit for the respective models was modest. With 3 % fibre content or greater a more noticeable increase in liquid limit determined was recorded. The plastic limit determination was carried out for the range of models tested, also showed an increase with increased fibre content; it was found that with increasing fibre content the plastic limit became increasing difficult to determine. Plastic limit values did not experience the same increase as those of the liquid limit for models with 3 % fibre content or greater. Plasticity index values showed that the presence of the fibrous material increased the plasticity of the soil models and lay with a range of intermediate to high plasticity.

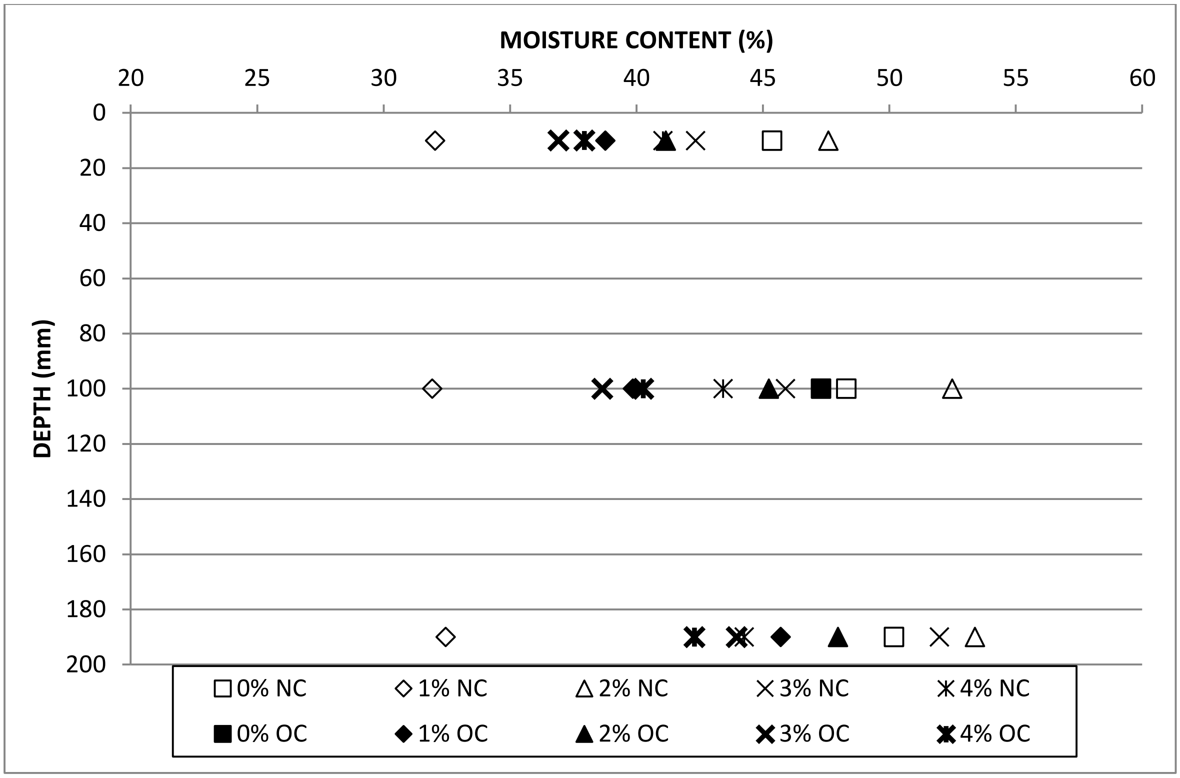

Figure 5.75: Moisture contents for the range of model tested for bearing capacity and shear strength.

5.6 Summary

Analysis and discussion of the centrifuge modelling programme, including bearing capacity and penetrometer profiling, have been presented in this chapter. Centrifuge modelling was comprised of two test series which investigated the effects of various parameters on the undrained shear strength of kaolin clay. Test Series 1 looked at normally consolidated models while the models in Test Series 2 were over consolidated. In each test series the fibre content of the models was varied from 0 to 4 %. The models were subjected to bearing capacity testing with various foundation shapes and sizes at an accelerated gravitational field of 25g for Test Series 1 and 2 respectively. The models were also profiled using the standard cone penetration test (CPT) and a full flow penetrometer (piezoball) to determine the undrained shear strength with depth and as a means of verifying the results of the bearing capacity tests. Various laboratory classification studies, including shear vane testing, were carried out on samples extracted from the consolidated models once centrifuge testing was completed.

Centrifuge modelling showed that varying the fibre content for both the normally consolidated and over consolidated test series had significant effects on the undrained shear strength and moisture content of the fibrous models. Analysis of the undrained shear strengths determined by back calculation from the bearing resistance showed that increasing the fibre content resulted in increased shear strength. This finding is similar to that of other studies such as Attom *et al* (2009), Al–Khafaji (1979) and Freitag (1986) where increased fibre content resulted in increased unconfined compressive and undrained shear strength. Models in Test Series 2 (over consolidated) showed greater undrained shear strength than models comprising Test Series 1 (normally consolidated). Over consolidated models produced an almost uniform shear strength increase for all fibre contents and footing types and was on average greater that the undrained shear strength results determined from normally consolidated models. The effect of over consolidation and anisotropy contributed to increased undrained shear strength, which concurred with studies such as that carried out by Attom and Al-Akhras (2008). Strength scatter was more pronounced for over consolidated models with high levels of fibre reinforcement, usually 2 % fibre content or greater. Normally consolidated models showed constant shear strength up to 3 % fibre content, upon reaching 4 % fibre content the undrained shear strength increased dramatically along with scatter in the results.

The increase in shear strength was also shown through analysis of the penetrometer results for the majority of models. Comparison of the CPT tests results with the undrained shear strength back calculated from bearing capacity testing produced a good relationship, with some scatter in the shear strength present. The relationship between the CPT and piezoball undrained shear strengths also produced a close correlation, similar to that found by Boylan *et al* (2011). Over consolidated models of low percentage fibre showed undrained shear strength levels twice that of the normally consolidation models. Analysis of the piezoball results showed a slightly higher undrained shear strength than that observed with the CPT; scatter was also reduced with the piezoball. Pore pressure data was recorded with the piezoball and was found to spike constantly with increasing depth. The spiked nature of the results may be attributed to positioning of the pore pressure filter located at the probe mid-face instead of a location closer to the piezoball shaft. Pore pressure was found to be negative in certain cases and could be explained by the possibility of the moisture being drawn into the micro cavities surrounding the fibres as the probe passes through the model. This could be similar to the process of dilation in over consolidated soil as described by Li and Meissner (2002), which cause negative pore pressures to occur. The factor N_{ball} was used to calculate the corrections necessary to determine q_{net} and was constant for determining the undrained shear strength of the normally and over consolidated models. As the shear strength determined from the CPT and piezoball are in close agreement with the findings from the back calculations of undrained shear strength, there is good reason to conclude that the correction factor used in this study was reasonably accurate and that little adjustment would be required.

Laboratory shear vane testing was carried out on model cores extracted from the centrifuge models. The shear vane showed that with increased fibre content the undrained shear strength of fibre models increased. This strength increase was only slightly greater for over consolidated models when compared to normally consolidated, indicating the shear vane directly measured the tensile strength of the fibrous matter and was influenced by the effects of consolidation to a lesser extent than that of profiling or bearing capacity analysis. This finding correlated well with that of Landva (1980) who discussed the interaction of fibres on the shearing plane created by conducting a shear vane test and the collection of fibres in front of the vane during testing. A poor correlation was found between the shear vane results and those from bearing capacity determination. The shear vane tests were conducted on model core at 1g compared to bearing capacity and profiling analysis which was carried out at 25g, thus the desk top analysis estimated the undrained shear strength of unconfined samples, where the effective stress was quite low.

Classification tests on samples extracted from centrifuge models demonstrated changing characteristics of kaolin clay, with fibre content. The liquid limit and plasticity were observed to increase with increased fibre content. Analysis of the liquid limit and plasticity index showed that the soil models created in this study were clays of intermediate to high plasticity. Completion of the classification tests such as the Atterberg limits proved to be difficult to complete with increasing fibre content. As the quantity of fibre in each model was chosen by weight this lead to a considerable volume of peat fibres in the 3 % and 4 % models. Objectivity in determining the plasticity index of the fibrous soils created was affected as high fibre content lead to crumbling of samples when handled; however classification was completed since a certain percentage of mineral content is required, as discussed by Edil (2001), when classifying peats or highly organic soil. Moisture content was observed to increase in the models with increasing depth, becoming more pronounced with increasing fibre content. On average, models with higher percentages of fibre reinforcement contained lower moisture contents than models of low fibre content. Consolidation ratio also impacted on moisture content, where normally consolidated models retained more moisture than corresponding over consolidated models. The effect of decreasing undrained shear strength with increasing moisture content could not be separated from the relationship of decreasing undrained shear strength and decreasing fibre content.

CHAPTER 6

CONCLUSIONS AND RECOMMENDATIONS

6.1 Introduction

This study outlined an investigation into the undrained shear strength of kaolin clay models containing organic peat fibres, using geotechnical centrifuge modelling and classification techniques. The results gathered during bearing capacity testing and profiling using standard penetrometers, provided an improved understanding of the shear strength of fibre reinforced soil.

6.2 Project summary

In the literature review, details of previous work on constructing a homogenous fibre sample and methods to determine the undrained shear strength of soil were outlined. Various organic materials have been trialled in fibre reinforcement studies along with numerous methods of mixing to achieve complete fibre dispersion within the soil. In cases of in-situ testing in peats, the presence of fibres can also lead to an elevated stress level in the soil mass when direct shear tests are conducted, particularly in applications of the shear vane (Flaate 1965b). Boylan *et al* (2011) found that the undrained shear strengths determined from the cone penetration test (CPT) were influenced by fibrous matter present in peats; accuracy was found to improve for the ball penetrometer (piezoball) as the full flow penetrometer allowed peat to flow around the sensor, equalising the penetration stresses (Boylan *et al* 2011). Studies identified that achieving a homogeneous soil fibre mass using most mechanical mixing methods can lead to localising of the fibre content and in some cases damage to the fibres became apparent; in contrast mixing by hand produced satisfactory results. Calculation methods relating the bearing capacity of the soil to its undrained shear strength were presented. Bearing capacity factors relevant to the foundations examined in this study were also presented.

The methods employed to construct fibrous centrifuge models and to complete tests utilizing the IT Sligo geotechnical centrifuge were outlined in Chapter 3. The clay used was kaolin as it has been used in geotechnical modelling previously and its responses are well established (Lowmass 2006). The kaolin clay was tested in accordance with BS 1377 (1990) to determine the liquid limit prior to model construction in an effort to ensure quality control of the clay. Fibre material was extracted from bulk peat samples due to the ease of availability and the relative simplicity of extraction; the fibrous material was classified in terms of average diameter and length. The centrifuge models consisted of kaolin clay and fibre quantities of between 0 to 4 % per dry weight of clay mixed together to form a slurry. To achieve normally consolidated models, consolidation and the testing programme was carried out at 25g; while an over consolidated ratio of 2 was achieved by consolidating at 25g and testing at 50 g to complete the second test series.

Undrained shear strength was back calculated from bearing capacity measured in the centrifuge for various foundations of different size and shape, while cone and ball penetrometers were also used to directly assess the undrained shear strength. Additional tests were carried out on cores and bulk samples retrieved from the centrifuge models at the end of testing. The liquid limit, plastic limit, plasticity index and moisture content properties were determined from bulk samples for each of the fibrous soils modelled during the course of this study. Laboratory shear vane testing was also carried out on the cores retrieved from the centrifuge models. The location of the ultimate bearing capacity and back calculated shear strength was determined at the point of maximum loading, along with a secondary failure location where depth of penetration was equal to 0.5 times the breadth or diameter of the foundation used.

6.3 Results from fibrous models

The fibre models used in this study varied in fibre content from 0 % to 4 % of the dry mass of kaolin clay for all models constructed. The analysis of centrifuge results to determine the undrained shear strength of fibrous models was carried out for two test series; Test Series 1 looked at normally consolidated soils while test series 2 investigated over consolidated models with an over consolidation ratio of 2.

The centrifuge modelling analysis and laboratory classification processes identified that increasing the organic fibre content in kaolin clay models, resulted in increased undrained shear strength. This concurred with studies such as Attom *et al* (2009), Al–Khafaji (1979) and Freitag (1986) who studied differing methods to increase shear strength through increased fibre content. Normally consolidated models showed relatively consistent undrained shear strengths determined for fibre contents of between 0 % and 3 %; strength was observed to increase rapidly for the 4 % fibre content normally consolidated model, for all methods used in this study. Strength gains became more pronounced for over consolidated models with 2 % fibre content and greater. Scatter in the undrained shear strength data increased considerably at 3 % fibre content for over consolidated models, and was also present for the 4 % fibre content model.

Comparison between undrained shear strengths associated with maximum load (the primary failure location) and at penetration depths of 0.5 times the foundation breath or diameter for a specific model (the secondary failure location), showed an increase in the undrained shear strength with depth in the majority of models. Strength increases in such cases may in part be attributed to strain hardening of the models. Some scatter of undrained shear strength was common for normally consolidated models, when bearing capacity tests of various foundation types were carried out. The occurrences of constant undrained shear strengths along with case of strain softening were more commonly encountered for normally consolidated models in Test Series 1. Shear strength at the locations of 0.5 B/D displayed diminished strength for some models such as the 3 % over consolidated model and can be related to cases of strain softening or a constant residual strength in the respective models. In the majority of cases, shear strengths determined at depth of 0.5 B/D displayed an increase in undrained shear strength, compared to that determined at maximum curvature.

The fibre content had a considerable effects on the shear strength profiles of the cone and to a lesser extent the ball penetrometer. For cone penetration testing, the strength profiles appeared to be particularly influenced by fibre contents interacting with the cone face and tip as was evident from the scatter present in the resistance profiles; becoming more pronounced with increasing fibre content. Such an action was experienced and commented on by Boylan *et al* (2011). The majority of CPT tests showed a reduction in undrained shear strength with depth, in both normally and over consolidated models. Piezoball strength profiles through the models were less affected by the fibre content as the probe's geometry allowed the fibrous soil to flow around the tip, equalizing the overburden pressure above and below the probe, thus reducing the data scatter, which is consistent with observations by Boylan *et al* (2011). Undrained shear strength for the piezoball showed a relatively constant profile with depth in the majority of cases in Test Series 1 and 2. Pore water pressure displayed significant scatter with depth for some fibre models, with negative pore pressure recorded. Negative pore pressure recordings varied from approximately 0 kPa to -10 kPa in some cases, the majority of negative pore pressure readings were found to be within the range of 0 to -3 kPa. Pore pressures profiles overall were not influenced greatly with increases in depth; where pore pressure was seen to increase, the pressure encountered was less than 15 kPa.

Comparison between the back calculated results of undrained shear strength from bearing capacity testing showed good correlation with the results of penetrometer testing. The undrained shear strength determined from bearing resistance testing were approximately twice that of CPT penetrometer strength results in some cases; that included over consolidated models and normally consolidated models with 3 % and 4 % fibre reinforcement. Normally consolidated models with low fibre levels produced an excellent correlation between the penetrometer and back calculated results. Piezoball results showed a closer relationship to back calculated bearing capacity shear strengths, with some scatter for models of high content and models that were over consolidated. Overall piezoball results determined that undrained shear strength to be higher than that of corresponding CPT results.

Comparison between the undrained shear strength of fibrous models determined during the centrifuge modelling series, which included back calculations of shear strength from bearing capacity results and penetrometer profiling did not correlate with the results of the laboratory shear vane results. Undrained shear strength between the control models of 0 % fibre content for normal and over consolidation were in reasonable agreement with the penetrometer and back calculated strength results; however, with increasing fibre content the shear strength determined from the vane increased only marginally in contrast to the other methods. This occurred as vane tests were carried out on model samples with low effective stress, i.e. unconfined samples.

In the fibrous models the moisture content increased with increased depth. Overall the models with a greater percentage of fibre held less moisture than models with a lower fibre content. This would suggest that the presence of fibres contributed to permeability of the models. Increased moisture content and permeability was the topic of investigation carried out by Mattone (2005) who found increased permeability with increasing fibre content. Over consolidated models also showed lower moisture content than normally consolidated models.

Other classification tests showed that with increasing fibre content the liquid limit, plastic limit and plasticity index increased almost linearly.

6.4 Main conclusions

The main conclusions of this study are as follows:

- The undrained shear strength of a fibre soil increased once a threshold quantity of fibres was present. Typically this was 4 % by dry unit weight of soil in normally consolidated soils and 2-3 % by dry unit weight of soil in over consolidated soils.
- Atterberg limits and plasticity indices increased almost linearly as the fibre content increased, but proved difficult to complete as detail by Edil (2001).
- CPT profiling of the fibrous soil resulted in a reduction in undrained shear strength profile with increased depth, along with some data spikes in the upper 20 mm of the model. Scatter of the undrained shear strength data was prominent in the CPT tests.
- Piezoball profiling of the fibrous soil was found to give consistent undrained shear strength results in the majority of cases with minimal scatter of data. This was a result of the ability of the fibrous soil to flow around the probe as described by Boylan *et al* (2011).
- Laboratory shear vane results on unconfined model samples showed poor correlation with back calculations of undrained shear strength results along with shear strength profiles from the CPT and piezoball tests. This is a result of laboratory shear vane testing at 1g where effective stress is low in comparison to the two centrifuge test series completed at 25g. Results of the shear vane analysis suggest that the shear vane is influenced more by fibre content, described by Landva (1980) than by the effects of consolidation.
- Mobilization of undrained shear strength decreased somewhat in the majority of cases with increased foundation size which is consistent with expectations from Eurocode 7.
- Back calculation of undrained shear strength from bearing capacity tests was found to be greater for over consolidated models compared to those normally consolidated. Scatter in the undrained shear strength profiles became considerable at 4 % and 3 % fibre content for the normally and over consolidated models respectively.

- The relationship between normally consolidated and over consolidated soil with fibre content showed that undrained shear strength from bearing capacity data was greater with over consolidated models with low fibre content but began to approach a good correlation with increased fibre content. The same trend was apparent for the CPT and piezoball data. Laboratory shear vane data showed a close correlation between normally and over consolidated models.

6.5 Recommendations for future work

This study has further added to the existing knowledge of organic soils with varying degrees of fibre content. There are still aspects of this topic that can be investigated:

- The peat fibre models in this study did not reach a peak undrained shear strength which would have translated to an optimum percentage of fibre content. Increasing the peat fibre content of centrifuge models to find the optimum percentage of organic fibre reinforcement should be investigated in a future study.
- Other forms of organic fibrous material would provide a comparison to the peat material trial in this study. Of particular interest would be the effects of the physical characteristics such as fibre length and surface texture; with the possibility of improved undrained shear strength for similar fibre contents. The preparation of peat fibre by hand proved to be a somewhat laborious task, other sources of organic fibrous matter could provide to be a more attainable source of material and achieve a better soil/fire shear strength.
- This study looked at fibrous soil at shallow depths of between 2.5 m and 5.0 m. Investigation of the effects of fibre content at depths greater than 5 m and with greater over consolidation of centrifuge models would perhaps lead to better understanding of fibrous soil at depth.
- This study looked at a uniform distribution of a single fibre quantity throughout a soil mass. It would be worth investigating the behaviour of several models, where fibre reinforcement varies between a series of separate layers and the resulting effects on undrained shear strength determined through a similar testing procedure. Care would be essential to ensure no discontinuity between the soil layers developed, thus effecting the homogeny of the models.

- Two penetrometer devices were utilized during the course of this study, a CPT and the piezoball. It would be worth investigating the performance of other penetrometers in fibrous soils in particular the effects of fibres on the accuracy of such probes.

REFERENCES

Aas, G., Lacasse, S., Lunne T. & Hoeg, K. 1986. Use of in situ tests for foundation design on clay. *Proceedings of the ASCE Specialty Conference In-Situ*, 1986.

Al-Khafaji, A.W.N. 1979. *Decomposition effects on engineering properties of fibrous organic soils*, PhD Thesis, Michigan State University.

Attom, M. F. & Al-Akhras, N.M. 2008. Investigating anisotropy in shear strength of clayey soils. *Proceedings of the Institute of Civil Engineers.* Geotechnical Engineering 161. Issue GE5, pp 269-273.

Attom, M. F., Al-Akhras, N. M. & Malkawi, A. I. H. 2009. The effect of fibre on the mechanical properties of clayey soil. *Proceedings of the Institution of Civil Engineers*, Geotechnical Engineering 162, Issue GE5, pp 277-282.

Bjerrum, L. 1973. Problems of soil mechanics and construction on soft clays. *Proceedings of the 8th International Conference on Soil Mechanics and Foundation Engineering*, Moscow, pp111-159.

Boylan, N. & Long, M. 2007. Characterisation of peat using full flow penetrometers. *Soft Soil Engineering*, Taylor & Francis Group, London. pp 403-414.

Boylan, N., Jennings, P. & Long, M. 2008. Peat slope failure in Ireland. *Quarterly Journal of Engineering Geology and Hydrogeology*, 41, pp 93-108. From, http://www.ucd.ie/bogland/publications/Boylan Peat Failures. (Accessed Nov 2011)

Boylan, N., Long, M. & Mathijssen, F.A.J.M. 2011. In situ strength characterisation of peat and organic soil using full flow penetrometers. *Canadian Geotechnical Journal*, 48, pp 1085-1099.

Broadbent & Sons 2010. *Layout of centrifuge equipped with drum, actuator, viewing window and rotary stack*, illustration from e-mail correspondence.

Broadbent & Sons 2010. *Cut-away of drum showing tool table, actuator and drive assembly*, illustration from e-mail correspondence.

Broadbent & Sons 2010. *Section through the radial actuator used for loading plate and penetrometer testing*, illustration from e-mail correspondence.

Broadbent & Sons 2010. *Location of CPT and Piezoball testing position, along with Core extraction position*, illustration from e-mail correspondence.

Broadbent & Sons 2010. *Funnel and spiral dispersion blade apparatus used to fill drum channel*, illustration from e-mail correspondence.

Broadbent & Sons 2010. *Location of various foundations along the model surface during each testing phase*, illustration.

BS1377-2 1990. *Methods of test for Soils for civil engineering purposes - Part 2: Classification tests*. British Standards Institute.

BS1377-7 1990. *Methods of test for Soils for civil engineering purposes - Part 7: Shear strength tests (total stress).* British Standards Institute.

BS5930 1999. *Code of practice for site investigations.* British Standards Institute.

Cassidy, M.J., Quah, C.K. & Foo, K.S. 2009. Experimental Investigation of the Reinstallation of Spudcan Footings Close to Existing Footprints. *Journal of Geotechnical and Geoenvironmental Engineering*, 135 (4), pp 474-486.

Cadling, L. & Odenstad, S. 1950. The vane borer: an apparatus for determineing the shear strength of clay soils directly in the ground. *Royal Swedish Geotechnical Institute*, Proc, 2.

Chia, L.S. 2004. Centrifuge Model study of Pile Foundation System for Oil Tank, *Degree of Masters of Engineering Thesis*, National University of Singapore.

Clough, G. W. & Hansen, L. A. 1981. Clay anisotropy and braced wall behavior. *Journal of the Geotechnical Engineering,* ASCE, 107, No. GT7, pp 893-913.

Connolly, J., Holden, N.M. & Ward, S.M. 2007. Mapping peatlands in Ireland using a rule-based methodology and digital data. *Soil Science Society of America Journal*, 71, pp 492-499.

Das, A., Jayashree, C. & Viswanadham, B.V.S. 2009. Effect of randomly distributed geofibers on the piping behaviour of embankments constructed with fly ash as a fill material. *Elsevier, Geotextiles and Geomembranes 27*, pp 341-349, From:www.elsevier.com/locate/geotexmem. (Accessed Jun 2012)

Dean, E.R.T., Hsu, Y.S., James, R.G., Sasakura, T., Schofield, A.N. & Tsukamoto, Y. 1997. Centrifuge Modeling of Jack-Ups and Spudcans on Drained and Partially Drained Silica Sand, *Elsevier, Marine Structures 10*, pp 221-241.

Eden, W.J. & Hamilton, J.J. 1957. The use of a field vane apparatus in sensitive clay. ASTM STP 193, pp 41-53.

Edil, T. B. 2001. Site characterisation in peat and organic soils. *Proceeding of the International Conference on In Situ Measurement of Soil Properties and Case Histories.* Bali, Indonesia, pp 49-59.

EN 1997-1:2005 Annex D. A sample analytical method for bearing resistance calculation.

Freitag, D.R. 1986. Soil randomly reinforced with fibers. *Journal of Geotechnical Engineering*, ASCE, 112 (8), pp 823-826.

Flaate, K. 1965b. Field vane tests with delayed shear. *Paper presented at 5th Pacific Area National Meeting of the ASTM* (Seattle).

Flaate, K. 1966. Factors influencing the results of vane tests. *Canadian Geotechnical Journal*, 3 (1), 18-31.

Gaudin, C., White, D.J., Boylan, N., Breen, J., Brown, T., De Catania, S. & Hortin, P. 2009. A wireless high-speed data acquisition system for geotechnical centrifuge model testing. *Meas. Sci. Technol.*, 20 (9), pp 1-11.

Gaudin, C., Cassidy, M.J., Bienen, B. & Hossain, M.S. 2011. Recent contributions of geotechnical centrifuge modelling to the understanding of jack-up spudcan behavior. Elsevier, Ocean Engineering, 38 (7), pp900-914.

Ghavami, K., Toledo F.R.D. & Barbosac, N.P. 1999. Behaviour of composite soil reinforced with natural fibres, *Elsevier, Cement and Concrete Composites*, pp 39-48.

Heineck, K.S., Coop, M.R. & Consoli, N.C. 2005. Effect of Micro reinforcement of Soils from very Small to very large shear strains. *Journal of Geotechnical and Geoenvironmental Engineering, (ASCE),* 131 (8), pp 1024-1033.

Hejazi, S.M., Sheikhzadeh, M., Abtahi, S.M., & Zadhoush, A. 2012. A simple review of soil reinforcement by using natural and synthetic fibers. *Elsevier, Construction and Building Materials 30,* pp 100–116, www.elsevier.com/locate/conbuildmat. (Accessed Nov 2012)

Helenelund, K. V. 1967. Vane tests and tension tests on fibrous peats, *Proceeding of the Geotechical Conference on shear strength properties of natural soils and rocks,* Oslo, pp 199-203.

Hobbs, N.B. 1986. Mire morphology and the properties and behaviour of some British and foreign peats. *Quarterly Journal of Engineering Geology,* 19, pp7-80.

Hossain, M. S., Hu, Y. & Randolph, M. F. 2003. Spudcan Foundation Penetration into Uniform Clay, *Proceedings of The Thirteenth (2003) International Offshore and Polar Engineering Conference Honolulu, Hawaii, USA*, pp 647-652.

Jacobson, B. 1955. Isotropy of clays. *Géotechnique*, 5 (3), pp 23-28

Kallstenius, T. 1963. Studies of clay samples taken with standard piston sampler. *Royal Swedish Geotechnical Institute Proc. 21.*

Knappett, J.A. & Craig, R.F. 2012. Craig's Soil Mechanics, 8th Edition, Spon Press, Taylor and Francis, New York and London.

Kelleher, P.J. & Randolph, M.F. (2005). Seabed geotechnical characterisation with the portable remotely controlled drill. *In Gourvenec S and Cassidy M (eds), Proceeding of the International Symposium on Frontiers in Offshore Geotechnics: ISFOG 2005.* London: Taylor and Francis, pp 365-371.

Kim, D.S., Kim, N.R., Choo, Y.W. & Cho, GC. 2013. A newly developed state-of-the-art geotechnical centrifuge in Korea. *KSCE Journal of Civil Engineering* 17 (1), 77-84. www.springer.com/12205. (Accessed Dec 2011)

Ladd, C. C. & Foott, R., 1974, "New Design Procedure for Stability of Soft Clays, *Journal of the Geotechnical Engineering Division,* Vol. 100, No. GT 7, pp. 763–786. http://www.maaconsultants.com/common/publications. (Accessed May 2014)

Landva, A.O. 1980. Vane testing in peat. *Canadian Geotechnical Journal* 17, pp1-19.

Lefebvre, G., Langlois, P., Lupien, C. & Lavallee, J. 1984. Laboratory testing on in situ behavior of peat as embankment foundation. *Canadian Geotechnical Journal*, 21, pp 322-337.

Li, T. & Meissner, H. 2002. Two Surface Plasticity Model for Cyclic Behaviour of Clays. *Journal of Geotechnical and Geo-environmental Engineering*, 128 (7).

Lindsay, R. & Bragg, O. 2003. Wind Farms and Blanket Peat. The Bog Slide of 16th October 2003 at Derrybrien, Co. Galway, Ireland. 2nd Edition. *School of Health and Biosciences, University of East London,* Romford Road, London.

Ling, H. I., Yue, D., Kaliakin, V.N. & Themelis, N. J. 2002. Anisotropic Elastoplastic Bounding Surface Model for Cohesive Soils. *Journal of Engineering Mechanics,* 128 (7), pp 748-758.

Long, M & Gudjonsson, G.T. 2004. T-bar testing in Irish soils. *Proceedings of 2nd International Conference on Geotechnical and Geophysical Site Characterization - ISC'2*. Porto, Millpress, pp 719-726.

Lowmass, A.C. 2006. *Installation and Keying of follower embedded Plate Anchors*. Master's Thesis, University of Western Australia.

Lunne, T., Robertson, P.K. & Powell, J.J.M. 1997. Cone Penetration Testing in Geotechnical Practice. Taylor and Francis Group.

Lunne, T., Randolph, M.F., Chung, S.F., Andersen, K.H. & Sjursen, M. 2005. Comparison of cone and T-bar factors in two onshore and one offshore clay sediments. *Frontiers in Offshore Geotechnics: ISFOG 2005*, Gourvenec and Cassidy, Perth, pp 981-989.

MacFarlane, I.C. & Rutka, A. 1962. An evaluaion of pavement performance over muskeg in northern Ontario. *Highway Researsch Boeard Bulletin*, 316, Washington, DC.

Maher, M. & Ho, Y. 1994. Mechanical properties of kaolinite/fiber soil composite. *Journal of Geotechnical Engineering*, ASCE, 120 (8), pp 1380-1392.

Mattone, R. 2005. Sisal fibre reinforced soil with cement or cactus pulp in Bahareque technique, *Elsevier, Cement and Concrete Composites,* pp 611-616. From;http:// sciencedirect.com (Accessed Jun 2012)

Meyerhof, G.G. 1951. The ultimate bearing capacity of foundations. *Geotechnique* 2: 301.

Meyerhof, G.G. 1963. Some recent research on the bearing capacity of foundations. *Canadian Geotechnical Journal*, 1 (1), pp 16-27.

Mitchell, J.K. 1993. Fundamentals of Soil Behaviour, 2nd Edition, Wiley, New York.

Ohde, J. 1938. Zur Theoris des Erddruckes unter besonderer Berücksic gung der Erddruckverteilung. (The theory of earth pressure with special reference to earth pressure distribution). *Die Bautechnik,* Vol. 16.

O'Loughlin, C.D., Naughton, P., Baker, N. & Ainsworth, A. 2010. *Establishing a beam centrifuge facility at the Institute of Technology, Sligo, Ireland.* Proceedings of the 7th International Conference on Physical Modelling in Geotechnics (ICPMG 2010), Zurich, Switzerland.

Powrie, W. 1997. Soil Mechanics Concepts and Applications, E & FN Spon, Chapman and Hall, London, UK.

Powrie, W. 2004. Soil Mechanics *Concepts and Applications* 2nd Edition, Spon Press Taylor and Francis Group, London and New York.

Prandtl, L. 1920. Uber die Härte plastischer Körper. (On the hardness of plastic bodies) Nachr. Kgl. G Wiss. Göttingen, Math.phys.Klasse, pp 74.

Puppala, A. & Musenda, C. 2000. Effects of fiber reinforcement on strength and volume change in expansive soils. *Transportation Research Record* 1736, pp 134-140.

Randolph, M.F. 2004. Characterisation of soft sediments for offshore applications. *Proceedings of the 2nd International Conference on Geotechnical and Geophysical Site Characterization - ISC'2*, Porto, 1, Millpress, pp 209-232.

Rankine, W.J.M. 1857. On the stability of Loose Earth, Phil. Trans. Royal Soc. London, Vol.147.

Rattley, M. J., Richards, D. J. & Lehane, B. M. 2008. Uplift Performance of Transmission Tower Foundations Embedded in Clay, *Journal of Geotechnical and Geoenvironmental Engineering*, 134 (4), pp 531-540.

Reissner, H. 1924. Zum Erddruckproblem (The earth pressure problem) *Proceedings of the First International Congregation of Applied Mechanics,* pp 295.

Schule, B.J., Morz, T. & Kreiter, S. 2011. Undrained shear strength properties of organic harbour mud at low consolidation stress levels. *Canadian Geotechnical Journal*, 48, pp 388-398.

Segetin, M., Jayaraman, K. & X, Xun. 2006. Harakeke reinforcement of soil–cement building materials, Manufacturability and properties. *Science Direct, Building and Environment*, 42, pp 3066-3079.

Sivakumar, V., Doran, I. G., Graham, J. & Johnson, A. 2001.The effect of anisotropic elasticity on the yielding characteristics of overconsolidated natural clay. *Canadian Geotechnical Journal*, 38, pp 125-137.

Sivakumar, V., Doran, I. G. & Graham, J. 2002. Particle orientation and its influence on the mechanical behavior of isotropically consolidated reconstituted clay. *Engineering Geology*, 66 (3–4), pp 197–209.

Skempton, A.W. 1951. *The bearing capacity of clays*, Proceedings, Building Research Congress, London.

Salgado, R., Lyamin, A.V., Sloan, S.W. & Yu, H.S. 2004. Two and three dimensional bearing capacity of foundations in clay, *Géotechnique*, 54 (5), pp 297–306.

Stewart, D.P. 1991. *Lateral Loading of Piled Bridge Abutments due to Embankment Construction*. PhD Thesis, University of Western Australia.

Stewart, D.P. & Randolph, M.F. 1991. A new site investigation tool for the centrifuge. *Proceeding of the International Conference on Centrifuge Modelling, Centrifuge 91*, Boulder, Colorado, pp 531 – 538.

Stewart, D.P. & Finnie, I.M.S. 2001. Spuncan-Footprint Interaction During Jack-Up Workovers, *Proceedings of the 11th International Offshore and Polar Engineering Conference, Stavanger, Norway*, pp 61-65.

Taylor, R. N. 1995. *Geotechnical Centrifuge Technology*, Taylor and Francis Group, London and New York.

Terzaghi, K. 1943. Theoretical soil mechanics. Wiley & Sons, New York.

Terzaghi, K., Peck, R.B., & Mesri, G. 1996. Soil Mechanics in Engineering Practice. 3rd Edition, John Wiley & Sons, New York.

Tessari, A., Sasanakul, I. & Abdoun, T. 2010. Advanced sensing in geotechnical centrifuge models, *Physical Modelling in Geotechnics*, Taylor and Francis Group, London.

Viswanadham, B.V.S., Phanikumar, B.R. & Mukherjee, R.V. 2009. Swelling behaviour of a geofiber-reinforced expansive soil, *Elsevier, Geotextiles and Geomembranes, 27*, pp 73-76. From:www.elsevier.com/locate/geotexmem. (Accessed Jun 2012)

Vesić, A.S. 1973. Analysis of Ultimate Loads of Shallow Foundations. *Journal of the Soil Mechanics and Foundation Division,* Proceedings of the American Society of Civil Engineers, 99, No. SMI.

Vey, E. 1955. Discussion of paper *Field vane shear testes of sensitive soils* by Hamilton Gray. *Proceedings.* ASCE 81, Paper 843, pp 17-20.

Whitlow, R. 2001. Basic Soil Mechanics, 4th Edition, Pearson Education Limited, Harlow, Essex, England.

APPENDIX A:

PAPER SUMMARY

Establishing a beam centrifuge facility at the Institute of Technology Sligo, Ireland.

O'Loughlin et al 2010.

The geotechnical centrifuge facility at the Institute of Technology, Sligo was installed and commissioned during July and August, 2009. The centrifuge, designed and manufactured by Thomas Broadbent & Sons, is a 9 g-tonne beam centrifuge. The centrifuge design permits a beam rotor to be interchanged with a drum channel, so that the centrifuge can be used in either beam or drum mode. The drum channel and tool table were designed and manufactured to rotate independently of each other. The 12 mm steel casing with an outer diameter of 1.7 m surrounding the rotating assembly is designed to contain debris, in the unlikely event of an accident. In beam mode the centrifuge is designed such that a strongbox is suspended from pivots at either end of the 0.75 m beam. Each strongbox acts as a counterweight to the other and doubles the available testing area. The strongboxes with perspex optical viewing windows either side of the model permits optical measurement of planar soil deformation using a high resolution digital compact camera. In drum mode the greater testing area permits a large number of foundation or profiling tests to be conducted from instrumentation attached to the tool table. A hinged window on the casing lid provides access to the assembly. When required the entire casing lid can be removed using the overhead gantry to allow the drum to be removed. The maximum rotational speed is 638 rpm, equivalent to an acceleration level of 300 g at the effective radius of the sample.

The centrifuge is driven by a 7.5 kW, 380/415 V, 3 phase AC motor. The motor is located vertically on the centrifuge casing and drive is transmitted from the motor to the centrifuge drive shaft via multiple V wedge belts. Variation in the centrifuge rotational speed is achieved using a solid state inverter located in the control/drive panel. The inverter is regenerative and can provide electrical braking to assist aerodynamic drag on the beam, allowing quick deceleration of the assembly. The centrifuge features a rotary stack that allows for the passage of fluid and air through 2 channels and electrical signals or power via 16 slip rings. The rotary stack is located centrally on top of the beam rotor/drum tool table and protrudes through the centre of the lid. The rotor of the slip ring stack is installed over a support column that is flange mounted to the top of the beam/drum hub. The power and data lines originating at the top plate of the stator, are fed down slots on the outside of the column terminating at connectors attached to the beam rotor/drum. Of the total 16 electrical slip rings, 4 are rated to 10 A and 12 rated to 2 A. The slip rings provide power to devices in flight such as the electrical actuator and data acquisition system. A two way fluid rotary union suitable for supplying both fluid and air up to 1 MPa is attached to the top of the support column. Fluid or air from the rotary union passes via transfer spools down the full length of the support column and emerges at tapped holes just above the beam hub.

An industrial programmable logic controller (PLC) controls all normal machine functions such as speed, start/stop sequences and also provide the first level of safety features such as access interlocks, and protection against overspeed and unbalance. Critical machine related safety functions such as emergency stop, overspeed and excessive unbalance are hardwired independently of the PLC to comply with current safety legislation. The centrifuge is operated from a local control panel that houses the PLC, an input/display touch screen and a series of push buttons for starting and stopping the centrifuge. The touch screen allows programming of the desired centrifuge speed and displays centrifuge status parameters. Centrifuge speed is measured by impulses from two proximity sensors attached to the bottom of the centrifuge drive shaft. To guard against faulty speed control, two independent speed monitoring systems are fitted, that bring the centrifuge to rest if the pulse speed exceeds preset limits. A number of wireless pinhole cameras are mounted at various locations within the centrifuge that facilitate visual safety checks and permits experiments to be viewed in real-time. Out of balance loading on the centrifuge beam causes small deflections of the centrifuge and the resultant vibration at the shaft rotational frequency is sensed by an accelerometer mounted on the connector ring at the top of the rotary stack. Software vibration limits initiate an alarm if the unbalance reaches 50% of the maximum permitted unbalance and a controlled stop and shutdown if the unbalance exceeds the maximum permitted unbalance. There is a hardwired protection feature that guards against PLC faults, initiating a controlled stop if unbalance exceeds 120 % of permitted limits.

A geotechnical centrifuge data acquisition system (DAS) is located on-board the rotating assembly close to the axis of rotation so as to minimise the g level experienced by the electronics. An extremely compact and robust wireless DAS has been developed by the University of Western Australia (UWA) for their drum centrifuge. Each logging unit is contained within a metal box 150 × 60 × 40 mm in size and is capable of powering and monitoring 8 instrument channels at a sampling rate of up to 1 MHz at 16-bit resolution. The UWA wireless DAS performs the full sequence of amplification, conditioning, digitization and storage on a single circuit board via an independent micro-controller allocated to each pair of instrumented channels (Gaudin et al. 2009). UWA have developed a similar wireless DAS for the ITS centrifuge, but with 2 units which allows up to 16 instrument channels to be logged simultaneously. Additional 8 channel logging units can be daisy-chained at a later date if required. 12 V DC power is provided to the DAS network switch via the electrical slip rings. The DAS and other test specific control systems are mounted on an instrumentation chassis plate that is mounted onto the tool table or the beam rotor at the axis of rotation.

An electronic linear actuator has been developed for conducting model characterisation and foundation tests. The location of the actuator in relation to the model is controlled manually prior to testing. The actuator has a stroke length of 145 mm and in flight has a loading capacity of 2 kN at a maximum actuator speed of 10 mm/s. The actuator drive motor is a 80 V DC brushless servo motor that drives a worm gearbox traveling nut screw jack via a toothed belt. Axial position is sensed by a non-contacting magneto-inductive linear transducer. The actuator is controlled via software from the laboratory PC.

APPENDIX B:

CENTRIFUGE MODELLING RESULTS

CPT

TEST SERIES 1

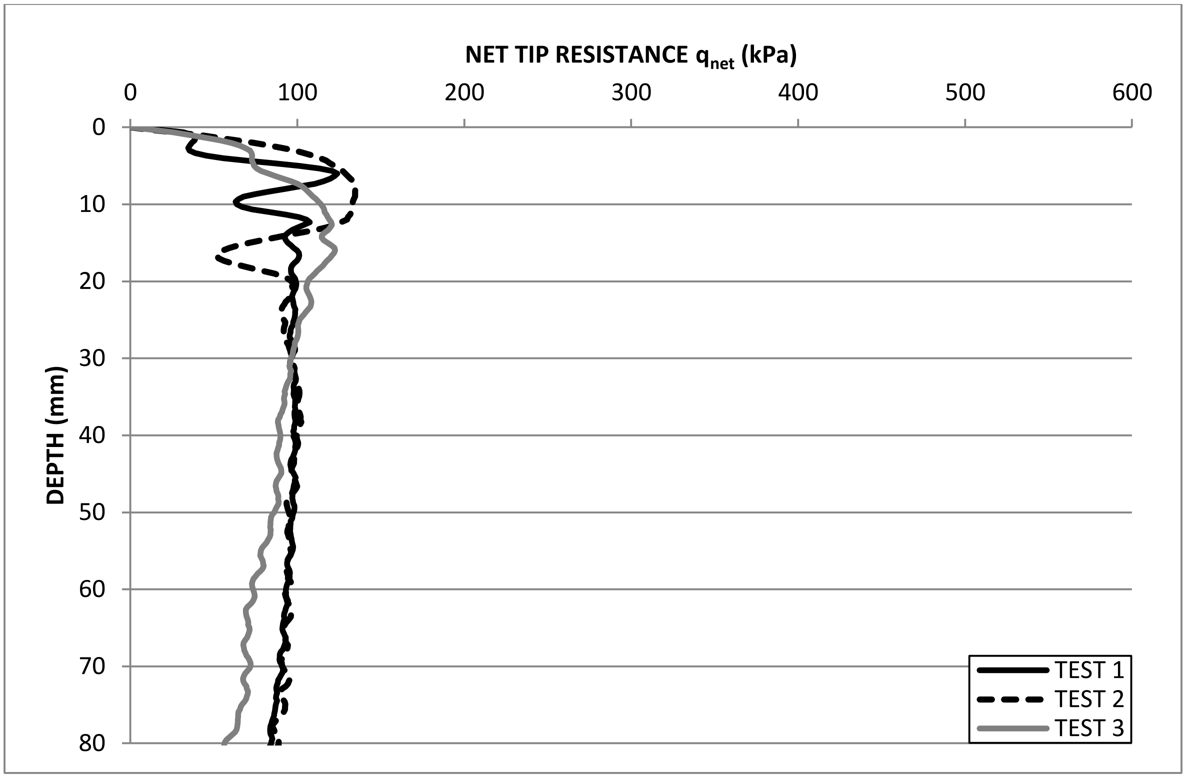

Figure B.1: CPT net tip resistance profile for 1 % fibre normally consolidated model.

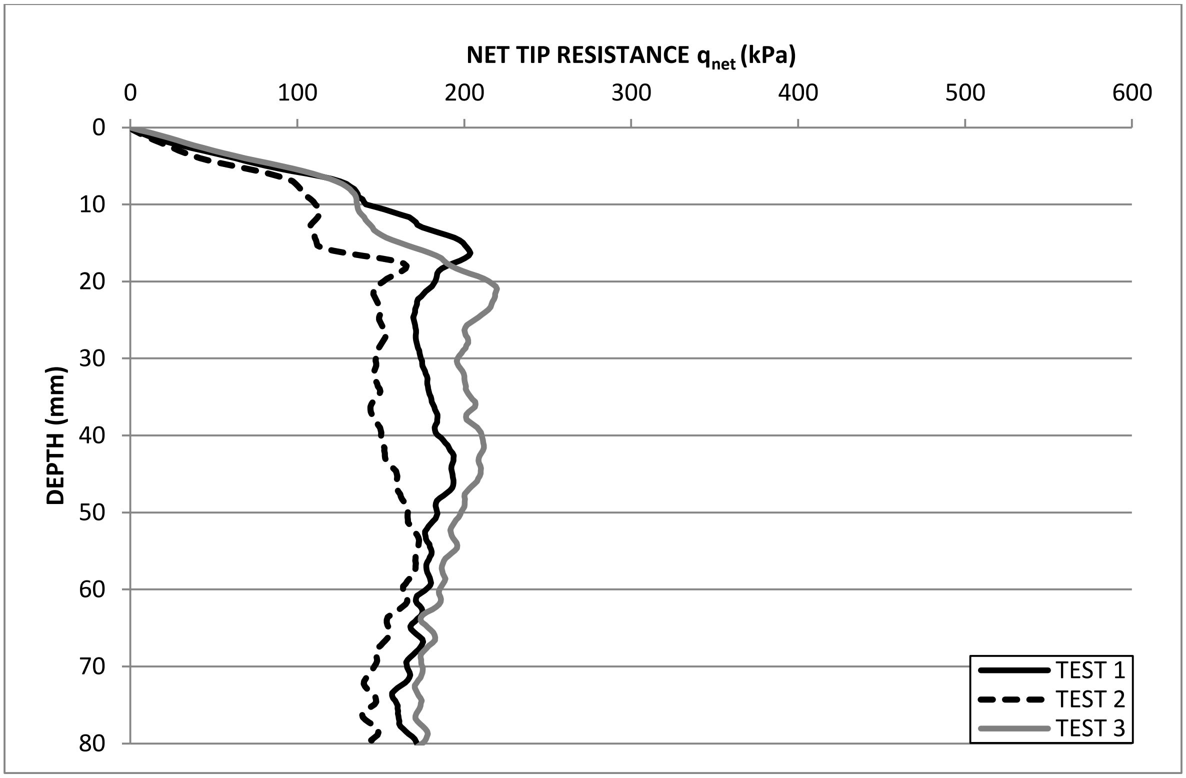

Figure B.2: CPT net tip resistance profile for 1 % fibre normally consolidated model.

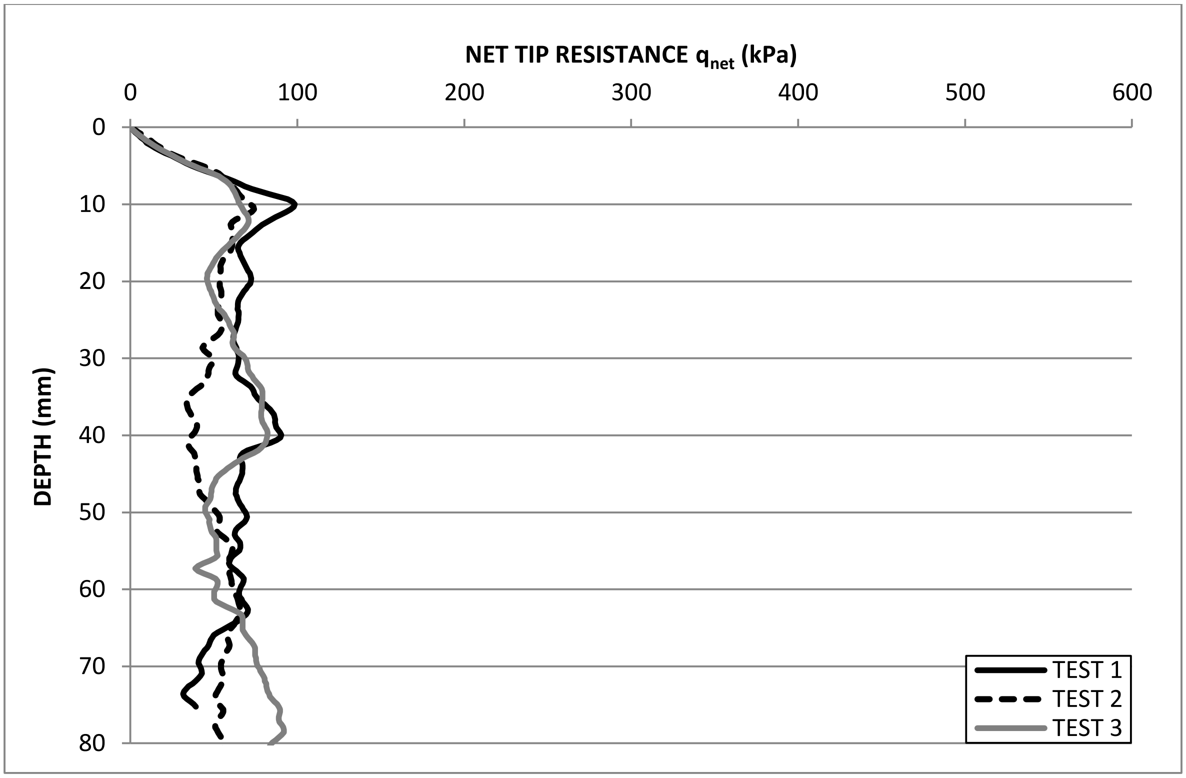

Figure B.3: CPT net tip resistance profile for 2 % fibre normally consolidated model.

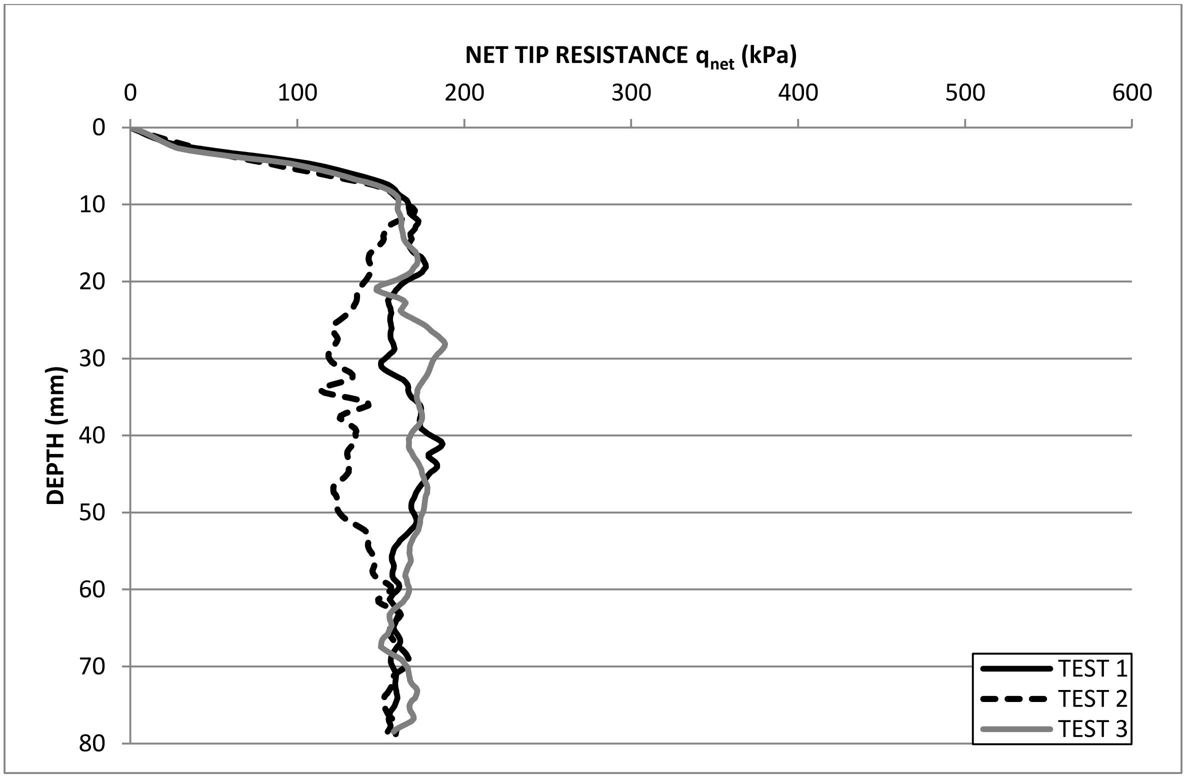

Figure B.4: CPT net tip resistance profile for 3 % fibre normally consolidated model.

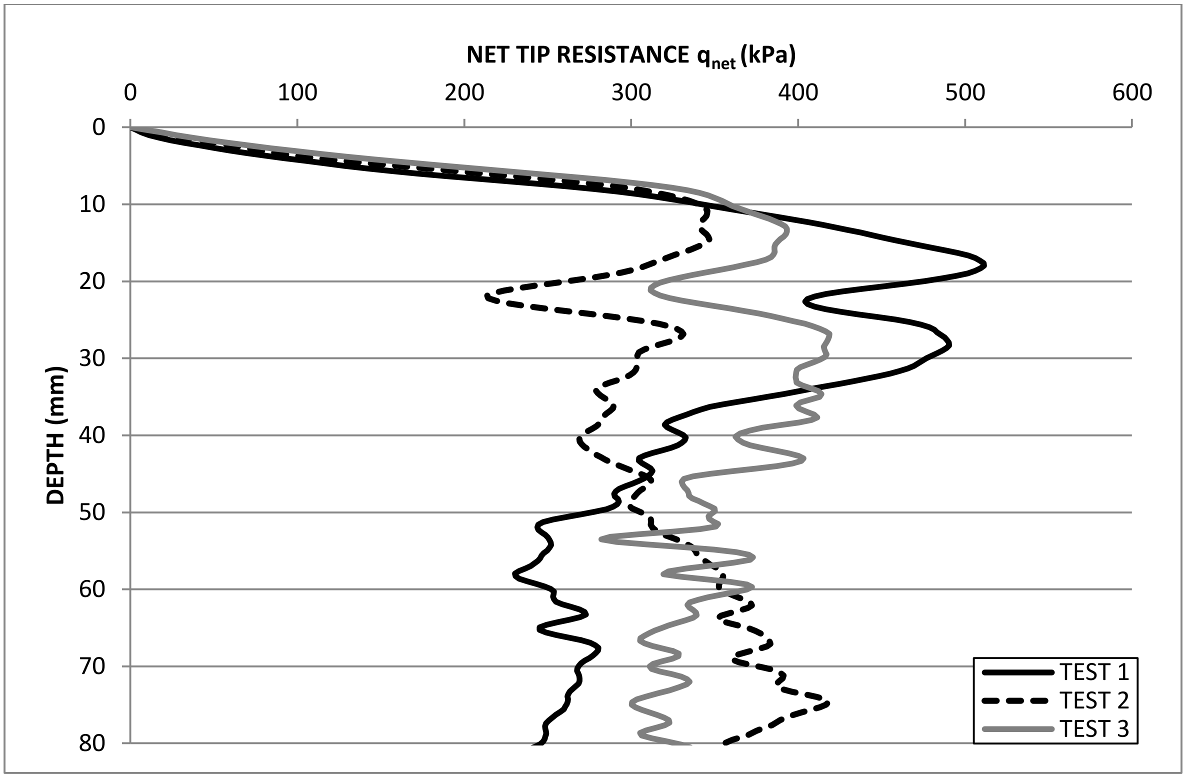

Figure B.5: CPT net tip resistance profile for 4 % fibre normally consolidated model.

APPENDIX C:

CENTRIFUGE MODELLING RESULTS

CPT

TEST SERIES 2

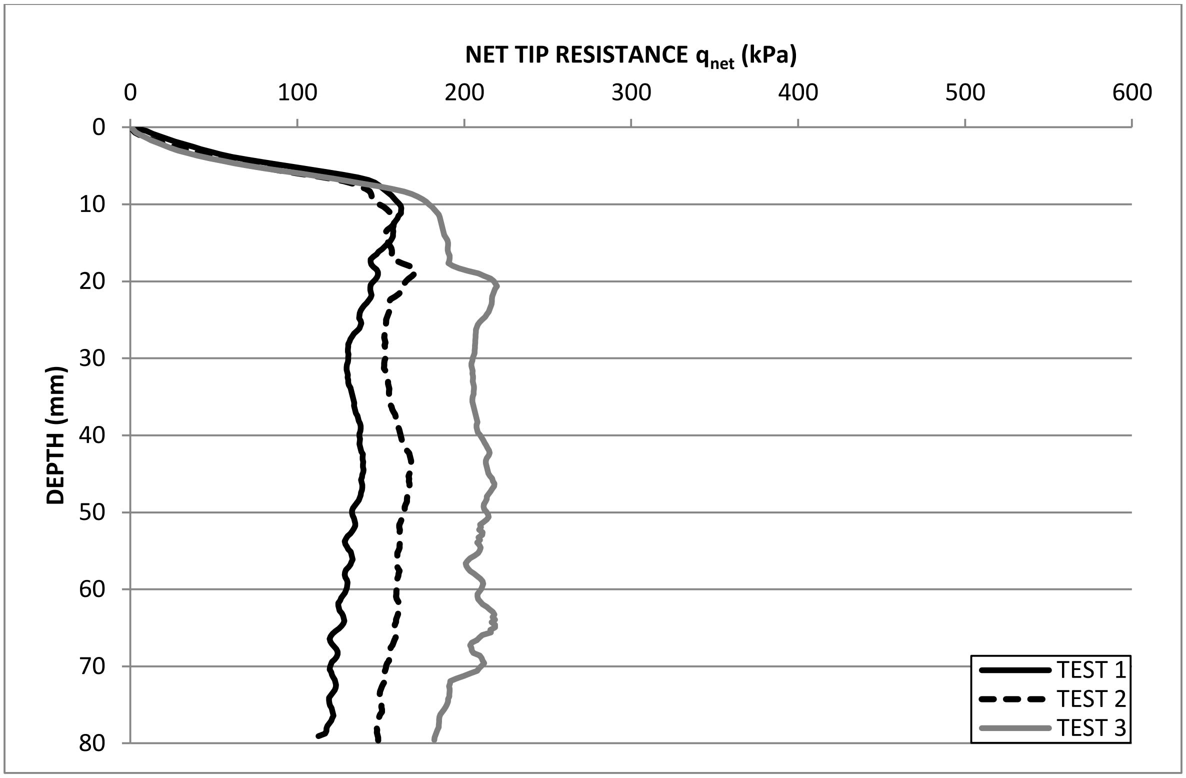

Figure C.1: CPT net tip resistance profile for 0 % fibre over consolidated model.

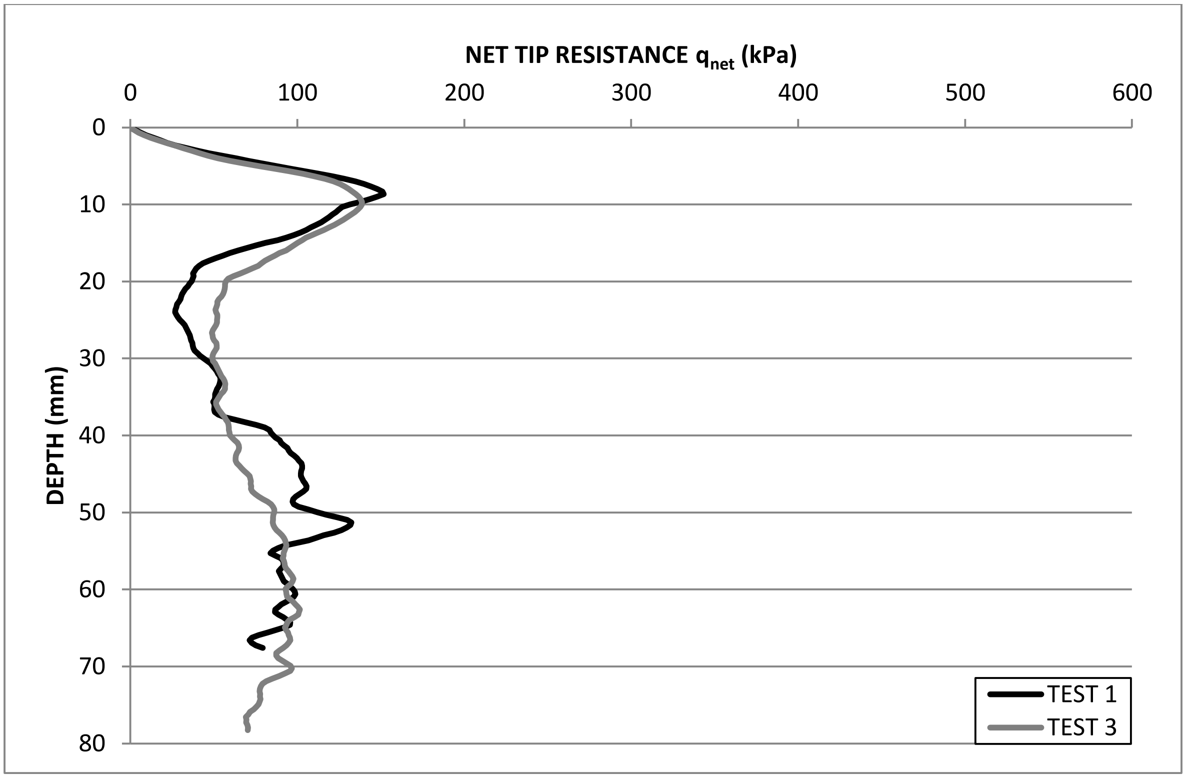

Figure C.2: CPT net tip resistance profile for 1 % fibre over consolidated model.

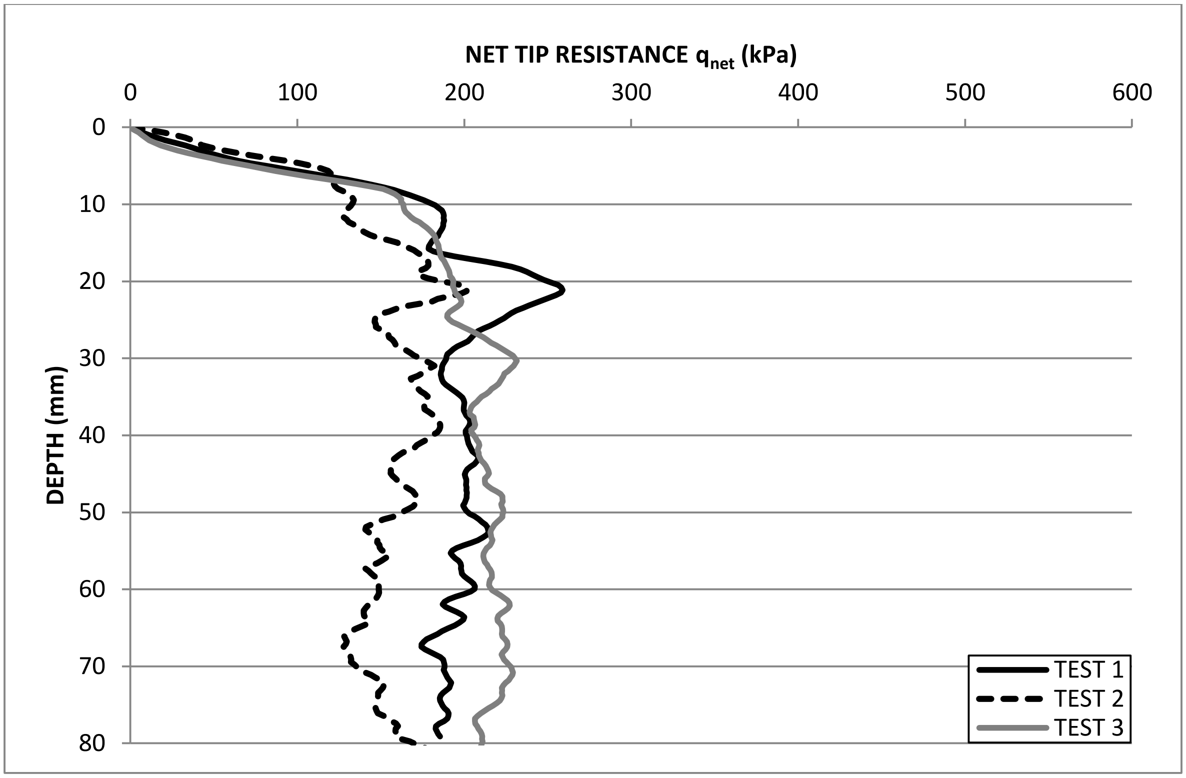

Figure C.3: CPT net tip resistance profile for 2 % fibre over consolidated model.

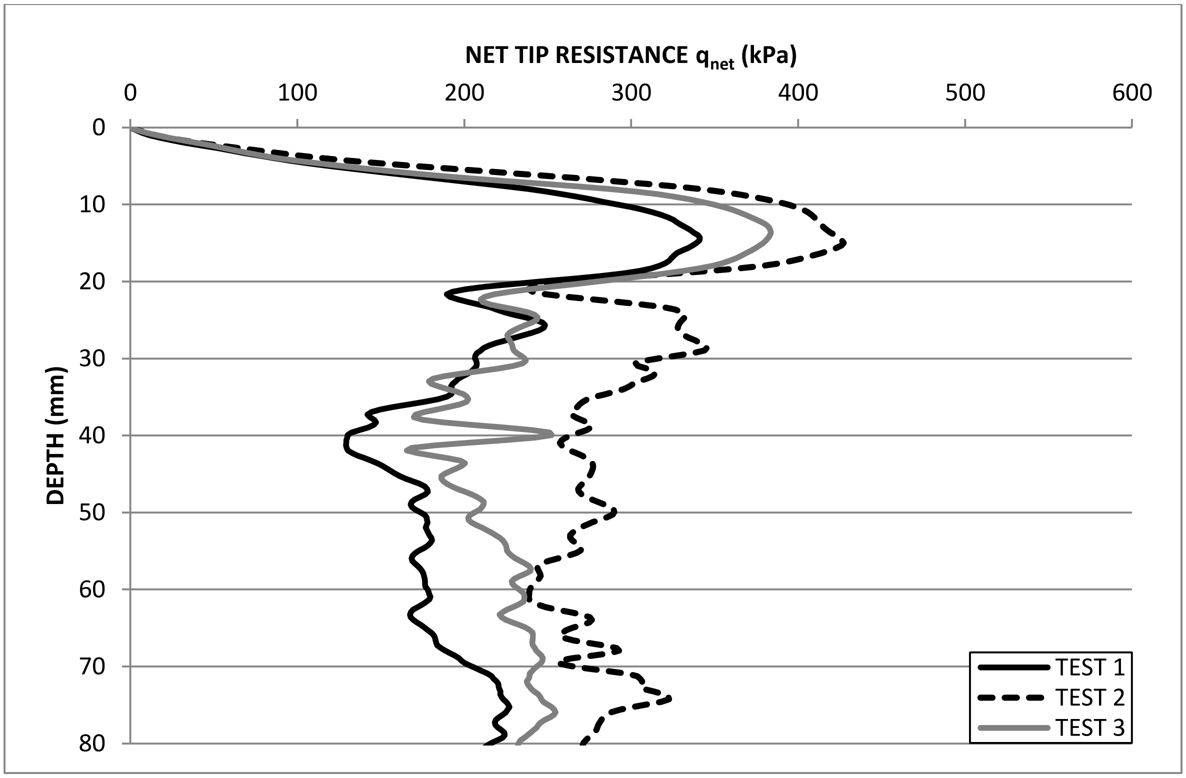

Figure C.4: CPT net tip resistance profile for 3 % fibre over consolidated model.

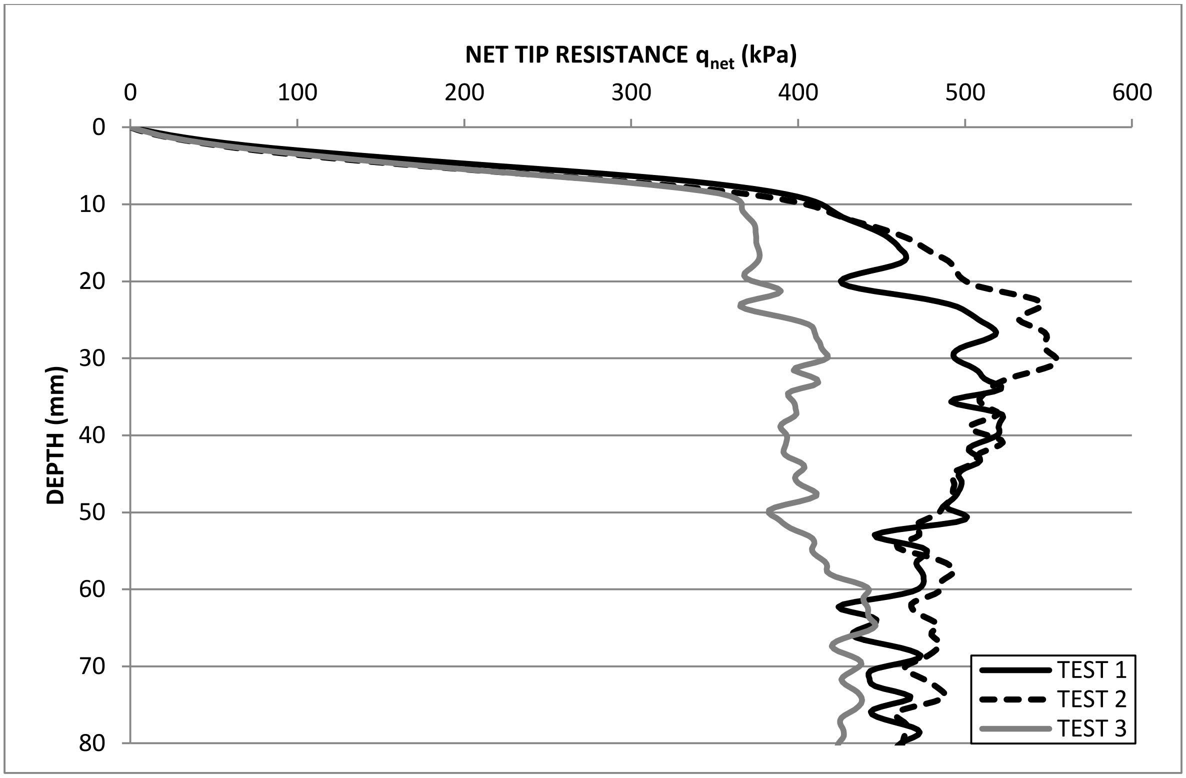

Figure C.5: CPT net tip resistance profile for 4 % fibre over consolidated model.

APPENDIX D:

CENTRIFUGE MODELLING RESULTS

PIEZOBALL TESTING

TEST SERIES 1

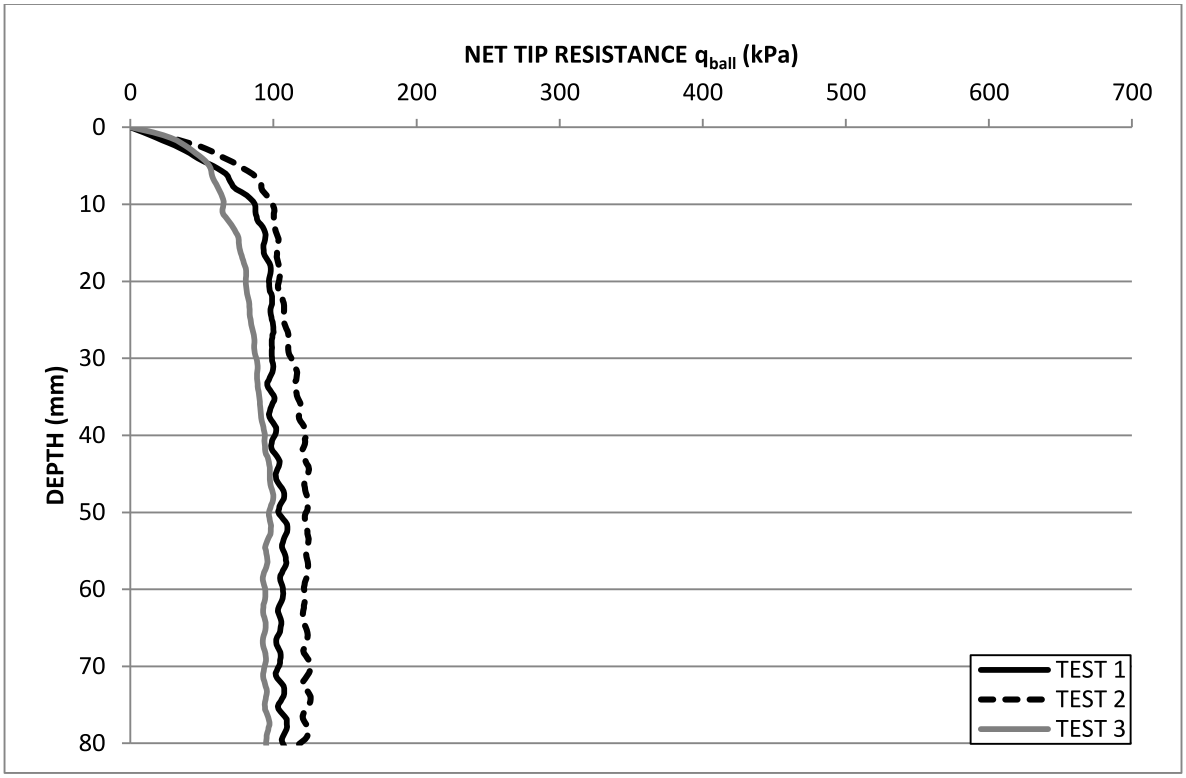

Figure D.1: Piezoball net tip resistance profile for 0 % fibre normally consolidated model.

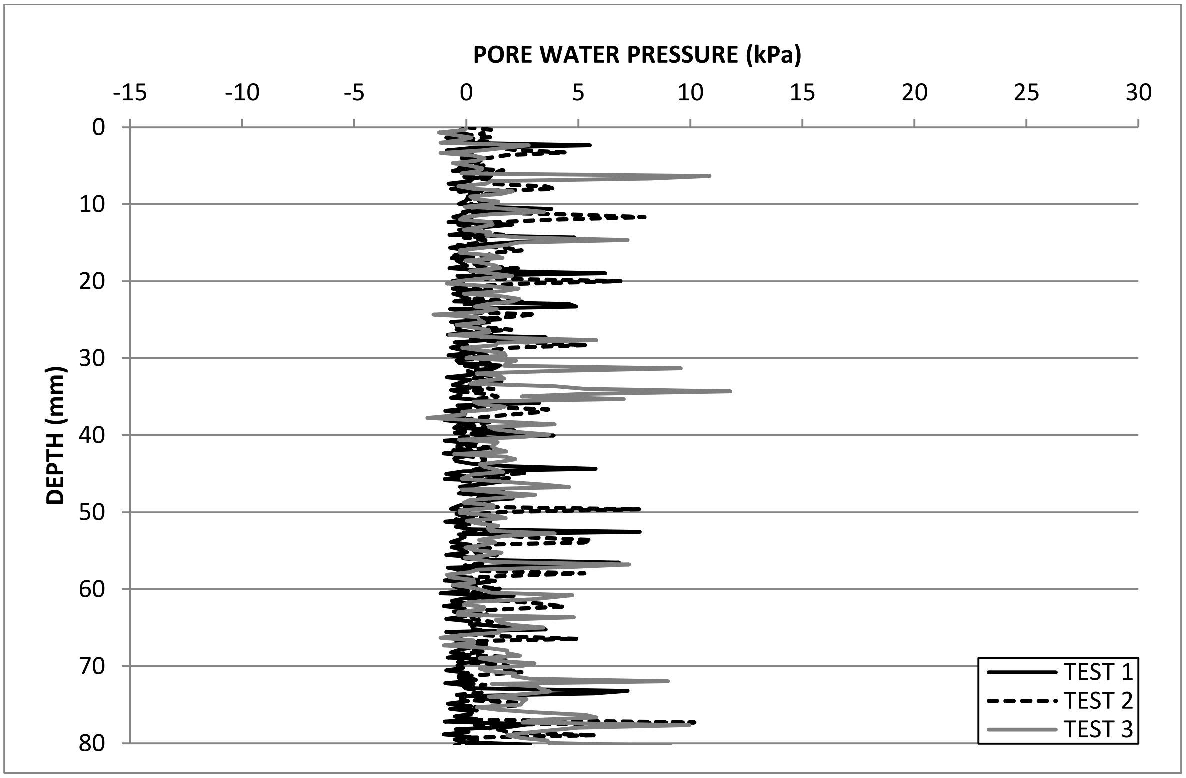

Figure D.2: Piezoball pore water pressure profile for 0 % fibre normally consolidated model.

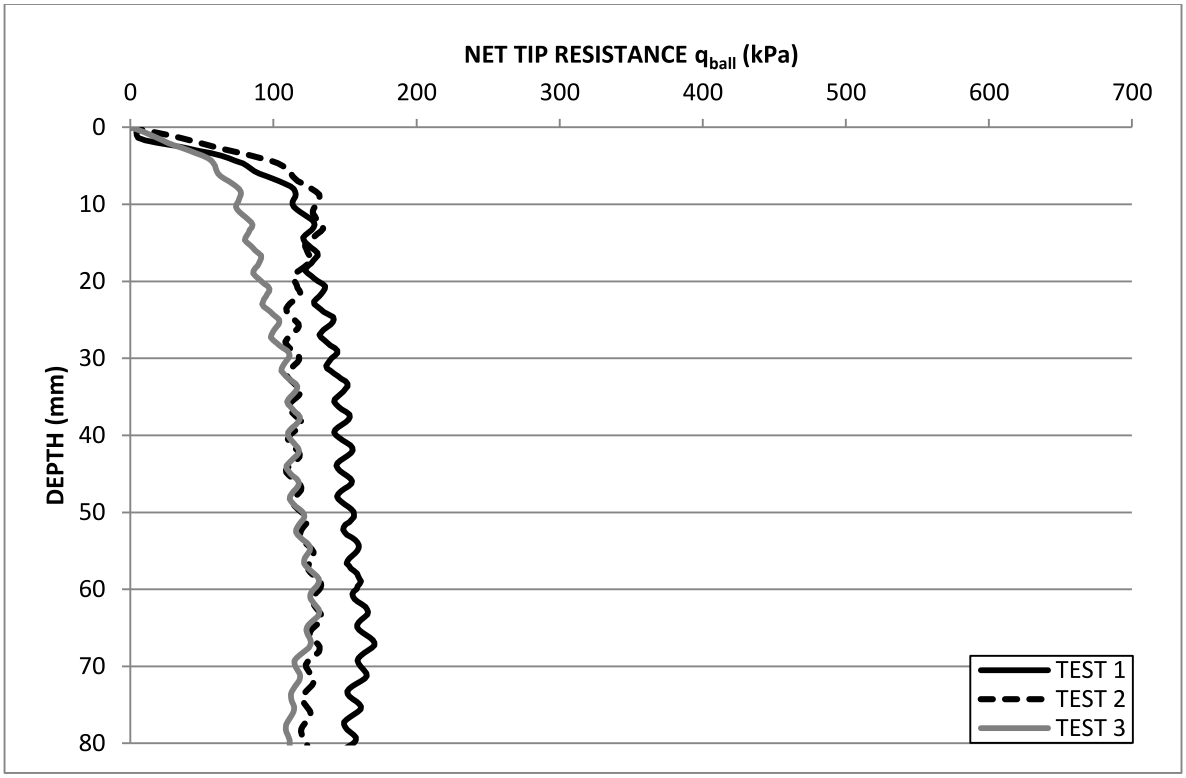

Figure D.3: Piezoball net tip resistance profile for 1 % fibre normally consolidated model.

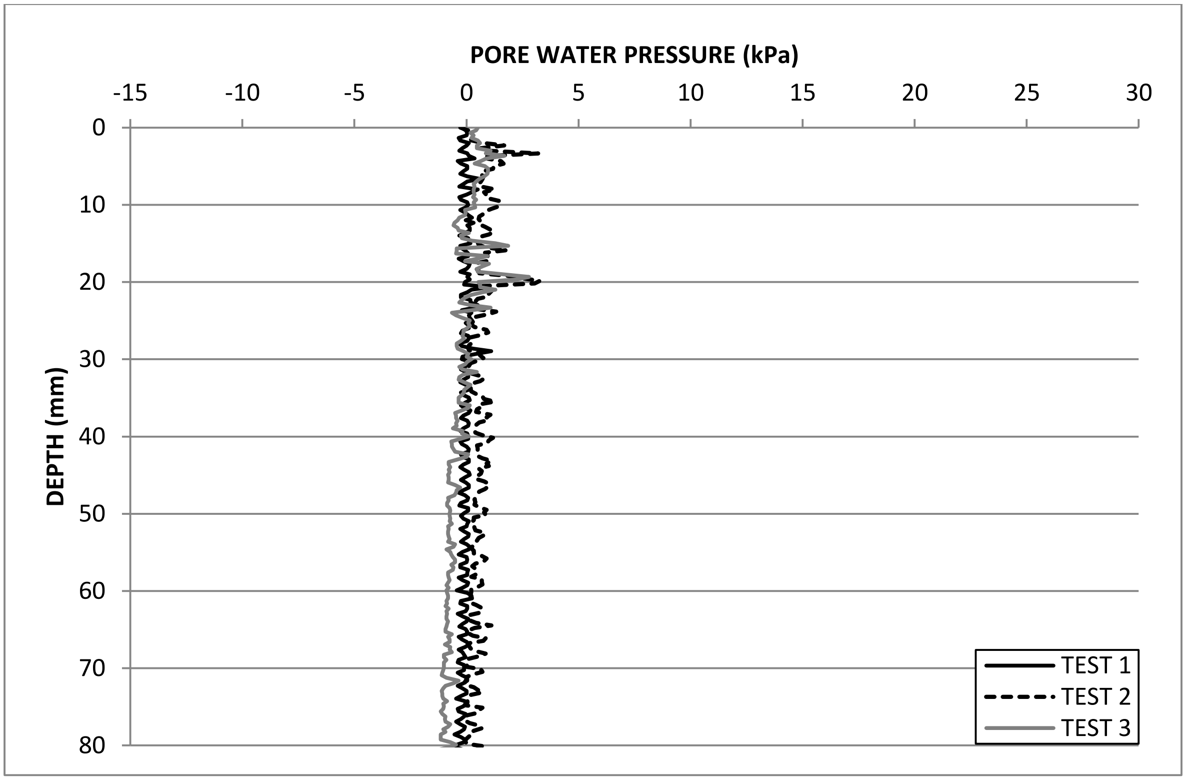

Figure D.4: Piezoball pore water pressure profile for 1 % fibre normally consolidated model.

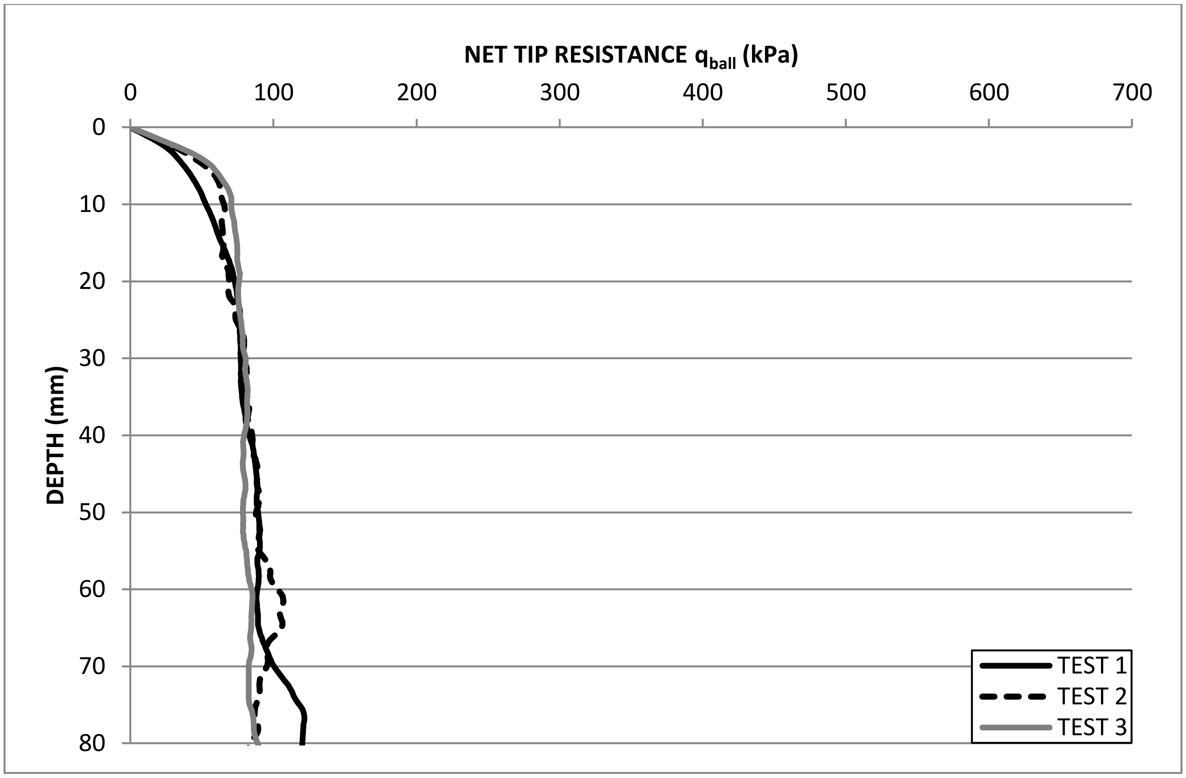

Figure D.5: Piezoball net tip resistance profile for 2 % fibre normally consolidated model.

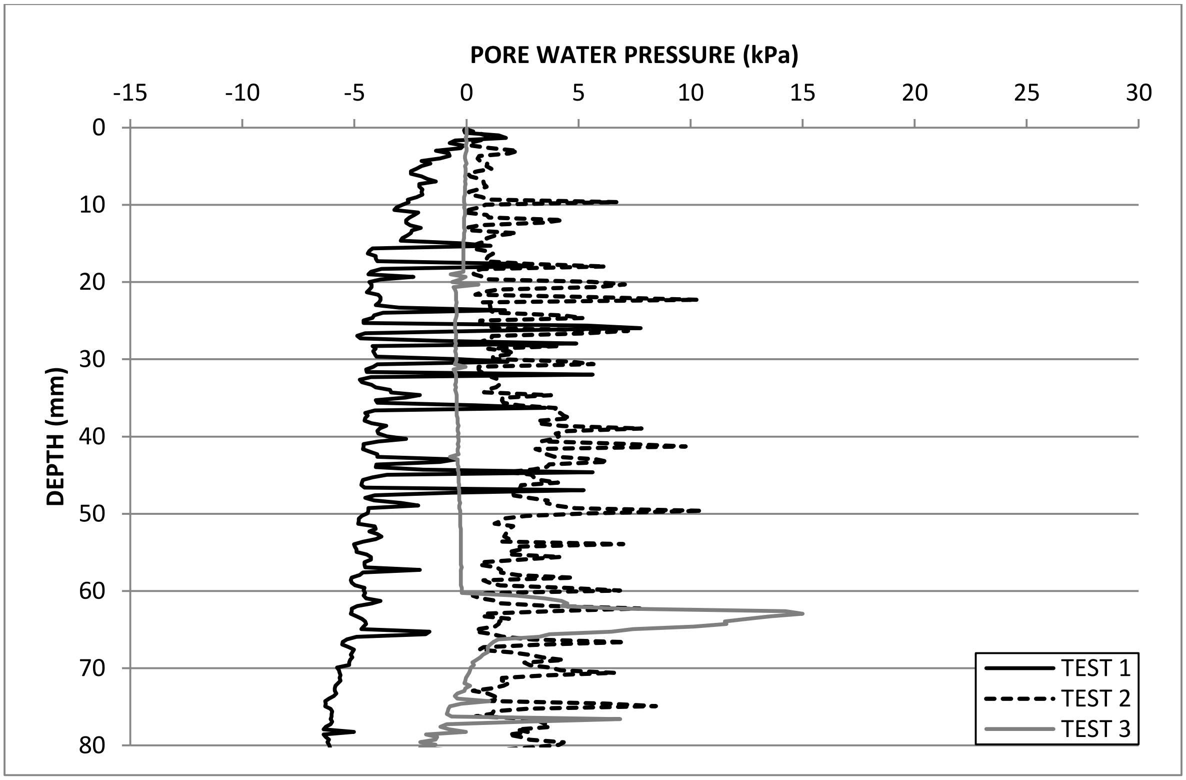

Figure D.6: Piezoball pore water pressure profile for 2 % fibre normally consolidated model.

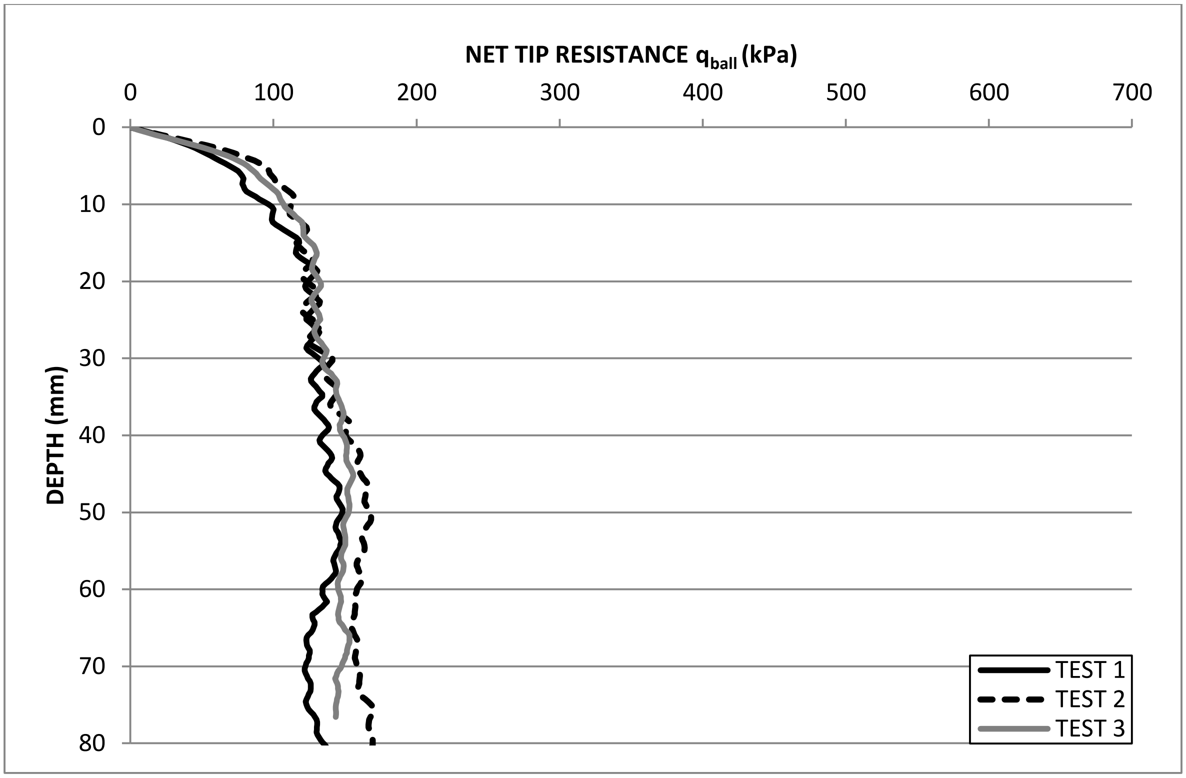

Figure D.7: Piezoball net tip resistance profile for 3 % fibre normally consolidated model.

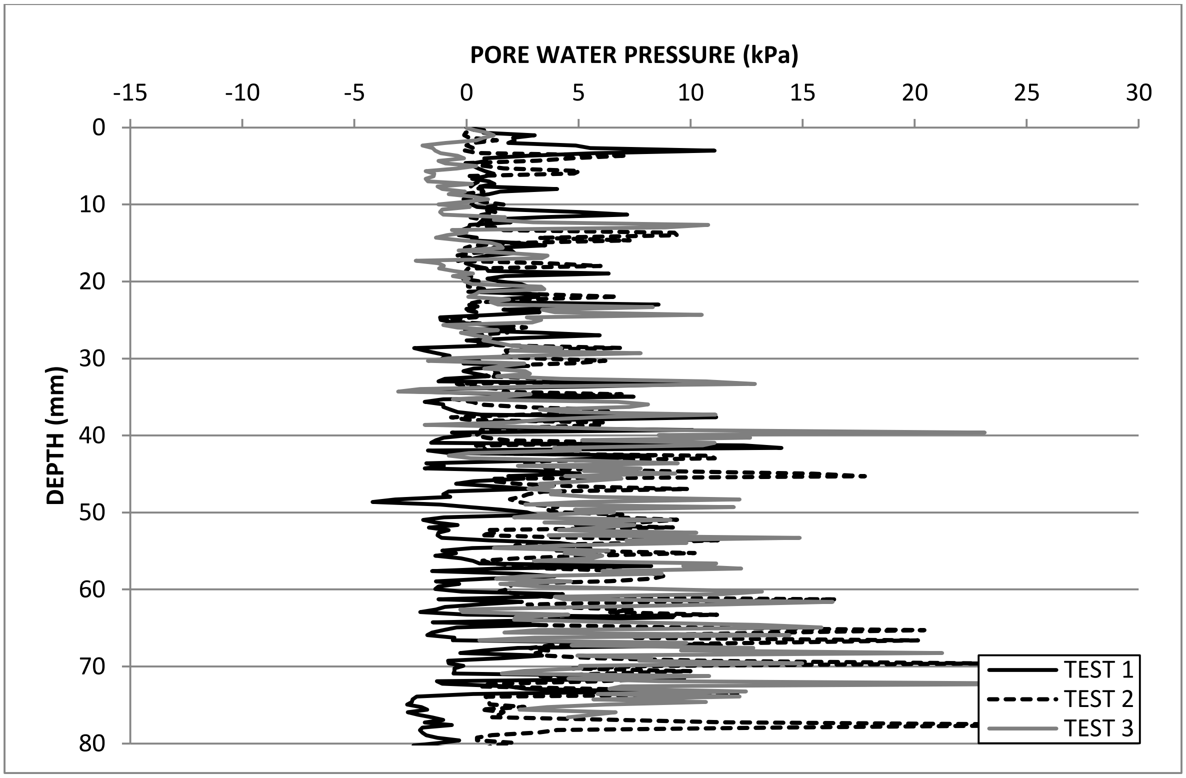

Figure D.8: Piezoball pore water pressure profile for 3 % fibre normally consolidated model.

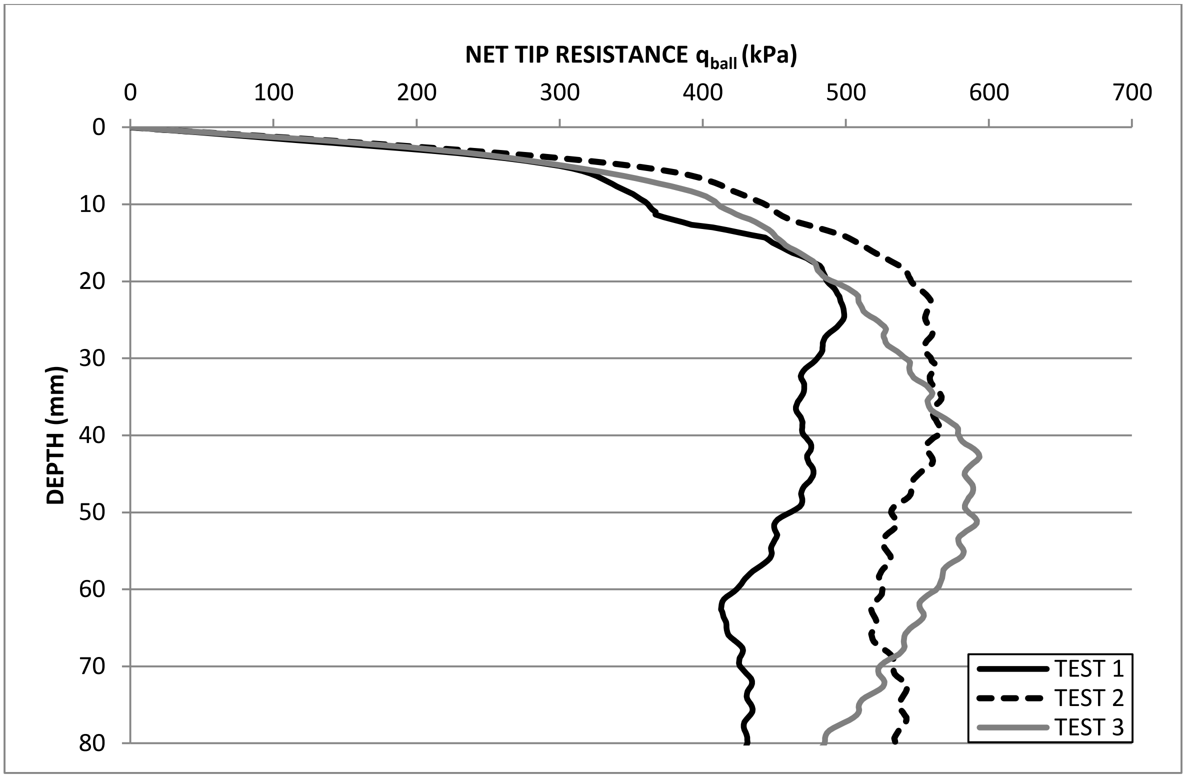

Figure D.9: Piezoball net tip resistance profile for 4 % fibre normally consolidated model.

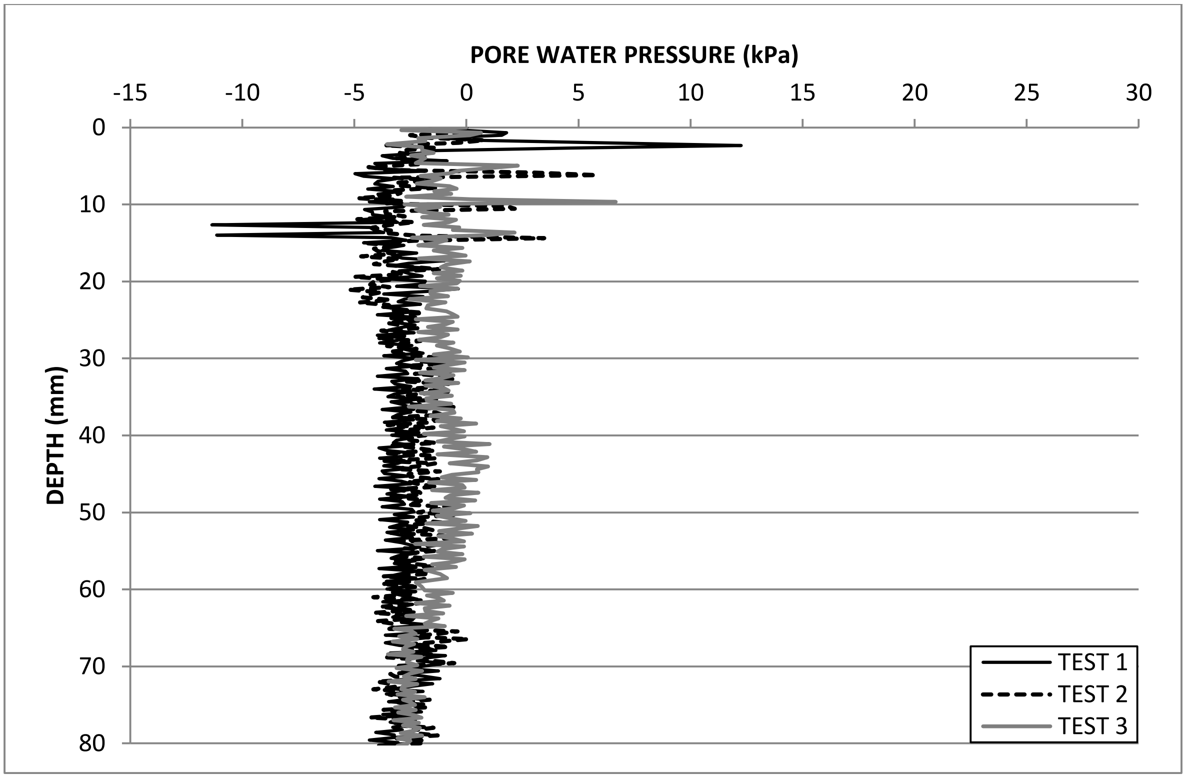

Figure D.10: Piezoball pore water pressure profile for 4 % fibre normally consolidated model.

APPENDIX E:

CENTRIFUGE MODELLING RESULTS

PIEZOBALL TESTING

TEST SERIES 2

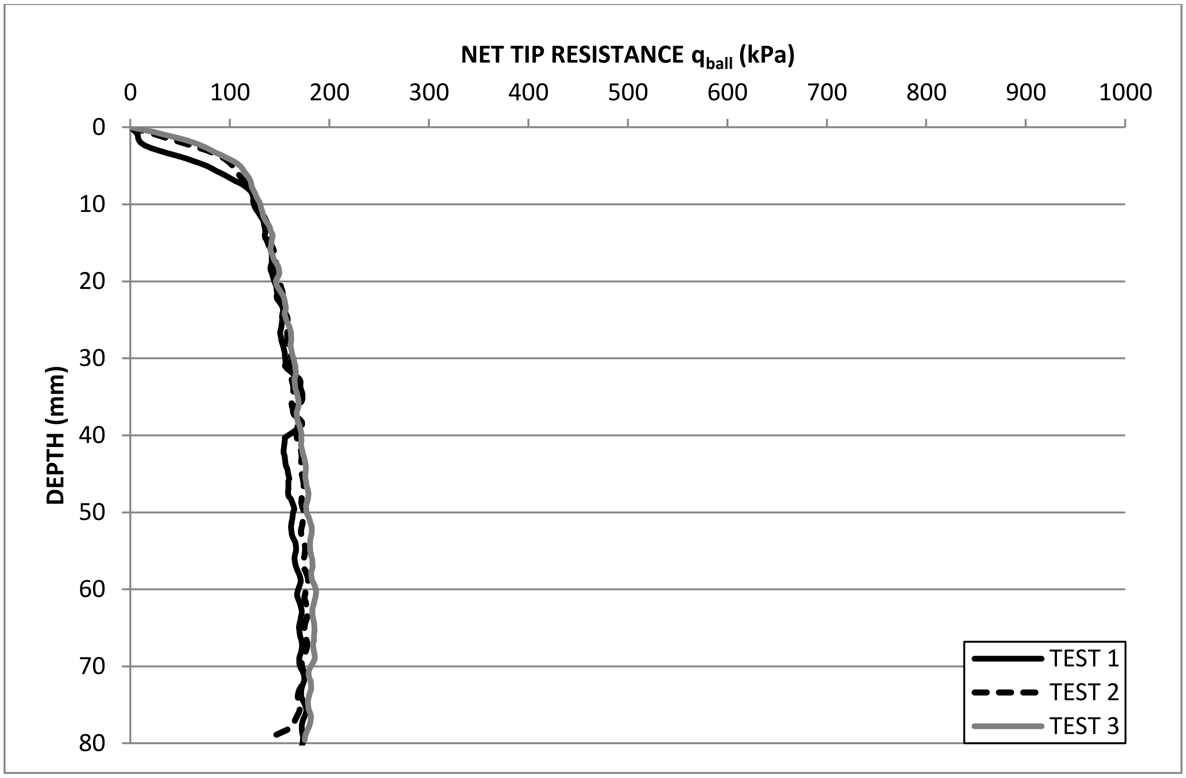

Figure E.1: Piezoball net tip resistance profile for 0 % fibre over consolidated model.

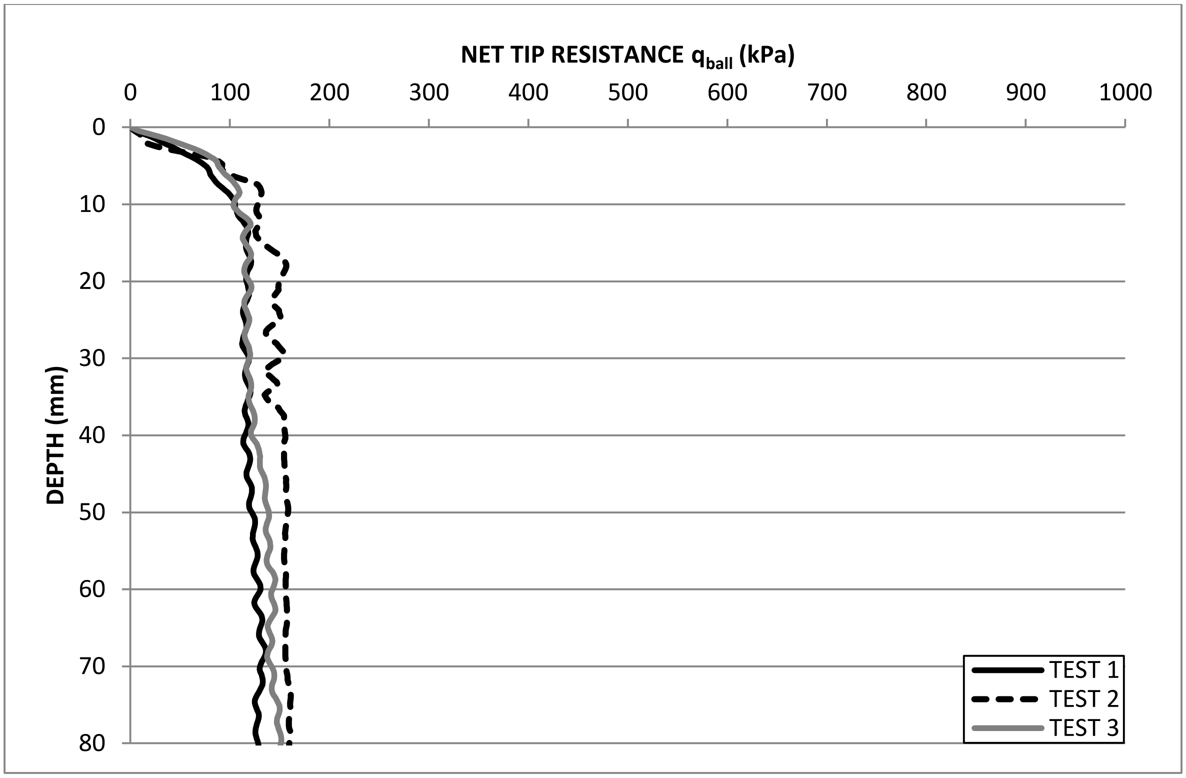

Figure E.2: Piezoball net tip resistance profile for 1 % fibre over consolidated model.

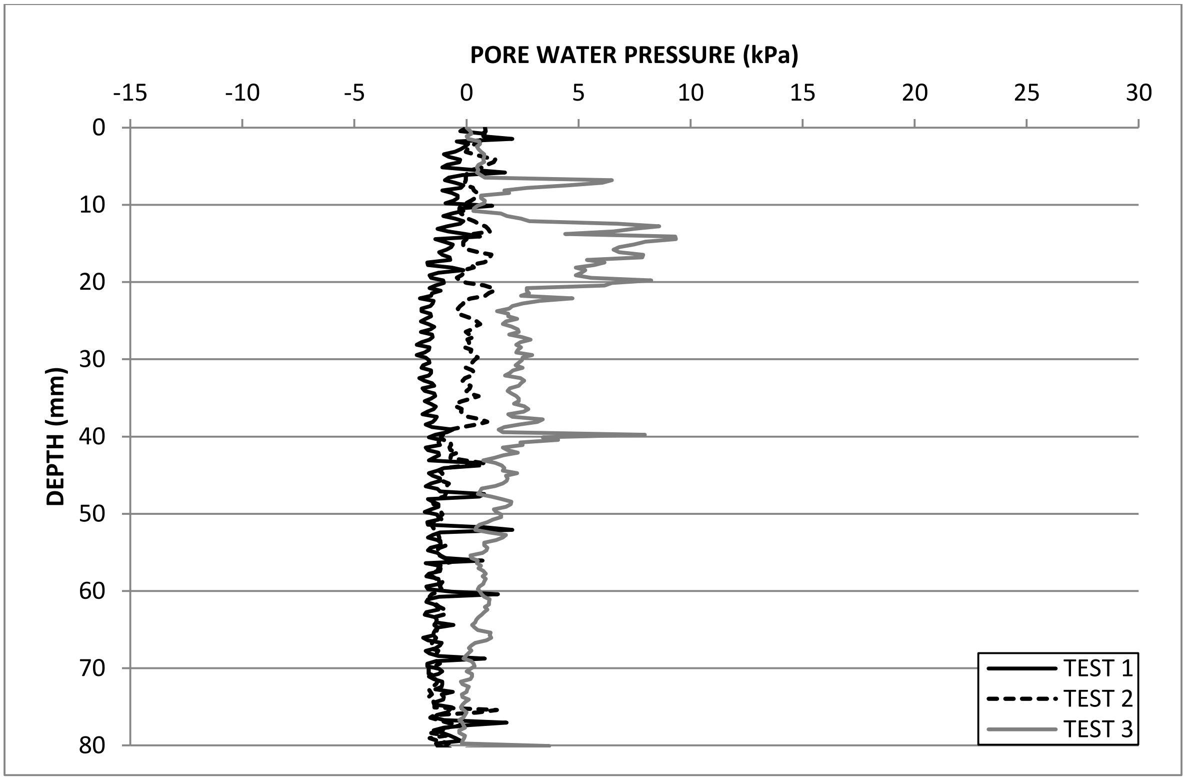

Figure E.3: Piezoball pore water pressure profile for 1 % fibre over consolidated model.

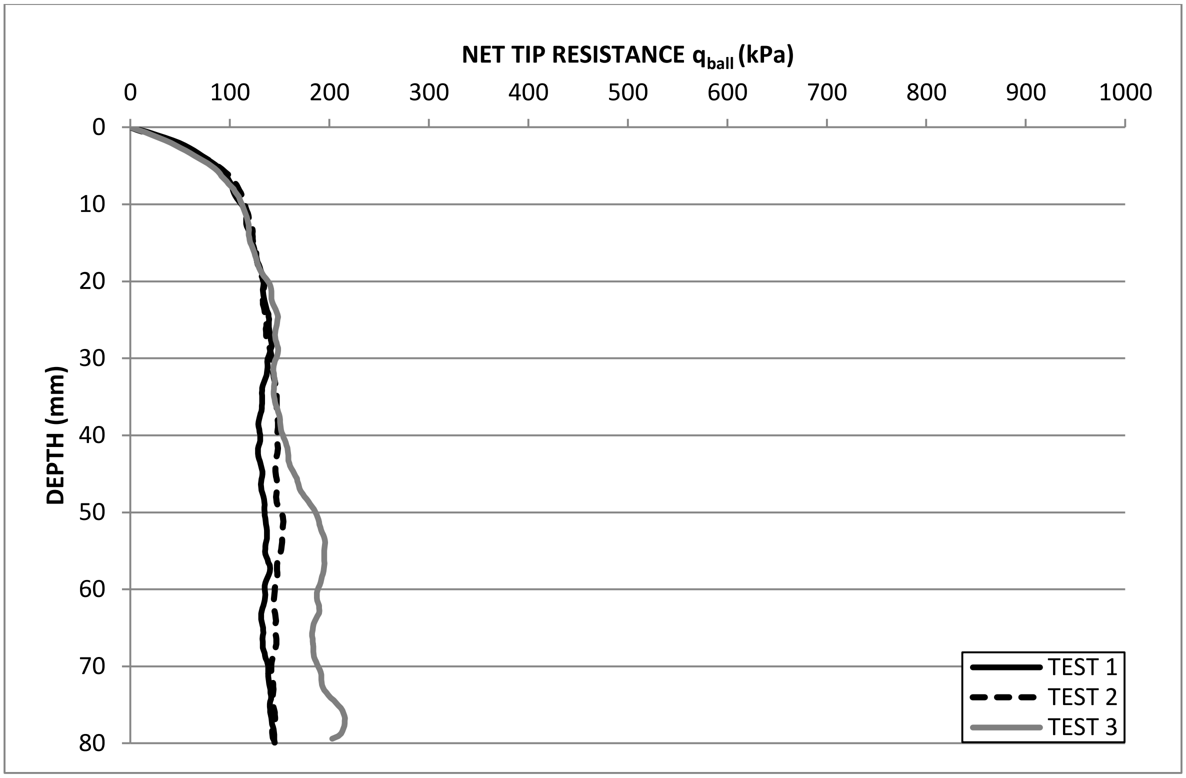

Figure E.4: Piezoball net tip resistance profile for 2 % fibre over consolidated model.

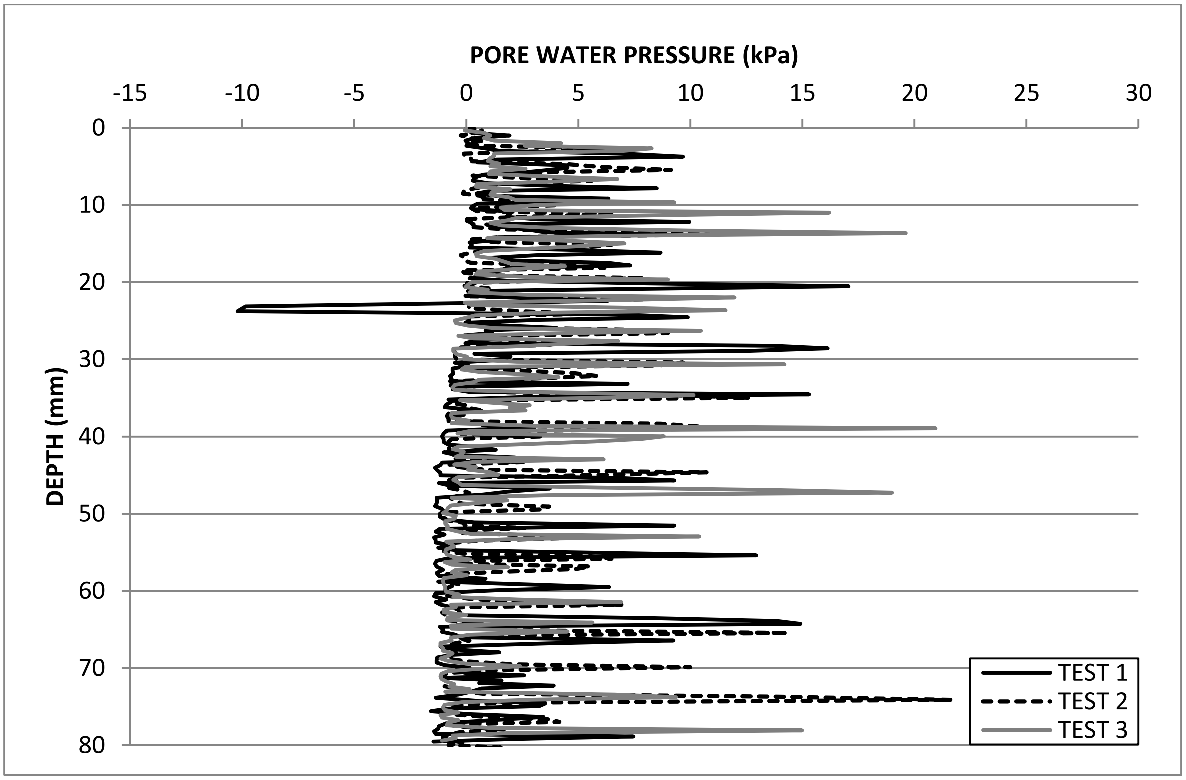

Figure E.5: Piezoball pore water pressure profile for 2 % fibre over consolidated model.

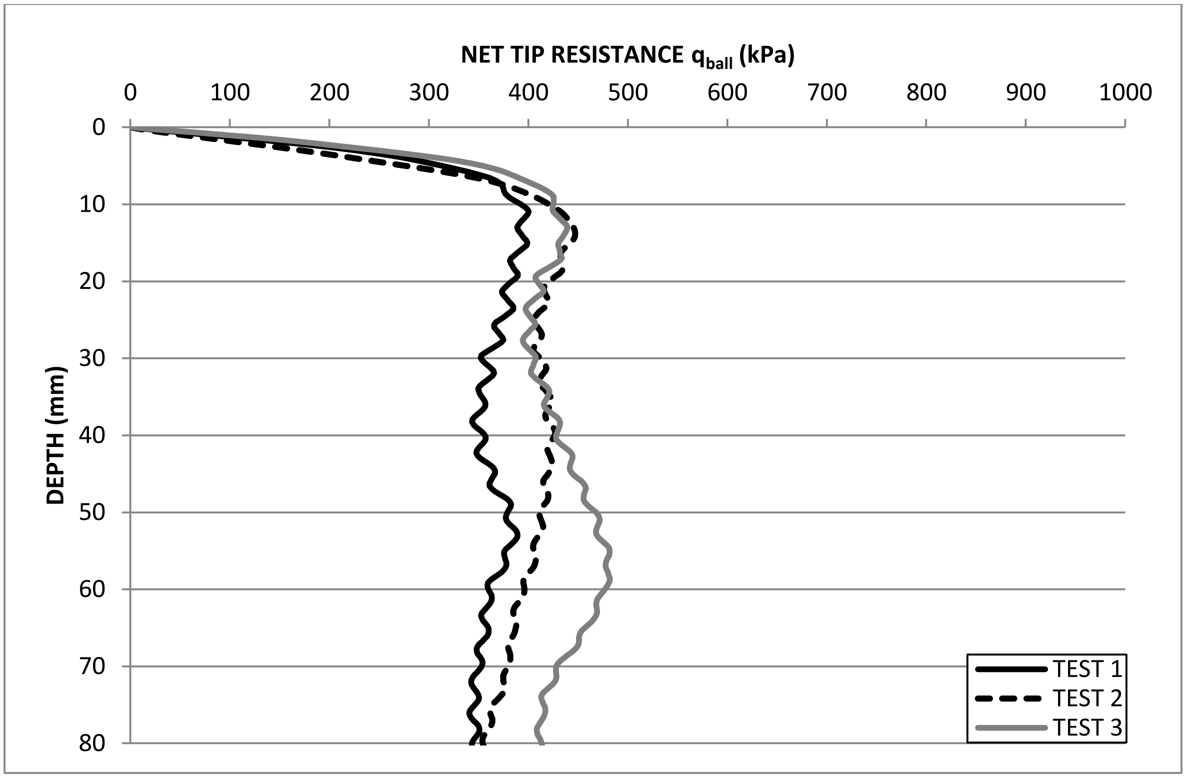

Figure E.6: Piezoball net tip resistance profile for 3 % fibre over consolidated model.

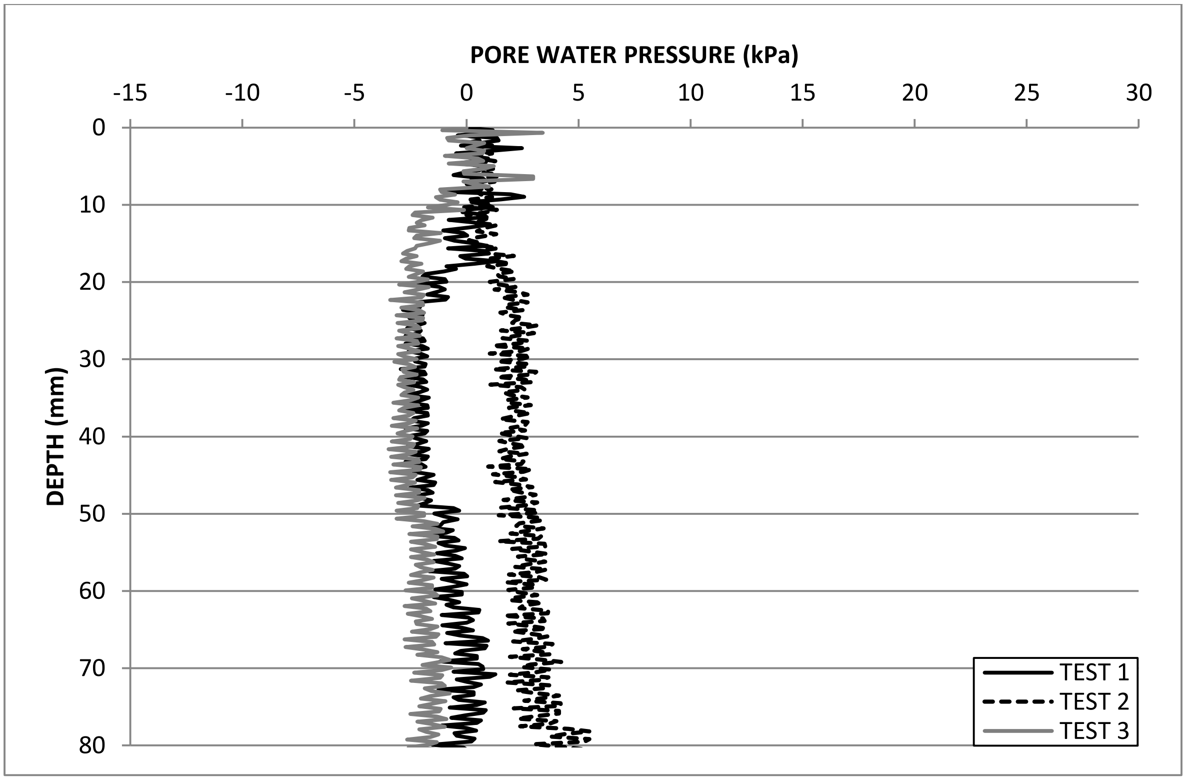

Figure E.7: Piezoball pore water pressure profile for 3 % fibre over consolidated model.

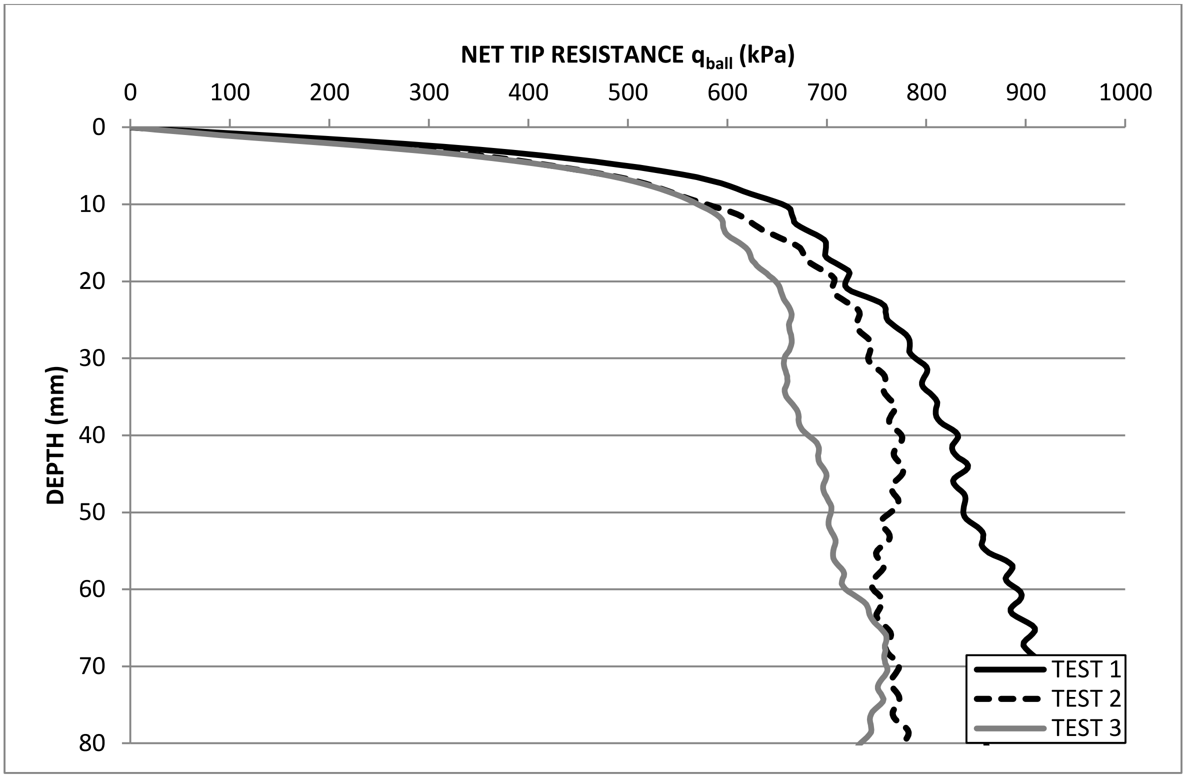

Figure E.8: Piezoball net tip resistance profile for 4 % fibre over consolidated model.

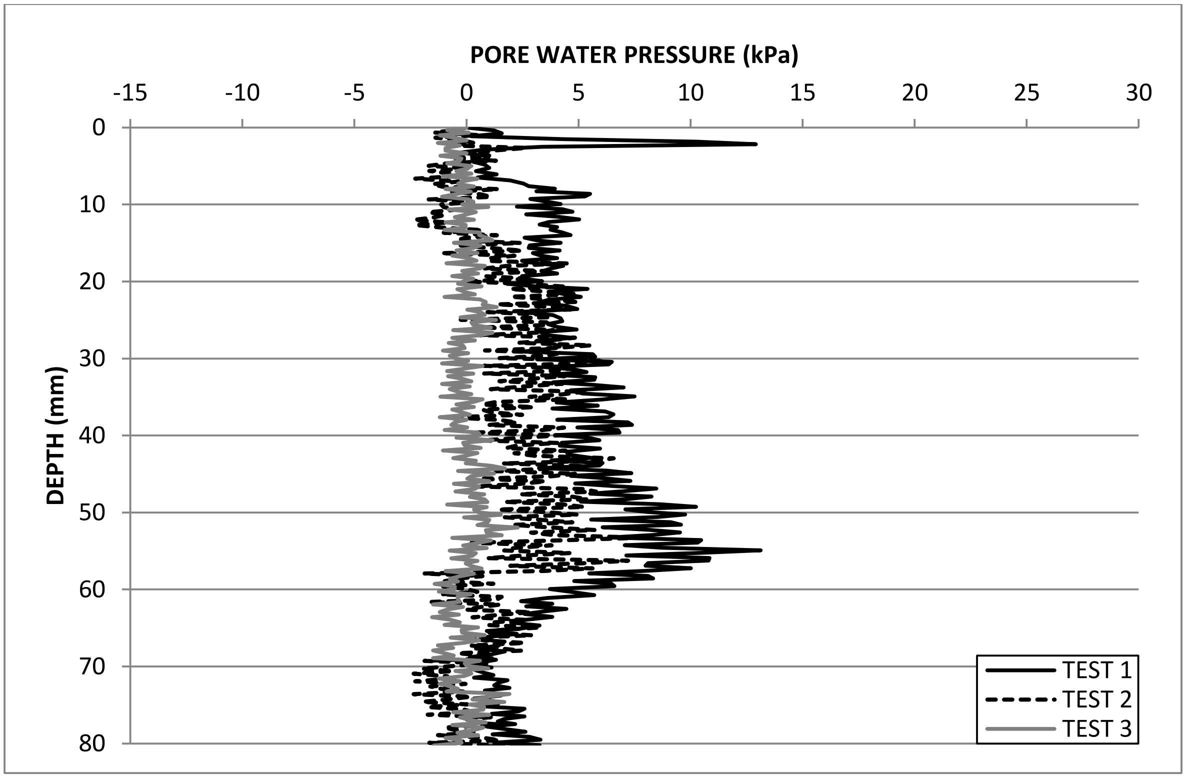

Figure E.9: Piezoball pore water pressure profile for 4 % fibre over consolidated model.

APPENDIX F:

CENTRIFUGE MODELLING RESULTS

BEARING CAPACITY

TEST SERIES 1

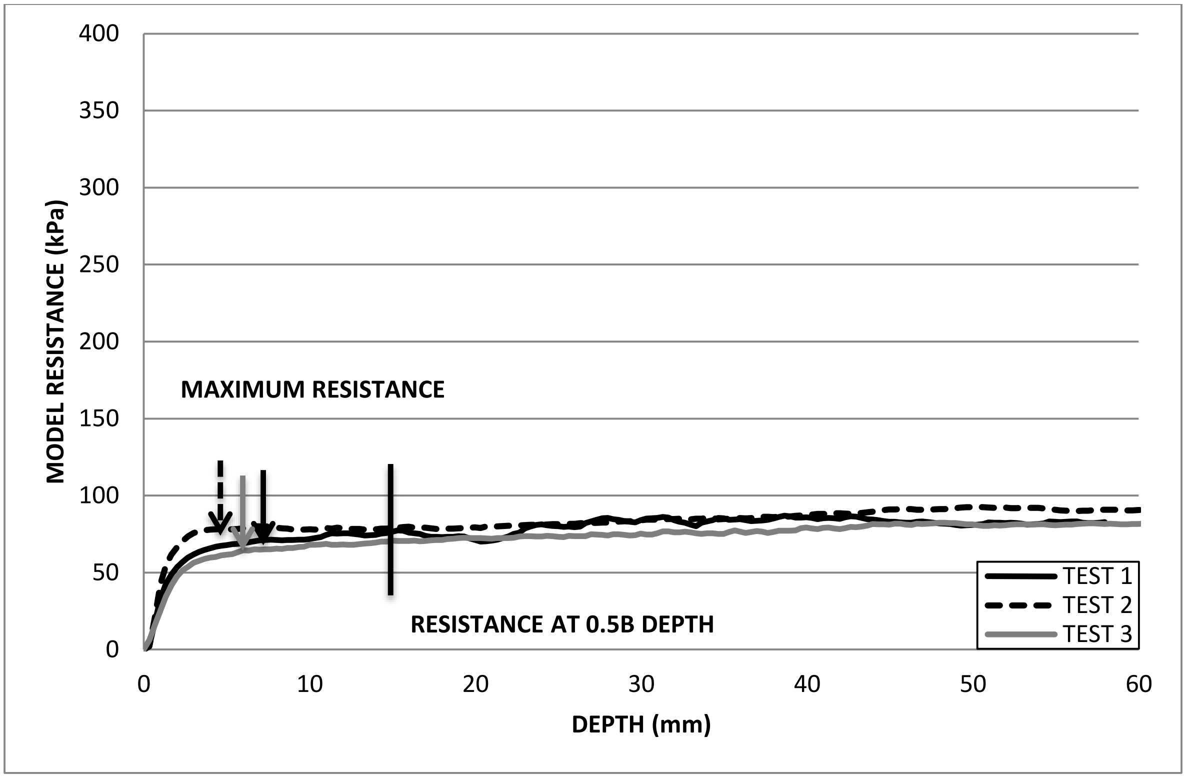

Figure F.1: Resistance profile for a 30 x 60 mm rectangular foundation tested on 0 % fibre normally consolidated model.

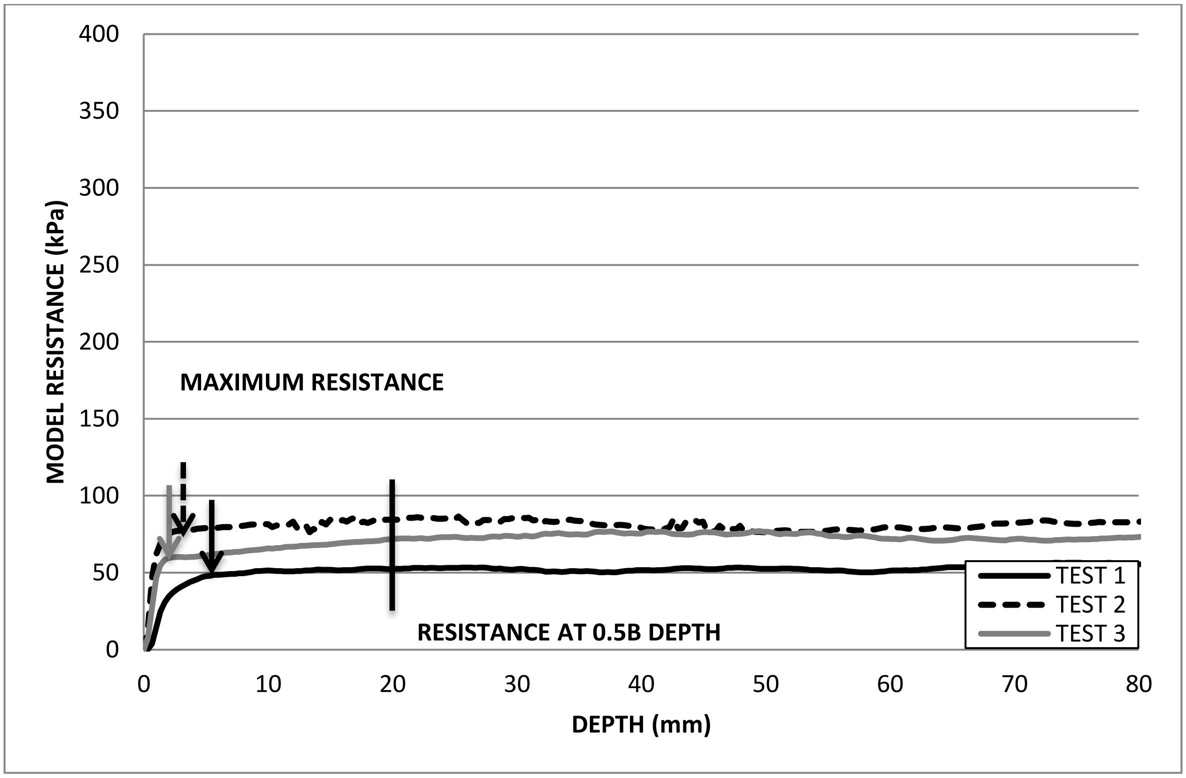

Figure F.2: Resistance profile for a 40 x 80 mm rectangular foundation tested on 0 % fibre normally consolidated model.

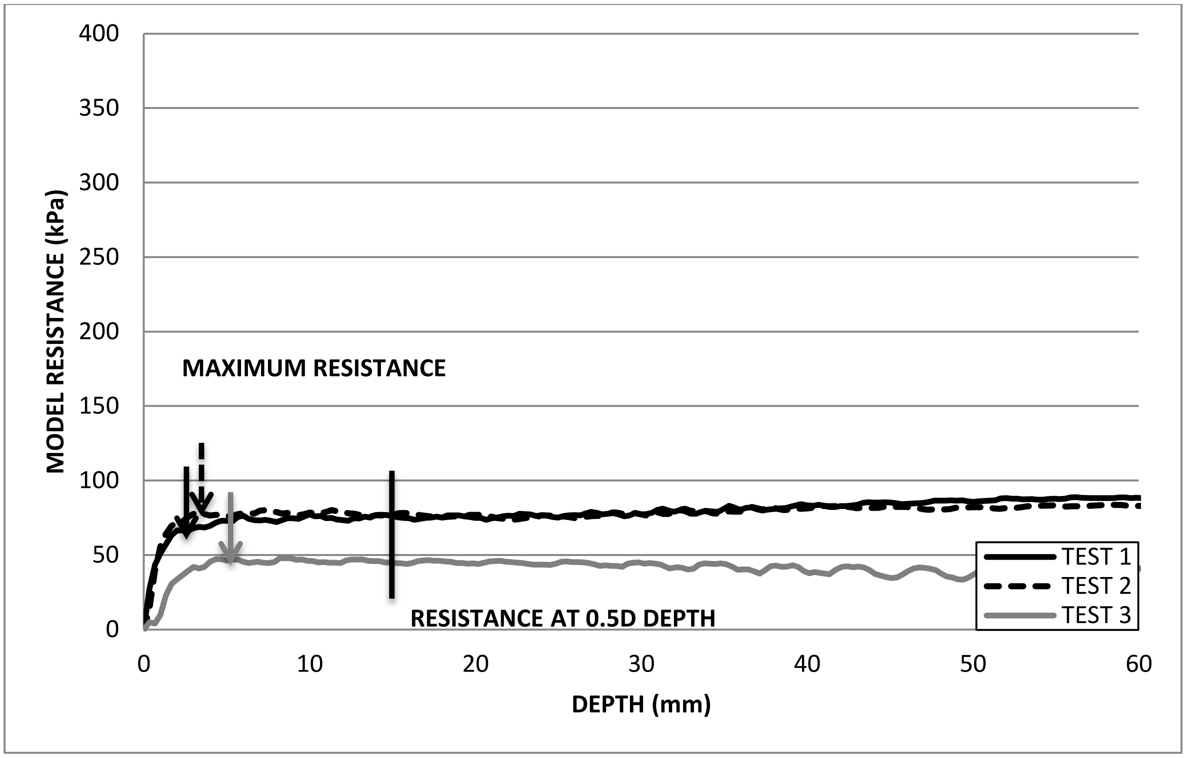

Figure F.3: Resistance profile for a 30 mm circular foundation tested on 0 % fibre normally consolidated model.

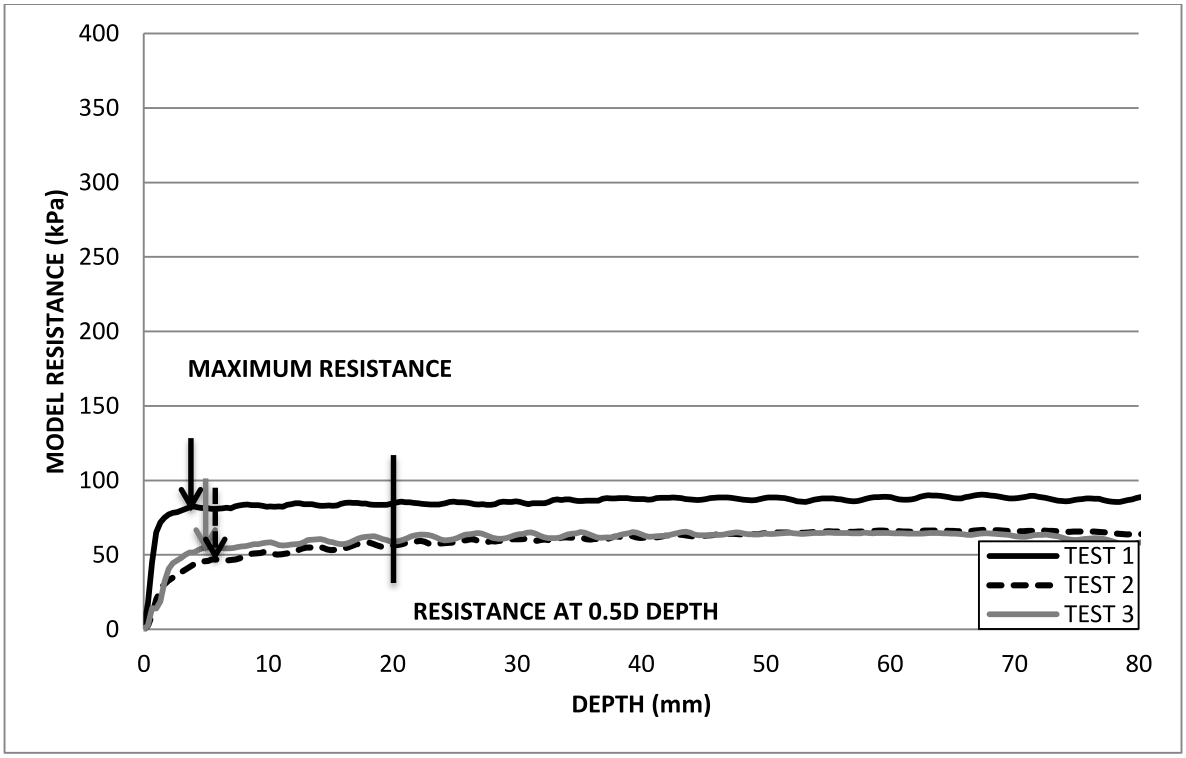

Figure F.4: Resistance profile for a 40 mm circular foundation tested on 0 % fibre normally consolidated model.

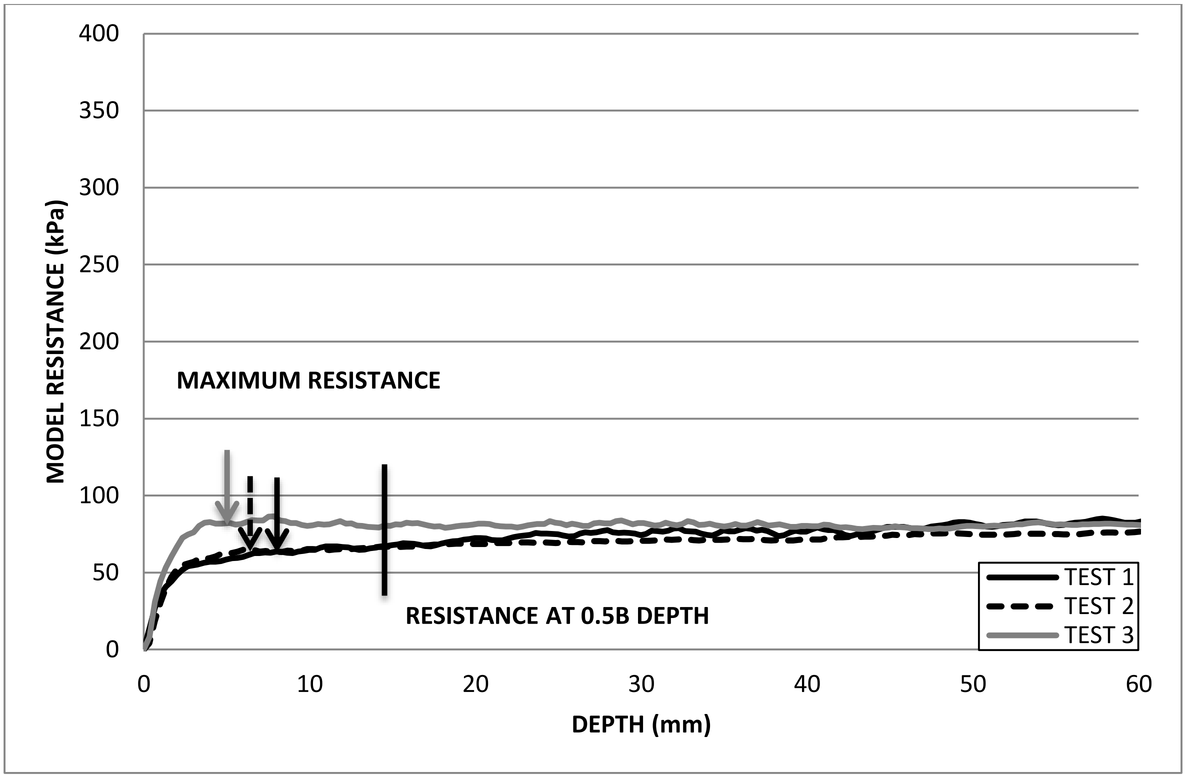

Figure F.5: Resistance profile for a 30 mm square foundation tested on 0 % fibre normally consolidated model.

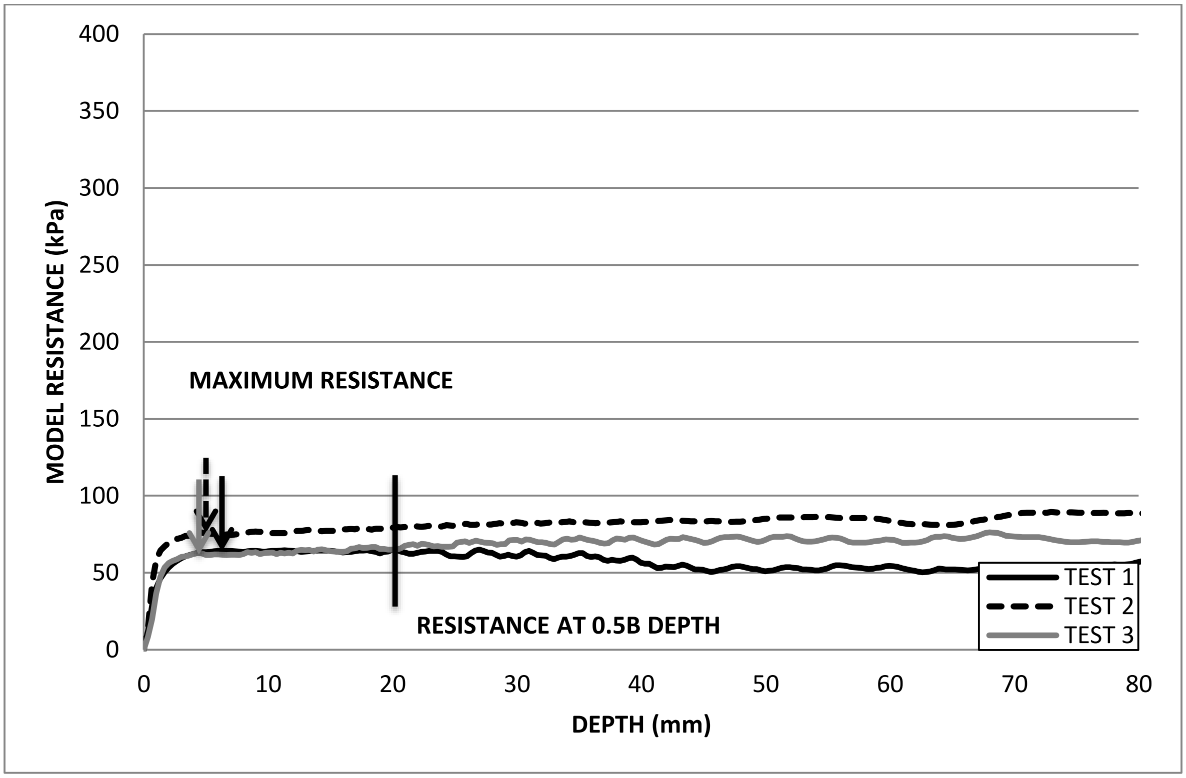

Figure F.6: Resistance profile for a 40 mm square foundation tested on 0 % fibre normally consolidated model.

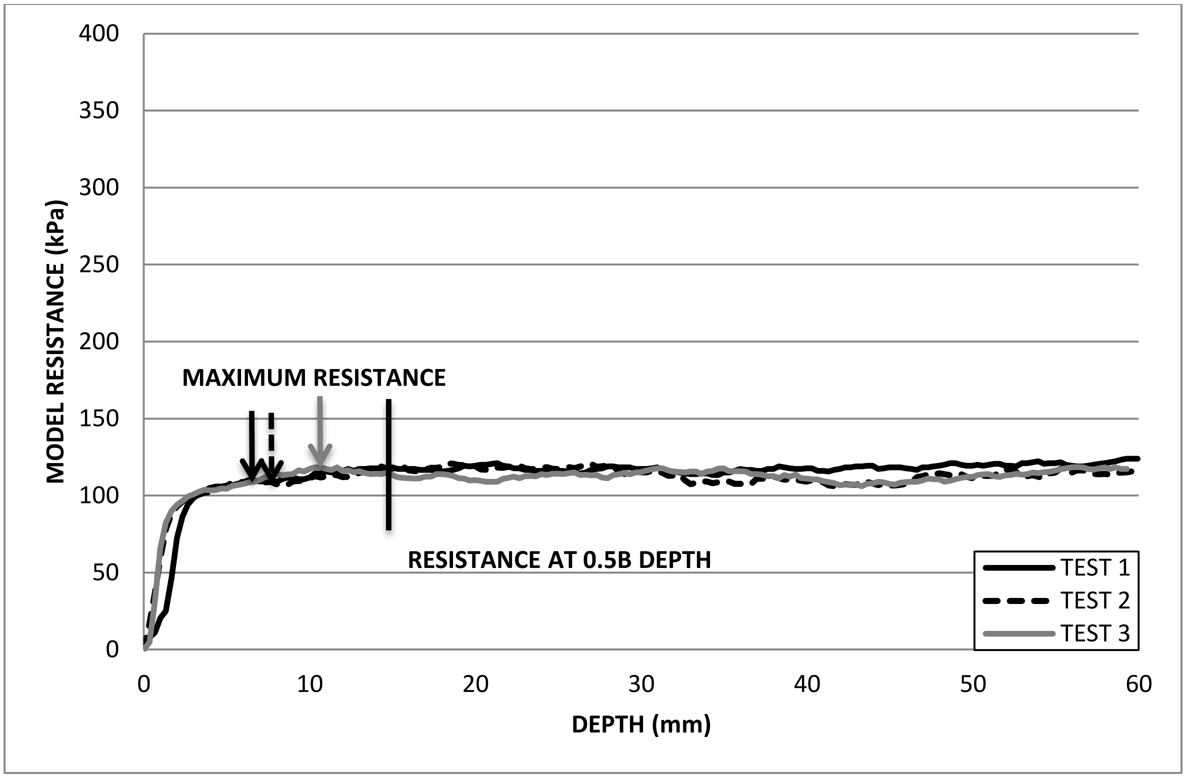

Figure F.7: Resistance profile for a 30 x 60 mm rectangular foundation tested on 1 % fibre normally consolidated model.

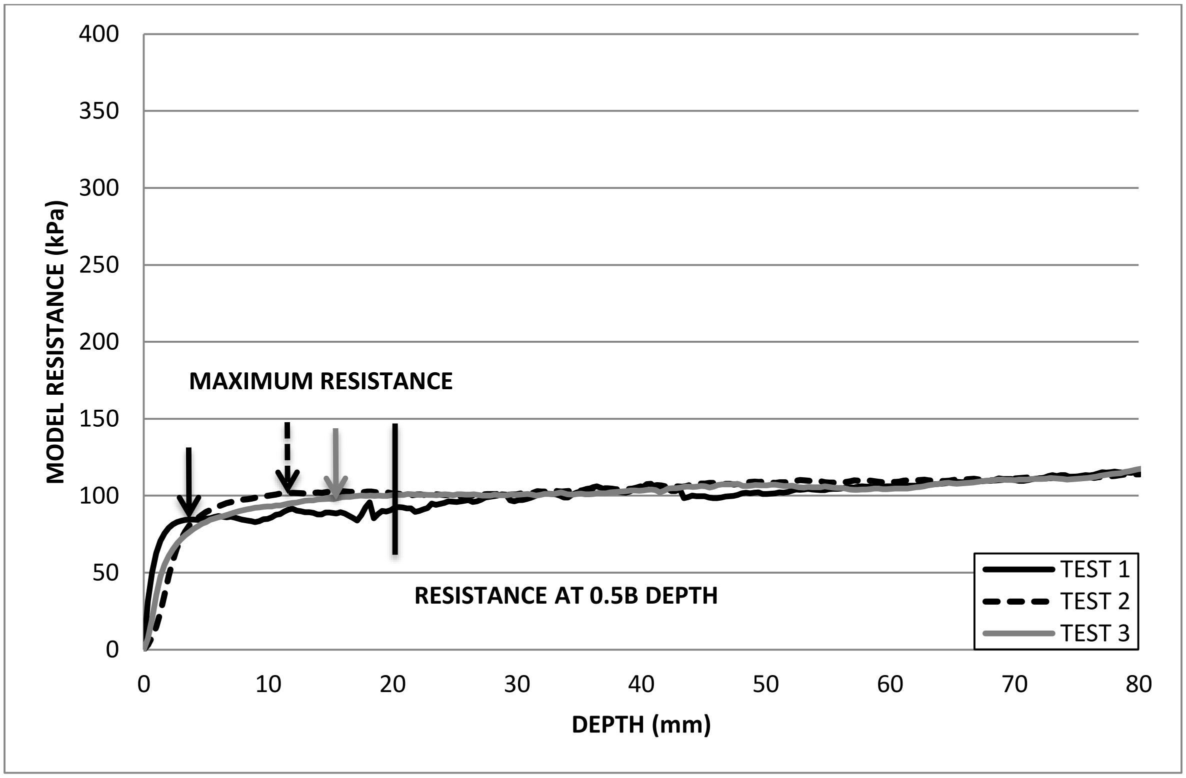

Figure F.8: Resistance profile for a 40 x 80 mm rectangular foundation tested on 1 % fibre normally consolidated model.

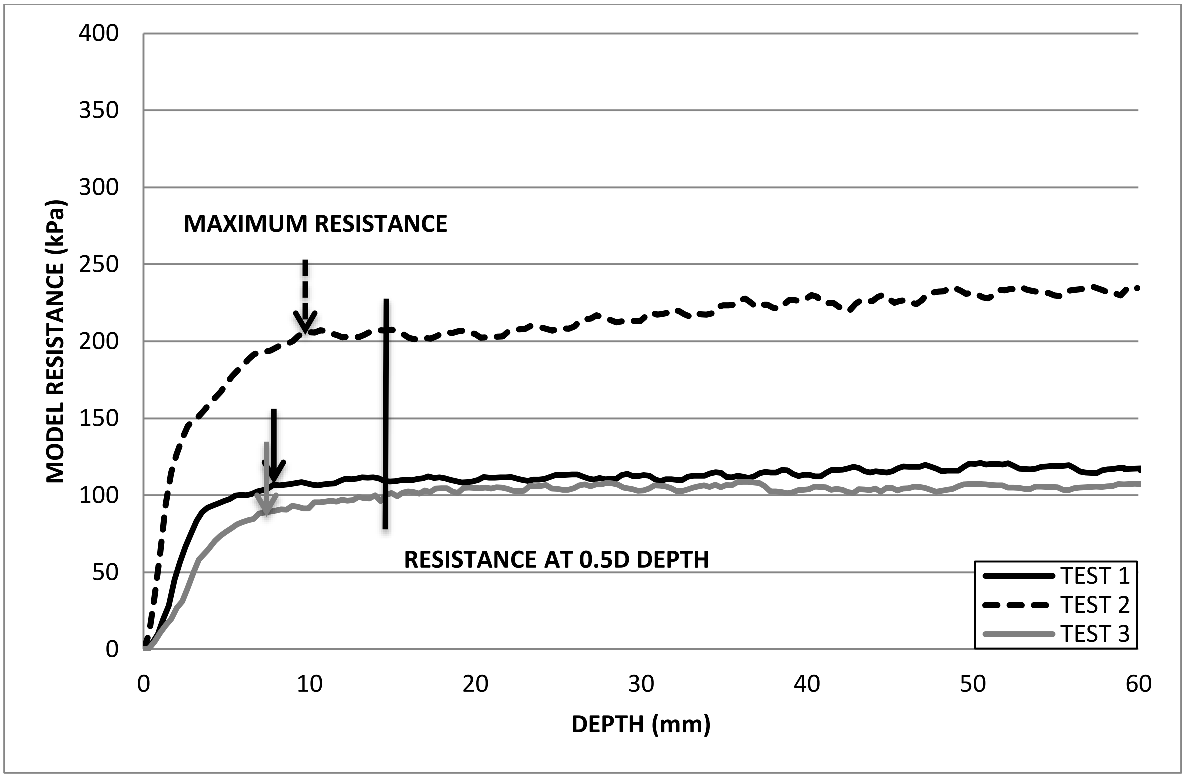

Figure F.9: Resistance profile for a 30 mm circular foundation tested on 1 % fibre normally consolidated model.

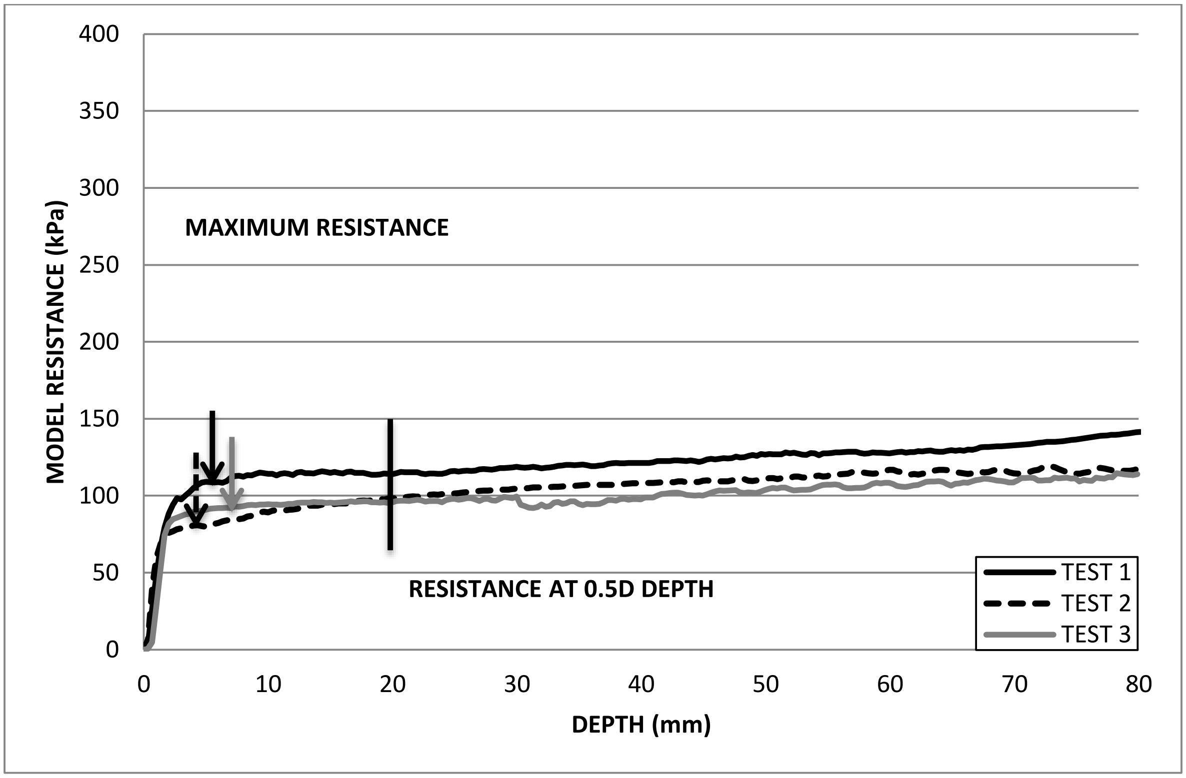

Figure F.10: Resistance profile for a 40 mm circular foundation tested on 1 % fibre normally consolidated model.

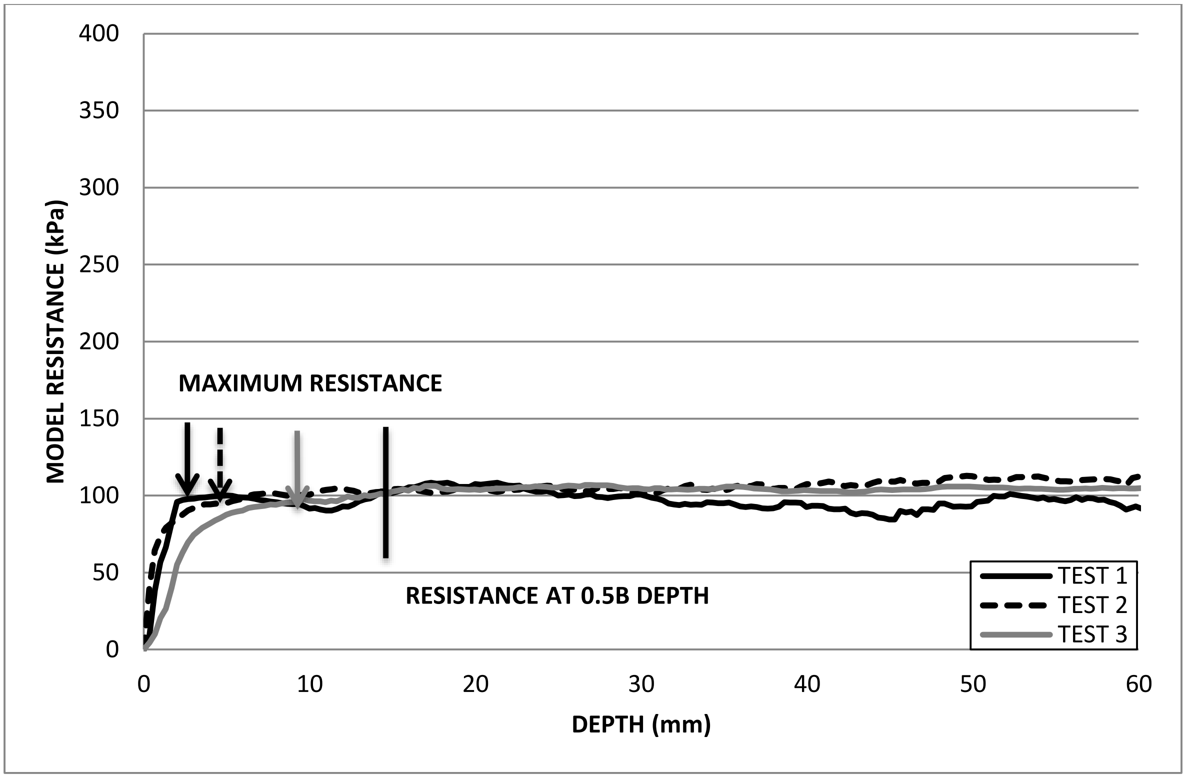

Figure F.11: Resistance profile for a 30 mm square foundation tested on 1 % fibre normally consolidated model.

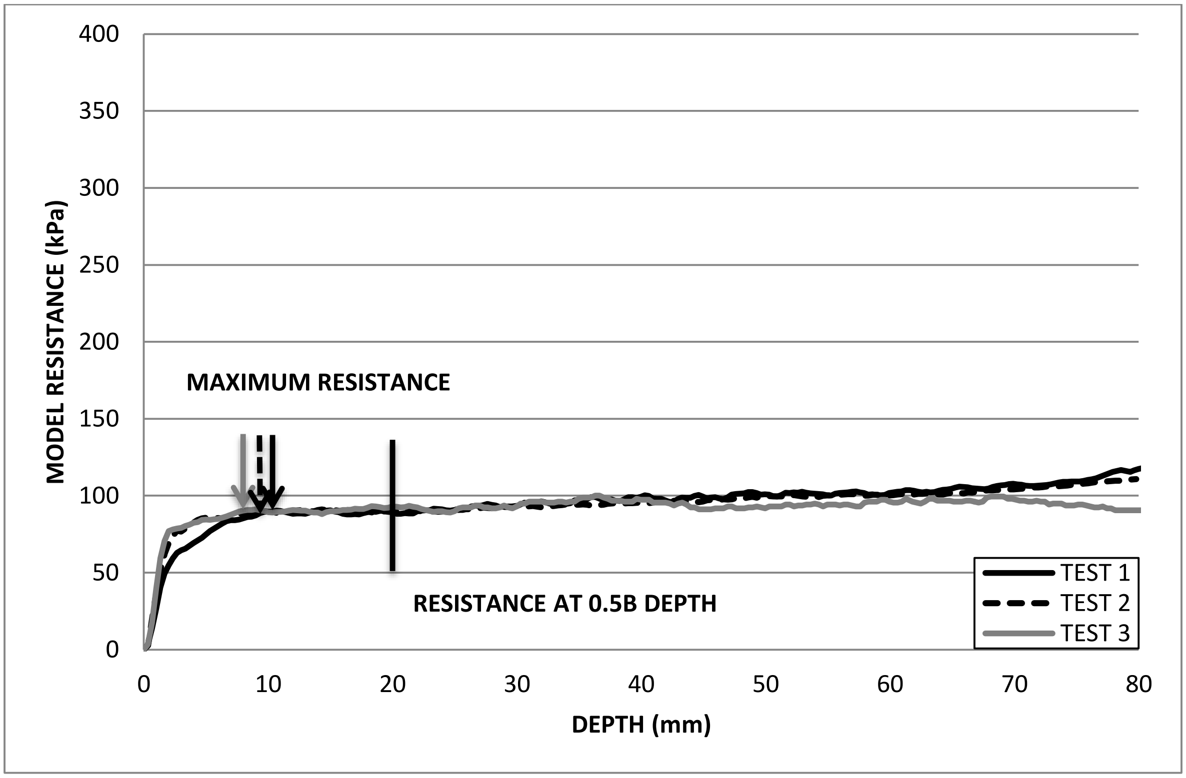

Figure F.12: Resistance profile for a 40 mm square foundation tested on 1 % fibre normally consolidated model.

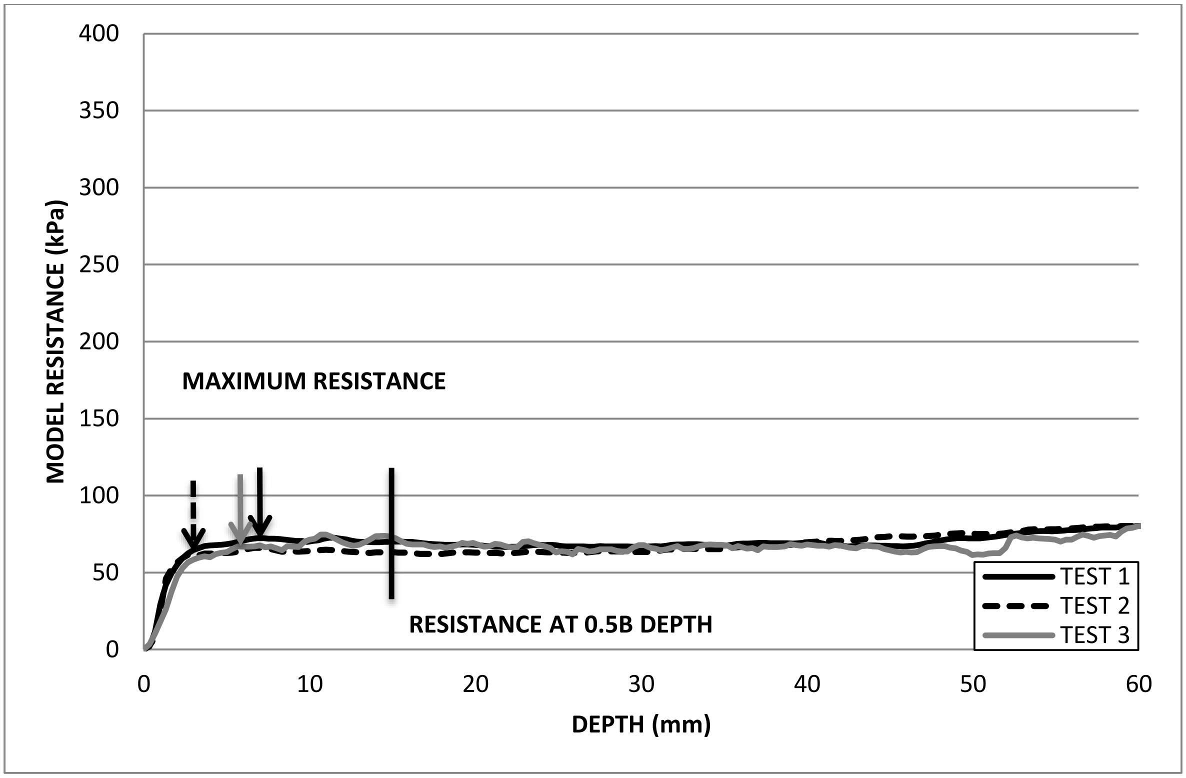

Figure F.13: Resistance profile for a 30 x 60 mm rectangular foundation tested on 2 % fibre normally consolidated model.

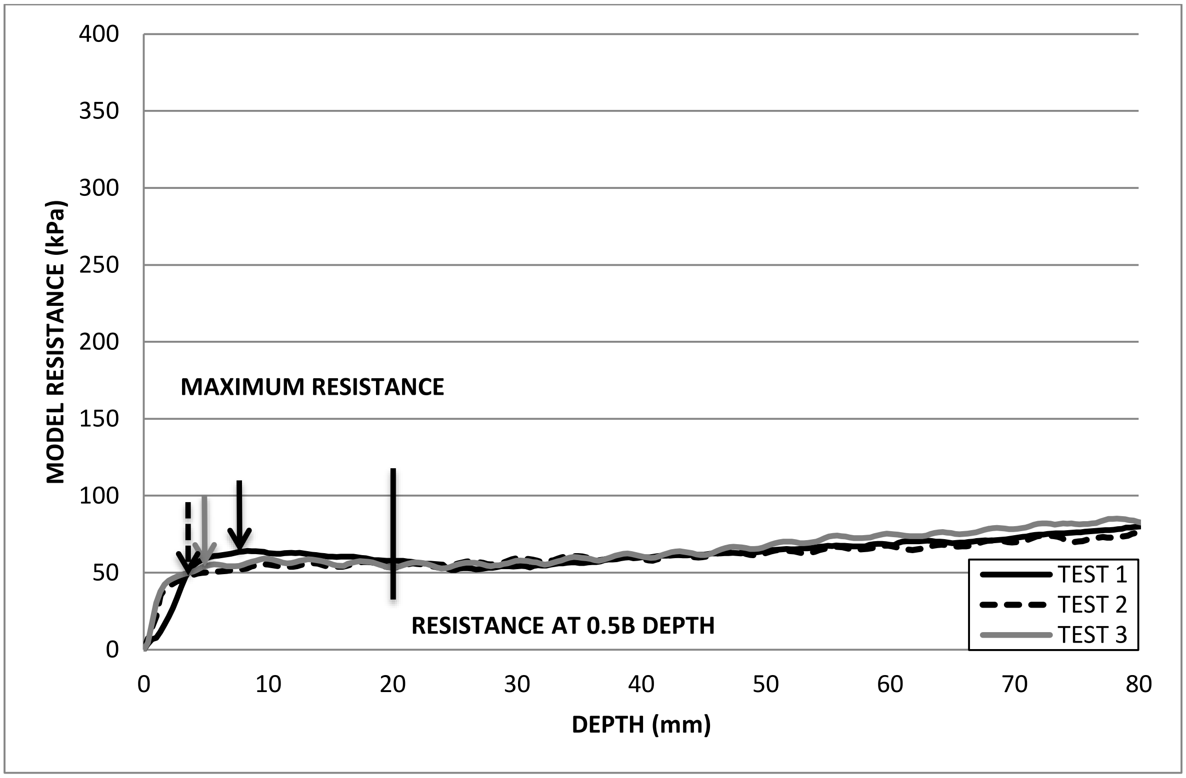

Figure F.14: Resistance profile for a 40 x 80 mm rectangular foundation tested on 2 % fibre normally consolidated model.

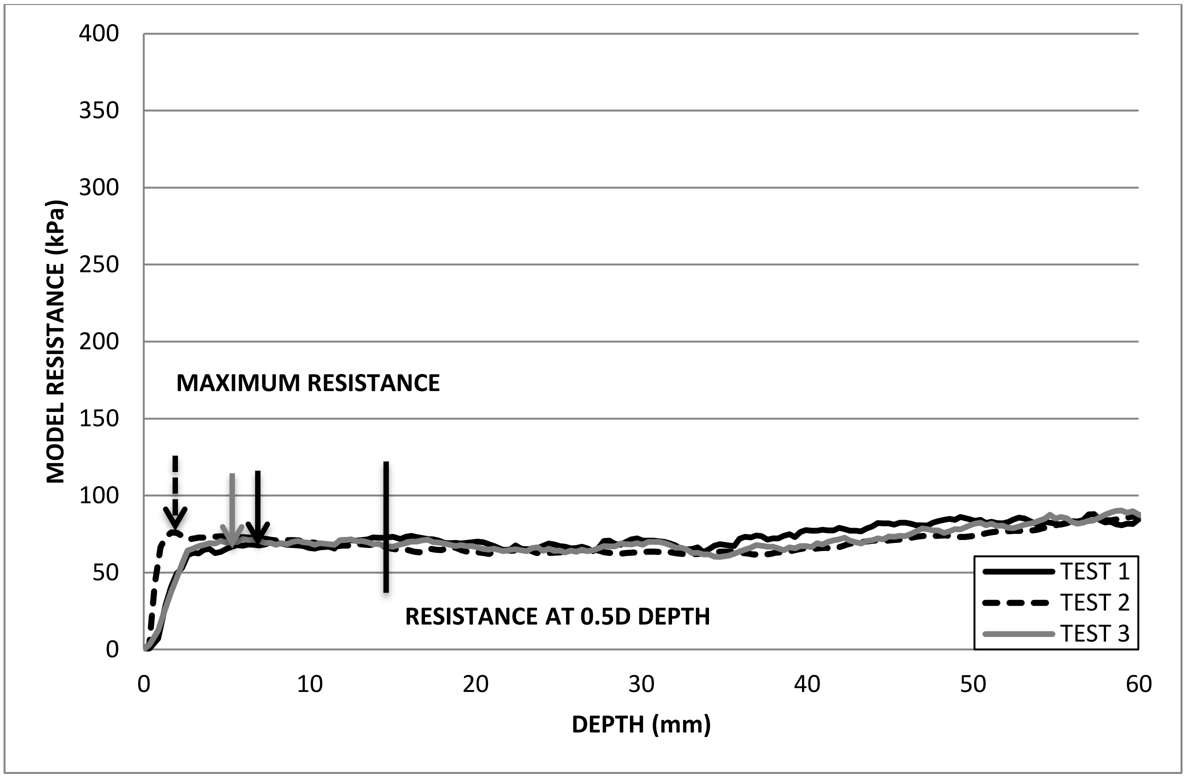

Figure F.15: Resistance profile for a 30 mm circular foundation tested on 2 % fibre normally consolidated model.

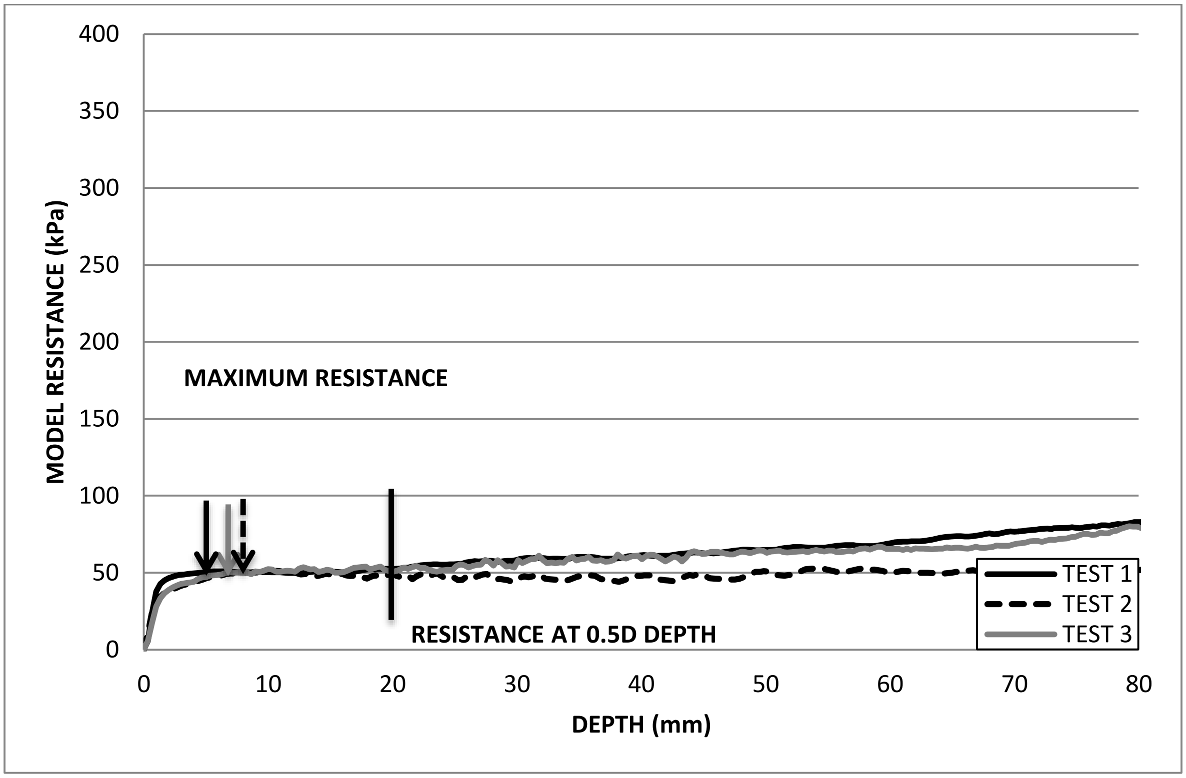

Figure F.16: Resistance profile for a 40 mm circular foundation tested on 2 % fibre normally consolidated model.

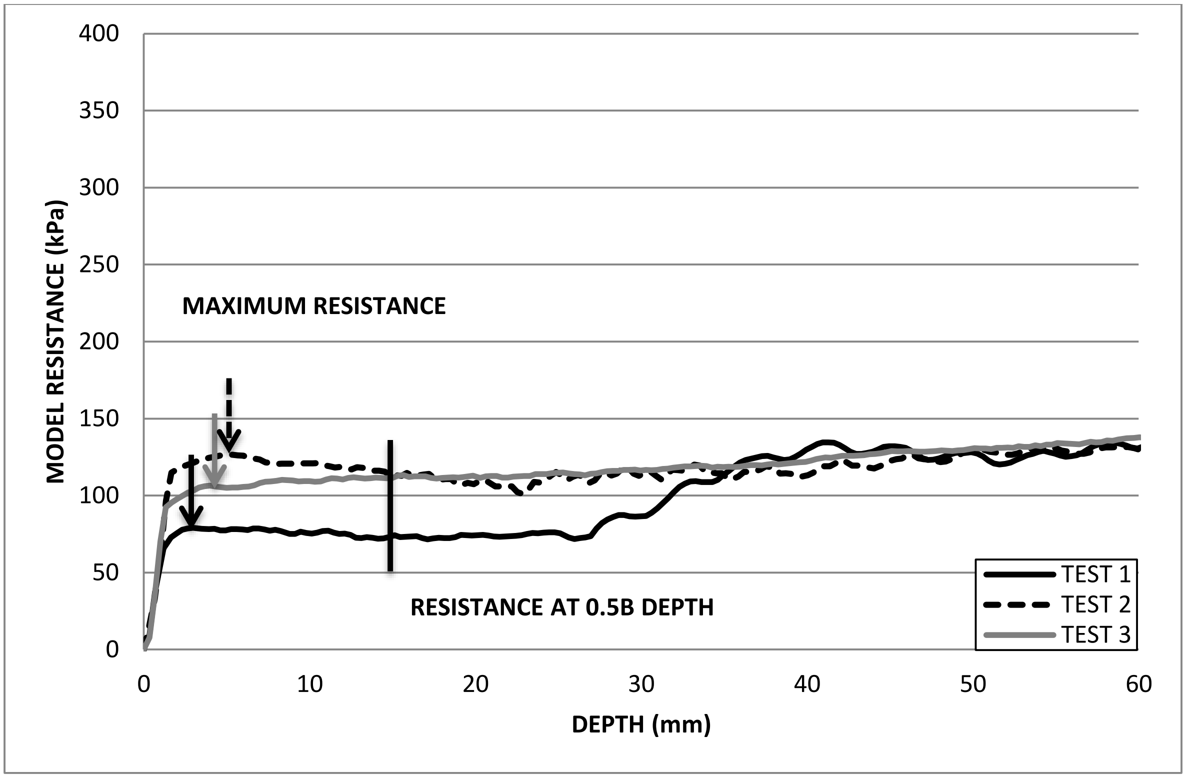

Figure F.17: Resistance profile for a 30 mm square foundation tested on 2 % fibre normally consolidated model.

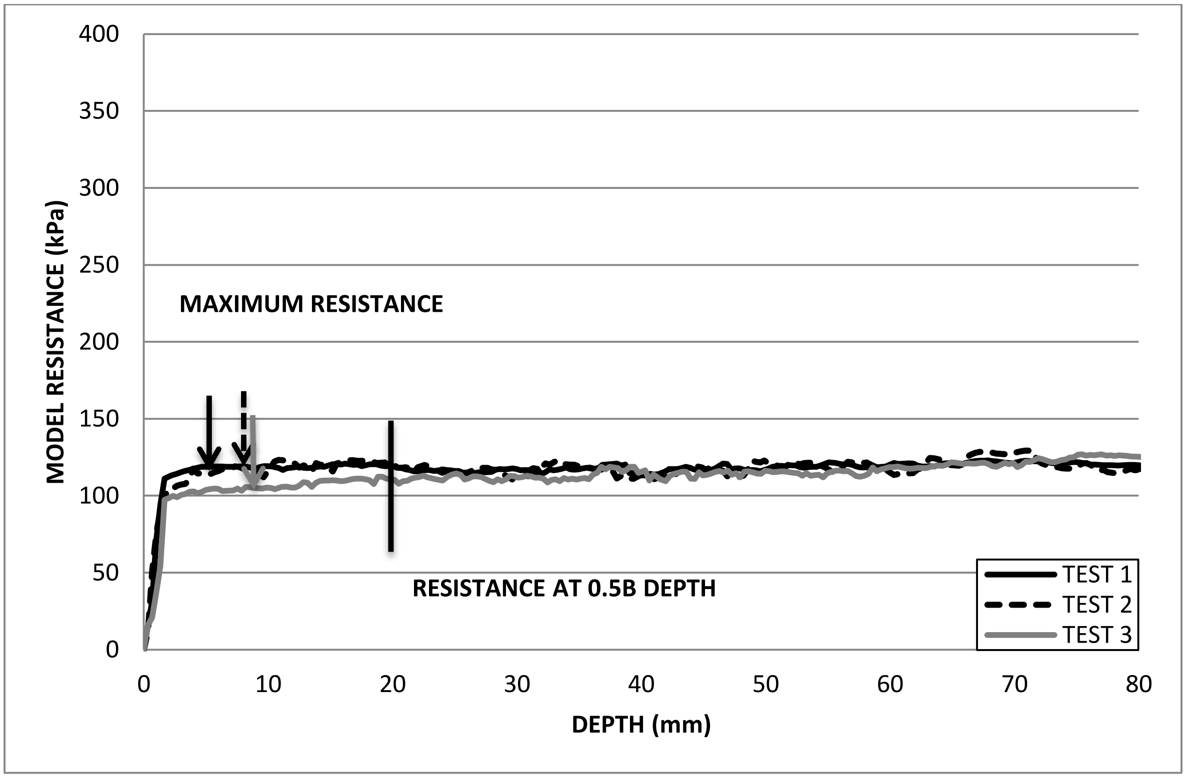

Figure F.18: Resistance profile for a 40 mm square foundation tested on 2 % fibre normally consolidated model.

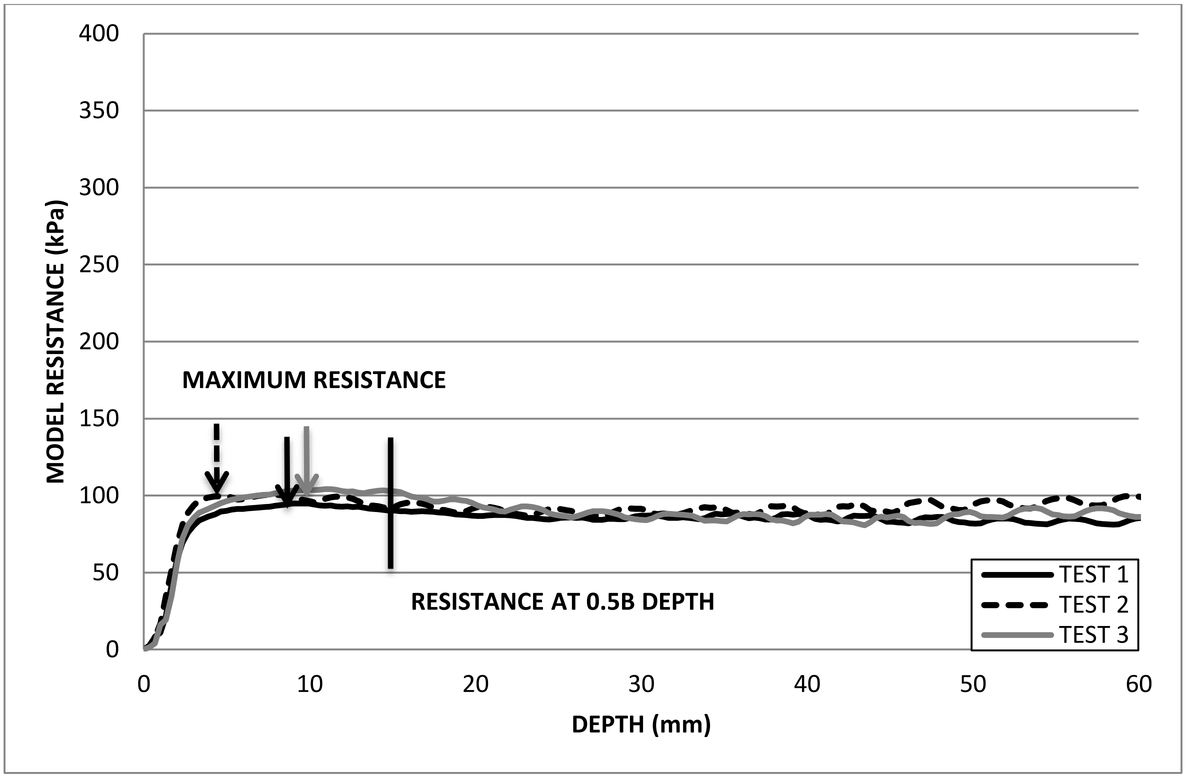

Figure F.19: Resistance profile for a 30 x 60 mm rectangular foundation tested on 3 % fibre normally consolidated model.

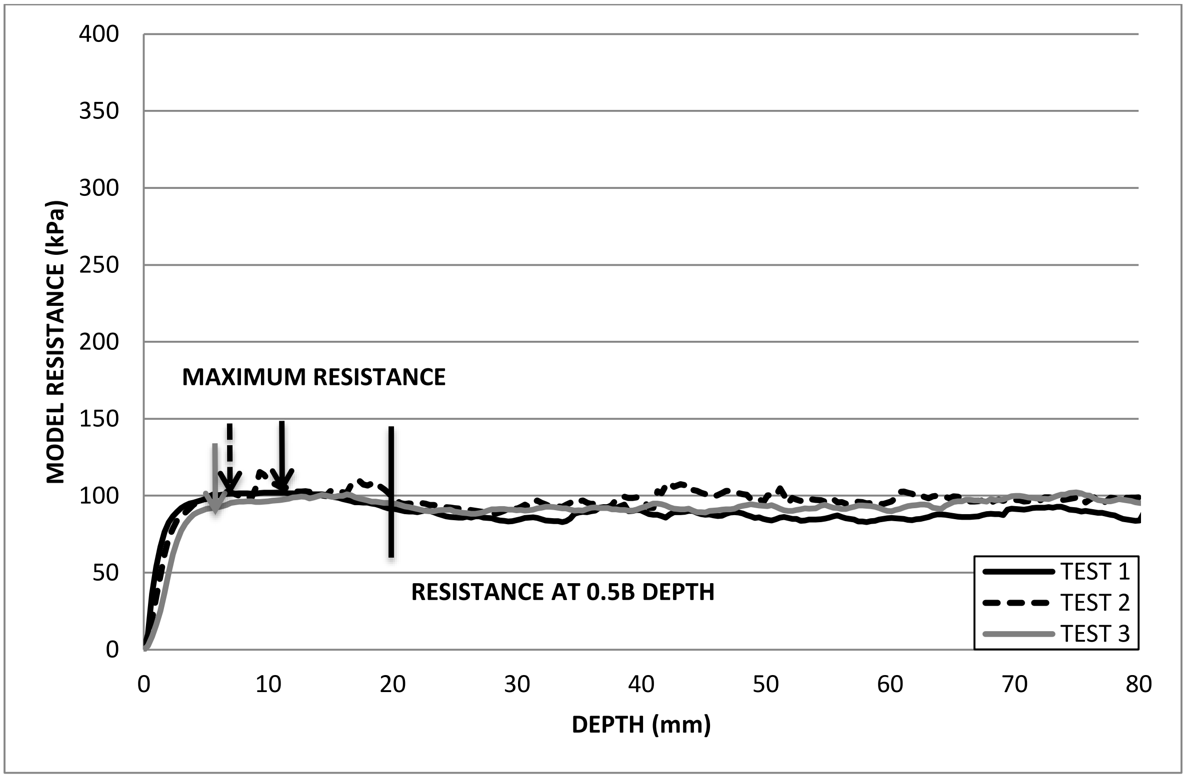

Figure F.20: Resistance profile for a 40 x 80 mm rectangular foundation tested on 3 % fibre normally consolidated model.

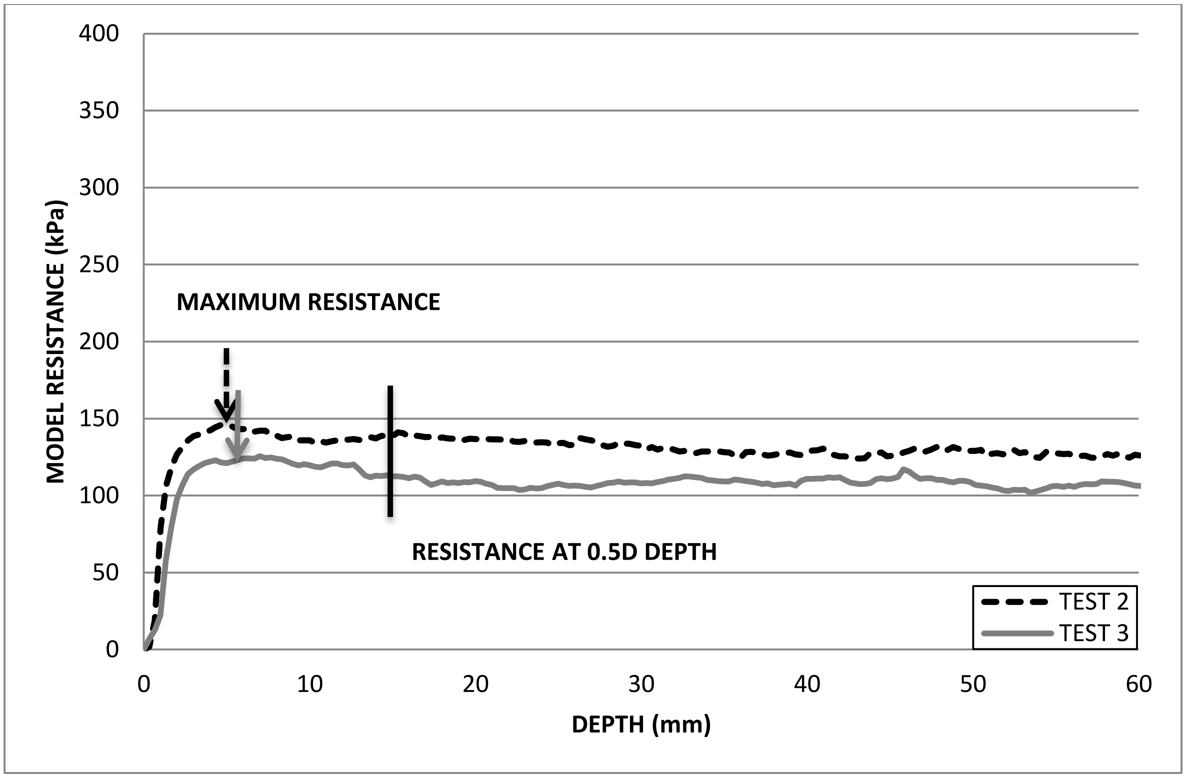

Figure F.21: Resistance profile for a 30 mm circular foundation tested on 3 % fibre normally consolidated model.

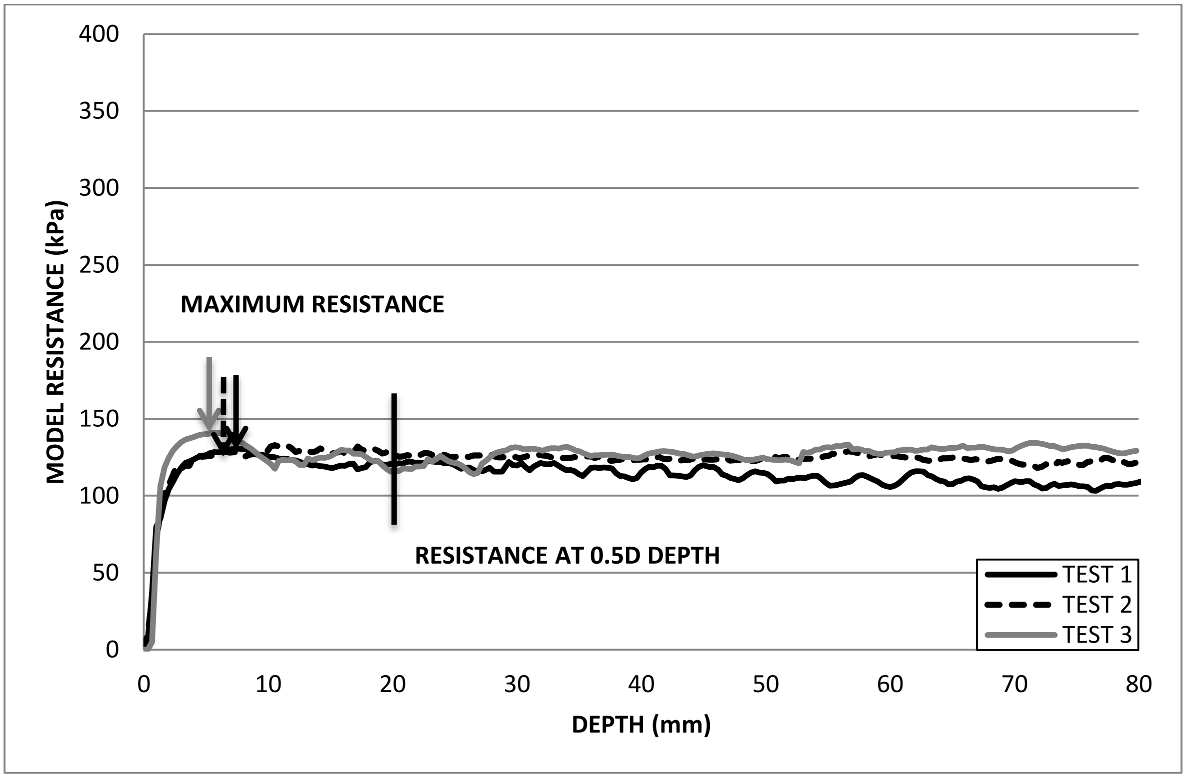

Figure F.22: Resistance profile for a 40 mm circular foundation tested on 3 % fibre normally consolidated model.

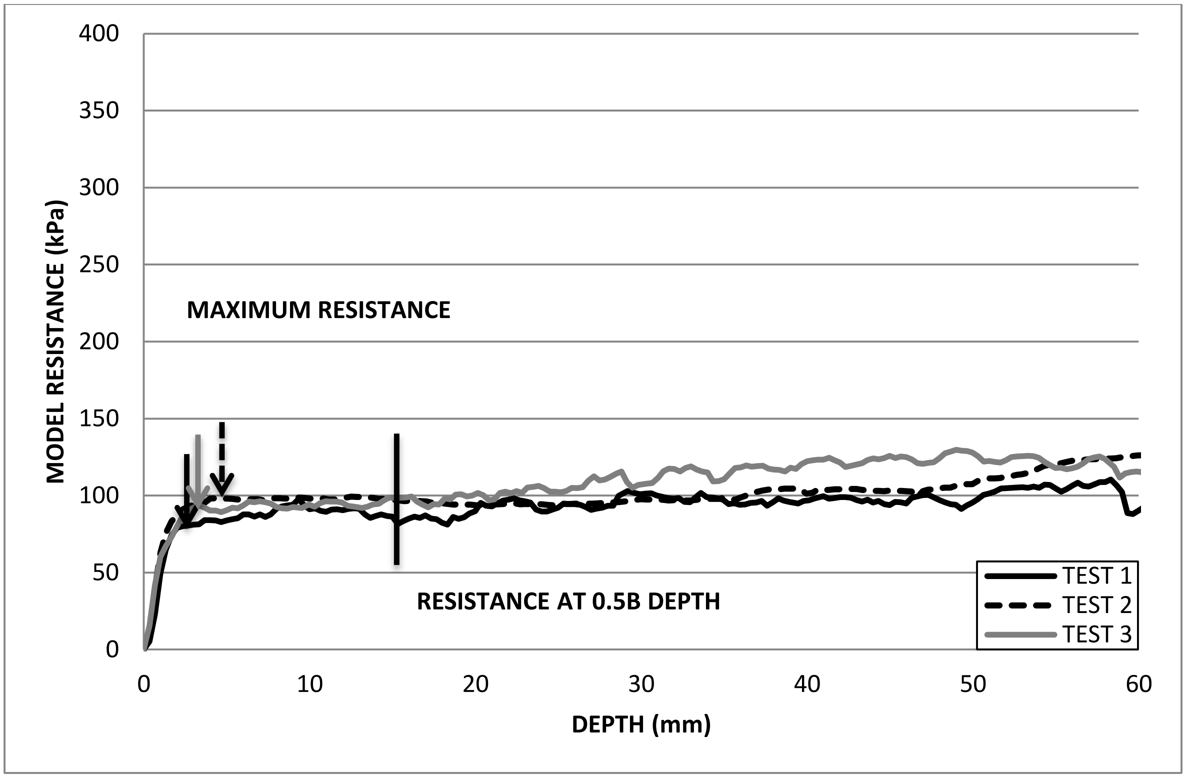

Figure F.23: Resistance profile for a 30 mm square foundation tested on 3 % fibre normally consolidated model.

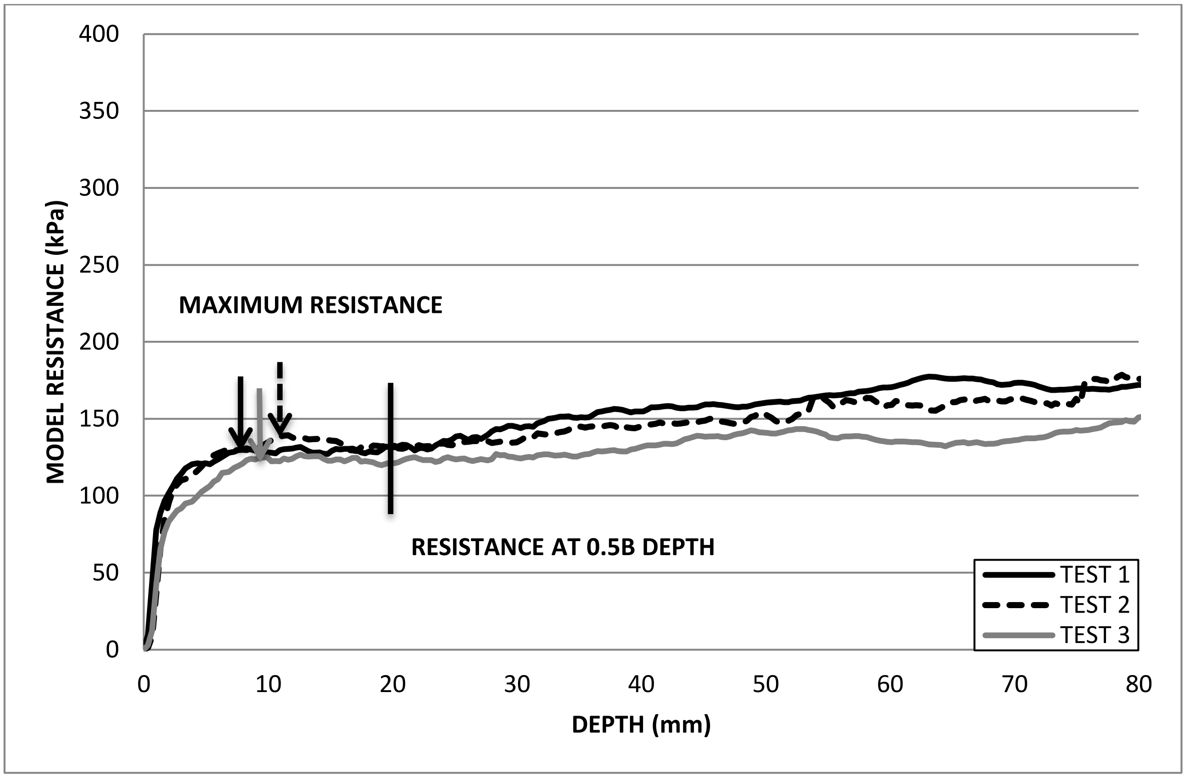

Figure F.24: Resistance profile for a 40 mm square foundation tested on 3 % fibre normally consolidated model.

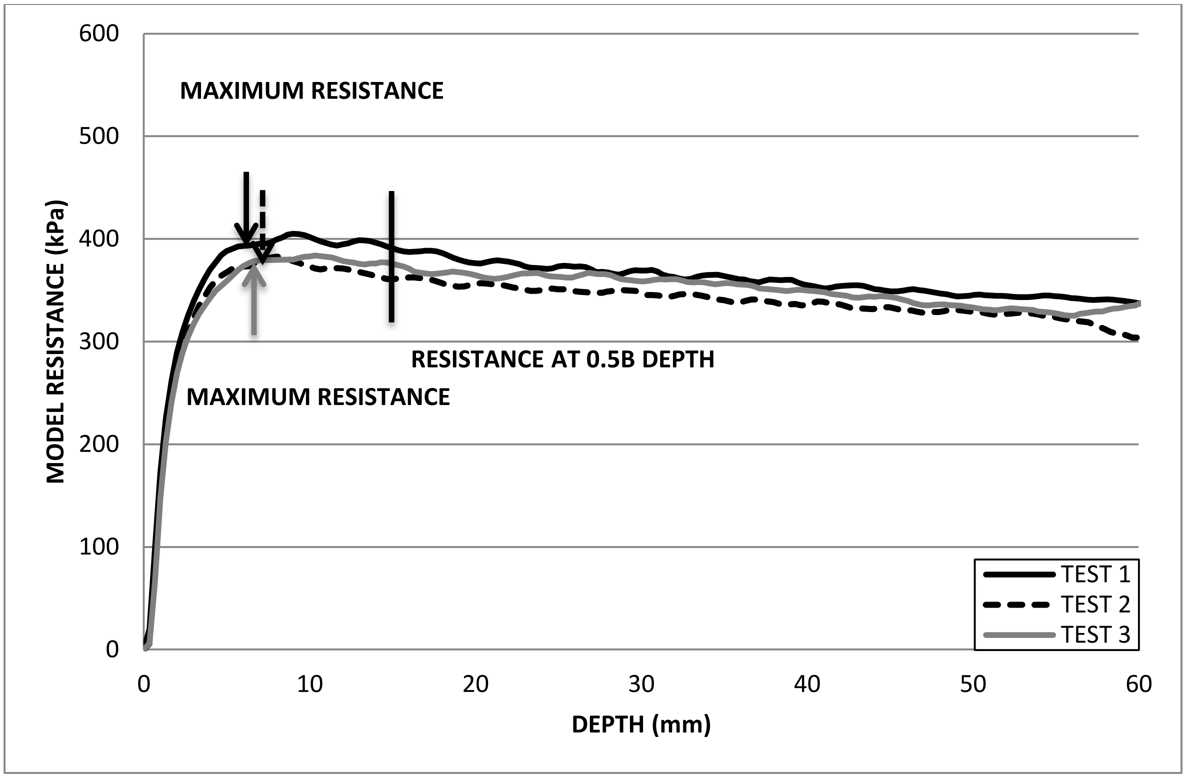

Figure F.25: Resistance profile for a 30 x 60 mm rectangular foundation tested on 4 % fibre normally consolidated model.

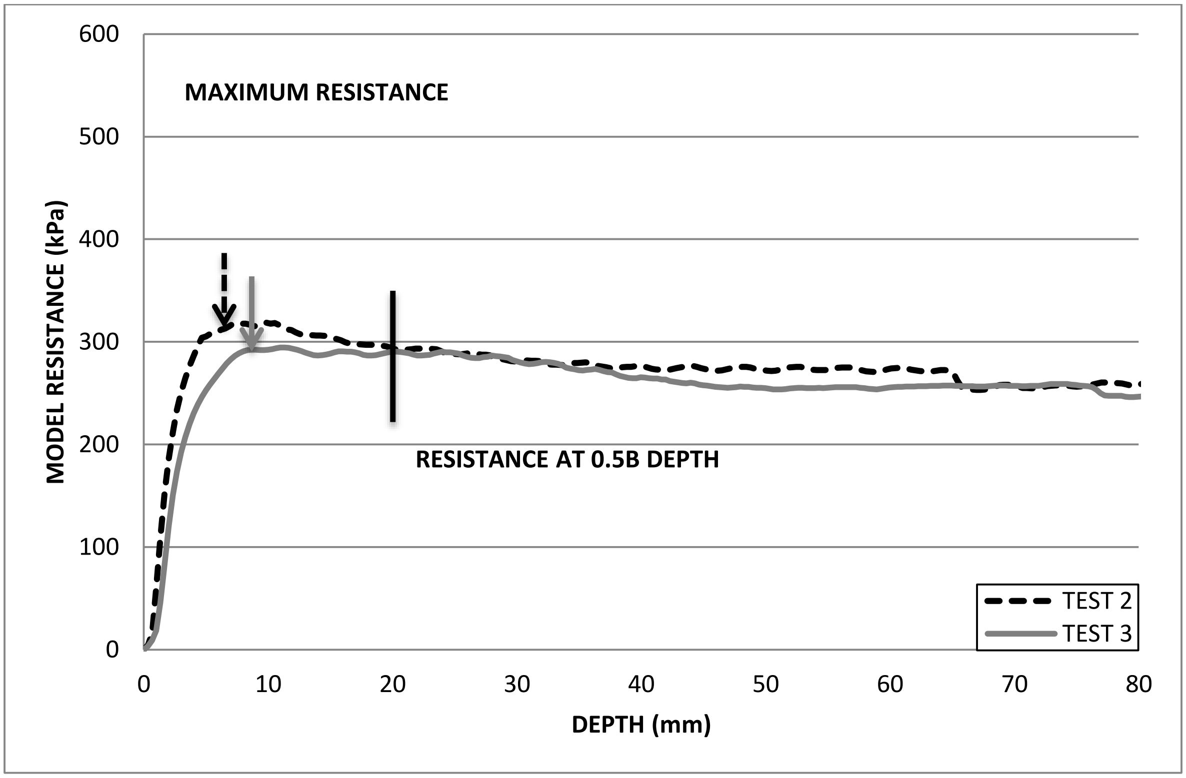

Figure F.26: Resistance profile for a 40 x 80 mm rectangular foundation tested on 4 % fibre normally consolidated model.

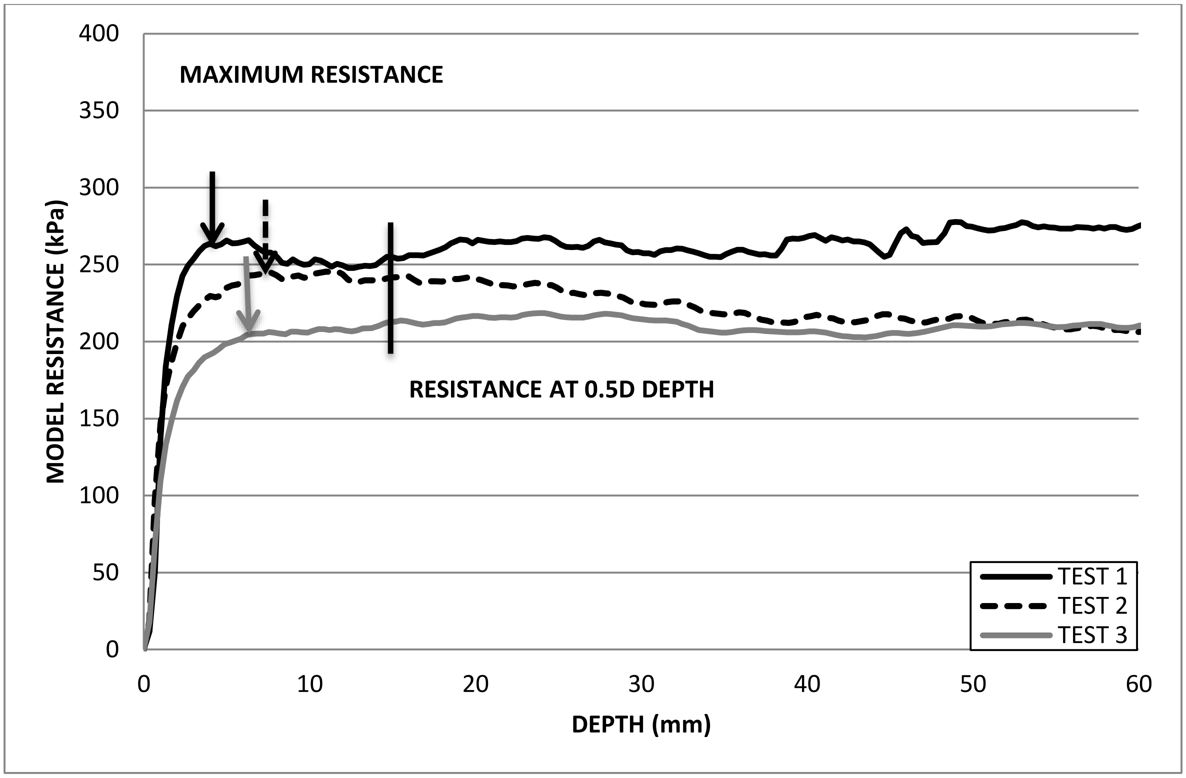

Figure F.27: Resistance profile for a 30 mm circular foundation tested on 4 % fibre normally consolidated model.

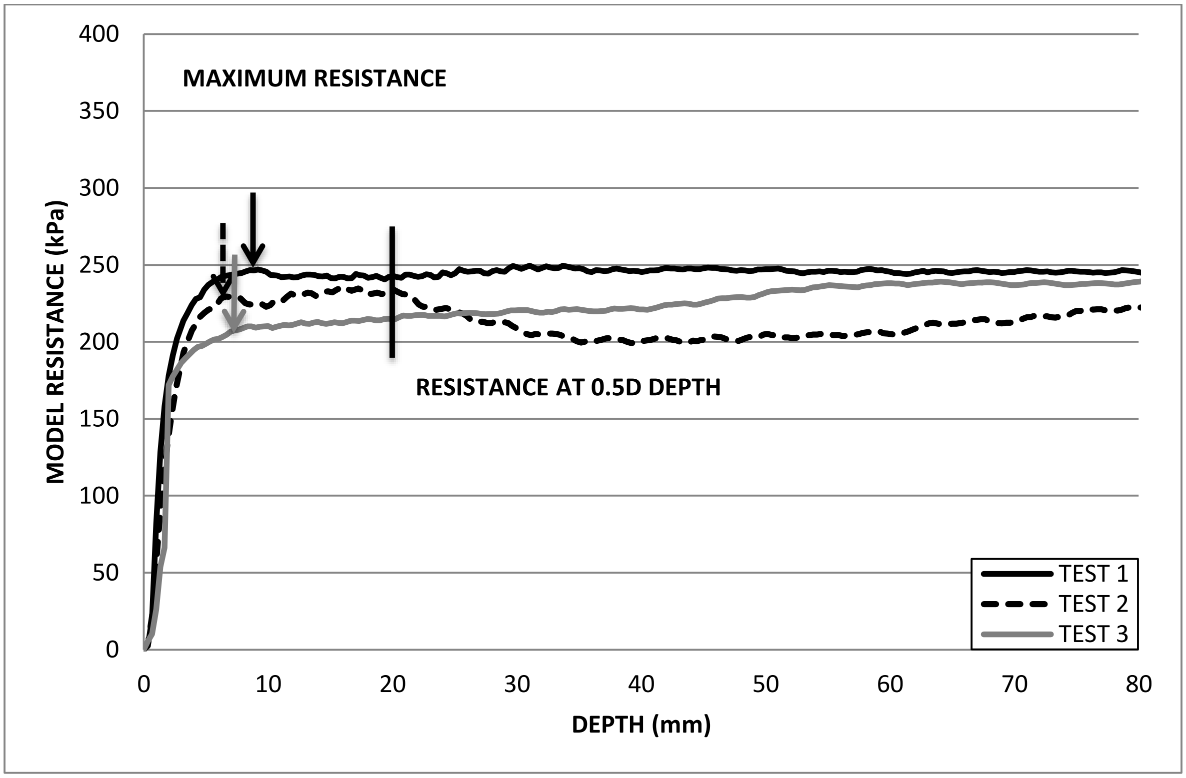

Figure F.28: Resistance profile for a 40 mm circular foundation tested on 4 % fibre normally consolidated model.

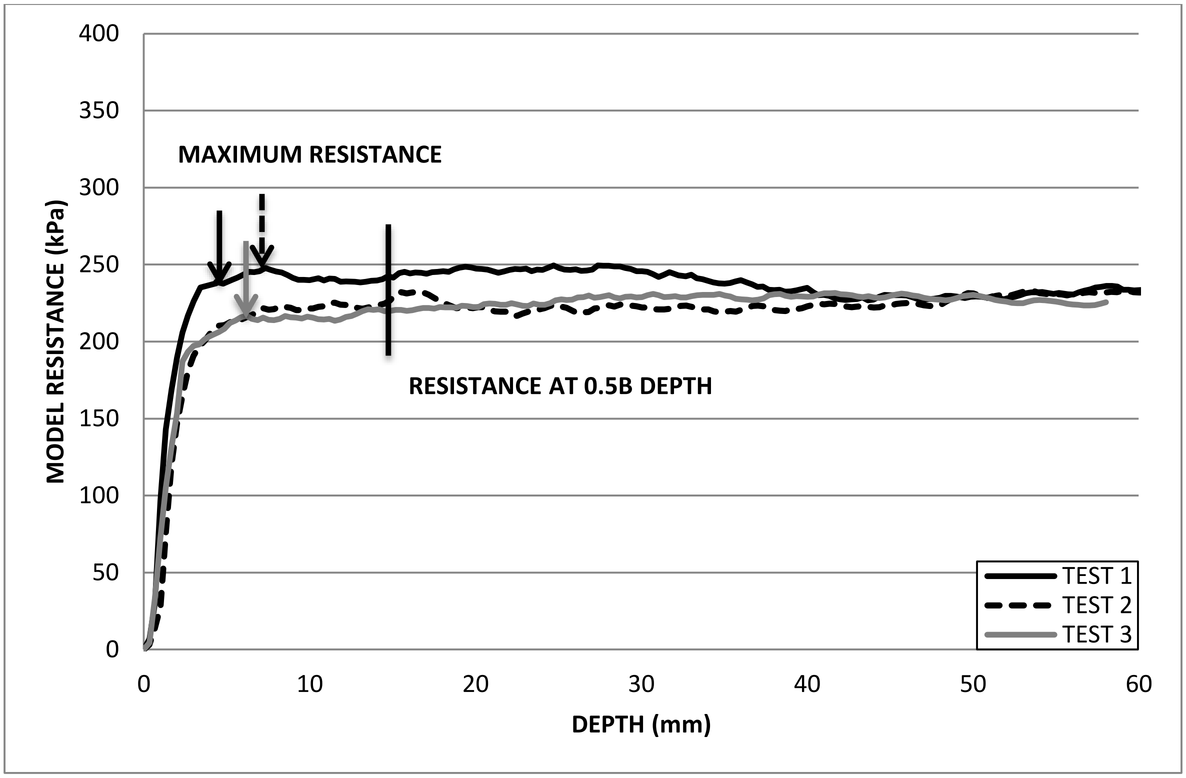

Figure F.29: Resistance profile for a 30 mm square foundation tested on 4 % fibre normally consolidated model.

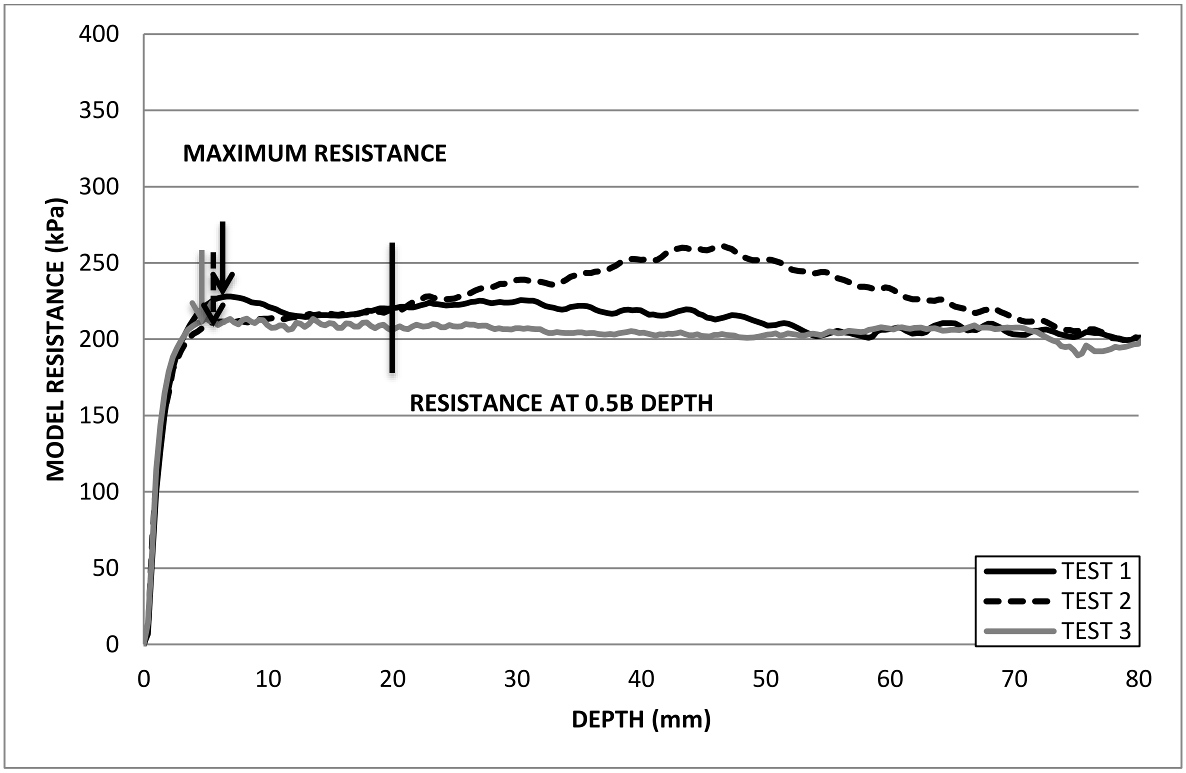

Figure F.30: Resistance profile for a 40 mm square foundation tested on 4 % fibre normally consolidated model.

APPENDIX G:

CENTRIFUGE MODELLING RESULTS

BEARING CAPACITY

TEST SERIES 2

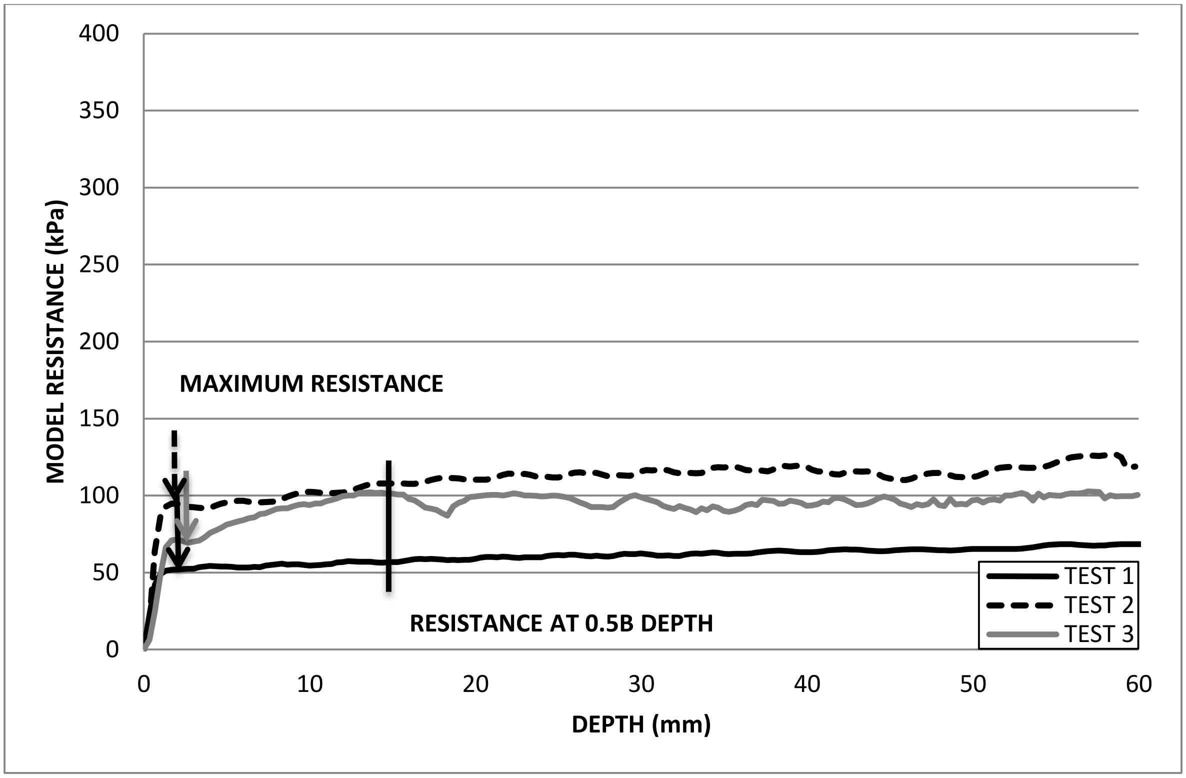

Figure G.1: Resistance profile for a 30 x 60 mm rectangular foundation tested on 0 % fibre over consolidated model.

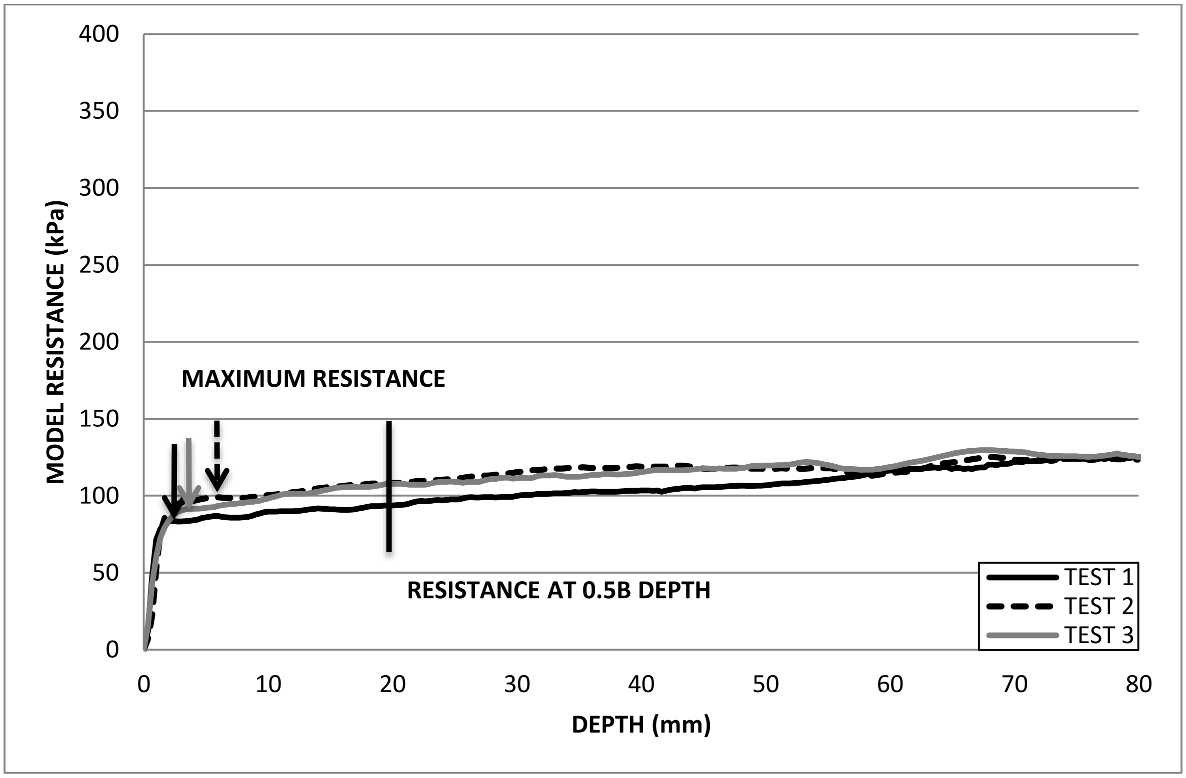

Figure G.2: Resistance profile for a 40 x 80 mm rectangular foundation tested on 0 % fibre over consolidated model.

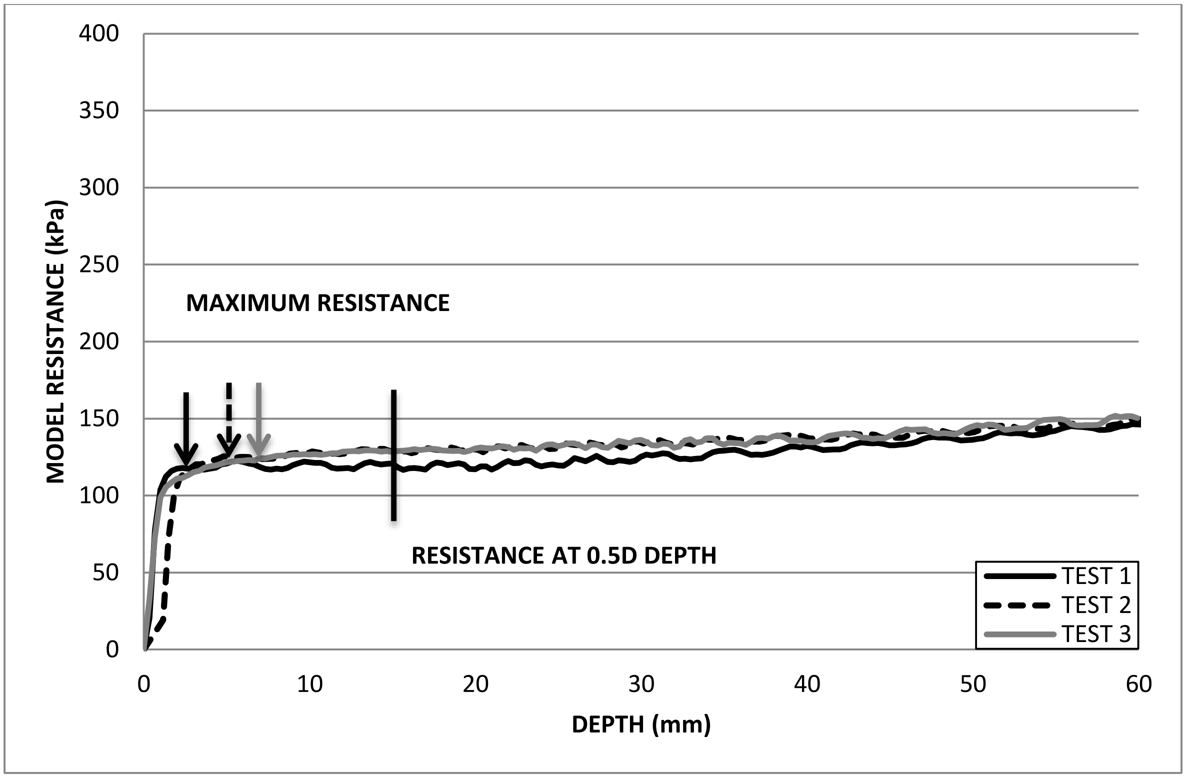

Figure G.3: Resistance profile for a 30 mm circular foundation tested on 0 % fibre over consolidated model.

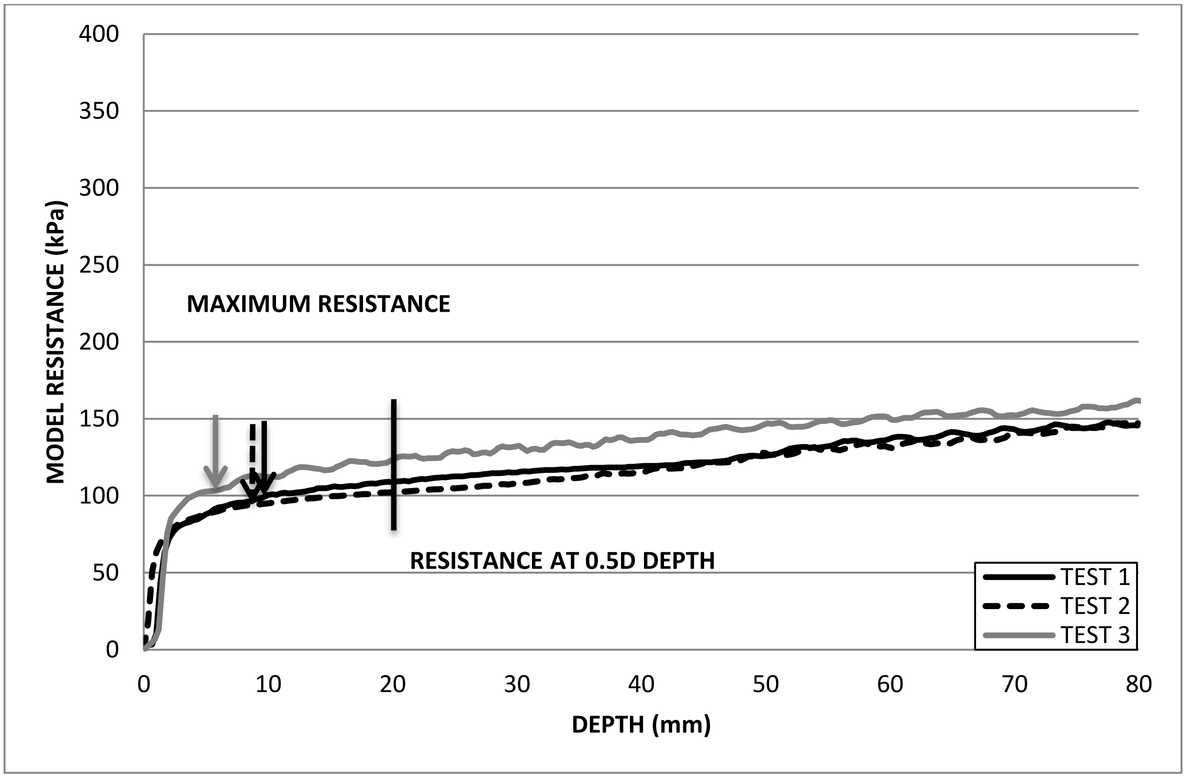

Figure G.4: Resistance profile for a 40 mm circular foundation tested on 0 % fibre over consolidated model.

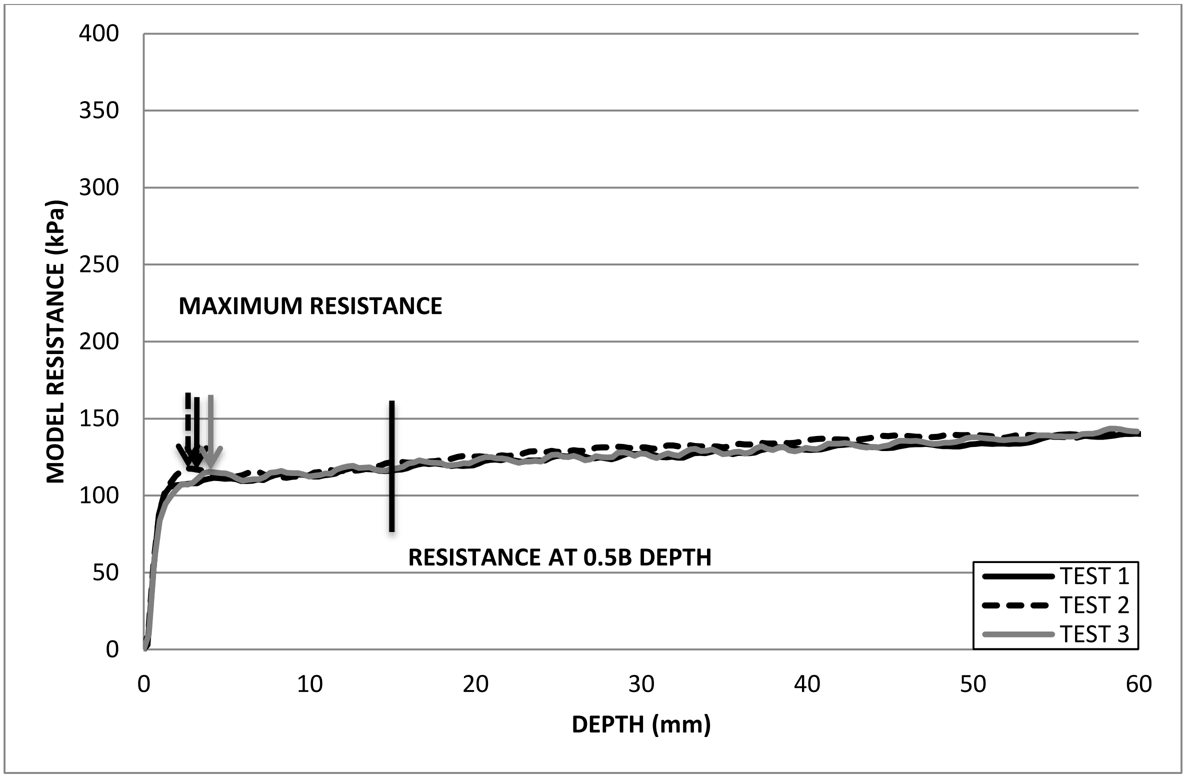

Figure G.5: Resistance profile for a 30 mm square foundation tested on 0 % fibre over consolidated model.

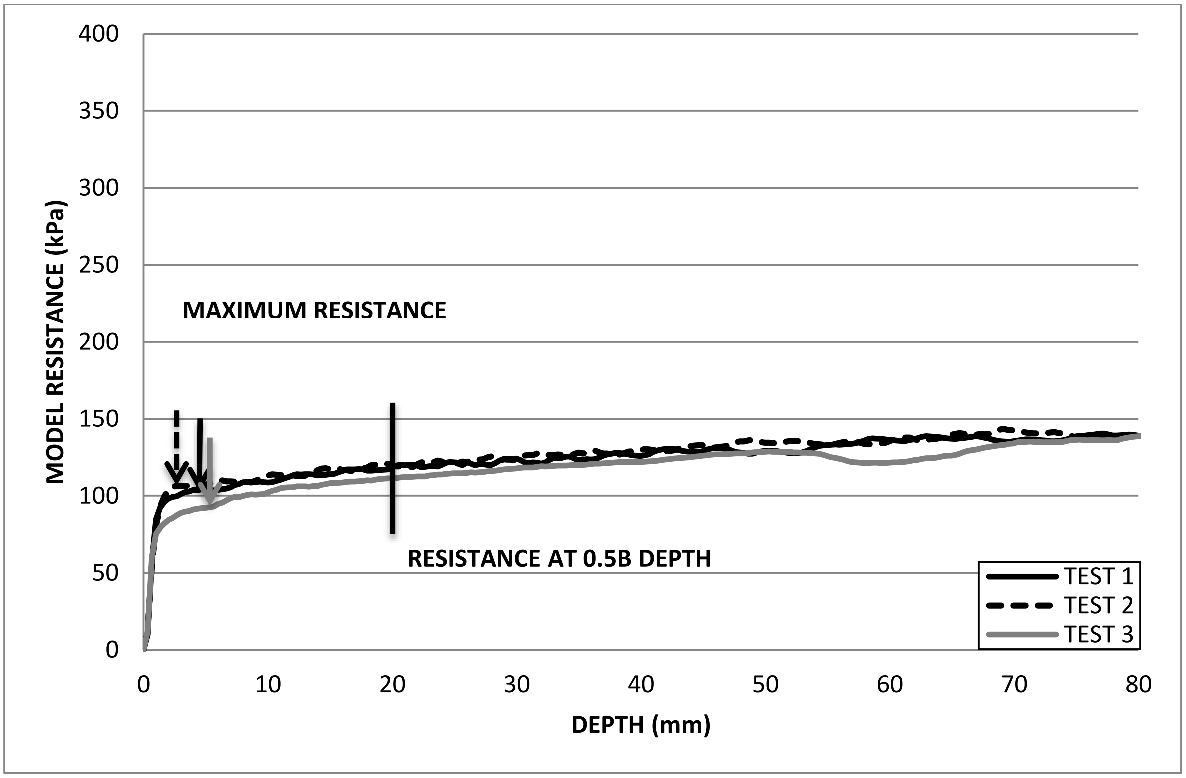

Figure G.6: Resistance profile for a 40 mm square foundation tested on 0 % fibre over consolidated model.

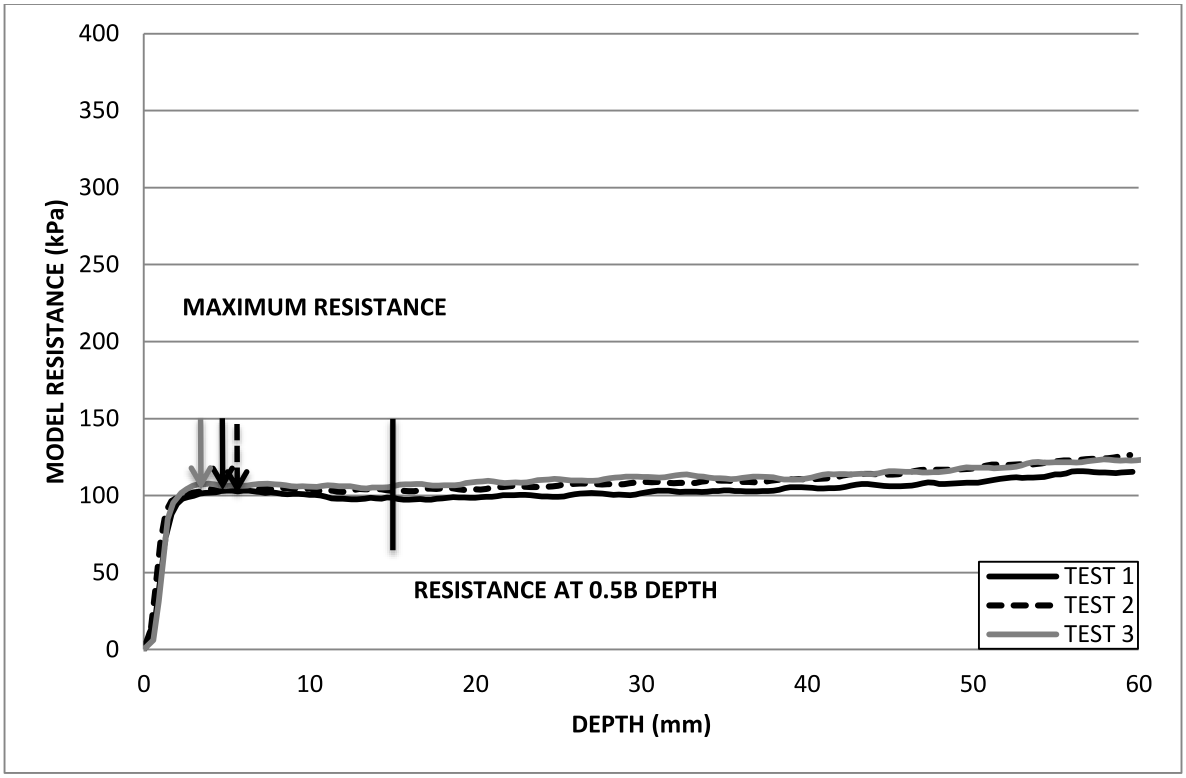

Figure G.7: Resistance profile for a 30 x 60 mm rectangular foundation tested on 1 % fibre over consolidated model.

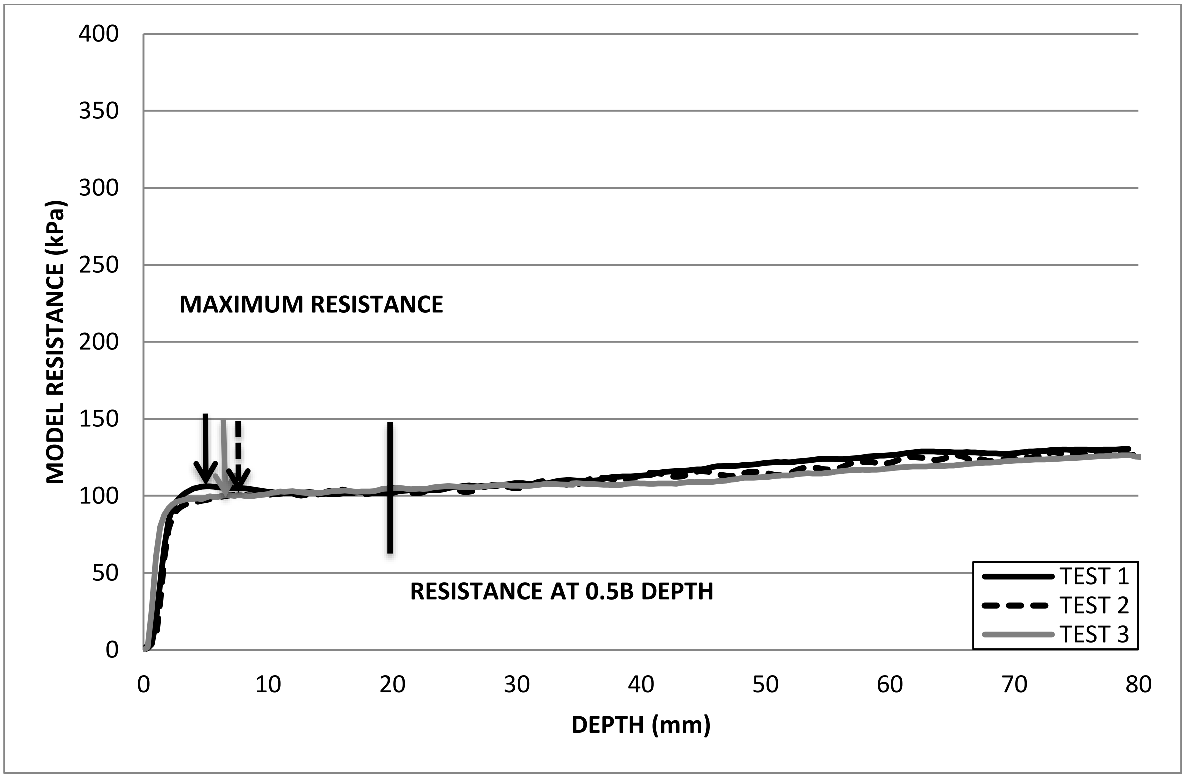

Figure G.8: Resistance profile for a 40 x 80 mm rectangular foundation tested on 1 % fibre over consolidated model.

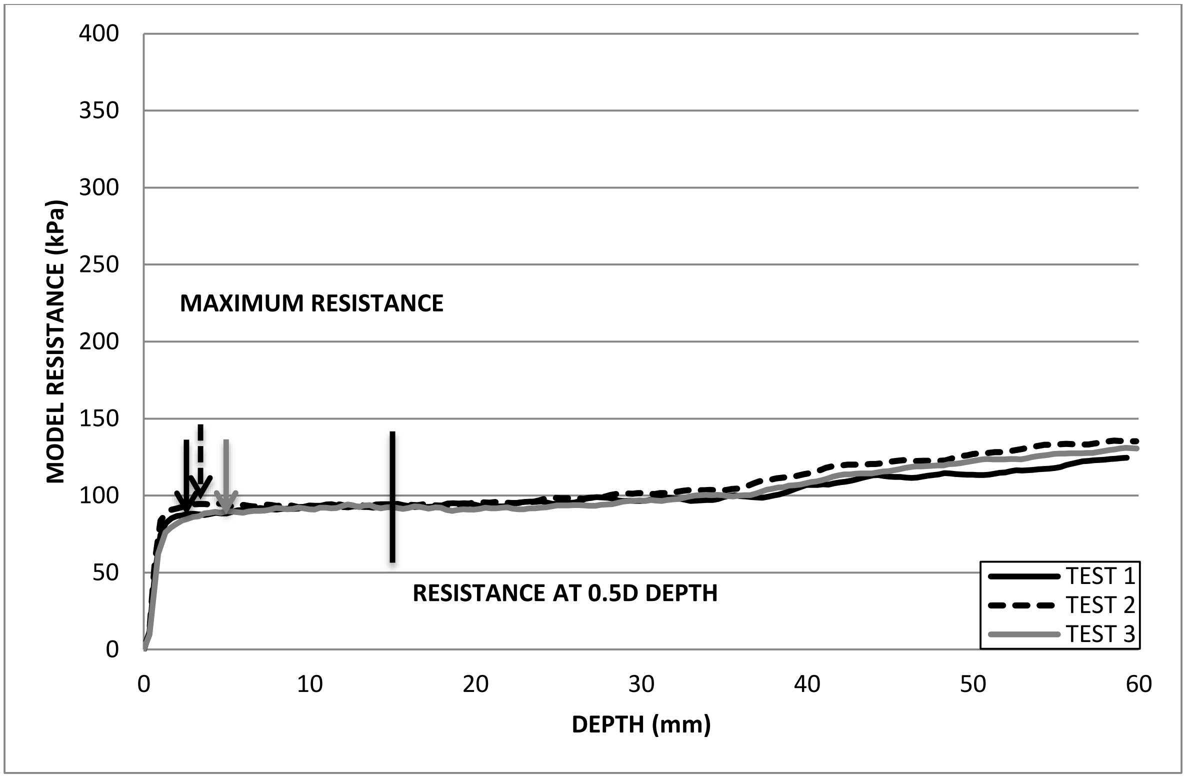

Figure G.9: Resistance profile for a 30 mm circular foundation tested on 1 % fibre over consolidated model.

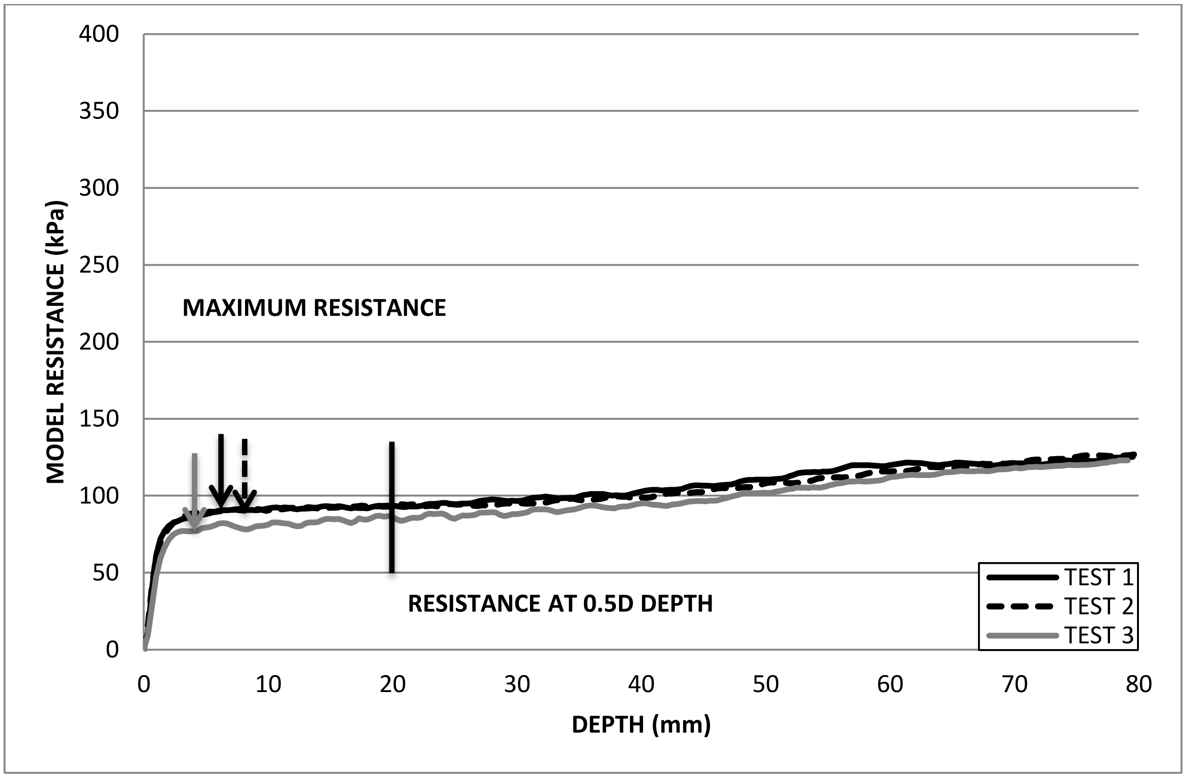

Figure G.10: Resistance profile for a 40 mm circular foundation tested on 1 % fibre over consolidated model.

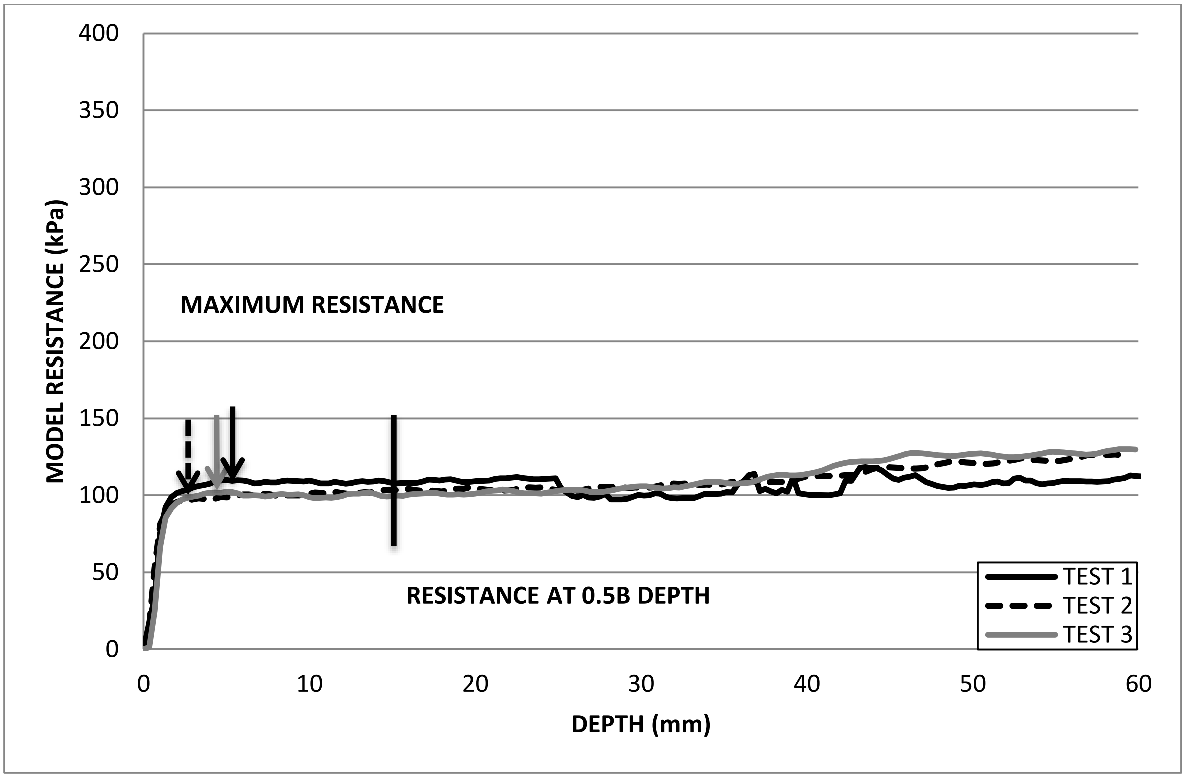

Figure G.11: Resistance profile for a 30 mm square foundation tested on 1 % fibre over consolidated model.

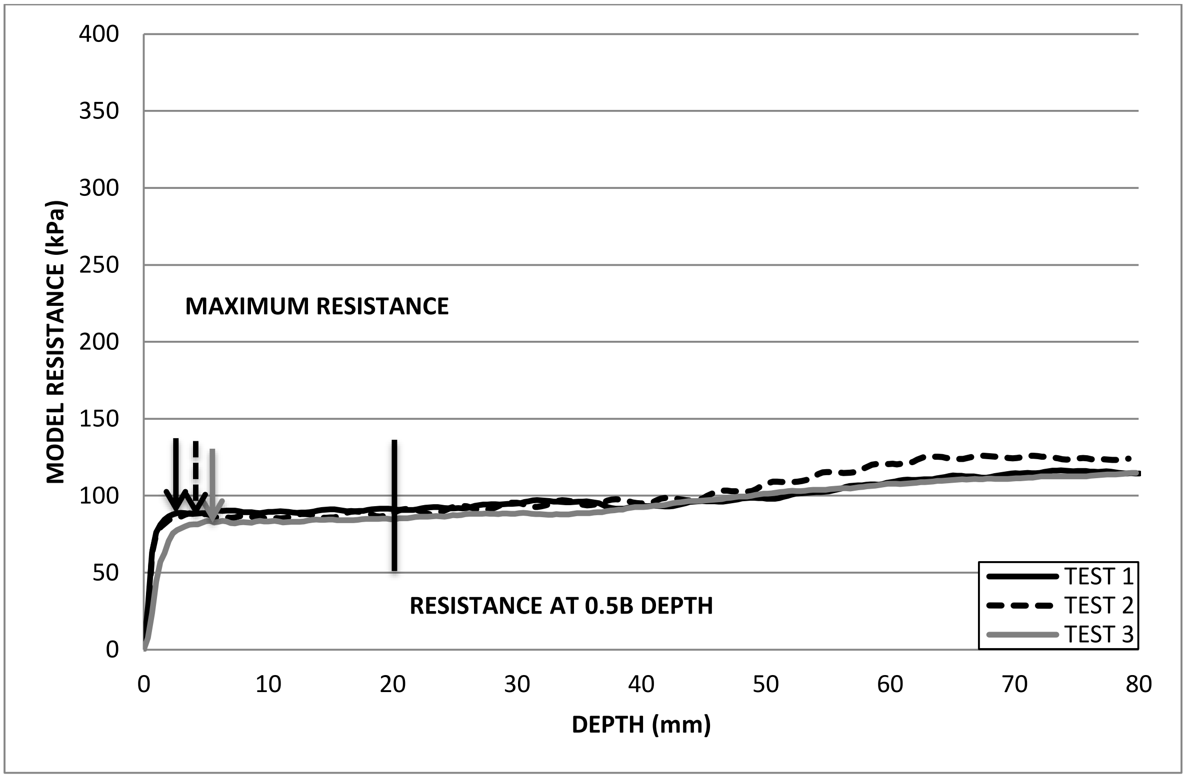

Figure G.12: Resistance profile for a 40 mm square foundation tested on 1 % fibre over consolidated model.

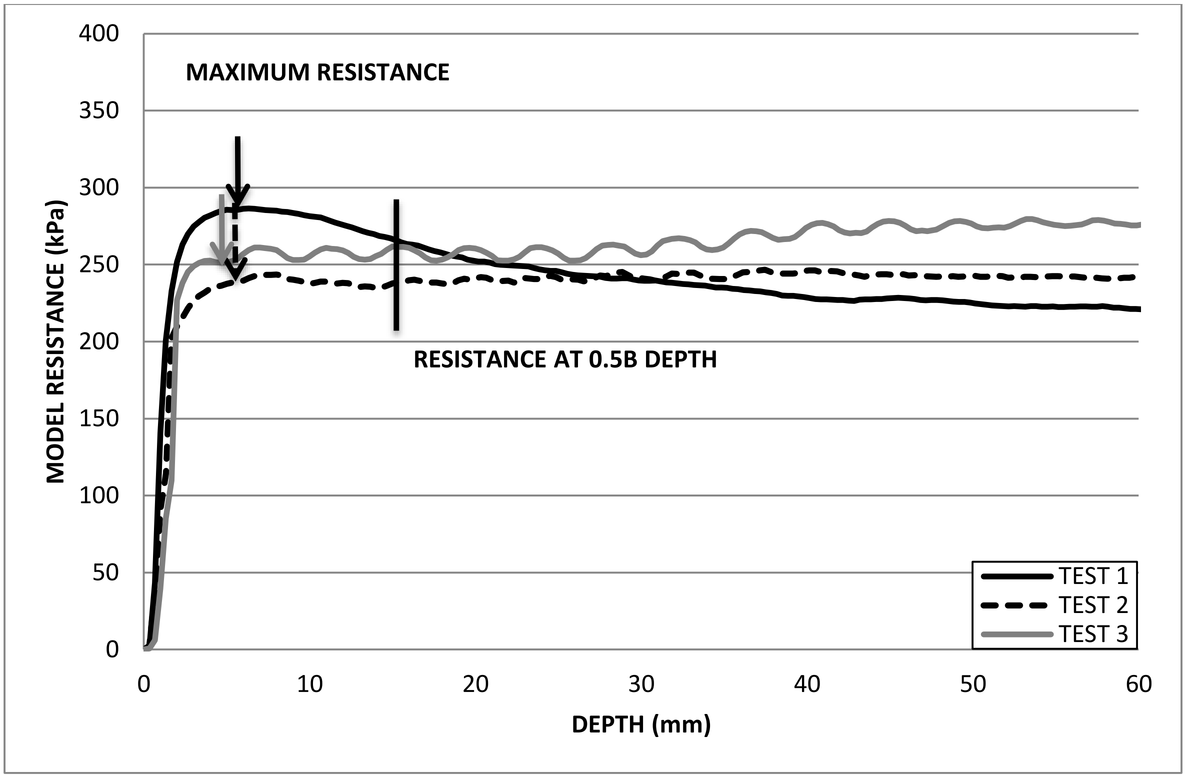

Figure G.13: Resistance profile for a 30 x 60 mm rectangular foundation tested on 2 % fibre over consolidated model.

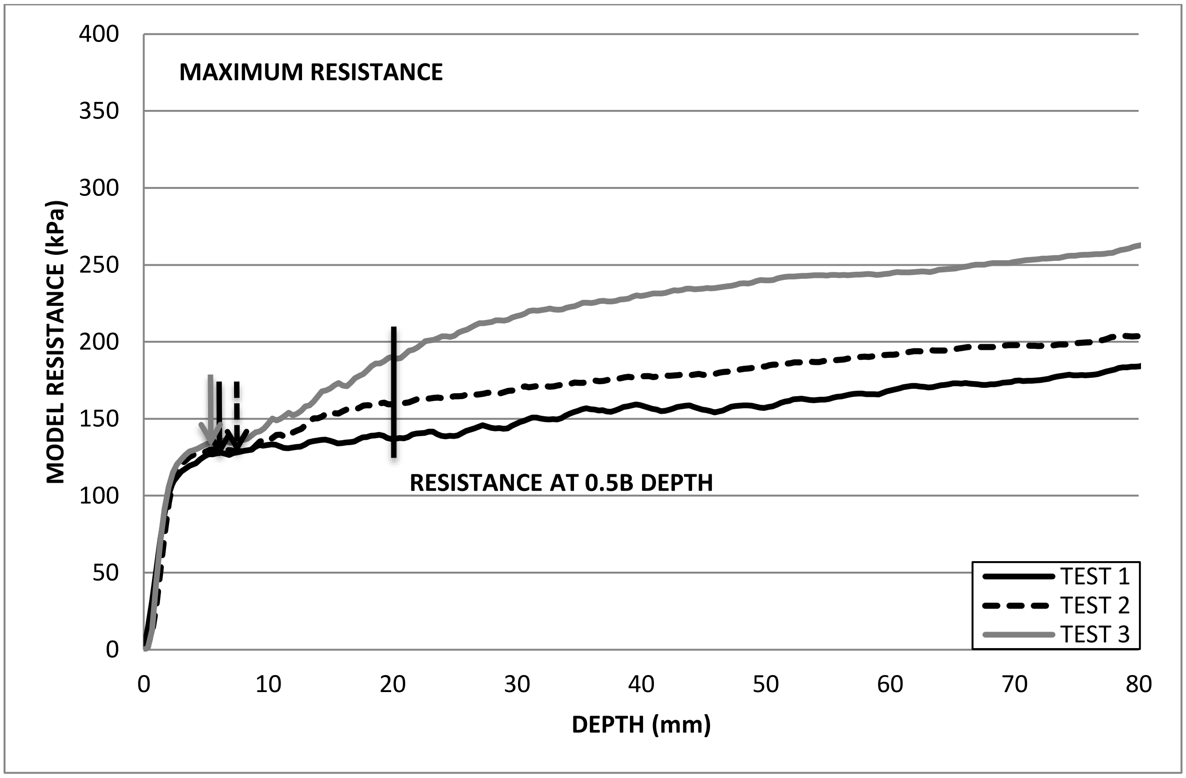

Figure G.14: Resistance profile for a 40 x 80 mm rectangular foundation tested on 2 % fibre over consolidated model.

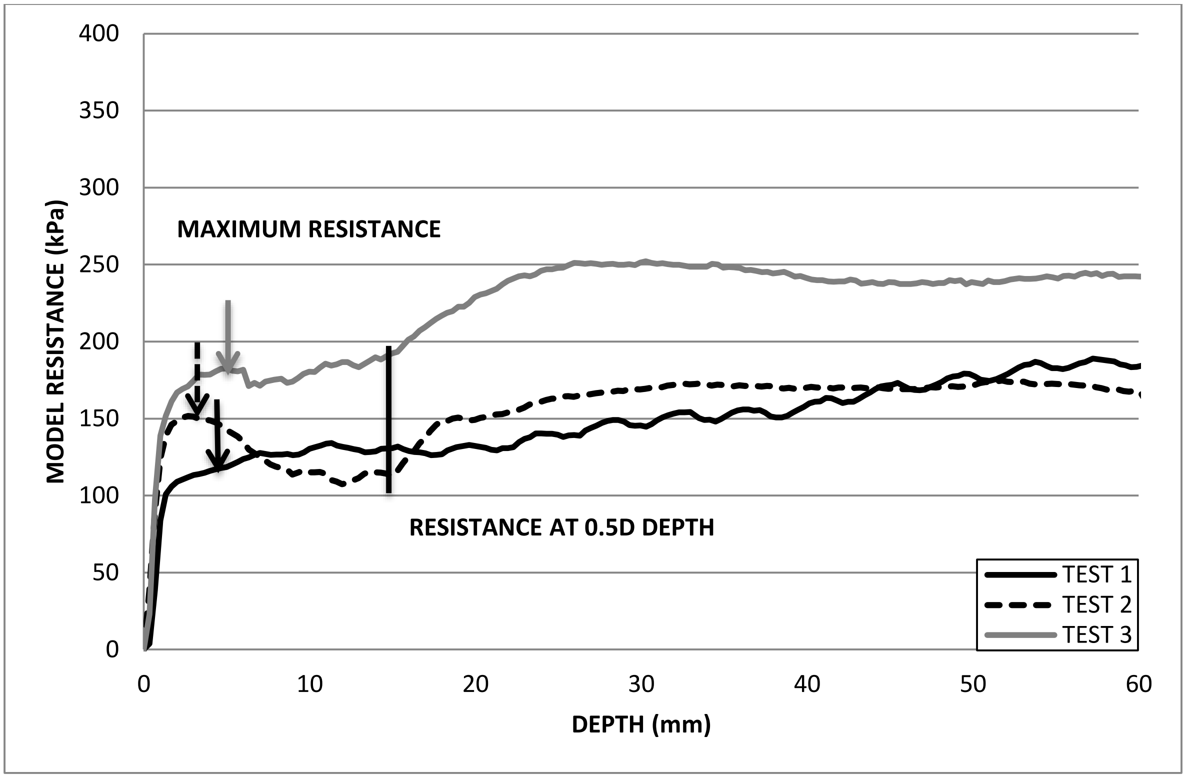

Figure G.15: Resistance profile for a 30 mm circular foundation tested on 2 % fibre over consolidated model.

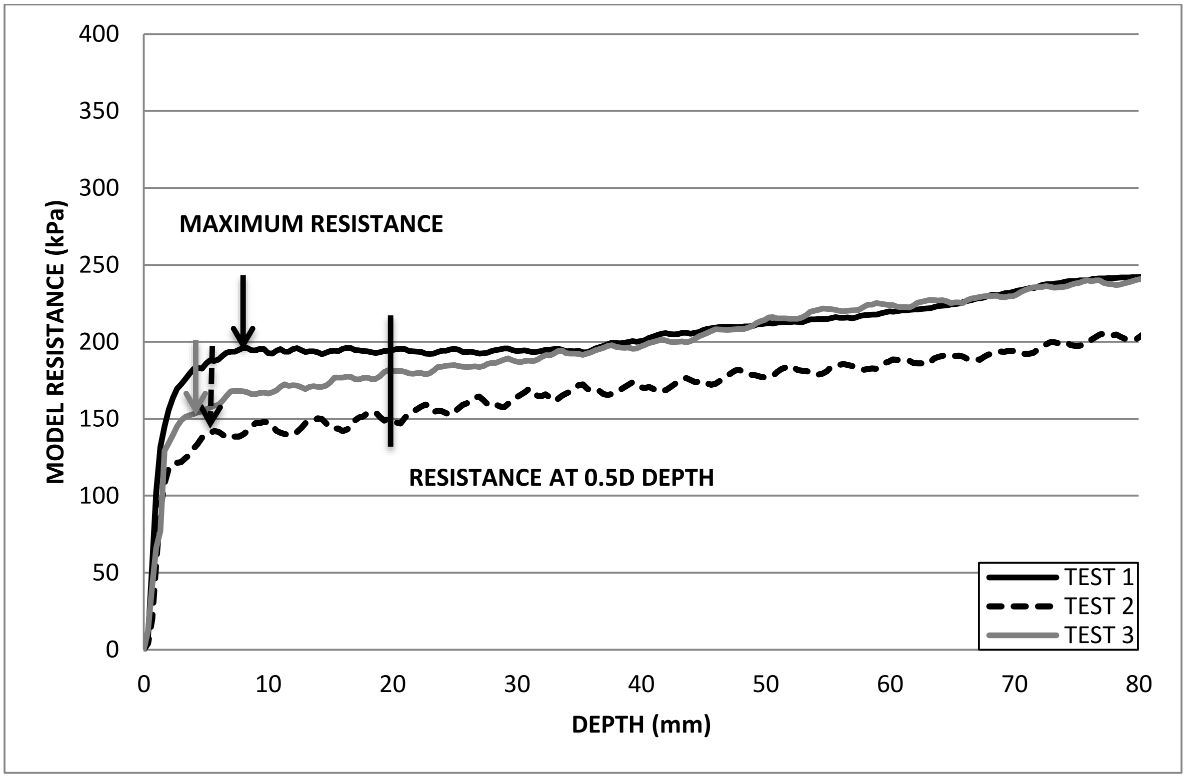

Figure G.16: Resistance profile for a 40 mm circular foundation tested on 2 % fibre over consolidated model.

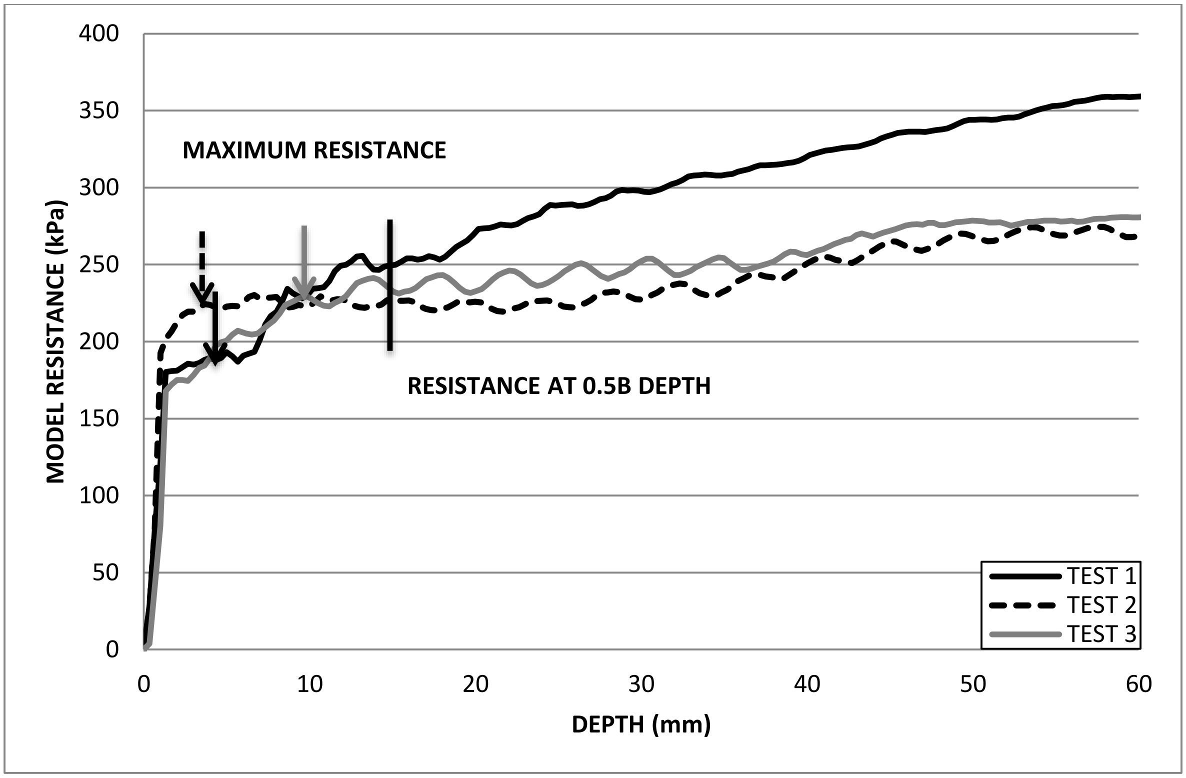

Figure G.17: Resistance profile for a 30 mm square foundation tested on 2 % fibre over consolidated model.

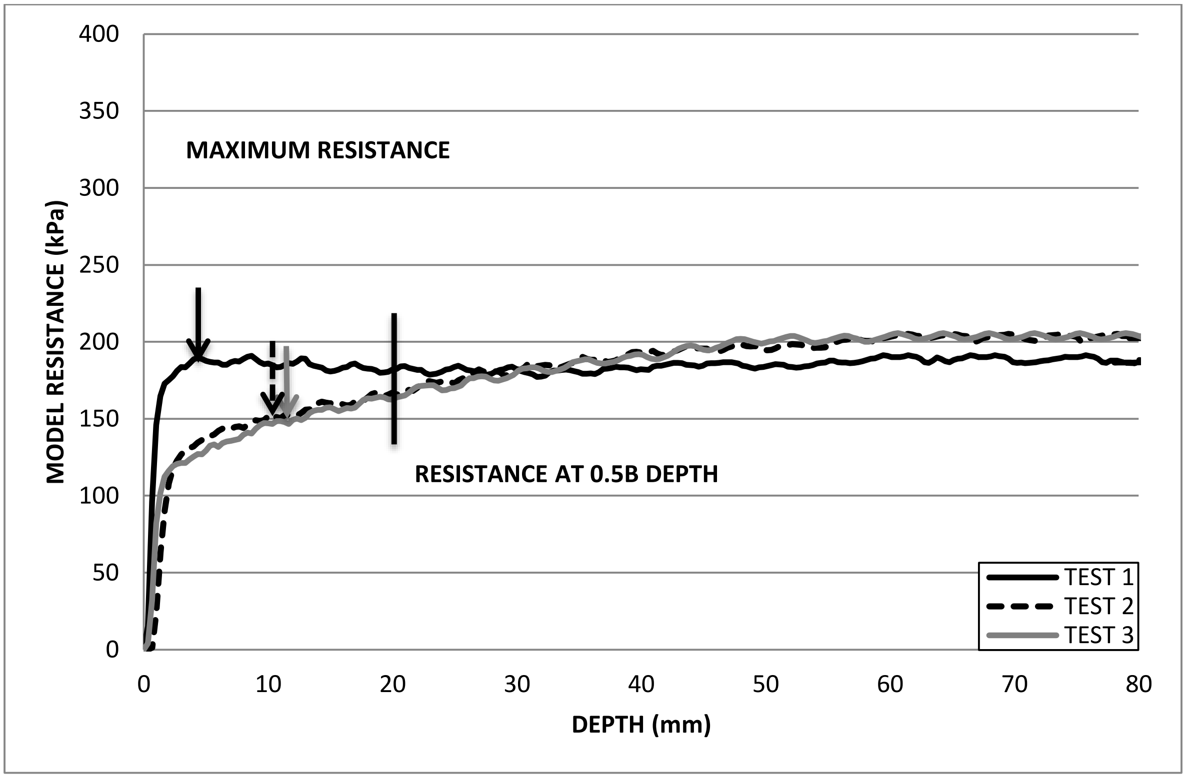

Figure G.18: Resistance profile for a 40 mm square foundation tested on 2 % fibre over consolidated model.

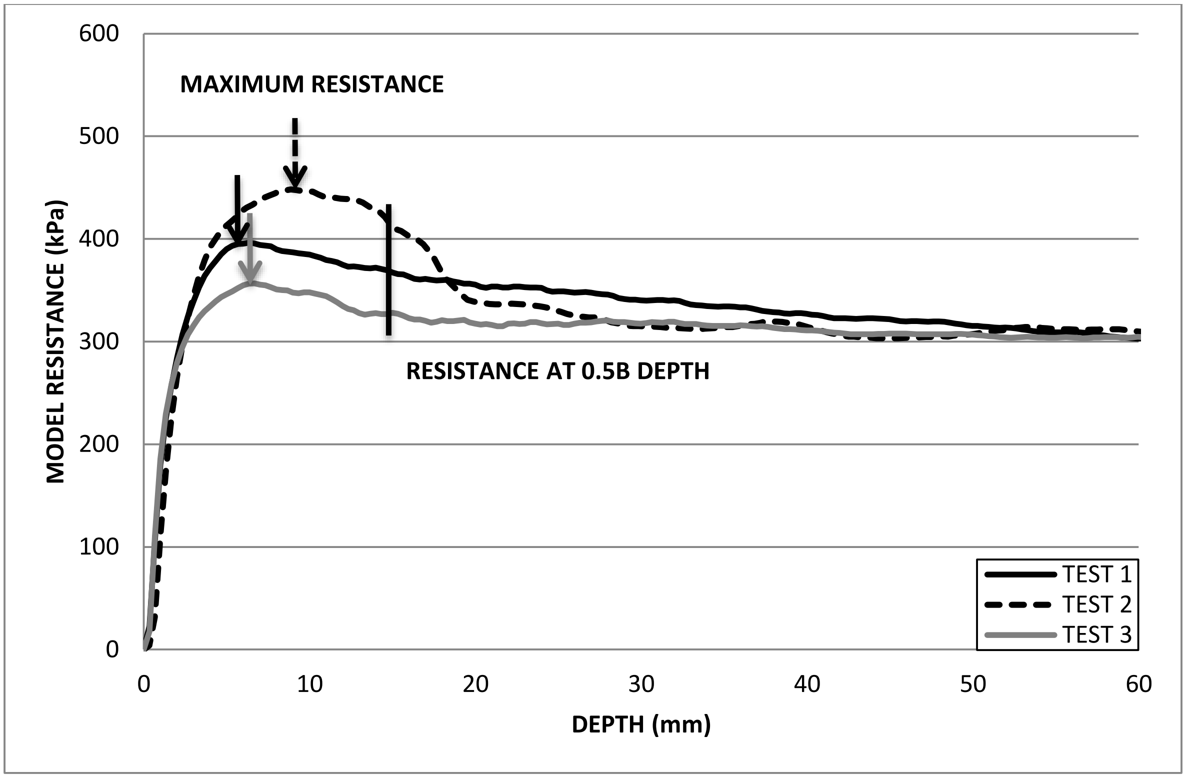

Figure G.19: Resistance profile for a 30 x 60 mm rectangular foundation tested on 3 % fibre over consolidated model.

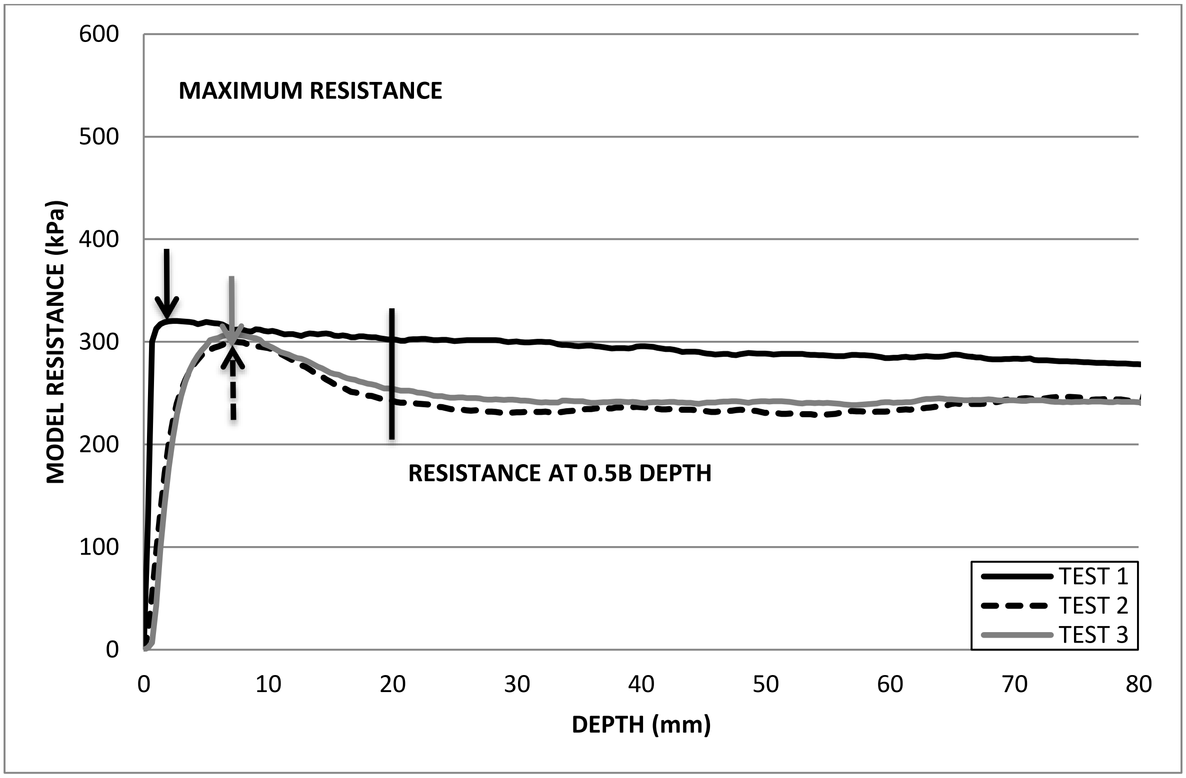

Figure G.20: Resistance profile for a 40 x 80 mm rectangular foundation tested on 3 % fibre over consolidated model.

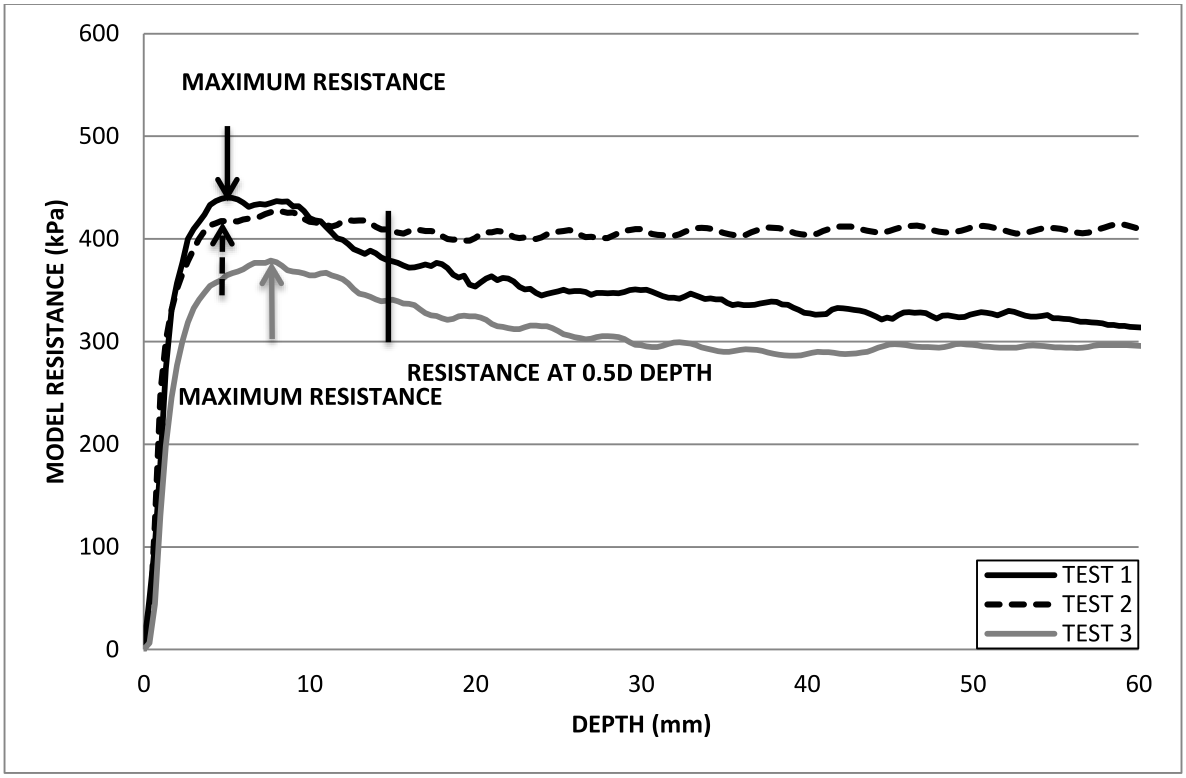

Figure G.21: Resistance profile for a 30 mm circular foundation tested on 3 % fibre over consolidated model.

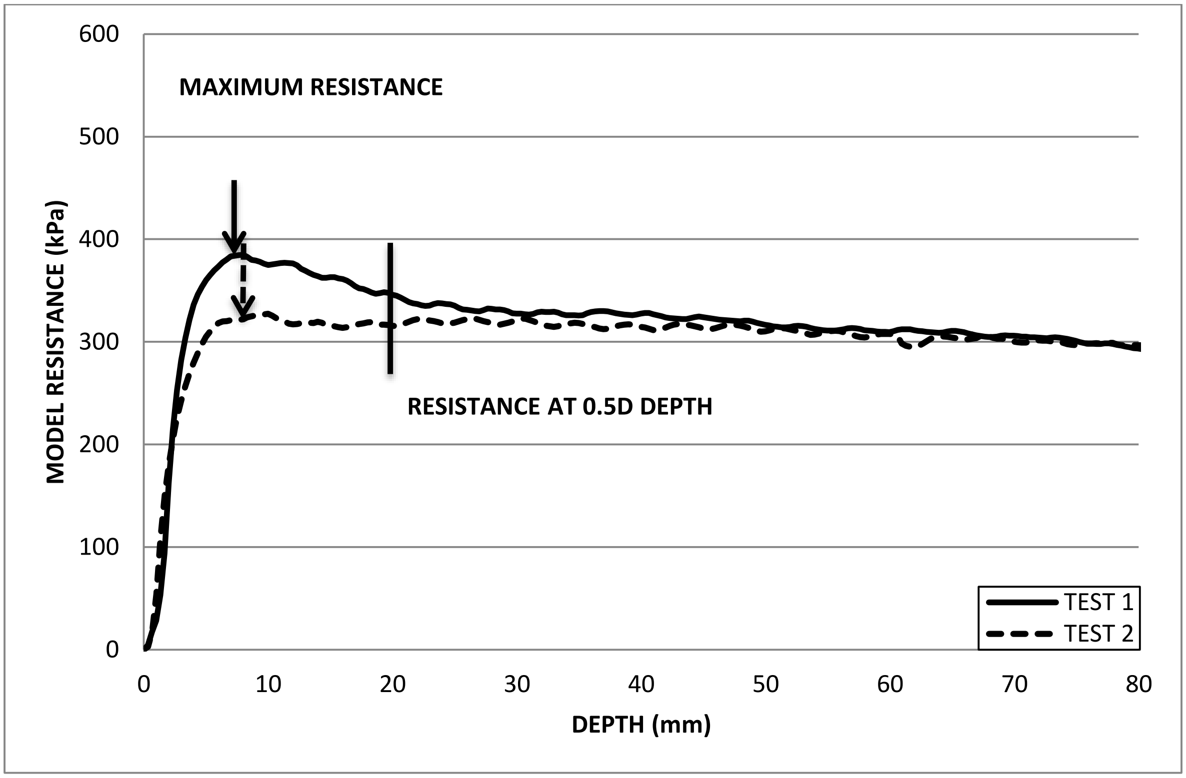

Figure G.22: Resistance profile for a 40 mm circular foundation tested on 3 % fibre over consolidated model.

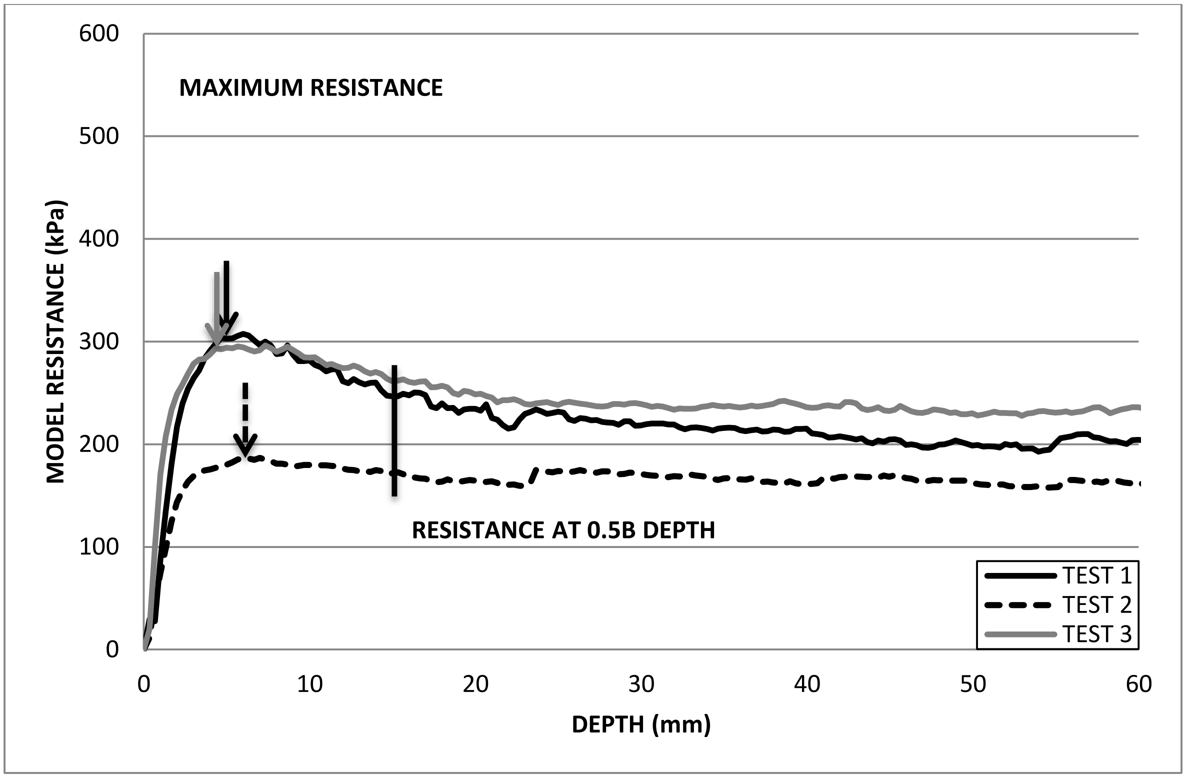

Figure G.23: Resistance profile for a 30 mm square foundation tested on 3 % fibre over consolidated model.

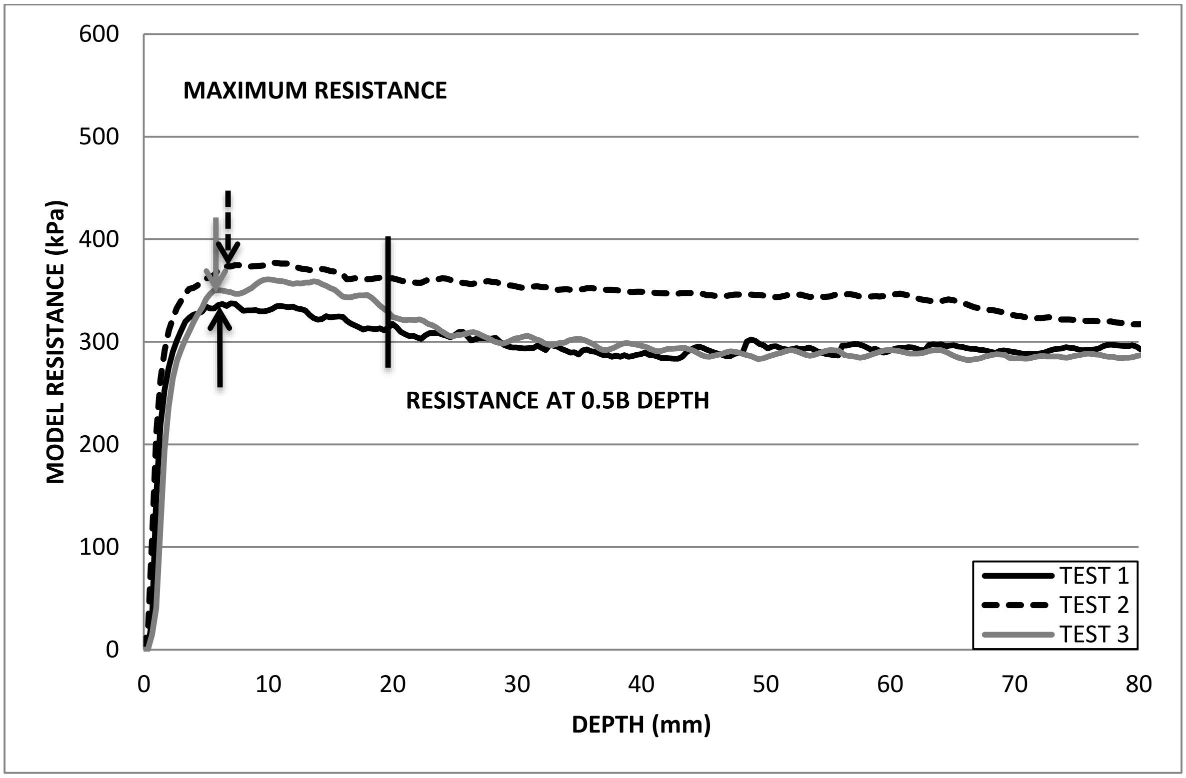

Figure G.24: Resistance profile for a 40 mm square foundation tested on 3 % fibre over consolidated model.

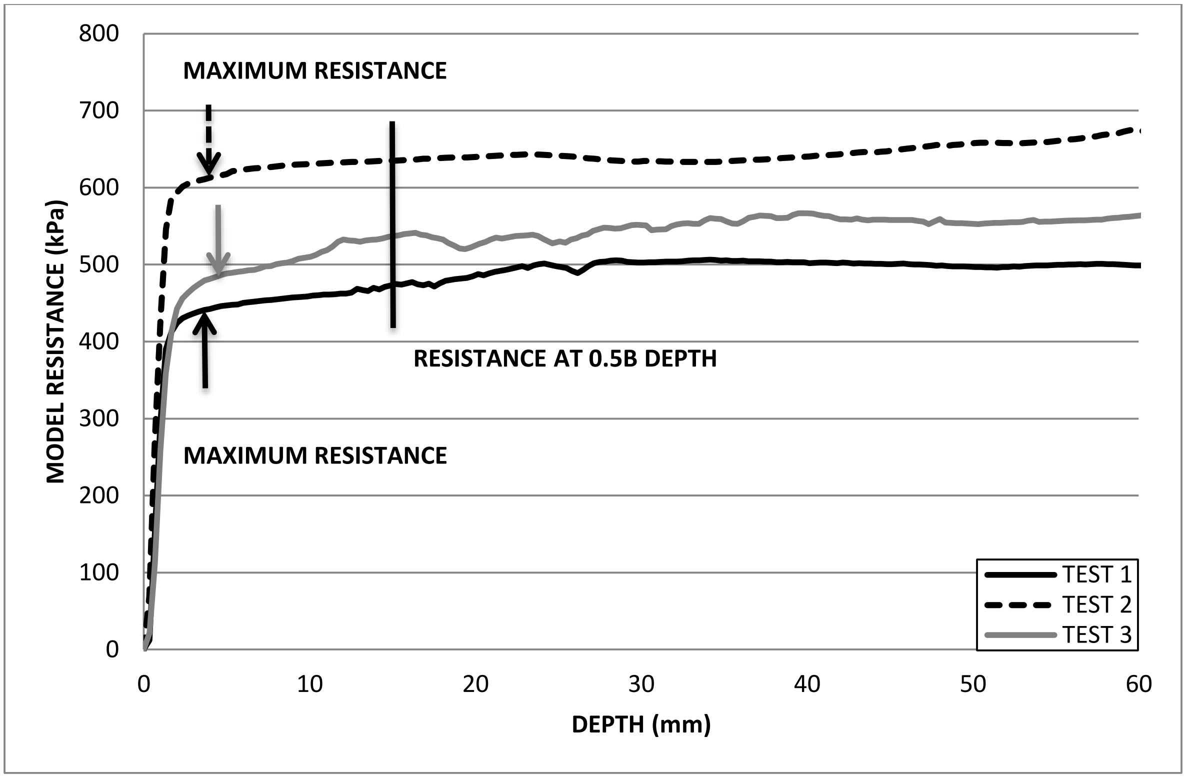

Figure G.25: Resistance profile for a 30 x 60 mm rectangular foundation tested on 4 % fibre over consolidated model.

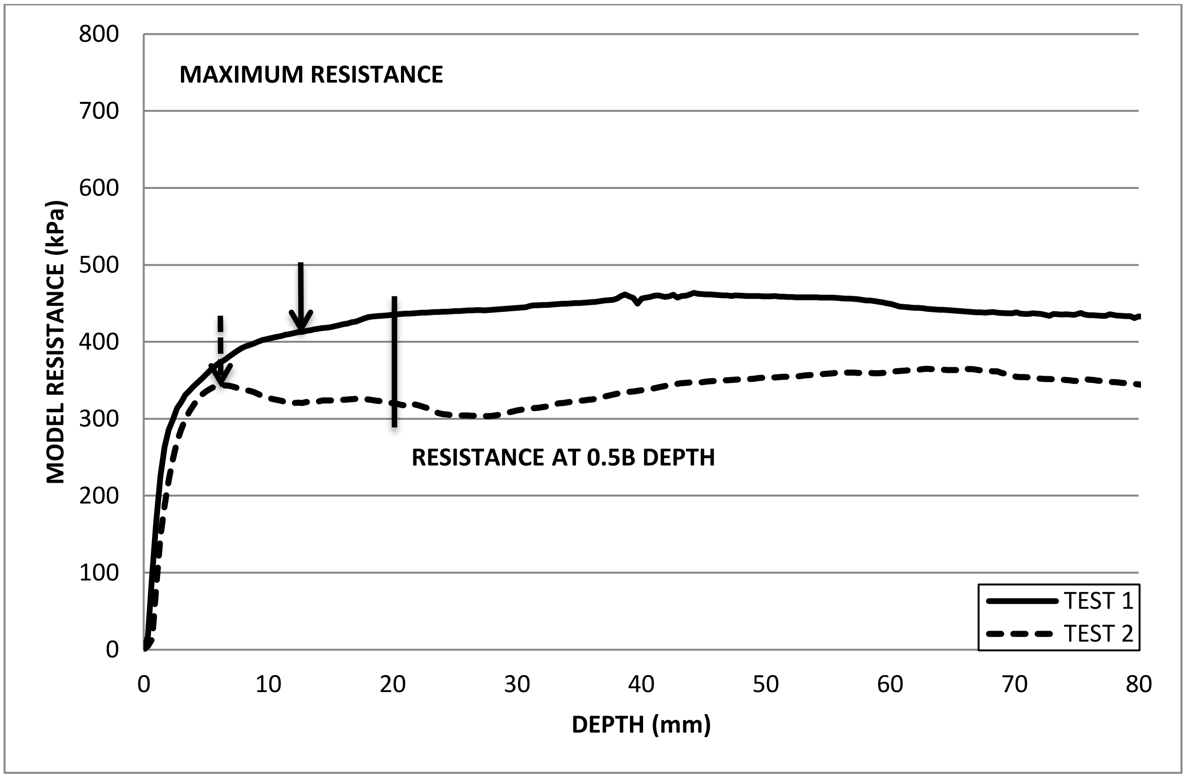

Figure G.26: Resistance profile for a 40 x 80 mm rectangular foundation tested on 4 % fibre over consolidated model.

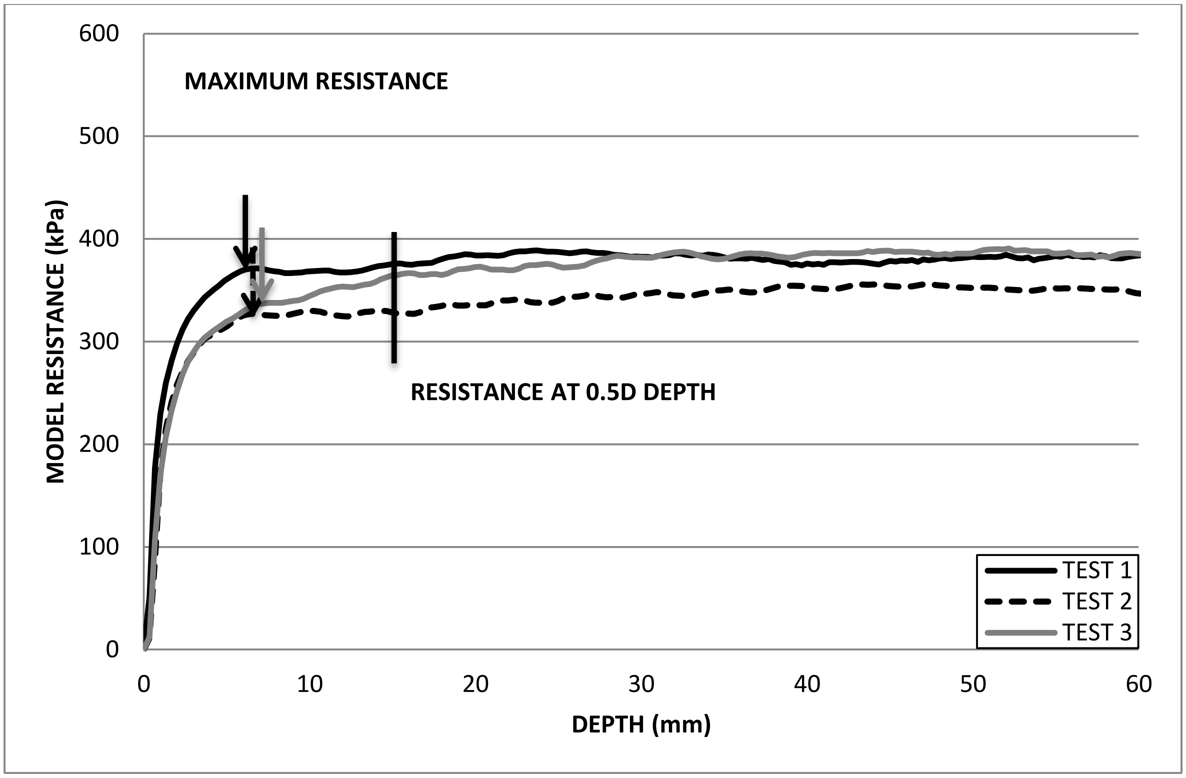

Figure G.27: Resistance profile for a 30 mm circular foundation tested on 4 % fibre over consolidated model.

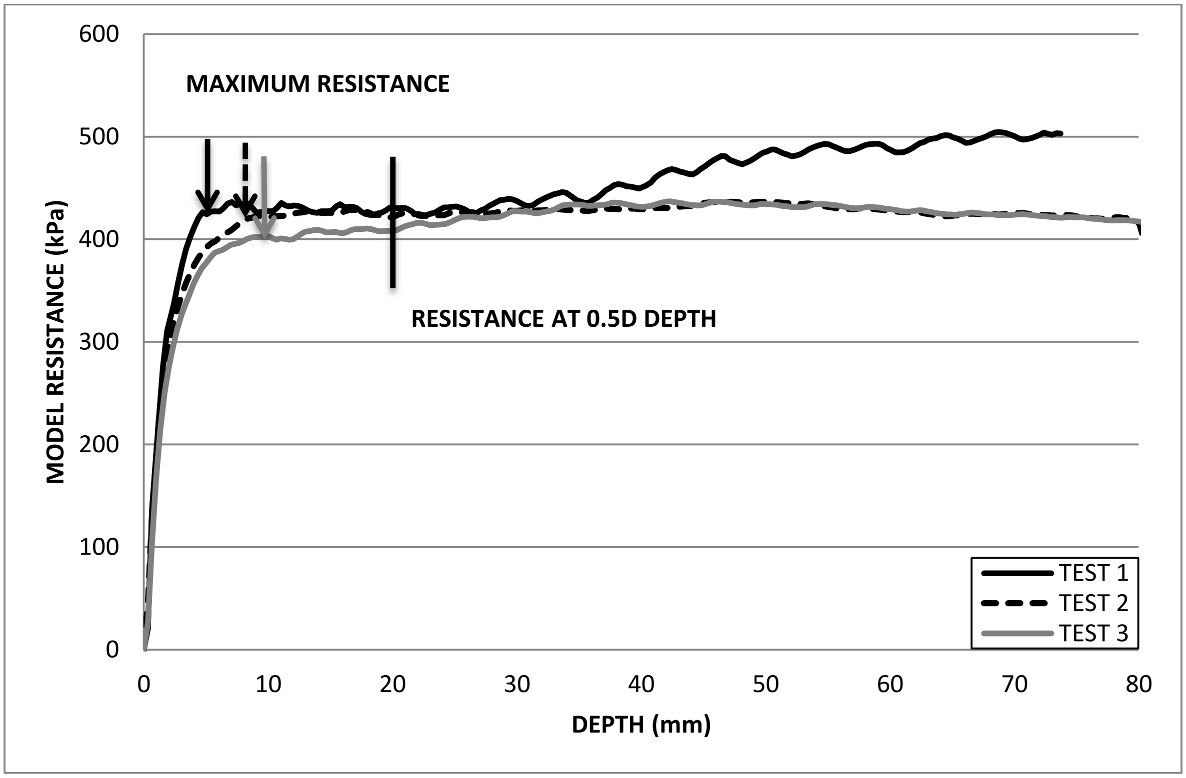

Figure G.28: Resistance profile for a 40 mm circular foundation tested on 4 % fibre over consolidated model.

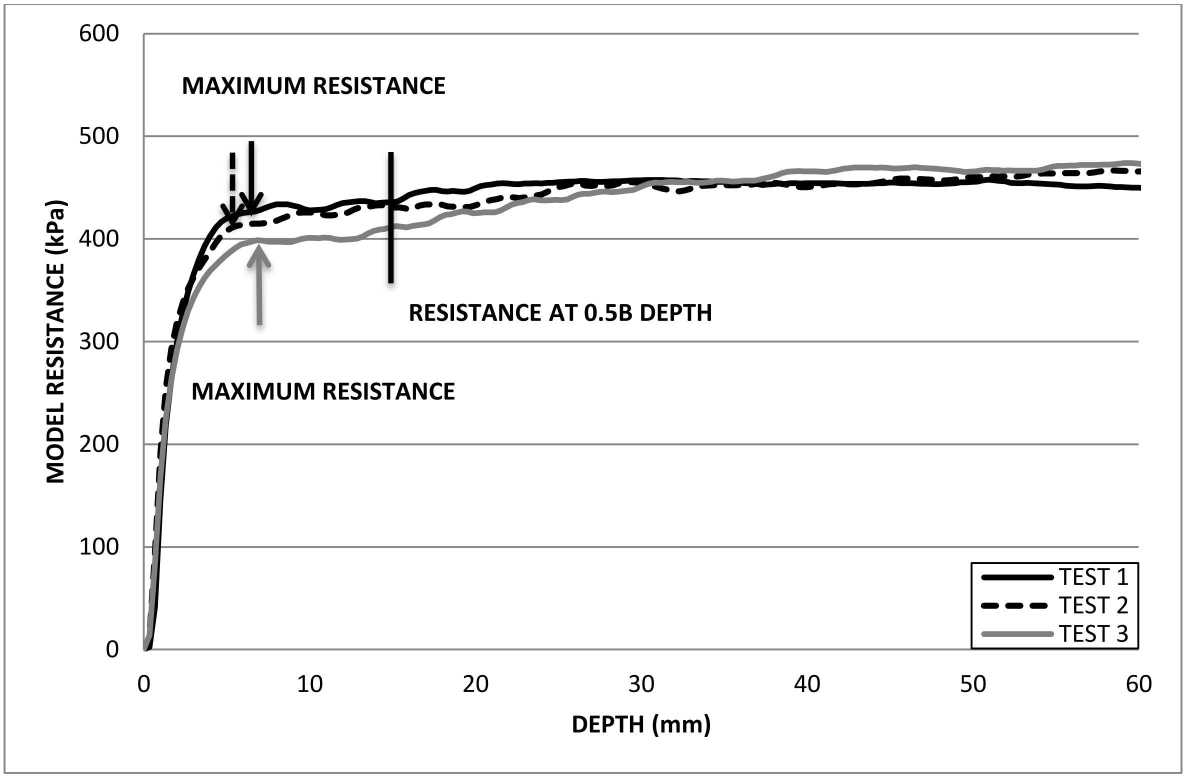

Figure G.29: Resistance profile for a 30 mm square foundation tested on 4 % fibre over consolidated model.

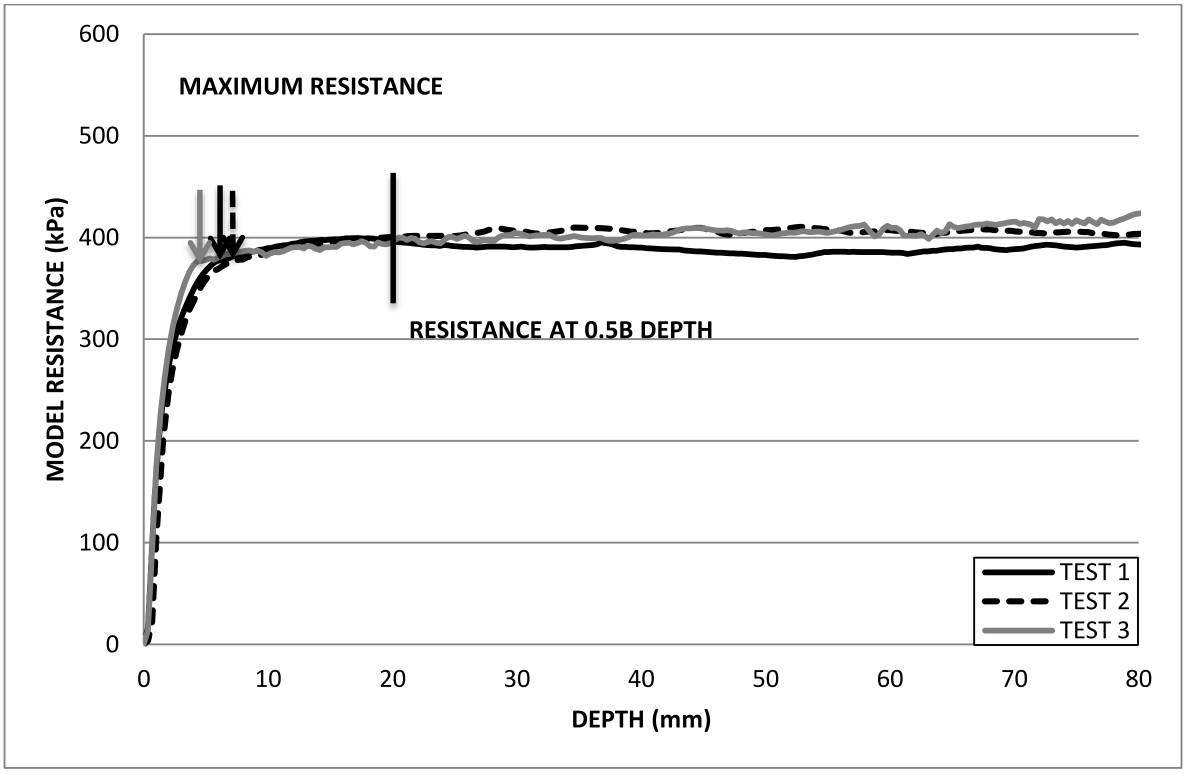

Figure G.30: Resistance profile for a 40 mm square foundation tested on 4 % fibre over consolidated model.

APPENDIX H:

CENTRIFUGE MODELLING RESULTS
COMPARATOR PROFILES
TEST SERIES 1 & 2

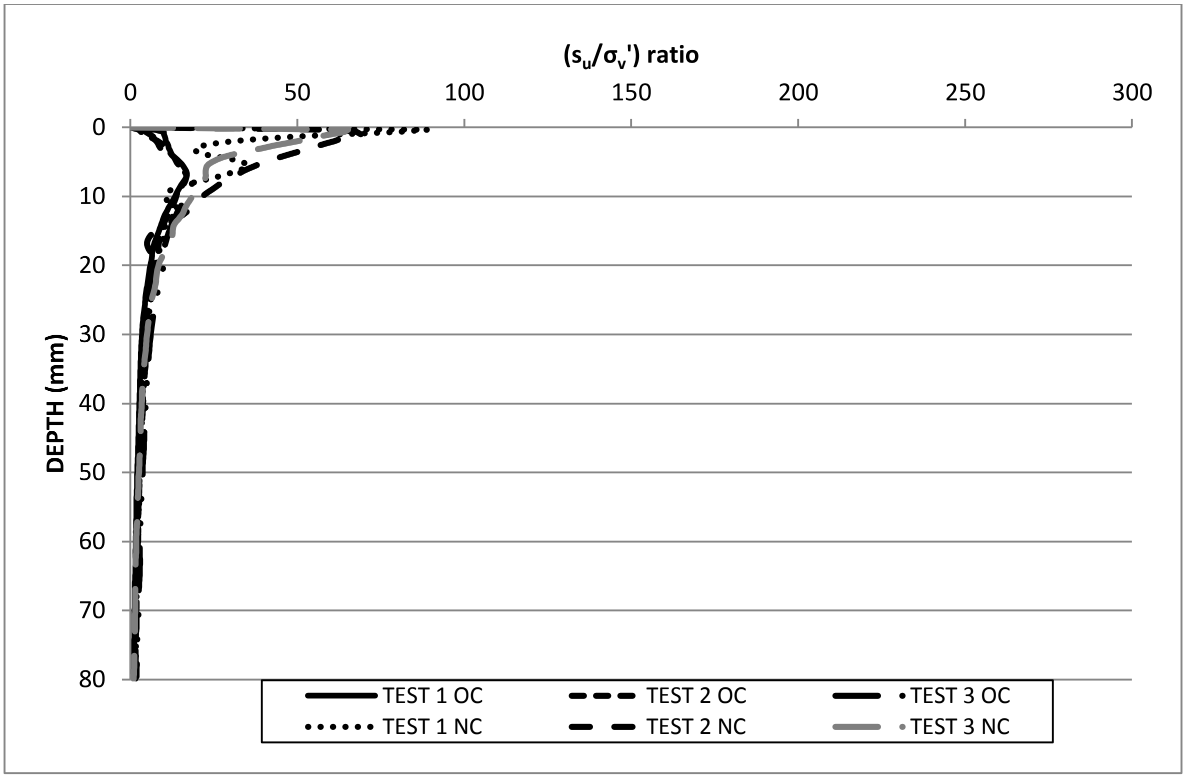

Figure H.1: $(s_u/\sigma_v')_{oc}$ and $OCR^{0.8}\,(s_u/\sigma_v')_{nc}$ comparator profiles for CPT tests completed on 0 % fibre normally and over consolidated models.

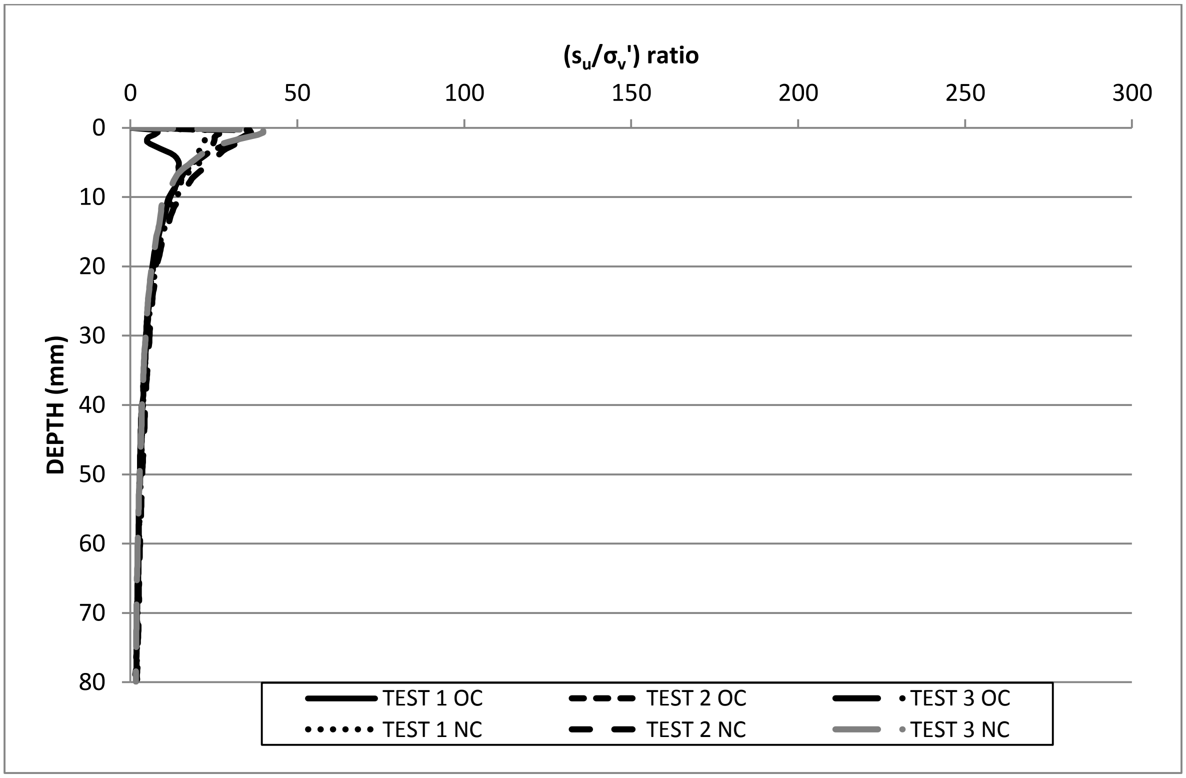

Figure H.2: $(s_u/\sigma_v')_{oc}$ and $OCR^{0.8}\,(s_u/\sigma_v')_{nc}$ comparator profiles for Piezoball tests completed on 0 % fibre normally and over consolidated models.

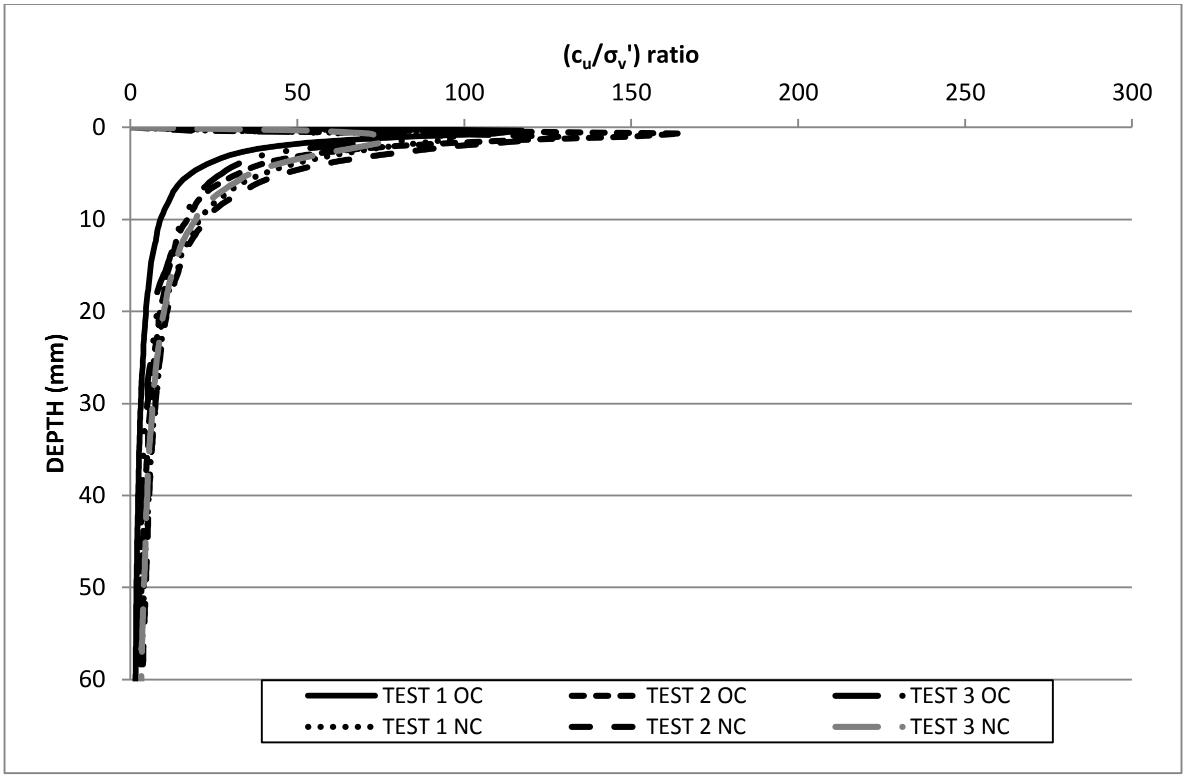

Figure H.3: $(c_u/\sigma_v')_{oc}$ and $OCR^{0.8}\,(c_u/\sigma_v')_{nc}$ comparator profiles for 30 x 60 mm rectangular foundation tests completed on 0 % fibre normally and over consolidated models.

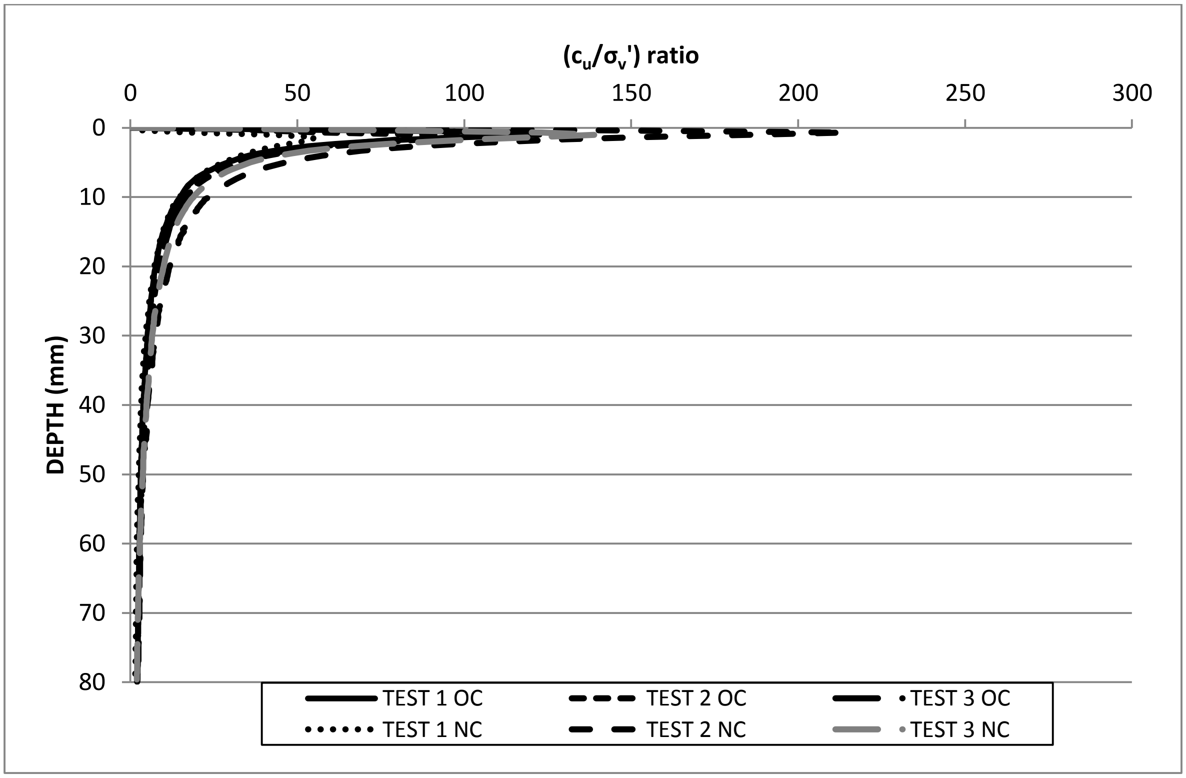

Figure H.4: $(c_u/\sigma_v')_{oc}$ and $OCR^{0.8}\,(c_u/\sigma_v')_{nc}$ comparator profiles for 40 x 80 mm rectangular foundation tests completed on 0 % fibre normally and over consolidated models.

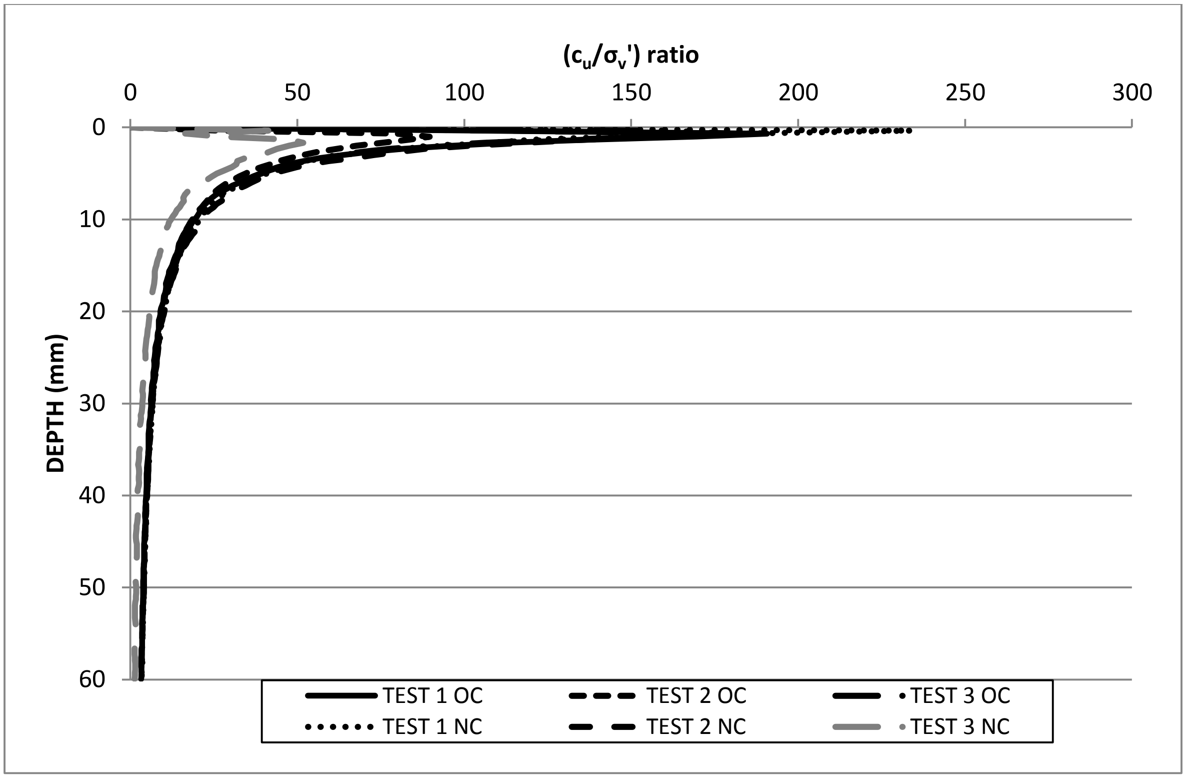

Figure H.5: $(c_u/\sigma_v')_{oc}$ and $OCR^{0.8}$ $(c_u/\sigma_v')_{nc}$ comparator profiles for 30 mm dia. circular foundation tests completed on 0 % fibre normally and over consolidated models.

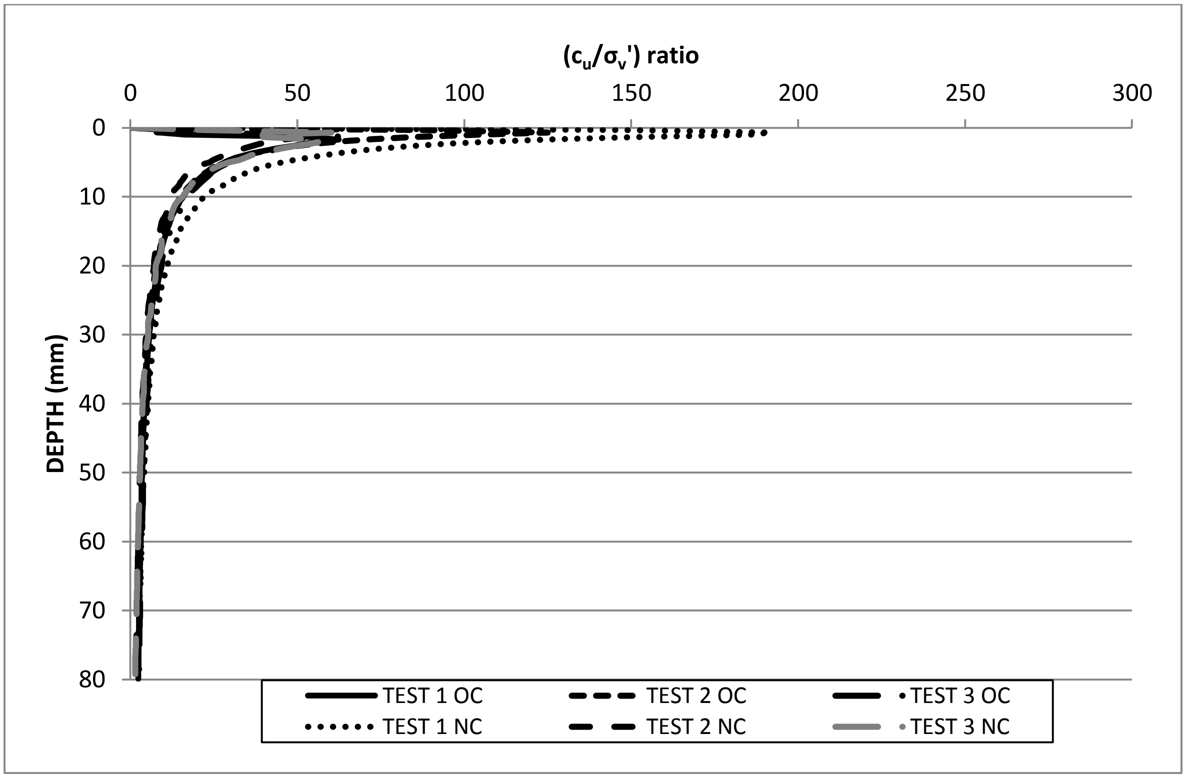

Figure H.6: $(c_u/\sigma_v')_{oc}$ and $OCR^{0.8}$ $(c_u/\sigma_v')_{nc}$ comparator profiles for 40 mm dia. circular foundation tests completed on 0 % fibre normally and over consolidated models.

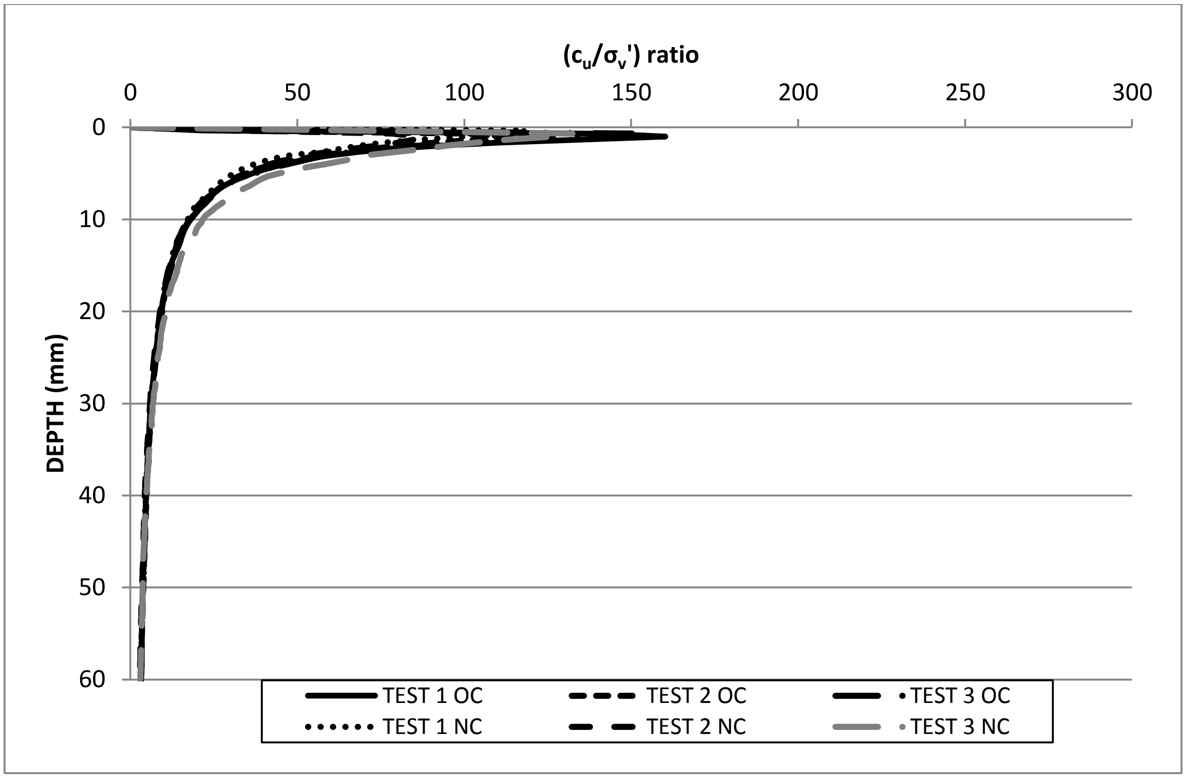

Figure H.7: $(c_u/\sigma_v')_{oc}$ and $OCR^{0.8}\,(c_u/\sigma_v')_{nc}$ comparator profiles for 30 mm square foundation tests completed on 0 % fibre normally and over consolidated models.

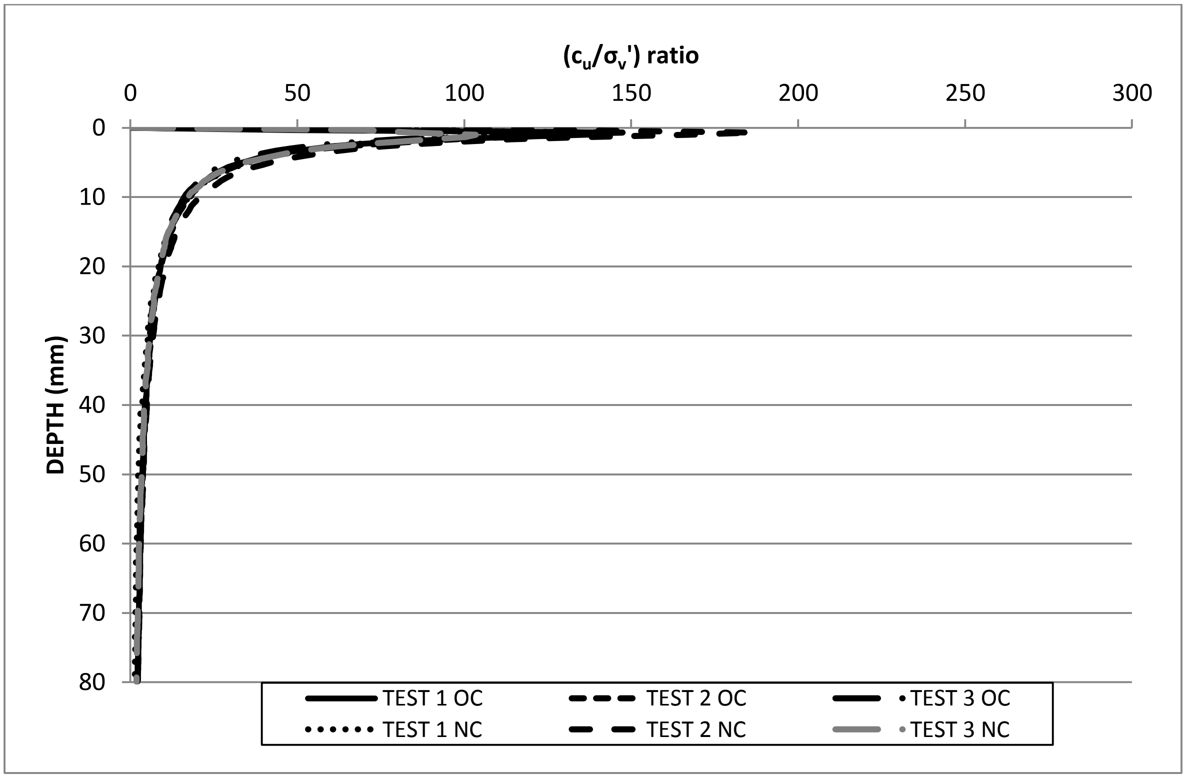

Figure H.8: $(c_u/\sigma_v')_{oc}$ and $OCR^{0.8}\,(c_u/\sigma_v')_{nc}$ comparator profiles for 40 mm square foundation tests completed on 0 % fibre normally and over consolidated models.

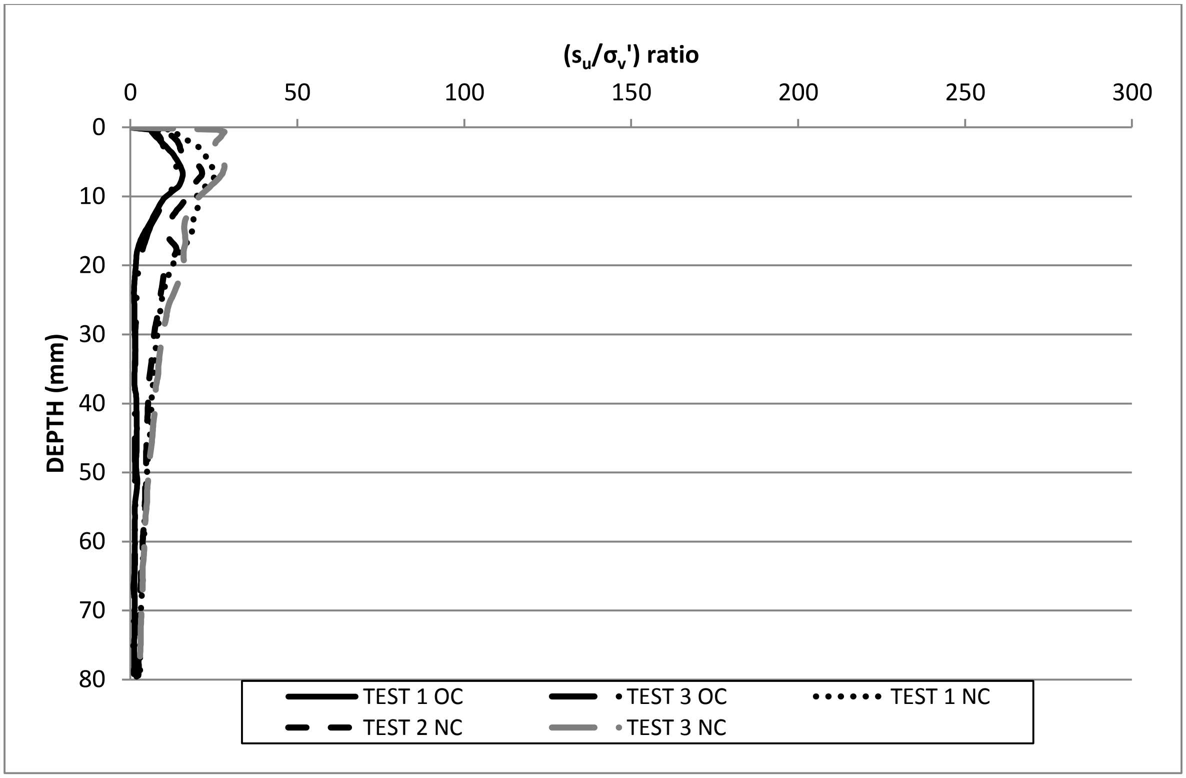

Figure H.9: $(s_u/\sigma_v')_{oc}$ and $OCR^{0.8}$ $(s_u/\sigma_v')_{nc}$ comparator profiles for CPT tests completed on 1 % fibre normally and over consolidated models.

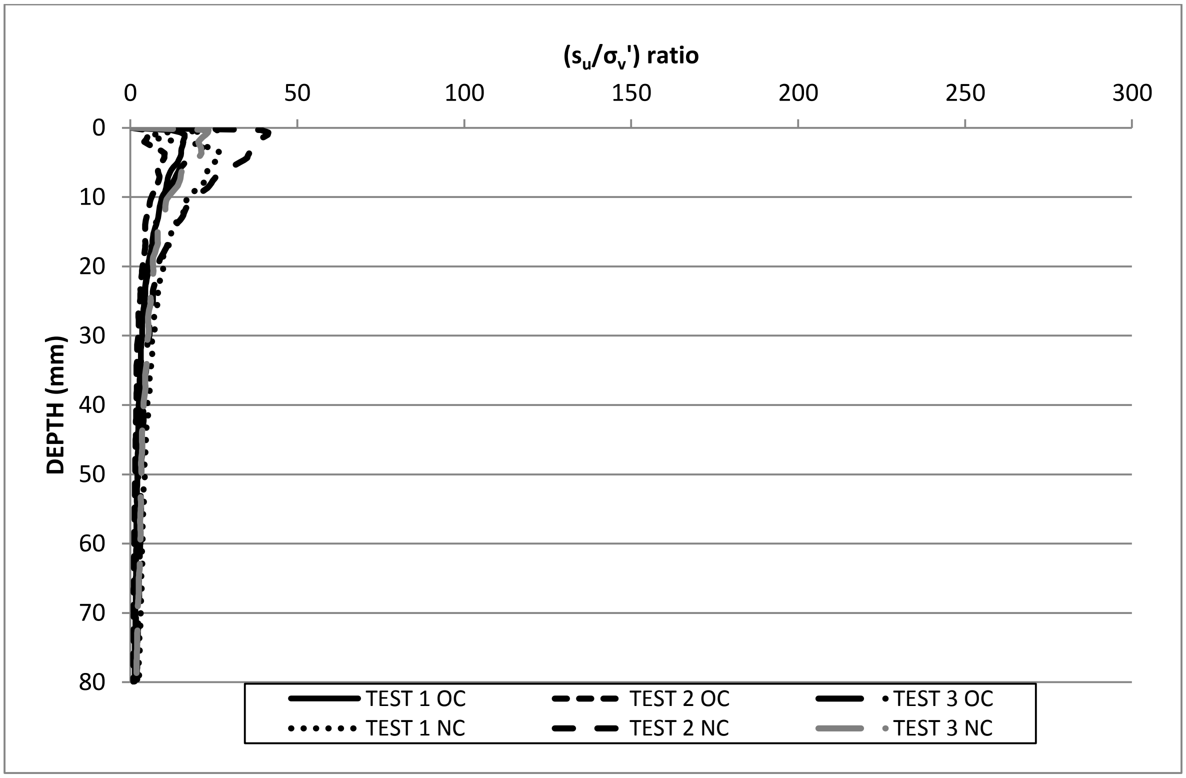

Figure H.10: $(s_u/\sigma_v')_{oc}$ and $OCR^{0.8}$ $(s_u/\sigma_v')_{nc}$ comparator profiles for Piezoball tests completed on 1 % fibre normally and over consolidated models.

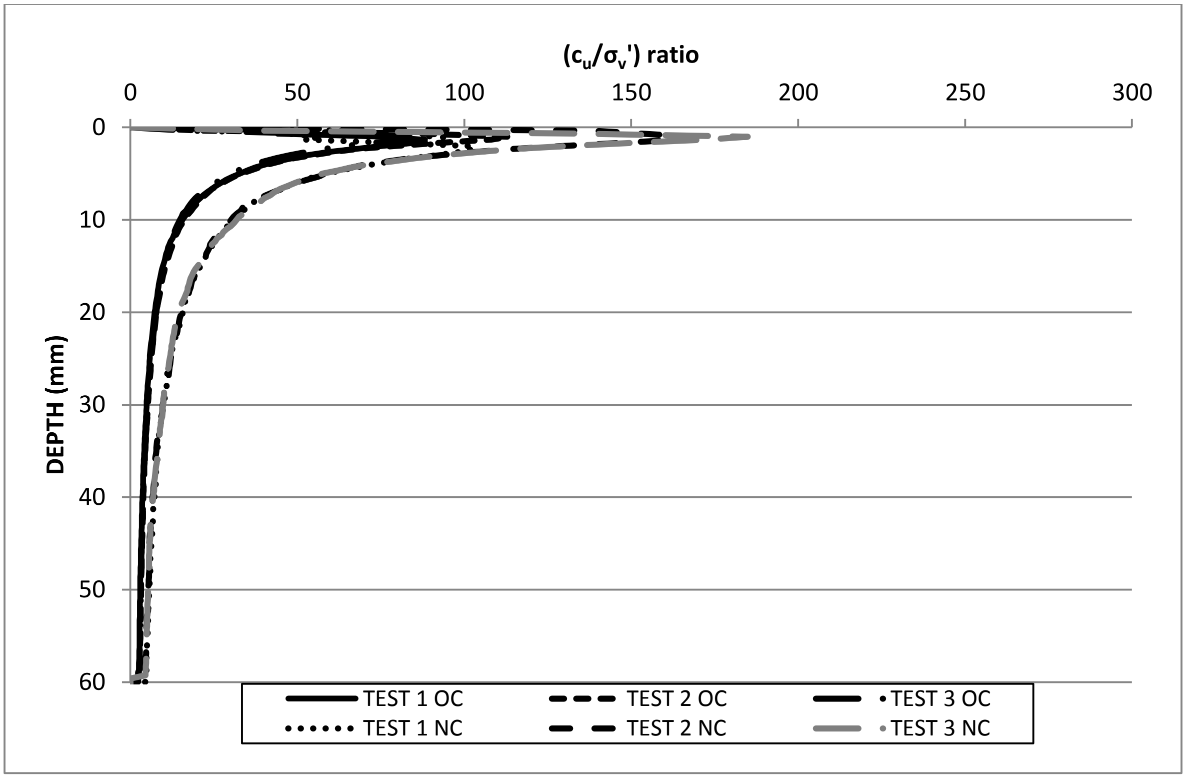

Figure H.11: $(c_u/\sigma_v')_{oc}$ and $OCR^{0.8}$ $(c_u/\sigma_v')_{nc}$ comparator profiles for 30 x 60 mm rectangular foundation tests completed on 1 % fibre normally and over consolidated models.

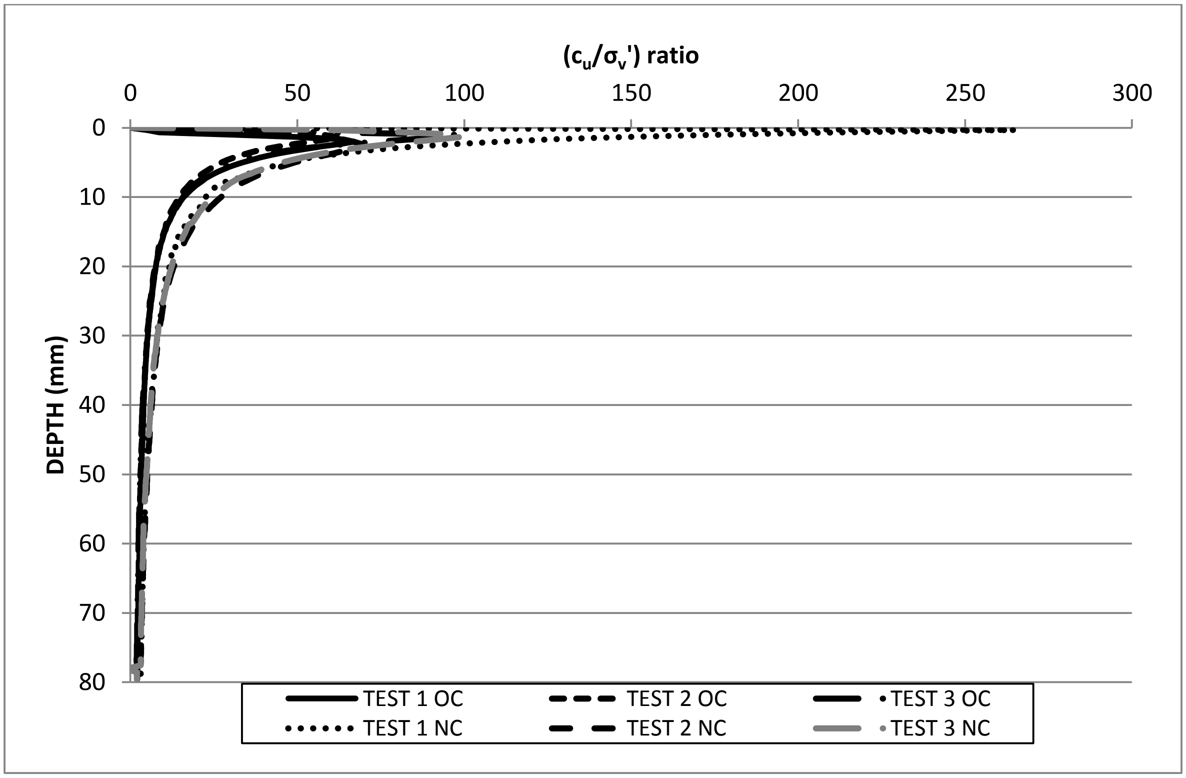

Figure H.12: $(c_u/\sigma_v')_{oc}$ and $OCR^{0.8}$ $(c_u/\sigma_v')_{nc}$ comparator profiles for 40 x 80 mm rectangular foundation tests completed on 1 % fibre normally and over consolidated models.

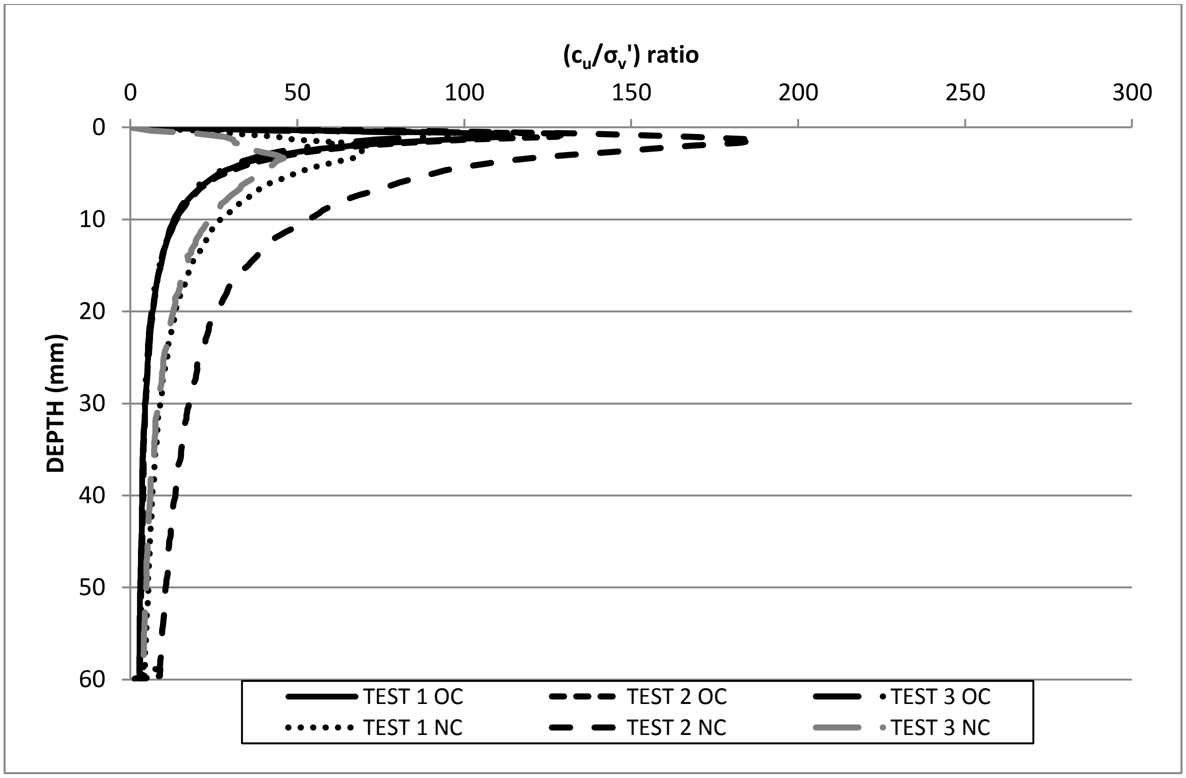

Figure H.13: $(c_u/\sigma_v')_{oc}$ and $OCR^{0.8}\,(c_u/\sigma_v')_{nc}$ comparator profiles for 30 mm dia. circular foundation tests completed on 1 % fibre normally and over consolidated models.

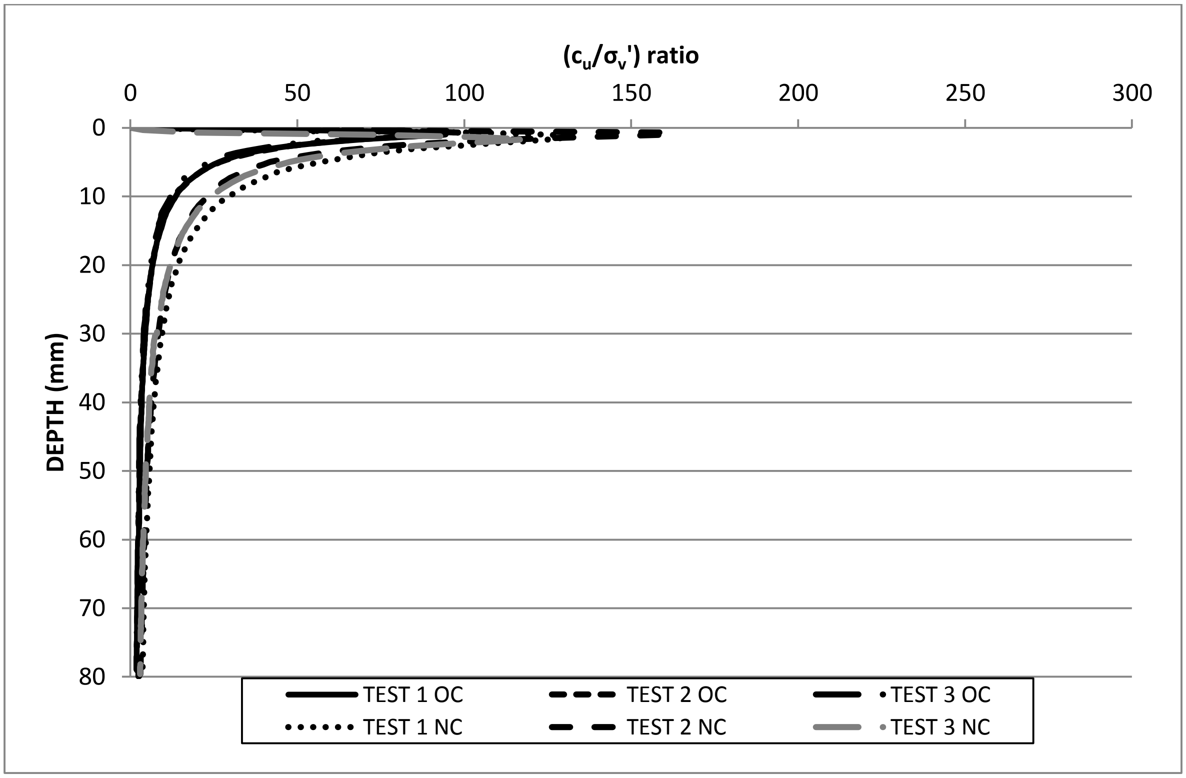

Figure H.14: $(c_u/\sigma_v')_{oc}$ and $OCR^{0.8}\,(c_u/\sigma_v')_{nc}$ comparator profiles for 40 mm dia. circular foundation tests completed on 1 % fibre normally and over consolidated models.

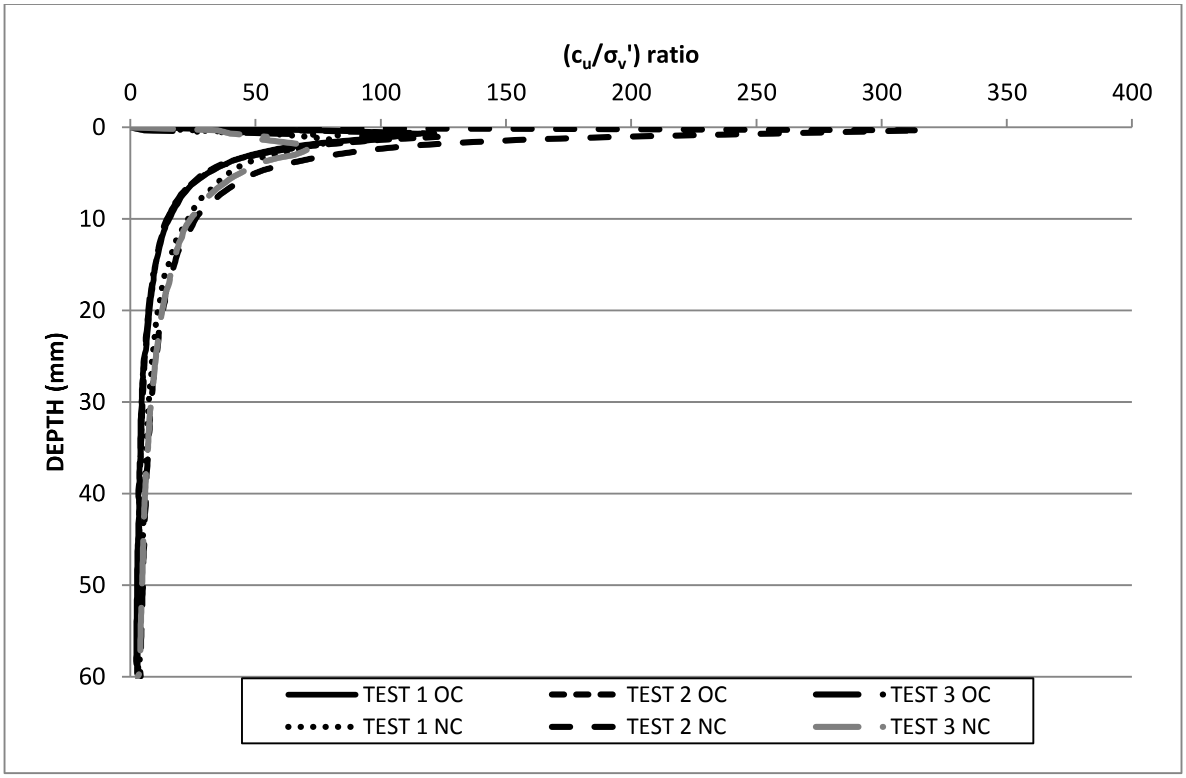

Figure H.15: $(c_u/\sigma_v')_{oc}$ and $OCR^{0.8}\,(c_u/\sigma_v')_{nc}$ comparator profiles for 30 mm square foundation tests completed on 1 % fibre normally and over consolidated models.

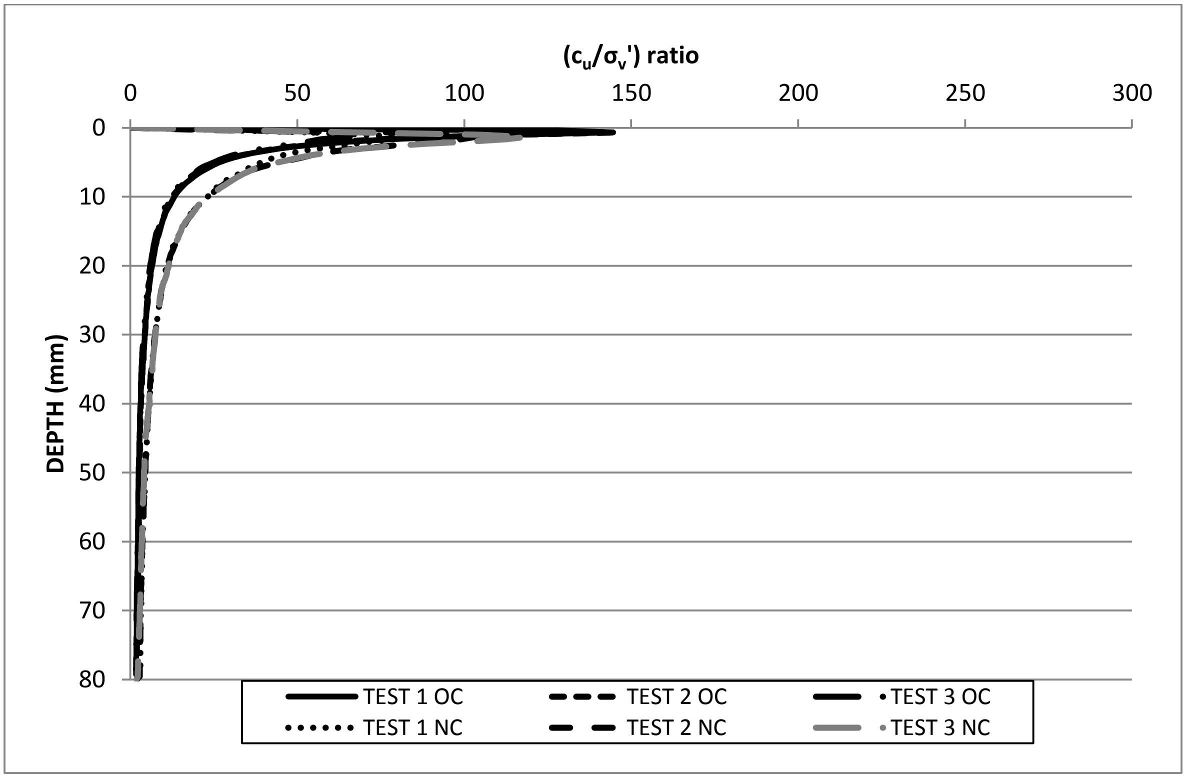

Figure H.16: $(c_u/\sigma_v')_{oc}$ and $OCR^{0.8}\,(c_u/\sigma_v')_{nc}$ comparator profiles for 40 mm square foundation tests completed on 1 % fibre normally and over consolidated models.

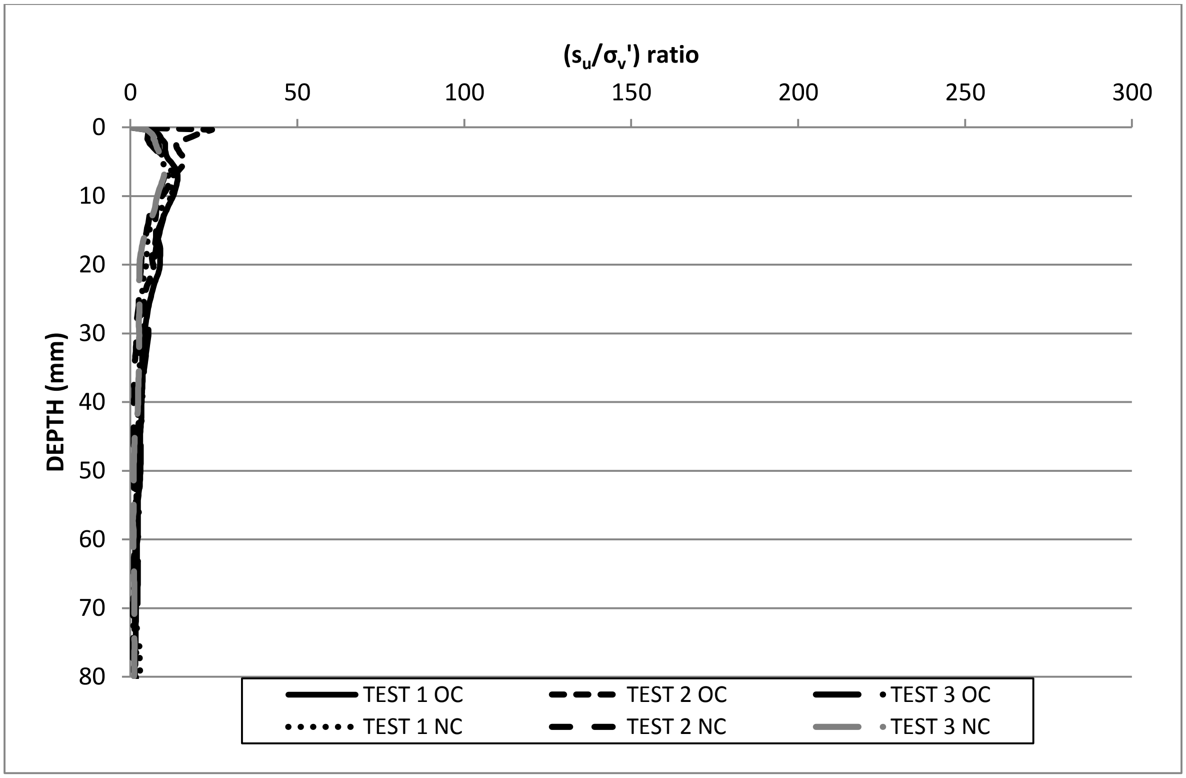

Figure H.17: $(s_u/\sigma_v')_{oc}$ and $OCR^{0.8}$ $(s_u/\sigma_v')_{nc}$ comparator profiles for CPT tests completed on 2 % fibre normally and over consolidated models.

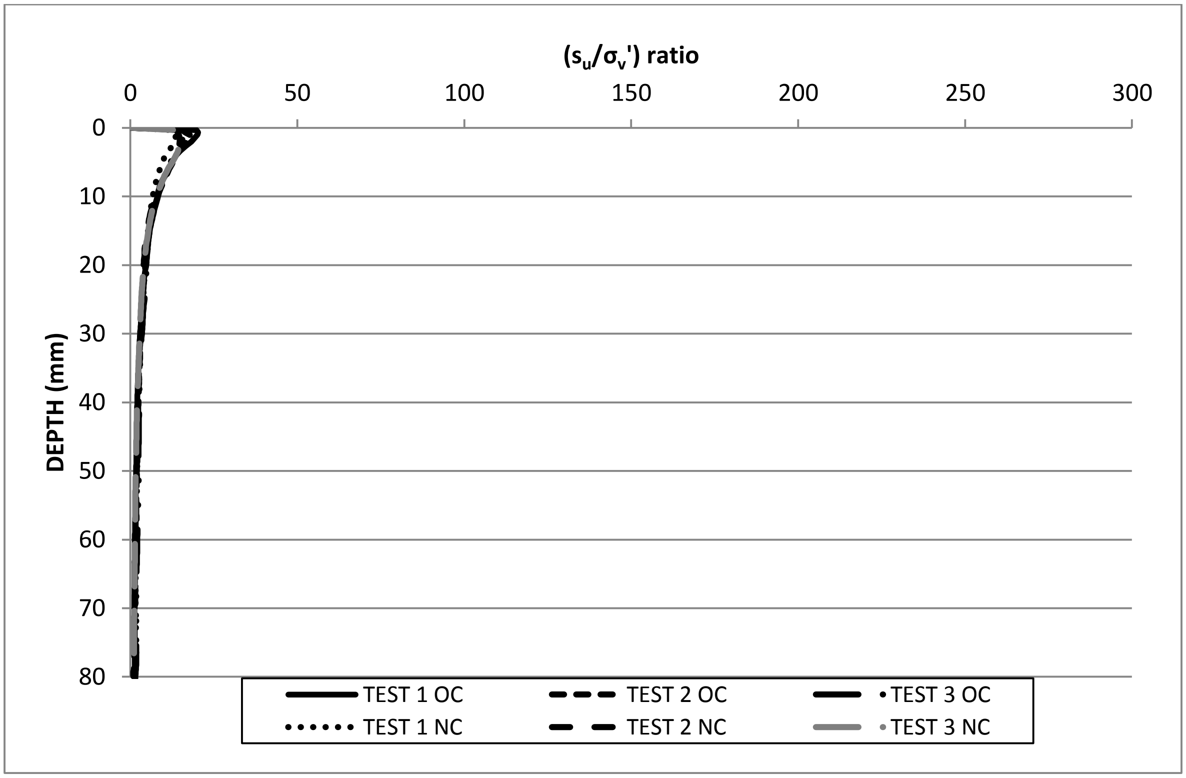

Figure H.18: $(s_u/\sigma_v')_{oc}$ and $OCR^{0.8}$ $(s_u/\sigma_v')_{nc}$ comparator profiles for Piezoball tests completed on 2 % fibre normally and over consolidated models.

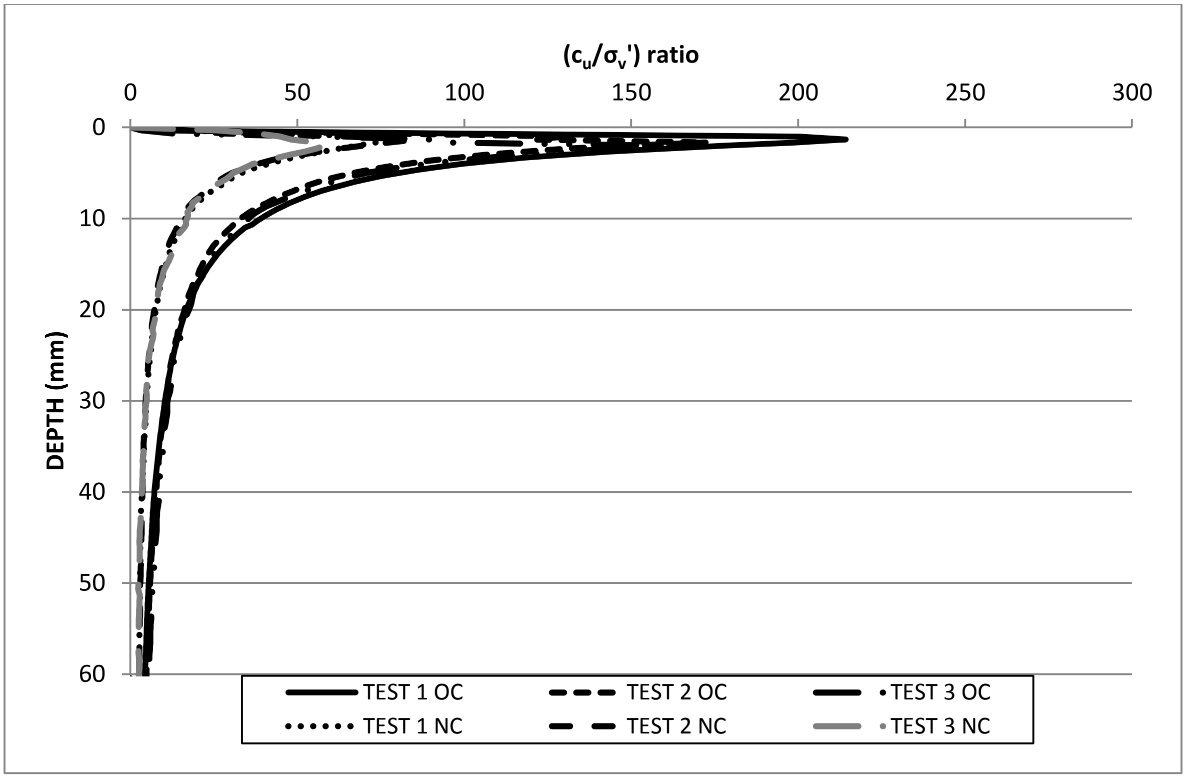

Figure H.19: $(c_u/\sigma_v')_{oc}$ and $OCR^{0.8}(c_u/\sigma_v')_{nc}$ comparator profiles for 30 x 60 mm rectangular foundation tests completed on 2 % fibre normally and over consolidated models.

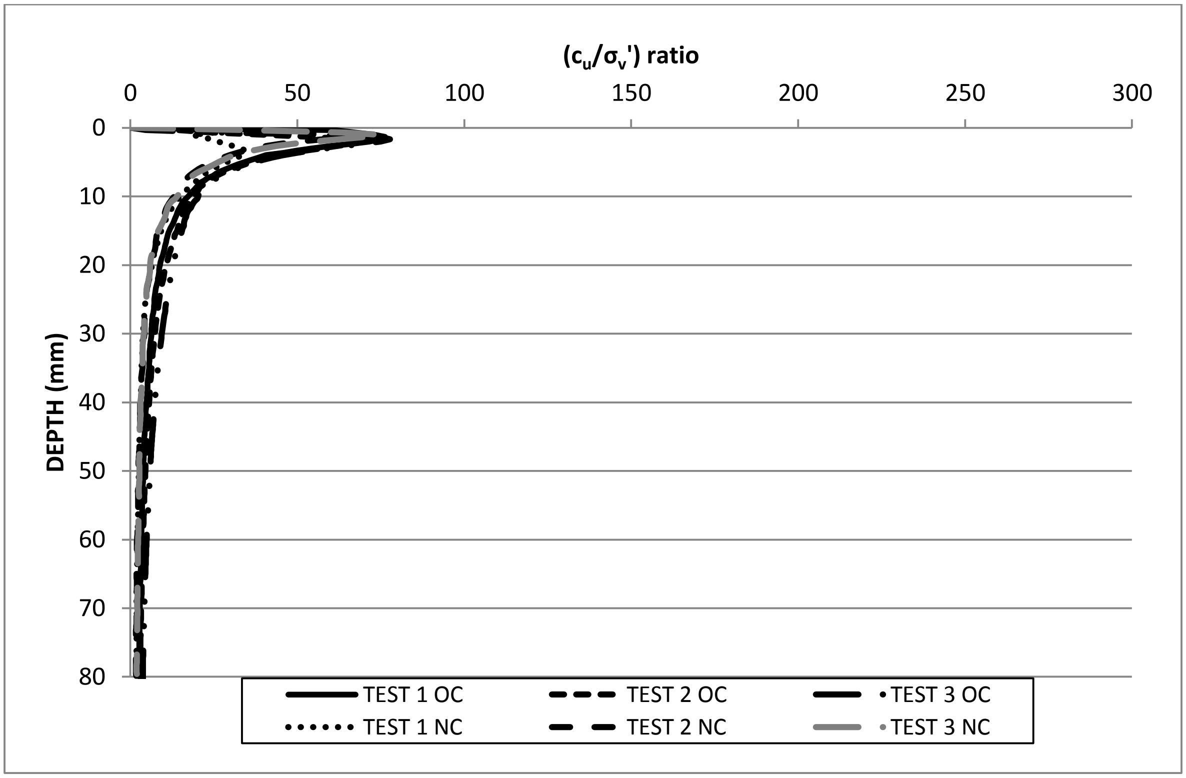

Figure H.20: $(c_u/\sigma_v')_{oc}$ and $OCR^{0.8}(c_u/\sigma_v')_{nc}$ comparator profiles for 40 x 80 mm rectangular foundation tests completed on 2 % fibre normally and over consolidated models.

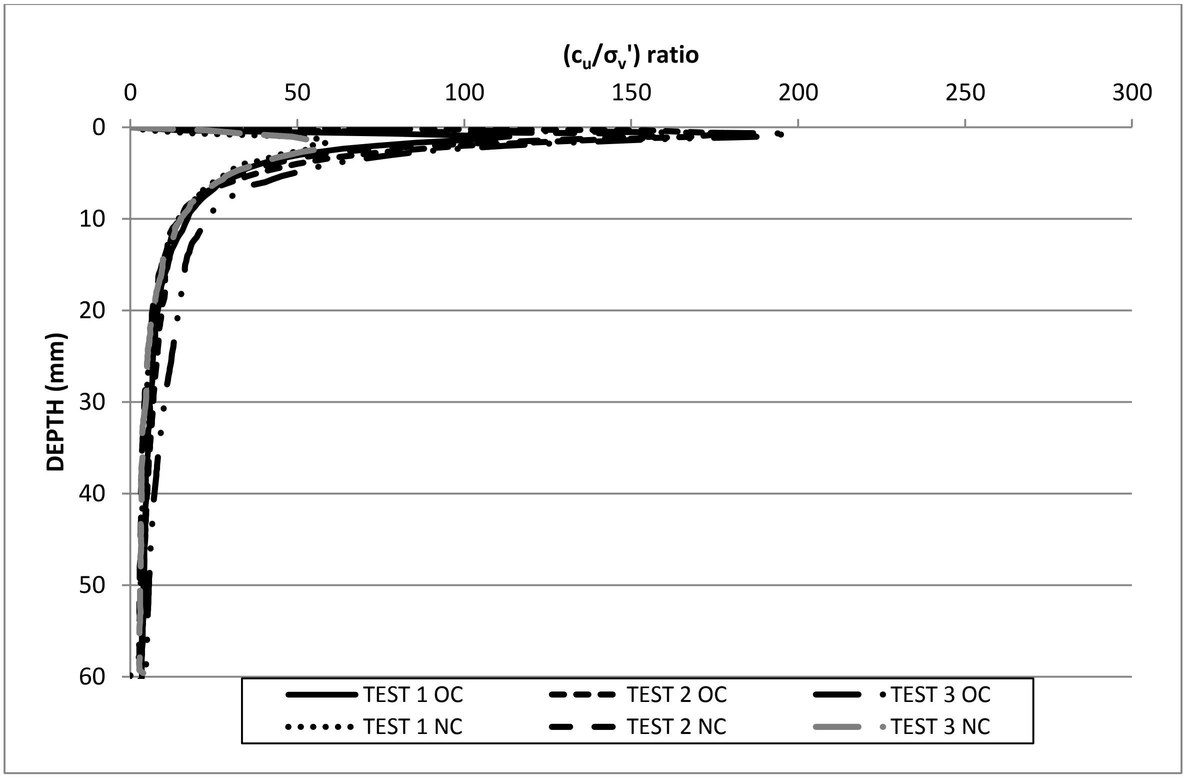

Figure H.21: $(c_u/\sigma_v')_{oc}$ and $OCR^{0.8}$ $(c_u/\sigma_v')_{nc}$ comparator profiles for 30 mm dia. circular foundation tests completed on 2 % fibre normally and over consolidated models.

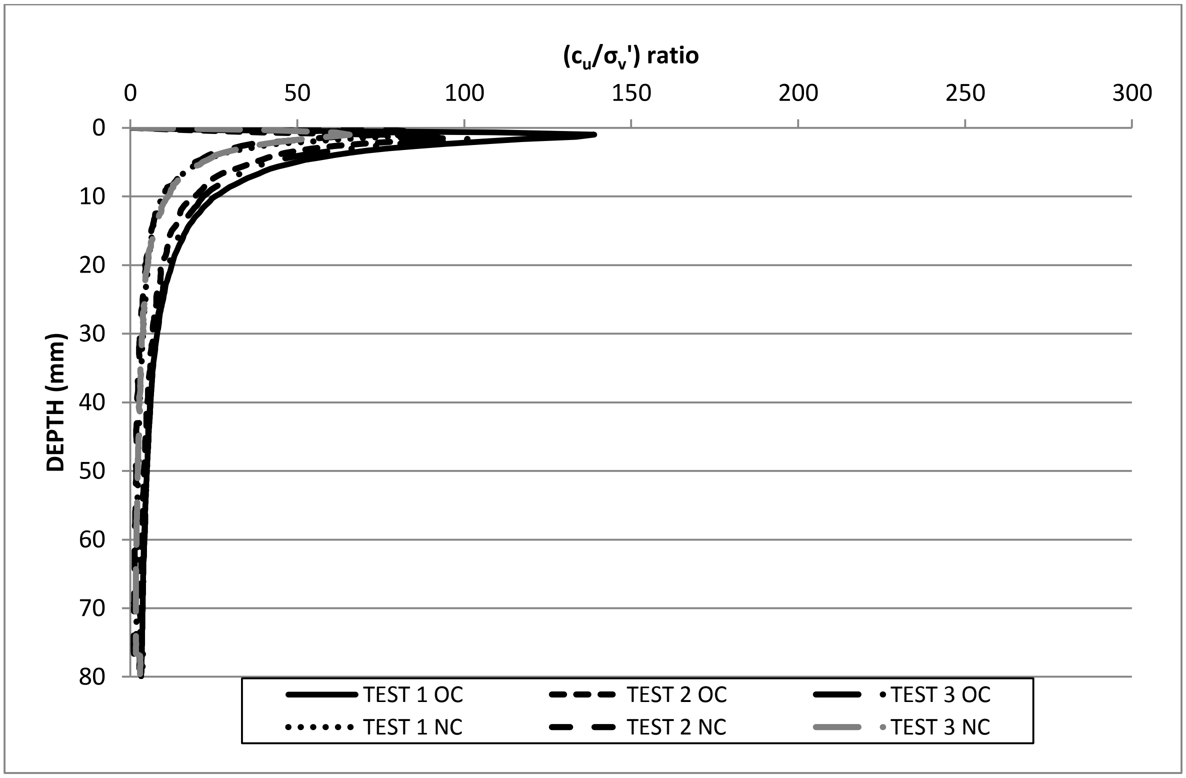

Figure H.22: $(c_u/\sigma_v')_{oc}$ and $OCR^{0.8}$ $(c_u/\sigma_v')_{nc}$ comparator profiles for 40 mm dia. circular foundation tests completed on 2 % fibre normally and over consolidated models.

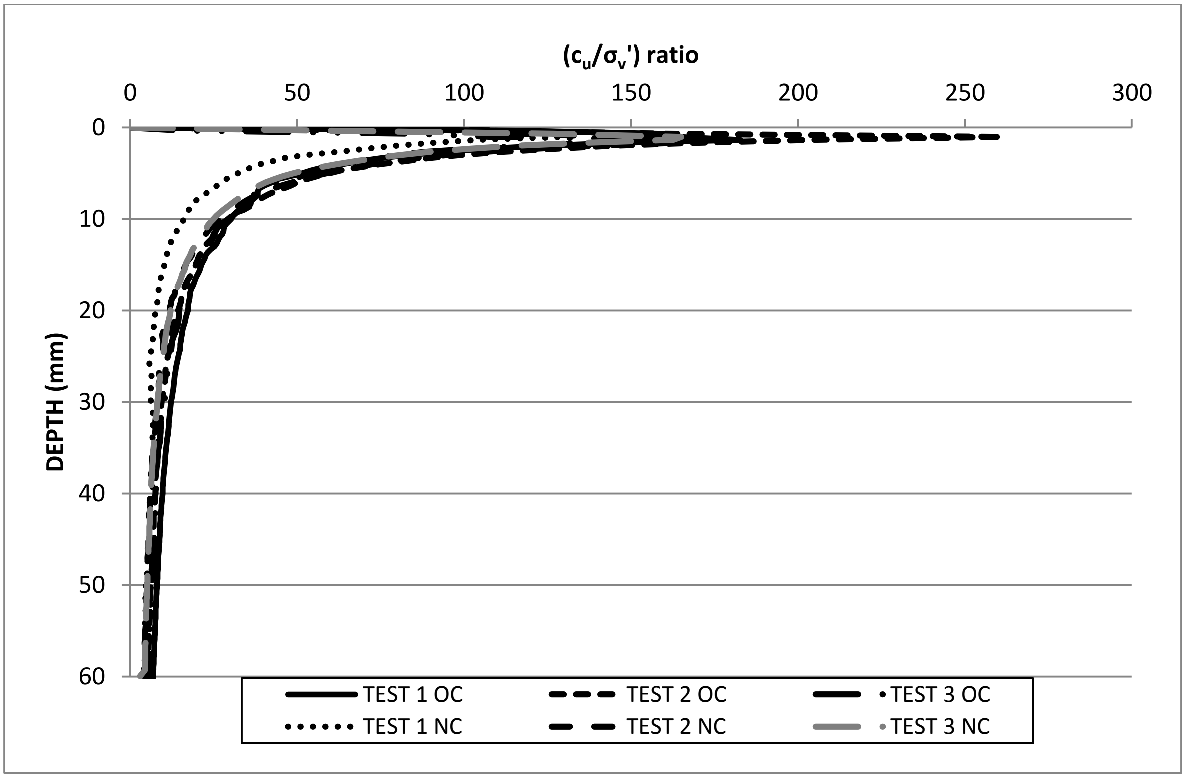

Figure H.23: $(c_u/\sigma_v')_{oc}$ and $OCR^{0.8}\,(c_u/\sigma_v')_{nc}$ comparator profiles for 30 mm square foundation tests completed on 2 % fibre normally and over consolidated models.

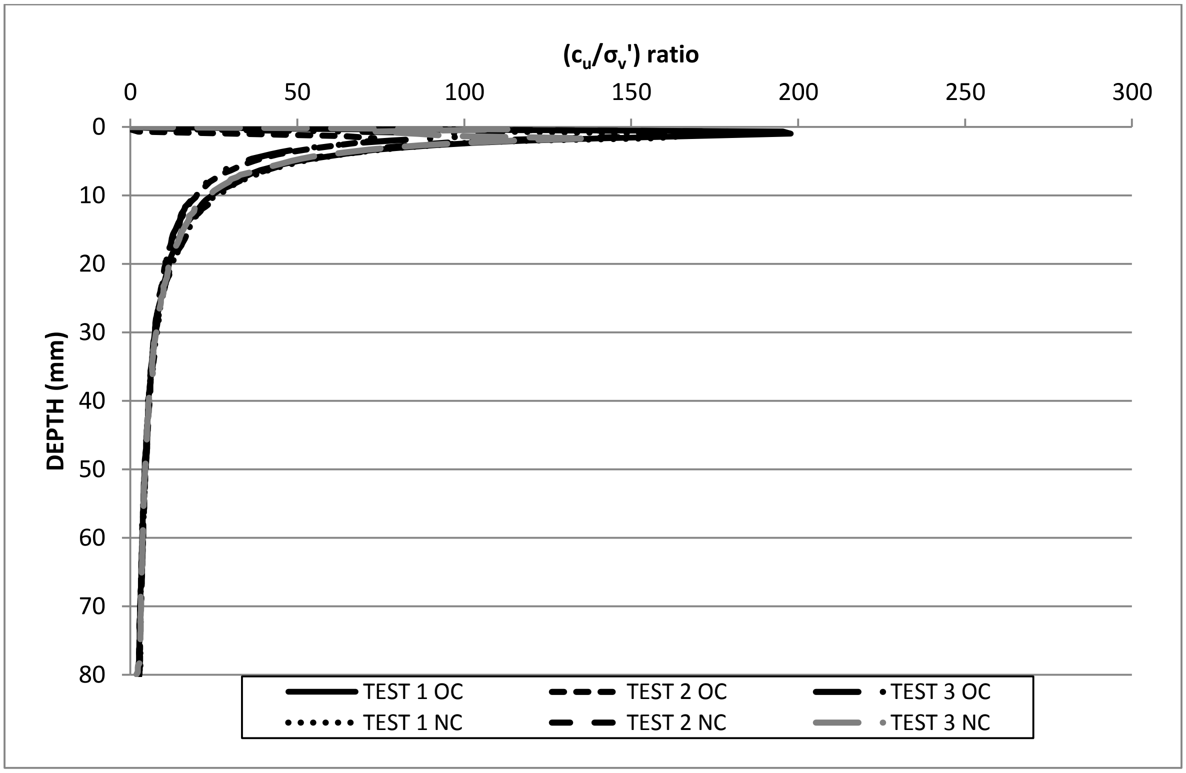

Figure H.24: $(c_u/\sigma_v')_{oc}$ and $OCR^{0.8}\,(c_u/\sigma_v')_{nc}$ comparator profiles for 40 mm square foundation tests completed on 2 % fibre normally and over consolidated models.

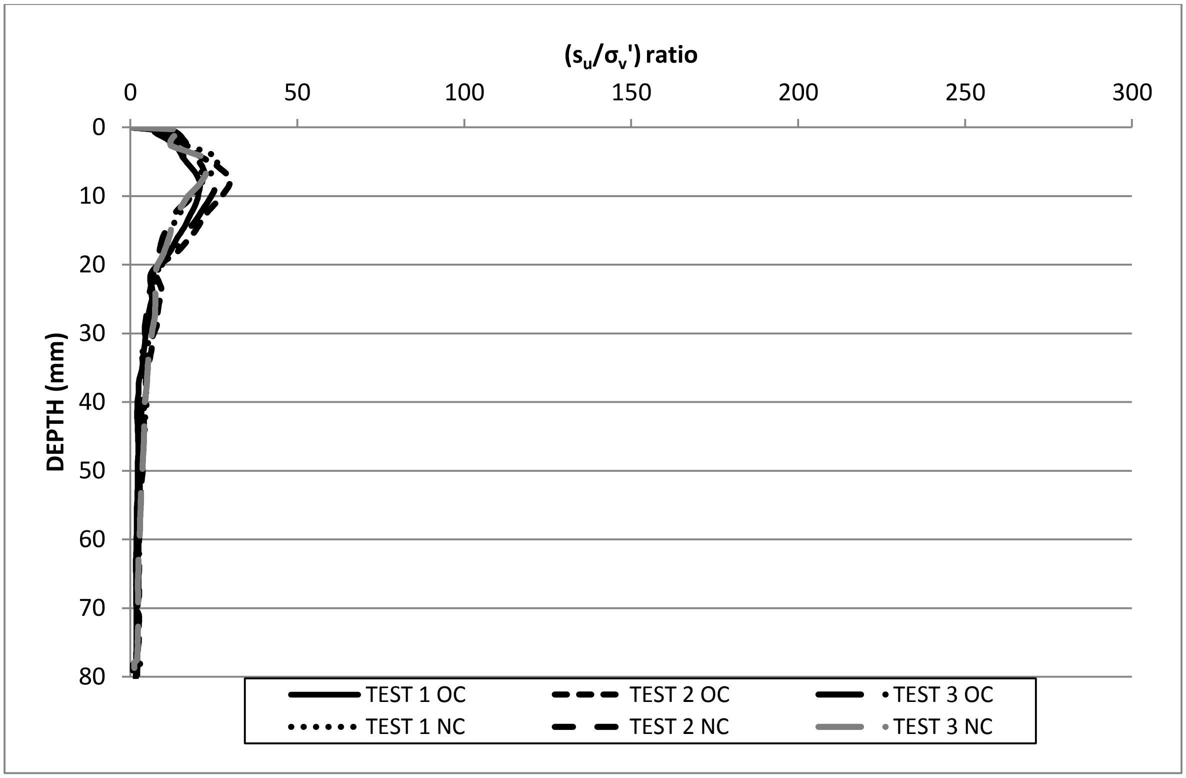

Figure H.25: $(s_u/\sigma_v')_{oc}$ and $OCR^{0.8}$ $(s_u/\sigma_v')_{nc}$ comparator profiles for CPT tests completed on 3 % fibre normally and over consolidated models.

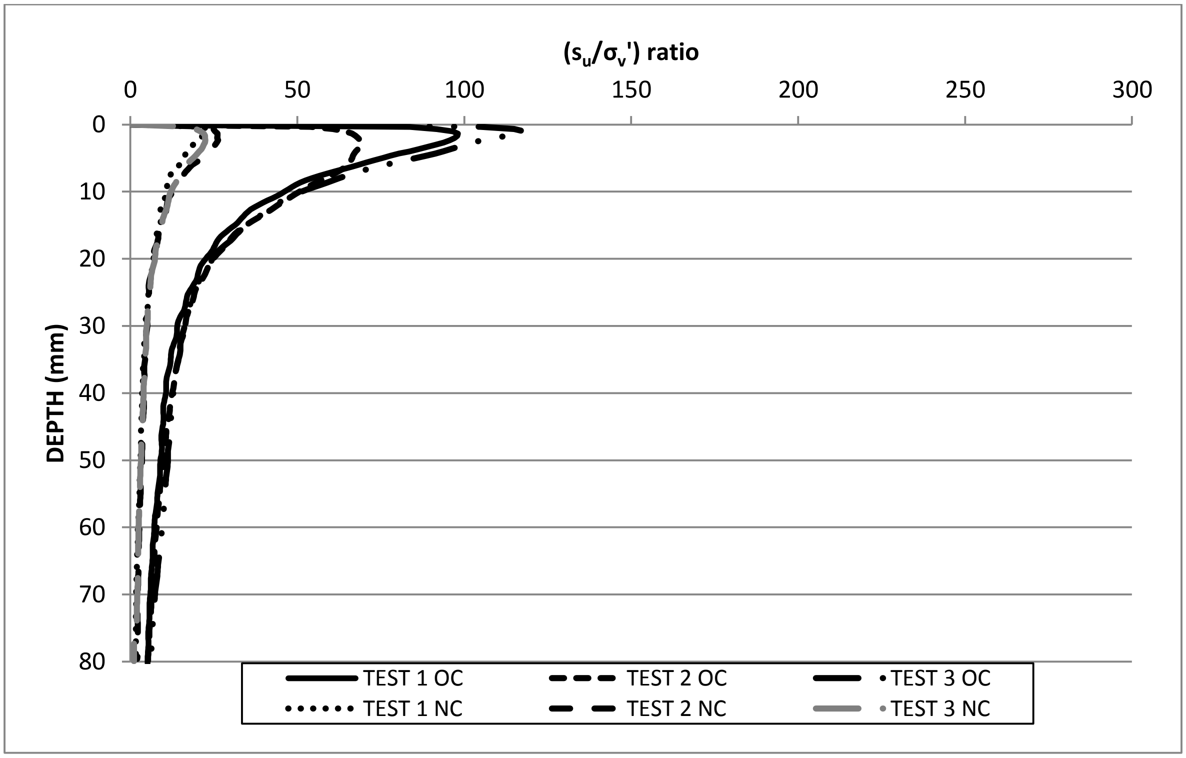

Figure H.26: $(s_u/\sigma_v')_{oc}$ and $OCR^{0.8}$ $(s_u/\sigma_v')_{nc}$ comparator profiles for Piezoball tests completed on 3 % fibre normally and over consolidated models.

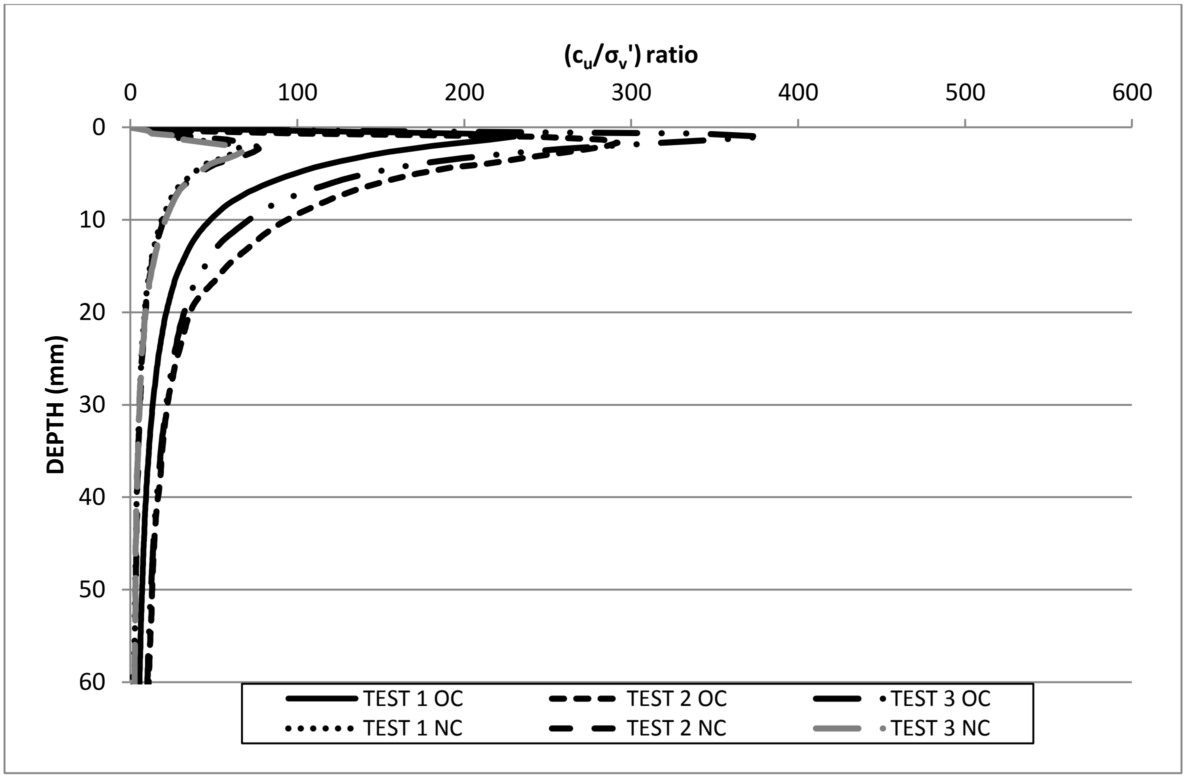

Figure H.27: $(c_u/\sigma_v')_{oc}$ and $OCR^{0.8}\,(c_u/\sigma_v')_{nc}$ comparator profiles for 30 x 60 mm rectangular foundation tests completed on 3 % fibre normally and over consolidated models.

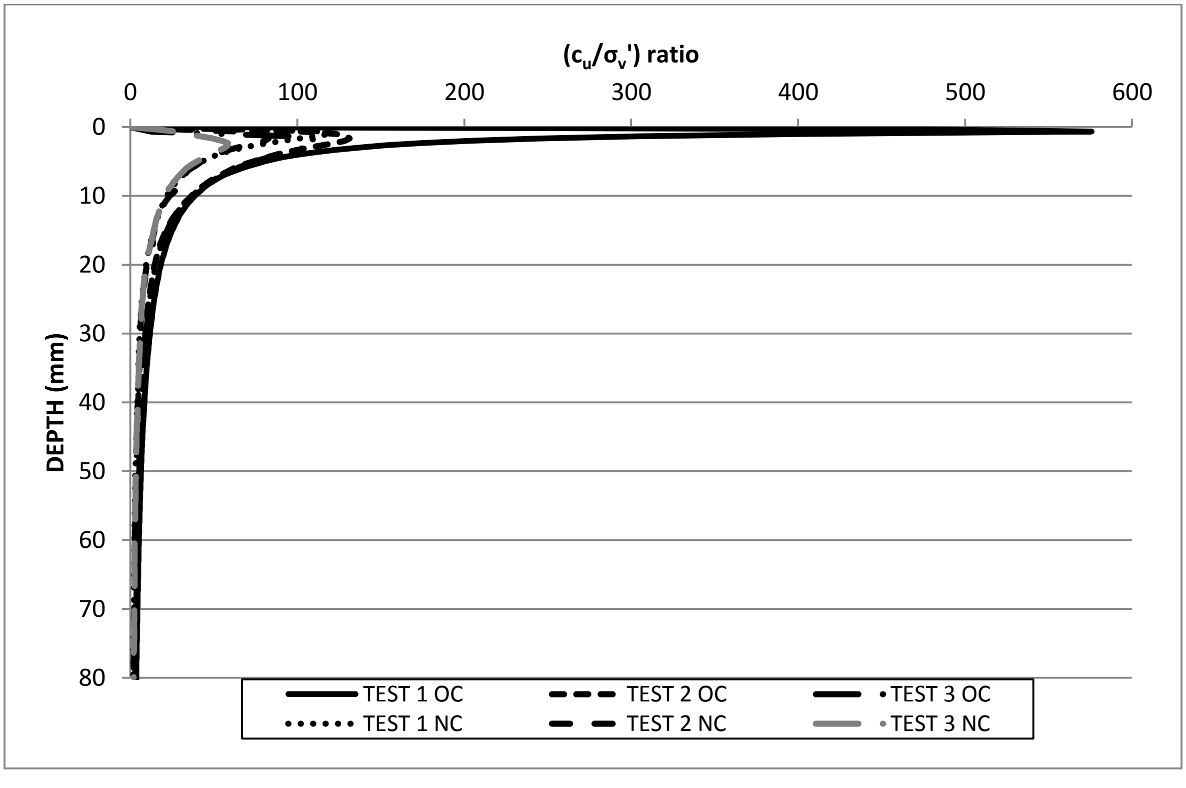

Figure H.28: $(c_u/\sigma_v')_{oc}$ and $OCR^{0.8}\,(c_u/\sigma_v')_{nc}$ comparator profiles for 40 x 80 mm rectangular foundation tests completed on 3 % fibre normally and over consolidated models.

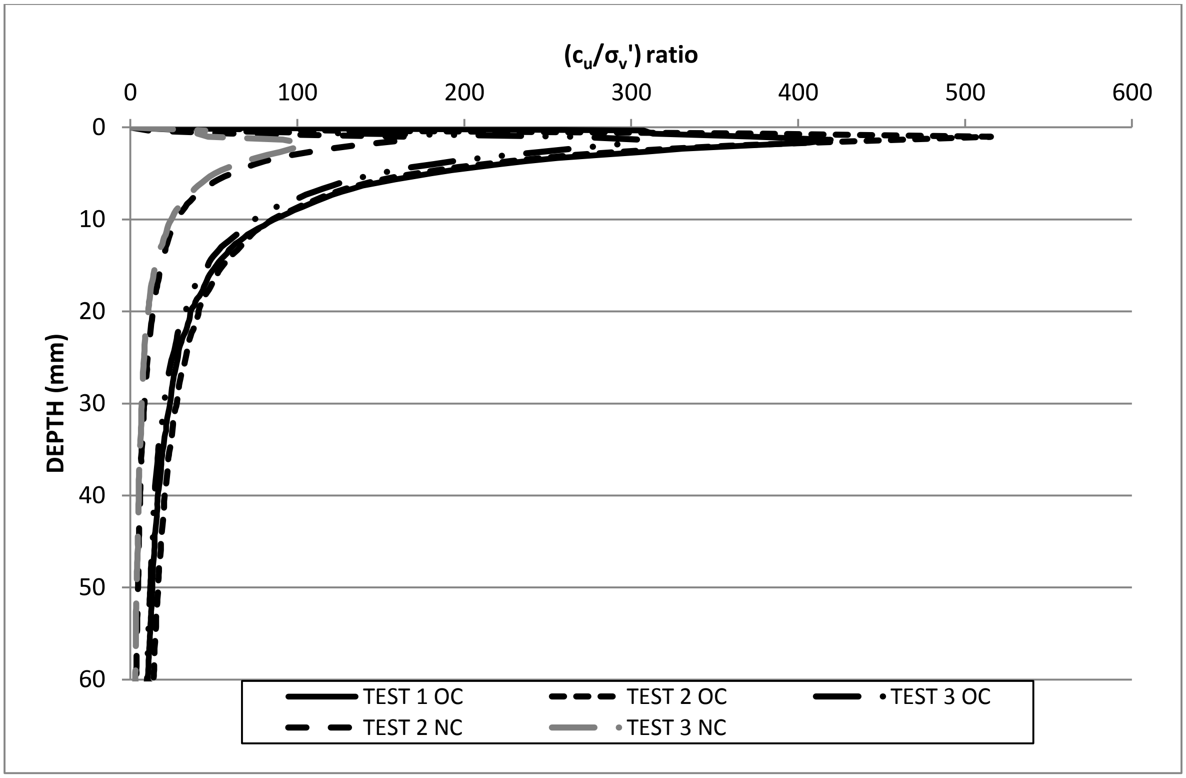

Figure H.29: $(c_u/\sigma_v')_{oc}$ and $OCR^{0.8}$ $(c_u/\sigma_v')_{nc}$ comparator profiles for 30 mm dia. circular foundation tests completed on 3 % fibre normally and over consolidated models.

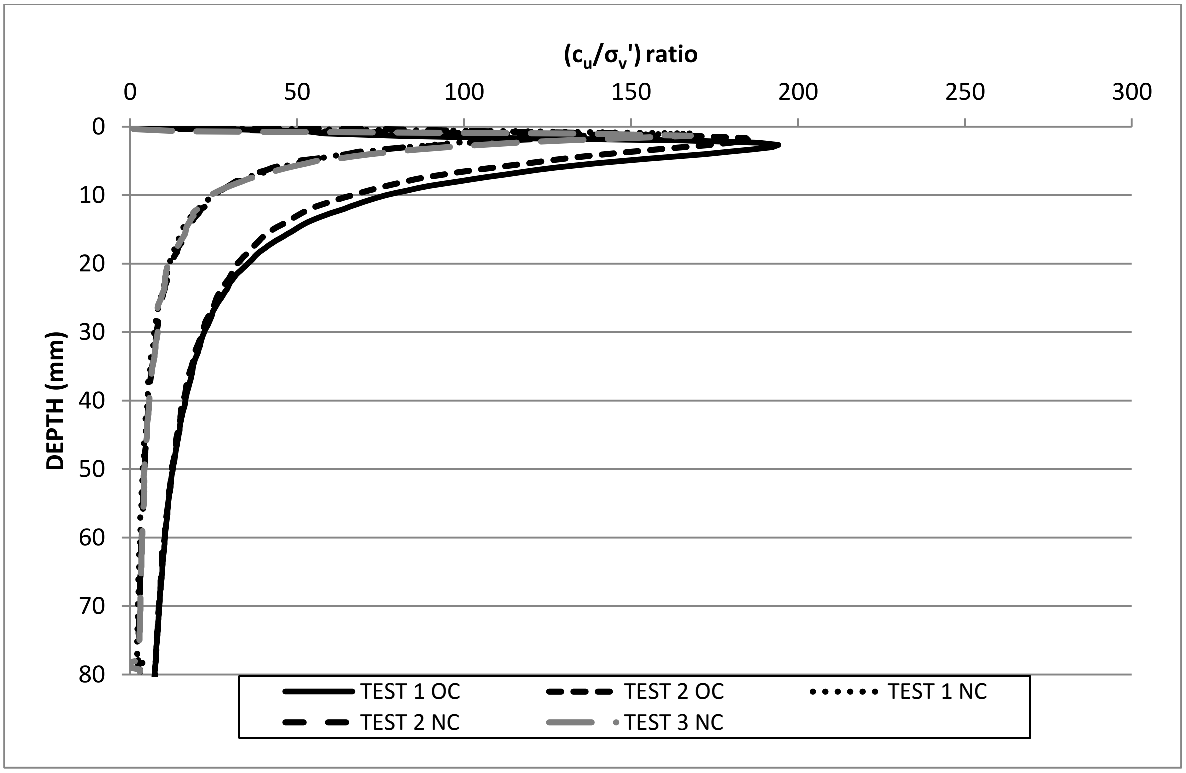

Figure H.30: $(c_u/\sigma_v')_{oc}$ and $OCR^{0.8}$ $(c_u/\sigma_v')_{nc}$ comparator profiles for 40 mm dia. circular foundation tests completed on 3 % fibre normally and over consolidated models.

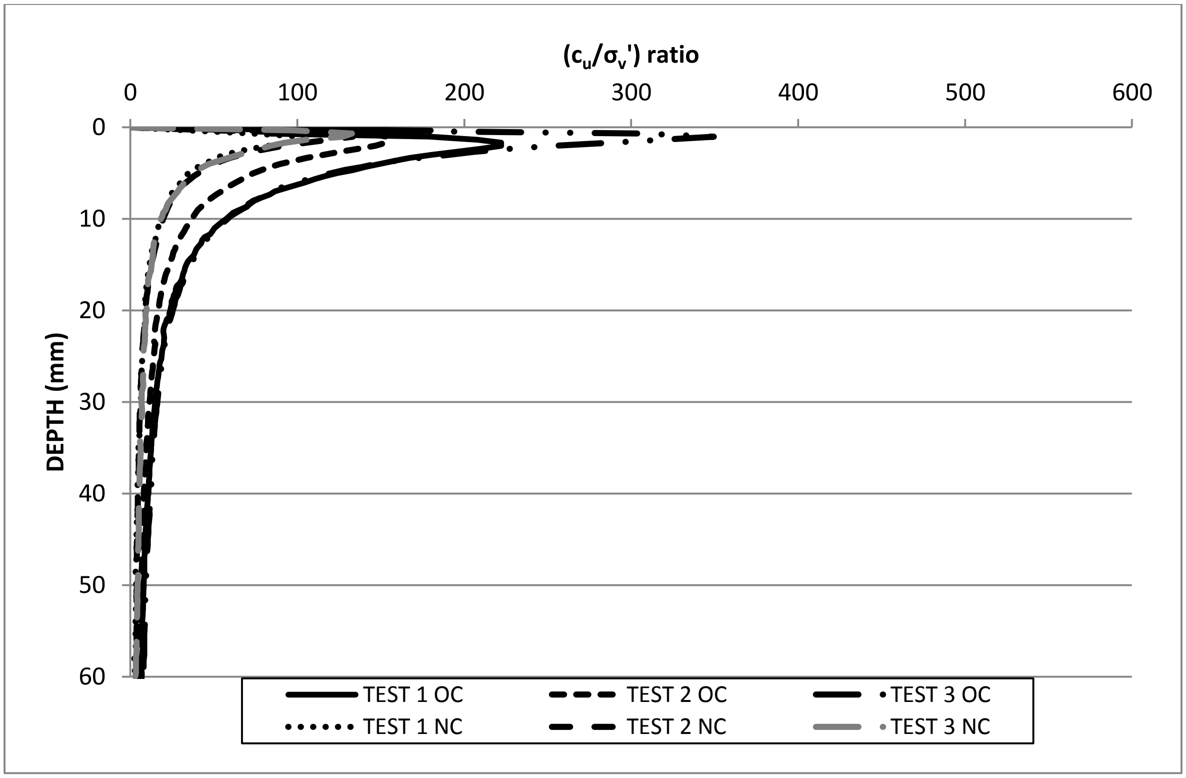

Figure H.31: $(c_u/\sigma_v')_{oc}$ and $OCR^{0.8}$ $(c_u/\sigma_v')_{nc}$ comparator profiles for 30 mm square foundation tests completed on 3 % fibre normally and over consolidated models.

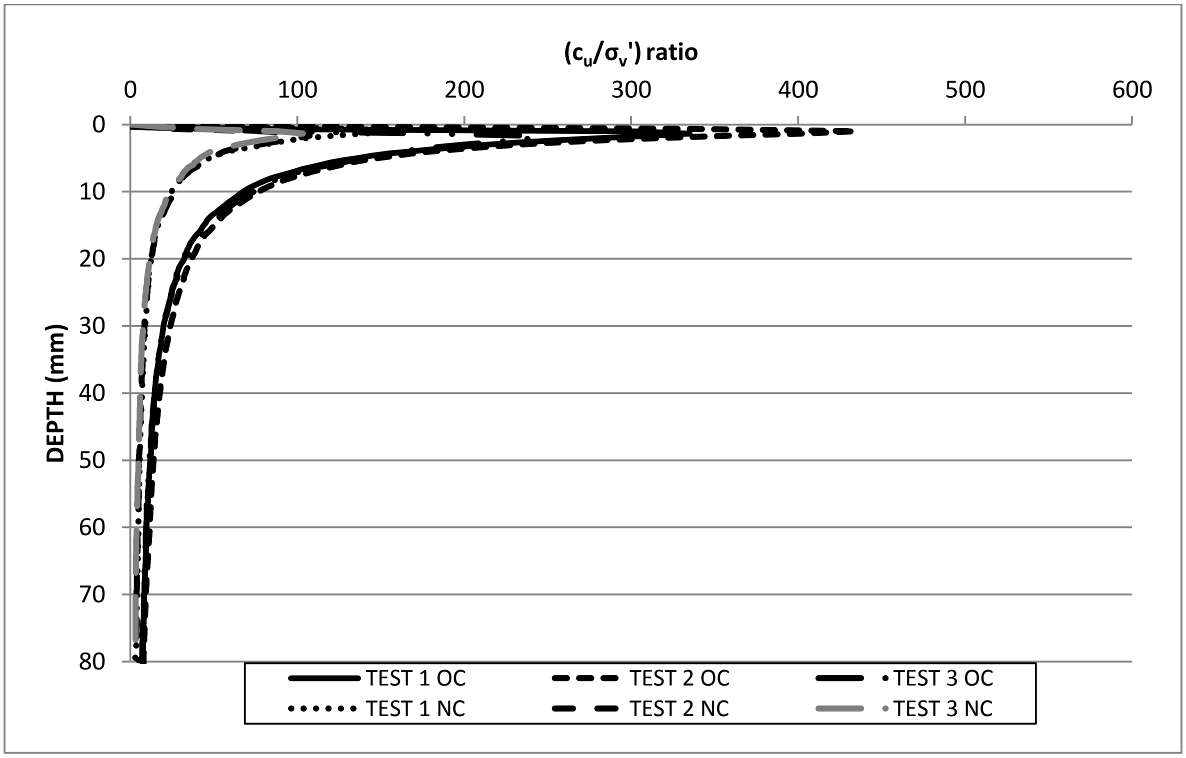

Figure H.32: $(c_u/\sigma_v')_{oc}$ and $OCR^{0.8}$ $(c_u/\sigma_v')_{nc}$ comparator profiles for 40 mm square foundation tests completed on 3 % fibre normally and over consolidated models.

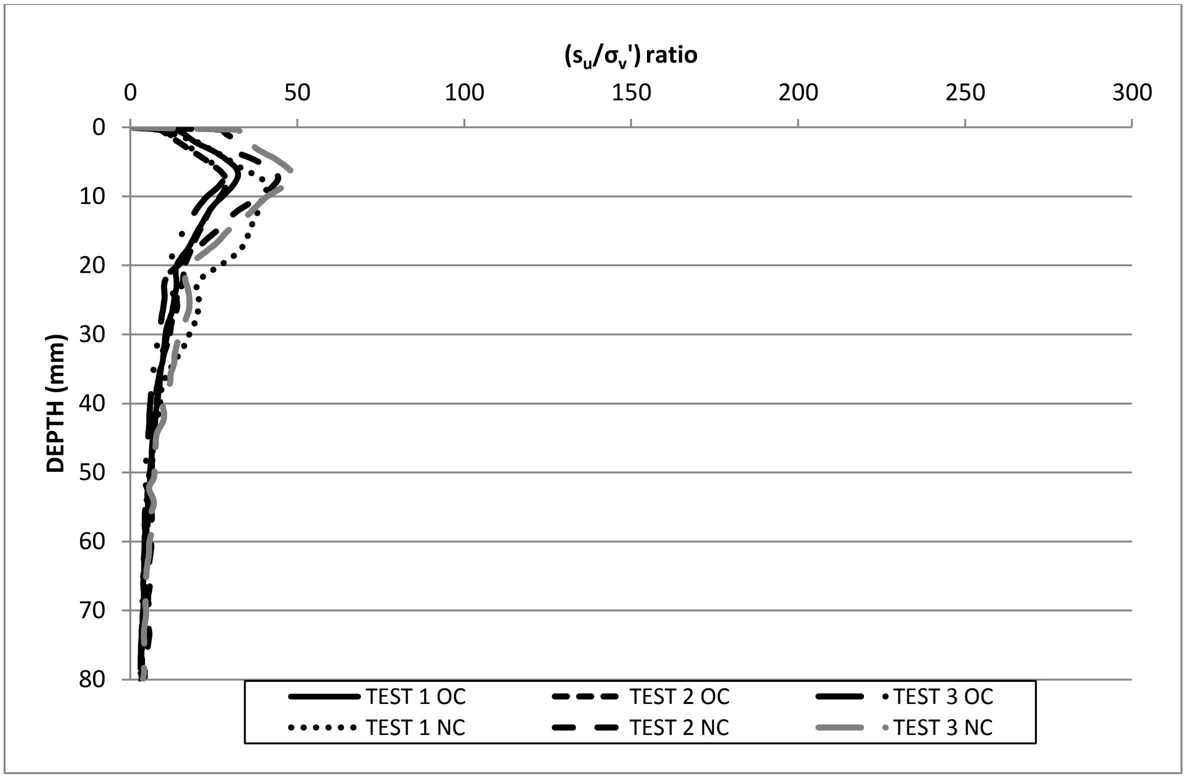

Figure H.33: $(s_u/\sigma_v')_{oc}$ and $OCR^{0.8}$ $(s_u/\sigma_v')_{nc}$ comparator profiles for CPT tests completed on 4 % fibre normally and over consolidated models.

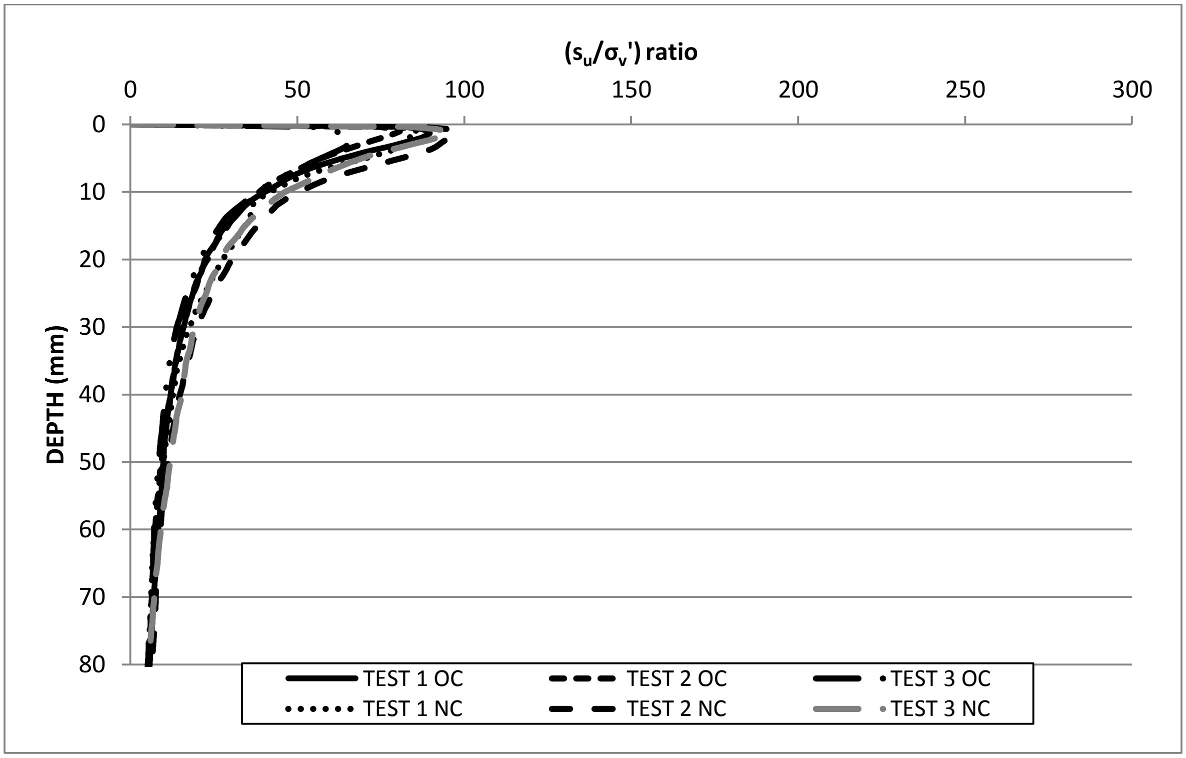

Figure H.34: $(s_u/\sigma_v')_{oc}$ and $OCR^{0.8}$ $(s_u/\sigma_v')_{nc}$ comparator profiles for Piezoball tests completed on 4 % fibre normally and over consolidated models.

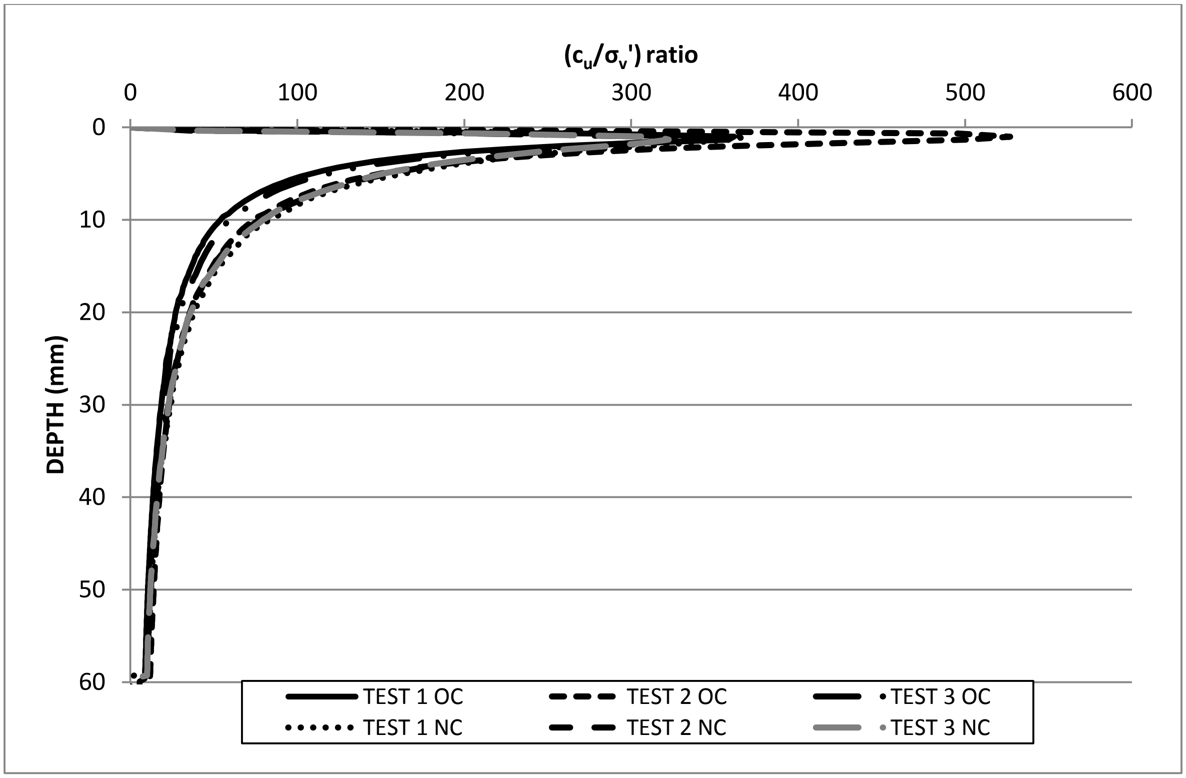

Figure H.35: $(c_u/\sigma_v')_{oc}$ and $OCR^{0.8}$ $(c_u/\sigma_v')_{nc}$ comparator profiles for 30 x 60 mm rectangular foundations tests completed on 4 % fibre normally and over consolidated models.

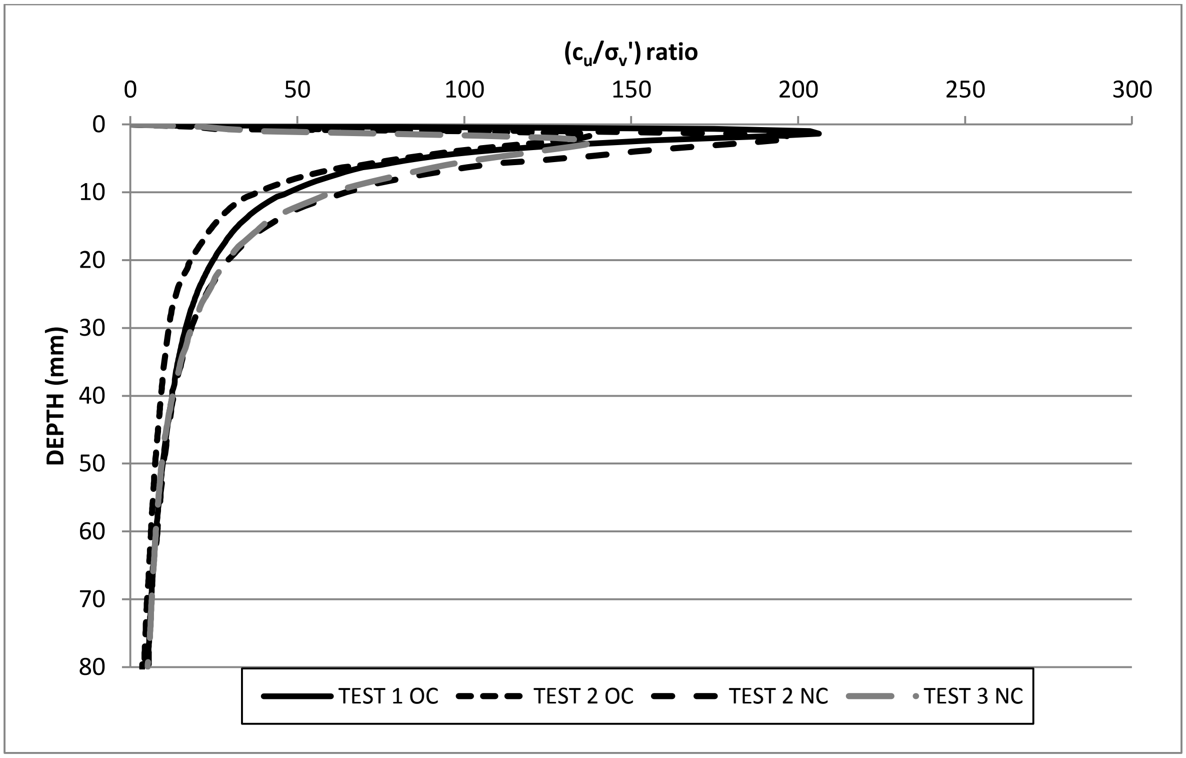

Figure H.36: $(c_u/\sigma_v')_{oc}$ and $OCR^{0.8}$ $(c_u/\sigma_v')_{nc}$ comparator profiles for 40 x 80 mm rectangular foundations tests completed on 4 % fibre normally and over consolidated models.

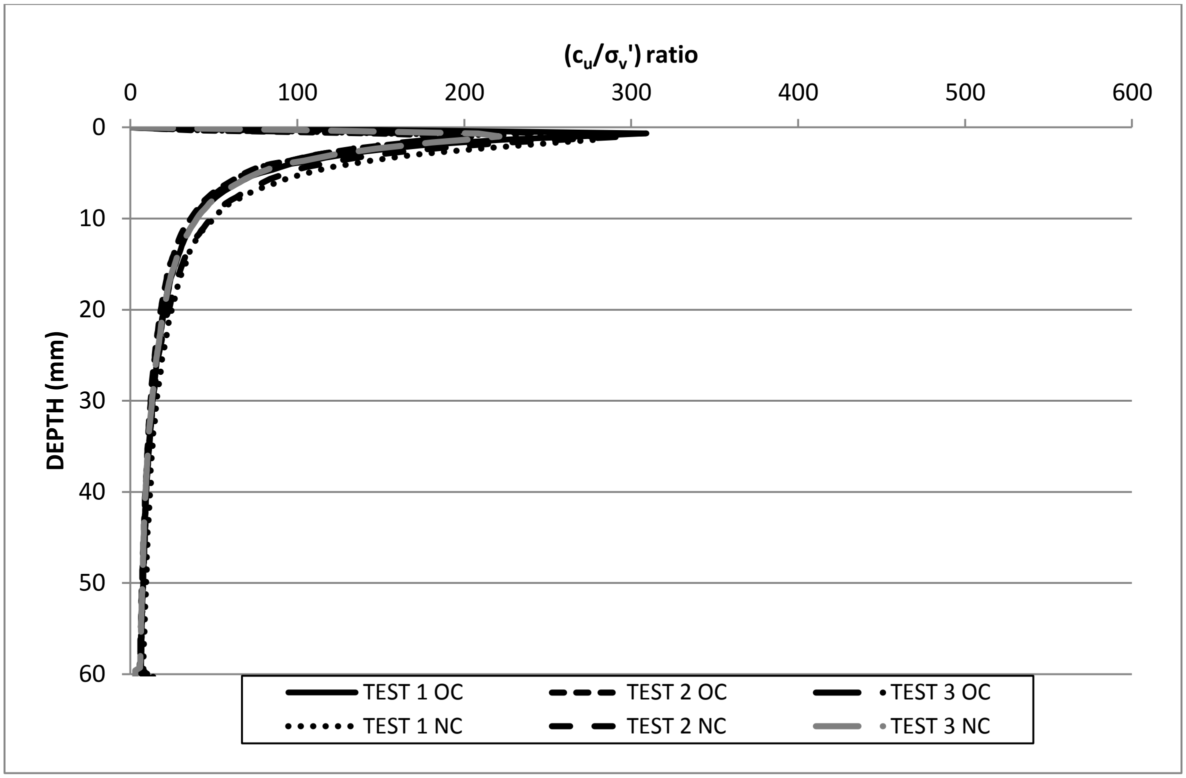

Figure H.37: $(c_u/\sigma_v')_{oc}$ and $OCR^{0.8}\,(c_u/\sigma_v')_{nc}$ comparator profiles for 30 mm dia. circular foundations tests completed on 4 % fibre normally and over consolidated models.

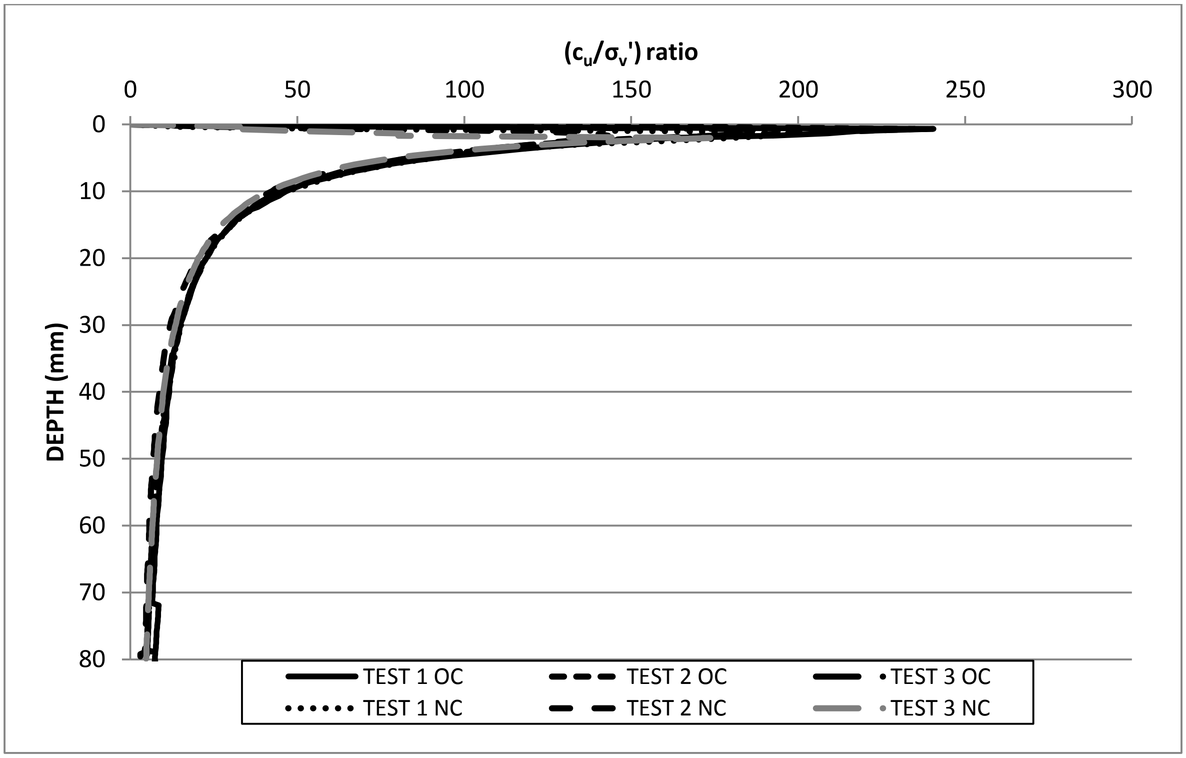

Figure H.38: $(c_u/\sigma_v')_{oc}$ and $OCR^{0.8}\,(c_u/\sigma_v')_{nc}$ comparator profiles for 40 mm dia. circular foundations tests completed on 4 % fibre normally and over consolidated models.

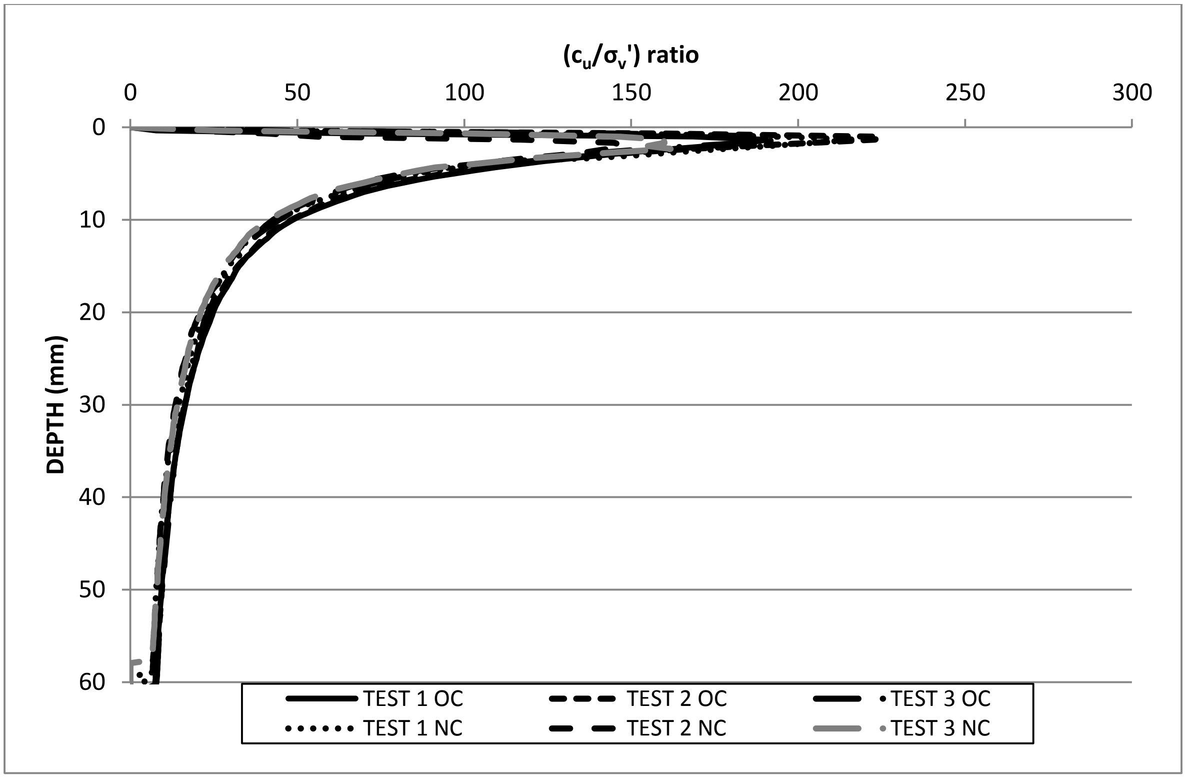

Figure H.39: $(c_u/\sigma_v')_{oc}$ and $OCR^{0.8}\,(c_u/\sigma_v')_{nc}$ comparator profiles for 30 mm square foundations tests completed on 4 % fibre normally and over consolidated models.

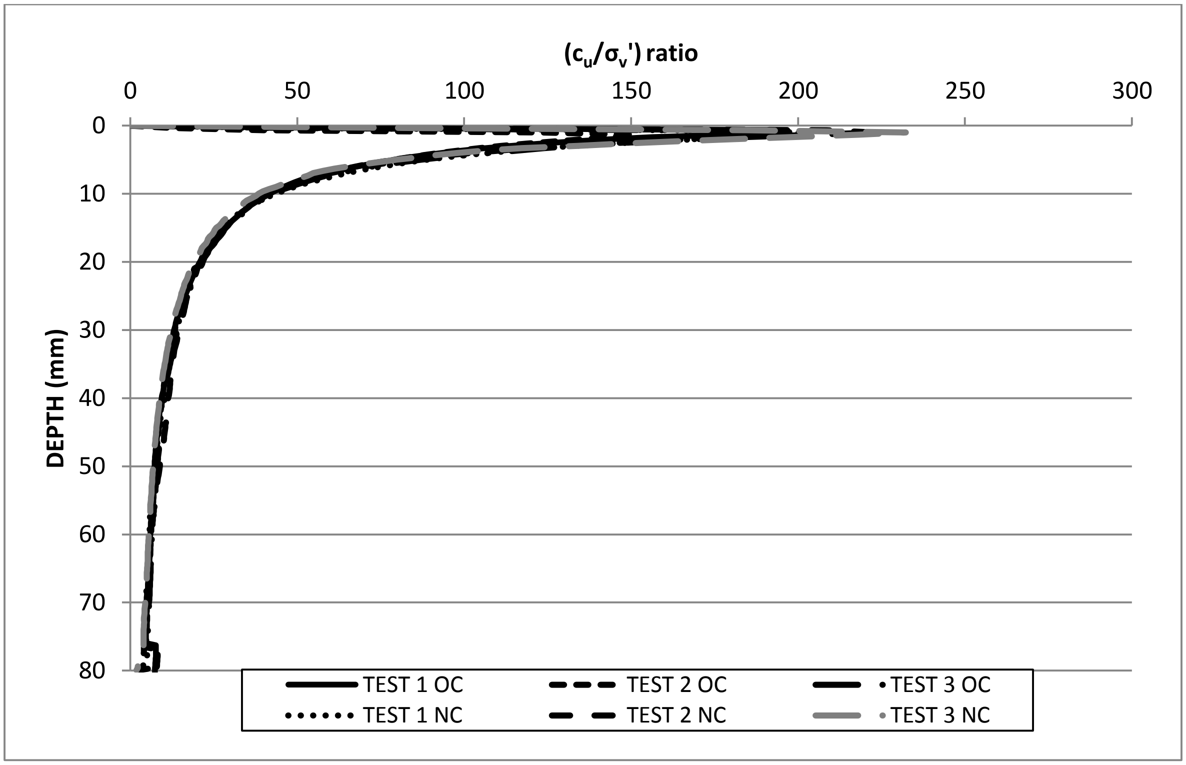

Figure H.40: $(c_u/\sigma_v')_{oc}$ and $OCR^{0.8}\,(c_u/\sigma_v')_{nc}$ comparator profiles for 40 mm square foundations tests completed on 4 % fibre normally and over consolidated models.